

Topics in Organometallic Chemistry 66

Shū Kobayashi *Editor*

Nanoparticles in Catalysis



Springer

66

Topics in Organometallic Chemistry

Series Editors

M. Beller, Rostock, Germany

P. H. Dixneuf, Rennes CX, France

J. Dupont, Porto Alegre, Brazil

A. Fürstner, Mülheim, Germany

F. Glorius, Münster, Germany

L. J. Goöben, Kaiserslautern, Germany

S. P. Nolan, Ghent, Belgium

J. Okuda, Aachen, Germany

L. A. Oro, Zaragoza, Spain

M. Willis, Oxford, UK

Q.-L. Zhou, Tianjin, China

Aims and Scope

The series *Topics in Organometallic Chemistry* presents critical overviews of research results in organometallic chemistry. As our understanding of organometallic structure, properties and mechanisms increases, new ways are opened for the design of organometallic compounds and reactions tailored to the needs of such diverse areas as organic synthesis, medical research, biology and materials science. Thus the scope of coverage includes a broad range of topics of pure and applied organometallic chemistry, where new breakthroughs are being achieved that are of significance to a larger scientific audience.

The individual volumes of *Topics in Organometallic Chemistry* are thematic. Review articles are generally invited by the volume editors. All chapters from Topics in Organometallic Chemistry are published Online First with an individual DOI. In references, Topics in Organometallic Chemistry is abbreviated as Top Organomet Chem and cited as a journal.

More information about this series at <http://www.springer.com/series/3418>

Shū Kobayashi

Editor

Nanoparticles in Catalysis

With contributions by

N. Akporji · J.-E. Bäckvall · M. Cortes-Clerget ·
I. J. S. Fairlamb · M. Haruta · T. Ishida · K. Jitsukawa ·
S. Kobayashi · E. Landstrom · B. H. Lipshutz ·
T. Mitsudome · H. Miyamura · N. W. J. Scott ·
B. S. Takale · A. Taketoshi · M. Tanabe · O. Verho ·
A. Wood · K. Yamamoto · T. Yasukawa



Springer

Editor

Shū Kobayashi
Department of Chemistry, School of Science
The University of Tokyo
Tokyo, Japan

ISSN 1436-6002

ISSN 1616-8534 (electronic)

Topics in Organometallic Chemistry

ISBN 978-3-030-56629-6

ISBN 978-3-030-56630-2 (eBook)

<https://doi.org/10.1007/978-3-030-56630-2>

© Springer Nature Switzerland AG 2020

This work is subject to copyright. All rights are reserved by the Publisher, whether the whole or part of the material is concerned, specifically the rights of translation, reprinting, reuse of illustrations, recitation, broadcasting, reproduction on microfilms or in any other physical way, and transmission or information storage and retrieval, electronic adaptation, computer software, or by similar or dissimilar methodology now known or hereafter developed.

The use of general descriptive names, registered names, trademarks, service marks, etc. in this publication does not imply, even in the absence of a specific statement, that such names are exempt from the relevant protective laws and regulations and therefore free for general use.

The publisher, the authors, and the editors are safe to assume that the advice and information in this book are believed to be true and accurate at the date of publication. Neither the publisher nor the authors or the editors give a warranty, expressed or implied, with respect to the material contained herein or for any errors or omissions that may have been made. The publisher remains neutral with regard to jurisdictional claims in published maps and institutional affiliations.

This Springer imprint is published by the registered company Springer Nature Switzerland AG.
The registered company address is: Gewerbestrasse 11, 6330 Cham, Switzerland

Preface

Metal nanoparticle catalysts are of great interest in both academia and industry, not only due to their large surface areas, producing high catalytic activity, but also for their quantum size effect, showing high activity and unique selectivity. This volume discusses the great potential of metal nanoparticle catalysts for complicated molecular synthesis and reviews the current progress of this field. The development of highly active and stable heterogeneous catalysts is a crucial subject in modern science. However, the development of heterogeneous catalysts for fine chemical synthesis has lagged far behind those for the bulk chemical process. Metal nanoparticle catalysts are an excellent candidate for the active and robust heterogeneous catalysts and this book overviews this possibility.

Recently, metal nanoparticle catalysts were widely studied and applied not only to a bulk chemical synthesis but also to various types of organic reactions. Many reviews or books about metal nanoparticles summarize their physical properties, surface structures, and/or catalytic behavior for relatively simple transformations as models and often categorized each topic by metal species. This volume summarizes recent progress on nanoparticle catalysis for various organic transformations from simple redox reactions to asymmetric C–C bond-forming reactions and also presents seminal studies on new technologies. In the chapters “Gold Nanoparticles for Oxidation Reactions: Critical Role of Supports and Au Particle Size” and “Metal Nanoparticles for Redox Reactions” of this volume, redox reactions are introduced as an investigation of metal nanoparticle catalysis for organic transformations. Several approaches to utilize earth-abundant metal nanoparticles that were recently reported are introduced in the chapter “Earth-Abundant and Precious Metal Nanoparticle Catalysis.” Precise synthesis of metal nanoclusters and their catalytic behavior including some mechanistic aspects such as active sites and effects of nanoparticle structure for catalytic activity are discussed in the chapter “Precise Synthesis of Nanoparticles and Their Catalytic Behavior.” Coupling reactions and C–H bond activations by metal nanoparticle catalysts are described in the chapter “Pd Nanoparticles in C–H Activation and Cross-Coupling Catalysis.” In the chapter “Nanoparticle Catalysts in Flow Systems,” the use of

nanoparticle catalysts under flow conditions directed toward organic synthesis is described. Finally, multidisciplinary fields such as biological applications (chapter “Nanocatalysis Meets Biology”) and asymmetric catalysis (chapter “Chiral Metal Nanoparticles for Asymmetric Catalysis”) are introduced. In those chapters, new ideas and technologies for more green and sustainable processes are discussed.

This volume comprehensively summarizes advances in metal nanoparticle catalysis across several aspects including reaction manners, mechanistic investigations, and new synthetic methodologies to encourage the use of metal nanoparticle catalysts for future organic synthesis. It can direct next-generation fine chemical synthesis.

I would like to thank all the authors for their great contributions. Professor Pierre Dixneuf (Rennes), who encouraged me strongly to make this volume, is greatly acknowledged. I am also grateful to Dr. Charlotte Hollingworth and Ms. Alamelu Damodharan (Springer Nature) for their continuous assistance to complete this volume.

Finally, I hope that this volume will lead to new ideas and research efforts in this field.

Tokyo, Japan
July 2020

Shū Kobayashi

Contents

Gold Nanoparticles for Oxidation Reactions: Critical Role of Supports and Au Particle Size	1
Tamao Ishida, Ayako Taketoshi, and Masatake Haruta	
Metal Nanoparticles for Redox Reactions	49
Koichiro Jitsukawa and Takato Mitsudome	
Earth-Abundant and Precious Metal Nanoparticle Catalysis	77
Margery Cortes-Clerget, Nnamdi Akporji, Balaram S. Takale, Alex Wood, Evan Landstrom, and Bruce H. Lipshutz	
Precise Synthesis of Nanoparticles and Their Catalytic Behavior	131
Makoto Tanabe and Kimihisa Yamamoto	
Pd Nanoparticles in C–H Activation and Cross-coupling Catalysis	171
Ian James Stewart Fairlamb and Neil Walter James Scott	
Nanoparticle Catalysts in Flow Systems	207
Hiroyuki Miyamura and Shū Kobayashi	
Nanocatalysis Meets Biology	243
Oscar Verho and Jan-E. Bäckvall	
Chiral Metal Nanoparticles for Asymmetric Catalysis	279
Tomohiro Yasukawa and Shū Kobayashi	

Gold Nanoparticles for Oxidation Reactions: Critical Role of Supports and Au Particle Size



Tamao Ishida, Ayako Taketoshi, and Masatake Haruta

Contents

1	Introduction	2
2	Oxidation of Alcohols to Aldehydes and Ketones	3
2.1	Reducible MO_x	5
2.2	Non-reducible MO_x	9
2.3	Non-oxides	10
2.4	Inorganic-Organic Hybrids	12
2.5	Carbonaceous and Organic Materials	14
2.6	Non-supported Au	17
3	Oxidation of Alcohols and Aldehydes to Carboxylic Acids	21
4	Oxidative Esterification of Alcohols and Aldehydes	23
5	Dehydrogenation of Alcohols in the Absence of O_2	25
6	Oxidation of Alkenes	28
7	Oxidation of Alkanes	32
8	Oxidative C–H Coupling Reaction	35
9	Conclusion	37
	References	38

T. Ishida (✉)

Department of Applied Chemistry for Environment, Graduate School of Urban Environmental Sciences, Tokyo Metropolitan University, Tokyo, Japan

Research Center for Gold Chemistry, Graduate School of Urban Environmental Sciences, Tokyo Metropolitan University, Tokyo, Japan
e-mail: tamao@tmu.ac.jp

A. Taketoshi

Department of Chemistry, Graduate School of Science and Engineering, Tokyo Metropolitan University, Tokyo, Japan

Research Center for Gold Chemistry, Graduate School of Urban Environmental Sciences, Tokyo Metropolitan University, Tokyo, Japan

M. Haruta

Research Center for Gold Chemistry, Graduate School of Urban Environmental Sciences, Tokyo Metropolitan University, Tokyo, Japan

Abstract Supported gold nanoparticles (Au NPs) exhibit unique catalytic properties for the oxidation of organic compounds. The catalytic activities and the selectivities of the supported Au catalysts largely depend on the kind of support and the particle size of Au. For oxidation of alcohols to aldehydes and ketones, the reducibility of metal oxide (MO_x) supports plays a prominent role, while the basicity of the supports or the size of Au particles are more important factors for non-reducible MO_x , non-oxides, and other supports. The size effect is more pronounced for dehydrogenation than aerobic oxidation because dehydrogenation takes place mainly on the low-coordinated edge and corner Au atoms. Oxidation of alkenes to epoxides using O_2 as a sole oxidant has been achieved by supported Au clusters having a diameter of 2 nm or less. For oxidation of cyclohexane using O_2 as a sole oxidant, the presence of Brønsted acid sites contributes to the production of K/A oil. The size of Au particles also largely affects the reaction rate and product selectivity; sub-nanometer Au clusters exhibited significantly higher catalytic activity and K/A oil selectivity than Au NPs.

Keywords Alcohol oxidation · Alkane oxidation · Alkene oxidation · Gold clusters · Gold nanoparticles · Oxidative coupling · Oxidative esterification

1 Introduction

Selective oxidation is of great importance in chemical industry, because oxidation reactions occupy ca. 30% of chemical processes. In particular, aerobic oxidation using O_2 or air as an oxidant is regarded as an environmentally benign reaction that can avoid use of harmful stoichiometric oxidants and minimize wastes. Thus, development of heterogeneous oxidation catalysts that have not only high catalytic activity but also high selectivity to a specific functional group in the substrates is highly desired.

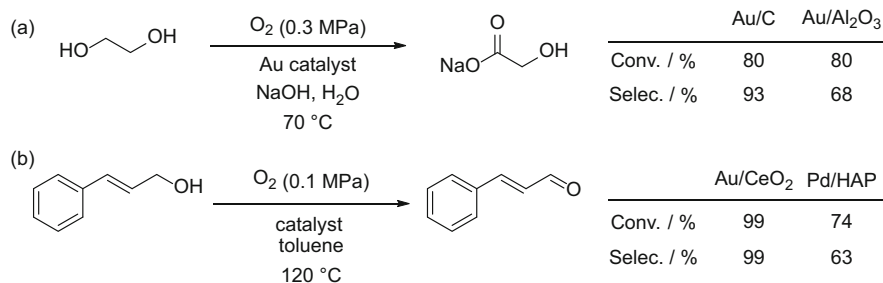
Since the discovery of catalysis by gold nanoparticles (Au NPs) in 1987 [1], Au has attracted growing interest in the field of catalysis [2–4]. In the early studies, reducible metal oxides (MO_x) supported Au NPs were revealed to exhibit very high catalytic activity for CO oxidation below room temperature, while supported Pd and Pt catalysts generally required higher reaction temperature such as 100°C [1, 5]. Au also exhibits unique catalysis for propylene oxidation to give propylene oxide directly and selectively in the presence of H_2 and O_2 [6] and then O_2 and H_2O [7]. Reducible MO_x , such as Fe_2O_3 , Co_3O_4 , NiO, and MnO_2 , are defined as that the MO_x have redox properties or have semiconducting properties. The oxygen atoms in the reducible MO_x are easily removed to form the oxygen vacancies on the surface. Because bare Au surface cannot dissociate O_2 in contrast to Pd and Pt [8], the oxygen vacancies near the Au NPs play an important role for O_2 activation in the gas-phase CO oxidation over Au catalysts. Namely, CO is adsorbed on Au NPs, and O_2 is activated at the oxygen vacancies of the reducible MO_x , so that the reaction of CO and O_2 takes place at the perimeter interface. Therefore, the catalytic activity of Au is significantly affected by the kind of supports in terms of O_2 storage-release capacity of the supports, and Au NPs on reducible MO_x

generally show superior catalytic activity to Au on non-reducible (inert) supports for CO oxidation. In addition, the perimeter length of Au NPs is proportional to $1/r^2$ (r : radius of Au particle), while the number of the surface Au atom is proportional to $1/r$. Thus, the size of Au NPs markedly influences the catalytic activity of Au for CO oxidation that takes place at the perimeter interface between Au and the supports. Au on inert supports that do not have the oxygen vacancies is less reactive and requires high reaction temperature. However, the presence of H_2O in the reaction gas remarkably enhances the CO oxidation over Au on inert supports due to the fact that H_2O can assist the O_2 activation [9, 10]. It means that the key factors to show high catalytic activity vary by the kind of supports.

In 1998, Prati and Rossi reported that supported Au NP catalysts could catalyze alcohol oxidation in liquid phase [11]. Since then, the selective oxidation for production of organic compounds in liquid phase has been intensively studied because of unique catalytic features. As observed in Au-catalyzed gas-phase reactions such as CO oxidation, Au-catalyzed reactions in liquid phase are markedly influenced by the kind of supports, the size of Au NPs, and the oxidation states in some cases. In this chapter, we chose several important oxidation reactions catalyzed by Au and focused on the role of supports and size specificity of Au.

2 Oxidation of Alcohols to Aldehydes and Ketones

Aerobic oxidation of alcohols is one of the most intensive research areas in liquid-phase organic reactions catalyzed by heterogeneous Au [12–15]. Prati and Rossi reported that Au/C and Au/ Al_2O_3 catalyzed the aerobic oxidation of 1,2-diols to glycolic acids under basic aqueous conditions (Scheme 1a) [11]. They demonstrated that these Au catalysts showed superior selectivity to supported Pd catalysts [16]. Later, various supports for Au NPs have been exploited for the aerobic oxidation of alcohols in the absence and presence of base. Corma et al. reported that Au/ CeO_2 catalyzed the aerobic oxidation of primary and secondary alcohols in the absence of base and showed higher selectivity than did supported Pd catalysts for the oxidation of unsaturated alcohols to the corresponding unsaturated ketones (Scheme 1b) [17, 18].



Scheme 1 Oxidation of 1,2-ethylene glycol to glycolic acid (a) [11, 16] and of cinnamyl alcohol to cinnamaldehyde (b) [17, 18]

Table 1 Oxidation of alcohols to aldehydes and ketones catalyzed by Au in liquid phase

	Support	nm	Key for high catalytic activity	Ref.
1. Reducible MO _x	Fe ₂ O ₃	5	Reducibility of supports	[19–21]
	MnO ₂ , NiO, CuO	3–4	Cationic Au species, surface oxygen vacancies	[22–24] [25]
	CeO ₂	2–5	Optimal surface acidity and redox properties	[17, 18, 26–28]
		Single-atom		Lattice oxygen atoms and oxygen vacancies
	TiO ₂	4–7	Size of Au, positively charged Au atoms	[30–37]
	SnO _x -SiO ₂	6	Low-coordinated Au active sites	[38]
2. Non-reducible MO _x	Al ₂ O ₃	2	Size of Au	[39]
	Ga ₂ O ₃ , Ga ₃ Al ₃ O ₉	4	High dehydrogenation activity of GaO _x	[40, 41]
	SiO ₂	5	Low coordinated sites on Au NPs	[42]
	MgO, MgZnAl ₂ O ₄ , MgFe ₂ O ₄ , Cu ₅ MgAl ₂ O _x	4–9	Basicity	[43–46]
3. Non-oxides	HT	2–3	Basicity, size of Au	[47–49]
	LDH	2–5	Defect-rich surface, basicity	[50, 51]
	HAP		Basicity	[52, 53]
	Cs ₂ CO ₃	30	Basicity	[54]
4. Hybrids	MOF	2–5	The selectivity can be tuned by the selection of supports	[55–60]
5. Organic materials	Carbon Polymer	3–4	Base is indispensable. Size of Au	[16, 61– 64]
6. Non-supported Au	NPG		Residual Ag in NPG	[65]
	Ligand-protected Au clusters and NPs		Negatively charged Au clusters. Sulfur and phosphine ligands poison the catalytic activity of Au	[66–73]

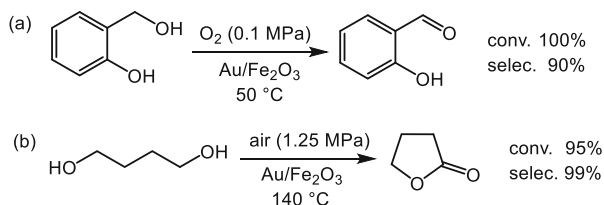
In principle, the catalytic performance of Au NPs is determined by the kind of supports and the size of Au NPs. We classified the supports as the following: (1) reducible MO_x, (2) non-reducible MO_x, (3) non-oxides (metal hydroxides, phosphates, and carbonates), (4) inorganic-organic hybrids (MOF), and (5) carbons and polymers. Inert materials including (2)–(4) also appeared to be effective supports for Au in application to alcohol oxidation in liquid-phase, but in order to show high catalytic activity, there are several key factors depending on the kind of supports. The key factors are summarized in Table 1.

2.1 Reducible MO_x

2.1.1 Role of Supports

Initially, Galvagno et al. reported that Au/Fe_2O_3 catalyzed the selective oxidation of *o*-hydroxybenzyl alcohol in the absence of base to give *o*-hydroxybenzaldehyde with 90% selectivity at a full conversion (Scheme 2a) [19]. The reducibility of Au/Fe_2O_3 prepared by CP influenced the catalytic activity of Au. Dai et al. examined Au NPs on several FeO_x (Fe_3O_4 , $\gamma\text{-}Fe_2O_3$, and $\alpha\text{-}Fe_2O_3$) for the oxidation of 1,4-butanediol (Scheme 2b) [20, 21]. As calcination temperature increased, the FeO_x crystalline structure changed from Fe_3O_4 to $\gamma\text{-}Fe_2O_3$ and then to $\alpha\text{-}Fe_2O_3$, while the size of Au NPs were almost similar for all the FeO_x . Au/FeO_x containing $\gamma\text{-}Fe_2O_3$ showed the highest activity, and Dai et al. explained that the presence of $Au^{\delta+}$ species was attributed to the high activity [20]. However, high Au^0 content on $\gamma\text{-}Fe_2O_3$ and the presence of $Au^{\delta+}$ species on $\alpha\text{-}Fe_2O_3$ also showed high catalytic activity [21].

Scheme 2 Oxidation of alcohols over Au/Fe_2O_3



Manganese oxides (MnO_x) are known as stoichiometric oxidants in organic syntheses and have also been utilized as a support for metal catalysts [22–24]. The morphology of MnO_x influenced the catalytic activity of Au NPs; $Au/\beta\text{-}MnO_2$ nanorod showed higher catalytic activity than $Au/\beta\text{-}MnO_2$ sphere for solvent-free benzyl alcohol oxidation (55% conversion, 97% benzaldehyde selectivity, metal-time yield (MTY) of 264 h^{-1}) [23]. The difference in the activity was ascribed to the presence of the higher amounts of positively charged Au and surface oxygen. Au/CuO was also reported to be highly active for the benzyl alcohol oxidation, and the redox cycles of $Au^0\text{-}Au^{\delta+}$ and $CuO\text{-}Cu_2O$ were considered to participate in the reaction mechanism [25].

CeO_2 [17, 18, 26–29] is also known as reducible MO_x due to facile redox properties and rich oxygen vacancies. The formation of oxygen vacancies varies by the size of CeO_2 particles, and Corma et al. reported that the deposition of small Au NPs (2–5 nm) onto nanocrystalline CeO_2 (5 nm) resulted in high activity and selectivity for the oxidation of alcohols to aldehydes and ketones under atmospheric O_2 in the absence of base and solvent [17, 18, 26]. Wang et al. investigated the effect of the crystalline plane of CeO_2 on the catalytic activity of Au/CeO_2 for the oxidation of benzyl alcohol [28]. Among CeO_2 nanorods, nanocubes, and nano-octahedra, the most active plane appeared to be (110) plane of nanorod CeO_2 . Raman spectroscopy was used to elucidate the formation of the oxygen vacancies, and the peak at

462 cm^{-1} corresponding to the fluorite phase was red-shifted, indicating the surface distortion caused by Au– CeO_2 interaction. The peak-shift was pronounced for nanorods rather than nano-octahedra and nanocube. Taking into account that the nanorod was largely enclosed by (110) planes, the interaction between Au and CeO_2 (110) plane would be stronger than (100) and (111) planes.

Recently, supported single Au atom catalysts have attracted growing interest because of the maximized atom efficiency. Qiao and Li et al. reported that single Au atoms on CeO_2 (Au_1/CeO_2) exhibited higher activity and selectivity for the solvent- and base-free benzyl alcohol oxidation (16% conversion, 98% selectivity, MTY of 3,091 h^{-1}) than Au NPs on CeO_2 (37% conversion, 72% selectivity, MTY of 216 h^{-1}) [29].

Au/TiO_2 has also been intensively studied for alcohol oxidations [30–37]. Hutchings et al. reported that Au/TiO_2 promoted the benzyl alcohol oxidation under solvent- and base-free conditions to give benzaldehyde in 55% selectivity at 68% conversion with TOF of 31,900 h^{-1} [30].

Solvent-free selective oxidation of benzyl alcohol to benzaldehyde is usually reported at low conversions, and an achievement of high selectivity at high conversions is rather difficult. Corma et al. demonstrated the corresponding aldehydes was obtained with excellent selectivity (98% conversion, 99% selectivity for cinnamaldehyde) by the oxidation of primary alcohol oxidation over Au/TiO_2 and Au/CeO_2 in organic solvents in the absence of base [34]. Baiker et al. screened organic solvents for benzyl alcohol oxidation over Au/TiO_2 , and mesitylene [35] or supercritical CO_2 was more suitable than toluene in terms of the selectivity of benzaldehyde.

Deposition of reducible MO_x onto inert supports has attempted to give highly dispersed reducible MO_x NPs, and Au NPs on reducible MO_x /inert supports, such as $\text{Au}/\text{Ce}-\text{SiO}_2$ [74], $\text{Au}/\text{SnO}_x-\text{SiO}_2$ [38], and $\text{Au}/\text{CeO}_2\text{-g-C}_3\text{N}_4$ [75], were reported. $\text{Au}/\text{SnO}_x-\text{SiO}_2$ showed superior catalytic activity (MTY of 15,248 h^{-1}) to those of Au/SiO_2 and $\text{Au}/\text{MoO}_x-\text{SiO}_2$ [38]. The high catalytic activity of $\text{Au}/\text{SnO}_x-\text{SiO}_2$ was due to the electron transfer between SnO_x and Au and the lattice distortion of Au, leading to more low-coordinated Au NPs. DFT calculation also suggested that the deposition of SnO_x onto Au would enhance the O_2 activation. On the other hand, no positive effect was observed for $\text{Au}/\text{MoO}_x-\text{SiO}_2$ due to weak interaction between MoO_x and Au.

2.1.2 Size Dependence

Rossi et al. studied the size effect of Au/TiO_2 and $\text{Au}/\text{Al}_2\text{O}_3$ having 3.8, 4.4, and 6.8 nm of Au NPs on the oxidation of ethylene glycol to glycolic acid and found that the catalytic activity increased as the size of Au NPs decreased [16]. Corma et al. examined the size effect of Au/TiO_2 having different size of Au NP in the range of 5–27 nm on the oxidation of cinnamyl alcohol to cinnamaldehyde [34]. The TOFs increased exponentially as the Au NPs became smaller (Fig. 1a). TOFs plotted as a function of the total number of surface Au atoms showed a linear relationship

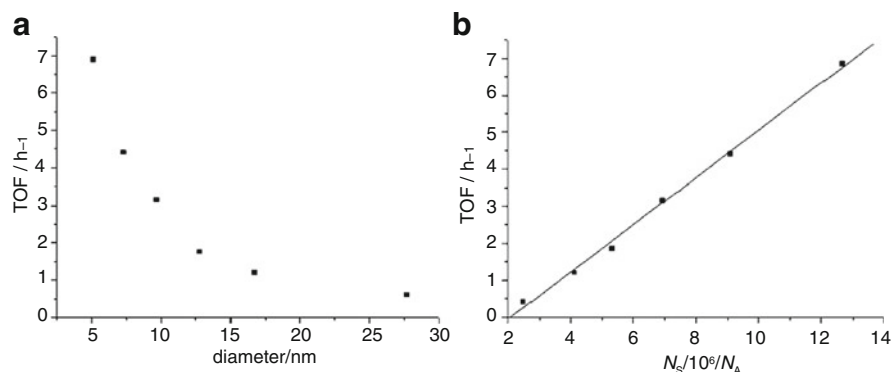


Fig. 1 Plots of TOFs as a function of the diameters of Au NPs (a) and the number of surface Au atoms (N_s) (N_A Avogadro's number) (b) for the oxidation of cinnamyl alcohol over Au/TiO₂. Adapted with permission from [34] Copyright 2008 Wiley-VCH Verlag GmbH & Co. KGaA, Weinheim

(Fig. 1b), indicating that the catalytic activity of each surface Au atoms did not alter by the size of Au NPs. On the other hand, Baiker et al. reported different size dependence on the oxidation of benzyl alcohol over Au/CeO₂ and Au/TiO₂ having 1.3, 2.1, 6.9, and 11.3 nm of Au NPs [35]. In their report, the medium size of Au NPs (6.9 nm) gave the highest activity irrespective to the MO_x, while the selectivity was not significantly influenced by the size of Au.

2.1.3 Reaction Mechanism

Christensen et al. [37] and Corma et al. [34] performed kinetic studies to discuss the reaction mechanism, respectively. Christensen et al. demonstrated a negative Hammett plot for the oxidation of *p*-substituted benzyl alcohols over Au/TiO₂, indicating that the reaction proceeds via the formation of a carbocation intermediate [37]. The same behavior was reported for Au/CeO₂ (Fig. 2) [28, 34]. According to the results that the reaction rate increased with an increase in the cationic Au content in Au/CeO₂, Xu et al. suggested that the interaction between Au and the oxygen vacancies gives Au^{δ+} species at the perimeter interface, which might favor for the formation of a carbocation-type intermediate, promoting the β-H elimination [28].

Isotopic experiments were also performed and the oxidation of deuterated benzyl alcohol- α,α -d₂ over Au/TiO₂ led to KIE (k_H/k_D) of 1.41 [37]. Corma et al. also performed isotopic experiments using α -monodeuterated benzyl alcohol and calculated the KIE to be 1.7–2.0 [34], indicating that the C–H bond cleavage was the rate-determining step (RDS). As shown in Fig. 3, the alcohol oxidation over Au/MO_x proceeds in the following order: (1) alkoxide formation on Au NPs or MO_x surface at the basic site, (2) β-hydride elimination on Au NPs (RDS), and (3) the abstraction of hydrogen atom or hydride from the Au NPs by O₂. Given that Au/MO_x catalyze alcohol oxidation in the absence of base, the surface OH group may participate in the

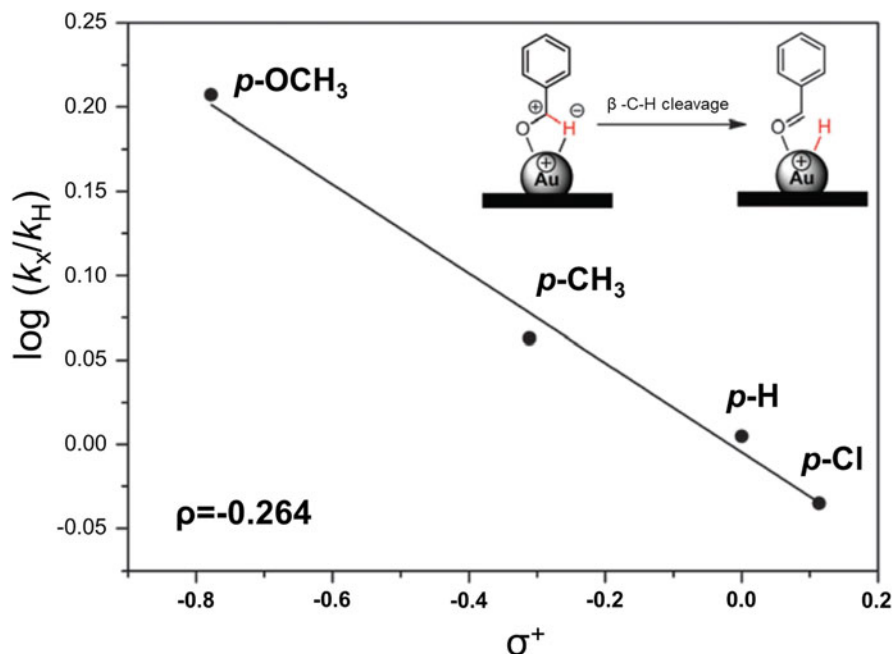


Fig. 2 Hammett plot for the oxidation of substituted benzyl alcohols over Au/CeO₂ nanorod [28]. Adapted with permission from [28] Copyright 2014 Royal Society of Chemistry

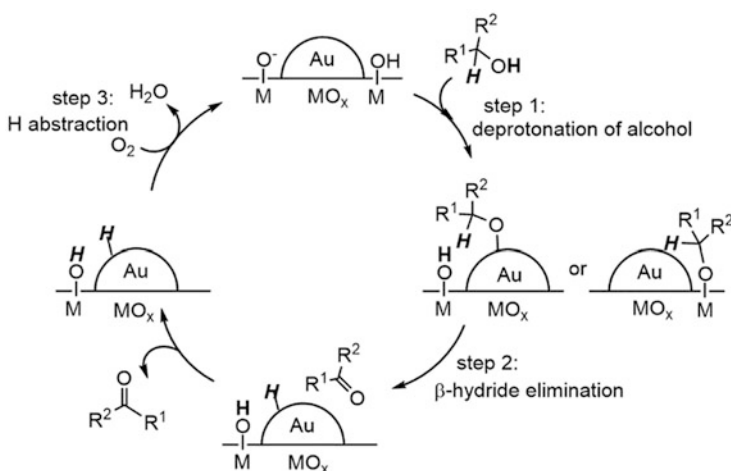


Fig. 3 A plausible reaction mechanism for alcohol oxidation over Au/MO_x

deprotonation step. In another case, MO_x provides positively charged Au atoms at the perimeter interface, which leads to form Au-alkoxides as an intermediate and accepting hydride species. The presence of the Au-H species was proved by spin trapping experiments [76].

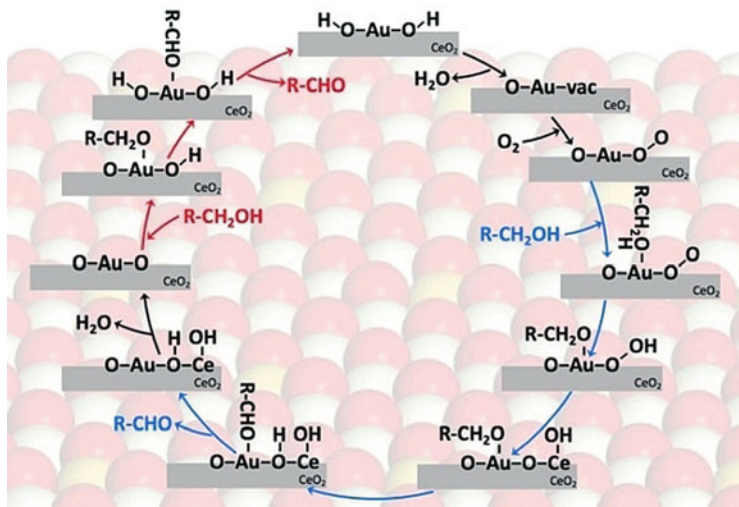


Fig. 4 A plausible reaction mechanism of alcohol oxidation over Au₁/CeO₂ [29]. Reproduced with permission from [29] Copyright 2018 Wiley-VCH Verlag GmbH&Co. KGaA, Weinheim

For highly reducible MO_x, O₂ is activated at the oxygen vacancies [17, 25, 26, 29, 34]; it is likely that the lattice oxygen was directly involved in the oxidation reaction. The H atom on the Au NPs after the β-H elimination would be abstracted by the lattice oxygen. The deposition of Au enhanced the formation of the oxygen vacancies or activated the lattice oxygen on the MO_x surface adjacent to the perimeter of the Au NPs.

Qiao and Li et al. performed kinetic studies for ethanol oxidation over Au₁/CeO₂ using ¹⁸O₂ and confirmed that H₂¹⁶O was formed together with H₂¹⁸O as a consequence of the alcohol oxidation, suggesting that the lattice oxygen of CeO₂ was used as an oxidant [29]. In addition, Au₁/CeO₂ produced a higher amount of H₂¹⁶O than did Au NPs on CeO₂ which produced more H₂¹⁸O. The results indicated that the lattice oxygen of CeO₂ was more activated by single Au atom and readily used for the oxidation, while ¹⁸O₂ was used directly over Au NPs on CeO₂. Given that the amount of the oxygen vacancies correlates to the catalytic activity of Au, Qiao and Li et al. proposed the reaction mechanism in which the lattice oxygen of MO_x may play a key role in the reaction via Mars-van Krevelen-like mechanism as shown in Fig. 4 [29].

2.2 Non-reducible MO_x

SiO₂ and Al₂O₃ are classified as non-reducible MO_x, because of the lack of redox properties, and Au on mesoporous SiO₂ [42] and Au/Al₂O₃ [39] were reported to be

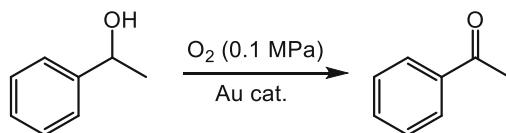
active for liquid-phase oxidations. In contrast to the Au/reducible MO_x catalysts, size of Au NPs and acid-base properties of MO_x become more important for Au/non-reducible MO_x catalysts. Low-coordinated sites on the Au NPs would be the active sites for O_2 activation and the adsorption sites of the substrate [77]. Au/ $\gamma\text{-Ga}_2\text{O}_3$ catalyzed base-free oxidation of benzyl alcohol in mesitylene to give benzaldehyde with 99% selectivity at >99% conversion [40]. In addition, the catalytic activity of Au/ $\gamma\text{-Ga}_2\text{O}_3$ exceeded those of Au/ TiO_2 , Au/ CeO_2 , and Au/ Fe_2O_3 . The remarkable high activity was speculated by dehydrogenation activity, and temperature-programmed surface reaction (TPSR) of 2-propanol was examined for Au/ $\gamma\text{-Ga}_2\text{O}_3$. As the temperature increased, 2-propanol adsorbed on the catalysts was converted to acetone together with the formation of H_2 . Accordingly, more intense H_2 desorption peak was observed for $\gamma\text{-Ga}_2\text{O}_3$ itself than those observed for Au/ CeO_2 (the H_2 desorption was not observed for Au/ TiO_2 and Au/ Fe_2O_3). In addition, H_2 desorption peak for Au/ $\gamma\text{-Ga}_2\text{O}_3$ was shifted to lower temperature from that for $\gamma\text{-Ga}_2\text{O}_3$ itself, indicating that $\gamma\text{-Ga}_2\text{O}_3$ has high activity for the dehydrogenation and Au NPs facilitate the reaction. Ga-Al mixed oxides were also examined and Au/ $\text{Ga}_3\text{Al}_3\text{O}_9$ showed the higher activity than Au/ Ga_2O_3 and other Au/ $\text{Ga}_x\text{Al}_y\text{O}_z$ catalysts. The catalytic activity order was consistent to the order of dehydrogenation activity which was elucidated by the amount of desorbed H_2 from 2-propanol by TPSR [41]. Au NPs supported on MgO [43], $\text{Mg}_x\text{Al}_y\text{O}_z$, Cu-containing $\text{Mg}_x\text{Al}_y\text{O}_z$ spinel-type oxides [44, 45], and MgFe_2O_4 [46] also promoted the oxidation of alcohols in the absence of base. For Cu-containing $\text{Mg}_x\text{Al}_y\text{O}_z$, the introduction of redox-active Cu might change the surface basicity, affect the electronic state of Au, and add the redox properties of Cu in some extent, which led to the improved activity from Au/ $\text{Mg}_x\text{Al}_y\text{O}_z$ without Cu [44].

2.3 Non-oxides

2.3.1 Role of Supports

Metal hydroxides, phosphates, and carbonates are classified as non-oxides inorganic supports. Au NPs on basic hydrotalcite (HT: $\text{Mg}_6\text{Al}_2(\text{OH})_{16}\text{CO}_3 \cdot n\text{H}_2\text{O}$) exhibited high catalytic activity for oxidation of various alcohols in the absence of base [47, 48]. Au/HT exhibited superior activity and selectivity (99% at 99% conversion) to Au/ Al_2O_3 and Au/MgO, reported by Kaneda et al. [47]. Au/MgCr-HT (Cr^{3+} substituted HT) improved the catalytic activity from Au/HT [49]. The oxidation of a primary aliphatic alcohol, 1-octanol, did not proceed to give octanal over Au/HT in the absence of base [47] but proceed over Au/MgCr-HT, whereas the conversion was lower than those for aromatic alcohols. Au/MgCr-HT also recorded extremely high TOF ($81,000 \text{ h}^{-1}$) for solvent-free oxidation of 1-phenyl ethanol to give acetophenone (Table 2).

A series of Au clusters (ca. 1.5 nm in diameters) on $\text{M}_3\text{Al-LDH}$ ($\text{M} = \text{Ni}, \text{Co}, \text{Mg}$) exhibited high catalytic activity for base-free oxidation of 1-phenylethanol to give TOF of $46,500 \text{ h}^{-1}$ over Au/ $\text{Ni}_3\text{Al-LDH}$ (Table 2) [50]. Both strong acidic and

Table 2 The comparison of TOFs for the solvent- and base-free oxidation of 1-phenylethanol over supported Au catalysts

Catalyst	Temp. (°C)	TOF (h ⁻¹)	Ref.
Au/MnO ₂	140	15,760	[23]
Au/CeO ₂	140	12,500	[26]
Au/Ga ₃ Al ₃ O ₉	160	25,000	[41]
Au/MgCr-HT	160	81,000	[49]
Au/Ni ₃ Al-LDH	160	46,500	[50]
PI Au	160	20,000	[83]

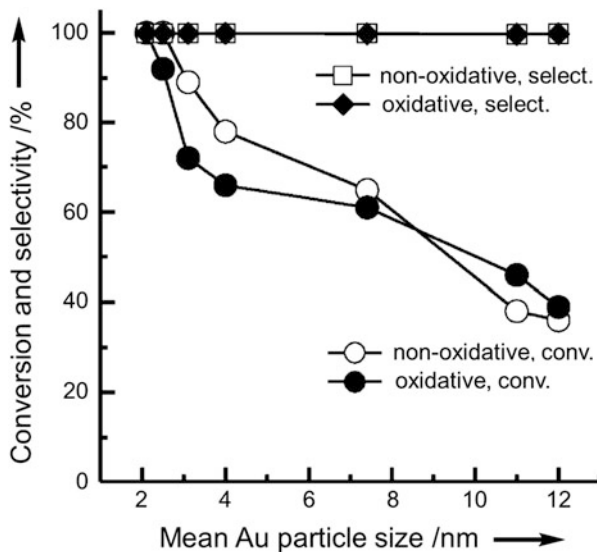
basic sites on the LDH surface would contribute to the alcohol oxidation; the surface basic sites (M–OH^{δ-}) would promote deprotonation from the OH group of the substrate alcohols, and the acidic sites would facilitate the removal of H species on the Au NPs [78].

Given that the early studies revealed that base is required to promote the alcohol oxidation for Au/C but not for Au/MO_x, the basic sites of MO_x and non-oxides are more important for the deprotonation of alcohols in the initial step. Wang et al. disclosed that Au/hydroxyapatite (HAP) showed the oxidative SMSI in which Au NPs were partly covered by HAP thin layer under oxidative thermal treatment [52], which is highly contrast to the conventional SMSI that occurs under reductive thermal treatment. The another unique feature of the oxidative SMSI of Au/HAP is to give positively charged Au species while the conventional SMSI leads to negatively charged metal species. They exploited Au/HAP for solvent- and base-free benzyl alcohol oxidation and evaluated the effect of SMSI [52]. Unfortunately, Au/HAP with SMSI showed lower catalytic activity than did Au/HAP without SMSI probably due to the decrease in the exposed Au surface. However, Au/HAP with SMSI improved the selectivity to benzaldehyde and reusability from Au/HAP without SMSI, and the catalytic activity of Au/HAP with SMSI exceeded the one without SMSI after the second run in the recycling test.

2.3.2 Size Dependence

The size dependence of Au/HT (2.1–12 nm) [48] and Au/HAP (1.7–7.7 nm) [53] were studied, and the catalytic activity increased with a decrease in the size of Au NPs. Zhang and Wang et al. reported that Au/HT promoted the benzyl alcohol oxidation not only under oxidative (O₂) but also non-oxidative (Ar) conditions [48]. The size dependence on the reaction rate was observed under both O₂ and Ar atmosphere (Fig. 5), although the degree of changes in the reaction rate was different between O₂ and Ar atmosphere due to much inferior activity under Ar. The size

Fig. 5 Conversion and selectivity as a function of Au particle size for the benzyl alcohol oxidation over Au/HT under oxidative (O₂ 0.1 MPa, flow) and non-oxidative (Ar 0.1 MPa, flow) conditions [48]. Note that 20 times amount of Au/HT was used for the non-oxidative reaction. Adapted with permission from [48] Copyright 2014 Wiley-VCH Verlag GmbH&Co. KGaA, Weinheim



dependence was studied in the range of 2.1–12 nm, and the TOF increased 4.3 times as the size of Au NPs decreased under Ar, whereas the TOF increased only 1.7 times under O₂, suggesting that the size dependence was pronounced for dehydrogenation. Zhang and Wang et al. speculated the different active sites varying by the reaction conditions. Given that the fractions of terrace, edge, and corner atoms alter by the Au particle size as shown in Fig. 6a, the logarithm of the reaction rates proportionally increased with the logarithm of the diameter of Au NPs as functions of $d^{-1.1}$ and $d^{-1.9}$ (d = diameter of Au NPs (nm)) for oxidative and non-oxidative reactions, respectively (Fig. 6b). These values were in accordance with the relationships between d and the fraction of terrace Au atoms and edge Au atoms (together with corner Au atoms) (Fig. 6a), respectively. Slight differences of the relationships in Fig. 6a, b indicated that the multiple Au sites contributed to the benzyl alcohol oxidation. These results suggest that the aerobic oxidation takes place mainly on the terrace Au atoms while non-aerobic oxidation (dehydrogenation) takes place mainly on the low-coordinated edge and corner Au atoms.

The KIEs for Au-/HT-catalyzed oxidation and dehydrogenation of benzyl alcohol were reported to be 2.9 and 2.2, respectively, indicating that the RDS of both of the reaction was the C–H bond cleavage [48].

2.4 Inorganic-Organic Hybrids

Metal-organic frameworks (MOFs) consisting of highly ordered nanometer-sized porous structure are promising materials for applications into not only gas storage materials but also supports for metal clusters. Au NPs could be deposited as NPs and

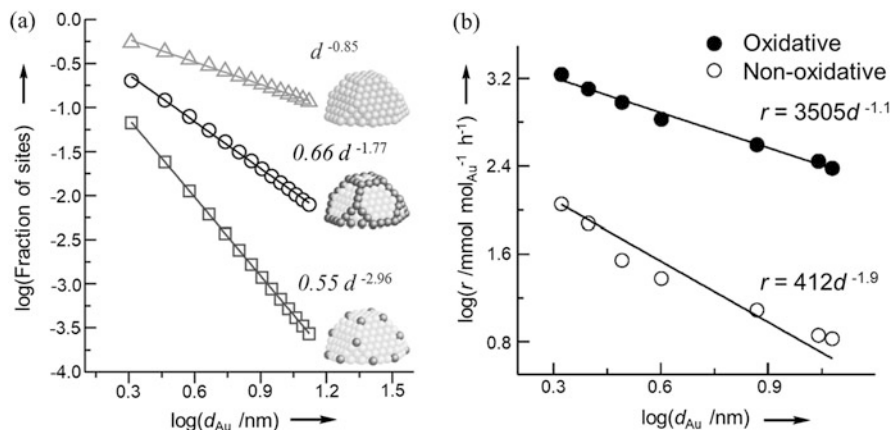
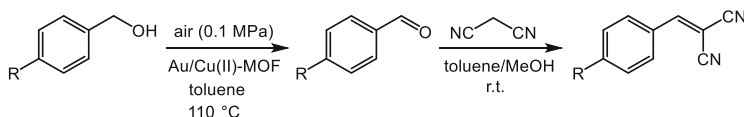


Fig. 6 Dependence of the fraction of terrace (triangles), edge (circles), and corner Au atoms (squares) on Au particle size in a truncated cuboctahedron (a) and dependence of the TOF for benzyl alcohol oxidation under oxidative and non-oxidative conditions (b) [48]. Adapted with permission from [48] Copyright 2014 Wiley-VCH Verlag GmbH&Co. KGaA, Weinheim

clusters onto several kinds of MOFs (MOF-5: $[\text{Zn}_4\text{O}(\text{bdc})_3]_n$ (bdc = benzene-1,4-dicarboxylate), Al-MIL-53: $[\text{Al}(\text{OH})(\text{bdc})]_n$, and CPL-2: $[\text{Cu}_2(\text{pzdc})_2(\text{bpy})]_n$ (pzdc = pyrazine-2,3-dicarboxylate, bpy = 4,4'-bipyridine)), and the resultant Au/MOFs were examined for the oxidation of alcohols in methanol in the absence of base [55]. The catalytic activity was much influenced on the kinds of MOFs rather than the size of Au particles: the catalytic activity for 1-phenylethanol oxidation increased in the order of Au/MOF-5 > Au/Al-MIL-53 > Au/CPL-2. The selectivity also varied by the kind of MOFs. When Au/MOF-5 and Au/Al-MIL-53 were used, methyl benzoate was selectively obtained, whereas benzaldehyde was obtained as a major product by Au/CPL-2. The size dependence of Au on the same MOF was studied for Au/MIL-101 prepared by different methods. The 2 nm of Au clusters on MIL-101 exhibited TOF of 258 h^{-1} , although the Au NPs larger than 6 nm showed very low TOF [56]. For Au/MOFs, the size of Au particles is more critically important for hydrogenation reactions [79, 80]. Au/MIL-101 ($\text{Cr}_3(\text{F},\text{OH})\text{O}(\text{bdc})_3$) [56] and Au/UiO-66 ($\text{Zr}_6\text{O}_4(\text{OH})_4(\text{bdc})_6$) [57–59] also exhibited high activity for oxidation of alcohols. Van der Voort et al. demonstrated the formation of oxygen ad-atoms (Au–O) and peroxy species (Au–OO) on Au/UiO-66 in a stream of O_2 by Raman spectroscopy [59]. It is also known that MOFs themselves work as heterogeneous acid catalysts. By combining the catalysis by Au and MOFs, Au/Cu(II)-MOF worked as a bifunctional catalyst to enable a one-pot reaction of benzyl alcohol oxidation followed by Knoevenagel condensation with malononitrile to obtain benzylidenemalononitrile (Scheme 3) [60].



Scheme 3 Oxidation–Knoevenagel condensation of benzyl alcohol over Au/Cu(II)-MOF [60]

2.5 Carbonaceous and Organic Materials

In the early stage of research, the deposition of Au NPs and clusters onto inert supports were difficult by conventional deposition-precipitation (DP) using HAuCl_4 as a precursor due to electrostatic repulsion between $[\text{Au}(\text{OH})_4]^-$ and negatively charged inert support surface. Therefore, colloid immobilization (CI) using ligand- or polymer-protected Au NPs had been usually exploited for the preparation of Au/C, and other new deposition techniques have also been developed to prepare Au/C and Au/polymers [81]. These Au catalysts have appeared to catalyze liquid-phase oxidation. Whereas Au/ MO_x and Au on basic non-oxides promote alcohol oxidations in the absence of base, base is often required for Au/C and Au/polymers under mild conditions. In early studies, more than stoichiometric amount of base was required for alcohol oxidations over Au/C [11].

Recently, Au on modified carbonaceous materials was reported to catalyze the alcohol oxidation even in the absence of base. Wang et al. reported that nitrogen-doped graphenes (NG) enable to deposit small Au NPs (ca. 3 nm), whereas the size of Au on the undoped graphene was much larger (>20 nm), and the resultant Au/NG promoted the base-free oxidation of alcohols [82].

Kobayashi et al. demonstrated that polymer-incarcerated Au cluster (1 nm) catalysts (PI Au) (Fig. 7) catalyzed the oxidation of 1-phenylethanol at room temperature in the presence of K_2CO_3 [83]. PI Au exhibited high catalytic activity (TOF of $20,000 \text{ h}^{-1}$) under solvent- and base-free oxidation of 1-phenylethanol at 160°C [26]. They also fabricated PI carbon-stabilized Au catalysts (PI/CB-Au) and performed the oxidation of various alcohols in the presence of base [84].

Recently, the rational design of organic materials enables Au/polymer catalysts to apply for base-free oxidation of alcohols. Shaabani et al. designed a supramolecular ionic liquid (IL)-grafted graphene in which Au NPs were stabilized in IL moiety

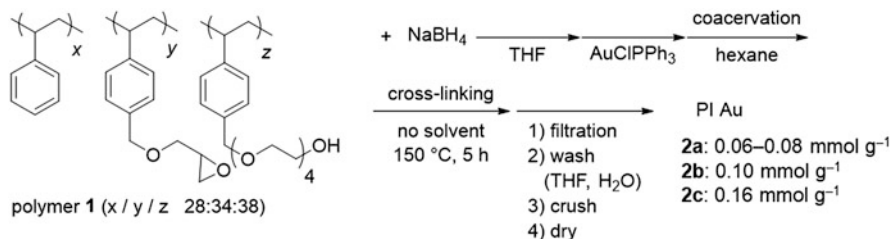


Fig. 7 Synthetic route of PI Au [83]. Adapted with permission from [83] Copyright 2007 Wiley-VCH Verlag GmbH&Co. KGaA, Weinheim

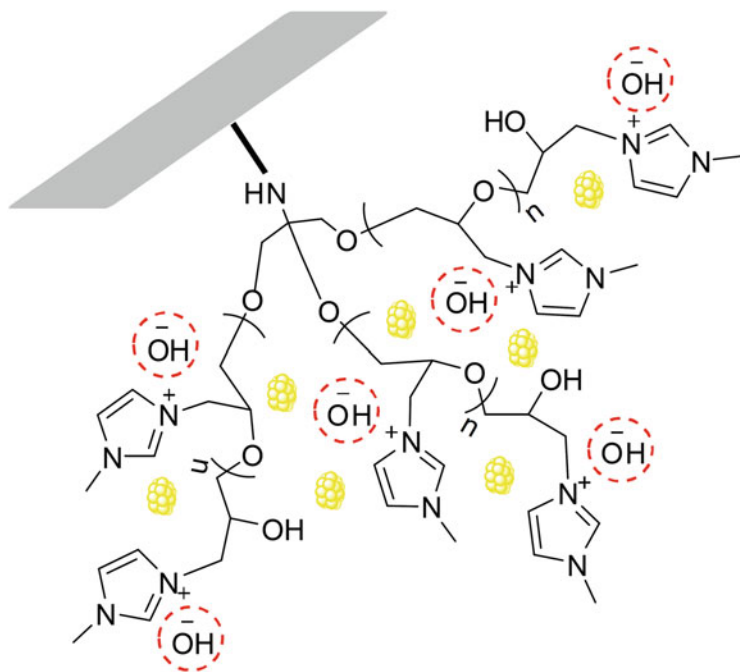


Fig. 8 Schematic image of Au NPs@SIL-g-G [61]. A gray sheet and yellow circles represent graphene and Au NPs, respectively. Adapted with permission from [61] Copyright 2013 Royal Society of Chemistry

(Au NPs@SIL-g-G, Fig. 8) and used Au NPs@SIL-g-G as a bifunctional catalyst for the base-free aerobic oxidation of various alcohols to the corresponding aldehydes and ketones at room temperature. The counter anion (OH^-) of the imidazolium unit in IL worked as a base to deprotonate the alcohol, and Au is responsible for the β -H elimination to give aldehydes or ketones [61]. Au NPs on basic ion-exchange resins also work as bifunctional catalysts in which the resin deprotonated the alcohol [85].

Nanoporous ionic organic networks (PIONs) having a high ionic density were also designed to stabilize Au NPs with a mean diameter of 2.2 nm (Fig. 9) [62]. The obtained Au/PION catalyzed the base-free oxidation of aliphatic secondary alcohols and 1-octanol to obtain ketones and octanal, respectively. For solvent- and base-free oxidation of cyclohexanol to cyclohexanone at 140°C , Au/PION showed comparable TOF ($2,064 \text{ h}^{-1}$) to Au/ TiO_2 ($2,517 \text{ h}^{-1}$) but much higher selectivity (95%) than 72% obtained by Au/ TiO_2 . High selectivity of Au/PION was explained by the suppression of O_2^- radical-induced over-oxidation according to the report that pyridinium/imidazolium cation could stabilize O_2^- radical [62, 86].

Dai et al. fabricated conjugated organic networks containing carbazole and pyridine units followed by quaternalization of the pyridine and anion-exchange to give P-CON-F and reported that the P-CON-F could stabilize small Au clusters (1.3 nm), whereas P-CON and P-CON-I resulted large Au NPs such as 12.7 and 2.8 nm, respectively (Fig. 10) [63]. The AuNCs@P-CON-F exhibited high catalytic activity for the base-free cyclohexanol oxidation ($\text{TOF } 129 \text{ h}^{-1}$).

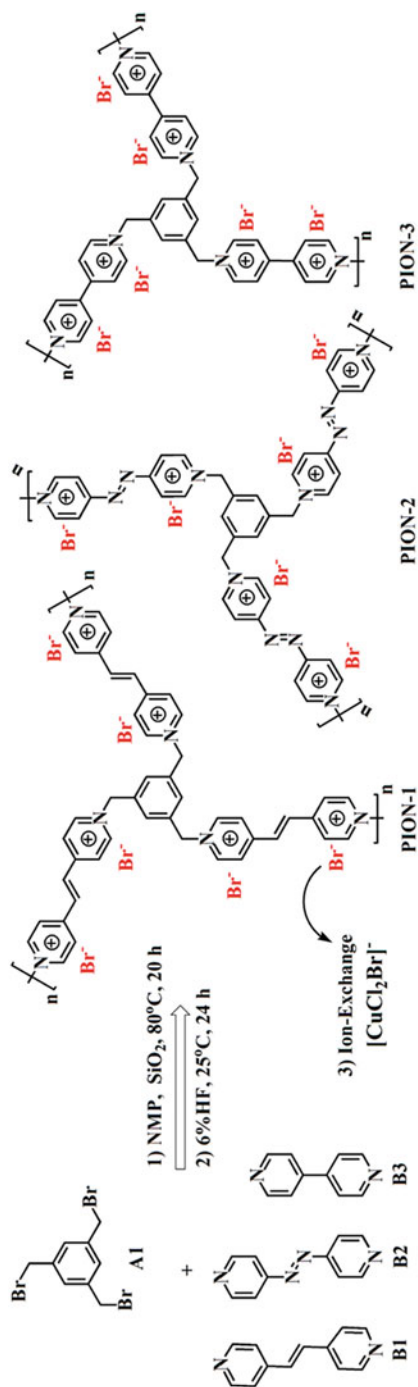


Fig. 9 Synthetic route of PIONs [62]. NMP *N*-methyl-2-pyrrolidone. Adapted from [62]

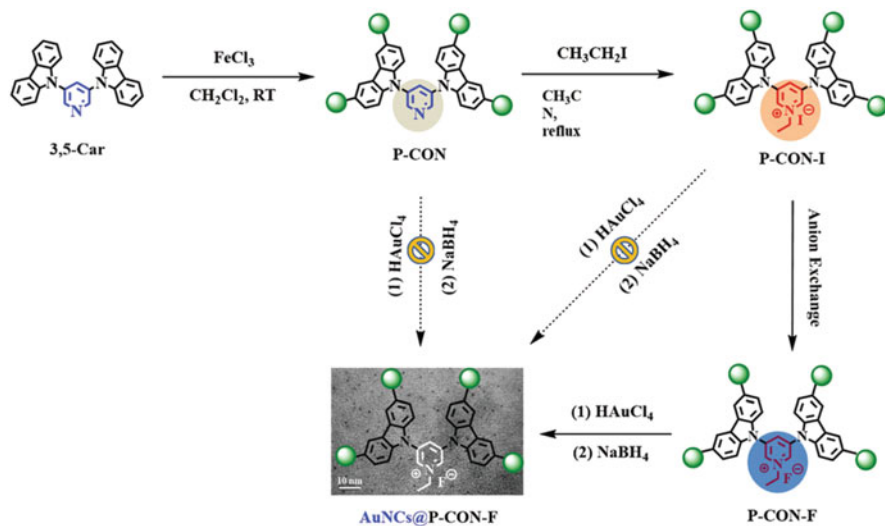


Fig. 10 Schematic image of the preparation of AuNCs@P-CON-F [63]. P-CON was prepared by FeCl₃-catalyzed polymerization. Reproduced with permission from [63] Copyright 2018 Royal Society of Chemistry

The size dependence was studied for Au/C (3.4 and 8.9 nm) [87] and Au/polymers (2.6–20 nm) [88, 89], and all the results suggested that the smaller Au NPs showed higher catalytic activity.

The TOFs for the oxidation of 1-phenylethanol under solvent- and base-free conditions are summarized in Table 2. Not only Au on highly reducible MO_x but also Au on non-reducible MO_x, non-oxides, and polymers can exhibit high catalytic activity by adding second metals into the supports or rational design of the supports.

2.6 Non-supported Au

2.6.1 Nanoporous Au

Nanoporous Au (NPG) has a three-dimensional having sponge-like morphology consisting of the interconnecting ligament with diameters in the range of 10–50 nm and is prepared by dealloying of Ag from the AuAg alloys. Asao et al. demonstrated that NPG catalyzed the base-free oxidation of alcohols in both batch and flow systems [65]. Ding et al. also reported that NPG catalyzed the glucose oxidation to gluconic acid, although the catalytic activity was inferior to other supported Au NPs [90]. They concluded that the corner and edge atoms of NPG might be the active sites for glucose oxidation, but it should be noted that the residual Ag remained in NPG, and the residual Ag were concentrated to the outer surface of NPG [91], and the Ag₂O on NPG surface should be taken into consideration. Wittstock et al. investigated the effect of the residual Ag content on the oxidations of methanol

and ethanol over NPG containing the residual Ag in the range of 1–10% [92, 93]. For methanol oxidation to give methyl formate, the highest activity was achieved by NPG containing Ag less than 1%, while the selectivity of methyl formate was always 100% irrespective to the Ag content. In contrast, for ethanol oxidation, acetaldehyde was obtained as a major product by NPG in which more than 2.5% Ag was contained, whereas ethyl acetate was obtained selectively by NPG in which less than 2.5% Ag was contained. This result suggests that the residual Ag is a determinant factor for the catalytic performance of NPG.

2.6.2 Polymer-Stabilized Au NPs and Clusters

The most intensively studied non-supported Au is ligand- or polymer-protected pseudo-homogeneous Au clusters and NPs. Poly(vinyl alcohol)-stabilized Au NPs have been also used to deposit carbons by colloid immobilization [11, 94]. Tsukuda et al. prepared poly(*N*-vinyl-2-pyrrolidone)-protected Au clusters (Au:PVP) and demonstrated the oxidation of benzylic alcohols in the presence of O₂ and K₂CO₃ at room temperature [66–68]. They performed several characterization and revealed that Au was negatively charged by the electron donation from PVP [67], which was also theoretically confirmed by Okumura et al. [95]. According to the behavior of Au cluster anions in the gas phase, they proposed the reaction mechanism in which O₂ is activated on the Au cluster by the electron transfer from anionic Au to O₂, generating superoxo- or peroxy-like species as shown in Fig. 11 [67, 68].

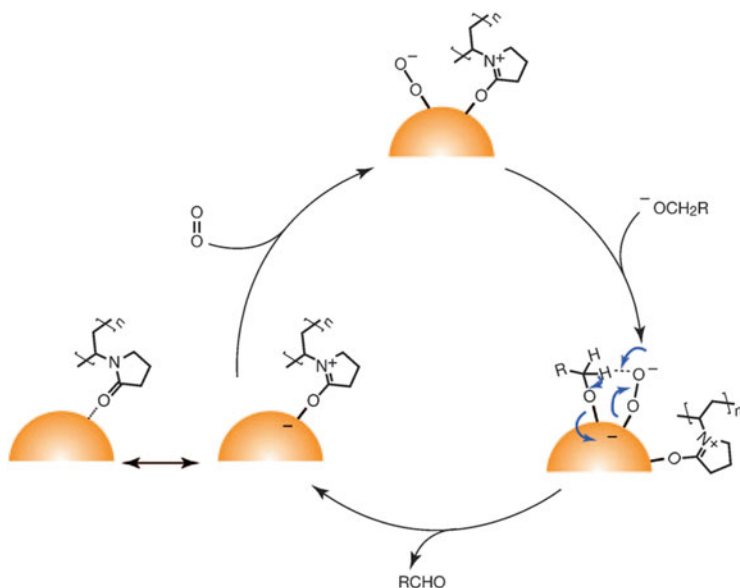


Fig. 11 A proposed reaction mechanism for the alcohol oxidation by Au:PVP [68]. Reproduced with permission from [68] Copyright 2011 Wiley-VCH Verlag GmbH&Co. KGaA, Weinheim

2.6.3 Atomically Precise Au Clusters Protected by Ligands

Conventional several preparation methods for heterogeneous Au catalysts such as DP and coprecipitation can obtain nanometer-sized Au particles with bare Au surfaces on metal oxide supports. However, the aggregation of Au during deposition or calcination cannot be completely avoided and leads to size distribution of Au NPs. On the other hand, phosphine- and thiolate-protected Au clusters consisting of precise number of Au atoms have been synthesized in organometallic chemistry and recently been focused on the catalytic performance of these atomically precise Au clusters as themselves or after the deposition onto supports.

For example, $\text{Au}_{25}(\text{SR})_{18}$ ($R = \text{alkyl or aryl}$) consists of a Au_{13} icosahedral core and a $\text{Au}_{12}(\text{SR})_{18}$ shell (Fig. 12) [69]. Li and Jin pointed out that the Au_{12} shell and the Au_{13} core are partly accessible to a substrate in catalytic reactions [69]. Indeed, $\text{Au}_{25}(\text{SR})_{18}$ clusters and their immobilized catalysts were reported to be catalytically active for the selective hydrogenation of α,β -unsaturated aldehydes and ketones to the corresponding unsaturated alcohols and oxidation of alkenes (discussed in the following section) even though the thiolate ligands remained. However, these ligands may poison the catalytic activity of Au for alcohol oxidations. In addition, the $\text{Au}_{25}(\text{SR})_{18}$ clusters have cationic characters because of the S–Au(I)–S bond at the Au_{12} shell. Phosphine-protected Au clusters such as $\text{Au}_9(\text{PPh}_3)_8(\text{NO}_3)_3$, $\text{Au}_{11}(\text{PPh}_3)_8\text{Cl}_3$ also possess counter anions (Cl^- and NO_3^-), resulting in the cationic Au characters. Therefore, the oxidation states of Au should be considered for the evaluation of catalytic properties of these ligand-protected atomically precise Au clusters.

For immobilized atomically precise Au cluster catalysts, various kinds of ligand-protected Au clusters, such as $\text{Au}_9(\text{PPh}_3)_8(\text{NO}_3)_3$, $\text{Au}_{11}(\text{PPh}_3)_8\text{Cl}_3$, and $\text{Au}_{25}(\text{SPh})_{18}$, have been exploited. The protected Au clusters deposited on supports are sometimes used as-prepared, but the protecting ligands are also removed by

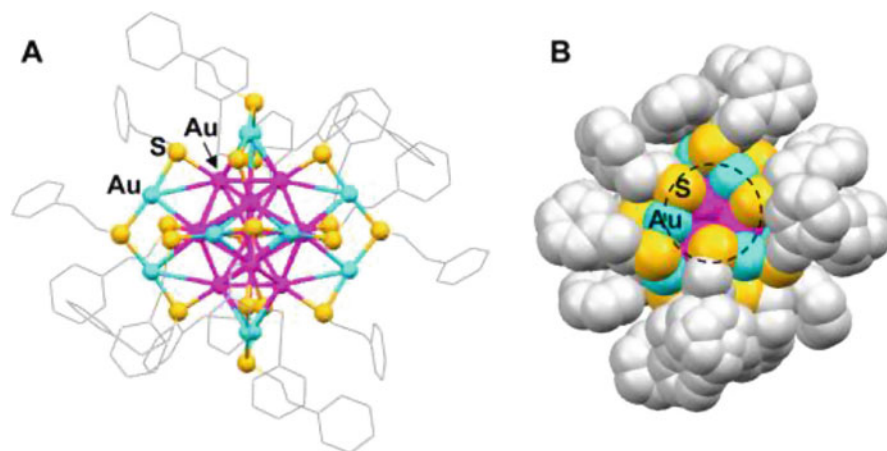


Fig. 12 Structure of $\text{Au}_{25}(\text{SCH}_2\text{CH}_2\text{Ph})_{18}$ clusters in ball-stick model (a) and space-filling model (b) [69]. Magenta: Au of the Au_{13} core, cyan: Au of Au_{12} shell, yellow: sulfur. Reproduced from [69]

calcination in air or H_2 to obtain bare Au surface. Removal of the ligands is performed at 200–400°C, which often causes aggregation of the Au clusters. Golovko et al. reported that TiO_2 supported $Au_9(PPh_3)_8(NO_3)_3$ and $Au_{101}(PPh_3)_{21}Cl_5$ was active for aerobic oxidation of benzyl alcohol, but the catalysts calcined in O_2 or followed by H_2 reduction exhibited much higher catalytic activity, whereas the size of Au particles of the calcined catalysts was significantly larger (2.5–5.7 nm) than those of the protected Au clusters [70]. The improved activity was ascribed to the change of the electronic state of Au, i.e., from cationic to metallic Au, by removal of phosphine ligands. In addition, $Au_{101}(PPh_3)_{21}Cl_5/TiO_2$ exhibited higher catalytic activity than $Au_9(PPh_3)_8(NO_3)_3/TiO_2$ in spite of larger Au cluster size even after calcination, indicating that the nitrate poisoned the catalytic activity of Au.

Protected Au clusters were also confined in the porous materials in order to avoid the aggregation of Au clusters during calcination. Tuel et al. prepared $Au_{25}(p\text{-aminobenzenethiolate})_{17}$ immobilized on the mesoporous silica, SBA-15, and examined the catalytic activity for benzyl alcohol oxidation [71]. The catalytic activity of $Au_{25}/SBA-15$ was markedly improved with calcination temperature owing to the removal of thiolate ligands and the change of the electronic state of Au, S-Au(I)-S to metallic Au, although the size of Au increased. Xie and Yang et al. attempted the removal of alkyl thiolate ligands by oxidation using *t*-butyl hydroperoxide (TBHP) under mild conditions [72]. The thiolate ligands of $Au_{25}(SC_{12}H_{25})_{18}/HAP$ were completely removed by TBHP at 50°C as sulfonic acid after 48 h while maintaining the Au cluster size (1.2–1.5 nm). They demonstrated that the presence of sulfur, even in a very small amount, significantly affected the catalytic activity of Au clusters.

Tsukuda et al. prepared $Au_{25}(SC_{12}H_{25})$ supported on carbon nanotubes (CNT) ($Au_{25}:SC_{12}/CNT$) and examined the catalytic activity for the benzyl alcohol oxidation in the presence of O_2 and K_2CO_3 [73]. The calcination of $Au_{25}:SC_{12}/CNT$ successfully removed the thiolate ligand without the aggregation of the Au clusters (Au_{25}/CNT). Although the $Au_{25}:SC_{12}/CNT$ was inactive, Au_{25}/CNT appeared to be active to produce benzaldehyde as a major product together with benzoic acid and benzyl benzoate. The doping of Pd into Au_{25}/CNT catalyst (Pd_1Au_{25}/CNT) significantly improved the catalytic activity, which was explained by the ligand effect in which Pd atoms modulated the electronic structure of Au by electron transfer from Pd to Au.

2.6.4 Size Dependence

Rossi et al. first reported the size dependence “naked” colloidal Au without protecting agents on the catalytic activity for the glucose oxidation (Scheme 4) in the range of 3–10 nm [96]. Naked Au NPs became catalytically active from the 5 nm of Au NPs, and the reaction rate increased with a decrease in the size of Au. However, the TOF did not alter by the size of Au, indicating that the apparent increase in the reaction rates was ascribed to an increase in the number of surface Au atoms.

Scheme 4 Oxidation of glucose to gluconic acid under basic conditions

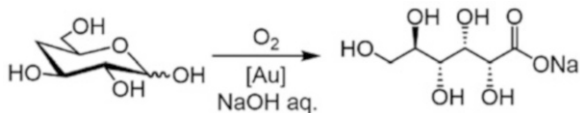
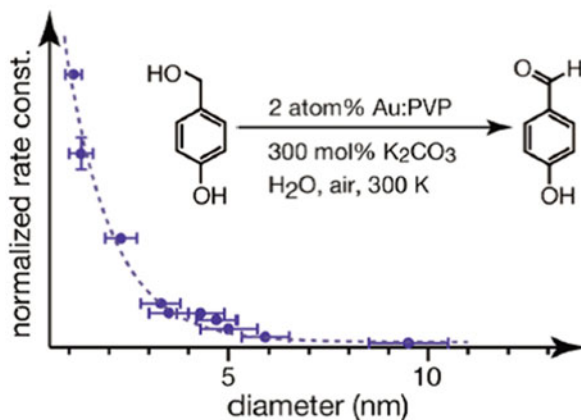


Fig. 13 Size dependence on Au:PVP for the aerobic oxidation of 4-hydroxybenzyl alcohol [67]. Reproduced from [67]



DFT calculation of the alcohol oxidation over naked Au_6 clusters suggested that the neutral Au_6 clusters did not activate O_2 , whereas the alkoxide or hydride adsorbed Au_6 clusters could activate O_2 because of the electron donation from anionic adsorbates to the Au_6 cluster [97].

Tsukuda et al. reported the size dependence of Au:PVP on the oxidation of 4-hydroxybenzyl alcohol [66, 67]. The rate constants per unit surface area of Au:PVP increased with a decrease in their size in the range of 1–5 nm, while Au:PVP consisting of Au NPs larger than 5 nm were poorly active and no size effect was observed (Fig. 13) [67]. This result suggested that the catalytic activity of the surface Au atoms changed depending on the size. XPS and IR using CO as a probe molecule measurements revealed that Au clusters possessed more negatively charged characters than Au NPs.

3 Oxidation of Alcohols and Aldehydes to Carboxylic Acids

For the production of carboxylic acid in the absence of base, oxidation of aldehydes proceeded to obtain the corresponding carboxylic acids in high yields (>90%) by Au/ CeO_2 [98] and Au/MgO [43]. Au/C also catalyzed the oxidation of aliphatic aldehydes to carboxylic acid in water in the absence of base, whereas the catalytic activity of Pt/C decreased rapidly by catalyst recycling due to Pt leaching [99].

The direct production of carboxylic acids from alcohols under base-free conditions is also an important issue because the reaction step can be reduced by the direct oxidation and the neutralization of the carboxylate salts after the reaction can be

avoided. However, supported Au catalysts often require base for the oxidation of alcohols to yield carboxylic acids irrespective to the kind of supports, and the reports on base-free oxidation of aliphatic alcohols to the corresponding carboxylic acids are still limited. Au/HT appeared to be highly active for 1-phenylethanol oxidation to give acetophenone under base-free conditions, but Au/HT gave unsatisfactory results for the oxidation of primary aliphatic alcohols, such as 1-octanol [47]. On the other hand, ethanol oxidation to acetic acid was achieved by Christensen et al. using Au/MgAl₂O₄ [100]. Au/MgAl₂O₄ gave acetic acid in 83% yield (86% selectivity), while Pd/MgAl₂O₄ and Pt/MgAl₂O₄ gave acetic acid with worse selectivity, 65 and 20%, respectively, at similar conversions due to the formation of acetaldehyde as a by-product. Several Au/MO_x, such as Au/TiO₂ [101], Au/ZnO [102], Au/SiO₂ [77], and Au/NiCuO_x [103], were also reported to be active and selective for the base-free ethanol oxidation to give acetic acid.

The oxidation of aliphatic alcohols having a long alkyl chain is a more challenging research target because these alcohols are less reactive than ethanol and benzylic alcohols. Au/NiO appeared to be active and selective for the base-free oxidation of 1-octanol to octanoic acid in aqueous solution, whereas Au/CeO₂ gave octyl octanoate as a major product [104]. Under the optimized conditions, the selectivity of octanoic acid reached to 97% at a full conversion. Due to the high hydrophilicity of NiO, octanal was hydrated to form geminal diol, which was readily oxidized to octanoic acid (Fig. 14), giving octanoic acid selectively. Au/Mg-doped ZnAl₂O₄ [45] and Au/NiTi-LDH [51] were also reported to give octanoic acid with 99% of selectivity at 99% conversion. The strong basic sites of Mg-doped ZnAl₂O₄ were suggested to be responsible for high activity and selectivity [45]. Not only abundant surface OH group of NiTi-LDH but also the defective Ti³⁺ species, forming the oxygen vacancies, would play an important role by fixing the oxygen atom of the substrate alcohol [51].

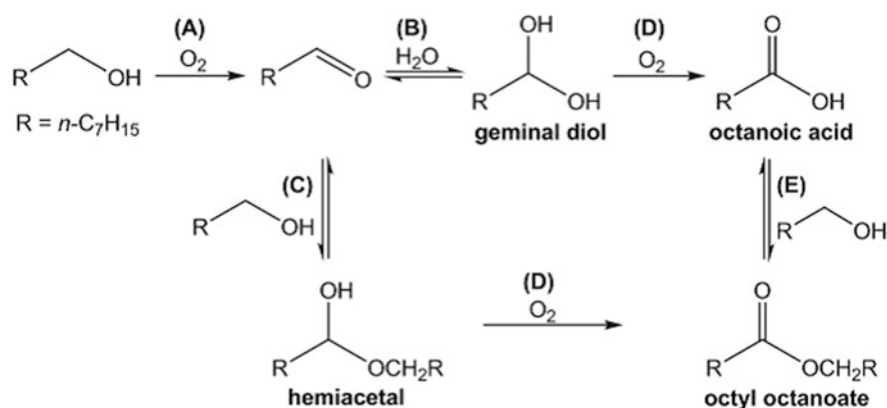
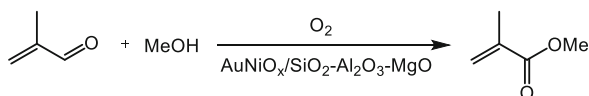


Fig. 14 Possible reaction pathways for the oxidation of 1-octanol over Au/NiO [104]. Reproduced with permission from [104] Copyright 2012 Wiley-VCH Verlag GmbH&Co. KGaA, Weinheim

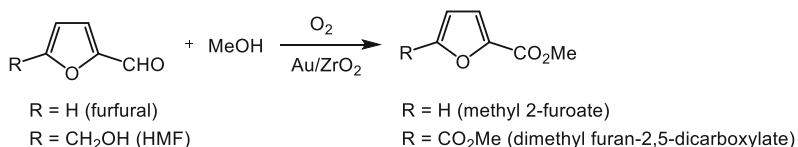
4 Oxidative Esterification of Alcohols and Aldehydes

Direct production of ester from alcohols or aldehydes is also important as well as direct oxidation of alcohols to carboxylic acid, because esters are produced from aldehydes by two steps: the oxidation of aldehyde to carboxylic acid followed by acid-catalyzed esterification. Oxidative esterification to produce methyl esters has been achieved by Au/TiO₂ [105–110], Au/Fe₂O₃ [111, 112], Au/Al₂O₃ [113, 114], Au/SiO₂ [115–117], Au/polymers [118, 119], Au/graphene oxide (GO) [120, 121], and Au/MOF [55, 122] in the presence of bases such as NaOMe, K₂CO₃, and Na₂CO₃.

Base-free oxidative esterification has been attempted by using basic supports; Au/MgO [123, 124], Au/La₂O₃ [125], Au/CeO₂ [126–129], and AuNiO_x/SiO₂-Al₂O₃-MgO [130] catalyzed the oxidative esterification of aldehydes in methanol to give the corresponding methyl esters in the absence of base. In particular, AuNiO_x/SiO₂-Al₂O₃-MgO produced methyl methacrylate selectively from methacrolein, which has been operated in the industrial process since 2008 by Asahi Kasei Corporation (Scheme 5). The oxidative esterification of biomass-derived compounds, such as furfural and 5-hydroxymethyl furfural (HMF), was performed over Au/ZrO₂ in the absence of base to obtain dimethyl furan-2,5-dicarboxylate and methyl 2-furoate, respectively (Scheme 6) [129, 131–137]. Au/β-Ga₂O₃ also exhibited high catalytic activity for the oxidative esterification of various alcohols in methanol to produce the corresponding methyl esters including benzyl alcohol [138]. Although the basic sites contribute to the activation of alcohols, the acidic sites activate the carbonyl group, facilitating the reaction.



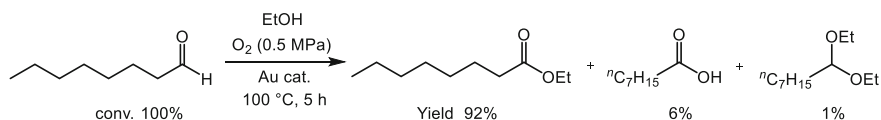
Scheme 5 Oxidative esterification of methacrolein with methanol to methyl methacrylate over Au/NiO_x/SiO₂-Al₂O₃-MgO [130]



Scheme 6 Oxidative esterification of furfural and HMF with methanol to give the corresponding methyl esters

Compared to the oxidative esterification for the synthesis of methyl esters, the production of ethyl esters is more challenging because of lower nucleophilicity of ethanol than that of methanol and easy oxidation of ethanol, which make difficult the selective oxidation of aldehydes or the substrate alcohols while ethanol is intact. Au/NiO_x/SiO₂-Al₂O₃-MgO catalyzed the oxidative esterification of methacrolein in

ethanol to obtain ethyl methacrylate, but the high selectivity (97%) was achieved at only low conversion (ca. 10%) [130]. For the oxidative esterification of octanal in ethanol, several Au/MO_x, such as Au/ZnO, Au/Al₂O₃, and Au/SiO₂, appeared to produce ethyl octanoate selectively in the absence of base (Scheme 7) [139]. In particular, Au/ZnO showed the highest selectivity (92%) at a full conversion.



Scheme 7 Oxidative esterification of octanal with ethanol to give ethyl octanoate over Au/ZnO [139]

Based on the NH₃- and CO₂-temperature programmed desorption (TPD) measurements, ZnO possessed both acidic and basic sites on the surface. The basic sites would facilitate the deprotonation of ethanol and the acidic sites would activate the carbonyl group of octanal (Fig. 15). The presence of suitable amount and strength of acidic and basic sites on ZnO surface resulted in the highest activity.

For the oxidative esterification to give ethyl octanoate from octanal [139] and to give methyl glycolate from ethylene glycol [140], the TOF did not change by the size of Au NPs in the range of 2–9 nm, which indicated that the reaction takes place on the Au surface. Pinna et al. proposed the presence of Au clusters (1.5 nm) on ZrO₂ was important because the O₂ dissociation on the Au clusters would be involved [132], whereas larger Au NPs on CeO₂ showed high catalytic activity [128]. The different size dependence between Au/ZrO₂ and Au/CeO₂ was explained by the different O₂

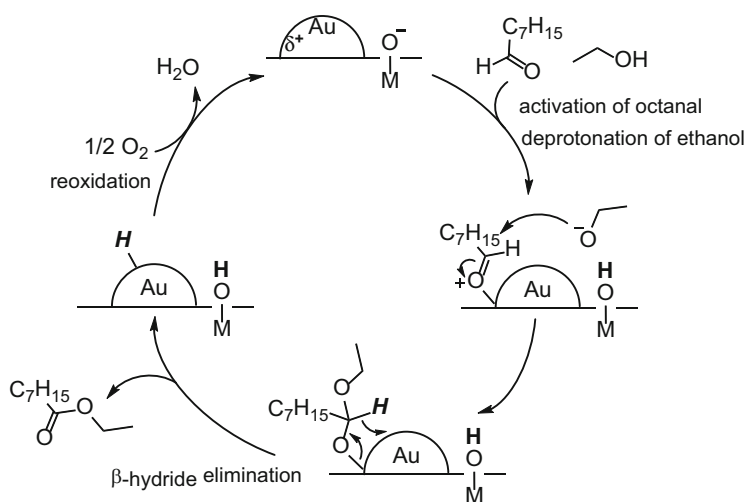


Fig. 15 A plausible reaction mechanism of the oxidative esterification of octanal in ethanol over Au/MO_x

activation mechanism. Namely, both O_2 is activated at the oxygen vacancies of CeO_2 without Au, whereas O_2 activation takes place at the Au– ZrO_2 interface, of which perimeter length is maximized by decreasing the size of Au particles.

Oxidative esterification of 1-octanol with methanol in the absence of a base has been reported for Au/ Mg_5Al -HT [141], Au/ MgO [124], and Au/ ZnO [139], and the selectivities of methyl octanoate exceeded 94%. In contrast, the oxidative esterification of 1-octanol with ethanol to give ethyl octanoate is very limited in the absence of base [139] and even in the presence of base [142]. For the base-free oxidative esterification of 1-octanol with ethanol, Au/ ZnO produced ethyl octanoate with 51% selectivity at 68% conversion. Although the oxidation of ethanol to form acetaldehyde could not be avoided to produce by-products such as ethyl acetate and octyl acetate, Au/ ZnO was selective to give ethyl octanoate as a major product [139]. It should be noted that the Au/ CeO_2 and Au/ ZrO_2 showed 45 and 50% selectivity to ethyl octanoate, respectively, at both 4% conversion even in the presence of base [142].

5 Dehydrogenation of Alcohols in the Absence of O_2

As mentioned in the Sect. 2.3.2, Zhang and Wang et al. reported that Au/HT catalyzed the dehydrogenation of benzyl alcohol, although the catalytic activity under inert atmosphere was much lower than that in the presence of O_2 [48]. In their following study, a full conversion was achieved for the benzyl alcohol dehydrogenation to give benzaldehyde in >99% selectivity with TOF of up to 800 h^{-1} under Ar, while Au/ Al_2O_3 and Au/HAP showed lower selectivity in spite of higher selectivity than did Au/HT [78]. The TOFs were plotted as a function of the mean Au particle size (Fig. 16a), which was in a good agreement with the plots of the fraction

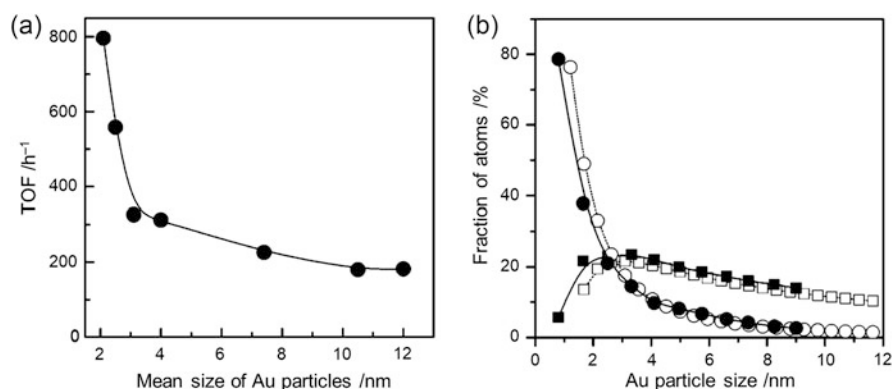


Fig. 16 TOF as a function of the mean diameter of Au NPs for the dehydrogenation of benzyl alcohol over Au/HT under Ar (a) and the calculated fractions of edge and corner Au atoms (\circ and \bullet) and terrace Au atoms (\square and \blacksquare) on the surface of Au NPs as a function of the mean diameter of Au NPs (b) [78]. \circ and \square : icosahedron particles. \bullet and \blacksquare : truncated octahedron particles. Adapted with permission from [78] Copyright 2011 Wiley-VCH Verlag GmbH&Co. KGaA, Weinheim

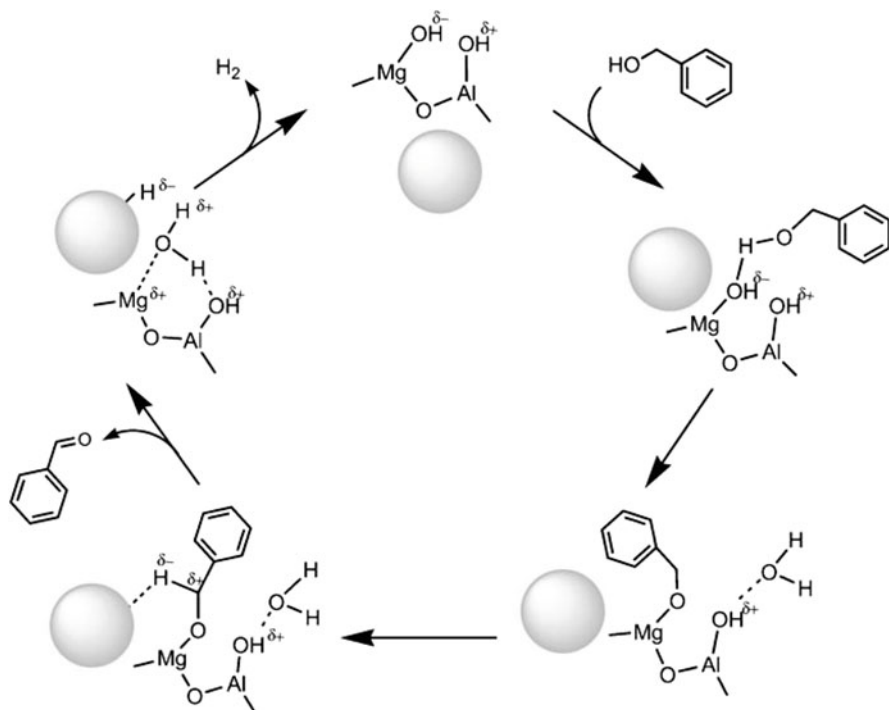


Fig. 17 A possible reaction mechanism for the dehydrogenation of benzyl alcohol over Au/HT under Ar [78]. Reproduced with permission from [78] Copyright 2011 Wiley-VCH Verlag GmbH&Co. KGaA, Weinheim

of edge and corner Au atoms as a function of the size of Au (Fig. 16b). This result suggested that the coordinatively unsaturated Au sites, i.e., edge and corner sites, were the active sites. The role of HT was also proposed in the reaction mechanism (Fig. 17). The basic sites ($\text{Mg-OH}^{\delta-}$) on HT promoted the deprotonation of benzyl alcohol to form a Mg-alkoxide intermediate. After $\beta\text{-H}$ elimination takes place on the corner and/or edge Au sites on the Au NPs to produce benzaldehyde, the Brønsted acid sites ($\text{AlO-H}^{\delta+}$) on HT would react with Au-H species to form H_2 .

Dehydrogenation of alcohols to give aldehydes was applied to one-pot reactions in the presence of a hydrogen acceptor, which is known as the hydrogen-borrowing strategy [143–148]. Cao et al. reported the one-pot reaction consisting of alcohol dehydrogenation, aldol condensation, and transfer hydrogenation to form higher ketones over Au/HT (Fig. 18) [143].

Imines formed in situ is also used as a hydrogen acceptor in one-pot *N*-alkylation, which consists dehydrogenation of alcohol to give aldehyde, dehydration of the aldehyde with primary amine to give imine, and reduction of the imine to secondary amine using the Au-H species (Fig. 19a) [79, 145, 146]. Au on basic supports such as CeO_2 proceeded the first dehydrogenation of benzyl alcohol smoothly, but further dehydrogenation to benzyl benzoate also took place, whereas Au on acidic supports

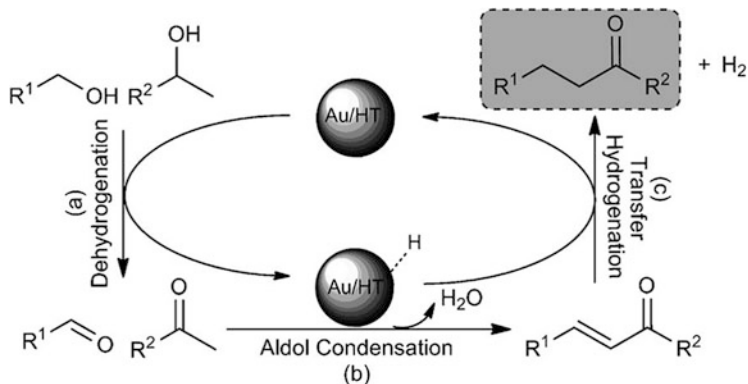


Fig. 18 One-pot reactions involving dehydrogenation of alcohols, aldol condensation, and transfer hydrogenation [143]. Reproduced with permission from [143] Copyright 2013 Wiley-VCH Verlag GmbH&Co. KGaA, Weinheim

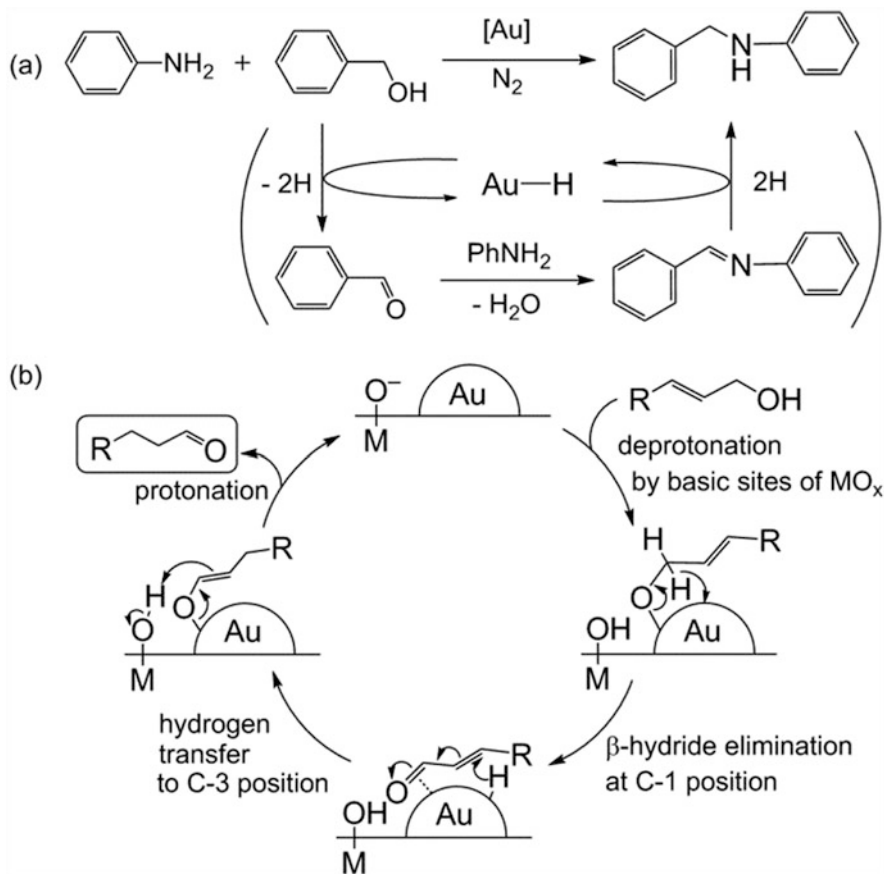


Fig. 19 One-pot reactions involving dehydrogenation of alcohols. N -Alkylation of primary amine (a) [145] and isomerization of allylic alcohol (b) [147] Reproduced with permission from [147] Copyright 2014 The Chemical Society of Japan & Wiley-VCH Verlag GmbH&Co. KGaA, Weinheim

such as WO_3 did not promote the dehydrogenation. In contrast, Au on basic supports gave worse results for the hydrogen transfer from imine to give secondary amine. As a result, Au on amphoteric ZrO_2 exhibited the highest selectivity of the secondary amine [145]. One-pot reaction using nitro group as a hydrogen acceptor was also reported [148].

Isomerization of allylic alcohols using an intramolecular hydrogen-borrowing strategy was achieved by Au/NiO and Au-/La-doped NiO (Fig. 19b) [147]. Doping of La into NiO reduced the size of Au particles from 2.5 nm for Au/NiO to 0.9 nm for Au-/La-doped NiO, resulting in a greatly improved catalytic activity. According to a DFT calculation using a Au_6 cluster, the β -hydride elimination of allylic alcohol at the C-1 position and the hydrogen transfer to the C-3 position would take place on the Au_6 cluster with low activation energy [97], suggesting that the Au clusters play a crucial role in hydrogen transfer, and the basicity of La-NiO would facilitate the deprotonation of the alcohol.

6 Oxidation of Alkenes

Au/ TiO_2 was first reported to catalyze the gas-phase epoxidation of propylene to propylene oxide (PO) in the presence of H_2 and O_2 in 1998 [6], and then the presence of Ti-isolated sites in Ti-containing SiO_2 supports improved the catalytic performance of Au for the epoxidation [149]. Au is responsible for the formation of H_2O_2 in situ from H_2 and O_2 , and the Ti site is responsible for the epoxidation via the formation of Ti-OOH from H_2O_2 formed on Au. Later, Au clusters deposited on titanosilicalite-1 (TS-1) enable the propylene epoxidation by only O_2 in the presence of H_2O [150].

The epoxidation of alkenes, such as cyclohexene and styrene, has been also studied in liquid phase. Early studies used radical initiators together with O_2 , but recently, O_2 has been used as a sole oxidant. The comparison of Au-catalyzed styrene oxidation using O_2 as a sole oxidant is shown in Table 3. Lambert et al. reported that $\text{Au}_{55}(\text{PPh}_3)_{12}\text{Cl}_6$ (1.5–1.6 nm) supported on boron nitride (BN) and on

Table 3 Styrene oxidation using O_2 as a sole oxidant catalyzed by supported Au catalysts

C=Cc1ccccc1.O=O>>C1OC1c2ccccc2.C=Oc3ccccc3.CC(=O)c4ccccc4

styrene oxide benzaldehyde acetophenone

Catalyst	Au size (nm)	Conv. (%)	Selectivity (%)			Ref.
			Styrene oxide	PhCHO	Acetophenone	
Au_{55}/BN	1.6	19	14	82	4	[151]
$\text{Au}_{55}/\text{SiO}_2$	1.5	26	12	82	6	[151]
Au/HNS	1.9 ± 0.3	46	69	23	8	[152]

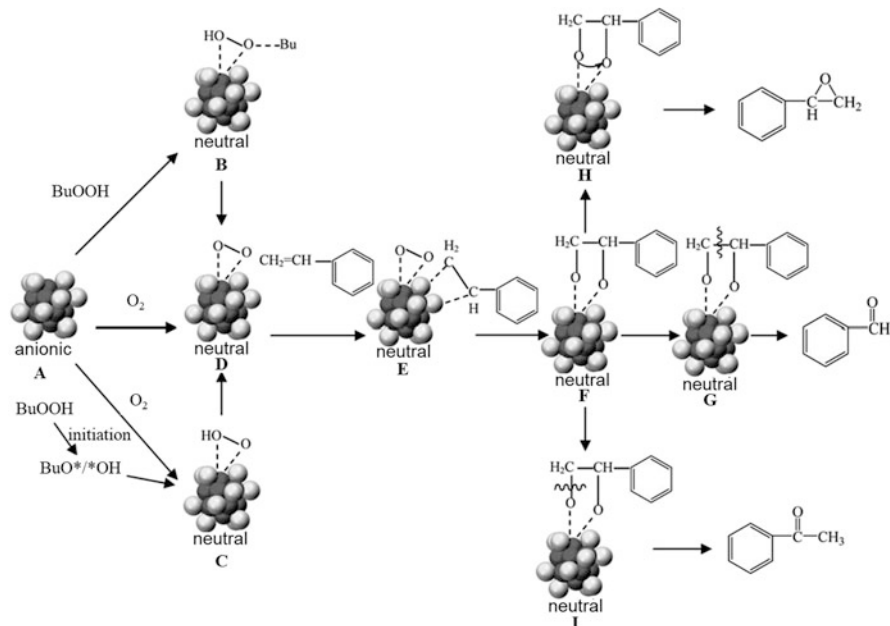


Fig. 20 A proposed reaction mechanism of the styrene oxidation over $\text{Au}_{25}(\text{SR})_{18}$ clusters [153]. The thiolate ligands are omitted for clarity. Dark gray, Au_{13} core; light gray, Au_{12} shell. Adapted with permission from [153] Copyright 2010 Wiley-VCH Verlag GmbH&Co. KGaA, Weinheim

SiO_2 promoted the oxidation of styrene to produce styrene oxide (14–27% selectivities) using O_2 as a sole oxidant, although benzaldehyde was obtained as a major product (64–82% selectivities). In contrast, SiO_2 -supported Au NPs larger than 2 nm were inactive [151]. XPS results revealed that the Au_{55} clusters were positively charged. Given that BN and SiO_2 were inert supports, they proposed that the Au_{55} clusters dissociatively adsorb O_2 to give O adatoms on Au, which is responsible for the epoxidation of styrene. The Au clusters (<2 nm) deposited on silica hollow nanosphere (HNS) also catalyzed the styrene epoxidation with O_2 as a sole oxidant and recorded the 69% selectivity to styrene oxide at a moderate conversion [152].

Thiolate-protected Au_{25} , Au_{38} , and Au_{144} clusters supported on HAP were reported to be active for the styrene oxidation to produce benzaldehyde and styrene oxide [153]. No obvious size effect was observed in the presence of TBHP, but the conversions of cyclohexene increased as Au clusters became smaller, $\text{Au}_{25} > \text{Au}_{38} > \text{Au}_{144}$ in the presence of O_2 without TBHP. They proposed the reaction mechanism depending on the oxidants as shown in Fig. 20. $\text{Au}_{25}(\text{SR})_{18}$ clusters have electron-rich Au_{13} cores and positively charged Au_{12} shells due to S–Au(I)–S bonds. O_2 activation would take place directly on the bare Au_{13} cores in the absence of TBHP (Fig. 20D), while the electron-rich C=C bond of styrene would be activated on the Au_{12} shells (Fig. 20E). The activated C=C bond would react with the activated O_2 on the Au_{13} core followed by O–O bond cleavage (Fig. 20F) to

Table 4 Cyclohexene oxidation using O₂ as a sole oxidant catalyzed by supported Au catalysts

Catalyst	Au size (nm)	Conv. (%)	Selectivity (%)				Ref.
			Cy-oxide	Cy-ol	Cy-one	Cy-OOH	
Au/OMS-2	10–20	40	3	36	52	–	[156]
K-OMS-2	–	29	3	43	43	–	[156]
Au/GaW ₁₁ -APTES@SiO ₂		69	5	57	29	–	[157]
GaW ₁₁ -APTES@SiO ₂	–	62	59	–	–	–	[157]
Au ₉ /SiO ₂	<1	43	7	12	19	51	[158, 159]
Au ₁₀₁ /SiO ₂	1.59 ± 0.04	39	7	11	17	54	[158, 159]
Au ₉ /WO ₃	<1	33	34	24	11	21	[158]
Au ₁₀₁ /WO ₃	2.25 ± 0.05	36	35	23	12	18	[158]
WO ₃	–	9	33	30	4	32	[158]

finally produce benzaldehyde, styrene oxide, and acetophenone. No size effect in the presence of TBHP was ascribed to the facile formation of peroxy species on the Au₁₃ core which leads to the intermediate B.

Hutchings et al. reported that Au/C containing ~5–50 nm Au NPs with the mean diameter of ~25 nm catalyzed the aerobic oxidation of cyclohexene to give cyclohexene oxide (Cy-oxide) as a major product with 50% selectivity at 30% conversion in the presence of O₂ and TBHP in 1,2,3,5-trimethylbenzene [154]. For *cis*-cyclooctene oxidation, Au/C produced *cis*-cyclooctene oxide with 81% selectivity at 8% conversion in the presence of O₂ and TBHP [154]. Au/Co-Al-LDH (Au 4–70 nm) significantly improved the selectivity of *cis*-cyclooctene oxide to 92% at 92% conversion [155].

The epoxidation of cyclohexene using O₂ without radical initiators is more challenging, and cyclohexene hydroperoxide (Cy-OOH), cyclohex-2-en-1-ol (Cy-ol), and cyclohexenone (Cy-one) are usually obtained instead of cyclohexene oxide (Cy-oxide). Table 4 summarizes the cyclohexene oxidation over heterogeneous Au catalysts using O₂ as a sole oxidant.

Zhu et al. reported that Cy-one was obtained as the major product together with Cy-ol by Au NPs on manganese oxide octahedral molecular sieve (OMS-2) [156]. K-OMS-2 produced Cy-one and Cy-ol without Au, and the deposition of Au increased the catalytic activity while the selectivity was almost the same. Keggin-type polyoxometalate (Na₉GaW₁₁O₃₉)-linked to nanometer-sized SiO₂ prepared from 3-aminopropyl triethoxysilane (APTES) and tetraethyl orthosilicate (GaW₁₁-APTES@SiO₂) also appeared to be active for cyclohexene oxidation and selective to Cy-oxide with high selectivity (59%) without Au. However, the selectivity of

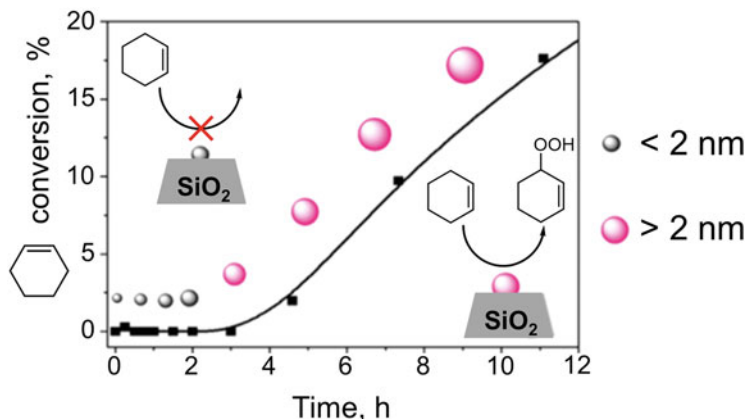
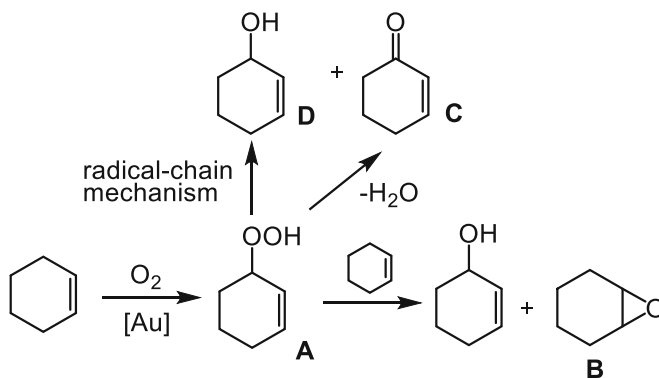


Fig. 21 Size dependence of Au on SiO₂ for the cyclohexene oxidation by O₂ [159]. Adapted with permission from [159] Copyright 2013 American Chemical Society

Cy-oxide significantly decreased after the deposition of Au, resulting in Cy-ol as a major product [157]. WO₃ also showed Cy-oxide selectivity without Au, and the deposition of Au onto WO₃ remarkably improved the conversion while keeping the Cy-oxide selectivity [158].

Golovko et al. also studied the size dependence on solvent-free cyclohexene oxidation with O₂ in the absence of radical initiators using Au₉(PPh₃)₈(NO₃)₃ and Au₁₀₁(PPh₃)₂₁Cl₅ supported on SiO₂ and their phosphine-free Au clusters supported on SiO₂ [159]. During the reaction, the Au clusters were gradually aggregated. They disclosed that Au clusters smaller than 2 nm were catalytically inactive irrespective to the presence or absence of the phosphine ligands, and Au⁰ NPs larger than 2 nm formed in situ appeared to be active, but further increase in the Au particle size decreased the activity due to a decrease in the exposed surface Au atoms (Fig. 21). The size dependence on cyclohexene oxidation was different from that on styrene oxidation [151, 153]. The allylic C–H bond of cyclohexene is more reactive, and the



Scheme 8 Oxidation of cyclohexene

cyclohexenyl radicals is formed to give cyclohexenyl hydroperoxide (Cy-OOH, **A**) as a major product under solvent-free conditions (Scheme 8). Therefore, the active sites for cyclohexene oxidation were the metallic Au particles, while the styrene oxidation requires Au clusters where O_2 is dissociated [159].

7 Oxidation of Alkanes

Oxidation of cyclohexane into the mixture of cyclohexanone and cyclohexanol (K/A oil) is an important reaction in chemical industry and currently produced by homogeneous catalysts such as Co salts under 1–2 MPa of O_2 at 150°C, affording ~4% conversion and 70–85% selectivity of K/A oil. Au catalysts have been also reported for the cyclohexane oxidation. For example, Au/Fe₂O₃ produced K/A oil in 14% yield with the K/A ratio of 1/99 in the presence of H₂O₂ as a radical initiator [160]. Au₃₈(SCH₂CH₂Ph)₂₄ clusters supported on CeO₂ gave 39% conversion at 250°C with 79% K/A oil selectivity (K/A ratio of 57/22) but also produced cyclohexanethiol in 15% selectivity in which the sulfur came from thiolate ligands [161].

Tsukuda et al. investigated the size dependence of Au_{*n*} clusters (*n* = 10, 18, 25, 39) supported on HAP on the cyclohexane oxidation in the presence TBHP as a radical initiator [162]. The size of Au clusters was maintained after calcination to remove glutathione ligands from the Au surface. The Au₃₉/HAP exhibited the highest TOF as shown in Fig. 22, suggesting that the catalytic activity of Au markedly change by the atomic size, while product selectivity did not change by the particle size.

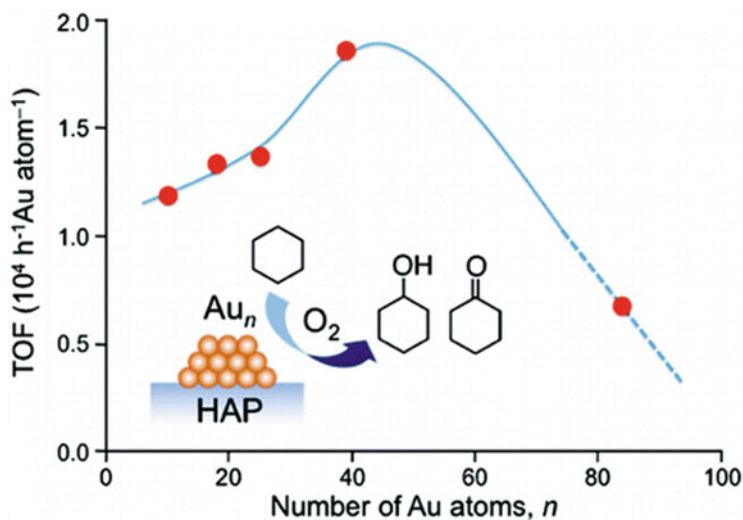
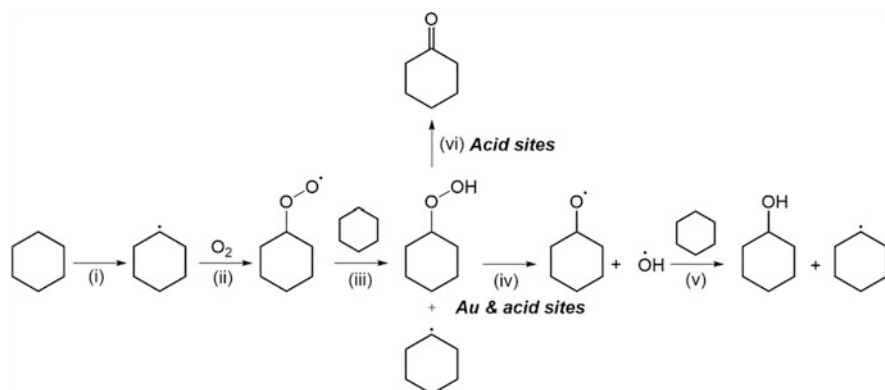


Fig. 22 Size dependence of Au_{*n*}/HAP for the oxidation of cyclohexane in the presence of TBHP [162]. Reproduced with permission from [162] Copyright 2011 American Chemical Society

As well as in alkene oxidation, alkane oxidation using O_2 as a sole oxidant is more challenging (Table 5). Au/ Al_2O_3 , Au/mesoporous SiO_2 , and Au/zeolite have been reported to be active for the cyclohexane oxidation with O_2 in the absence of radical initiators. Au/ Al_2O_3 showed cyclohexanol selectivity [163], whereas Au NPs on mesoporous SiO_2 (MCM-41) [164] and on zeolite (ZSM-5) [163, 165] showed cyclohexanone selectivity. Sivakumar et al. prepared Au NPs confined in the ZSM-5 shell (Au@ZSM-5) and demonstrated that Au@ZSM-5 gave ca. 40% conversion with ca. 80% K/A oil selectivity, whereas ZSM-5 without Au also promoted the oxidation with lower conversion and selectivity [166]. The radical-chain mechanism for the cyclohexane oxidation involves (i) C–H bond cleavage to form cyclohexyl radical, (ii) reaction of the cyclohexyl radical with O_2 to form peroxy radical, (iii) chain propagation of the peroxy radical with cyclohexane to form Cy-OOH and the cyclohexyl radical, (iv) O–O bond cleavage of Cy-OOH to form cyclohexyloxy radical and/or cyclohexanone, and (v) the chain propagation of the cyclohexyloxy radical with cyclohexane to give cyclohexanol (Scheme 9) [166]. Given that ZSM-5 having strong acidic sites also catalyzed the cyclohexane oxidation to produce cyclohexanone selectively (vi) and showed higher catalytic activity than commercial ZSM-5, Sivakumar et al. concluded that both Au NPs and the Brønsted acid sites of ZSM-5 accelerated the O–O bond cleavage of Cy-OOH (step iv) and the Brønsted acid sites also promoted the Cy-one formation [166].



Scheme 9 Radical-chain reaction mechanism for cyclohexane oxidation [166]

Corma et al. exploited MCM-22 to confine Au clusters inside the pore [167]. The resultant Au@MCM-22-S (Au 0.025 wt%) and Au@MCM-22-L (Au 0.11 wt%) contains sub-nanometer Au clusters and small Au NPs (1–2 nm) and exhibited markedly improved catalytic activity and selectivity to KA-oil, whereas Au NPs (1.2–2.5 nm) supported on MCM-22 showed much low catalytic activity and the selectivity to Cy-OOH (Fig. 23) [167]. From these results, sub-nanometer Au clusters would be responsible for the K/A oil production by means of O_2 activation to form oxygen radical species on the Au species (Table 5).

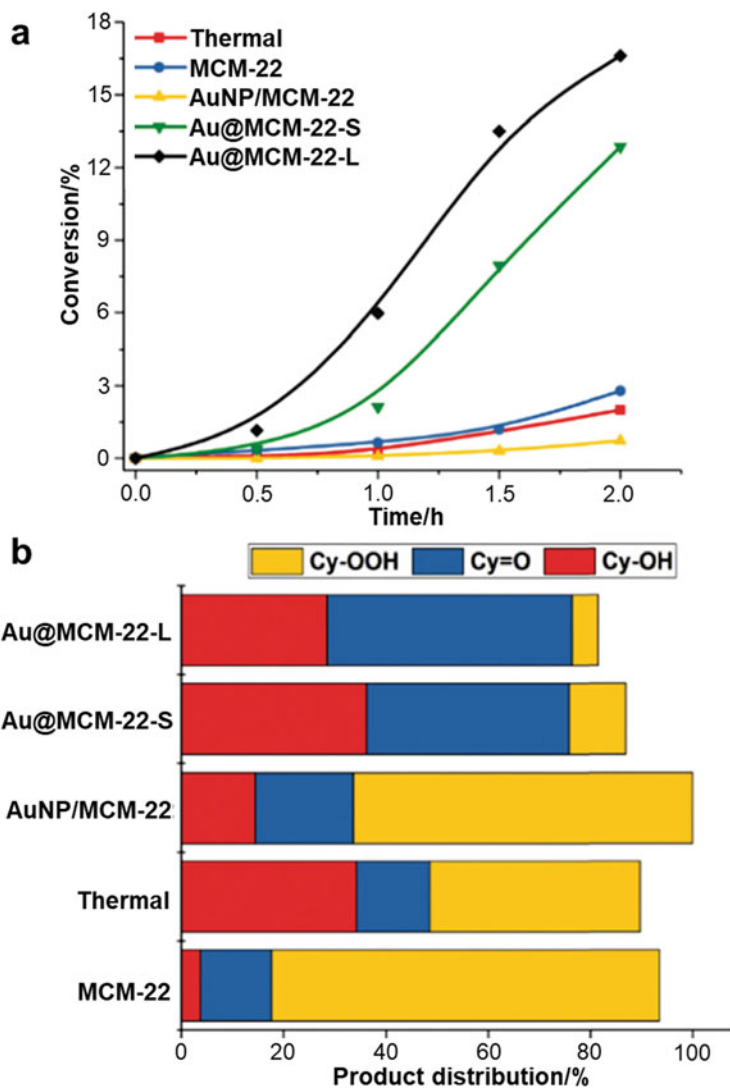


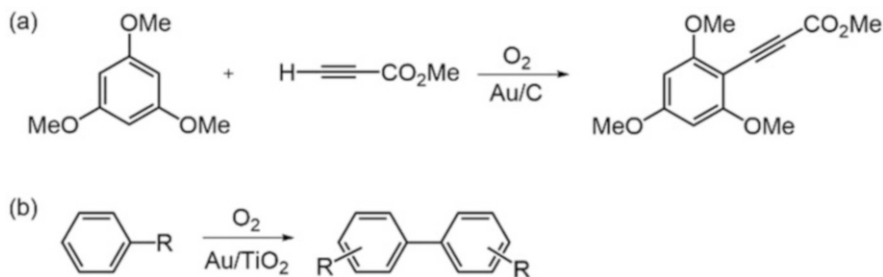
Fig. 23 Time-conversion curves for the cyclohexane oxidation over Au@MCM-22-S and -L (a) and product distributions after 2 h reaction at 150°C under 1 MPa of O₂ (b). The “thermal” represents the blank test in the absence of catalyst [167]. Adapted with permission from [167] Copyright 2019 Royal Chemical Society

Table 5 Cyclohexane oxidation using O₂ as a sole oxidant catalyzed by supported Au catalysts

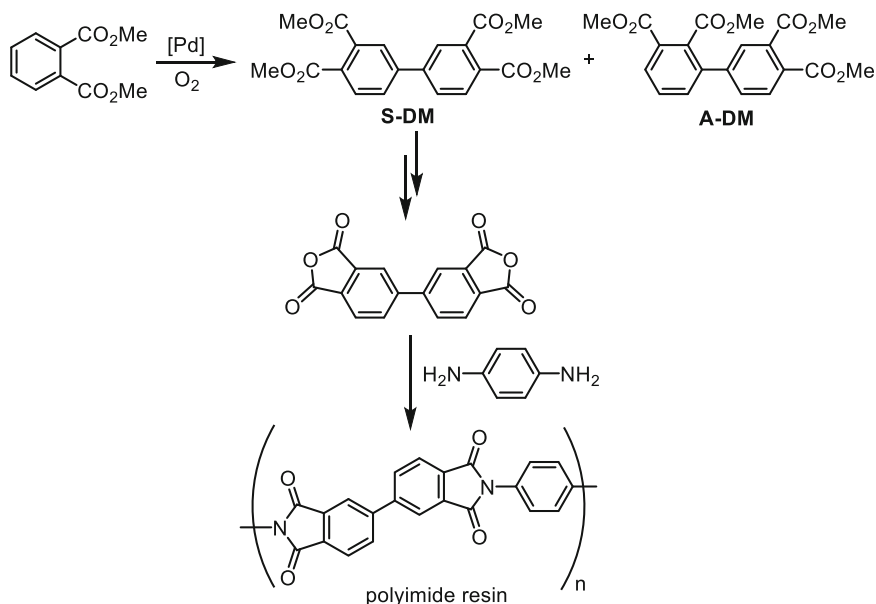
Catalyst	Au size (nm)	Conv. (%)	Selectivity (%)				Ref.
			Cy-one	Cy-ol	Cy-OOH	K/A oil	
Au/Al ₂ O ₃	3–6	13	32	53	4	85	[163]
Au/ZSM-5	–	7	55	36	–	91	[163]
Au/ZSM-5	–	16	67	25	–	92	[165]
Au@ZSM-5	>20	~42	–	–	–	~80	[166]
Au/MCM-41	4.4	13	68	27	–	95	[164]
Au@MCM-22-S	<2	13	~40	~35	~10	~75	[167]
Au@MCM-22-L	<2	17	~45	~30	~5	~75	[167]
AuNP/MCM-22		<1	~15	~3	~75	~18	[167]

8 Oxidative C–H Coupling Reaction

Metal-catalyzed C–C bond coupling reactions have been one of the most important research topics in organic chemistry. In particular, direct C–H bond functionalization to transform into C–C bond has been rapidly growing interest owing to the high atom efficiency and environmentally friendly reactions. Corma et al. reported the coupling of electron-rich arene and propiolate over Au/C in the presence of O₂ (Scheme 10a) [168]. They also reported a direct oxidative homocoupling of aryl C–H bonds to produce biaryls (Scheme 10b) [169]. For these reactions, H₂O is the only by-product, and transformation of unreactive C–H bonds into reactive C–X (X = halogen) or C–M (M = transition metal) bonds in advance of the coupling reaction can be avoided. However, the yield of biaryl is very low, and the regioselectivity could not be controlled [169]. The oxidative C–H homocoupling to synthesize biaryls is currently used in industry for the production of tetramethyl (1,1'-biphenyl)-3,3',4,4'-tetracarboxylate (S-DM) which leads to high thermally stable polyimide resin using homogenous Pd catalysts with Cu co-catalyst (Scheme 11). However, the conversion is controlled to not exceed 10% to avoid trimerization, and a bulky ligand is required to achieve high regioselectivity to S-DM. Au/MO_x, such as Au/Co₃O₄, Au/ZrO₂, and Au/TiO₂ appeared to catalyze the oxidative C–H coupling of dimethyl phthalate to produce S-DM with excellent regioselectivity in the absence of either co-catalysts or ligands even at high conversions [170]. In particular, Au/Co₃O₄ showed 98% dimer selectivity (total yield of S-DM and A-DM) and 94% regioselectivity to S-DM at 49% conversion. Au/ZrO₂ showed 83% dimer selectivity and 95% regioselectivity to S-DM at 88% conversion. It is worth to note that PdO/Co₃O₄ showed almost negligible catalytic activity. Pd(OH)₂/Co₃O₄ showed catalytic activity but was much less active and low regioselectivity (67%).



Scheme 10 Coupling of electron-rich arene and propiolate (a) [168] and homocoupling of arenes to biaryls (b) [169]



Scheme 11 Conventional Pd-catalyzed oxidative coupling of dimethyl phthalate to tetramethyl (1,1'-biphenyl)-3,3',4,4'-tetracarboxylate (S-DM) which is the intermediate for the production of polyimide resin [170]. Reproduced with permission from [170] Copyright 2015 Wiley-VCH Verlag GmbH&Co. KGaA

Given that Co(III) species in Au/Co₃O₄ was reduced to Co(II) after the C–H homocoupling under N₂ to give the biaryls, the redox properties of Co₃O₄ facilitate the reaction. Kinetic studies suggested that the C–H homocoupling takes place by an electrophilic aromatic substitution pathway (Fig. 24). The aromatic ring would react with cationic Au sites located at the perimeter interface between Au and MO_x to make Au–C bond followed by C–H bond cleavage. After the second electrophilic substitution takes place, the reductive elimination produces biaryl and the reduced

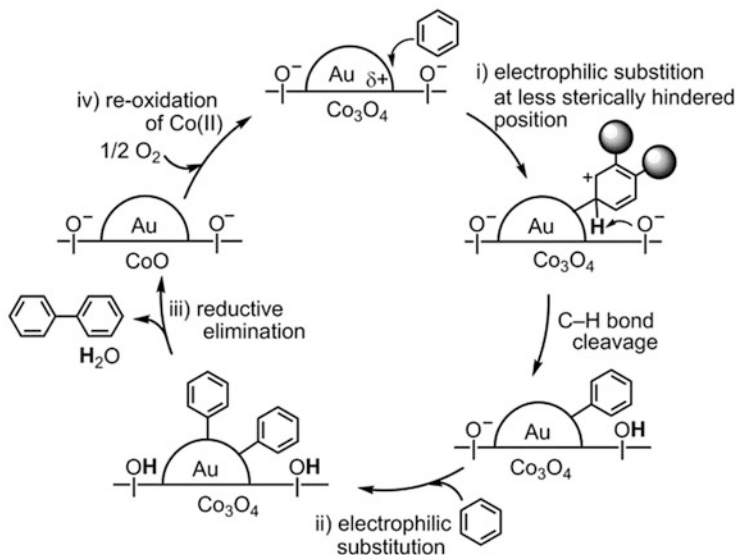


Fig. 24 A plausible mechanism for the oxidative C–H/C–H homocoupling of aromatic compounds over Au/Co₃O₄ [170]. Reproduced with permission from [170] Copyright 2015 Wiley-VCH Verlag GmbH&Co. KGaA

CoO species. The high regioselectivity was probably ascribed to that Au NPs that acted as a bulky ligand and suppressed the C–H bond cleavage at sterically hindered positions.

9 Conclusion

It is clear that the types of supports greatly influence the catalytic performance of Au for many reactions. For aerobic alcohol oxidation, the redox properties of MO_x and the surface acid/base properties of support materials are the crucial factors to determine the catalytic activity of Au. High reducibility of MO_x contributes to accelerate the alcohol oxidation via a Mars-van Krevelen-like mechanism. Basic sites would facilitate the deprotonation of the OH group of the substrate alcohol, and acidic sites would promote to remove the H-species on the Au particles. For alkene oxidation, inert and acidic supports such as WO₃ led to high selectivity to epoxide. Alkane oxidation required acidic supports such as zeolites of which the acidic sites probably participate in the decomposition of hydroperoxy intermediate. The redox properties of MO_x also contribute to the oxidative C–H coupling of arenes to give biaryls.

The size of Au particles also affects the catalytic activity depending on the kinds of reactions and supports. For aerobic alcohol oxidation, an obvious size effect in terms of TOF was not observed for Au/MO_x, suggesting that the surface Au atoms

seem to be the active sites, whereas the presence of small Au particles becomes more important to show high activity for Au on inert materials and ligand-protected Au clusters. For dehydrogenation of alcohols under inert atmosphere, the TOF sharply increased with a decrease in the size of Au, reflecting that the active site would change to the edge and corner Au atoms. For the alkene oxidation, conflicting results was reported; Au clusters were important for styrene oxidation but Au NPs larger than 2 nm were active for cyclohexene oxidation. The difference was explained by the substrate structure, i.e., allylic oxidation of cyclohexene readily takes place, which do not need O₂ activation. Atomically precise Au clusters protected by phosphine or thiolate ligands are one of the hot research topics due to small Au particle size and narrow size distributions. For cyclohexane oxidation, a unique size dependence was observed; Au₃₉/HAP exhibited the highest catalytic activity among smaller or larger ones. However, the ligands remained on the Au clusters even after calcination affected the catalytic properties of Au, which sometimes make difficult to elucidate the true size effect of Au. For alkane oxidation, the presence of sub-nanometer-sized Au clusters would be a crucial factor which is probably responsible for the O₂ activation to form oxygen radical species on the sub-nano Au clusters.

To understand the role of supports and the size effect of Au more precisely for each reaction will help us to design more efficient and sophisticated Au catalysts. In order to discuss these effects, the developments of preparation method to deposit Au as sub-nm clusters with narrow size distributions, new support materials, and of characterization techniques including in situ measurements are highly demanded.

References

1. Haruta M, Kobayashi T, Sano H, Yamada N (1987) Novel gold catalysts for the oxidation of carbon monoxide at a temperature far below 0 °C. *Chem Lett* 16:405–408. <https://doi.org/10.1246/cl.1987.405>
2. Takei T, Akita T, Nakamura I, Fujitani T, Okumura M, Okazaki K, Huang J, Ishida T, Haruta M (2012) Heterogeneous catalysis by gold. *Adv Catal* 55:1–126. <https://doi.org/10.1016/B978-0-12-385516-9.00001-6>
3. Okumura M, Fujitani T, Huang J, Ishida T (2015) A career in catalysis: Masatake Haruta. *ACS Catal* 5:4699–4707. <https://doi.org/10.1021/acscatal.5b01122>
4. Ishida T, Koga H, Okumura M, Haruta M (2016) Advances in gold catalysis and understanding the catalytic mechanism. *Chem Rec* 16:2278–2293. <https://doi.org/10.1002/tcr.201600046>
5. Haruta M, Yamada N, Kobayashi T, Iijima S (1989) Gold catalysts prepared by coprecipitation for low-temperature oxidation of hydrogen and of carbon monoxide. *J Catal* 115:301–309. [https://doi.org/10.1016/0021-9517\(89\)90034-1](https://doi.org/10.1016/0021-9517(89)90034-1)
6. Hayashi T, Tanaka K, Haruta M (1998) Selective vapor-phase epoxidation of propylene over Au/TiO₂ catalysts in the presence of oxygen and hydrogen. *J Catal* 178:566–575. <https://doi.org/10.1006/jcat.1998.2157>
7. Huang J, Akita T, Faye J, Fujitani T, Takei T, Haruta M (2009) Propene epoxidation with dioxygen catalyzed by gold clusters. *Angew Chem Int Ed Engl* 48:7862–7866. <https://doi.org/10.1002/anie.200903011>
8. Hammer B, Norskov JK (1995) Why gold is the noblest of all the metals. *Nature* 376:238–240. <https://doi.org/10.1038/376238a0>

9. Fujitani T, Nakamura I, Haruta M (2014) Role of water in CO oxidation on gold catalysts. *Catal Lett* 144:1475–1486. <https://doi.org/10.1007/s10562-014-1325-2>
10. Saavedra J, Doan HA, Pursell CJ, Grabow LC, Chandler BD (2014) The critical role of water at the gold-titania interface in catalytic CO oxidation. *Science* 345:1599–1602. <https://doi.org/10.1126/science.1256018>
11. Prati L, Rossi M (1998) Gold on carbon as a new catalyst for selective liquid phase oxidation of diols. *J Catal* 176:552–560. <https://doi.org/10.1006/jcat.1998.2078>
12. Liu L, Corma A (2018) Metal catalysts for heterogeneous catalysis: from single atoms to nanoclusters and nanoparticles. *Chem Rev* 118:4981–5079. <https://doi.org/10.1021/acs.chemrev.7b00776>
13. Sharma AS, Kaur H, Shah D (2016) Selective oxidation of alcohols by supported gold nanoparticles: recent advances. *RSC Adv* 6:28688–28727. <https://doi.org/10.1039/c5ra25646a>
14. Castro PR, Garcia AS, de Abreu WC, de Sousa AA, de Moura VR, Costa CS, de Moura EM (2018) Aerobic oxidation of benzyl alcohol on a strontium-based gold material: remarkable intrinsic basicity and reusable catalyst. *Catalysts* 8:83. <https://doi.org/10.3390/catal8020083>
15. Hui Y, Zhang S, Wang W (2019) Recent progress in catalytic oxidative transformations of alcohols by supported gold nanoparticles. *Adv Synth Catal* 361(10):2215–2235. <https://doi.org/10.1002/adsc.201801595>
16. Bianchi C, Porta F, Prati L, Rossi M (2000) Selective liquid phase oxidation using gold catalysts. *Top Catal* 13:231–236. <https://doi.org/10.1023/A:1009065812889>
17. Abad A, Almela C, Corma A, García H (2006) Efficient chemoselective alcohol oxidation using oxygen as oxidant. Superior performance of gold over palladium catalysts. *Tetrahedron* 62:6666–6672. <https://doi.org/10.1016/j.tet.2006.01.118>
18. Abad A, Almela C, Corma A, García H (2006) Unique gold chemoselectivity for the aerobic oxidation of allylic alcohols. *Chem Commun* 30:3178–3180. <https://doi.org/10.1039/b606257a>
19. Milone C, Ingoglia R, Neri G, Pistone A, Galvagno S (2001) Gold catalysts for the liquid phase oxidation of o-hydroxybenzyl alcohol. *Appl Catal A Gen* 211:251–257. [https://doi.org/10.1016/S0926-860X\(00\)00875-9](https://doi.org/10.1016/S0926-860X(00)00875-9)
20. Huang J, Dai WL, Fan K (2008) Support effect of new Au/FeO_x catalysts in the oxidative dehydrogenation of α,ω -diols to lactones. *J Phys Chem C* 112:16110–16117. <https://doi.org/10.1021/jp8043913>
21. Huang J, Dai WL, Fan K (2009) Remarkable support crystal phase effect in Au/FeO_x catalyzed oxidation of 1,4-butanediol to γ -butyrolactone. *J Catal* 266:228–235. <https://doi.org/10.1016/j.jcat.2009.06.011>
22. Wang LC, Liu YM, Chen M, Cao Y, He HY, Fan KN (2008) MnO₂ nanorod supported gold nanoparticles with enhanced activity for solvent-free aerobic alcohol oxidation. *J Phys Chem C* 112:6981–6987. <https://doi.org/10.1021/jp711333t>
23. Wang LC, He L, Liu Q, Liu YM, Chen M, Cao Y, He HY, Fan KN (2008) Solvent-free selective oxidation of alcohols by molecular oxygen over gold nanoparticles supported on β -MnO₂ nanorods. *Appl Catal A Gen* 344:150–157. <https://doi.org/10.1016/j.apcata.2008.04.013>
24. Alhumaimess M, Lin Z, He Q, Lu L, Dimitratos N, Dummer NF, Conte M, Taylor SH, Bartley JK, Kiely CJ, Hutchings GJ (2014) Oxidation of benzyl alcohol and carbon monoxide using gold nanoparticles supported on MnO₂ nanowire microspheres. *Chem Eur J* 20:1701–1710. <https://doi.org/10.1002/chem.201303355>
25. Wang H, Fan W, He Y, Wang J, Kondo JN, Tatsumi T (2013) Selective oxidation of alcohols to aldehydes/ketones over copper oxide-supported gold catalysts. *J Catal* 299:10–19. <https://doi.org/10.1016/j.jcat.2012.11.018>
26. Abad A, Concepción P, Corma A, García H (2005) A collaborative effect between gold and a support induces the selective oxidation of alcohols. *Angew Chem Int Ed Engl* 44:4066–4069. <https://doi.org/10.1002/anie.200500382>

27. Sudarsanam P, Malleshm B, Durgasri DN, Reddy BM (2014) Physicochemical and catalytic properties of nanosized Au/CeO₂ catalysts for eco-friendly oxidation of benzyl alcohol. *J Ind Eng Chem* 20:3115–3121. <https://doi.org/10.1016/j.jiec.2013.11.053>
28. Wang M, Wang F, Ma J, Li M, Zhang Z, Wang Y, Zhang X, Xu J (2014) Investigations on the crystal plane effect of ceria on gold catalysis in the oxidative dehydrogenation of alcohols and amines in the liquid phase. *Chem Commun* 50:292–294. <https://doi.org/10.1039/c3cc46180g>
29. Li T, Liu F, Tang Y, Li L, Miao S, Su Y, Zhang J, Huang J, Sun H, Haruta M, Wang A, Qiao B, Li J, Zhang T (2018) Maximizing the number of interfacial sites in single-atom catalysts for the highly selective, solvent-free oxidation of primary alcohols. *Angew Chem Int Ed Engl* 57:7795–7799. <https://doi.org/10.1002/anie.201803272>
30. Dimitratos N, Lopez-Sanchez JA, Morgan D, Carley A, Prati L, Hutchings GJ (2007) Solvent free liquid phase oxidation of benzyl alcohol using Au supported catalysts prepared using a sol immobilization technique. *Catal Today* 122:317–324. <https://doi.org/10.1016/j.cattod.2007.01.002>
31. Zheng N, Stucky GD (2007) Promoting gold nanocatalysts in solvent-free selective aerobic oxidation of alcohols. *Chem Commun* 1:3862–3864. <https://doi.org/10.1039/b706864f>
32. Kimmerle B, Grunwaldt JD, Baiker A (2007) Gold catalysed selective oxidation of alcohols in supercritical carbon dioxide. *Top Catal* 44:285–292. <https://doi.org/10.1007/s11244-007-0301-0>
33. Huang J, Dai WL, Li H, Fan K (2007) Au/TiO₂ as high efficient catalyst for the selective oxidative cyclization of 1,4-butanediol to γ -butyrolactone. *J Catal* 252:69–76. <https://doi.org/10.1016/j.jcat.2007.09.011>
34. Abad A, Corma A, García H (2008) Catalyst parameters determining activity and selectivity of supported gold nanoparticles for the aerobic oxidation of alcohols: the molecular reaction mechanism. *Chem Eur J* 14:212–222. <https://doi.org/10.1002/chem.200701263>
35. Haider P, Kimmerle B, Krumeich F, Kleist W, Grunwaldt JD, Baiker A (2008) Gold-catalyzed aerobic oxidation of benzyl alcohol: effect of gold particle size on activity and selectivity in different solvents. *Catal Lett* 125:169–176. <https://doi.org/10.1007/s10562-008-9567-5>
36. Yang X, Wang X, Liang C, Su W, Wang C, Feng Z, Li C, Qiu J (2008) Aerobic oxidation of alcohols over Au/TiO₂: an insight on the promotion effect of water on the catalytic activity of Au/TiO₂. *Catal Commun* 9:2278–2281. <https://doi.org/10.1016/j.catcom.2008.05.021>
37. Fristrup P, Johansen LB, Christensen CH (2008) Mechanistic investigation of the gold-catalyzed aerobic oxidation of alcohols. *Catal Lett* 120:184–190. <https://doi.org/10.1007/s10562-007-9301-8>
38. Xu J, Wang Y, Cao Y, He Z, Zhao L, Etim UJ, Bai P, Yan Z, Wu P (2019) What is the effect of Sn and Mo oxides on gold catalysts for selective oxidation of benzyl alcohol? *New J Chem* 43:2591–2599. <https://doi.org/10.1039/C8NJ05642K>
39. Berndt H, Pitsch I, Evert S, Struve K, Pohl MM, Radnik J, Martin A (2003) Oxygen adsorption on Au/Al₂O₃ catalysts and relation to the catalytic oxidation of ethylene glycol to glycolic acid. *Appl Catal A Gen* 244:169–179. [https://doi.org/10.1016/S0926-860X\(02\)00575-6](https://doi.org/10.1016/S0926-860X(02)00575-6)
40. Su FZ, Chen M, Wang LC, Huang XS, Liu YM, Cao Y, He HY, Fan KN (2008) Aerobic oxidation of alcohols catalyzed by gold nanoparticles supported on gallia polymorphs. *Catal Commun* 9:1027–1032. <https://doi.org/10.1016/j.catcom.2007.10.010>
41. Su FZ, Liu YM, Wang LC, Cao Y, He HY, Fan KN (2008) Ga-Al mixed-oxide-supported gold nanoparticles with enhanced activity for aerobic alcohol oxidation. *Angew Chem Int Ed Engl* 47:334–337. <https://doi.org/10.1002/anie.200704370>
42. Huang R, Fu Y, Zeng W, Zhang L, Wang D (2017) The facile approach to fabricate gold nanoparticles and their application on the hydration and dehydrogenation reactions. *J Organomet Chem* 851:46–51. <https://doi.org/10.1016/j.jorganchem.2017.09.016>
43. Choudhary VR, Dumbre DK (2011) Solvent-free selective oxidation of primary alcohols-to-aldehydes and aldehydes-to-carboxylic acids by molecular oxygen over MgO-supported nano-gold catalyst. *Catal Commun* 13:82–86. <https://doi.org/10.1016/j.catcom.2011.07.001>

44. Haider P, Baiker A (2007) Gold supported on Cu-Mg-Al-mixed oxides: strong enhancement of activity in aerobic alcohol oxidation by concerted effect of copper and magnesium. *J Catal* 248:175–187. <https://doi.org/10.1016/j.jcat.2007.03.007>
45. Li S, Li W, Li Y, Fan G, Li F (2017) Structure-dependent base-free aerobic oxidation of benzyl alcohol over high-surface-area Mg-doped ZnAl₂O₄ spinel supported gold nanoparticles. *ChemPlusChem* 82:270–279. <https://doi.org/10.1002/cplu.201600500>
46. De Moura EM, Garcia MAS, Gonçalves RV, Kiyohara PK, Jardim RF, Rossi LM (2015) Gold nanoparticles supported on magnesium ferrite and magnesium oxide for the selective oxidation of benzyl alcohol. *RSC Adv* 5:15035–15041. <https://doi.org/10.1039/c4ra16159a>
47. Mitsudome T, Noujima A, Mizugaki T, Jitsukawa K, Kaneda K (2009) Efficient aerobic oxidation of alcohols using a hydrotalcite supported gold nanoparticle catalyst. *Adv Synth Catal* 351:1890–1896. <https://doi.org/10.1002/adsc.200900239>
48. Chen J, Fang W, Zhang Q, Deng W, Wang Y (2014) A comparative study of size effects in the Au-catalyzed oxidative and non-oxidative dehydrogenation of benzyl alcohol. *Chem Asian J* 9:2187–2196. <https://doi.org/10.1002/asia.201402238>
49. Liu P, Guan Y, Santen RAV, Li C, Hensen EJM (2011) Aerobic oxidation of alcohols over hydrotalcite-supported gold nanoparticles: the promotional effect of transition metal cations. *Chem Commun* 47:11540–11542. <https://doi.org/10.1039/c1cc15148g>
50. Li L, Dou L, Zhang H (2014) Layered double hydroxide supported gold nanoclusters by glutathione-capped Au nanoclusters precursor method for highly efficient aerobic oxidation of alcohols. *Nanoscale* 6:3753–3763. <https://doi.org/10.1039/c3nr05604j>
51. Liu M, Fan G, Yu J, Yang L, Li F (2018) Defect-rich Ni-Ti layered double hydroxide as a highly efficient support for Au nanoparticles in base-free and solvent-free selective oxidation of benzyl alcohol. *Dalton Trans* 47:5226–5235. <https://doi.org/10.1039/c7dt04229a>
52. Tang H, Wei J, Liu F, Qiao B, Pan X, Li L, Liu J, Wang J, Zhang T (2016) Strong metal-support interactions between gold nanoparticles and nonoxides. *J Am Chem Soc* 138:56–59. <https://doi.org/10.1021/jacs.5b11306>
53. Haesuwannakij S, Poonsawat T, Noikham M, Somsook E, Yakiyama Y, Dhital RN, Sakurai H (2017) Size-controlled preparation of gold nanoclusters on hydroxyapatite through trans-deposition method. *J Nanosci Nanotechnol* 17:4649–4657. <https://doi.org/10.1166/jnn.2017.13777>
54. Karimi B, Kabiri Esfahani F (2009) Gold nanoparticles supported on Cs₂CO₃ as recyclable catalyst system for selective aerobic oxidation of alcohols at room temperature. *Chem Commun* 37:5555–5557. <https://doi.org/10.1039/b908964k>
55. Ishida T, Nagaoka M, Akita T, Haruta M (2008) Deposition of gold clusters on porous coordination polymers by solid grinding and their catalytic activity in aerobic oxidation of alcohols. *Chem Eur J* 14:8456–8460. <https://doi.org/10.1002/chem.200800980>
56. Liu H, Liu Y, Li Y, Tang Z, Jiang H (2010) Metal-organic framework supported gold nanoparticles as a highly active heterogeneous catalyst for aerobic oxidation of alcohols. *J Phys Chem C* 114:13362–13369. <https://doi.org/10.1021/jp105666f>
57. Zhu J, Wang PC, Lu M (2014) Selective oxidation of benzyl alcohol under solvent-free condition with gold nanoparticles encapsulated in metal-organic framework. *Appl Catal A Gen* 477:125–131. <https://doi.org/10.1016/j.apcata.2014.03.013>
58. Luan Y, Qi Y, Gao H, Zheng N, Wang G (2014) Synthesis of an amino-functionalized metal-organic framework at a nanoscale level for gold nanoparticle deposition and catalysis. *J Mater Chem A* 2:20588–20596. <https://doi.org/10.1039/c4ta04311a>
59. Leus K, Concepcion P, Vandichel M, Meledina M, Grirrane A, Esquivel D, Turner S, Poelman D, Waroquier M, Van Speybroeck V, Van Tendeloo G, García H, Van Der Voort P (2015) Au@UiO-66: a base free oxidation catalyst. *RSC Adv* 5:22334–22342. <https://doi.org/10.1039/c4ra16800c>
60. Wang JS, Jin FZ, Ma HC, Li XB, Liu MY, Kan JL, Chen GJ, Dong YB (2016) Au@Cu(II)-MOF: highly efficient bifunctional heterogeneous catalyst for successive oxidation-condensation reactions. *Inorg Chem* 55:6685–6691. <https://doi.org/10.1021/acs.inorgchem.6b00925>

61. Mahyari M, Shaabani A, Bide Y (2013) Gold nanoparticles supported on supramolecular ionic liquid grafted graphene: a bifunctional catalyst for the selective aerobic oxidation of alcohols. *RSC Adv* 3:22509–22517. <https://doi.org/10.1039/c3ra44696d>
62. Zhang P, Qiao ZA, Jiang X, Veith GM, Dai S (2015) Nanoporous ionic organic networks: stabilizing and supporting gold nanoparticles for catalysis. *Nano Lett* 15:823–828. <https://doi.org/10.1021/nl504780j>
63. Ding S, Tian C, Zhu X, Wang H, Wang H, Abney CW, Zhang N, Dai S (2018) Engineering nanoporous organic frameworks to stabilize naked Au clusters: a charge modulation approach. *Chem Commun* 54:5058–5061. <https://doi.org/10.1039/c8cc02966k>
64. Porta F, Rossi M (2003) Gold nanostructured materials for the selective liquid phase catalytic oxidation. *J Mol Catal A Chem* 204–205:553–559. [https://doi.org/10.1016/S1381-1169\(03\)00338-8](https://doi.org/10.1016/S1381-1169(03)00338-8)
65. Asao N, Hatakeyama N, Menggenbateer, Minato T, Ito E, Hara M, Kim Y, Yamamoto Y, Chen M, Zhang W, Inoue A (2012) Aerobic oxidation of alcohols in the liquid phase with nanoporous gold catalysts. *Chem Commun* 48:4540–4542. <https://doi.org/10.1039/c2cc17245c>
66. Tsunoyama H, Sakurai H, Negishi Y, Tsukuda T (2005) Size-specific catalytic activity of polymer-stabilized gold nanoclusters for aerobic alcohol oxidation in water. *J Am Chem Soc* 127:9374. <https://doi.org/10.1021/JA052161E>
67. Tsunoyama H, Ichikuni N, Sakurai H, Tsukuda T (2009) Effect of electronic structures of Au clusters stabilized by poly(*N*-vinyl-2-pyrrolidone) on aerobic oxidation catalysis. *J Am Chem Soc* 131:7086–7093. <https://doi.org/10.1021/ja810045y>
68. Tsukuda T, Tsunoyama H, Sakurai H (2011) Aerobic oxidations catalyzed by colloidal nanogold. *Chem Asian J* 6:736–748. <https://doi.org/10.1002/asia.201000611>
69. Li G, Jin R (2013) Atomically precise gold nanoclusters as new model catalysts. *Acc Chem Res* 46:1749–1758. <https://doi.org/10.1021/ar300213z>
70. Adnan RH, Andersson GG, Polson MIJ, Metha GF, Golovko VB (2015) Factors influencing the catalytic oxidation of benzyl alcohol using supported phosphine-capped gold nanoparticles. *Catal Sci Technol* 5:1323–1333. <https://doi.org/10.1039/c4cy01168f>
71. Lavenn C, Demessence A, Tuel A (2014) Au 25 (SPh- p NH 2) 17 nanoclusters deposited on SBA-15 as catalysts for aerobic benzyl alcohol oxidation. *J Catal* 322:130–138. <https://doi.org/10.1016/j.jcat.2014.12.002>
72. Zhang B, Fang J, Li J, Lau JJ, Mattia D, Zhong Z, Xie J, Yan N (2016) Soft, oxidative stripping of alkyl thiolate ligands from hydroxyapatite-supported gold nanoclusters for oxidation reactions. *Chem Asian J* 11:532–539. <https://doi.org/10.1002/asia.201501074>
73. Xie S, Tsunoyama H, Kurashige W, Negishi Y, Tsukuda T (2012) Enhancement in aerobic alcohol oxidation catalysis of Au 25 clusters by single Pd atom doping. *ACS Catal* 2:1519–1523. <https://doi.org/10.1021/cs300252g>
74. Kotolevich Y, Martynyuk O, Martínez-González S, Tiznado H, Pestryakov A, Avalos Borja M, Cortés Corberán V, Bogdanchikova N (2019) Novel route of synthesis of ultra-small Au nanoparticles on SiO₂ supports. *Fuel* 236:589–597. <https://doi.org/10.1016/j.fuel.2018.09.050>
75. Kohantorabi M, Gholami MR (2018) Fabrication of novel ternary Au/CeO₂@g-C₃N₄ nanocomposite: kinetics and mechanism investigation of 4-nitrophenol reduction, and benzyl alcohol oxidation. *Appl Phys A Mater Sci Process* 124:1–17. <https://doi.org/10.1007/s00339-018-1858-0>
76. Conte M, Miyamura H, Kobayashi S, Chechik V (2009) Spin trapping of Au-H intermediate in the alcohol oxidation by supported and unsupported gold catalysts. *J Am Chem Soc* 131:7189–7196. <https://doi.org/10.1021/ja809883c>
77. Sun KQ, Luo SW, Xu N, Xu BQ (2008) Gold nano-size effect in Au/SiO₂ for selective ethanol oxidation in aqueous solution. *Catal Lett* 124:238–242. <https://doi.org/10.1007/s10562-008-9507-4>

78. Fang W, Chen J, Zhang Q, Deng W, Wang Y (2011) Hydrotalcite-supported gold catalyst for the oxidant-free dehydrogenation of benzyl alcohol: studies on support and gold size effects. *Chem Eur J* 17:1247–1256. <https://doi.org/10.1002/chem.201002469>
79. Ishida T, Kawakita N, Akita T, Haruta M (2009) One-pot *N*-alkylation of primary amines to secondary amines by gold clusters supported on porous coordination polymers. *Gold Bull* 42:267–274. <https://doi.org/10.1007/BF03214948>
80. Ishida T, Kawakita N, Akita T, Haruta M (2010) Deposition of gold clusters onto porous coordination polymers by solid grinding. In: *Studies in surface science and catalysis*. Elsevier, Amsterdam, pp 839–842
81. Takei T, Akita T, Nakamura I, Fujitani T, Okumura M, Okazaki K, Huang J, Ishida T, Haruta M (2012) Heterogeneous catalysis by gold. In: *Advances in catalysis*. Academic Press, Cambridge, pp 1–126
82. Xie X, Long J, Xu J, Chen L, Wang Y, Zhang Z, Wang X (2012) Nitrogen-doped graphene stabilized gold nanoparticles for aerobic selective oxidation of benzylic alcohols. *RSC Adv* 2:12438. <https://doi.org/10.1039/c2ra21291a>
83. Miyamura H, Matsubara R, Miyazaki Y, Kobayashi S (2007) Aerobic oxidation of alcohols at room temperature and atmospheric conditions catalyzed by reusable gold nanoclusters stabilized by the benzene rings of polystyrene derivatives. *Angew Chem Int Ed Engl* 46:4151–4154. <https://doi.org/10.1002/anie.200700080>
84. Lucchesi C, Inasaki T, Miyamura H, Matsubara R, Kobayashi S (2008) Aerobic oxidation of alcohols under mild conditions catalyzed by novel polymer-incarcerated, carbon-stabilized gold nanoclusters. *Adv Synth Catal* 350:1996–2000. <https://doi.org/10.1002/adsc.200800319>
85. Ishida T, Okamoto S, Makiyama R, Haruta M (2009) Aerobic oxidation of glucose and 1-phenylethanol over gold nanoparticles directly deposited on ion-exchange resins. *Appl Catal A Gen* 353:243–248. <https://doi.org/10.1016/j.apcata.2008.10.049>
86. Ahmed OU, Mjalli FS, Al-Wahaibi T, Al-Wahaibi Y, Alnashef IM (2015) Stability of superoxide ion in phosphonium-based ionic liquids. *Ind Eng Chem Res* 54:2074–2080. <https://doi.org/10.1021/ie504893k>
87. Wang S, Wang J, Zhao Q, Li D, Wang JQ, Cho M, Cho H, Terasaki O, Chen S, Wan Y (2015) Highly active heterogeneous 3 nm gold nanoparticles on mesoporous carbon as catalysts for low-temperature selective oxidation and reduction in water. *ACS Catal* 5:797–802. <https://doi.org/10.1021/cs501896c>
88. Han J, Liu Y, Li L, Guo R (2009) Poly(*o*-phenylenediamine) submicrosphere-supported gold nanocatalysts: synthesis, characterization, and application in selective oxidation of benzyl alcohol. *Langmuir* 25:11054–11060. <https://doi.org/10.1021/la901373t>
89. Wang Y, Yan R, Zhang J, Zhang W (2010) Synthesis of efficient and reusable catalyst of size-controlled Au nanoparticles within a porous, chelating and intelligent hydrogel for aerobic alcohol oxidation. *J Mol Catal A Chem* 317:81–88. <https://doi.org/10.1016/j.molcata.2009.10.026>
90. Yin H, Zhou C, Xu C, Liu P, Xu X, Ding Y (2008) Aerobic oxidation of *D*-glucose on support-free nanoporous gold. *J Phys Chem C* 112:9673–9678. <https://doi.org/10.1021/jp8019864>
91. Wittstock A, Neumann B, Schaefer A, Dumbuya K, Kübel C, Biener MM, Zielasek V, Steinrück HP, Gottfried JM, Biener J, Hamza A, Bäumer M (2009) Nanoporous Au: an unsupported pure gold catalyst? *J Phys Chem C* 113:5593–5600. <https://doi.org/10.1021/jp808185v>
92. Lackmann A, Bäumer M, Wittstock G, Wittstock A (2018) Independent control over residual silver content of nanoporous gold by galvanodynamically controlled dealloying. *Nanoscale* 10:17166–17173. <https://doi.org/10.1039/c8nr03699c>
93. Lackmann A, Mahr C, Schowalter M, Fitzek L, Weissmüller J, Rosenauer A, Wittstock A (2017) A comparative study of alcohol oxidation over nanoporous gold in gas and liquid phase. *J Catal* 353:99–106. <https://doi.org/10.1016/j.jcat.2017.07.008>
94. Prati L, Porta F (2005) Oxidation of alcohols and sugars using Au/C catalysts: part I. Alcohols. *Appl Catal A Gen* 291:199–203. <https://doi.org/10.1016/j.apcata.2004.11.050>

95. Okumura M, Kitagawa Y, Kawakami T, Haruta M (2008) Theoretical investigation of the hetero-junction effect in PVP-stabilized Au₁₃ clusters. The role of PVP in their catalytic activities. *Chem Phys Lett* 459:133–136. <https://doi.org/10.1016/j.cplett.2008.04.120>
96. Comotti M, Della Pina C, Matarrese R, Rossi M (2004) The catalytic activity of “naked” gold particles. *Angew Chem Int Ed Engl* 43:5812–5815. <https://doi.org/10.1002/anie.200460446>
97. Sakata K, Koga H, Ishida T, Aimoto J, Tokunaga M, Okumura M (2015) Theoretical investigation for isomerization of allylic alcohols over Au₆ cluster. *Gold Bull* 48:31–37. <https://doi.org/10.1007/s13404-015-0157-1>
98. Corma A, Domine ME (2005) Gold supported on a mesoporous CeO₂ matrix as an efficient catalyst in the selective aerobic oxidation of aldehydes in the liquid phase. *Chem Commun* 32:4042–4044. <https://doi.org/10.1039/b506685a>
99. Biella S, Prati L, Rossi M (2003) Gold catalyzed oxidation of aldehydes in liquid phase. *J Mol Catal A Chem* 197:207–212. [https://doi.org/10.1016/S1381-1169\(02\)00618-0](https://doi.org/10.1016/S1381-1169(02)00618-0)
100. Christensen CH, Jørgensen B, Rass-Hansen J, Egeblad K, Madsen R, Klitgaard SK, Hansen SM, Hansen MR, Andersen HC, Riisager A (2006) Formation of acetic acid by aqueous-phase oxidation of ethanol with air in the presence of a heterogeneous gold catalyst. *Angew Chem Int Ed Engl* 45:4648–4651. <https://doi.org/10.1002/anie.200601180>
101. Jørgensen B, Egholm Christiansen S, Dahl Thomsen ML, Christensen CH (2007) Aerobic oxidation of aqueous ethanol using heterogeneous gold catalysts: efficient routes to acetic acid and ethyl acetate. *J Catal* 251:332–337. <https://doi.org/10.1016/j.jcat.2007.08.004>
102. Tembe SM, Patrick G, Scurrall MS (2009) Acetic acid production by selective oxidation of ethanol using Au catalysts supported on various metal oxide. *Gold Bull* 42:321–327. <https://doi.org/10.1007/BF03214954>
103. Takei T, Suenaga J, Ishida T, Haruta M (2015) Ethanol oxidation in water catalyzed by gold nanoparticles supported on NiO doped with Cu. *Top Catal* 58:295–301. <https://doi.org/10.1007/s11244-015-0370-4>
104. Ishida T, Ogihara Y, Ohashi H, Akita T, Honma T, Oji H, Haruta M (2012) Base-free direct oxidation of 1-octanol to octanoic acid and its octyl ester over supported gold catalysts. *ChemSusChem* 5:2243–2248. <https://doi.org/10.1002/cssc.201200324>
105. Nielsen IS, Taarning E, Egeblad K, Madsen R, Christensen CH (2007) Direct aerobic oxidation of primary alcohols to methyl esters catalyzed by a heterogeneous gold catalyst. *Catal Lett* 116:35–40. <https://doi.org/10.1007/s10562-007-9086-9>
106. Marsden C, Taarning E, Hansen D, Johansen L, Klitgaard SK, Egeblad K, Christensen CH (2008) Aerobic oxidation of aldehydes under ambient conditions using supported gold nanoparticle catalysts. *Green Chem* 10:168–170. <https://doi.org/10.1039/B712171G>
107. Taarning E, Nielsen IS, Egeblad K, Madsen R, Christensen CH (2008) Chemicals from renewables: aerobic oxidation of furfural and hydroxymethylfurfural over gold catalysts. *ChemSusChem* 1:75–78. <https://doi.org/10.1002/cssc.200700033>
108. Liu G, Li G, Song H (2009) Direct synthesis of methyl propionate from n-propyl alcohol and methanol using gold catalysts. *Catal Lett* 128:493–501. <https://doi.org/10.1007/s10562-008-9782-0>
109. Pazhavelikkakath Purushothaman RK, van Haveren J, van Es DS, Melián-Cabrera I, Heeres HJ (2012) The oxidative esterification of glycerol to methyl glycerate in methanol using gold on oxidic supports: an insight in product selectivity. *Green Chem* 14:2031. <https://doi.org/10.1039/c2gc35226e>
110. Kotionova T, Lee C, Miedziak PJ, Dummer NF, Willock DJ, Carley AF, Morgan DJ, Knight DW, Taylor SH, Hutchings GJ (2012) Oxidative esterification of homologous 1,3-propanediols. *Catal Lett* 142:1114–1120. <https://doi.org/10.1007/s10562-012-0872-7>
111. Taarning E, Madsen AT, Marchetti JM, Egeblad K, Christensen CH (2008) Oxidation of glycerol and propanediols in methanol over heterogeneous gold catalysts. *Green Chem* 10:408. <https://doi.org/10.1039/b714292g>

112. Gawande MB, Rathi AK, Tucek J, Safarova K, Bundaleski N, Teodoro OMND, Kvitek L, Varma RS, Zboril R (2014) Magnetic gold nanocatalyst (nanocat-Fe-Au): catalytic applications for the oxidative esterification and hydrogen transfer reactions. *Green Chem* 16:4137–4143. <https://doi.org/10.1039/C4GC00774C>
113. Rautiainen S, Simakova O, Guo H, Leino AR, Kordás K, Murzin D, Leskelä M, Repo T (2014) Solvent controlled catalysis: synthesis of aldehyde, acid or ester by selective oxidation of benzyl alcohol with gold nanoparticles on alumina. *Appl Catal A Gen* 485:202–206. <https://doi.org/10.1016/j.apcata.2014.08.003>
114. Chng LL, Yang J, Ying JY (2015) Efficient synthesis of amides and esters from alcohols under aerobic ambient conditions catalyzed by a Au/mesoporous Al₂O₃ nanocatalyst. *ChemSusChem* 8:1916–1925. <https://doi.org/10.1002/cssc.201403469>
115. Bernini R, Cacchi S, Fabrizi G, Niembro S, Prastaro A, Shafir A, Vallribera A (2009) Perfluoro-tagged gold nanoparticles immobilized on fluorosilica gel: a reusable catalyst for the benign oxidation and oxidative esterification of alcohols. *ChemSusChem* 2:1036–1040. <https://doi.org/10.1002/cssc.200900211>
116. Oliveira RL, Kiyohara PK, Rossi LM (2009) Clean preparation of methyl esters in one-step oxidative esterification of primary alcohols catalyzed by supported gold nanoparticles. *Green Chem* 11:1366. <https://doi.org/10.1039/b902499a>
117. Hao Y, Chong Y, Li S, Yang H (2012) Controlled synthesis of Au nanoparticles in the nanocages of SBA-16: improved activity and enhanced recyclability for the oxidative esterification of alcohols. *J Phys Chem C* 116:6512–6519. <https://doi.org/10.1021/jp2093252>
118. Buonerba A, Noschese A, Grassi A (2014) Highly efficient direct aerobic oxidative esterification of cinnamyl alcohol with alkyl alcohols catalysed by gold nanoparticles incarcerated in a nanoporous polymer matrix: a tool for investigating the role of the polymer host. *Chem Eur J* 20:5478–5486. <https://doi.org/10.1002/chem.201303880>
119. Buonerba A, Impemba S, Litta AD, Capacchione C, Milione S, Grassi A (2018) Aerobic oxidation and oxidative esterification of 5-hydroxymethylfurfural by gold nanoparticles supported on nanoporous polymer host matrix. *ChemSusChem* 11:3139–3149. <https://doi.org/10.1002/cssc.201801560>
120. Mondal P, Salam N, Mondal A, Ghosh K, Tuhina K, Islam SM (2015) A highly active recyclable gold-graphene nanocomposite material for oxidative esterification and Suzuki cross-coupling reactions in green pathway. *J Colloid Interface Sci* 459:97–106. <https://doi.org/10.1016/j.jcis.2015.07.072>
121. Gawande MB, Rathi AK, Gawande MB, Datta KKR, Ranc V, Cepe K, Petr M, Varma RS, Kvitek L, Zboril R (2016) Gold nanoparticle-decorated graphene oxide: synthesis and application in oxidation reactions under benign conditions. *J Mol Catal A Chem* 424:121–127. <https://doi.org/10.1016/j.molcata.2016.07.047>
122. Ning L, Liao S, Liu X, Guo P, Zhang Z, Zhang H, Tong X (2018) A regulatable oxidative valorization of furfural with aliphatic alcohols catalyzed by functionalized metal-organic frameworks-supported Au nanoparticles. *J Catal* 364:1–13. <https://doi.org/10.1016/j.jcat.2018.04.030>
123. Costa VV, Estrada M, Demidova Y, Prosvirin I, Kriventsov V, Cotta RF, Fuentes S, Simakov A, Gusevskaya EV (2012) Gold nanoparticles supported on magnesium oxide as catalysts for the aerobic oxidation of alcohols under alkali-free conditions. *J Catal* 292:148–156. <https://doi.org/10.1016/j.jcat.2012.05.009>
124. Wan X, Deng W, Zhang Q, Wang Y (2014) Magnesia-supported gold nanoparticles as efficient catalysts for oxidative esterification of aldehydes or alcohols with methanol to methyl esters. *Catal Today* 233:147–154. <https://doi.org/10.1016/j.cattod.2013.12.012>
125. Paul B, Khatun R, Sharma SK, Adak S, Singh G, Das D, Siddiqui N, Bhandari S, Joshi V, Sasaki T, Bal R (2019) Fabrication of Au nanoparticles supported on one-dimensional La₂O₃ nanorods for selective esterification of methacrolein to methyl methacrylate with molecular oxygen. *ACS Sustain Chem Eng* 7:3982–3994. <https://doi.org/10.1021/acssuschemeng.8b05291>

126. Casanova O, Iborra S, Corma A (2009) Biomass into chemicals: one pot-base free oxidative esterification of 5-hydroxymethyl-2-furfural into 2,5-dimethylfuroate with gold on nanoparticulated ceria. *J Catal* 265:109–116. <https://doi.org/10.1016/j.jcat.2009.04.019>
127. Wang X, Zhao G, Zou H, Cao Y, Zhang Y, Zhang R, Zhang F, Xian M (2011) The base-free and selective oxidative transformation of 1,3-propanediol into methyl esters by different Au/CeO₂ catalysts. *Green Chem* 13:2690. <https://doi.org/10.1039/c1gc15588a>
128. Manzoli M, Menegazzo F, Signoretto M, Cruciani G, Pinna F (2015) Effects of synthetic parameters on the catalytic performance of Au/CeO₂ for furfural oxidative esterification. *J Catal* 330:465–473. <https://doi.org/10.1016/j.jcat.2015.07.030>
129. Menegazzo F, Manzoli M, di Michele A, Ghedini E, Signoretto M (2018) Supported gold nanoparticles for furfural valorization in the future bio-based industry. *Top Catal* 61:1877–1887. <https://doi.org/10.1007/s11244-018-1003-5>
130. Suzuki K, Yamaguchi T, Matsushita K, Iitsuka C, Miura J, Akaogi T, Ishida H (2013) Aerobic oxidative esterification of aldehydes with alcohols by gold-nickel oxide nanoparticle catalysts with a core-shell structure. *ACS Catal* 3:1845–1849. <https://doi.org/10.1021/cs4004084>
131. Signoretto M, Menegazzo F, Contessotto L, Pinna F, Manzoli M, Boccuzzi F (2013) Au/ZrO₂: an efficient and reusable catalyst for the oxidative esterification of renewable furfural. *Appl Catal B Environ* 129:287–293. <https://doi.org/10.1016/j.apcatb.2012.09.035>
132. Pinna F, Olivo A, Trevisan V, Menegazzo F, Signoretto M, Manzoli M, Boccuzzi F (2013) The effects of gold nanosize for the exploitation of furfural by selective oxidation. *Catal Today* 203:196–201. <https://doi.org/10.1016/j.cattod.2012.01.033>
133. Menegazzo F, Fantinel T, Signoretto M, Pinna F, Manzoli M (2014) On the process for furfural and HMF oxidative esterification over Au/ZrO₂. *J Catal* 319:61–70. <https://doi.org/10.1016/j.jcat.2014.07.017>
134. Menegazzo F, Signoretto M, Pinna F, Manzoli M, Aina V, Cerrato G, Boccuzzi F (2014) Oxidative esterification of renewable furfural on gold-based catalysts: which is the best support? *J Catal* 309:241–247. <https://doi.org/10.1016/j.jcat.2013.10.005>
135. Menegazzo F, Signoretto M, Marchese D, Pinna F, Manzoli M (2015) Structure-activity relationships of Au/ZrO₂ catalysts for 5-hydroxymethylfurfural oxidative esterification: effects of zirconia sulphation on gold dispersion, position and shape. *J Catal* 326:1–8. <https://doi.org/10.1016/j.jcat.2015.03.006>
136. Ampelli C, Centi G, Genovese C, Papanikolaou G, Pizzi R, Perathoner S, van Putten RJ, Schouten KJP, Gluhoi AC, van der Waal JC (2016) A comparative catalyst evaluation for the selective oxidative esterification of furfural. *Top Catal* 59:1659–1667. <https://doi.org/10.1007/s11244-016-0675-y>
137. Ampelli C, Barbera K, Centi G, Genovese C, Papanikolaou G, Perathoner S, Schouten KJ, van der Waal JK (2016) On the nature of the active sites in the selective oxidative esterification of furfural on Au/ZrO₂ catalysts. *Catal Today* 278:56–65. <https://doi.org/10.1016/j.cattod.2016.04.023>
138. Su FZ, Ni J, Sun H, Cao Y, He Y, Fan KN (2008) Gold supported on nanocrystalline β-Ga₂O₃ as a versatile bifunctional catalyst for facile oxidative transformation of alcohols, aldehydes, and acetals into esters. *Chem Eur J* 14:7131–7135. <https://doi.org/10.1002/chem.200800982>
139. Taketoshi A, Ishida T, Murayama T, Honma T, Haruta M (2019) Applied catalysis A, general oxidative esterification of aliphatic aldehydes and alcohols with ethanol over gold nanoparticle catalysts in batch and continuous flow reactors. *Appl Catal A Gen* 585:117169. <https://doi.org/10.1016/j.apcata.2019.117169>
140. Ke Y, Qin X, Liu C, Yang R, Dong W (2014) Oxidative esterification of ethylene glycol in methanol to form methyl glycolate over supported Au catalysts. *Catal Sci Technol* 4:3141–3150. <https://doi.org/10.1039/C4CY00556B>
141. Liu P, Li C, Hensen EJM (2012) Efficient tandem synthesis of methyl esters and imines by using versatile hydrotalcite-supported gold nanoparticles. *Chem Eur J* 18:12122–12129. <https://doi.org/10.1002/chem.201202077>

142. Wei H, Li J, Yu J, Zheng J, Su H, Wang X (2015) Gold nanoparticles supported on metal oxides as catalysts for the direct oxidative esterification of alcohols under mild conditions. *Inorganica Chim Acta* 427:33–40. <https://doi.org/10.1016/j.ica.2014.11.024>
143. Liu X, Ding RS, He L, Liu YM, Cao Y, He HY, Fan KN (2013) C-C cross-coupling of primary and secondary benzylic alcohols using supported gold-based bimetallic catalysts. *ChemSusChem* 6:604–608. <https://doi.org/10.1002/cssc.201200804>
144. Kim S, Bae SW, Lee JS, Park J (2009) Recyclable gold nanoparticle catalyst for the aerobic alcohol oxidation and C-C bond forming reaction between primary alcohols and ketones under ambient conditions. *Tetrahedron* 65:1461–1466. <https://doi.org/10.1016/j.tet.2008.12.005>
145. Ishida T, Takamura R, Takei T, Akita T, Haruta M (2012) Support effects of metal oxides on gold-catalyzed one-pot N-alkylation of amine with alcohol. *Appl Catal A Gen* 413–414:261–266. <https://doi.org/10.1016/j.apcata.2011.11.017>
146. Demidova YS, Suslov EV, Simakova IL, Mozhajcev ES, Korchagina DV, Volcho KP, Salakhutdinov NF, Simakov A, Murzin DY (2018) One-pot monoterpene alcohol amination over Au/ZrO₂ catalyst: effect of the substrate structure. *J Catal* 360:127–134. <https://doi.org/10.1016/j.jcat.2018.01.020>
147. Ishida T, Aimoto J, Hamasaki A, Ohashi H, Honma T, Yokoyama T, Sakata K, Okumura M, Tokunaga M (2014) Formation of gold clusters on La-Ni mixed oxides and its catalytic performance for isomerization of allylic alcohols to saturated aldehydes. *Chem Lett* 43:1368–1370. <https://doi.org/10.1246/cl.140369>
148. Peng Q, Zhang N, Shi F, Deng Y (2011) Fe₂O₃-supported nano-gold catalyzed one-pot synthesis of N-alkylated anilines from nitroarenes and alcohols. *Chem Commun* 47:6476–6478. <https://doi.org/10.1039/c1cc11057h>
149. Qi C, Akita T, Okumura M, Haruta M (2001) Epoxidation of propylene over gold catalysts supported on non-porous silica. *Appl Catal A Gen* 218:81–89. [https://doi.org/10.1016/S0926-860X\(01\)00621-4](https://doi.org/10.1016/S0926-860X(01)00621-4)
150. Huang J, Akita T, Faye J, Fujitani T, Takei T, Haruta M (2009) Propene epoxidation with dioxygen catalyzed by gold clusters. *Angew Chem Int Ed* 48:7862–7866. <https://doi.org/10.1002/anie.200903011>
151. Turner M, Golovko VB, Vaughan OPH, Abdulkin P, Berenguer-Murcia A, Tikhov MS, Johnson BFG, Lambert RM (2008) Selective oxidation with dioxygen by gold nanoparticle catalysts derived from 55-atom clusters. *Nature* 454:981–983. <https://doi.org/10.1038/nature07194>
152. Zheng Y, Zhang X, Yao Y, Chen X, Yang Q (2015) Ultra-small Au nanoparticles stabilized by silica hollow nanospheres for styrene oxidation with oxygen. *RSC Adv* 5:105747–105752. <https://doi.org/10.1039/c5ra21997c>
153. Zhu Y, Qian H, Jin R (2010) An atomic-level strategy for unraveling gold nanocatalysis from the perspective of Au_n(SR)_m nanoclusters. *Chem Eur J* 16:11455–11462. <https://doi.org/10.1002/chem.201001086>
154. Hughes MD, Xu YJ, Jenkins P, McMorn P, Landon P, Enache DI, Carley AF, Attard GA, Hutchings GJ, King F, Stitt EH, Johnston P, Griffin K, Kiely CJ (2005) Tunable gold catalysts for selective hydrocarbon oxidation under mild conditions. *Nature* 437:1132–1135. <https://doi.org/10.1038/nature04190>
155. Leandro SR, Fernandes CI, Viana AS, Mourato AC, Vaz PD, Nunes CD (2019) Catalytic performance of bulk and colloidal Co/Al layered double hydroxide with Au nanoparticles in aerobic olefin oxidation. *Appl Catal A Gen* 584:117155. <https://doi.org/10.1016/j.apcata.2019.117155>
156. Cai ZY, Zhu MQ, Chen J, Shen YY, Zhao J, Tang Y, Chen XZ (2010) Solvent-free oxidation of cyclohexene over catalysts Au/OMS-2 and Au/La-OMS-2 with molecular oxygen. *Catal Commun* 12:197–201. <https://doi.org/10.1016/j.catcom.2010.09.014>

157. Jameel U, Zhu M, Chen X, Chen H, Iqbal N, Tong Z, Timayo SJ (2017) Novel gallium polyoxometalate/nano-gold hybrid material supported on nano-sized silica for mild cyclohexene oxidation using molecular oxygen. *Bull Korean Chem Soc* 38:614–624. <https://doi.org/10.1002/bkcs.11135>
158. Ovoshchnikov DS, Donoeva BG, Williamson BE, Golovko VB (2014) Tuning the selectivity of a supported gold catalyst in solvent- and radical initiator-free aerobic oxidation of cyclohexene. *Catal Sci Technol* 4:752–757. <https://doi.org/10.1039/C3CY01011B>
159. Donoeva BG, Ovoshchnikov DS, Golovko VB (2013) Establishing a Au nanoparticle size effect in the oxidation of cyclohexene using gradually changing Au catalysts. *ACS Catal* 3:2986–2991. <https://doi.org/10.1021/cs400701j>
160. Dias Ribeiro de Sousa Martins LM, Carabineiro SAC, Wang J, Rocha BGM, Maldonado-Hódar FJ, Latourrette de Oliveira Pombeiro AJ (2017) Supported gold nanoparticles as reusable catalysts for oxidation reactions of industrial significance. *ChemCatChem* 9:1211–1221. <https://doi.org/10.1002/cctc.201601442>
161. Zhang B, Kaziz S, Li H, Hevia MG, Wodka D, Mazet C, Bürgi T, Barrabés N (2015) Modulation of active sites in supported Au₃₈(SC₂H₄Ph)₂₄ cluster catalysts: effect of atmosphere and support material. *J Phys Chem C* 119:11193–11199. <https://doi.org/10.1021/jp512022v>
162. Liu Y, Tsunoyama H, Akita T, Xie S, Tsukuda T (2011) Aerobic oxidation of cyclohexane catalyzed by size-controlled Au clusters on hydroxyapatite: size effect in the sub-2 nm regime. *ACS Catal* 1:2–6. <https://doi.org/10.1021/cs100043j>
163. Xu LX, He CH, Zhu MQ, Fang S (2007) A highly active Au/Al₂O₃ catalyst for cyclohexane oxidation using molecular oxygen. *Catal Lett* 114:202–205. <https://doi.org/10.1007/s10562-007-9058-0>
164. Lu GM, Zhao R, Qian G, Qi YX, Wang XL, Suo JS (2004) A highly efficient catalyst Au/MCM-41 for selective oxidation cyclohexane using oxygen. *Catal Lett* 97:115–118. <https://doi.org/10.1023/B:CATL.0000038571.97121.b7>
165. Zhao R, Ji D, Lv G, Qian G, Yan L, Wang X, Suo J (2004) A highly efficient oxidation of cyclohexane over Au/ZSM-5 molecular sieve catalyst with oxygen as oxidant. *Chem Commun* 7:904–905. <https://doi.org/10.1039/B315098D>
166. Saxena S, Singh R, Pala RGS, Sivakumar S (2016) Sinter-resistant gold nanoparticles encapsulated by zeolite nanoshell for oxidation of cyclohexane. *RSC Adv* 6:8015–8020. <https://doi.org/10.1039/c5ra20734g>
167. Liu L, Arenal R, Meira DM, Corma A (2019) Generation of gold nanoclusters encapsulated in an MCM-22 zeolite for the aerobic oxidation of cyclohexane. *Chem Commun* 55:1607–1610. <https://doi.org/10.1039/c8cc07185c>
168. Leyva-Pérez A, Oliver-Meseguer J, Cabrero-Antonino JR, Rubio-Marqués P, Serna P, Al-Resayes SI, Corma A (2013) Reactivity of electron-deficient alkynes on gold nanoparticles. *ACS Catal* 3:1865–1873. <https://doi.org/10.1021/cs400362c>
169. Serna P, Corma A (2014) Towards a zero-waste oxidative coupling of nonactivated aromatics by supported gold nanoparticles. *ChemSusChem* 7:2136–2139. <https://doi.org/10.1002/cssc.201402061>
170. Ishida T, Aikawa S, Mise Y, Akebi R, Hamasaki A, Honma T, Ohashi H, Tsuji T, Yamamoto Y, Miyasaka M, Yokoyama T, Tokunaga M (2015) Direct C-H arene homocoupling over gold nanoparticles supported on metal oxides. *ChemSusChem* 8:695–701. <https://doi.org/10.1002/cssc.201402822>

Metal Nanoparticles for Redox Reactions



Koichiro Jitsukawa and Takato Mitsudome

Contents

1	Introduction	50
2	Metal NP-Catalyzed Selective Reductions Using H ₂	51
2.1	Design of Core–Shell NPs	51
2.2	Nitrogen or Sulfur Modification of Metal NP Surface	58
3	Metal NP-Catalyzed Selective Oxidations Using O ₂	62
3.1	Aerobic Oxidation of Alcohols Using Pd NPs	62
3.2	Bimetallic NP-Catalyzed Alcohol Oxidation	65
3.3	Base Metal NP-Catalyzed Alcohol Oxidation	67
3.4	Wacker-Type Oxidation Using Pd NPs	68
4	Summary	72
	References	73

Abstract Reduction and oxidation reactions (redox reactions) are fundamental and important transformation of chemicals in both laboratory and industrial chemistries. With regard to atom economy and the environmental demands, an ultimate goal of these reactions is to employ molecular hydrogen (H₂) or molecular oxygen (O₂). High-performance heterogeneous catalysts with high activity, selectivity, recoverability, and reusability are ideal for the development of green sustainable processes using H₂ or O₂. Moreover, the heterogeneous catalyst systems are the promising approach to solve the disadvantage of homogeneous ones, such as short lifetimes (low stability), risk of contaminating products with metals (low recoverability), tedious workups for reuse (low reusability), and so on. For the design of high-performance heterogeneous catalysts under liquid-phase redox reactions, metal nanoparticles (NPs) is the most promising strategy because of their unusual properties compared to bulk metal. This review provides an overview of metal NP heterogeneous catalysts developed for redox reactions using H₂ or O₂. The state-of-the-art metal NP catalysts show higher activity and selectivity for the

K. Jitsukawa (✉) and T. Mitsudome

Department of Materials Engineering Science, Graduate School of Engineering Science, Osaka University, Toyonaka, Osaka, Japan
e-mail: jitkk@cheng.es.osaka-u.ac.jp

chemoselective hydrogenations of carbonyl, nitro, and alkynyl compounds while retaining C=C bonds, and the aerobic oxidation of alcohols and the Wacker type oxidation of alkenes, which overcome the limitations of the conventional catalyst systems. This improved catalytic performance is due to significant advances in the precise fabrication of nanoscale metals, which has made it possible to explore novel catalysis and design metal active centers.

Keywords Catalyst · Hydrogenation · Metal · Nanoparticle · Oxidation

1 Introduction

Reduction and oxidation reactions (redox reactions) are fundamental and important transformations in both laboratory and industrial chemistries. In conventional redox reaction systems, metal hydrides, such as NaBH_4 and LiAlH_4 , or heavy metal salts, such as permanganate and dichromate, have been employed as reducing or oxidizing agents. As these stoichiometric reagents have serious drawbacks, including high costs, toxicity, and producing large amounts of waste, the development of promising catalytic systems to replace these stoichiometric reactions has attracted much attention. With regard to atom economy and the environmental demands of chemical reactions, an ultimate goal of redox reactions is to employ molecular hydrogen (H_2) or molecular oxygen (O_2) [1–6]. These inexpensive reagents are abundant and can avoid the use of harmful reagents. In this context, transition metal complexes have traditionally been employed as catalysts, because they are dissolved in reaction media, which makes all active sites accessible to substrates, leading to exhibit high catalytic activities. Despite these advantages, homogeneous catalyst systems have fundamental problems, including short lifetimes (low stability), risk of contaminating products with metals (low recoverability), and tedious workups for reuse (low reusability). Although heterogeneous catalysts are the most promising approach to solving the above issues, they generally show low activity and require harsh reaction conditions and have mainly been applied in gas-phase reactions. Therefore, high-performance heterogeneous catalysts with high activity, selectivity, recoverability, and reusability would be ideal, leading to the development of green sustainable redox reaction processes using H_2 or O_2 .

Using metal nanoparticles (NPs) is among the most promising strategies for the design of high-performance heterogeneous catalysts because of their unusual properties compared to bulk metal. To date, metal NP catalysts have been employed to refine petroleum, manufacture petrochemicals, clean exhaust gas, and produce renewable clean energy, especially in gas-phase reactions [7–9]. Recently, the advance of nanoengineering has enabled the precise construction of metal NP catalysts. Sophisticated metal NP catalysts, obtained by controlling particle sizes and shapes, tuning metal electronic states, and modulating metal–support

interactions [10–14], have achieved high activity and selectivity in fine chemical synthesis under mild conditions. Accordingly, this review provides an overview of metal NP heterogeneous catalysts developed for redox reactions using H_2 or O_2 under liquid-phase conditions. As many reviews and reports on heterogeneous catalysts for hydrogenation [15–17] and aerobic oxidation [18–21] have been published, herein we have focused on state-of-the-art metal NP catalysts, which overcome the limitations of conventional catalysts in selective redox reactions.

2 Metal NP-Catalyzed Selective Reductions Using H_2

Selective hydrogenations are important methods in fine chemical synthesis. However, the chemoselective hydrogenation of targeted functional groups in the presence of other reducible groups is difficult. In particular, chemoselective hydrogenation in the presence of easily reducible alkene groups represents a significant challenging. To date, various approaches using metal NP catalysts to achieve high chemoselectivity have been proposed through the design of metal size, surface, shape, and components. In this section, rationally designed and developed novel metal NP catalysts for the chemoselective hydrogenation of nitro, carbonyl, and alkyne moieties while retaining easily reducible alkene groups are discussed.

2.1 Design of Core–Shell NPs

The hydrogenation of aromatic nitro compounds bearing other reducible groups is important for the direct synthesis of functionalized aniline derivatives, which are useful feedstocks in the chemical industry. In 2005, Corma et al. discovered that a Au/TiO_2 catalyst promoted the chemoselective hydrogenation of 3-nitrostyrene to give 3-aminostyrene with 98.5% conversion and 95.9% selectivity [22]. Since this pioneering report, many catalysts have been developed for the chemoselective hydrogenation of functionalized aromatic nitro compounds [23]. However, these catalysts suffer from overhydrogenation of aminostyrene to ethylaniline at high conversion levels. This is due to the chemoselectivity often being derived from preferential adsorption of the nitro moiety over the alkene moiety, resulting in alkene hydrogenation occurring prior to nitro hydrogenation at low nitro compound concentrations. Therefore, a new catalyst design strategy for the chemoselective hydrogenation of nitro compounds is needed as an alternative to the preferential adsorption method.

Au or Ag NPs and basic metal oxide support are known to cooperatively dissociate H_2 into polar hydrogen species $H^{\delta+}$ and $H^{\delta-}$, which straddle the interfacial perimeter sites [24, 25]. These polar hydrogen species show favorable reactivity with nitro groups compared to that with alkene groups [26]. Mitsudome et al. developed a novel core–shell nanostructured catalyst, $Ag@CeO_2$, for the chemoselective

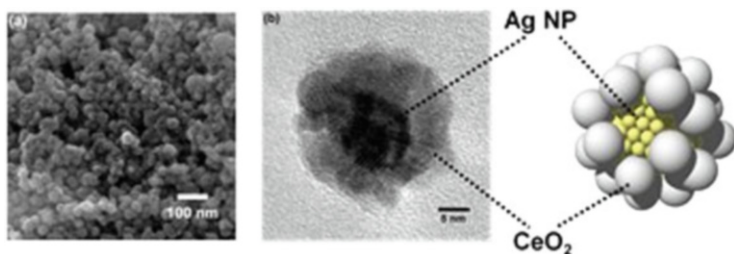


Fig. 1 Electron micrographs of Ag@CeO₂: (a) SEM image of Ag@CeO₂; (b) HRTEM image of single Ag@CeO₂ particle

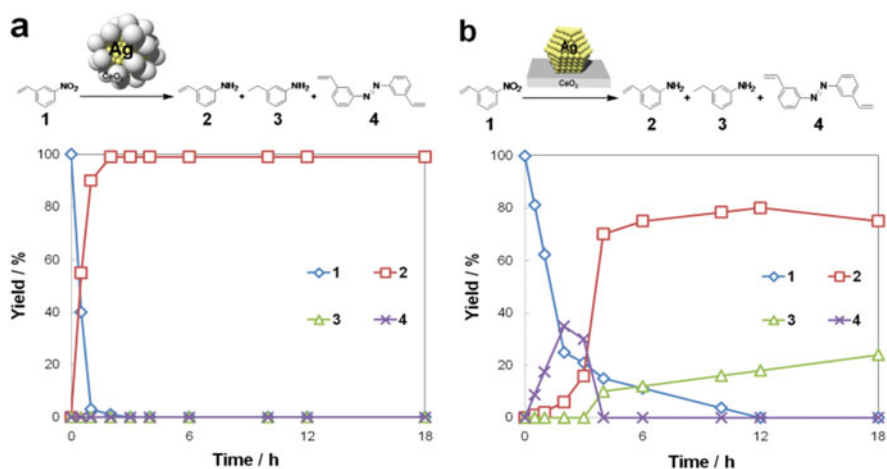


Fig. 2 Time course of 3-nitrostyrene reduction with H₂ using (a) Ag@CeO₂ and (b) Ag/CeO₂. Reprinted with permission from [27]. Copyright 2012 Wiley-VCH

hydrogenation of nitrostyrene [27]. Ag@CeO₂ comprised a core of Ag NPs with a mean diameter of 10 nm and a shell assembled from CeO₂ NPs with diameters of 3–5 nm. The shell had nanopores among the CeO₂ NPs that enabled the reactants to access AgNPs in the core (Fig. 1).

The core–shell Ag@CeO₂ catalyst structurally maximizes the interface area between the AgNPs and basic metal oxide CeO₂ while simultaneously minimizing the area of bare AgNPs. Therefore, Ag@CeO₂ is expected to enable the selective formation of polar hydrogen species at the interface between AgNPs and the basic sites of CeO₂ through heterolytic dissociation of H₂ while suppressing the unfavorable formation of nonpolar hydrogen species on bare AgNPs through homolytic dissociation of H₂, which react with alkene groups. This precise design strategy for NP catalysts enabled the selective generation of polar hydrogen species that promote complete chemoselective hydrogenation of nitro groups while retaining C=C bonds (Fig. 2). Ag@CeO₂ catalyst exhibited excellent selectivity toward the nitro hydrogenation of 3-nitrostyrene, affording 3-aminostyrene in 98% yield with >99%

Fig. 3 Activities of Au@CeO₂ and Ag/CeO₂ toward styrene

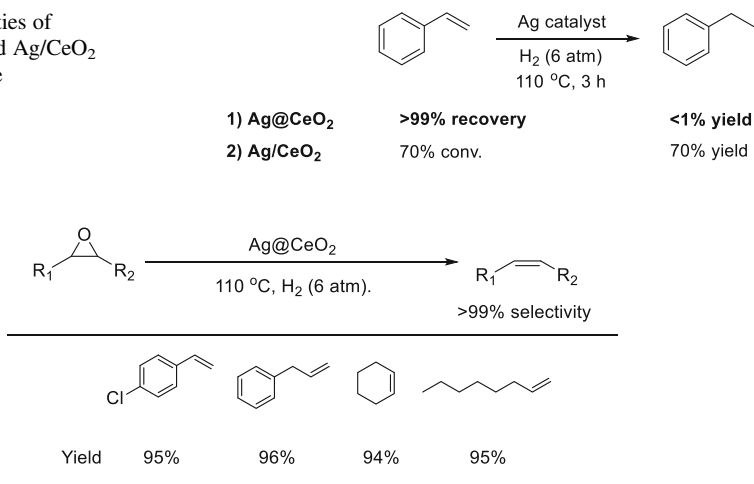


Fig. 4 Ag@CeO₂-catalyzed deoxygenation of epoxides to give alkenes using H₂

selectivity without alkene hydrogenation occurring. Interestingly, the C=C bond of 3-aminostyrene showed no hydrogenation when the reaction time was prolonged.

The efficiency of the Ag@CeO₂ core-shell structure was also demonstrated in the hydrogenation of styrene. Styrene was not hydrogenated using this catalyst but was hydrogenated using CeO₂-supported Ag NPs without a core-shell structure (Ag/CeO₂) (Fig. 3). Furthermore, the Ag@CeO₂ catalyst could be recovered through simple filtration from the reaction mixture after the reaction and reused without any loss of activity or selectivity [28].

Ag@CeO₂ also promoted the unique deoxygenation reaction of epoxides to give the corresponding alkenes. Various epoxides, including aromatic, aliphatic, and alicyclic epoxides, were smoothly converted into the corresponding alkenes with >99% selectivity (Fig. 4). This represented the first reported Ag-catalyzed chemoselective deoxygenation of epoxides to alkenes using H₂.

The design strategy of Ag@CeO₂ for the exclusive hydrogenation of a polar functional group while retaining alkene groups was further demonstrated by the selective hydrogenation of unsaturated aldehydes to give the corresponding unsaturated alcohols, which are important intermediates in fragrances and pharmaceuticals. Highly dispersed Ag@CeO₂ on a CeO₂ support (Ag@CeO₂-D), which represents a modified version of Ag@CeO₂, efficiently converted a wide range of aldehydes, including not only terpenes and aliphatic and aromatic α,β -unsaturated aldehydes but also unconjugated aldehydes, to the corresponding allylic alcohols with high selectivity at high conversion levels (Fig. 5). Ag@CeO₂ also operated well under gram-scale reaction conditions to produce unsaturated alcohols in high yields.

The semihydrogenation of alkynes is among the most important and fundamental reactions for the synthesis of (*Z*)-alkenes, which are important building blocks of fine chemicals, including bioactive molecules, flavors, and natural products

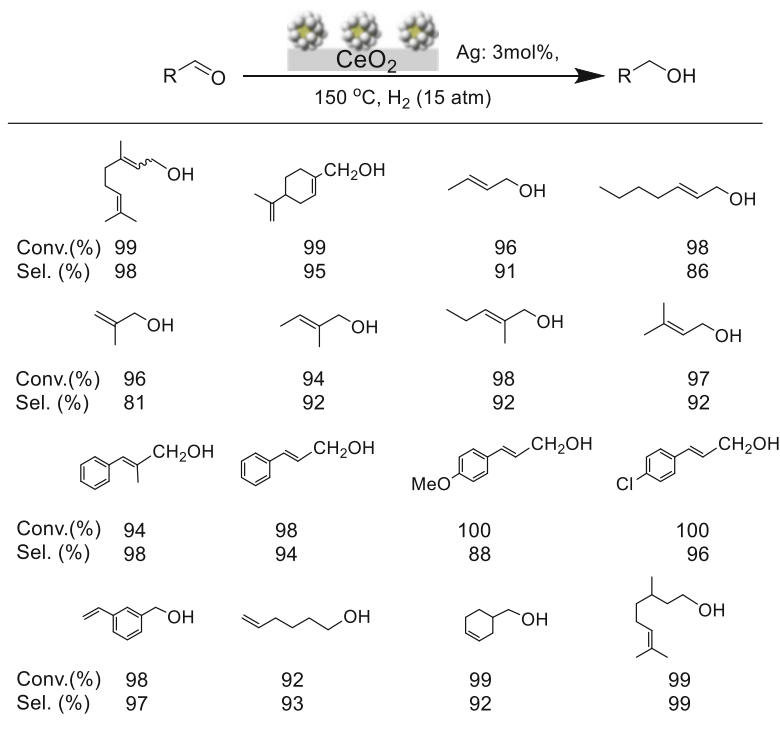


Fig. 5 Chemoselective hydrogenations of unsaturated aldehydes using Ag@CeO₂-D

[29, 30]. Although Lindlar catalyst (Pb(OAc)₂-treated Pd/CaCO₃ with large amounts of quinoline) has been widely used in these reactions [31], this method has serious drawbacks, including requiring a toxic Pb salt and large amounts of quinoline to suppress overhydrogenation of alkenes. Furthermore, when applied to terminal alkynes, Lindlar catalyst causes rapid overhydrogenation of the terminal alkene products. To establish more environmentally benign catalyst systems, a number of Pb-free catalysts involving Pd [32, 33], Fe [34, 35], Ni [36–38], Cu [39], and Ru [40] metals have been reported. Among the reported Pd NP catalysts, the addition of dimethylsulfoxide (DMSO) is a simple and effective approach alternative to Lindlar catalyst, in which DMSO drastically suppresses the overhydrogenation and isomerization of the alkene products [41]. This is caused by the suitable coordination ability of DMSO with Pd NPs, where DMSO adsorbed on the Pd NP surface inhibits the coordination of alkenes to Pd NPs, while alkynes can adsorb onto the Pd NP surfaces due to their higher coordination ability compared with that of DMSO.

Based on the above DMSO effect, Mitsudome et al. designed core–shell nanocomposites of SiO₂-supported Pd NPs covered with a DMSO-like matrix of methyl-3-trimethoxysilylpropylsulfoxide (MPSO) (Pd@MPSO/SiO₂) [42]. Pd@MPSO/SiO₂ had Pd NPs with a mean diameter of 17 nm covered by a MPSO matrix shell with a thickness of 4 nm (Pd@MPSO/SiO₂-1) or 19 nm

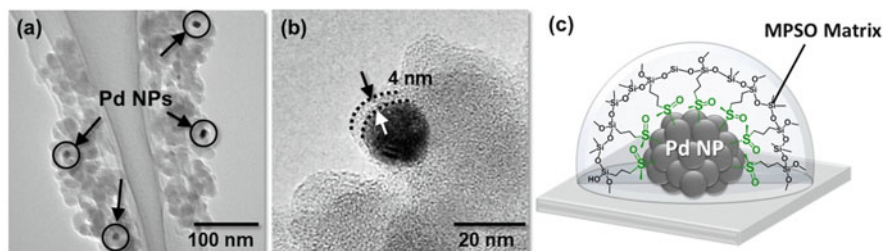


Fig. 6 TEM images of (a, b) Pd@MPSO/SiO₂-1 and (c) illustration of the core-shell structured Pd@MPSO/SiO₂

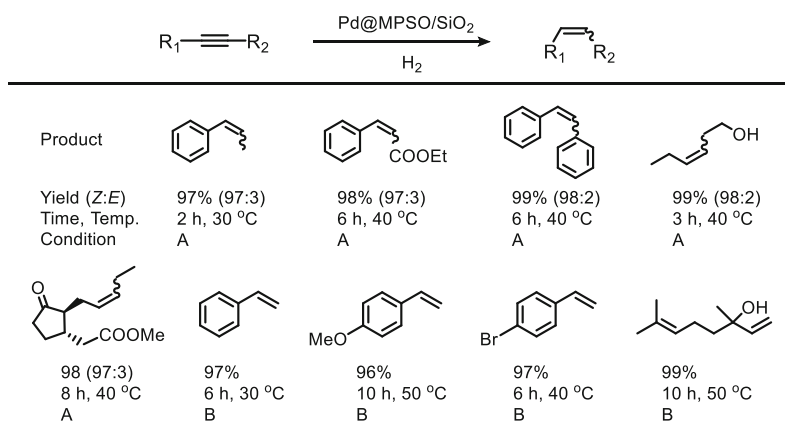


Fig. 7 Semihydrogenation of internal and terminal alkynes using Pd@MPSO/SiO₂. Reaction conditions: (a) Pd@MPSO/SiO₂-1 (Pd, 0.2 mol%), H₂ (1 atm); (b) Pd@MPSO/SiO₂-2 (Pd, 0.2 mol%), H₂ (1 atm)

(Pd@MPSO/SiO₂-2), which was controlled by the amount of MPSO. Energy-dispersive X-ray spectroscopy (EDX) of Pd@MPSO/SiO₂ proved the existence of sulfur and Si atoms in the shell matrix (Fig. 6). The Pd@MPSO/SiO₂ shell consisted of an alkyl sulfoxide network that allowed the exclusive coordination of alkynes to the Pd NP active center, promoting the selective semihydrogenation of various terminal and internal alkynes (Fig. 7).

The design of bimetallic catalysts comprising a core of Pd NPs and a Ag nanolayer shell provides another strategy for core-shell metal NP arrangement for the selective semihydrogenation of alkynes. Unmodified Pd NP catalysts have intrinsically high activity for alkyne hydrogenation but low selectivity for alkene products owing to the overhydrogenation of alkenes to alkanes. Ag NP catalysts, in contrast, exhibit low activity for hydrogenation despite having inherent high alkene selectivity [43–45]. Mitsudome et al. envisioned that the design of core-Pd/shell-Ag nanocomposite catalysts (Pd@Ag) could avoid the trade-off between activity and selectivity for Pd and Ag NPs in semihydrogenation [46]. The construction of a

Fig. 8 Design concept of complementary bimetallic core-Pd/shell-Ag catalyst for selective semihydrogenation of alkynes

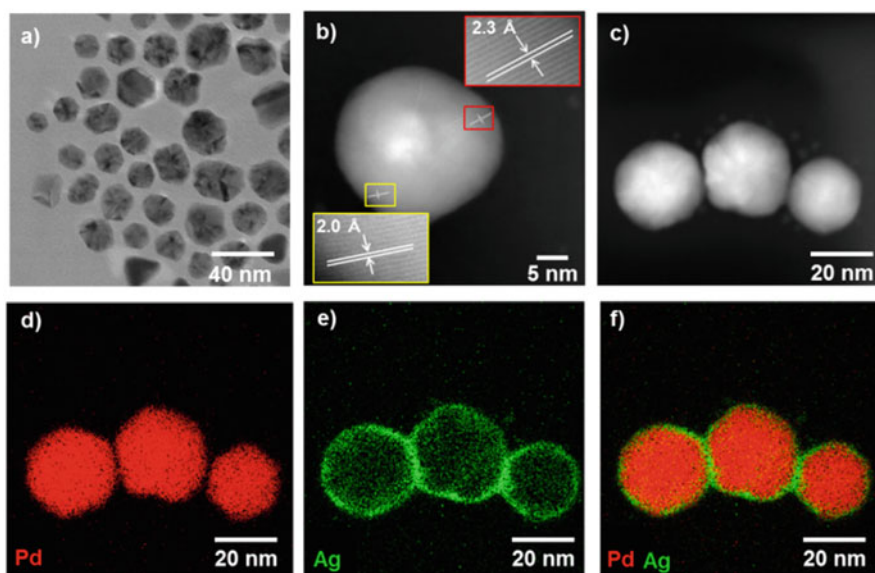
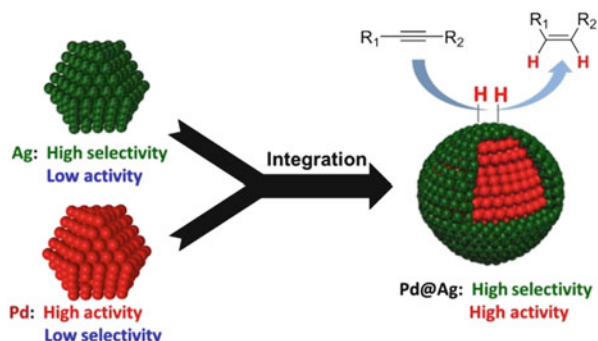


Fig. 9 Compositional and structural analysis of Pd@Ag. (a) TEM image; (b, c) HAADF-STEM images; (d, e) elemental mapping images of (d) Pd and (e) Ag; and (f) composite overlay image formed from (d) and (e). Reprinted with permission from [46]. Copyright 2016 American Chemical Society

core-shell nanocomposite would significantly improve the low activity of Ag NPs owing to a ready supply of hydrogen from the core of Pd NPs to Ag nanolayer shell in a synergistic manner. Meanwhile, coating the core Pd NPs with a Ag nanolayer would suppress overhydrogenation of alkenes at the Pd surface (Fig. 8). This cooperative catalysis between the Pd core and Ag shell was expected to lead to the selective semihydrogenation of alkynes under mild reaction conditions.

According to the above catalyst design concept, Pd@Ag comprising of Pd NPs with a mean diameter of 26.2 nm in the core and a Ag nanolayer with a thickness of approx. 1 nm as the shell was synthesized (Fig. 9) and demonstrated excellent alkene

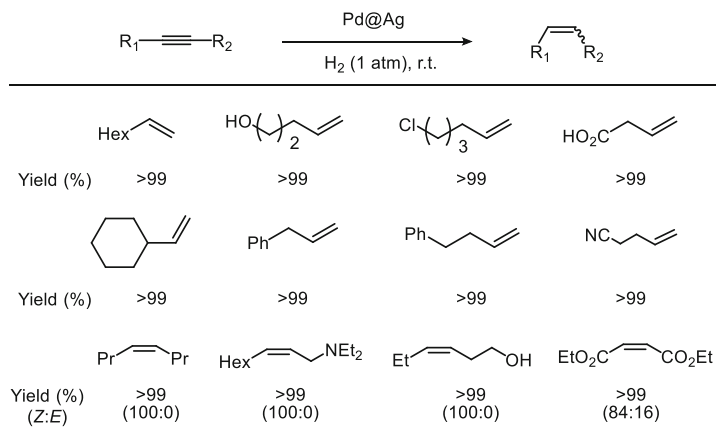
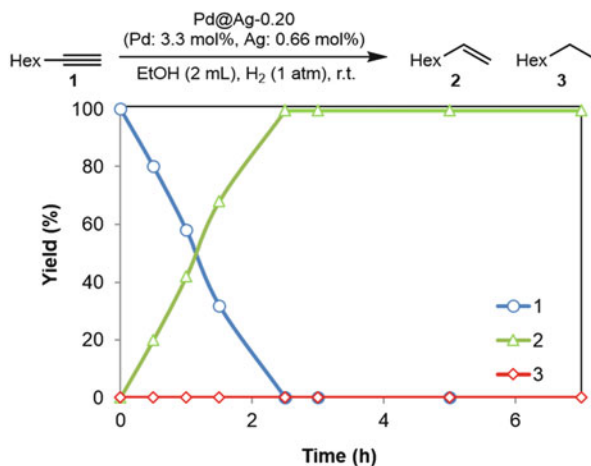


Fig. 10 Pd@Ag-catalyzed semihydrogenation of alkenes under ambient conditions

Fig. 11 Time profile of semihydrogenation of 1-octyne using Pd@Ag



selectivity for a wide range of alkynes under mild reaction conditions (room temperature and 1 atm of H_2) (Fig. 10). Notably, Pd@Ag successfully inhibited the overhydrogenation of alkenes even after the full conversion of alkynes. This result was quite different from those obtained using other previously reported catalysts, in which rapid overhydrogenation of alkenes occurred at a high alkyne conversion level (Fig. 11). Furthermore, Pd@Ag was separable from the reaction mixture and reusable without a loss of catalytic activity or selectivity. Furthermore, Pd@Ag was also suitable for use in a column flow reactor, demonstrating its practical utility.

2.2 Nitrogen or Sulfur Modification of Metal NP Surface

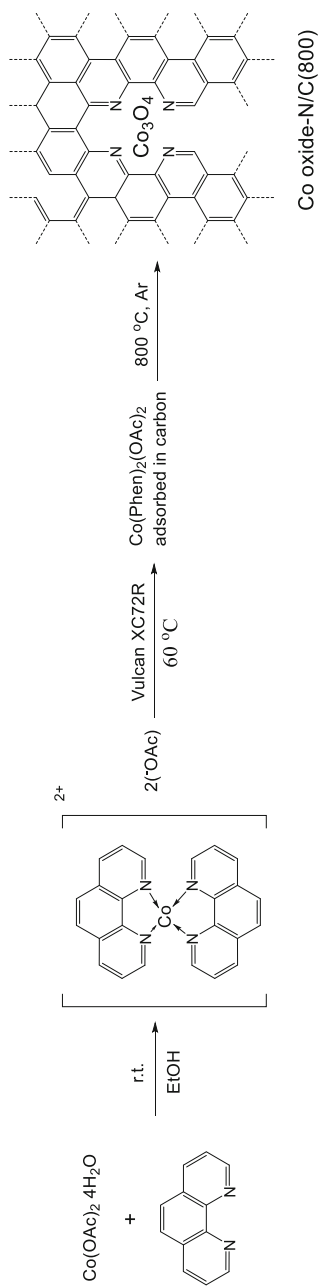
Although heterogeneous metal NP catalysts have many advantages over homogeneous catalysts, such as high stability and easy separation and reuse, fine-tuning the active metal center remains difficult. Beller et al. reported the heterogenization of well-defined organometallic complex catalysts via immobilization and pyrolysis on activated carbon [47]. The synthetic scheme for novel cobalt oxide NPs is shown in Fig. 12. The deposition of cobalt(II) acetate–phenanthroline complex onto commercially available carbon followed by pyrolysis under inert conditions provided cobalt oxide NPs coated with *N*-doped graphene (Co oxide–*N*/C).

The synthesized novel *N*-ligated Co oxide NPs showed high chemoselectivity for nitroarenes bearing easily reducible moieties including alkenes, alkynes, aldehydes, and ketones (Fig. 13). Furthermore, this heterogeneous Co catalyst was reusable without a significant decrease in activity during the recycling experiments, although an initial loss of activity was observed.

Beller et al. also showed that the convenient pyrolysis heterogenization method of well-defined organometallic complex catalysts could be applied to the most earth-abundant metal, iron [48], because the development of efficient and cost-effective catalyst systems is greatly needed in current chemical research. The pyrolysis of iron–phenanthroline complexes adsorbed on carbon at 800°C provided stable Fe₂O₃ NPs surrounded by a nitrogen-doped carbon layer (Fe-phen/C-800). The Fe-phen/C-800 catalyst promoted more than 80 examples of structurally diverse nitroarenes, giving the corresponding functionalized anilines in good to excellent yields under industrially acceptable conditions (Fig. 14).

One rational design approach toward metal NP catalysts involves metal modification with self-assembled monolayers (SAMs) to create a favorable surface environment for selective formation of the desired products [49, 50]. SAMs are organic assemblies of molecules containing a headgroup that noncovalently bind to the metal, producing ordered and stable monolayer films on the metal surface. A unique property of SAM modification is the formation of highly ordered assembly structures on metal surfaces, where modifiers with different tail structures can finely tune the metal surface environment to facilitate specific interactions between reactants and metal NPs.

Medlin et al. showed that SAMs on metal NP surfaces can act as “molecular recognition monolayers” to give the reactant a desirable orientation, which greatly improves the catalytic performance for hydrogenation reactions [51]. For example, in the hydrogenation of cinnamaldehyde, modification of a Pt NP catalyst with 3-phenylpropanethiol significantly improved the selectivity for cinnamyl alcohol to over 95% compared with 25% selectivity using uncoated Pt catalysts [52]. This high chemoselectivity was attributed to the favorable orientation of cinnamaldehyde in the vertical configuration through aromatic stacking interactions between the modifier and reactant. The proposed adsorption mechanism on SAMs is shown in Fig. 15. This represents the first successful demonstration of using specific

**Fig. 12** Synthetic scheme for Co oxide-N/C

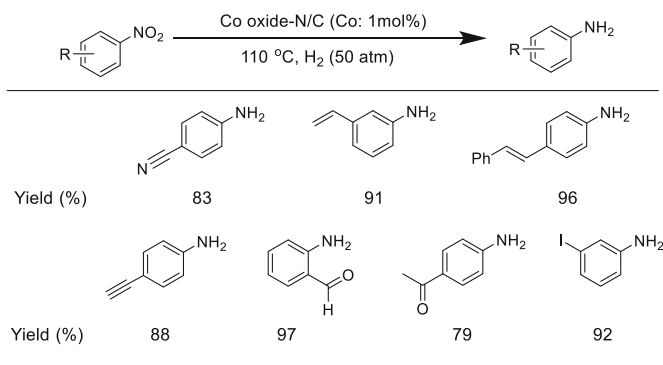


Fig. 13 Chemoselective hydrogenation of substituted nitroarenes using Co oxide-N/C

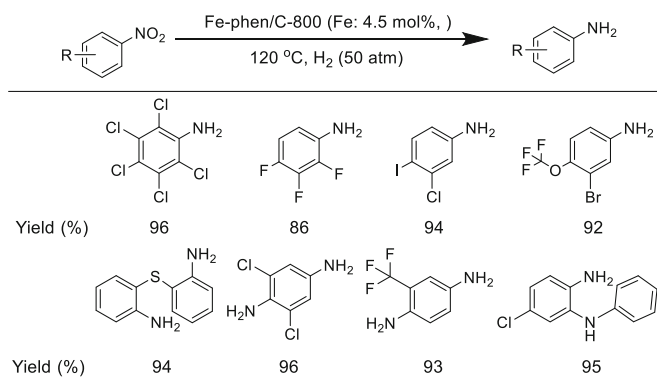


Fig. 14 Fe-phen/C-800-catalyzed selective hydrogenation of substituted nitroarenes

noncovalent interactions to orient the reactant to promote aldehyde-selective hydrogenation.

Pt catalysts are not chemoselective for the hydrogenation of nitro groups in nitro aromatic compounds bearing other reducible groups. However, the thiol-modification approach transforms nonchemoselective Pt catalysts into highly chemoselective Pt catalysts for the hydrogenation of 4-nitrostyrene to 4-aminostyrene [53]. The TiO₂-supported Pt NPs with a mean diameter of 1.4 nm treated with some thiols, such as thioglycerol, 1,6-hexanedithiol, and α -lipoic acid, gave 100% selectivity for aminostyrene at conversion levels close to 100%. In contrast, an unmodified Pt/TiO₂ catalyst provided C=C bond-hydrogenated products, 4-ethylnitrobenzene, and 4-ethylaniline. Therefore, thiol modification produced a 100% switch in selectivity to 4-aminostyrene.

As shown above, surface modification through SAMs construction on the metal NP surface is a powerful method to improve the selectivity of hydrogenations. However, the modifiers often suppressed diffusion and the adsorption of reactants and protected active sites, unavoidably resulting in the low activity of metal NPs.

Fig. 15 Proposed adsorption model depicting favorable orientation of cinnamaldehyde induced by 3-phenylpropanethiol SAM modifiers. Reprinted with permission from [58]. Copyright 2014 American Chemical Society

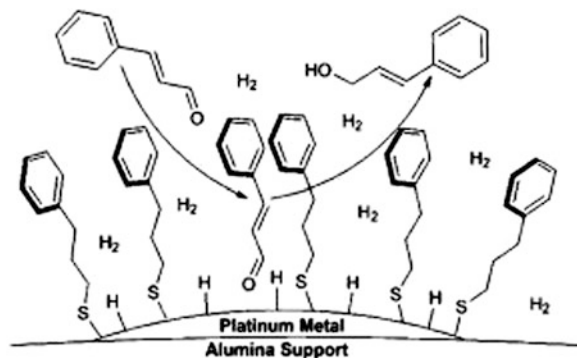
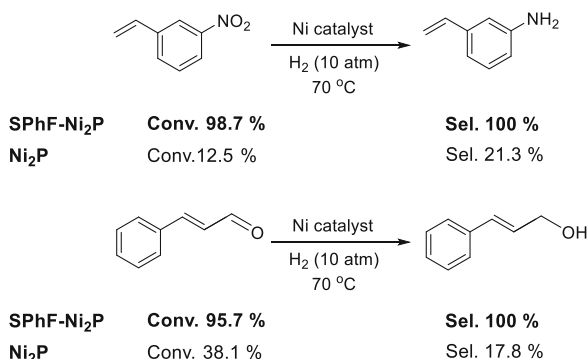


Fig. 16 Performance-boosting effect of SPhF modification on chemoselective hydrogenation



Therefore, high selectivity is usually achieved at the expense of activity, resulting in a trade-off relationship between the activity and selectivity. Therefore, the development of surface-modified metal NPs with both high selectivity and activity is a great challenge in chemoselective hydrogenation.

Recently, Zou et al. succeeded in breaking the trade-off between activity and selectivity in chemoselective hydrogenations using Ni NPs modified by *p*-fluorothiophenol (SPhF) [54]. SPhF-chelated dinickel phosphide nanosheets (SPh-Ni₂P) with activity nearly 12-fold higher than that of unmodified Ni₂P in the hydrogenations of 3-nitrostyrene and cinnamaldehyde selectively gave 3-aminostyrene and cinnamyl alcohol, respectively. Furthermore, the selectivity for desired products significantly improved from 38.1% and 21.3% to nearly 100%. Importantly, the effect of SPhF modification has broad applicability to other metal catalysts, such as Pt, Pd, and commercially available metal catalysts. For example, commercial catalysts like Raney Ni modified with SPhF exhibit twice higher activity with enhanced selectivity from 21–23% to nearly 100% in the above hydrogenations (Fig. 16). Experimental results and density functional theory calculations showed that both the steric and electronic effects of SPhF modification can provide superior catalytic performance. Namely, the confined flat adsorption of ordered SPhF-arrays onto the metal surface and downshifted d-band center of the

catalysts lead to prohibited undesired hydrogenation of the alkene group and accelerative H₂ activation, respectively.

3 Metal NP-Catalyzed Selective Oxidations Using O₂

The selective oxidation of organic compounds is a fundamental challenge in synthetic chemistry. Although the economic and environmental advantages of molecular oxygen as a chemical oxidant are apparent, few reports on the selective introduction of oxygen functions into organic compounds exist because oxygenation often involves radical reactions that are difficult to control. The oxidation reactivity of organic compounds greatly varies depending on their structures. For example, in the oxidation of ethylene using silver catalyst, ethylene oxide is produced using molecular oxygen through a silver-superoxo intermediate. In contrast, when the substrate is changed from ethylene to propylene, propylene is not converted to propylene oxide but completely oxidized to CO₂ and H₂O. This is attributed to the low bond dissociation energy of the allylic C–H bond. Preferential dissociation of the allylic C–H bond in organic compounds generally induces unselective reactions or combustion. Therefore, only limited compounds with tertiary or benzylic C–H bonds can undergo selective oxygenation reactions.

The Wacker oxidation of alkenes is an important oxygenation reaction. The Wacker oxidation is conducted under an oxygen atmosphere, but the carbonyl oxygen introduced into the product is derived from water, not molecular oxygen. Molecular oxygen reoxidizes the metal and is not added into the substrate. An oxygen nucleophile from water attacks the positively charged C=C double bond through coordination to the metal center to form methyl ketones. Alternatively, the resulting metal–hydrogen species generated from the substrate through dehydrogenation is oxidized by molecular oxygen, completing the catalytic cycle. In this reaction, high selectivity for methyl ketone products can be achieved because the radical character of oxygen is not involved.

Some oxidation reactions that use molecular oxygen as an oxidant give low selectivity for oxygenated compounds, while oxidations involving dehydrogenation give high selectivity. In this section, we describe metal NP-catalyzed selective oxidation reactions involving dehydrogenation, in which molecular oxygen acts as an oxidant but is not incorporated into the substrate.

3.1 *Aerobic Oxidation of Alcohols Using Pd NPs*

There have been numerous reports on the catalytic oxidation of alcohols under an oxygen atmosphere [55]. In particular, Pd had been used as a metal center both in homogeneous and heterogeneous systems [56]. PdHAP, in which a mononuclear Pd species is adsorbed to hydroxyapatite (HAP), was reduced to a Pd NP (~5 nm)

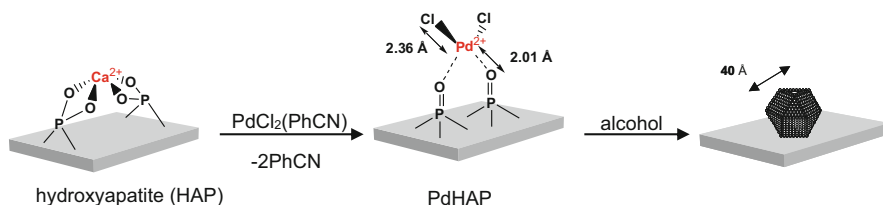


Fig. 17 PdHAP preparation method

Fig. 18 PdHAP-catalyzed aerobic oxidation of 1-phenylethanol under solvent-free conditions

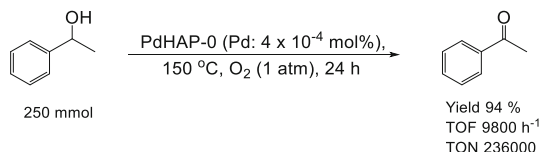
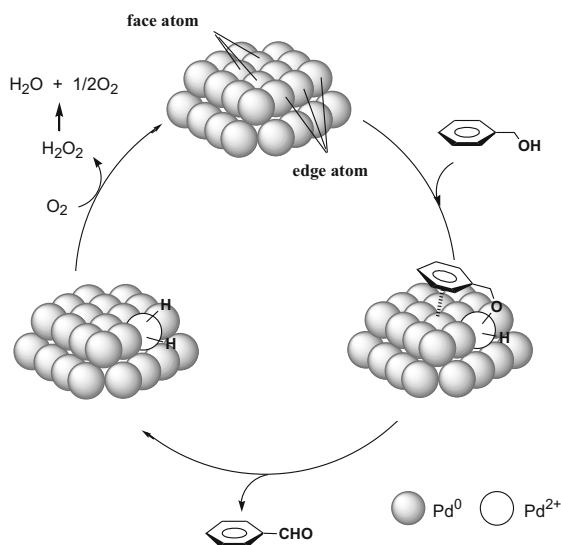


Fig. 19 Proposed reaction mechanism for the PdHAP-catalyzed aerobic oxidation of alcohols. Reprinted with permission from [58]. Copyright 2004 American Chemical Society



during alcohol oxidation (Fig. 17), catalyzing the aerobic oxidation of a wide range of alcohols without any need for additives [57, 58]. The use of HAP as catalyst supports has the following advantages: (1) well-defined monomeric active species can be immobilized on their surface owing to its high ion-exchange ability and adsorption capacity; (2) the nonporous structure can help overcome the problems regarding mass transfer limitations; and (3) weak acid–base properties prohibit side reactions induced by the support itself.

Typically, PdHAP promoted well in the aerobic oxidation of 1-phenylethanol under solvent-free conditions, showing a remarkably high TON of up to 236,000 with an excellent TOF of approximately 9,800 h⁻¹ (Fig. 18).

A possible reaction pathway is shown in Fig. 19. Initially, oxidative addition of an alcohol O–H bond to the coordinately unsaturated Pd⁰ species at the edge of the NP

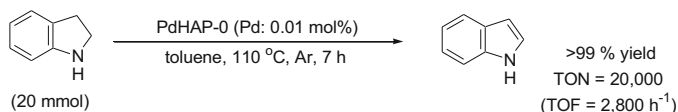


Fig. 20 PdHAP-catalyzed dehydrogenation of indoline

affords a Pd-alcoholate species, which undergoes β -hydride elimination to produce the corresponding carbonyl compounds and Pd-hydride species. The hydride species mediated on the Pd NPs was oxidized by O₂ along with the formation of O₂ and H₂O through H₂O₂ as an intermediate. The kinetic isotope effect for the intramolecular competitive oxidation of α -deuterio-*p*-methylbenzyl alcohol gave a k_H/k_D value of 2.0, indicating that the elimination of β -hydride from the Pd-alcoholate species might be the rate-determining step.

Interestingly, the PdHAP catalyst also promoted dehydrogenation of various indolines to indole, which serves as an important and versatile intermediate for the synthesis of pharmaceuticals and agrochemicals [59]. The applicability of PdHAP was demonstrated in a 20-mmol scale reaction of indole, as shown in Fig. 20. Dehydrogenation was completed within 6 h to afford **2** in 99% yield, in which the TON based on Pd approached up to 20,000 with an excellent TOF of approximately 2,800 h⁻¹. These TON and TOF values were significantly higher than those reported for other catalytic systems.

Pd NPs supported on inorganic materials often give undergo leaching from the support or aggregate to generate inactive larger NPs during the reaction. Park et al. found that small Pd NPs with a diameter of 2–3 nm entrapped into an aluminum hydroxide matrix showed high catalytic activity and durability in the oxidation of alcohols [60]. The oxidation of 1-phenylethanol under solvent-free conditions proceeded smoothly in the presence of 0.005 mol% aluminum hydroxide-entrapped Pd NPs at 150 °C, giving acetophenone in 98% yield. This highly dispersed Pd NP catalyst was also reusable at least ten times without activity loss.

Kantam et al. reported the aerobic oxidation of alcohols at room temperature under aerobic conditions using nanocrystalline magnesium oxide-supported Pd NPs (NAP-Mg-Pd(0)) [61]. Although most Pd NP catalysts require high temperatures (65–150 °C) for alcohol oxidation, these Pd NPs with a diameter of 5–7 nm highly dispersed on the surface of NAP-Mg showed a wide substrate scope for alcohols under mild conditions through a cooperative effect between the basic support and active metal NPs. Benzylic, allylic, aliphatic, and alicyclic alcohols were oxidized at room temperature under air, giving the corresponding carbonyl compounds from good to excellent yields. This NAP-Mg-Pd(0) catalyst was able to be recycled four times without loss of catalytic efficiency.

From both a practical and economic standpoint, using water in organic reactions has significant advantages, including the low cost, abundance, safety (nonexplosive, non-flammable, and nontoxic), easily controlled reaction temperatures owing to the high heat capacity of water, and ease of phase separation [62–65]. Uozumi et al. synthesized polymer-supported Pd NPs with a mean diameter of 9 nm (ARP-Pd) via

Fig. 21 Preparation of amphiphilic resin-dispersed Pd NPs (ARP-Pd)

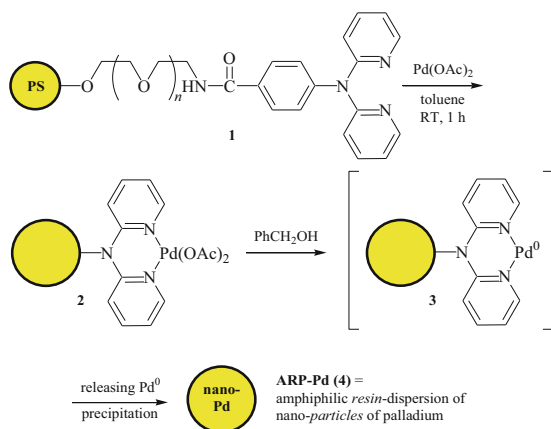
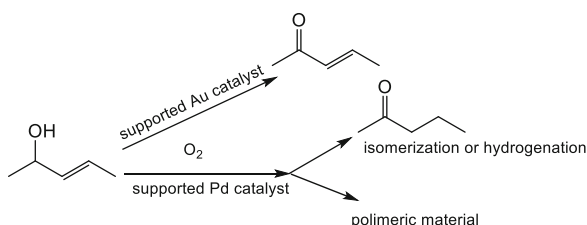


Fig. 22 Differences in product distribution for the aerobic oxidation of allylic alcohols catalyzed by Au and Pd catalysts



the reduction of a polystyrene-polyethylene glycol (PS-PEG) resin-supported bipyridyl palladium(II) complex, which efficiently promoted the aerobic oxidation of alcohols in aqueous media (Fig. 21) [66]. ARP-Pd was used in aqueous media to show that alcohols as substrates would diffuse into the hydrophobic ARP-Pd matrix to give a highly concentrated reaction field, where the active Pd NPs in the polymer matrix would efficiently oxidize the trapped alcohols.

Pd NP catalysts generally show low chemoselectivity for the oxidation of allylic alcohols to α,β -unsaturated carbonyl compounds compared with Au NPs, which was due to the formation of other byproducts arising from the isomerization and hydrogenation of C=C bonds and/or polymerization (Fig. 22) [67]. The different stabilities and steady-state concentrations of the metal hydrides (Au-H and Pd-H) are probably the cause of such a result. The Au-H species generated during oxidation is much more reactive with O₂ than the Pd-H species, preventing C=C bond hydrogenation or isomerization.

3.2 Bimetallic NP-Catalyzed Alcohol Oxidation

A combined system composed of plural metal species exhibit interesting catalytic activity compared with single metal species. Au-Pd/TiO₂ showed a wide substrate

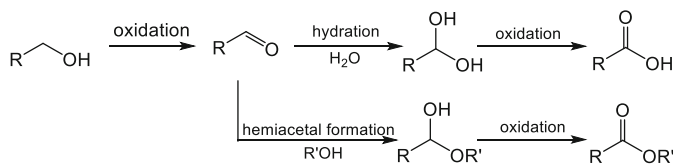


Fig. 23 Two reaction pathways for alcohol oxidation

scope with high TOFs in the aerobic oxidation, in which the choice of metal oxide support significantly influenced the product distribution in the oxidation of benzyl alcohol [68]. The side reaction, involving disproportionation of two molecules of benzyl alcohol to produce benzaldehyde and toluene, occurred when using TiO₂-, Nb₂O₅-, and activated carbon-supported Au–Pd NPs. In contrast, MgO- and ZnO-supported Au–Pd NPs were superior to the above catalysts for the selective oxidation of benzyl alcohol, giving benzaldehyde in more than 99% selectivity. Similarly, Kobayashi et al. reported that polymer-incarcerated Au–Pt alloyed bimetallic NPs (PI Pt/Au) exhibited higher catalytic activity than single metal Au or Pt NPs in the aerobic oxidation of alcohols [69]. PI Pt/Au worked well without additional base in water at room temperature, although PI Au, as a single metal species, required a large amount of K₂CO₃ to promote oxidation, in which water acted as a hydrogen transporter in the hydrophobic polystyrene surroundings, therefore aiding α-hydrogen abstraction.

The same group also developed carbon black-stabilized polymer-incarcerated bimetallic catalysts (PI-CB catalysts) [70]. Notably, PI-CB containing Au and Pt NP catalysts (PI-CB/Au–Pt) showed high catalytic activity and selectivity in the oxidation of primary aliphatic alcohols to the corresponding aldehydes under mild reaction conditions. This high catalytic activity could not be obtained using monometallic PI-CB catalysts, such as PI-CB/Au and PI-CB/Pt. The reactivity and selectivity were strongly dependent on the combination of metals and solvent system, with the overoxidation of 1-octanol to octanoic acid suppressed under neutral conditions. Furthermore, PI-CB/Au–Pd showed completely different activity and selectivity compared with PI-CB/Au–Pt, with direct oxidative methyl ester formation catalyzed by PI-CB/Au–Pd proceeding in methanol/H₂O in the presence of K₂CO₃. The oxidation to carboxylic acids or esters is dependent on hydration of, or hemiacetal formation from, the aldehyde (Fig. 23).

Au@NiOx NP catalyst with a core–shell structure was developed for the oxidative esterification of aldehydes with alcohols [71]. The Au@NiOx NP catalyst, in which 20 mol% Au in the core was covered by nickel oxide (NiOx) supported on silica-alumina-magnesia, provided an environmentally benign method for ester synthesis, because the side product was water and molecular oxygen is the ideal oxidant. In this method, the reaction with various aldehydes and primary alcohols gave the corresponding esters with good selectivity. Typically, this catalyst can promote aerobic esterification of acrolein with methanol, providing methyl methacrylate as an important raw material for polymer chemistry.

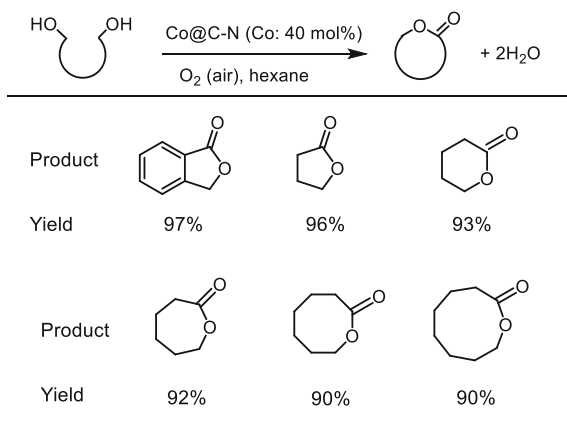
3.3 Base Metal NP-Catalyzed Alcohol Oxidation

From an economic efficiency standpoint, some non-noble transitional metals catalysts, such as Co [72–75], Mn [76, 77], Fe [78–80], V [81], and Cu [82, 83], have been explored in the aerobic oxidation of alcohols. Yingwei et al. reported that Co NPs stabilized by N-doped carbon composite (Co/C–N) acted as highly efficient heterogeneous catalysts for the synthesis of carbonyl compounds from the aerobic oxidation of alcohols [84]. Co/C–N could be synthesized by the one-pot thermal decomposition of Co-containing metal–organic frameworks (MOFs). Co NPs with a particle size of 9.8 ± 2.6 nm were highly dispersed on N-doped carbon. Importantly, N-doping into Co/C–N played a dual role, not only in enhancing the basic properties, which is crucial for promoting the activity of the liquid-phase aerobic oxidation of alcohols, but also in reducing the Co particle size. The Co/C–N catalyst showed a broad substrate scope for both aryl and alkyl alcohols in water under an atmospheric pressure of air and base-free conditions. Furthermore, the Co/C–N catalyst could be separated from the reaction system using an external magnetic field and reused. The Co NPs with surface-oxidized CoO species incorporated into N-doped carbon were applicable to the esterification of primary alcohols under mild conditions with air or 1 bar of O₂ [85, 86]. A broad substrate scope was observed for aromatic and aliphatic alcohols, as well as diols, giving their corresponding esters in good to excellent yields (Fig. 24).

Based on the above results, a possible reaction mechanism for the oxidative esterification of alcohols over Co–CoO incorporated into N-doped carbon is illustrated in Fig. 25. Firstly, alcohols are oxidized to aldehydes by O₂ through the abstraction of β-hydride from alcohols. Secondly, aldehydes and methanol undergo a condensation reaction to give hemiacetal species. Finally, the hemiacetal intermediate is oxidized by Co catalyst giving an ester product.

Although heterogeneous catalysts of inexpensive and reusable transition metals are attractive alternatives to homogeneous catalysts, the relatively low activity of

Fig. 24 Lactonization of various diols using Co NP catalyst



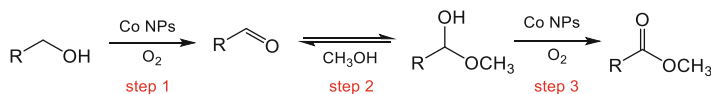


Fig. 25 Proposed reaction pathway for direct oxidative esterification of alcohols using Co NP catalysts

transition metal NPs represents a hurdle to their practical application. Li et al. reported that a nitrogen-rich carbon-coated cobalt NPs (Co@NC) catalyst, synthesized by direct polycondensation in the presence of $g\text{-C}_3\text{N}_4$ powder, exhibited a high TOF of 8.12 for the direct base-free aerobic oxidation of benzyl alcohols to methyl benzoate. This TOF was 30-fold higher than those of state-of-the-art transition metal-based nanocatalysts previously reported [87].

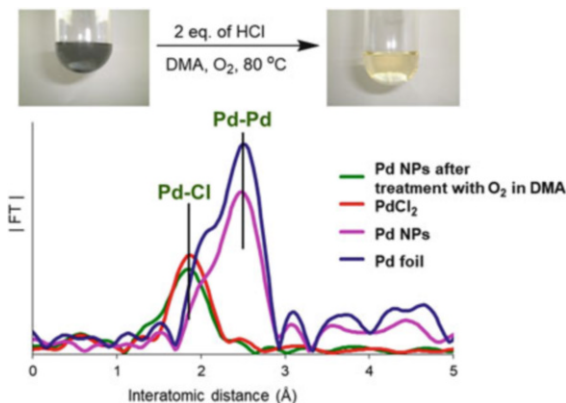
Nitrogen-rich carbon, which has a higher band potential than that of metallic Co materials, will accept electrons from Co NPs until their Fermi level reaches equilibrium, described as the Mott–Schottky effect. The resulting electron-poor Co NPs sufficiently attract and activate O_2 for proton removal from the Co–H intermediates to accelerate the whole reaction process. N-doped carbon could also act as a strengthened Lewis base to accelerate the deprotonation process of alcohols. Conclusively, the Co@NC-x-based Mott–Schottky catalysts not only boosted the oxidative power of the Co NPs but also enabled the reaction to proceed in the absence of bases, constituting an overall mild and additive-free catalytic system.

Continuous flow technology has attracted much attention because it can maximize catalyst efficiency in the simple workup procedure. Heterogeneous catalysts also have a significant advantage in the application to the use in column flow reactor. Kappe et al. found that iron oxide NPs stabilized on a mesoporous aluminosilicate support acted as highly efficient catalysts for the selective aerobic oxidation of a primary alcohol in continuous flow reactor [88]. In a single pass of the reactor, benzyl alcohol as a model substrate was selectively converted to benzaldehyde. This catalyst was highly stable and did not leach from support under the investigated conditions, providing solid evidence for the participation of a heterogeneous iron species in the catalytic cycle.

3.4 Wacker-Type Oxidation Using Pd NPs

Ethylene and palladium chloride react in the presence of water under atmospheric conditions to produce a stoichiometric amount of acetaldehyde with simultaneous formation of the precipitates of Pd (0) (Pd black) [89]. When copper dichloride (CuCl_2) is added to this system, in situ-formed Pd(0) species are reoxidized to Pd (II) by Cu(II), and then O_2 oxidizes the resulting Cu(I) back to Cu(II), thereby allowing this catalytic cycle. This method is called the Wacker process, which is limited to the synthesis of acetaldehydes through ethylene oxidation [90]. Using *N,N*-dimethylformamide (DMF) as a solvent in this process allowed the substrates to

Fig. 26 Direct oxidation of colloidal Pd NPs coordinated by *N,N*-dimethylacetamide (DMA) by O₂



be extended to the terminal alkenes. This process, the Wacker–Tsuji reaction, is an effective means of selective methyl ketone synthesis from a wide range of terminal alkenes [91].

Recently, Mitsudome et al. found that colloidal Pd NPs in *N,N*-dimethylacetamide (DMA) solution can be directly oxidized by O₂ as sole oxidant to homogeneous Pd(II) species in the presence of hydrochloric acid (Fig. 26). Pd K-edge XAFS analysis proved that the peak attributed to the Pd–Pd bond in the Fourier transforms (FT) of k^3 -weighted EXAFS disappeared and that a new peak derived from the Pd–Cl bond appeared after treating Pd NPs with DMA in the presence of two equivalents of HCl at 80 °C under O₂ at atmospheric pressure.

This unique phenomenon would be applicable to developing the Cu-free Wacker oxidation system because in situ-generated Pd(0) species from the reaction of Pd(II) with alkenes can be readily reoxidized to Pd(II) by O₂ without the necessity of Cu [92]. In fact, the Cu-free Wacker oxidation of various terminal alkenes could proceed using a PdCl₂/DMA catalyst system, affording the corresponding methyl ketones under O₂ at atmospheric pressure without substrate isomerization (Fig. 27).

This PdCl₂-DMA-O₂ system can be used for the oxidation of not only terminal alkenes but also internal alkenes, where various internal alkenes were efficiently converted to the corresponding ketones with 99% selectivity (Fig. 28) [93]. Although the conventional Wacker oxidation suffers from limited reactivity toward internal alkenes, this catalyst system overcame this limitation and provided a new and efficient methodology for catalyzing the oxidation of internal alkenes to carbonyl compounds.

The regioselective introduction of ketone oxygen functions was also possible using substrates containing functional groups [94]. Various nonenyl acetates were tested in this system, as shown in Fig. 29, and the ketone oxygen atom was selectively introduced into the carbon distal from the acetoxy group.

This breakthrough in the limitations of the conventional Wacker oxidation was attributed to the development of a Cu-free catalyst system because Cu strongly

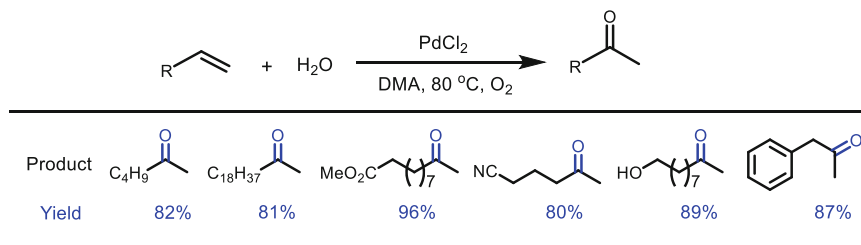


Fig. 27 O₂-coupled Wacker oxidation system without copper

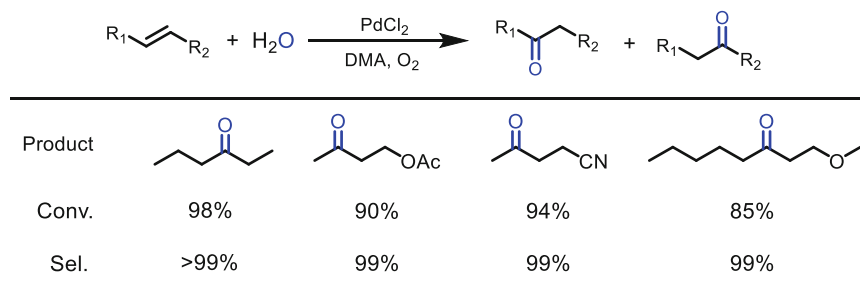


Fig. 28 Cu-free Wacker oxidation of internal alkenes

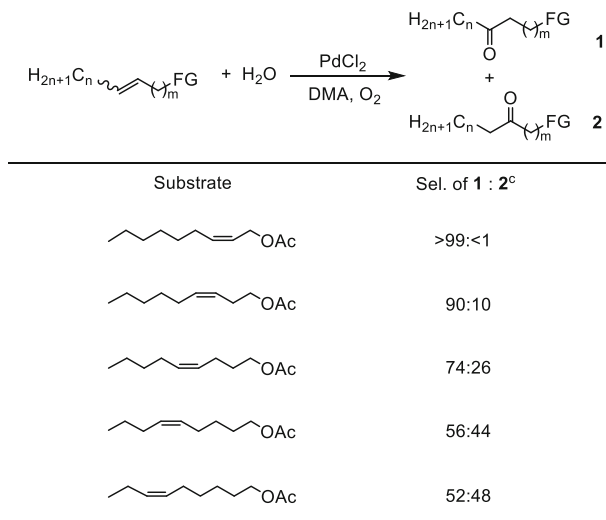


Fig. 29 Wacker-type oxidation of nonenyl acetates

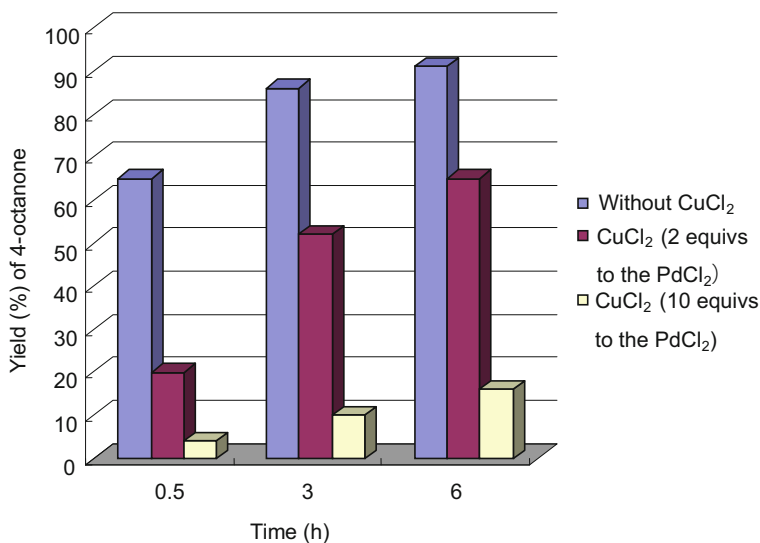


Fig. 30 Effect of CuCl₂ amounts on the oxidation of 4-octene. Reprinted with permission from [93]. Copyright 2010 Wiley-VCH

suppresses the oxidation of internal alkenes. As shown in Fig. 30, the reactivity of the internal alkene for oxidation was strongly suppressed by adding CuCl₂ to the PdCl₂-DMA-O₂ system, while that of the terminal alkene was not suppressed. This was probably due to the formation of a bulky Pd/Cu complex [95], which is difficult to coordinate to internal alkenes.

In the previous Wacker reaction, molecular oxygen acted to reoxidize palladium through the redox cycle of Cu(I) and Cu(II) and was not incorporated into the substrate. In this PdCl₂-DMA-O₂ system, ¹⁸O₂ was not incorporated into the product ketones, and the oxygen atom introduced into the ketone was derived from water. The selective oxygenation of alkenes to ketones was achieved using oxygen nucleophiles derived from water. Interestingly, methanol can be used as a nucleophile instead of water. In this case, using the PdCl₂-DMA-O₂-methanol system, the oxidation of α,β -unsaturated carbonyl compounds gave β -methoxy- α,β -unsaturated compounds that were easily hydrolyzed to the corresponding β -carbonyl compounds, as shown in Fig. 31 [96].

The PdCl₂-DMA-O₂-methanol-TsOH-H₂O system realized the simple oxidation process of converting α,β -unsaturated carbonyl compounds to β -carbonyl compounds (Fig. 32). As described above, this reinvestigation of the Wacker process provides a new and highly selective oxygenation method for converting various internal alkenes to ketones.

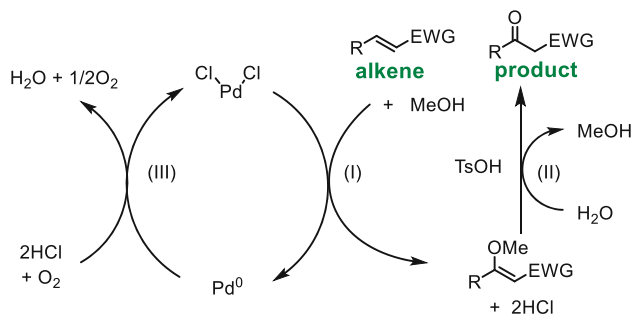


Fig. 31 Reaction pathway and reaction formulas of the PdCl₂-DMA-MeOH-TsOH catalyst system

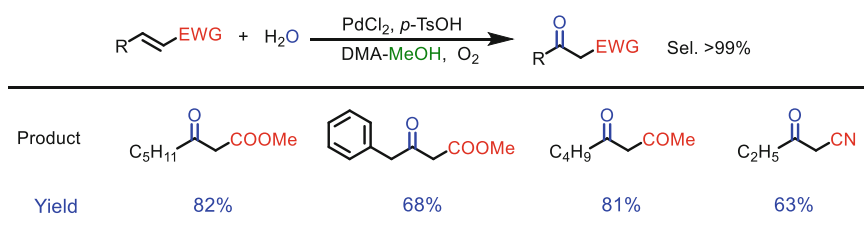


Fig. 32 Wacker-type oxidation of α,β -unsaturated carbonyl compounds to β -carbonyl compounds using PdCl₂-DMA-O₂-methanol-TsOH-H₂O system

4 Summary

The selective transformation of organic compounds through reduction and/or oxidation is a fundamental challenge in synthetic chemistry. This review focused on recently developed high-performance metal NP catalysts for selective reduction and oxidation under liquid-phase conditions using molecular hydrogen and molecular oxygen, respectively. Traditional heterogeneous catalysts, including metal NP catalysts, have significant intrinsic advantages of easy separation and robustness but generally show lower catalytic performance (activity and selectivity) and require harsh reaction conditions, such as high temperature, compared with homogeneous catalysts. Compared with premodern heterogeneous catalysts, the state-of-the-art metal NP catalysts introduced here have higher activity and selectivity for the chemoselective hydrogenations of carbonyl, nitro, and alkynyl compounds while retaining C=C bonds and the aerobic oxidation of alcohols and the Wacker oxidation of alkenes. This improved catalytic performance is due to significant advances in the precise fabrication of nanoscale metals, which has made it possible to explore novel catalysis and design metal active centers. The rapid expansion of characterization methods for the nanostructured catalysts has also greatly contributed to catalytic improvement. Spectroscopic analysis, especially operant analysis, enabled deep understanding of the role of supports and the relationship between structure and

activity, leading to the development of more sophisticated catalysts with high performance. Although the catalytic performance of heterogeneous metal NP catalysts has been greatly advanced in the last decade, research on heterogeneous catalysts for fine chemistry is still in the development stage. The development of more efficient metal NP catalysts that promote selective hydrogenation and aerobic oxidation using lower amounts of active metals under milder reaction conditions without any additives and solvents remains vital. We believe that advances in both nanotechnology for the fine-tuning of metal NPs and a deep understanding of the complicated structure of heterogeneous catalysts play key roles in the development of next-generation metal NP catalysts for selective redox reactions in environmentally friendly fine chemistry.

References

1. Trost BM (1991) *Science* 254:1471
2. Anastas PT, Warner JC (1998) *Green chemistry, theory and practice*. Oxford University Press, Oxford
3. Sheldon RA, Wallau M, Arends IWCE, Schuhardt U (1998) *Acc Chem Res* 31:485
4. Clark JH (1999) *Green Chem* 1:1
5. Sheldon RA (2000) *Green Chem* 2:G1
6. Anastas PT, Bartlett LB, Kirchoff MM, Williamson TC (2000) *Catal Today* 55:11
7. Hagen J (1999) *Industrial catalysis: a practical approach*. Wiley, Weinheim
8. Ertl G, Knözinger H, Schüth F, Weitkamp J (2008) *Handbook of heterogeneous catalysis*. 2nd edn. Wiley, Weinheim
9. Astruc D (2008) *Nanoparticles and catalysis*. Wiley, Weinheim
10. Tauster SJ, Fung SC, Baker RT, Horsley JA (1981) *Science* 211:1121
11. Schubert MM, Hackenberg S, van Veen AC, Muhler M, Plzak V, Behm RJ (2001) *J Catal* 197:113
12. Bell AT (2003) *Science* 299:1688
13. Tian N, Zhou Z-Y, Sun S-G, Ding Y, Wang ZL (2007) *Science* 316:732
14. Somorjai GA, Park JY (2008) *Angew Chem Int Ed* 47:9212
15. Astruc D, Lu F, Aranzaes JR (2005) *Angew Chem Int Ed* 44:7852
16. Johnson BF (2003) *Top Catal* 24:147
17. Mitsudome T, Kaneda K (2013) *Green Chem* 15:2636
18. Mallat T, Baiker A (2004) *Chem Rev* 104:3037
19. Zhan BZ, Thompson A (2004) *Tetrahedron* 60:2917
20. Matsumoto T, Ueno M, Wang N, Kobayashi S (2008) *Chem Asian J* 3:196
21. Vinod CP, Wilson K, Lee AF (2011) *J Chem Technol Biotechnol* 86:161
22. Serna P, Corma A (2006) *Science* 313:332
23. Serna P, Corma A (2015) *ACS Catal* 5:7114
24. Mitsudome T, Noudjima A, Mikami Y, Mizugaki T, Jitsukawa K, Kaneda K (2010) *Angew Chem Int Ed* 49:5545
25. Noudjima A, Mitsudome T, Mizugaki T, Jitsukawa K, Kaneda K (2011) *Angew Chem Int Ed* 50:2986
26. Shimizu K, Miyamoto Y, Satsuma A (2010) *J Catal* 270:86
27. Mitsudome T, Mikami Y, Matoba M, Mizugaki T, Jitsukawa K, Kaneda K (2012) *Angew Chem Int Ed* 51:136
28. Mitsudome T, Matoba M, Mizugaki T, Jitsukawa K, Kaneda K (2013) *Chem Eur J* 19:5255

29. Derrien ML (1986) Catalytic hydrogenation. In: Červený L (ed) *Studies in surface science and catalysis*, vol 27. Elsevier, Amsterdam, p 613
30. Piringer OG, Baner AL (2008) *Plastic packaging: interactions with food and pharmaceuticals*. 2nd edn. Wiley, Weinheim
31. Lindlar H (1952) *Helv Chim Acta* 35:446
32. van Laren MW, Elsevier CJ (1999) *Angew Chem Int Ed* 38:3715
33. Yabe Y, Yamada T, Nagata S, Sawama Y, Monguchi Y, Sajiki H (2012) *Adv Synth Catal* 354:1264
34. Armbrüster M, Kovnir K, Friedrich M, Teschner D, Wowsnick G, Hahne M, Gille P, Szentmiklósi L, Feuerbacher M, Heggen M, Girgsdies F, Rosenthal D, Schlögl R, Grin Y (2012) *Nat Mater* 11:690
35. Torres Galvis HM, Bitter JH, Khare CB, Ruitenbeek M, Dugulan AI, de Jong KP (2012) *Science* 335:835
36. Brown CA, Ahuja VK (1973) *J Chem Soc Chem Commun* 38:553
37. Studt F, Abild-Pedersen F, Bligaard T, Sørensen RZ, Christensen CH, Nørskov JK (2008) *Science* 320:1320
38. Carencó S, Leyva-Pérez A, Concepción P, Boissière C, Mézailles N, Sanchez C, Corma A (2012) *Nano Today* 7:21
39. Semba K, Fujihara T, Xu T, Terao J, Tsuji Y (2012) *Adv Synth Catal* 354:1542
40. Niu M, Wang Y, Li W, Jiang J, Jin Z (2013) *Catal Commun* 38:77
41. Takahashi Y, Hashimoto N, Hara T, Shimazu S, Mitsudome T, Mizugaki T, Jitsukawa K, Kaneda K (2011) *Chem Lett* 40:405
42. Mitsudome T, Takahashi Y, Ichikawa S, Mizugaki T, Jitsukawa K, Kaneda K (2013) *Angew Chem Int Ed* 52:1481
43. Sárkány A, Révay Z (2003) *Appl Catal A Gen* 243:347
44. Vilé G, Baudouin D, Remediakis IN, Copèret C, López N, Pérez-Ramírez J (2013) *ChemCatChem* 5:3750
45. Oakton E, Vilé G, S. Levine D, Zoicher E, Baudouin D, Pérez-Ramírez J, Copèret C (2014) *Dalton Trans* 43:15138
46. Mitsudome T, Urayama T, Yamazaki K, Maehara Y, Yamasaki J, Gohara K, Maeno Z, Mizugaki T, Jitsukawa K, Kaneda K (2016) *ACS Catal* 6:666
47. Westerhaus FA, Jagadeesh RV, Wienhofer G, Pohl MM, Radnik J, Surkus AE, Rabeah J, Junge K, Junge H, Nielsen M, Bruckner A, Beller M (2013) *Nat Chem* 5:537
48. Jagadeesh RV, Surkus AE, Junge H, Pohl MM, Radnik J, Rabeah J, Huan HM, Schunemann V, Bruckner A, Beller M (2013) *Science* 342:1073
49. Schwartz DK (2001) *Annu Rev Phys Chem* 52:107
50. Love JC, Estroff LA, Kriebel JK, Nuzzo RG, Whitesides GM (2005) *Chem Rev* 105:1103
51. Schoenbaum CA, Schwartz DK, Medlin JW (2014) *Acc Chem Res* 47:1438
52. Kahsar KR, Schwartz DK, Medlin JW (2014) *J Am Chem Soc* 136:520
53. Makosch M, Lin WI, Bumbálek V, Sá J, Medlin JW, Hungerbühler K, van Bokhoven JA (2012) *ACS Catal* 2:2079
54. Gao R, Pan L, Wang H, Yao Y, Zhang X, Wang L, Zou J-J (2019) *Adv Sci* 6:1900054
55. Mitsudome T, Kaneda K (2013) Oxidation of alcohols using nano-catalysts. In: *Nanocatalysis: synthesis and applications*. Wiley, Weinheim, pp 287–332
56. Stahl SS (2004) *Angew Chem Int Ed* 43:3400
57. Mori K, Yamaguchi K, Hara T, Mizugaki T, Ebitani K, Kaneda K (2002) *J Am Chem Soc* 124:11572
58. Mori K, Hara T, Mizugaki T, Ebitani K, Kaneda K (2004) *J Am Chem Soc* 126:10657
59. Hara T, Mori K, Mizugaki T, Ebitani K, Kaneda K (2003) *Tetrahedron Lett* 44:6207
60. Kwon MS, Kim N, Park CM, Lee JS, Kang KY, Park J (2005) *Org Lett* 7:1077
61. Layek K, Maheswaran H, Arundhathi R, Kantam ML, Bhargava SK (2011) *Adv Synth Catal* 353:606
62. Chanda A, Fokin VV (2009) *Chem Rev* 109:725

63. Minakata S, Komatsu M (2009) *Chem Rev* 109:71
64. Grieco PA (1998) *Organic synthesis in water*. Blackie, London
65. Li CJ, Chan T-H (1997) *Organic reaction in aqueous media*. Wiley, New York
66. Uozumi Y, Nakao R (2003) *Angew Chem Int Ed* 42:194
67. Abad A, Almela C, Corma A, García H (2006) *Chem Commun* 30:3178
68. Sankar M, Nowicka E, Tiruvalam R, He Q, Taylor SH, Kiely CJ, Bethell D, Knight DW, Hutchings GJ (2011) *Chem Eur J* 17:6524
69. Miyamura H, Matsubara R, Kobayashi S (2008) *Chem Commun* 17:2031
70. Kaizuka K, Miyamura H, Kobayashi S (2010) *J Am Chem Soc* 132:15096
71. Suzuki K, Yamaguchi T, Matsushita K, Itsuka C, Miura J, Akaogi T, Ishida H (2013) *ACS Catal* 3:1845
72. Zhu J, Faria JL, Figueiredo JL, Thomas A (2011) *Chem Eur J* 17:7112
73. Zhu J, Kailasam K, Fischer A, Thomas A (2011) *ACS Catal* 1:342
74. Shimizu K-I, Kon K, Seto M, Shimura K, Yamazaki H, Kondo JN (2013) *Green Chem* 15:418
75. Zhang G, Vasudevan KV, Scott BL, Hanson SK (2013) *J Am Chem Soc* 135:8668
76. Sun HY, Hua Q, Guo F-F, Wang Z-Y, Huang WX (2012) *Adv Synth Catal* 354:569
77. Raisanen MT, Al-Hunaiti A, Atosuo E, Kemell M, Leskela M, Repo T (2014) *Cat Sci Technol* 4:2564
78. Song H, Kang B, Hong SH (2014) *ACS Catal* 4:2889
79. Li R, Zhao J, Yang F, Zhang Y, Ramella D, Peng Y, Luan Y (2017) *RSC Adv* 7:51142
80. Rajabi F, Pineda A, Naserian S, Balu AM, Luque R, Romero AA (2013) *Green Chem* 15:1232
81. Hanson SK, Baker RT, Gordon JC, Scott BL, Sutton AD, Thorn DL (2009) *J Am Chem Soc* 131:428
82. Chen C, Liu B, Chen W (2013) *Synthesis* 45:3387
83. Liu L, Ma J, Ji L, Wei Y (2008) *J Mol Catal A Chem* 291:1
84. Cuihua B, Ai Qin L, Xianfang Y, Hongli L, Yingwei L (2016) *Green Chem* 18:1061
85. Zhou YX, Chen YZ, Cao L, Lu J, Jiang HL (2015) *Chem Commun* 51:8292
86. Wei Z, Hongli L, Cuihua B, Shijun L, Yingwei L (2015) *ACS Catal* 5:1850–1856
87. Su H, Zhang KX, Zhang B, Wang HH, Yu QY, Li XH, Antonietti M, Chen JS (2017) *J Am Chem Soc* 139:811
88. Obermayer D, Balu AM, Romero AA, Goessler W, Luque R, Kappe CO (2013) *Green Chem* 15:1530
89. Phillip FC (1894) *Am Chem J* 16:255
90. Smidt J, Hafner W, Jira R, Sieber R, Sedlmeier J, Sabel A (1962) *Angew Chem Int Ed Engl* 1:80
91. Tsuji J (1984) *Synthesis* 1984:369
92. Mitsudome T, Umetani T, Nosaka N, Mori K, Mizugaki T, Ebitani K, Kaneda K (2006) *Angew Chem Int Ed* 45:481
93. Mitsudome T, Mizumoto K, Mizugaki T, Jitsukawa K, Kaneda K (2010) *Angew Chem Int Ed* 49:1238
94. Mitsudome T, Yoshida S, Tsubomoto T, Mizugaki T, Jitsukawa K, Kaneda K (2013) *Tetrahedron Lett* 54:1596
95. Hosokawa T, Nomura T, Murahashi S-I (1998) *J Organomet Chem* 551:387
96. Mitsudome T, Yoshida Y, Mizugaki T, Jitsukawa K, Kaneda K (2013) *Angew Chem Int Ed* 52:5961

Earth-Abundant and Precious Metal Nanoparticle Catalysis



Margery Cortes-Clerget, Nnamdi Akporji, Balaram S. Takale, Alex Wood, Evan Landstrom, and Bruce H. Lipshutz

Contents

1	Introduction	78
2	Palladium	78
3	Nickel	89
4	Platinum	94
5	Copper	97
6	Gold	103
7	Rhodium	110
8	Ruthenium	113
9	Cobalt	115
10	Iron	116
11	Summary	122
	References	122

Abstract This chapter is an overview focusing on the preparation and use of transition metal-containing nanoparticles (NPs) described in the literature over the past decade or so. It is organized according to the metal, including NPs that feature catalysis based on Pd, Ni, Pt, Cu, Au, Rh, Ru, Co, and Fe. Nanoparticles that involve metals on various supports are discussed, as are those derived solely from precursor metals salts. Experimental procedures from these reports detailing both the preparation and use of several of these NPs are also contained herein.

M. Cortes-Clerget

Department of Chemistry and Biochemistry, University of California, Santa Barbara, CA, USA

Chemical and Analytical Development, Novartis Pharma AG, Basel, Switzerland

e-mail: margery.cortes@novartis.com

N. Akporji, B. S. Takale, A. Wood, E. Landstrom, and B. H. Lipshutz (✉)

Department of Chemistry and Biochemistry, University of California, Santa Barbara, CA, USA

e-mail: nnamdi@ucsb.edu; balaram_takale@ucsb.edu; abwood@ucsb.edu;

evanlandstrom@ucsb.edu; lipshutz@chem.ucsb.edu

Exciting developments associated with mixed metal NPs and their applications that highlight synergistic effects of synthetic value offer a glimpse of what is likely to be an increasingly important direction for catalysis in the near future.

Keywords Catalysis · Nanoparticles · Synergistic effects between metals · Transition metals

1 Introduction

Metal nanoparticle technology applied to organic synthesis continues to blossom. New materials for catalysis are being introduced on a regular basis, while methods for their analyses have become increasingly sophisticated, offering insights that have led to many of these advances. Technically, even in cases where these materials are quite small, including metal clusters, metal nanoparticles (NPs), and even species containing single atoms, they are all categorized within the area of heterogeneous catalysis. A timely and extensive review by Liu and Corma in 2018 highlighted the important factors that can influence metal catalysts of these types, drawing attention to parameters such as size and shape, among several others (e.g., metal support, their chemical make-up, the influence of additives such as other metals, etc.) [1]. At stake, of course, are the resulting key issues of reactivity and selectivity and, ultimately, synthetic utility. Hence, this review focuses on not only the development of new NPs but also the synthetic applications that have appeared over the past decade, discussed according to metal.

2 Palladium

Palladium occupies a unique position among transition metals in the field of catalysis. Although a costly precious metal, it remains world-renowned for its ability to catalyze formation of new C-C bonds, such as Heck cross-coupling reactions to form new substituted olefins; the Suzuki-Miyaura, Kumada, and Stille couplings, which can afford, e.g., new biaryls; Negishi couplings that facilitate introduction of alkyl groups onto carbon sp^2 centers; and Sonogashira reactions which can afford substituted alkynes [2–8]. Moreover, gases such as CO and CO₂ can also be used in tandem with palladium catalysts to generate carbonyl-containing products [9, 10]. Palladium is also the “go-to” metal in many hydrogenation reactions [11]. The products of these numerous types of reactions oftentimes contain structural motifs present in natural products, polymers, and a wide array of pharmaceuticals and other targets within the fine chemical industry [12].

The high surface area to volume ratio of Pd NPs makes them especially reactive [13]. Heterogeneous Pd NPs as catalysts are finding increased use due to their overall stability, as avoidance of phosphine ligands on Pd in solution is readily appreciated given their potential instability, toxicity, and susceptibility to oxidation. Thus, there has been increased interest in ligand-free palladium nanoparticles. On the other hand, many examples exist where phosphines have been incorporated into palladium complexes and their derived NPs, since the presence of a ligand can significantly affect both reactivity and selectivity associated with the reaction of interest. Preparations of palladium NPs can oftentimes be straightforward and, in most cases of interest, are well documented. The flexibility in their preparation leading to NPs of different sizes and their demonstrated recyclability and catalytic efficiency make them attractive alternatives to traditional methods involving homogeneous catalysis. A general mechanistic understanding as to the exact location of catalysis in many cases, however, remains for the future [8].

A report in 2015 in *Science* disclosed that a mixture composed of an inexpensive Fe^{III} salt doped with ppm levels of Pd and a suitable phosphine ligand could be converted upon the addition of MeMgCl in THF into highly active NPs capable of catalyzing Suzuki-Miyaura couplings in micellar media under very mild conditions [14]. Each component of the catalyst proved to be critical to its activity. Anhydrous FeCl_3 , 320–500 ppm $\text{Pd}(\text{OAc})_2$ (relative to 0.5 mmol of halide substrate), and MeMgCl were optimal, while alternative alkyl or aryl Grignard reagents were found to afford far less effective catalysts. The inclusion of a suitable phosphine ligand, SPhos in this case, was crucial for high catalyst activity, with other phosphine ligands leading to inferior levels of conversion. This observation is of particular note, since phosphine ligands traditionally tend to play a critical role in *homogeneous* catalysis, but less so in heterogeneous processes.

Remarkably, these NPs were found to contain ca. 40% THF by weight, which was later observed to be essential for catalytic activity. TGA analysis revealed a sharp loss of mass from ca. 60 to 145°C. While the material itself maintained thermal stability from 145 to 380°C, the catalytic activity dropped precipitously after loss of THF. Analyses of these aqueous reaction mixtures by cryo-TEM revealed the association of the NPs with nanomicelles of designer surfactant TPGS-750-M (Fig. 1), where the MPEG present stabilizes the metal NPs (rods), while the (spherical) nanomicelles present deliver the coupling partners localized within

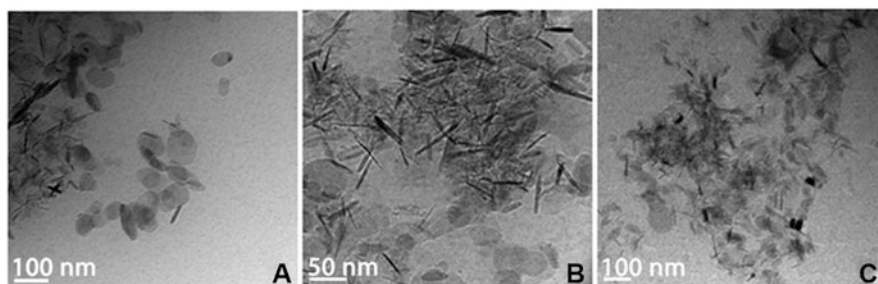


Fig. 1 Cryo-TEM images of Fe/Pd nanoparticles in the presence of aqueous TPGS-750-M

their inner cores. This so-called “nano-to-nano” effect [15] may be responsible for the observed activity, where heating is not needed notwithstanding the heterogeneous nature of the catalysis.

This NP catalyst is very effective in accommodating numerous substrate combinations. An array of functionality within either the electrophilic or boron-containing partner is tolerated, including as examples labile perfluoroarylboronic acids, complex uracil derivatives, and *O*-, *N*-, and *S*-containing heterocycles. A variety of chlorides, bromides, and iodides are amenable, while Bpin, BMIDA, BF_3K , and boronic acid reagents have all been successfully coupled using this NP catalyst under mild aqueous conditions (Fig. 2).

By replacing SPhos with XPhos and MeMgCl with MeMgBr as reductant, modified NPs are formed that can successfully catalyze Sonogashira couplings with similar efficacy on complex heterocyclic substrates [16]. This catalyst shows desirable selectivity toward oxidative addition with iodides preferentially over bromides, although in the absence of an iodide-bearing substrate, bromides can be smoothly and efficiently coupled. Notably, no copper is required in these transformations. This catalyst system was utilized in the synthesis of an intermediate en route to the antitumor agent ponatinib (Fig. 3). In all cross-coupling cases utilizing these Fe/Pd nanoparticles, residual palladium in the products is at or below the FDA threshold (10 ppm), bypassing the need for Pd scrubbing of the products.

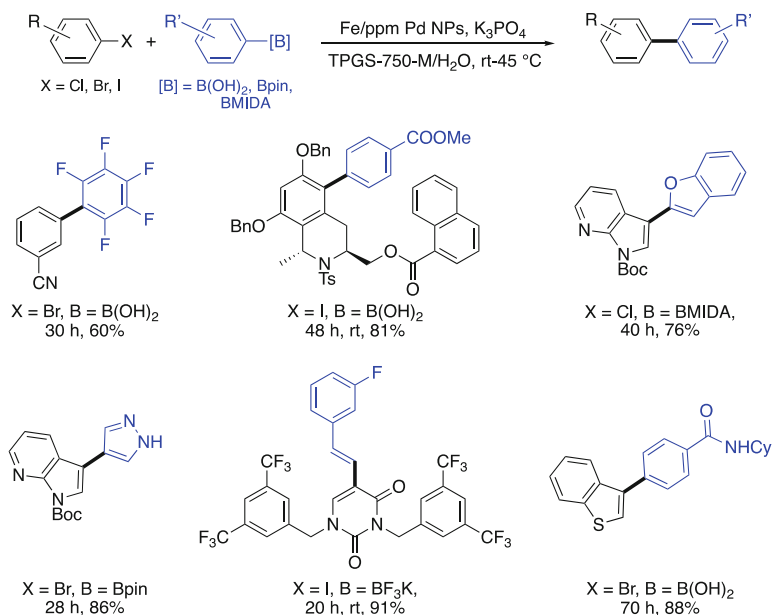


Fig. 2 Representative substrates synthesized using Fe/ppm Pd NPs

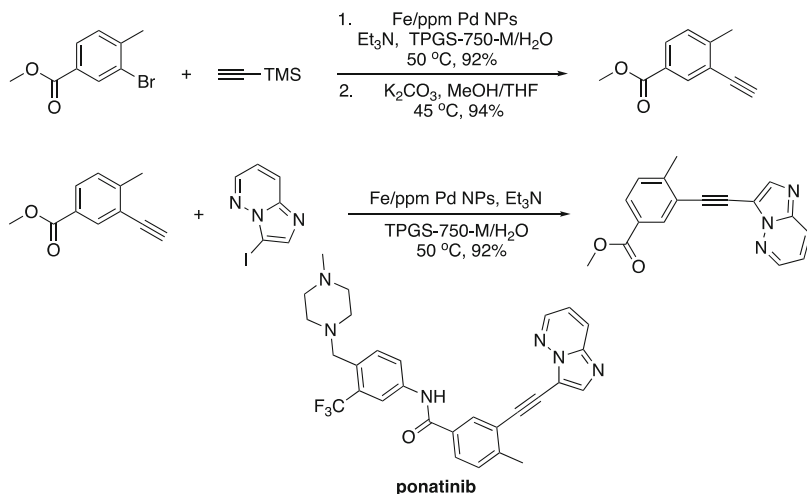


Fig. 3 Fe/ppm-Pd NPs used in the synthesis of a ponatinib intermediate

In Situ Preparation and Use of Fe/ppm Pd NPs for Sonogashira Couplings.

In a flame-dried 4 mL microwave reaction vial, pure FeCl₃ (4.1 mg, 5 mol%) and XPhos (7.1 mg, 3 mol%) were added under anhydrous conditions. The reaction vial was sealed with a rubber septum, and the mixture was evacuated and backfilled with argon. Dry THF (1.0 mL) was added to the vial, and Pd(OAc)₂ (500 ppm) was then added using a 5 mM solution of Pd(OAc)₂ in dry THF. Then the mixture was stirred for 20 min at rt. after which dissolution and complexation of iron chloride was clearly visualized by a color change to dark brown. While maintaining an inert atmosphere, THF was evaporated under reduced pressure at rt. MeMgBr (0.25 mL, 10 mol%, 0.2 M) was added to the reaction mixture, after which it was stirred at rt. for 1 min. An aqueous solution of 2 wt% TPGS-750-M (1.0 mL) was added to the vial followed by sequential addition of an aryl halide (0.5 mmol, 1.0 equiv), alkyne (0.75 mmol, 1.5 equiv), and Et₃N (101 mg, 1.0 mmol, 2.0 equiv). The reaction vial was sealed with a rubber septum under argon and stirred at 45 °C until complete consumption of starting material as monitored by TLC or GCMS. The reaction mixture was then allowed to cool to rt, and EtOAc (1.0 mL) was added and the mixture stirred gently for 1 min. The organic layer was allowed to separate from the aqueous layer with the help of a centrifuge, if needed. The organic layer was decanted using a pipette. The same extraction procedure was applied by using an additional 1.0 mL EtOAc. The combined organic extracts were dried over anhydrous Na₂SO₄. Volatiles were removed under reduced pressure to obtain crude product, which were further purified by flash chromatography over silica gel using EtOAc/hexanes as eluent.

During the screening of optimized reaction parameters for Fe/ppm Pd NP catalyzed cross-couplings, it was noted that in the absence of a phosphine ligand and with NaBH₄ serving as reductant, catalyst activity toward C-C bond formation was retarded in favor of reduction of nitro groups within aromatic or heteroaromatic substrates to their corresponding anilines [17]. Reductions of this functional group proceed smoothly at room temperature and pressure with only 80 ppm

Pd doped into these ligandless Fe/ppm Pd NPs. An extensive array of highly functionalized educts readily participated, leading to the corresponding amines in high yields (Fig. 4). Akin to other NPs of this type, optimal activity was realized when used in conjunction with a 2 wt% solution of aqueous TPGS-750-M. Classical methods for nitro group reductions (e.g., H_2 with Pd/C) typically require high temperatures, pressures, and catalyst loadings, necessitating specialized reaction vessels to mitigate potential safety hazards. Reductions using Fe/Pd NPs in the presence of either $NaBH_4/KCl$ or KBH_4 can be accomplished without the need for any specialized equipment, allowing for ready scalability of these reactions from 0.5 mmol up to 100 mmol [18].

Nitro Group Reductions: Preparation of Fe/ppm Pd NPs In an oven-dried two-necked round-bottomed flask, anhydrous 99.99% pure $FeCl_3$ (487.5 mg, 3 mmol), $Pd(OAc)_2$ (2.2 mg, 0.01 mmol) (or other commercially available $FeCl_3$ that contains ppm levels of Pd) was added under an atmosphere of dry argon. The flask was covered with a septum, and dry THF (15 mL) was added. The reaction mixture was stirred for 20 min at rt. While maintaining a dry atmosphere at rt., 0.5 M solution of $MeMgCl$ in THF (6 mL, 3 mmol) was very slowly (1 drop/2 s) added to the reaction mixture. After complete addition of Grignard reagent, the mixture was stirred for an additional 20 min at rt. Appearance of a yellow-brown color was indicative of generation of nanomaterial. The mixture was then quenched with pentane (containing traces of water). The THF was then evaporated under reduced pressure at rt. Removal of THF was followed by triturating the mixture with pentane to provide yellow-brown colored nanomaterial as a powder (trituration was repeated 3–4 times). The Fe nanoparticles obtained were dried under reduced pressure at rt for 10 min yielding 1.5 g Fe/ppm Pd nanoparticles. The material was used as such for subsequent reactions under micellar conditions. Note: These iron

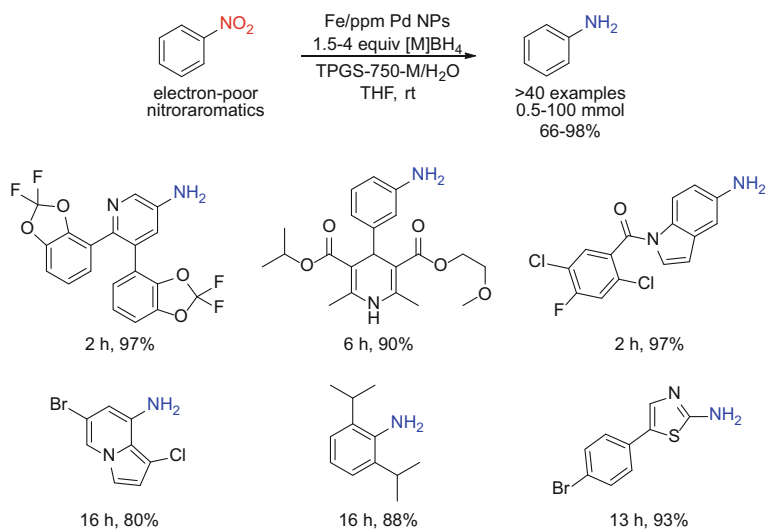


Fig. 4 First-generation Fe/ppm Pd nanoparticles for nitro group reductions

nanoparticles are best stored under argon in a refrigerator; otherwise, the color may change indicative of a drop in reactivity.

General Procedure for Reductions Iron-based nanomaterial (6 mg) was added to an oven-dried 10 mL round-bottomed flask (RBF) containing a PTFE-coated magnetic stir bar. An aqueous solution of 2 wt% TPGS-750-M (0.5 mL) was added via syringe, and NaBH_4 (28.5–59.0 mg, 0.75–1.50 mmol) was added to the reaction mixture. (Caution: NaBH_4 should be added slowly, especially for large-scale reactions, i.e., >1 mmol.) During addition of NaBH_4 , the reaction mixture turned black with evolution of hydrogen gas. The reaction flask was covered with a rubber septum, and the mixture was stirred for 2 min at rt. The nitro group-containing substrate (0.5 mmol, pre-dissolved or dispersed in mixture of 0.5 mL aqueous TPGS-750-M and 0.1 mL THF in advance) was then added to the catalyst suspension via syringe (substrates which are not soluble in aqueous TPGS solution were first dissolved in a minimum amount of THF (160 μL for 0.5 mmol of educt)). The RBF was filled with argon and covered again with a rubber septum. Finally, the reaction mixture was vigorously stirred at rt. Progress of the reaction was monitored by TLC or GCMS. After complete consumption of starting material as monitored by TLC, the septum was removed, and argon was bubbled through the mixture. Minimal amounts of an organic solvent (EtOAc, *i*-PrOAc, Et_2O , MTBE, etc.) were added, and the mixture was stirred gently for 2 min. Stirring was stopped, and the organic layer was then allowed to separate, after which it was removed via pipette. The same extraction procedure was repeated, and the combined organic extracts were dried over anhydrous Na_2SO_4 . Volatiles were evaporated under reduced pressure, and semi-pure product was purified by flash chromatography over silica gel. Caution: Never use acetone for TLC monitoring or column chromatography. Occasionally during the progress of the reaction, the reaction vial requires gentle shaking to avoid adherence of reaction material to the glass. Always use fresh and good quality NaBH_4 .

Further optimization of these NPs led to an improved catalyst exhibiting synergistic effects between Pd (80 ppm) and Ni (1,600 ppm) [19]. While electron-rich nitroaromatics on occasion showed sluggish behavior toward the initially reported catalyst, the second-generation Fe/Pd/Ni NPs are, in general, far more reactive. Ether-, thioether-, and aniline-containing nitroaromatics were reduced in good-to-excellent yields with remarkable chemoselectivity (Fig. 5). For example, despite the presence of super-stoichiometric amounts of borohydride, reduction of aryl hydrazones to their corresponding hydrazines was not observed. EXAFS analysis of the first-generation NPs revealed high shell scattering indicative of tight Pd-Pd interactions. The nickel-containing particles contained no such feature. It is postulated that the presence of nickel dilutes the palladium on the surface of the NPs inhibiting clustering (i.e., Pd-Pd interactions) and therefore increasing the availability of highly reactive single atoms of Pd.

In 2018, Ming Bao and co-workers reported that allylboronates can be used as a carbon-based ligand for in situ generation of Pd NPs [20]. These have been shown to be useful in carboxylative Suzuki-Miyaura coupling reactions of benzylic chlorides with allylpinacolborate (Fig. 6). The reaction conditions were relatively

Fig. 5 Second-generation Fe/ppm-Pd + Ni nanoparticles for nitro group reductions

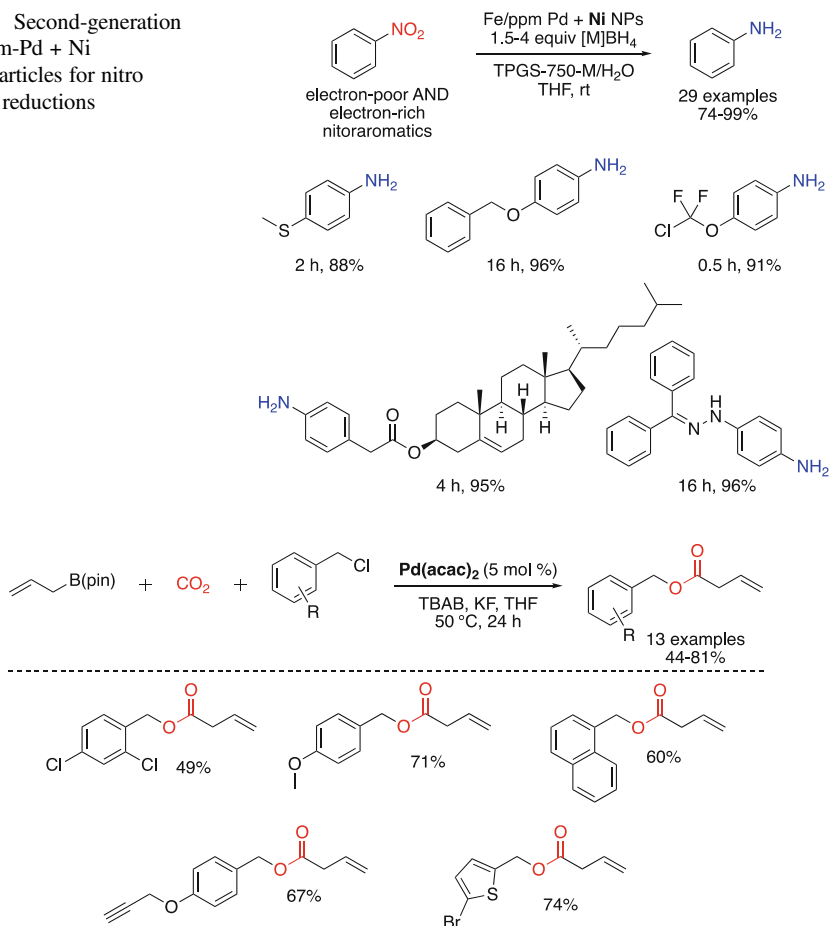


Fig. 6 Carboxylative Suzuki coupling reactions of benzylic chlorides with allyl borates catalyzed by palladium NPs

mild with low pressures of CO₂ compared to previous methods. Halogen atoms present on aromatic rings as part of the substrates were also unaffected, adding credence to the selectivity as well as allowing products to undergo further transformations. Electron-donating substituents on the benzene were also suitable. Thiophenes, likewise, participated in this chemistry, affording satisfactory yields.

Z-Selective semi-hydrogenations of alkynes (i.e., Lindlar reductions) have been reported using Pd NPs in water [21]. These time-honored reductions typically rely on Pd that has been “poisoned” by toxic lead and quinoline, thereby preventing over-reduction to the alkane. By contrast, this nanoparticle-nanomicelle system requires no such manipulation of the Pd catalyst. Key to the efficacy of this catalyst was the nature of both the Pd salt and the surfactant. Optimal results were achieved with 1 mol% Pd(OAc)₂, a 2 wt% solution of TPGS-750-M in water, and

pre-reduction of the Pd salt with 0.05 equivalents of NaBH_4 (followed by 0.35 equivalents for alkyne reduction). Cryo-TEM imaging of the catalyst solution revealed Pd nanoparticles (Fig. 7 – dark particles) surrounded by micellar aggregates (light gray particles). The catalyst could be generated in situ or stored for later use. Replacement of $\text{Pd}(\text{OAc})_2$ with PdCl_2 and use of alternative surfactant Brij 30 with $\text{Pd}(\text{OAc})_2$ both resulted in complete reduction to the alkane.

Of particular note is the excellent chemoselectivity associated with use of these NPs. Esters, ketones (in the presence of Pd), silyl protected alcohols, THP-protected alcohols, 1,4-unsaturated systems, Cbz-protected amines, and epoxides remained untouched during the reduction of the alkyne while proceeding in excellent isolated yields (>95%) and stereoselectivity (>95% *Z*) (Fig. 8). The catalyst and reaction medium could be effectively recycled five times without loss in efficiency. The E Factor determined for these conversions was only 3.4.

Fig. 7 Cryo-TEM image of Pd nanoparticles aggregated around nanomicelles in water

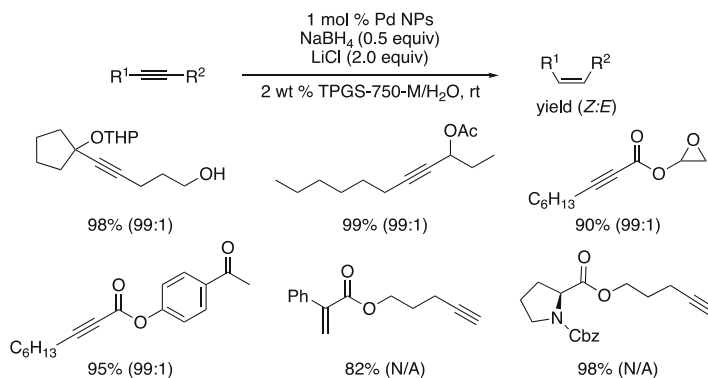
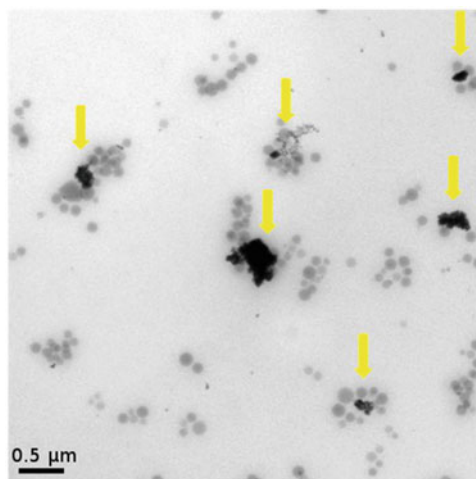


Fig. 8 Representative examples of Pd NP-catalyzed semi-hydrogenations

Roulland and coworkers [22] relied on palladium NPs for the stereo-retentive insertion of a methyl residue in their total synthesis of the aglycon of tiacumicin B. The NPs were generated in situ by mixing $\text{Pd}_2(\text{dba})_3$ with Grignard reagent MeMgBr (Fig. 9). While stereodefined, poly-substituted alkenes are found in a wide array of drug targets and natural products [23], most routes of entry rely on nickel to catalyze couplings with alkenyl halides. In the case of a bulky leaving group like a vinyl sulfide, use of Ni-mediated substitutions has been sparse due to their sensitivity to steric hindrance around the mercaptide moiety, as well as lack of stereo-control [22]. In this case, use of NPs derived from $\text{Pd}_2(\text{dba})_3$ in the absence of a phosphine ligand afforded the best yields. It was also noted that the vicinal unprotected hydroxyl group played an important role, potentially facilitating insertion of a Pd^0 species via chelation of magnesium between the alcoholate and the proximal sulfur atom, in turn activating the C-S bond. Transmission electron microscopy (TEM) confirmed the presence of NPs ranging from 1.5 to 2.0 nm in diameter. Reaction conditions were optimized at 1 mol% loading of palladium, since higher loadings (2.5 mol%) led to formation of undesired by-products and lower isolated yields.

Palladium nanoparticles have been used to catalyze couplings between aryllithium reagents and various aryl and heteroaryl bromides. Feringa and co-workers [24] generated these NPs in situ, and using molecular oxygen to form stable n^2 -peroxo complexes, they observed rapid conversions to the coupled products on timescales of 2–5 min. Via NMR studies of intermediates and TEM analysis of the reaction medium, rapid formation of palladium NPs was observed upon addition of the organolithium. The possibility that a monoligated palladium [Pd-PR_3] is the active catalytic species was excluded based on (a) the lack of

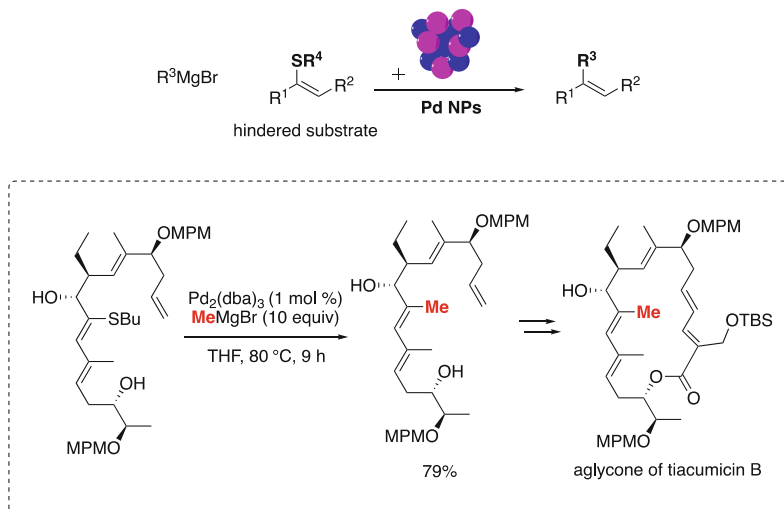


Fig. 9 Stereo-retentive cross-couplings of vinyl sulfides with Grignard reagents

reactivity with aryl chlorides, and (b) no inhibitory effect was observed from the addition of excess *t*-Bu₃P on the outcome of the cross-coupling products. Both electron-poor and electron-rich substrates gave good yields with high selectivities. The reaction proved to be selective toward aryl bromides, as aryl and benzylic chlorides present within the substrate remained untouched. Sensitive functional groups, including those bearing acidic protons, are unreactive, such as phenols, epoxides, and silyl protected pyrroles. This method was applied to time-sensitive reactions, such as synthesis of the [¹¹C]-labeled PET tracer celecoxib (Fig. 10). The expedient coupling of [¹¹C]-methyl lithium to the drug precursor greatly increases the yield of the overall reaction, given the low half-life of the alkyllithium reagent ($t_{1/2}({}^{11}\text{C}) = 20 \text{ min}$).

Wei and co-workers showcased the ability of Al(OH)₃-supported palladium NPs, generated in situ, to facilitate ligand and copper-free Sonogashira and Heck cross-coupling reactions (Fig. 11, left) [25]. In their studies, they noted that nanoparticles generated in situ showed higher reactivity than catalysts prepared via co-precipitation. For Sonogashira reactions, couplings proceeded best in DMSO with the addition of TBAB (tetrabutylammonium bromide). The Pd loading was quite low at 0.2 mol% (2,000 ppm). The base also played an important role in this chemistry, as NaOAc yielded the best results over more common bases such as K₂CO₃ and K₃PO₄. The reaction ran smoothly on a range of aryl and heteroaryl bromides, including pyridines, thiophenes, and quinolines. The scope of the alkyne, however, was limited to mostly phenylacetylenes among the examples screened.

Using the same NPs, Heck reactions were also investigated, in these cases using only a 0.1 mol% loading of palladium (Fig. 11, right) [25]. A solution of TBAB in DMF was the chosen reaction medium. Both electron-rich and electron-poor aryl bromides gave the desired product using the enoate of choice, butyl acrylate. Some aryl chlorides did undergo the coupling; however, the aryl ring present contained a strongly activating nitro group. For both reaction types, high

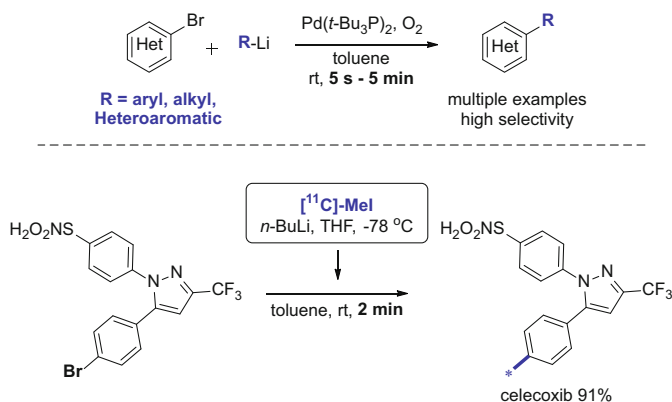


Fig. 10 Synthesis of radiolabeled celecoxib via a Pd NP-catalyzed coupling

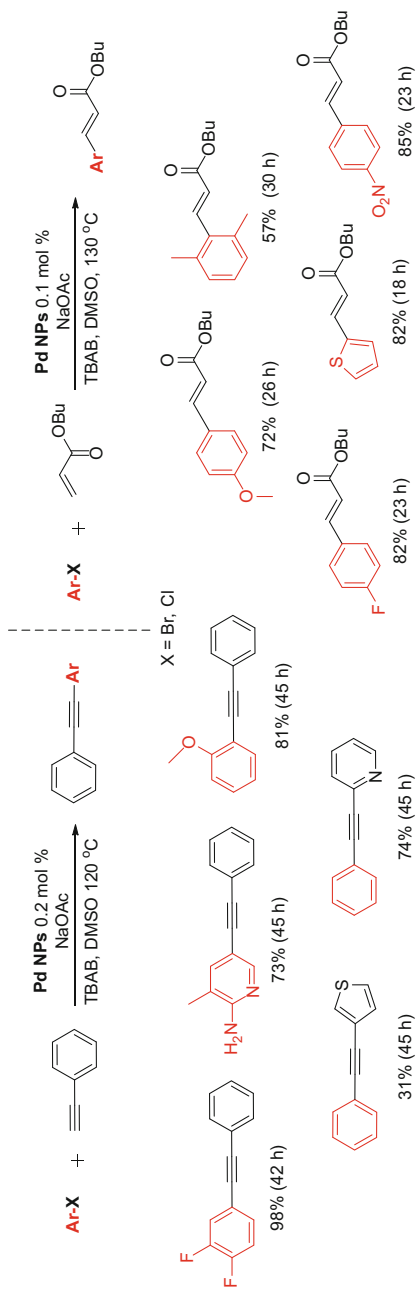


Fig. 11 Ligand and copper-free Pd NP-catalyzed Sonogashira and Heck cross-couplings

temperatures on the order of 130°C were needed. Nonetheless, the catalyst could be recovered and reused, as demonstrated for Sonogashira couplings. Membrane filtration led to catalyst recovery, which showed no apparent detriment to the yields after six consecutive cycles.

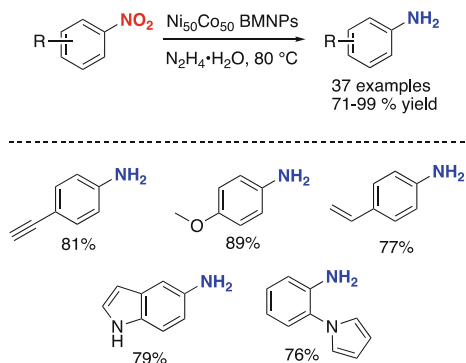
3 Nickel

There has been a significant increase in the use of nickel in synthesis over the past few decades. This can be attributed to the natural abundance of this metal which accounts for its low cost compared to that of other transition metals that are far more commonly used. Moreover, its ability to function in several oxidation states, as well as its increased nucleophilicity due to its size, has made it a desirable alternative, especially relative to palladium [26, 27]. Its place within the group 10 metals has enticed chemists to further investigate the ability of this base metal to facilitate valued organic transformations, including reductions and C-C bond formations. Substituting the more abundant nickel in reactions that mostly utilize palladium and platinum would reduce costs of various chemical processes, as well as open the door to new reactivities of the metal and its complexes.

As with palladium, use of heterogeneous nickel NPs for catalysis has gained interest for several good reasons. For example, the metal has been utilized with other metals to create bimetallic nanoparticles which appear to have a synergistic effect that can greatly contribute to the overall reactivity, as well as generality, of the reactions that it can catalyze (e.g., see Fig. 5; Fe/ppm Pd + Ni NPs).

Cai et al. introduced Ni-Co bimetallic nanoparticles (BMNPs) for chemoselective transfer hydrogenation of nitroarenes (Fig. 12) [28]. Their BMNPs were prepared in ethanol with a 1:1 mixture of nickel and cobalt salts and PVP as stabilizer. They noted that this was the ratio that afforded the best results under optimized conditions. Reduction of the metal salts to NPs with NaBH₄ under inert atmosphere was sufficient to form well-dispersed BMNPs with an average diameter of 2.5 nm, confirmed by TEM. The catalyst suspension was suitable for up to one week if stored

Fig. 12 Chemoselective reduction of nitroarenes by bimetallic Ni-Co NPs



under inert atmosphere. The bimetallic properties of these NPs also provided insight regarding their reactivity. They noted that the BMNPs are of a smaller particle size than the individual Ni and Co NPs, suggesting that greater surface area is available on which the reactions take place.

Hydrazine hydrate was chosen as the hydrogen donor en route to these BMNPs due to its ease of handling as well as the inert by-product formed after use. Temperature played a crucial role in this transformation; when run at 60°C, poor conversion was noted, while higher temperatures led to aggregation of the NPs resulting in reaction inhibition. A temperature of 70°C seemed to be the optimal compromise. Water or ethanol served as the reaction medium depending upon the solubility of the substrates. Electron-rich as well as electron-poor nitroarenes were smoothly converted to the corresponding amines. Halogenated anilines could also be obtained with no dehalogenation observed. Dinitro compounds were fully consumed to the desired diamine products upon addition of excess hydrazine hydrate. Most importantly, the nitro groups were reduced in the presence of olefins, alkynes, and nitrile groups indicative of the selectivity of this process. However, formyl substituents under the reaction conditions afforded the derived primary alcohol.

Preparation of Ni₅₀Co₅₀ BMNPs NiCl₂·6H₂O (0.5 mg), CoCl₂ (0.26 mg), and PVP (160 mg, average molecule weight = 40,000) were dissolved in ethanol (1.5 mL) and charged into a 10 mL reactor with a magnetic stirrer. Then, a freshly prepared ethanol solution of NaBH₄ (0.8 mg, in 0.5 mL in ethanol) was added into the reactor quickly under vigorous stirring (1,000 rpm) at rt. (25°C) under argon. The color of the colloidal mixture turned to black immediately which indicates that metal salts have been reduced to metal particles. The catalysts prepared were directly used for reactions, as overexposure of catalysts containing Ni to air will result in significantly decreased activity due to oxidation.

Typical Procedure Hydrazine hydrate (4 equiv) was added into the reactor which contains freshly prepared catalyst, as described above. Then, the reactor was placed into a pre-heated oil bath with a stirring speed of 500 rpm, and the substrate (1 mmol) dissolved in 1 mL ethanol was added dropwise under argon. The reactions were monitored by TLC. After the reaction, the mixture was vacuum filtered through a pad of silica on a glass-fritted funnel, and an additional 15 mL of EtOAc (5 mL portions) was used to rinse the product from the silica. The filtrate was concentrated in vacuo and analyzed by GC. Products were purified by column chromatography and identified by ¹H NMR and ¹³C NMR.

Although reductive amination via metal hydrides or catalytic hydrogenation has long been reported [29], uses of hydrogen transfer to facilitate the reaction are sparse in the literature and often employ hydrazine or borohydride as the hydrogen source. However, Yus and co-workers reported that Ni NPs can catalyze reductive amination of aldehydes by hydrogen transfer using a relatively environmentally benign 2-propanol as both solvent and reductant in the absence of base (Fig. 13) [30]. Their nanoparticles were prepared by mixing anhydrous

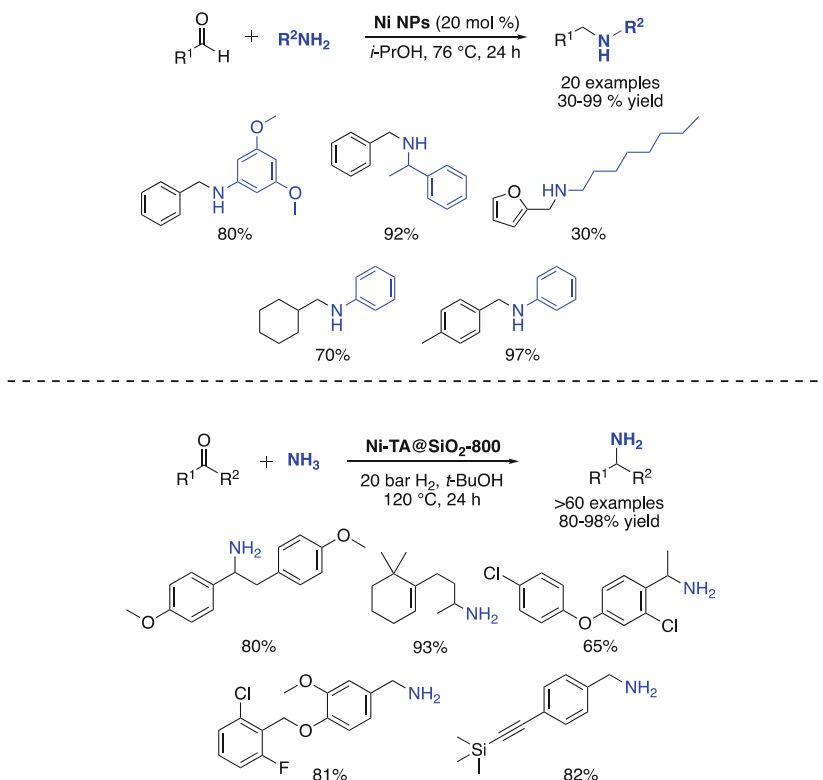


Fig. 13 Nickel NP-catalyzed reductive aminations of aldehydes

nickel(II) chloride with lithium powder and a catalytic amount of DTBB (5 mol%) in THF, which yielded NPs with an average diameter of 2.5 nm.

Reactions of benzaldehydes with primary amines and anilines smoothly afforded the desired benzylic amines under these conditions. *N*-Benzylamines, as well as *ortho*-, *meta*-, and *para*-substituted anilines, were easily obtained. Alkylamines also efficiently participated in this reaction, although phenethylamine exhibited reduced reactivity affording the corresponding product in modest yield. Substituted benzaldehydes, especially with an electron-donating component, also led to diminished yields. Advantages of this methodology include the avoidance of step-wise, preformation of the imine, as well as the source of hydrogen being both inexpensive and environmentally friendly (i.e., isopropanol). Recently, Jagadeesh and coworkers documented the scope of nickel NPs generated in situ for reductive amination [31]. Their method also allows for a range of ketones to undergo this transformation. Although their substrate scope is far more expansive in terms of complexity, the reaction requires high pressures of hydrogen as the donor and temperatures upward of 120°C.

Adholeya et al. showcased a magnetically recoverable, silica-based nickel catalyst, *Ni-TC@ASMNPs*, that could be used to catalyze Suzuki-Miyaura cross-coupling reactions [32]. The NPs were prepared via co-precipitation; iron salts were initially combined with ammonium hydroxide. Then, a coating of silica was applied in order to inhibit the aggregation of the NPs. The silica-coated NPs were then further functionalized with an NH_2 linker to provide the solid support. Finally, the material was stirred in a solution of $\text{NiCl}_2 \cdot 6\text{H}_2\text{O}$ to form the Ni NPs which were easily separated using a magnet. Their analysis by TEM indicated an average diameter of 10–12 nm.

Upon optimization of these couplings, it was found that dioxane was the preferred solvent. K_3PO_4 was utilized as base, being far superior to other bases tested. Reaction temperatures lower than 100°C led to longer reaction times. The presence of PPh_3 was essential, as no reaction occurred in the absence of this ligand. It was postulated that the ligand may be stabilizing $\text{Ni}(0)$ prior to oxidative addition. A range of aryl halides and pseudo-halides (Br, Cl, I, OTs) were all amenable to this transformation (Fig. 14). Aryl bromides were able to smoothly couple in good-to-excellent yields regardless of the electronic properties of the ring. Due to the magnetic properties of the NPs, the nickel catalyst could be cleanly separated from the reaction mixture using a permanent magnet. The same catalyst could be recycled for six subsequent reactions without noticeable loss of activity, as well as with negligible leaching of nickel.

Preparation of Catalyst *Ni-TC@ASMNPs* $\text{Fe}_2(\text{SO}_4)_3$ (6.0 g) and FeSO_4 (4.2 g) were dissolved in 250 mL of water and stirred at 60°C to give a yellowish orange solution. NH_4OH solution (25%, 15 mL) was added into the solution with vigorous stirring, and the color of the bulk solution turned black. Stirring was continued for another 30 min, and the precipitated MNPs were separated using an external magnet and washed several times with deionized water and ethanol.

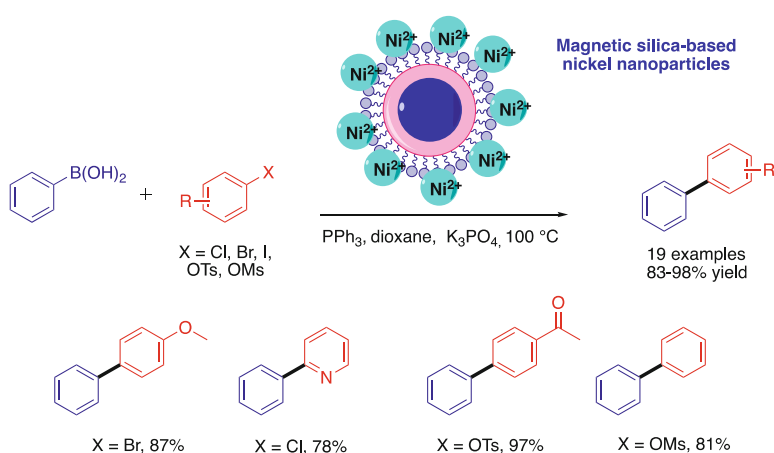


Fig. 14 Nickel-catalyzed Suzuki-Miyaura cross-couplings

Silica coating over these MNPs was achieved via a sol-gel approach. A dispersed solution of 5.0 g of activated MNPs with 0.1 M HCl (2.2 mL) in 200 mL of ethanol and 50 mL of water was obtained via sonication. Then, 5 mL of 25% NH₄OH solution was added to the suspension at rt., followed by the addition of 1 mL of TEOS, and the solution was kept under constant stirring at 60°C for 6 h. The obtained SMNPs were magnetically separated, washed with ethanol, and dried under vacuum. The obtained SMNPs were further functionalized using APTES to afford ASMNPs. This was done by adding APTES to a dispersed solution of 0.1 g of SMNP in 100 mL of ethanol under sonication, and the resulting mixture was stirred at 50°C for 6 h. For covalent grafting of the ligand on SMNPs, 1 g of ASMNP was refluxed with TC in dried methanol along with molecular sieves at 70°C for 3 h. The obtained product was washed with methanol and dried under vacuum. Finally, 1 g of grafted TC@ASMNPs was stirred with a solution of 4 mmol of NiCl₂·6H₂O in methanol for 3 h. The resulting Ni-TC@ASMNPs were separated magnetically and thoroughly washed with deionized water and dried under vacuum.

Representative Procedure for Cross-Couplings Catalyst Ni-TC@ASMNP (15 mg) was placed into an oven-dried round-bottom flask, and PPh₃ (20 mol%), aryl halide (0.5 mmol), and phenylboronic acid (0.6 mmol) were added. After this, K₃PO₄ (0.75 mmol) was added, followed by the addition of 1 mL of dioxane. The reaction mixture was kept under a N₂ atmosphere and was stirred at 100°C until completion of the reaction. The catalyst was recovered using a permanent magnet. The reaction was monitored by TLC, and the products were extracted using EtOAc, dried over sodium sulfate, concentrated under reduced pressure, and analyzed by GC-MS.

In 2015, Lipshutz et al. introduced a new nickel nanoparticle catalyst for mild and efficient Suzuki-Miyaura couplings in micellar media. This catalyst was formed by the addition of one equivalent of MeMgBr to NiCl₂ ligated by either dppf or dipf [33]. Cryo-TEM imaging of the NPs revealed needle-like particles situated in and around nanomicelles of TPGS-750-M (Fig. 15). It was postulated that the efficacy of these particles under the mild reaction conditions (22–45°C and 0.35 equiv. K₃PO₄) could be due to the close proximity of

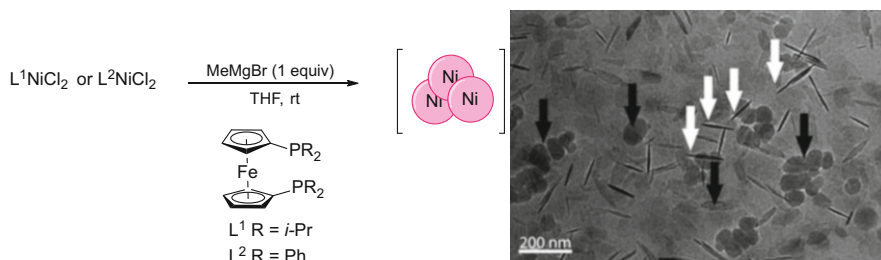


Fig. 15 Synthesis of Ni nanoparticles (left). Rod-shaped Ni nanoparticles and spherical TPGS-750-M nanomicelles (right)

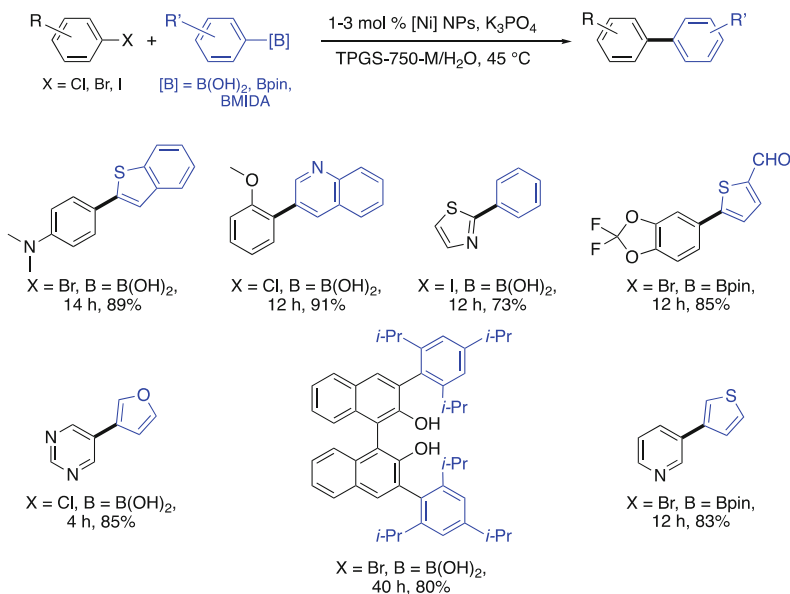


Fig. 16 Representative biaryl products prepared using Ni NPs

each type of nanoparticle, where the nanomicelles delivered relatively high local concentrations of educt to the metal NP catalyst. Counterintuitively, arylboronic esters (Bpin) were more reactive, only requiring 22 °C vs 45 °C for the corresponding boronic acids. The expansive substrate scope contains a wide variety of electron-rich and electron-poor aryl and heteroaryl chlorides, bromides, while the boron-containing partners included boronic acids, Bpin, and BMIDA derivatives, resulting in good-to-excellent isolated yields of products (Fig. 16). The aqueous reaction medium could be recycled six times while maintaining yields >94% (albeit with additional catalyst required) and an E Factor of only 3.8.

4 Platinum

Platinum is yet another metal that has played a crucial role in catalysis. Its use in a wide array of hydrogenation reactions as well as its applications toward various catalytic processes in the industrial setting cannot be overstated. Being the rarest of the group 10 metals, reduction in the amount of platinum utilized in chemical processes needs to be addressed. Hence, platinum nanoparticles may play a major role in addressing both the cost and endangered metal status. Bimetallic nanoparticles containing Pt have already been shown to have remarkable catalytic activity in a wide array of transformations, and further investigation into the use of Pt NPs in heterogeneous catalysis may advance their utility in organic synthesis [34].

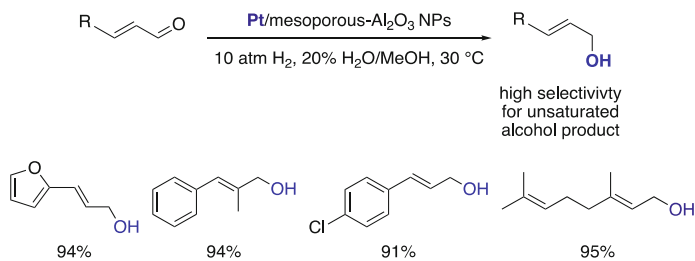


Fig. 17 Selective hydrogenation of enals

Han and co-workers utilized Pt nanoparticles immobilized on a nonporous Al_2O_3 support stabilized by aspartic acid for the selective hydrogenation of unsaturated aldehydes to allylic alcohols at room temperature (Fig. 17) [35]. Upon centrifugation of the reaction medium, the catalyst could also be recycled up to five times without noticeable decline in activity. Both the presence of aspartic acid and the nonporous properties of the support played key roles in enhancing catalyst reactivity. The aspartic acid not only inhibits formation of aggregates but also aided in the observed chemoselectivity of hydrogenation, reducing only the aldehyde over the olefin attributed to steric hindrance. The average size of the NPs according to TEM analysis was ca. 4 nm. The amount of platinum embedded in the nanoparticles, analyzed via a chemisorption method, was 0.68%.

Reaction conditions involved an atmospheric pressure of hydrogen, along with a 20% mixture of water in methanol over a ca. 3 h period. The catalyst, 30 mg, was employed for a 1 mmol scale reaction of aldehyde. Aliphatic and aromatic substrates tolerate these conditions. The reaction proceeded with selectivity of over 90% producing the unsaturated alcohol among the various substrates examined.

Like nickel, platinum, as one metal within a bimetallic NP, seems to exhibit both higher reactivity and stability as compared to the reactivity of the monometal nanoparticle counterpart. This was illustrated by work from Lee and co-workers in which they performed silylations of aryl halides catalyzed by magnetically recyclable bimetallic Pd/Pt Fe_3O_4 nanoparticles (Fig. 18) [36]. Classical introduction of the silyl moiety into organic molecules typically relies on either organolithium reagents or a Grignard reagent together with a silicon-based electrophile. This approach can be of limited scope due to base-sensitive functional groups that may be present in the molecule of interest [37, 38]. These bimetallic NPs were synthesized through a solution phase reduction process [39] that is often employed in the making of a wide array of NPs. In this case, the catalyst was composed of 4.10 wt% Pd and 9.60 wt% Pt, determined via plasma atomic emission spectroscopy.

Conditions for these silylations relied on NMP as solvent and diisopropylethylamine as base at 70°C , yielding the best results after optimization. Substrates well-suited for this method typically contained an electron-withdrawing component, as electron-rich substrates tested on both aryl iodides and bromides gave poor yields. Primarily alkylsilanes, such as triethyl- and trihexylsilane, converted smoothly to silylated aromatics in most cases, while diphenylmethylsilane led to

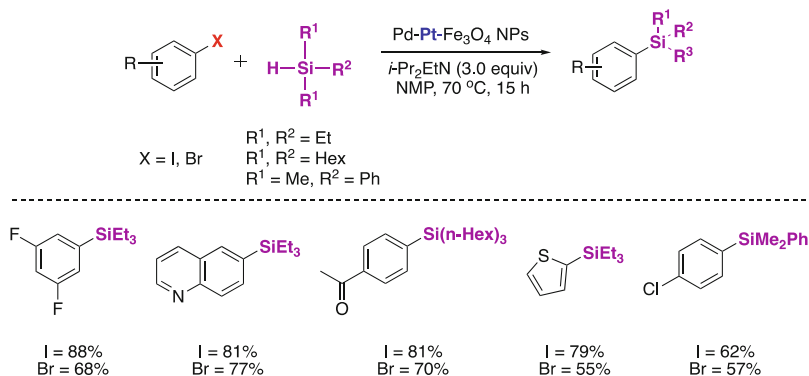


Fig. 18 Silylation of aryl halides

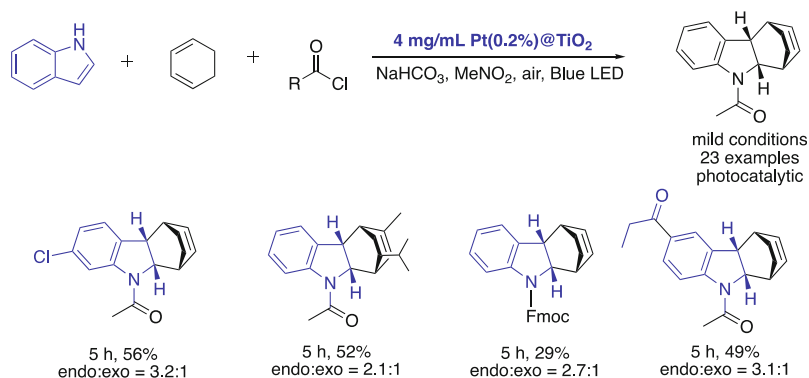


Fig. 19 Photocatalytic indole Diels-Alder cycloadditions

somewhat lower yields. With the use of a magnet, the nanoparticles could be recovered and recycled up to 20 times. It was estimated that an average of only 0.03% Pd and 0.08% Pt was lost with each recycle. Control studies with the Pd-Fe₃O₄ and Pt-Fe₃O₄ NPs showed a dramatic decrease in the rates of these reactions, as well as the amount of metal lost after each recycle (0.26% Pd and 0.55% Pt liberated), indicating the increased stability and reactivity of this bimetallic system.

Photoredox catalysis used in tandem with bimetallic NPs was studied by Tehshik et al., focused on radical cation Diels-Alder reactions of indoles [40]. Although photooxidation of indoles is well established, the common use of harsh UV irradiation can limit the reaction's scope due to functional group compatibility issues. They postulated that the use of a heterogeneous catalytic system might overcome some of these limitations, as well as introduce recyclability. Thus, the combination of a Pt(0.2%)@TiO₂ NP system together with visible light irradiation (with a 10 W blue LED) promoted generation of the desired tetrahydrocarbazoles (Fig. 19).

The presence of an acyl trapping agent was crucial, since the unprotected cycloadduct can rapidly trigger oxidative fragmentation to undesired products. Other protecting groups including Boc and Fmoc were examined, but they resulted in diminished yields. The Pt in the system was proposed to inhibit back electron transfer to the indole by acting as an electron sponge, resulting in a more efficient catalytic system. The reaction tolerates a wide range of electron-donating or electron-withdrawing functionality at the C5 and C6 positions of the indole ring. Halides, as well as a pinacolboron group, were also unreactive, opening the door to further functionalization of the cycloaddition product. It was observed that nitro- and azaindoles did not participate in this reaction. Centrifugation could be used to separate catalyst from reaction mixture, whereupon its drying under vacuum allowed for reuse in subsequent reactions. However, loss in activity was observed, most likely due to poisoning by the indole derivatives.

5 Copper

Opportunities to apply relatively inexpensive organocopper chemistry [41] in the form of nanoparticles as catalysts have also been the focus of several recent investigations. Significant efforts have been dedicated to improving the efficiency of copper located within NPs, notably toward reducing metal loading ($\leq 1,000$ ppm) as well as developing an alternative to more toxic and/or precious metals. One driving force behind reducing the loading of copper can be seen in the case of biologically relevant couplings, such as the copper(I)-catalyzed alkyne-azide cycloaddition (CuAAC) or other click reactions, where excess metal may interfere with applications of the triazole products. Additionally, valuable transformations such as C-C or C-heteroatom formation as well as reduction [41] or oxidation [42] processes have been reported.

Historically, alkyne-azide cycloaddition (AAC) reactions usually lead to mixtures of 1,4- and 1,5-disubstituted triazoles. Work by Sharpless and Meldal, in 2002 [43, 44], highlighted the positive impact of adding Cu(I) to the pot, leading to regiocontrol strongly favoring the 1,4-isomer. In this regard, the emergence of CuNPs as recoverable and recyclable catalysts has begun to address the sustainability aspects of this important reaction. Radivoy et al. described both unsupported and supported CuNPs for the CuAAC reaction [45]. In the case of unsupported CuNPs, despite superior activities compared to commercial copper catalysts, the NPs had the tendency to dissolve under optimal conditions, posing a problem for recycling and residual metal to be found in the final product [46]. Later, the same group reported on supported NPs, using carbon or MagSilica. Isolation and manipulation of the organic azide needed for the Cu-catalyzed AAC could be avoided by its in situ generation via a multicomponent process from anilines, aryldiazonium salts, alkenes [47], epoxides [48], or halides [49]. Thus, both waste reduction and safer processes were achieved. Simultaneously, the CuAAC reaction could be effected in the presence of 0.5–5 mol% of CuNPs on carbon or MagSilica at 70°C in water or acetonitrile [50]. Applications of

the silica-coated maghemite (CuNPs/MagSilica) to homocoupling of terminal alkynes, as well as three-component reactions to arrive at propargylamines from aldehydes, amines, and terminal alkynes (A^3 coupling), have also been studied (Fig. 20) [49].

Astruc et al. reported PEG-2000-stabilized copper NPs [51], the formation of which required reduction of $\text{CuSO}_4 \cdot 5\text{H}_2\text{O}$ using sodium naphthalenide in acetonitrile, followed by an aqueous DCM extraction resulting in pure, stabilized copper nanoparticles (designated as Cu(0)NP-PEG). Interestingly, UV detection of the catalyst after brief exposure to air showed the formation of Cu_2O on the surface of the catalyst (designated Cu(I)NP-PEG). The activity of the three catalysts, the unpurified catalyst (Cu(0)-PEG-1), Cu(0)-PEG, and Cu(I)NP-PEG, was then used in water in a model reaction between phenylacetylene and benzyl azide at room temperature. At 50 ppm copper, a significant increase in conversion is seen using Cu(I)NP-PEG relative to that using purified Cu(0)-PEG (32%) air-free catalyst, or relative to the conversion noted using oxidized Cu(I)NP-PEG (75%). The unpurified catalyst afforded only traces of the product. Furthermore, increasing the catalyst loading of Cu(I)NP-PEG from 50 to 100 ppm resulted in 100% conversion and 97% isolated yield of the desired click product. By immobilizing the optimal oxidized catalyst onto a mesoporous type of silica (SBA-15) as solid support, syntheses of three bioactive molecules requiring only 1,000 ppm of Cu catalyst could be accomplished (Fig. 21). No leaching was detected at 50°C using a 1:1 H_2O to *t*-BuOH mixture as solvent.

In 2017, Lipshutz et al. developed a novel nanoparticle catalyst for click chemistry [52], prepared using 1,000 ppm of a Cu(I) salt in place of Pd in the Fe NPs previously described [14]. A wide variety of benzyl and alkyl azide/alkyne combinations were efficiently cyclized at room temperature. The use of 2 wt% TPGS-750-M in water facilitated the reaction of even highly water-insoluble alkynes such as those derived from α -tocopherol (84%) and solanesol (88%; Fig. 22). The active catalyst is bench-stable when stored in an aqueous medium containing ascorbic acid.

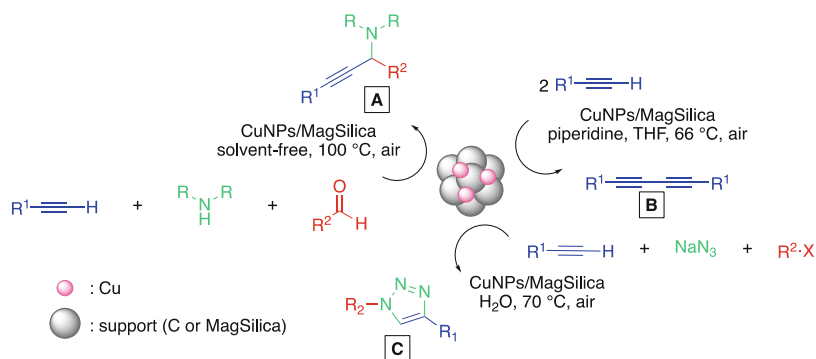


Fig. 20 CuNPs/support applied to a three-component reaction (a), an alkyne homocoupling (b), and a Cu-catalyzed AAC reaction (c)

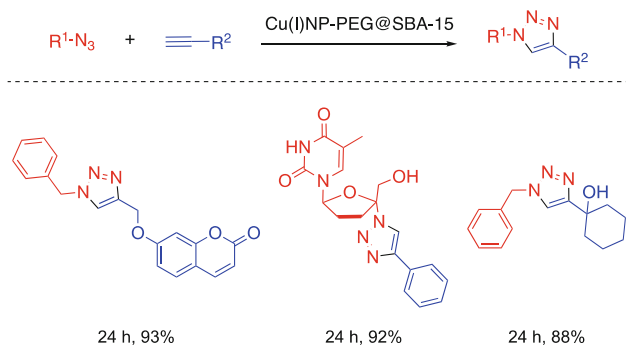
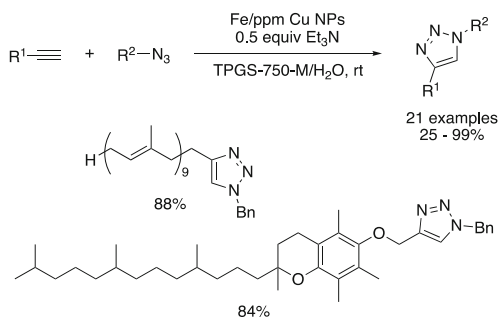


Fig. 21 ppm level of PEG-2000-stabilized CuNPs for CuAAC reactions

Fig. 22 CuAAC reactions using Fe/ppm CuNPs



Preparation of Fe/ppm Cu Nanoparticles In a tared, flame-dried two-neck round-bottomed flask, anhydrous pure $FeCl_3$ (121.7 mg, 0.75 mmol) and $CuOAc$ (1.839 mg, 0.015 mmol) were placed under an atmosphere of dry argon. The flask was closed with a septum, and dry THF (10 mL) was added. The reaction mixture was stirred for 10 min at rt. While maintaining a dry atmosphere at rt., $MeMgCl$ (2.25 mL, 1.125 mmol; 0.5 M solution) in THF was very slowly (1 drop/2 s) added to the reaction mixture. After complete addition of the Grignard reagent, the reaction mixture was stirred for an additional 30 min at rt. An appearance of a dark brown coloration was indicative of generation of nanomaterial. The stir bar was removed, and THF was evaporated under reduced pressure at rt. followed by washing the mixture with dry pentane to provide a light brown-colored nanopowder. The nanomaterial was dried under reduced pressure at rt. for 10 min (603 mg) and could then be used directly for CuAAC reactions under micellar conditions. Dividing the starting mass of $CuOAc$ by the final weight in the flask yields $CuOAc$ concentration in the isolated catalyst: $1.839\ mg\ CuOAc/603\ mg\ NPs = 0.305\ mg\ CuOAc/100\ mg\ NPs$ which equates to 0.061 mg (1,000 ppm Cu for 0.5 mmol substrate)/20 mg NPs.

General Procedure for CuAAC Reactions In a flame-dried 10 mL microwave reaction vial, $FeCl_3$ (4.1 mg, 5 mol%) was added under anhydrous conditions. The reaction vial was closed with a rubber septum, and the mixture was evacuated

and backfilled with argon three times. Dry THF (0.7 mL) and CuOAc in THF (0.061 mL, 1,000 ppm; 1 g/L) were added to the vial, and the mixture was stirred for 10 min at rt., after which MeMgCl in THF (0.75 mL, 7.5 mol%; 0.5 M) was added to the reaction mixture. While maintaining an inert atmosphere, THF was evaporated under reduced pressure. An aqueous solution of 2 wt% TPGS-750-M (1.0 mL) was then added to the vial followed by sequential addition of alkyne (0.5 mmol), azide (0.6 mmol, 1.2 equiv), and triethylamine (0.0349 mL, 0.25 mmol, 0.5 equiv). The mixture was stirred vigorously at rt. After complete consumption of starting material, as monitored by TLC or GC-MS, EtOAc (1 mL) was added to the reaction mixture, which was then stirred gently for 5 min (NOTE: vigorous stirring or shaking in the reaction flask or in a separatory funnel during the extraction process resulted in the formation of an intractable emulsion with consequent reductions in isolated yields). Stirring was stopped, and the organic layer was separated with the aid of a centrifuge. The organic layer was removed, and the extraction process was repeated two additional times. The combined organic layers were dried over anhydrous magnesium or sodium sulfate or flushed through a plug of dried silica gel. The solvent was then evacuated under reduced pressure to obtain crude material which was purified by flash chromatography over silica gel using EtOAc/hexanes as eluent.

Among the virtues associated with supported NPs is their assumed re-isolation and reuse once a reaction is complete, indicative of a greener and potentially sustainable process. However, their small size may, upon filtration, block the filter pores or may not be retained at all. Magnetic separation of an active core catalyst dispersed onto a ferromagnetic surface may solve this problem. In this scenario, the nanoparticle catalyst would be simply retained on a magnet, while the bulk product mixture is separated from the system.

In that vein, Hosseini and co-workers reported the use of silica-coated Fe₃O₄ NPs applied to click chemistry [53]. The surface of the stabilized NPs was modified with a polymer [3-(trimethoxysilyl)propylmethacrylate/ILs] matrix for immobilization of copper sulfate. The cycloaddition between azides and alkynes was performed with only 0.2 mol% of catalyst, in water at room temperature affording products with yields typically surpassing 82% (Fig. 23).

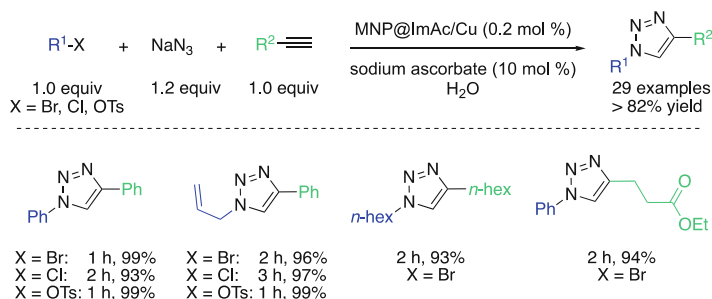


Fig. 23 Copper-loaded polymeric magnetic nanocatalysts for CuAAC reactions

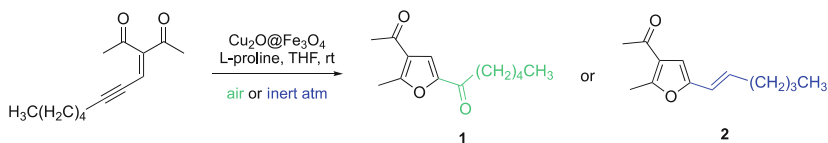


Fig. 24 Rearrangement of a diketoenyne catalyzed by magnetic CuNPs

Further advancement of related NP technology has been pursued by Liu et al. recently using magnetic, iron-supported cupric oxide nanoparticles for rearrangements of a diketoenyne to substituted furans [54]. They began by testing an array of copper (II) salts dispersed onto Fe_3O_4 as support, finding that Cu_2O led to the most active catalyst for the formation of diketofuran **1**. Further optimization using additives such as L-proline and solvent such as THF resulted in formation of the intended product **1**, along with side product **2**. Interestingly, they discovered that the atmosphere of the reaction played a crucial role: running the reaction under air resulted in the highest yield (88%) of **1**, while using an inert atmosphere afforded the highest yield of **2** (89%) (Fig. 24).

Evaluation of substrate scope for both types of optimized domino processes leading to furans indicated that high yields are formed in general, in reactions leading to *bis*-keto products **1** (78–87%), while keto-olefin products **2** formed in yields ranging from 41 to 87%. In terms of NP recovery, the catalyst was found to be deposited onto the magnetic stir bar leading to 99% recovery. Remarkably, the recovered catalyst could be reused eight more times, resulting in only a modest drop in yield of **1** under standard conditions to 72%. The results of this report, as well as those from others pursuing similar magnetic NP technology, provide industrially interesting prospects at the process level due to these facile, economical, and “green” methods that have been developed of late.

Mesoporous polymers (MP) have also attracted a lot of attention due to their large surface area and their high stability to acidic and basic conditions. Zhang et al. described a green synthesis of mesoporous polymer-supported CuNPs and their applications to a Sonogashira-like reaction between acyl chlorides and terminal alkynes [55]. These NPs were obtained via melt infiltration of copper nitrate hydrates into a phenol-formaldehyde polymer, followed by a pyrolysis-induced reduction of Cu(II) ions. Subsequent use of a capping agent or additional reduction process was not needed. This catalyst was used for the synthesis of seven alkynes under mild conditions (solvent-free, 40°C) with good-to-excellent yields (71–99%; Fig. 25). The coupling provides access to ynones, a structural array found in several natural products. The material can be recycled at least six times with no decrease of reactivity. ICP analysis revealed that only 0.17% Cu had leached from the catalyst after ten cycles, making it a good candidate for pharmaceutical applications.

CuNPs have also been utilized for reduction processes. Notably, the original work from Zamani et al. involved use of renewable and low-cost biomass containing cellulose and lignin as the support. Indeed, crushed walnut shells have been used to support and stabilize the metal (Fig. 26) [41].

Fig. 25 Sonogashira-like reaction catalyzed by CuNPs supported on a mesoporous polymer

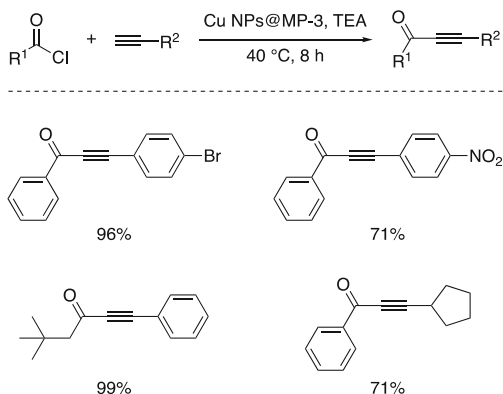


Fig. 26 Copper nanoparticles on walnut shell for reduction reactions

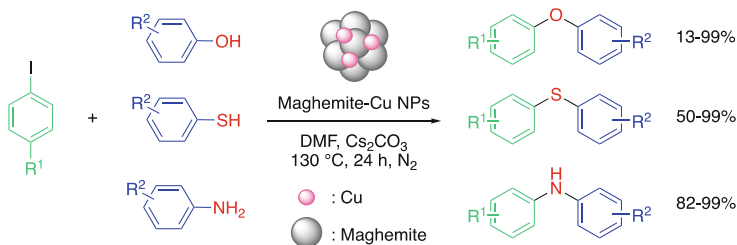
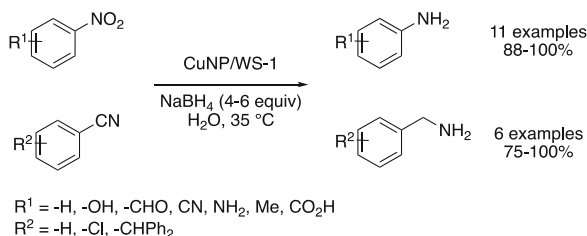


Fig. 27 C-Heteroatom bond formation with Cu-maghemite NPs

Gawande et al. reported the use of magnetic CuNPs for various C-heteroatom bond constructions [56]. Copper was uniformly dispersed on the surface of maghemite thereby gaining access to new C-O, C-S, and C-N bonds in moderate-to-excellent yields despite high temperatures and catalyst loadings (~3–6 mol%). These NPs could be recovered magnetically, washed with ethanol, dried at 60 °C under vacuum, and then reused six times with unaltered efficiency (Fig. 27).

One-pot, multicomponent reactions (MCRs) are of great industrial importance, offering expeditious routes toward complicated target molecules, as illustrated by Ugi [57, 58], Passerini [59], Biginelli [60, 61], and others. The processes involved usually enjoy the benefits of environmental friendliness, as the number of downstream processing and purification steps is typically significantly reduced.

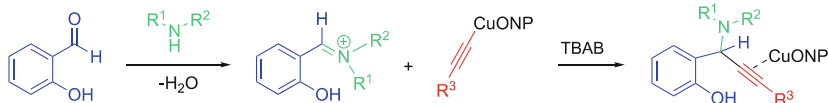


Fig. 28 Reaction between 2-hydroxybenzaldehyde, a secondary amine, and an alkyne catalyzed by Cu(I) oxide NPs

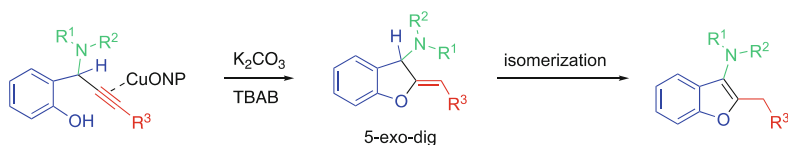


Fig. 29 Solvent-free synthesis of substituted benzofurans catalyzed by Cu(I) oxide NPs

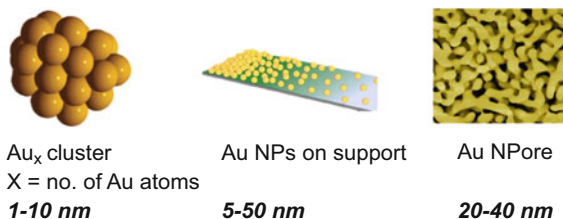
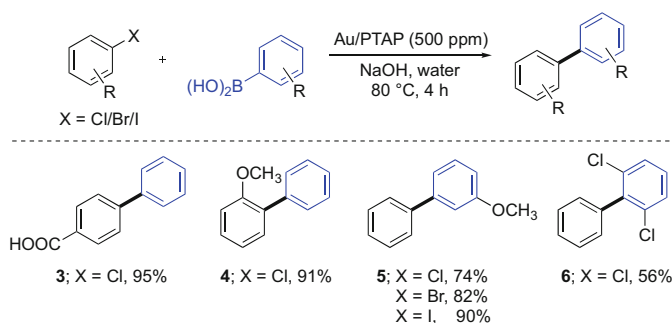
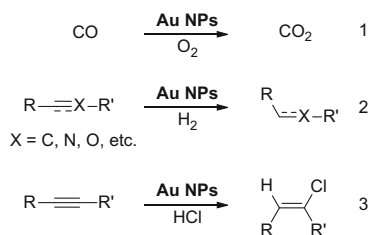
Therefore, the combination of both MCR and non-noble nanoparticle catalysis, as well as neat reaction conditions, represents a synthetic strategy as a means to “green-up” an approach to functionalized, complex cores. A recent example of the combination of MCR and copper(I) oxide NPs was described by Sharghi et al. for construction of functionalized benzofurans [62]. This involved a three-step, one-pot process, wherein a secondary amine condenses onto a salicylaldehyde, forming an iminium intermediate in the presence of tetra-*n*-butylammonium bromide (TBAB), followed by 1,2-addition of a copper-(NP)-acetylide to form the corresponding tertiary amine (Fig. 28).

Key to this sequence is the combination of the deprotonation of the phenol along with activation of the alkyne by the copper nanoparticles. Subsequent 5-*exo-dig* cyclization affords the immediate precursor to the final aromatic benzofuran product (Fig. 29).

Optimization of the catalyst for this transformation led to copper(I) NPs as the best source of copper, compared to copper(II) salts. The nanoparticles were then prepared using a route developed by Tang et al. [63, 64]. Screening solvents showed that the reaction run neat at 100°C gave the best result for the cyclized product (91% yield) in less than 2 h. Recycling of these nanoparticles for the same reaction reduced efficiency in product formation by only 8% after five consecutive runs (90% yield for the first run, 82% for the fifth run). Analysis of the catalyst showed loss of copper of 7% after five runs. Ultimately, this reaction provides an example of the combination of two “green” technologies: multicomponent reactions and low-cost copper NP catalysis.

6 Gold

Heterogeneous gold catalysts as used in organic synthesis have appeared in three main forms (Fig. 30). These are not only different in appearance and reactivity but also in their preparation. The first two, metal clusters and Au NPs on a

Fig. 30 Heterogeneous gold catalysts**Fig. 31** Heterogeneous gold catalysis**Fig. 32** Heterogeneous gold catalysis

support, are prepared from metal salts, while the third is prepared essentially from bulk gold possessing silver or other less noble metal impurities [64, 65].

The most notable applications of gold catalysis were mainly based on fundamental reactions (Fig. 31), such as CO oxidation (Eq. 1) [66, 67], hydrogenation (Eq. 2) [68–71], and hydrochlorination of alkynes (Eq. 3) [72]. These heterogeneous reactions have been widely investigated and reviewed over time. What has been most intriguing of late, however, is how gold NPs function as an alternative to copper, palladium, or other transition metals for C-C and C-N couplings, in addition to other complex catalytic reactions (vide infra).

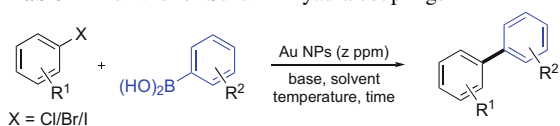
Suzuki-Miyaura (SM) coupling reactions are highly dominated by palladium catalysts, attributed to the extensive work done on fine-tuning of ligands that allows for couplings of even especially challenging reaction partners. On the other hand, gold has only recently been introduced for this purpose by Guo et al. [73] who reported the first gold nanoparticle-mediated SM couplings of aryl halides (chlorides, bromides, and iodides) with boronic acids (Fig. 32). Nanoparticles

of ca. 1 nm in size were supported or stabilized by polyaminothiophenol (PTAP) and were easily prepared by mixing the appropriate precursors. Reactions could be performed in water using only 500 ppm of gold catalyst, albeit at 80°C. Although trace amounts of gold were leached into the solution leading to debate regarding the homo- vs. heterogeneity of the reaction, the catalyst was recycled six times without noticeable differences in chemical yield. The chemistry can be done with electron-poor (**3**) or electron-rich (**4**) chlorides. The normal reactivity trend of I > Br > Cl was also followed to arrive at product **5**. A bulky, *di-ortho*-halo-substituted boronic acid also gave product (**6**), although in this case the yield was modest. The size of gold NPs has considerable effect on the reactivity, where 5 nm gold particles led to only trace amounts (ca. 10%) of product.

Preparation of the Polymer-Supported Au Catalyst 2-Aminothiophenol (100.0 mg, 0.4 mmol) was dispersed in aqueous HCl solution (1.0 M, 20 mL) with magnetic stirring at rt. for 1 h to obtain a uniform solution. After that, the mixture was maintained at 20°C for 0.5 h before oxidative polymerization. Then, a quantitative amount of an aqueous HAuCl₄ solution (0.1 M) was added to the above mixture in one portion. The resulting solution was stirred for another 0.5 min to ensure complete mixing, and then the reaction was allowed to proceed with agitation for 24 h at 20°C. Finally, the product was washed with deionized water until the filtrate became colorless and then dried under vacuum at 60°C for 24 h.

General Procedure for Suzuki-Miyaura Cross-Coupling The aryl halide (225.0 mg, 2.0 mmol), phenylboronic acid (292.6 mg, 2.4 mmol), and NaOH (320.0 mg, 8.0 mmol) were added to 40 mL of deionized water. The solution was stirred at 80°C until the chemicals were completely dissolved. Then, an aqueous solution of the Au catalyst (1.0 mM, 1.0 mL, 0.05 mol%) was added to the stirred solution in one portion, and the reaction mixture was stirred for another 4 h at this temperature. After the mixture had cooled to rt., the organic product was extracted with Et₂O (3 × 20 mL). The organic layer was dried with anhydrous Na₂SO₄. After filtration, all volatiles were removed under reduced pressure to yield the final product.

Following this initial discovery, applications of Au NPs toward SM couplings have gained attention from the synthetic community (Table 1). In this context, Corma, Garcia, and co-workers [74] used Au-platelets grafted on graphene (Au/*fl*-G) for SM couplings of aryl halides with phenylboronic acid in water (entry 1). Interesting is the reactivity of aryl halides in the order of Cl > Br > I, which is contrary to expectations based on C-X bond strength. DFT calculations suggested that such reactivity could be observed due to a poisoning effect of halide on gold, with iodide having a greater effect than bromide and much higher than chloride. Thomas et al. [75] prepared a composite of gold NPs with strontium, cross-linked alginate carboxymethyl cellulose, and graphene oxide (Sr/Alg/CMC/GO/Au) and utilized 50 ppm of this catalyst for SM couplings of chlorobenzene with phenylboronic acid in water at 80°C, leading to a 76% yield of the desired product (entry 2). Nemygina et al. [76] have

Table 1 Au NPs for Suzuki-Miyaura couplings

Entry	Au NPs (ppm)	X/R ¹ /R ²	Base	Solvent	Temperature (°C)/ time (h)	Yield (%)
1	Au/fI-G (N/A)	Cl/H/H	NaOH	H ₂ O	80/24	65
2	Sr/Alg/CMC/GO/Au (50)	Cl/H/H	NaOH	H ₂ O	80/4	76
3	Au-Pd/HPS (N/A)	Br/4-Ome/H	NaOH	EtOH/ H ₂ O	60/3	71
4	Fe ₃ O ₄ -Au@SF-SBA-15 (6400)	Cl/H/H	K ₂ CO ₃	EtOH/ H ₂ O	80/1.3	95

Table 2 Au NPs used for Heck and Sonogashira couplings

X = Cl/Br/I

entry	Au NPs (ppm)	X/R ¹ /R ²	base	solvent	temperature (°C)/time (h)	yield (%)
1	Au-Pd NPs-1 (2000)	I/H/H	K ₂ CO ₃	H ₂ O	80/8	94
2	Au-Pd NPs-2 (2000)					
3	Au/SiO ₂ (30,000)	I/H/H	K ₂ CO ₃	DMF	~130/4	87
4	Au/Pd ₂ -Sn NRs (N/A)					

shown that bimetallic Au-Pd core-shell NPs stabilized with hyper-cross-linked polystyrene (Au-Pd/HPS) could be used for SM couplings of 4-bromoanisole with phenylboronic acid in an EtOH/water mixture at 60°C under light irradiation using a 300 W filament lamp (entry 3). Very recently, Khodaei and Dehghan [77] explored comparatively complex Fe₃O₄-Au@SF-SBA-15 NPs for couplings of chlorides, bromides, and iodides at 80°C in aqueous ethanol (entry 4). In this case, recycling this catalyst seven times showed limited reduction in yield.

Gold catalysis using NPs is also applicable to both Heck and Sonogashira reactions, which are alternative ways of preparing internal alkenes and alkynes, respectively (Table 2). Nasrollahzadeh et al. [78] used 2,000 ppm Au-Pd bimetallic nanoparticles (Au-PdNPs-1), prepared by reducing gold and palladium salts using *Euphorbia condylocarpa* plant extract, for Heck couplings between aryl iodides and styrene derivatives in water at 80°C (entry 1). The catalyst was reused over four cycles, giving essentially the same chemical yields. Moreover [79], they also prepared bimetallic Au-Pd nanoparticles (Au-PdNPs-2) by

electrochemical reduction of the corresponding salts. Interestingly, 3,000 ppm of metal within these NPs was sufficient to catalyze Heck couplings of bromides under close to the same conditions as used for Au-PdNPs-1 (entry 2). The authors did not perform control experiments with only Au NPs or Pd NPs; hence, the need for a bimetallic system is still an open question. Experiments that test the extent of leaching of metals, however, were carried out to establish the heterogeneous nature of these reactions.

De Souza et al. [80] have used 3 mol% (30,000 ppm) gold nanoparticles supported on silica (Au/SiO₂) for copper-free Sonogashira couplings of iodobenzene with phenylacetylene under microwave conditions in DMF (entry 3). This educt gave an 87% yield of the alkyne within 1 h, while bromobenzene afforded a 61% yield and required a longer reaction time (3.5 h). Recently, Nafria et al. [81] used gold nanoparticles supported on Pd₂-Sn nanorods (Au/Pd₂-Sn NRs), prepared by growing gold dots on nanorods for Sonogashira coupling between iodobenzene and phenylacetylene in hot DMF (entry 4). Apart from the desired product, both partial and complete reduction of the initially coupled product alkyne was observed, where the hydrogen for reduction was coming from DMF.

Three-component couplings that rely on gold NPs involve 1-pot, 2-bond (C-C/C-N) formations leading to highly valued propargylamines [82]. As examples, this reaction represents a key step in the synthesis of an intermediate toward the naamine family of natural products [83], as well as a lactone intermediate used to prepare other natural products (Fig. 33, left) [84]. The mechanism of this reaction is believed to be similar to that of other metal-catalyzed A³ couplings. Auophilic interaction of Au NPs with the alkyne leads to formation of a Au-acetylide complex, which then attacks an iminium ion formed from the amine and aldehyde to give the desired product, releasing the Au NPs. In the process, a molecule of water is lost (Fig. 33, right).

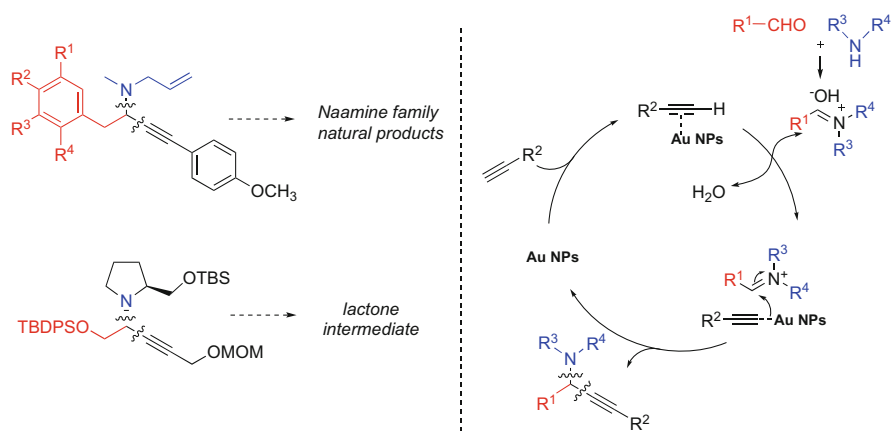


Fig. 33 Targeted products using Au NPs (left) and a proposed mechanism of A³-couplings (right)

Although the mechanism is not fully established, considerable research has been done in this regard on heterogeneous gold catalysts following the first report by Kidwai and co-workers [85]. In this work, gold NPs of varying sizes (10–70 nm) were prepared. It was then observed that Au NPs of size 10 nm showed the best activity. The only drawback anticipated was the need for excessive amounts of these NPs (10 mol%), used in methanol at 75–80°C. Nevertheless, a wide variety of substrates was studied (Fig. 34; e.g., **7**), most affording excellent chemical yields. Following this discovery, Huang et al. [86] used robust gold NPs supported on thiol-modified cellulose nanocrystallite Au/HS-CNC (4.4 mol%) for this same reaction type but under solvent-free conditions to arrive at a wide variety of propargylamines (e.g., **8**) in good-to-moderate yields. In 2016, Haruta's [87] group prepared phosphine-/phenylacetylide-protected gold clusters on TiO_2 ($\text{Au}_{25}(\text{PPh}_3)_{10}(\text{PA})_5\text{X}_2/\text{TiO}_2$) and applied these to A^3 couplings in water at 100°C to give the desired product in 90% yield (see **9**). Yields were similar for the first (90%) and second (88%) recycles. This catalyst has been applied to several substrates leading to products in good-to-excellent yields, although in the case of aliphatic aldehydes, yields dropped significantly (~30%). Recently, Veisi and co-workers [88] described an eco-friendly method to prepare Au NPs by reducing gold salts with *Stachys lavandulifolia* (*Au/S. lavandulifolia*). Such nanoparticles were utilized for similar A^3 -couplings to give a variety of products (e.g., **10**).

Corma and Hashmi [89] reported that gold nanoparticles supported on CeO_2 (Au/CeO_2) could be utilized for alkyne activation of ω -alkynylfurans, leading to the cyclized phenols in high yields (Fig. 35). Analysis of the extent of leaching showed that 25 ppm of gold had been released into solution, questioning heterogeneity of the reaction.

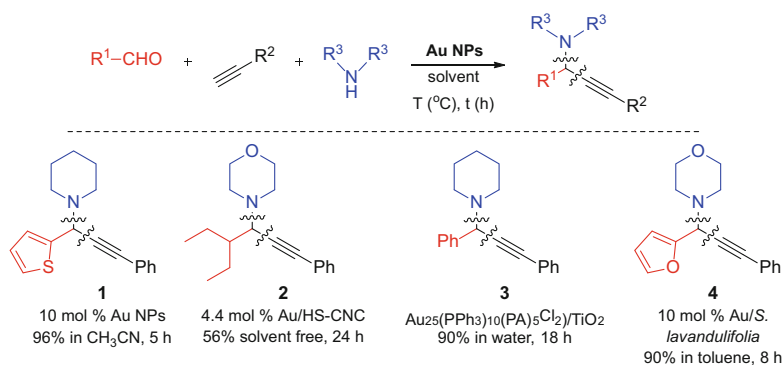
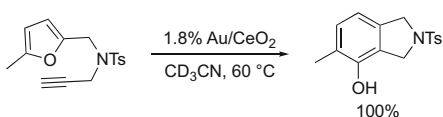


Fig. 34 Representative examples of A^3 -coupling using different Au NPs

Fig. 35 Cyclization of alkynylfuran to phenol using Au NPs



Oh and Han [90] described spherical monodispersed Au(III) NPs for use in a cascade-type cyclization, leading to an interesting polycyclic ring system (Fig. 36). The mechanism proposed is akin to that characteristic of homogeneous gold catalysis. Alkyne activation with gold leads to a zwitterionic intermediate, which further undergoes [3 + 2] cyclization with the tethered allene to give the final oxabicyclic product.

Stratakis and co-workers [91] used 1.2 mol% of TiO₂-supported Au NPs (Au/TiO₂) for cyclization of enynes (Fig. 37). The desired product was obtained in 92% yield after a 4-day reaction period. The mechanism was found to involve a cyclopropyl gold carbene complex, which then undergoes ring expansion and isomerizes to the desired product by eventual loss of the Au catalyst.

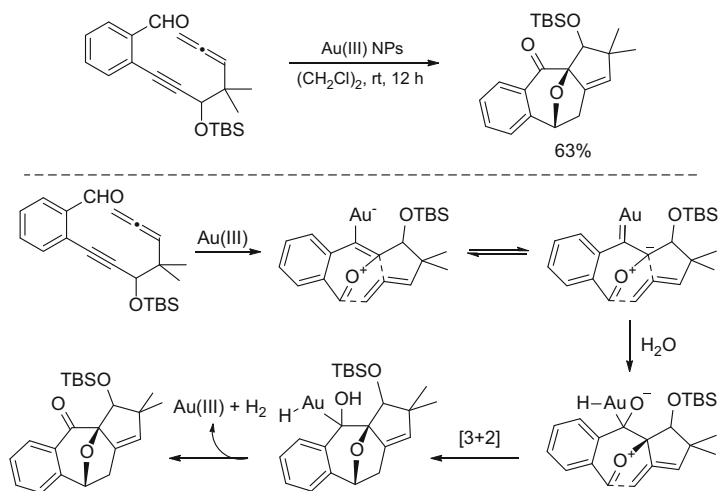


Fig. 36 Cascade intramolecular cyclization of an alkyne benzaldehyde + allene using Au NPs

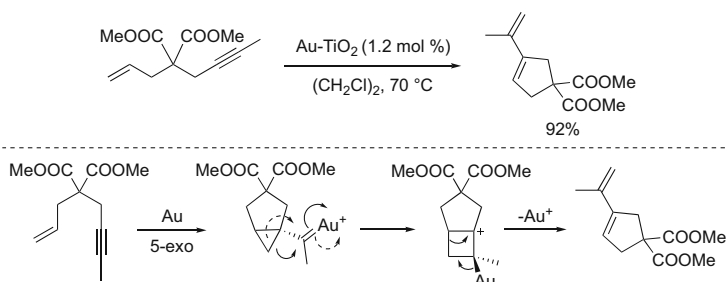


Fig. 37 Cycloaddition of enynes using Au NPs

7 Rhodium

Given that rhodium is among the rarest and most expensive precious metals, use of heterogeneous Rh NPs as highly reactive, robust, and reusable platforms can be especially attractive, perhaps most notably in the pharmaceutical industry where the residual contamination by Rh is limited to <100 µg/day (oral PDE) [92].

While Suzuki-Miyaura and Sonogashira cross-couplings are dominated by Pd-catalyzed processes, some examples mediated by Rh have been reported [93–95], illustrating the versatility of rhodium NPs. Most applications described, however, involve hydrogenation and hydroformylation reactions.

In 2016, Karakulina et al. described the cooperative effect of Rh NPs and acidic ionic liquids (ILs) for the chemoselective reduction of quinolines, as well as pyridine and benzofuran derivatives, to access the corresponding heterocycles [96]. To avoid harsh conditions (i.e., temperatures >150°C, high catalyst loadings, etc.), a chlorozincate-[bmim][BF₄] IL medium was found not only to stabilize and support the NPs but also to participate in the reaction. It is postulated that the Lewis acid IL coordinates to the heteroatom and facilitates hydrogenation of the ring under milder conditions (80°C, 30 bars of H₂). Indeed, in the absence of the chlorozincate, lower conversions were observed (Fig. 38). Both electron-donating and electron-withdrawing substituents, as well as halides, are well tolerated. The catalyst has been recycled six times without substantial loss of reactivity (90 → 84%, over 6 cycles). This method is remarkable given its chemoselectivity, as the aromatic rings remained untouched, leading to reduction of only the heteroaromatic.

The work of Kobayashi and co-workers involves Rh/Ag bimetallic NPs stabilized by nanocomposites of cross-linked polystyrene-based copolymers, and carbon black has been introduced as a new strategy for Rh immobilization [97]. This polymer-incarcerated metal platform (PI/CB Rh/Ag) shows high catalytic activity, robustness insofar as recyclability and reactivation are concerned, and no metal leaching. A first application of this system to asymmetric 1,4-additions of

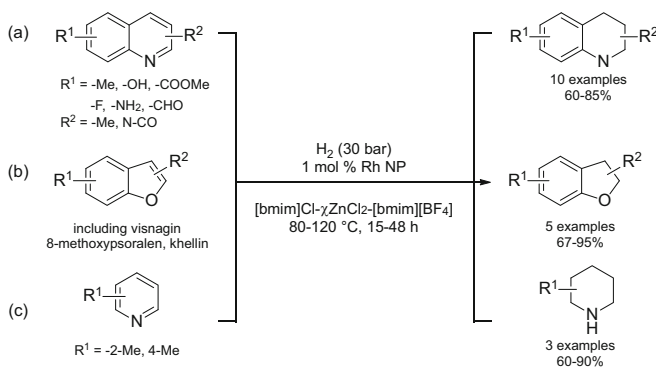
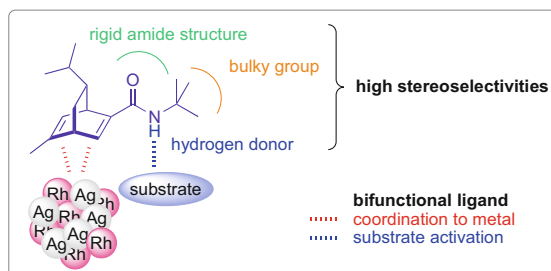
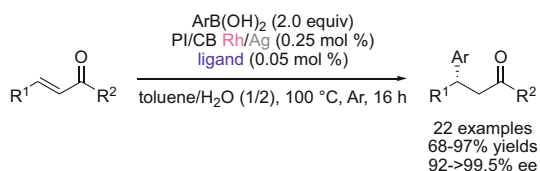


Fig. 38 Rh NP/[bmim]Cl-γZnCl₂-[bmim][BF₄] (*c* = 0.67) catalyzed hydrogenation of quinolines (a), pyridine derivatives (b), and benzofuran derivatives (c)

arylboronic acids to enones has been reported [98]. A bifunctional chiral diene ligand was used to simultaneously bind the metal and activate the substrate through Brønsted acid activation. While (*S*)-BINAP was initially investigated, a significant amount of Rh leaching was observed, ultimately suppressed by the use of this diene ligand (Fig. 39) [99]. The proximity of the substrate to the metal and the bulkiness of the chiral ligand allowed the reaction to proceed with high yields and stereoselectivities. Compared to homogeneous systems, the heterogeneous NPs showed superior performance, even with a lesser amount of ligand (0.05 mol % vs. 0.11 mol %). Use of a bimetallic system impacted greatly the surface distribution of Rh. Indeed, STEM analysis and EDS mapping revealed aggregation of Rh within the monometallic Rh NPs, while rhodium was more dispersed in the bimetallic Rh/Ag system.

Several examples, including three biologically important molecules, were prepared using this approach. Recycling of the NPs (up to six times) showed no significant loss of reactivity or selectivity. Comparison between heterogeneous and homogeneous catalysis showed that, despite a long induction period for the NP version, they are stable and ultimately lead to completion even at lower concentrations, while use of homogeneous catalysis plateaued, leading to lower yields. The mechanism is postulated to follow a redox process between the arylboronic acid and the surface of the NPs, as the induction period was reduced by incubation with the NPs. Coordination of the ligand to the reduced surface may then follow different pathways. In the case of hydrogenation, the reaction would happen directly at those sites, but in the case of C-C bond formation, the mechanism is more controversial. A smaller entity could detach from the NPs as a form of an active metal cluster or complex, which could reaggregate as NPs after the reaction. The second theory suggests that some degree of homogeneous metal complex leached into solution. As no leaching was detected by inductively coupled plasma (ICP) or a hot-filtration test, the latter hypothesis is unlikely [100].

Fig. 39 Asymmetric 1,4-addition reaction with PI/CB Rh/Ag NPs and bifunctional ligand



The same system has been applied to asymmetric arylations of imines (Fig. 40) [101]. Aryl tosylimines substituted by electron-withdrawing or electron-donating groups can be arylated in high yields and stereoselectivities. In the case of aliphatic imines, being more prone to hydrolysis, an induction period to activate the catalyst at 100°C in the presence of the arylboronic acid (reductant) helped to diminish this side reaction and led to the desired products with 99% ee's despite low yields. The NPs could be recovered by simple filtration and reused, along with ligand addition and reactivation at 150°C, up to five cycles.

Use of heterobimetallic NPs is also of high interest as they usually show improved performances compared to the monometallic NPs, alone, or combined. The same group recently reported Rh/Pt NPs, supported on alumina and polysilane (DMPSi), for hydrogenation of arenes (Fig. 41) [102]. The NPs have been used both in batch and under flow conditions. Very high activity was observed in the batch system, under mild conditions (0.00625 mol%, 30–50°C, 1 atm H₂). These Rh-Pt/(DMPSi-Al₂O₃) NPs could be recycled via simple filtration and reused ten times. In the case of decreased activity, drying the NPs under argon was sufficient to reactivate them. Even greater activity was noted when applied to flow processes, especially for highly coordinating substrates.

Prof. Chung and co-workers have extensively studied the application of Co/Rh heterobimetallic nanoparticles in carbonylation-related reactions (Fig. 42) [103, 104]. These NPs were prepared by mixing Co₂Rh₂(CO)₁₂ and Co₃Rh(CO)₁₂ clusters in a solution of *o*-dichlorobenzene, oleic acid, and trioctylphosphine oxide at 180°C, over 2 h. After removal of solvent, the resulting NPs were suspended in THF and either used directly or immobilized by refluxing them in

Fig. 40 Asymmetric arylations of imines catalyzed by PI/CB Rh/Ag NPs

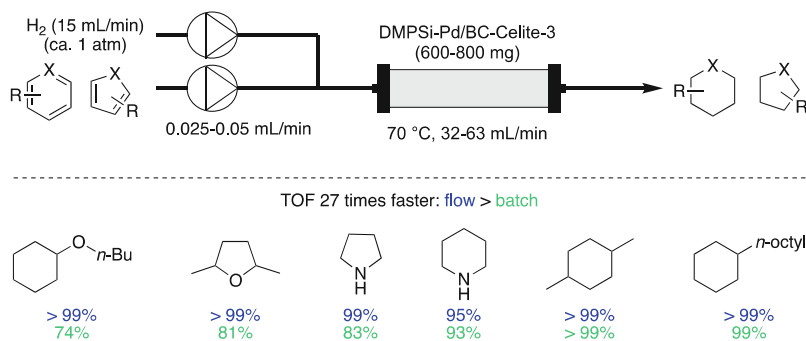


Fig. 41 Arene hydrogenation catalyzed by Rh-Pt NPs under batch and flow conditions

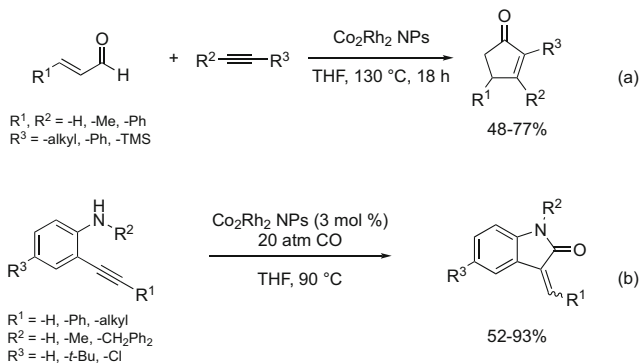


Fig. 42 Co₂Rh₂ NPs as catalysts for carbonylation-type reactions: (a) Pauson-Khand-type reaction using an olefinic aldehyde as CO source; (b) carbonylation cycloaddition of 2-alkynylanilines to oxindoles

THF in the presence of flame-dried charcoal for 12 h, followed by filtration and then drying. As determined by ICP-AES, the ratios of Co:Rh were 1.09:1 and 2.93:1, respectively [105].

Application to [2 + 2 + 1] Pauson-Khand cycloaddition reactions confirmed the synergistic effect of these bimetallic structures. Indeed, the intramolecular reaction of allyl propargyl ether under one atmosphere of CO afforded 87 and 88% yields, with Co/Rh and supported CO/Rh NPs, respectively. The solid support did not affect the outcome of the reaction and allowed five recycles without significant loss of reactivity. On the other hand, no reaction was observed with supported Co/C NPs, and low-to-moderate yields were reported using (Rh₄) and Co₃Rh/C (23 and 65%, respectively). A mixture of both Co NPs and Rh NPs led to only 12% yield, confirming the synergistic effect. Perhaps more important than the recycling aspect of this technology is the residual amount of metal found in the final product. ICP-AES elemental analysis showed less than 0.1 ppm of leached metals after reaction completion. The FDA limitation for the orally permitted daily exposure for Rh and Co in drugs is 100 and 50 µg/day, respectively. These NPs have also recently been applied to reductive aminations [106, 107] and reductive cyclizations to access indoles [108].

8 Ruthenium

Ruthenium has an especially broad number of oxidation states and, thus, various coordination geometries, making it a versatile catalyst. Hara et al. reported aminations of carbonyl compounds in the presence of ammonia as nitrogen source and hydrogen gas as reductant, catalyzed by highly active and structurally controlled ruthenium NPs (Fig. 43) [109]. The morphology of the catalyst was the key to access primary amines with high reaction rates. Flat-shaped pristine

Fig. 43 Reductive amination catalyzed by Ru NPs

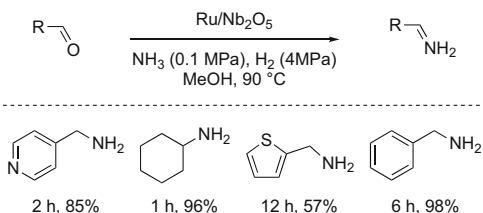
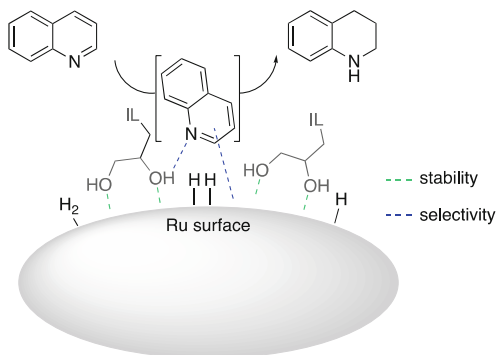


Fig. 44 Selective reduction of quinolines by Ru-diol-functionalized-ILs



fcc (face-centered cubic) ruthenium NP performance was in most cases superior to that previously described using Ru/Nb₂O₅ [110]. Indeed, reaction rates have been reported to be 5–7 times higher. While both catalysts are supported by a weakly electron-donating material, the flat Ru NPs present a larger surface of Ru(0). Functional groups such as halides, aryl, and heterocycles are well tolerated. The nanoparticles have been recycled four times without loss of reactivity.

Prechtl and co-workers have described use of ruthenium NPs in multifunctional ILs for selective hydrogenation of quinolines [111]. Here again, the nature of the IL was crucial for obtaining good selectivity. Diol-functionalized ILs have been found to play a significant role as chemoselective controllers as well as stabilizers for the hydrogenation of *N*-heterocyclic compounds. The 1–3 nm Ru NP surface is believed to be coated by the diols, which activate the heteroaromatic within the substrate (Fig. 44). In the absence of these functionalities, up to 9% of the side-product 5,6,7,8-tetrahydroquinoline was detected. Pyridines, pyrimidines, pyrroles, and pyrazoles have been successfully reduced. By contrast, indoles and carbazoles, being less basic, are less prone to be involved in hydrogen bonding with the diols and, hence, are typically fully reduced. Both methods, using Rh as reported by Dyson et al. (vide supra) [96] and Ru as catalyst for the selective hydrogenation of *N*-heterocycles, require similar conditions (pressure, temperature, reaction time), but a slightly lower loading was necessary with Rh (1 vs. 2 mol%).

Preparation of NPs for Hydrogenations A screw-capped vial with butyl/PTFE septum was loaded with [Ru(2-methylallyl)₂COD] (12.1 mg, 0.038 mmol) and the appropriate ionic liquid (0.3 g) under argon. The suspension was heated to 90 °C and

stirred under argon for 18 h resulting in a black suspension. The NP suspension was evaporated under reduced pressure to remove volatile by-products from the decomposition of the organometallic precursor. The monometallic Ru NPs in $[C_1C_1(EG)IM]NTf_2$ were prepared adapted from a literature method using a concentration of 0.1 M precursor in the IL. The monometallic Ru NPs in $[C_2OHMIM]NTf_2$ were synthesized using 0.1 M precursor in IL suspension at 90°C for 18 h.

Representative Hydrogenation Reaction To freshly prepared Ru NPs in an IL was added 1.9 mmol of the N-heteroaromatic compound. Then, the vial was placed in a stainless-steel autoclave; the reactor was sealed, charged with hydrogen, and was then placed into a preheated aluminum heating block (600 rpm) at the appropriate temperature. For certain compounds, mesitylene was added as cosolvent for better solubility of the substrate. After the appropriate reaction time the reactor was cooled to rt. For work-up, the reaction mixture was extracted with 5×2 mL of n-pentane or diethyl ether, the solvent was evaporated under reduced pressure, and 20 μ L (0.01 mmol) of hexamethyldisilane as internal standard was added.

9 Cobalt

Hydroquinolines are present in many pharmaceuticals and agrochemicals. While rhodium NPs can selectively hydrogenate *N*-heterocyclic compounds, an alternative approach using an earth-abundant metal under mild conditions is desirable. Beller et al. have developed cobalt oxide-derived NPs featuring nitrogen-doped (e.g., phenanthroline) graphene layers on alumina [112]. While reduction of quinoline failed using the homogeneous catalyst $Co(OAc)_2 \cdot 4H_2O/1,10$ -phenanthroline, these NPs, obtained via pyrolysis, led to reduction of the heterocyclic ring in good-to-excellent yields (Fig. 45). The NPs have been reused six times with only a slight loss in reactivity. Hydrogenation of indoles to indolines was also reported.

Semi-hydrogenation of alkynes in the presence of hydrogen gas is an attractive route to access alkenes, for both economic and environmental reasons. Cobalt NPs have also proven to be efficient for selective semi-hydrogenation of alkynes without over-reduction to the corresponding alkanes (Fig. 46) [113]. Computational studies

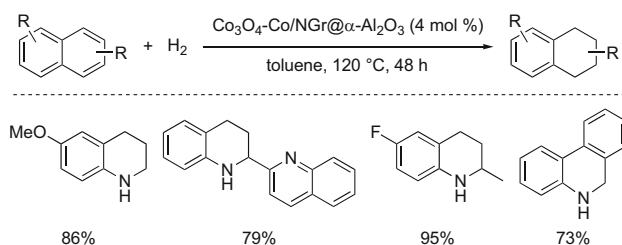


Fig. 45 Semi-hydrogenation of heteroarenes by Co NPs

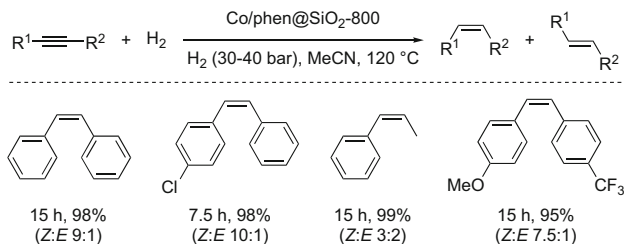


Fig. 46 Semi-hydrogenation of alkynes catalyzed by Co NPs

show that over-reduction of the alkene to the alkane is forbidden. After alkene insertion to form the alkylcobalt(I) intermediate, β -H elimination is energetically favored over protonation of the Co-C bond [114].

10 Iron

Iron, the fourth most abundant element on Earth, is attractive not only as an economical choice of metal but for its magnetic and catalytic properties. Fe(0) and iron oxides, namely, maghemite ($\gamma\text{-Fe}_2\text{O}_3$) and magnetite (Fe_3O_4), are the two dominant forms of iron NPs encountered in the literature (Fig. 47). Use of the reduced, less stable form in synthesis is still very early in its development. Indeed, Fe(0) NPs are pyrophoric upon contact with oxidizing agents; hence, working with a pre-oxidized form is far more convenient. Surprisingly, while iron is commonly used on large scale for catalytic hydrogenation (e.g., the Haber-Bosch process), its applications to pharmaceuticals and fine chemical synthesis are still minimal and should be investigated further for obvious environmental and economic reasons.

A sustainable iron-catalyzed (Z)-selective alkyne semi-hydrogenation in ionic liquids has been reported by Gieshoff et al. [116]. To avoid use of expensive and endangered Pd, or other platinumoids or group ten metals, as well as toxic $\text{Pb}(\text{OAc})_2$, Lindlar-type catalysts involving Fe NPs, stabilized by ionic liquids and a suitable ligand, acetonitrile, have been developed. The nanoparticles were prepared by reduction of FeCl_3 with EtMgCl . The presence of a nitrile function in, e.g., CH_3CN , either directly involved with the ILs or as an additive, was required to control the reactivity of the catalyst and to avoid over-reduction to the alkane. The solvent plays a crucial role here, as the ILs allow not only for catalyst recycling but also stabilization of the NPs. Indeed, the catalyst lost activity after 48 h in the absence of ILs (Fig. 48). Transmission electron microscopy (TEM) of the Fe NPs in ILs showed that their initial diameter of 4–5 nm enlarged to 8–20 nm under hydrogenation conditions. Optimized conditions were applied to numerous alkynes and are well tolerated by numerous functional groups, including free

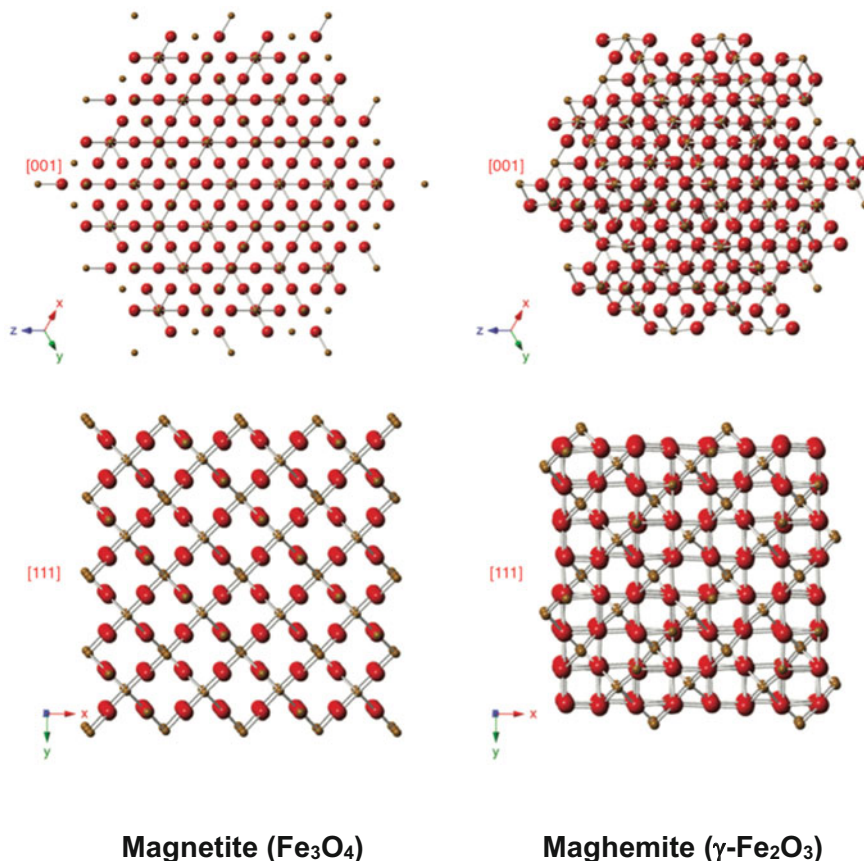


Fig. 47 Crystal structure of magnetite (Fe₃O₄) and maghemite (γ-Fe₂O₃) – reproduction from ref. [115]

amines, esters, halides, and alkenes. Terminal alkynes gave a mixture of alkanes and alkenes. Finally, after extraction, the catalyst layer could be reused without loss of reactivity for up to seven cycles.

In Situ Preparation of the Fe(0) NP Catalyst A 10 mL flask was charged with FeCl₃ (0.20 mmol, 33.1 mg) and THF (3.6 mL) in a glovebox. Under vigorous stirring, EtMgCl in THF (2 M, 0.80 mmol, 0.40 mL) was added dropwise. The resulting dark mixture was stirred at rt. for 30 min before use.

Hydrogenation of Alkynes with [Fe(0)]/IL-1/MeCN A 4 mL vial with screw cap and PTFE septum was charged with [BMIM][NTf₂] (IL-1) (150 μL) and 0.50 mL of the freshly prepared catalyst solution in a glove box and the mixture was stirred for 2 min before THF was evaporated under reduced pressure (oil pump). The vial was transferred back into the glove box, charged with an alkyne (0.50 mmol), dry acetonitrile (0.50 mmol), and dry n-heptane (0.50 mL), and

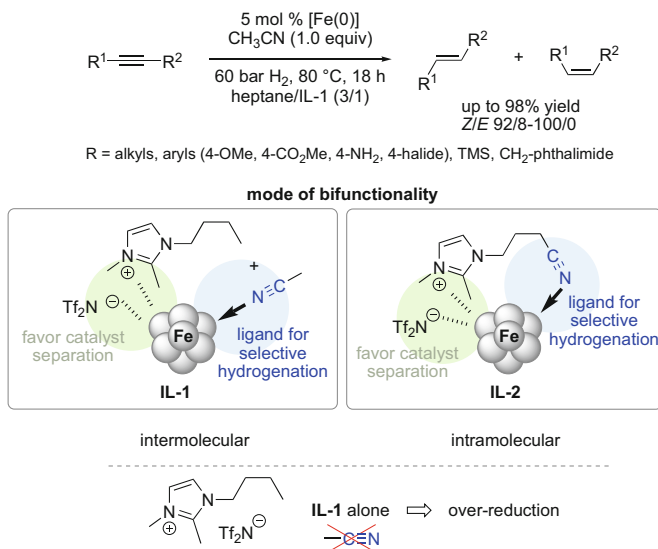


Fig. 48 Stereoselective Fe-catalyzed alkyne semi-hydrogenation in ionic liquids

then placed into a high-pressure reactor and punctured with a short needle, and the reactor was then sealed. The reactor was purged three times with hydrogen and pressurized with 53 bar of H₂, heated to 80°C by a heating jacket (resulting pressure 60 bar) and stirred with an external magnetic stirrer for 18 h. The reactor was then depressurized, the vial removed, the heptane phase separated by decantation, and the catalyst phase washed 2 × 1 mL with *n*-heptane. The product mixture was analyzed by GC and proton NMR. Quantifications were done via proton NMR vs. hexamethyldisiloxane as internal standard. For identification of *E/Z* stereochemistry of the resulting alkenes, the characteristic vinyl signals were analyzed and compared with literature data.

More recently, Corma and co-workers described a biomimetic approach using planar Fe(II)/(III) oxide nanoparticles supported on a slightly acidic material for the same reaction [117]. The support plays the role of a donor/acceptor entity, a functionality found in the active sites of hydrogenases. The nature of the support and the mode of preparation of the Fe-solid assembly are crucial, as only Fe deposited on TiO₂, ZrO₂, and ZnO by oxidative dispersion gave satisfactory results. Numerous alkynes have been reduced to the corresponding *Z*-alkenes, while aldehydes, with halides and nitro groups, remained unaffected. Although this method is not as selective as Lindlar-like catalysts, it is a useful tool for flow semi-hydrogenation of acetylene during ethylene manufacturing processes. The mechanism (Fig. 49) is believed to start with the adsorption of H₂ in the *n*FeOx catalytic sites, while adsorption of the alkyne occurs in both the Brønsted acid and *n*FeOx catalytic sites. Dihydrogen then dissociates heterolytically through

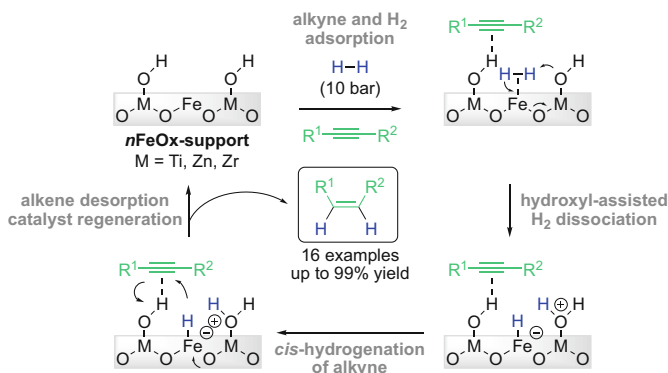
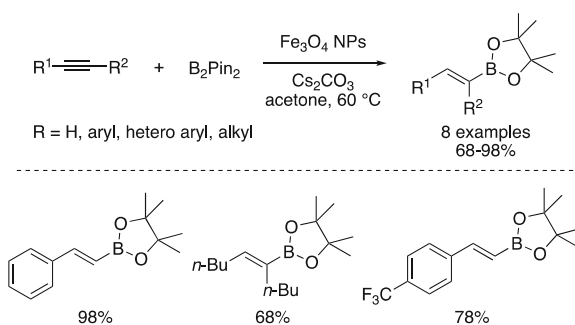


Fig. 49 Postulated mechanism for the *Z*-selective semi-hydrogenation of alkynes with *n*FeOx-supported catalysts

Fig. 50 Borylation of alkynes catalyzed by magnetic Fe NPs



a hydroxyl-assisted pathway. The alkyne is then *cis*-hydrogenated by the resulting hydride carried by the iron species, as well as the hydroxyl proton. Ti, Zn, or Zr are interesting metallic elements to constitute the solid support, as their electronegativity is substantially lower than Fe (1.3–1.6 vs. 1.8).

In 2014, Rawat et al. reported the regioselective borylation of alkynes to access *E*-vinylboronates (Fig. 50) [118]. Aryl, heteroaryl, as well as internal and external alkynes afforded good-to-excellent yields, while moderate yields were obtained with aliphatic substrates. The Fe₃O₄ NPs that perform this reaction could be isolated with an external magnetic field and reused without loss of reactivity (six recycles).

Magnetic silica-supported iron oxide (Fe₃O₄/SiO₂) NPs have also been employed for multicomponent syntheses of diazepines-2-carboxamides (Fig. 51) [119]. The reaction performed on model substrates showed significant improvement by using these NPs compared to non-supported Fe₃O₄ (92 vs. 35% yield, respectively). Yields ranged from 86 to 98% on 15 examples. After completion, the catalyst could be magnetically re-isolated, allowing its recycling for six cycles without loss of activity.

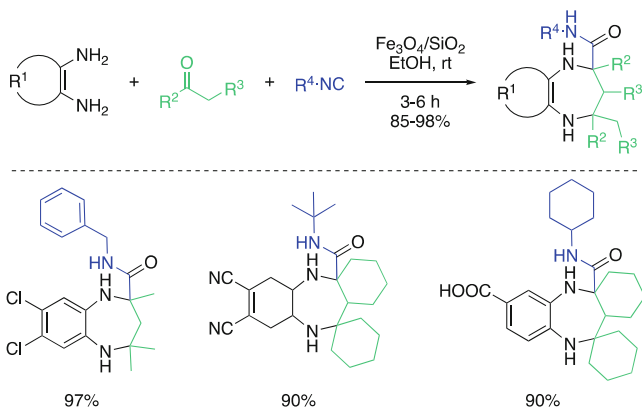


Fig. 51 Multicomponent diazepine-2-carboxamide synthesis catalyzed by $\text{Fe}_3\text{O}_4/\text{SiO}_2$ NPs

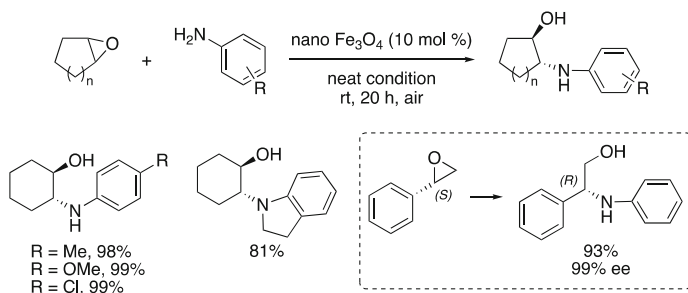


Fig. 52 Aminolysis of epoxides in presence of magnetic Fe_3O_4 NPs

A green route to access β -amino-alcohols, by ring-opening of epoxides with amines, has been reported by Kumar and co-workers [120]. Magnetically separable Fe_3O_4 NPs, under solvent-free and ambient conditions, catalyzed the reaction with high *trans*-selectivity. The NPs were recycled ten times with only a slight decrease in activity. In the case of chiral epoxides, a total inversion of the stereochemistry was noted, indicative of an $\text{S}_{\text{N}}2$ -type mechanism (Fig. 52).

A synergistic effect between unmodified κ -carrageenan (a sulfated polysaccharide naturally present in red seaweed) and Fe_3O_4 nanoparticles has been observed on Michael additions of aldehydes, in their neat state, to nitroalkenes [121]. While the hybrid magnetic material showed good reactivity, individual species showed no catalytic activity. Despite a chiral environment induced by the polysaccharide, no enantioselectivity has been detected. Thus, the authors reported the functionalization of the hybrid material using a nonracemic proline derivative (**1**, Fig. 53), leading to good-to-excellent enantioselectivities.

Iron oxide-containing NPs have also been developed as recoverable, magnetically supported materials for asymmetric organocatalysis, such as those derived from L-proline, but are outside the scope of this chapter [122].

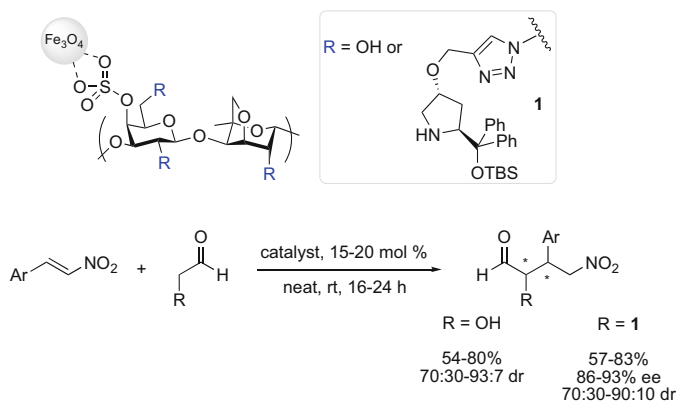


Fig. 53 Michael additions catalyzed by hybrid κ -carrageenan/ Fe_3O_4 NPs

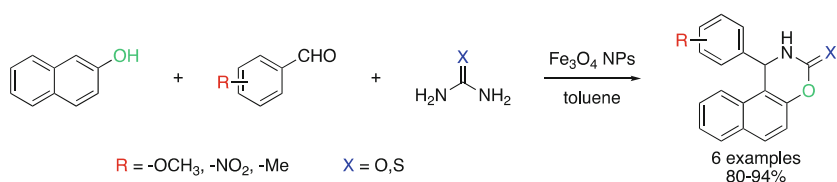


Fig. 54 Fe_3O_4 NPs applied to syntheses of benzoxazinones and benzthioxazinones

Common methods to prepare iron oxide-based NPs rely on toxic and, usually, reactive reductants such as NaBH_4 or hydrazine hydrate. Thus, more environmentally sound and safe routes are important to explore. Basavegowda et al. described a greener method for magnetite NP preparation using dried powder derived from naturally occurring *A. annua* leaves. A 5 mL aqueous filtrated infusion of the plant extract, rich in hydroxylated bioactive molecules, was mixed with 50 mL of a 2 mM aqueous solution of iron(III) chloride (FeCl_3), turning immediately into a black solution presumably forming Fe_3O_4 NPs [123], as the mechanism of NP formation by plant extracts remains unclear. A combination of several phytochemicals with redox properties (polyphenols, flavonoids, tannic acids, terpenoids, sugars, etc.) may be responsible for these reductions. Moreover, they can also act as capping agents that stabilize the particles [124]. These magnetite NPs have been tested in multicomponent syntheses of benzoxazinones and benzthioxazinones, compounds of interest given the variety of their biological activities. In one example, reaction of 2-naphthol with benzaldehyde derivatives and (thio)urea in the presence of 5 mol% of Fe_3O_4 NPs in refluxing toluene led to the desired products in good-to-excellent yields (Fig. 54).

11 Summary

This review highlights some of the advances in metal nanoparticle technology that have been made of late. Clearly, several of both the precious and base types of metals show considerable promise for inclusion into various NP formations, whether as their derived clusters or embedded on a solid support. Examples of mixed metal NPs are particularly exciting, as new synergistic activities have been uncovered leading to NP catalysts that show enhanced activities, suggestive of many more discoveries to come along these lines. Several reaction parameters addressed by the examples discussed herein, such as use of alternative reaction media (e.g., water, ILs, etc.), minimization of precious metals (e.g., platinoids), and attention to residual metals in products formed, all point to the potential for these catalysts to provide solutions to modern-day needs in catalysis. Indeed, based on these studies, the lines between homogeneous and heterogeneous catalysis have already begun to blur. And when considered together with environmental considerations taken into account in many of these reports, the future for NP technologies is not only very bright, but may figure prominently from the sustainability perspective of organic synthesis.

References

1. Liu L, Corma A (2018) Metal catalysts for heterogeneous catalysis: from single atoms to nanoclusters and nanoparticles. *Chem Rev* 118:4981–5079. <https://doi.org/10.1021/acs.chemrev.7b00776>
2. Phan NTS, van der Sluys M, Jones CW (2006) On the nature of the active species in palladium catalyzed Mizoroki–Heck and Suzuki–Miyaura couplings – homogeneous or heterogeneous catalysis, a critical review. *Adv Synth Catal* 348:609–679. <https://doi.org/10.1002/adsc.200505473>
3. Zhang D, Wang Q (2015) Palladium catalyzed asymmetric Suzuki–Miyaura coupling reactions to axially chiral biaryl compounds: chiral ligands and recent advances. *Coord Chem Rev* 286:1–16. <https://doi.org/10.1016/j.ccr.2014.11.011>
4. Lennox AJJ, Lloyd-Jones GC (2014) Selection of boron reagents for Suzuki–Miyaura coupling. *Chem Soc Rev* 43:412–443. <https://doi.org/10.1039/C3CS60197H>
5. Beletskaya IP, Cheprakov AV (2000) The heck reaction as a sharpening stone of palladium catalysis. *Chem Rev* 100:3009–3066. <https://doi.org/10.1021/cr9903048>
6. Rodríguez N, Goossen LJ (2011) Decarboxylative coupling reactions: a modern strategy for C–C-bond formation. *Chem Soc Rev* 40:5030–5048. <https://doi.org/10.1039/C1CS15093F>
7. Littke AF, Fu GC (2002) Palladium-catalyzed coupling reactions of aryl chlorides. *Angew Chem Int Ed* 41:4176–4211. [https://doi.org/10.1002/1521-3773\(20021115\)41:22<4176::AID-ANIE4176>3.0.CO;2-U](https://doi.org/10.1002/1521-3773(20021115)41:22<4176::AID-ANIE4176>3.0.CO;2-U)
8. Trzeciak AM, Augustyniak AW (2019) The role of palladium nanoparticles in catalytic C–C cross-coupling reactions. *Coord Chem Rev* 384:1–20. <https://doi.org/10.1016/j.ccr.2019.01.008>
9. Wu X-F, Neumann H, Beller M (2013) Synthesis of heterocycles via palladium-catalyzed carbonylations. *Chem Rev* 113:1–35. <https://doi.org/10.1021/cr300100s>
10. Gautam P, Bhanage BM (2015) Recent advances in the transition metal catalyzed carbonylation of alkynes, arenes and aryl halides using CO surrogates. *Cat Sci Technol* 5:4663–4702. <https://doi.org/10.1039/C5CY00691K>

11. Durand J, Teuma E, Gómez M (2008) An overview of palladium nanocatalysts: surface and molecular reactivity. *Eur J Inorg Chem* 2008:3577–3586. <https://doi.org/10.1002/ejic.200800569>
12. Torborg C, Beller M (2009) Recent applications of palladium-catalyzed coupling reactions in the pharmaceutical, agrochemical, and fine chemical industries. *Adv Synth Catal* 351:3027–3043. <https://doi.org/10.1002/adsc.200900587>
13. Narayanan R, El-Sayed MA (2003) Effect of catalysis on the stability of metallic nanoparticles: Suzuki reaction catalyzed by PVP-palladium nanoparticles. *J Am Chem Soc* 125:8340–8347. <https://doi.org/10.1021/ja035044x>
14. Handa S, Wang Y, Gallou F, Lipshutz BH (2015) Sustainable Fe–ppm Pd nanoparticle catalysis of Suzuki–Miyaura cross-couplings in water. *Science* 349:1087. <https://doi.org/10.1126/science.aac6936>
15. Lipshutz BH (2017) The ‘Nano-to-Nano’ effect applied to organic synthesis in water. *Johns Matthey Technol Rev* 61:196
16. Handa S, Jin B, Bora PP, Wang Y, Zhang X, Gallou F, Reilly J, Lipshutz BH (2019) Sonogashira couplings catalyzed by Fe nanoparticles containing ppm levels of reusable Pd, under mild aqueous Micellar conditions. *ACS Catal* 9:2423–2431. <https://doi.org/10.1021/acscatal.9b00007>
17. Feng J, Handa S, Gallou F, Lipshutz BH (2016) Safe and selective nitro group reductions catalyzed by sustainable and recyclable Fe/ppm Pd nanoparticles in water at room temperature. *Angew Chem Int Ed* 55:8979–8983. <https://doi.org/10.1002/anie.201604026>
18. Gabriel CM, Parmentier M, Riegert C, Lanz M, Handa S, Lipshutz BH, Gallou F (2017) Sustainable and scalable Fe/ppm Pd nanoparticle nitro group reductions in water at room temperature. *Org Process Res Dev* 21:247–252. <https://doi.org/10.1021/acs.oprd.6b00410>
19. Pang H, Gallou F, Sohn H, Camacho-Bunquin J, Delferro M, Lipshutz BH (2018) Synergistic effects in Fe nanoparticles doped with ppm levels of (Pd + Ni). A new catalyst for sustainable nitro group reductions. *Green Chem* 20:130–135. <https://doi.org/10.1039/C7GC02991H>
20. Sun J, Wang J, Feng X, Yamamoto Y, Almansour AI, Arumugam N, Kumar RS, Bao M (2018) Carboxylative Suzuki coupling reactions of benzyl chlorides with allyl pinacolborate catalyzed by palladium nanoparticles. *Chin J Catal* 39:1258–1262. [https://doi.org/10.1016/S1872-2067\(18\)63045-1](https://doi.org/10.1016/S1872-2067(18)63045-1)
21. Slack ED, Gabriel CM, Lipshutz BH (2014) A palladium nanoparticle–nanomicelle combination for the stereoselective semihydrogenation of alkynes in water at room temperature. *Angew Chem Int Ed* 53:14051–14054. <https://doi.org/10.1002/anie.201407723>
22. Jeanne-Julien L, Astier E, Lai-Kuen R, Genta-Jouve G, Roulland E (2018) Palladium nanoparticle-catalyzed stereoretentive cross-coupling of alkenyl sulfides with grignard reagents. *Org Lett* 20:1430–1434. <https://doi.org/10.1021/acs.orglett.8b00208>
23. Dictionary of Natural Products (2007) Chapman and Hall/CRC, Boca Raton. Internet resource
24. Heijnen D, Tosi F, Vila C, Stuart MCA, Elsinga PH, Szymanski W, Feringa BL (2017) Oxygen activated, palladium nanoparticle catalyzed, ultrafast cross-coupling of organolithium reagents. *Angew Chem Int Ed* 56:3354–3359. <https://doi.org/10.1002/anie.201700417>
25. Li X, Gong X, Li Z, Chang H, Gao W, Wei W (2017) Ligand- and copper-free Sonogashira and Heck couplings of (Het)aryl chlorides and bromides catalyzed by palladium nanoparticles supported on in situ generated Al(OH)₃. *RSC Adv* 7:2475–2479. <https://doi.org/10.1039/C6RA25416K>
26. Gao W-Z, Xu Y, Chen Y, Fu W-F (2015) Highly efficient and selective photocatalytic reduction of nitroarenes using the Ni₂P/CdS catalyst under visible-light irradiation. *Chem Commun* 51:13217–13220. <https://doi.org/10.1039/C5CC04030B>
27. Cai S, Duan H, Rong H, Wang D, Li L, He W, Li Y (2013) Highly active and selective catalysis of bimetallic Rh₃Ni₁ nanoparticles in the hydrogenation of nitroarenes. *ACS Catal* 3:608–612. <https://doi.org/10.1021/cs300689w>

28. Zhang J, Lu G, Cai C (2016) Chemoselective transfer hydrogenation of nitroarenes by highly dispersed Ni-Co BMNPs. *Catal Commun* 84:25–29. <https://doi.org/10.1016/j.catcom.2016.05.023>
29. Bódis J, Lefferts L, Müller TE, Pestman R, Lercher JA (2005) Activity and selectivity control in reductive amination of butyraldehyde over noble metal catalysts. *Catal Lett* 104:23–28. <https://doi.org/10.1007/s10562-005-7431-4>
30. Alonso F, Riente P, Yus M (2008) Hydrogen-transfer reductive amination of aldehydes catalysed by nickel nanoparticles. *Synlett*:1289–1292. <https://doi.org/10.1055/s-2008-1072748>
31. Jagadeesh R, Murugesan K, Beller M (2019) Reusable nickel nanoparticles-catalyzed reductive amination for selective synthesis of primary amines. *Angew Chem Int Ed*. <https://doi.org/10.1002/anie.201812100>
32. Sharma RK, Yadav M, Gaur R, Monga Y, Adholeya A (2015) Magnetically retrievable silica-based nickel nanocatalyst for Suzuki–Miyaura cross-coupling reaction. *Cat Sci Technol* 5:2728–2740. <https://doi.org/10.1039/C4CY01736F>
33. Handa S, Slack ED, Lipshutz BH (2015) Nanonickel-catalyzed Suzuki–Miyaura cross-couplings in water. *Angew Chem Int Ed* 54:11994–11998. <https://doi.org/10.1002/anie.201505136>
34. Sankar M, Dimitratos N, Miedziak PJ, Wells PP, Kiely CJ, Hutchings GJ (2012) Designing bimetallic catalysts for a green and sustainable future. *Chem Soc Rev* 41:8099–8139. <https://doi.org/10.1039/C2CS35296F>
35. Liu H, Mei Q, Li S, Yang Y, Wang Y, Liu H, Zheng L, An P, Zhang J, Han B (2018) Selective hydrogenation of unsaturated aldehydes over Pt nanoparticles promoted by the cooperation of steric and electronic effects. *Chem Commun* 54:908–911. <https://doi.org/10.1039/C7CC08942B>
36. Jang J, Byun S, Kim BM, Lee S (2018) Arylsilylation of aryl halides using the magnetically recyclable bimetallic Pd–Pt–Fe₃O₄ catalyst. *Chem Commun* 54:3492–3495. <https://doi.org/10.1039/C7CC09926F>
37. Heiss C, Schlosser M (2003) Organometallic control over the regioselectivity of functionalization reactions: 1,2,3-trifluorobenzene and bromo derivatives thereof as substrates. *Eur J Org Chem* 2003:447–451. <https://doi.org/10.1002/ejoc.200390078>
38. Luliński S, Serwatowski J (2003) Regiospecific metalation of oligobromobenzenes. *J Org Chem* 68:5384–5387. <https://doi.org/10.1021/jo0340511>
39. Zeng J (2012) A simple eco-friendly solution phase reduction method for the synthesis of polyhedra platinum nanoparticles with high catalytic activity for methanol electrooxidation. *J Mater Chem* 22:3170–3176. <https://doi.org/10.1039/C1JM14413H>
40. Pitre SP, Scaiano JC, Yoon TP (2017) Photocatalytic Indole Diels–Alder cycloadditions mediated by heterogeneous platinum-modified titanium dioxide. *ACS Catal* 7:6440–6444. <https://doi.org/10.1021/acscatal.7b02223>
41. Zamani A, Poursattar Marjani A, Nikoo A, Heidarpour M, Dehghan A (2018) Synthesis and characterization of copper nanoparticles on walnut shell for catalytic reduction and C–C coupling reaction. *Inorg Nano-Met Chem* 48:176–181. <https://doi.org/10.1080/24701556.2018.1503676>
42. He J, Zhang M, Primo A, García H, Li Z (2018) Selective photocatalytic benzene hydroxylation to phenol using surface-modified Cu₂O supported on graphene. *J Mater Chem A* 6:19782–19787. <https://doi.org/10.1039/C8TA07095D>
43. Rostovtsev VV, Green LG, Fokin VV, Sharpless KB (2002) A stepwise Huisgen cycloaddition process: copper(I)-catalyzed regioselective “ligation” of azides and terminal alkynes. *Angew Chem Int Ed* 41:2596–2599. [https://doi.org/10.1002/1521-3773\(20020715\)41:14<2596::AID-ANIE2596>3.0.CO;2-4](https://doi.org/10.1002/1521-3773(20020715)41:14<2596::AID-ANIE2596>3.0.CO;2-4)
44. Tornøe CW, Christensen C, Meldal M (2002) Peptidotriazoles on solid phase: [1,2,3]-triazoles by regioselective copper(I)-catalyzed 1,3-dipolar cycloadditions of terminal alkynes to azides. *J Org Chem* 67:3057–3064. <https://doi.org/10.1021/jo011148j>
45. Alonso F, Moglie Y, Radivoy G (2015) Copper nanoparticles in click chemistry. *Acc Chem Res* 48:2516–2528. <https://doi.org/10.1021/acs.accounts.5b00293>

46. Astruc D, Lu F, Aranzas JR (2005) Nanoparticles as recyclable catalysts: the frontier between homogeneous and heterogeneous catalysis. *Angew Chem Int Ed* 44:7852–7872. <https://doi.org/10.1002/anie.200500766>
47. Alonso F, Moglie Y, Radivoy G, Yus M (2013) Alkenes as azido precursors for the one-pot synthesis of 1,2,3-triazoles catalyzed by copper nanoparticles on activated carbon. *J Org Chem* 78:5031–5037. <https://doi.org/10.1021/jo400110m>
48. Alonso F, Moglie Y, Radivoy G, Yus M (2011) Multicomponent click synthesis of 1,2,3-triazoles from epoxides in water catalyzed by copper nanoparticles on activated carbon. *J Org Chem* 76:8394–8405. <https://doi.org/10.1021/jo2016339>
49. Nador F, Volpe MA, Alonso F, Feldhoff A, Kirschning A, Radivoy G (2013) Copper nanoparticles supported on silica coated maghemite as versatile, magnetically recoverable and reusable catalyst for alkyne coupling and cycloaddition reactions. *Appl Catal A Gen* 455:39–45. <https://doi.org/10.1016/j.apcata.2013.01.023>
50. Alonso F, Moglie Y, Radivoy G, Yus M (2010) Multicomponent synthesis of 1,2,3-triazoles in water catalyzed by copper nanoparticles on activated carbon. *Adv Synth Catal* 352:3208–3214. <https://doi.org/10.1002/adsc.201000637>
51. Fu F, Martinez A, Wang C, Ciganda R, Yate L, Escobar A, Moya S, Fouquet E, Ruiz J, Astruc D (2017) Exposure to air boosts CuAAC reactions catalyzed by PEG-stabilized Cu nanoparticles. *Chem Commun* 53:5384–5387. <https://doi.org/10.1039/C7CC02504A>
52. Adenot A, Landstrom EB, Gallou F, Lipshutz BH (2017) Fe/ppm Cu nanoparticles as a recyclable catalyst for click reactions in water at room temperature. *Green Chem* 19:2506–2509. <https://doi.org/10.1039/C7GC00883J>
53. Pourjavadi A, Tajbakhsh M, Farhang M, Hosseini SH (2015) Copper-loaded polymeric magnetic nanocatalysts as retrievable and robust heterogeneous catalysts for click reactions. *New J Chem* 39:4591–4600. <https://doi.org/10.1039/C4NJ02134G>
54. Liu Y, Liu Z, Cui Y (2015) An efficient nanoparticle-supported and magnetically recoverable copper(I) catalyst for synthesis of furans from Ene-Yne-Ketone. *Chin J Chem* 33:175–180. <https://doi.org/10.1002/cjoc.201400730>
55. Wang K, Yang L, Zhao W, Cao L, Sun Z, Zhang F (2017) A facile synthesis of copper nanoparticles supported on an ordered mesoporous polymer as an efficient and stable catalyst for solvent-free Sonogashira coupling reactions. *Green Chem* 19:1949–1957. <https://doi.org/10.1039/C7GC00219J>
56. Sharma RK, Gaur R, Yadav M, Rathi AK, Pechousek J, Petr M, Zboril R, Gawande MB (2015) Maghemite-copper nanocomposites: applications for ligand-free cross-coupling (C–O, C–S, and C–N) reactions. *ChemCatChem* 7:3495–3502. <https://doi.org/10.1002/cctc.201500546>
57. Ugi I, Meyr R, Fetzer U (1959) Versammlungsberichte. *Angew Chem* 71:373–388. <https://doi.org/10.1002/ange.19590711110>
58. Ugi I, Steinbrückner C (1960) Über ein neues Kondensations-Prinzip. *Angew Chem* 72:267–268. <https://doi.org/10.1002/ange.19600720709>
59. Passerini M, Simone L (1921) Sopra gli isonitrili (I). Composto del p-isonitril-azobenzolo con acetone ed acido acetico. *Gazz Chim Ital* 51:126–129
60. Biginelli P (1891) Ueber aldehyduramide des acetessigäthers. *Ber Dtsch Chem Ges* 24:1317–1319. <https://doi.org/10.1002/cber.189102401228>
61. Biginelli P (1891) Ueber aldehyduramide des acetessigäthers. II. *Ber Dtsch Chem Ges* 24:2962–2967. <https://doi.org/10.1002/cber.189102402126>
62. Sharghi H, Shirri P, Aberi M (2014) A solvent-free and one-pot strategy for eco-compatible synthesis of substituted-benzofurans from various salicylaldehydes, secondary amines, and nonactivated alkynes catalyzed by copper(I) oxide nanoparticles. *Synthesis* 46:2489–2498. <https://doi.org/10.1055/s-0034-1378206>
63. Li J-H, Tang B-X, Tao L-M, Xie Y-X, Liang Y, Zhang M-B (2006) Reusable copper-catalyzed cross-coupling reactions of aryl halides with organotin in inexpensive ionic liquids. *J Org Chem* 71:7488–7490. <https://doi.org/10.1021/jo061220j>

64. Tang B-X, Wang F, Li J-H, Xie Y-X, Zhang M-B (2007) Reusable Cu₂O/PPH₃/TBAB system for the cross-couplings of aryl halides and heteroaryl halides with terminal alkynes. *J Org Chem* 72:6294–6297. <https://doi.org/10.1021/jo070538o>
65. Takale BS, Bao M, Yamamoto Y (2014) Gold nanoparticles (Au NPs) and gold nanopore (Au NPore) catalysts in organic synthesis. *Org Biomol Chem* 12:2005–2027
66. Haruta M, Yamada N, Kobayashi T, Iijima S (1989) Gold catalysts prepared by coprecipitation for low-temperature oxidation of hydrogen and of carbon monoxide. *J Catal* 115:301–309. [https://doi.org/10.1016/0021-9517\(89\)90034-1](https://doi.org/10.1016/0021-9517(89)90034-1)
67. Fujita T, Guan P, McKenna K, Lang X, Hirata A, Zhang L, Tokunaga T, Arai S, Yamamoto Y, Tanaka N et al (2012) Atomic origins of the high catalytic activity of nanoporous gold. *Nat Mater* 11:775
68. Ferlin F, Cappelletti M, Vivani R, Pica M, Piermatti O, Vaccaro L (2019) Au@zirconium-phosphonate nanoparticles as an effective catalytic system for the chemoselective and switchable reduction of nitroarenes. *Green Chem* 21:614–626. <https://doi.org/10.1039/C8GC03513J>
69. Takale BS, Feng X, Lu Y, Bao M, Jin T, Minato T, Yamamoto Y (2016) Unsupported nanoporous gold catalyst for chemoselective hydrogenation reactions under low pressure: effect of residual silver on the reaction. *J Am Chem Soc* 138:10356–10364. <https://doi.org/10.1021/jacs.6b06569>
70. Takale BS, Tao SM, Yu XQ, Feng XJ, Jin T, Bao M, Yamamoto Y (2014) Exclusive chemoselective reduction of imines in the coexistence of aldehydes using AuNPore catalyst. *Org Lett* 16:2558–2561. <https://doi.org/10.1021/ol500958p>
71. Takale BS, Wang S, Zhang X, Feng X, Yu X, Jin T, Bao M, Yamamoto Y (2014) Chemoselective reduction of α,β -unsaturated aldehydes using an unsupported nanoporous gold catalyst. *Chem Commun* 50:14401–14404. <https://doi.org/10.1039/C4CC07068B>
72. Johnston P, Carthey N, Hutchings GJ (2015) Discovery, development, and commercialization of gold catalysts for acetylene hydrochlorination. *J Am Chem Soc* 137:14548–14557. <https://doi.org/10.1021/jacs.5b07752>
73. Han J, Liu Y, Guo R (2009) Facile synthesis of highly stable gold nanoparticles and their unexpected excellent catalytic activity for Suzuki–Miyaura cross-coupling reaction in water. *J Am Chem Soc* 131:2060–2061. <https://doi.org/10.1021/ja808935n>
74. Candu N, Dhakshinamoorthy A, Apostol N, Teodorescu C, Corma A, Garcia H, Parvulescu VI (2017) Oriented Au nanoplatelets on graphene promote Suzuki–Miyaura coupling with higher efficiency and different reactivity pattern than supported palladium. *J Catal* 352:59–66. <https://doi.org/10.1016/j.jcat.2017.04.034>
75. Thomas M, Sheikh MUD, Ahirwar D, Bano M, Khan F (2017) Gold nanoparticle and graphene oxide incorporated strontium crosslinked alginate/carboxymethyl cellulose composites for o-nitroaniline reduction and Suzuki–Miyaura cross-coupling reactions. *J Colloid Interface Sci* 505:115–129. <https://doi.org/10.1016/j.jcis.2017.05.051>
76. Nemygina NA, Nikoshvili LZ, Tiamina IY, Bykov AV, Smirnov IS, LaGrange T, Kaszkur Z, Matveeva VG, Sulman EM, Kiwi-Minsker L (2018) Au Core–Pd shell bimetallic nanoparticles immobilized within hyper-cross-linked polystyrene for mechanistic study of Suzuki cross-coupling: homogeneous or heterogeneous catalysis? *Org Process Res Dev* 22:1606–1613. <https://doi.org/10.1021/acs.oprd.8b00272>
77. Khodaei MM, Dehghan M (2019) A green and cost-effective approach for the production of gold nanoparticles using corn silk extract: a recoverable catalyst for Suzuki–Miyaura reaction and adsorbent for removing of dye pollutants. *Polyhedron* 162:219–231. <https://doi.org/10.1016/j.poly.2019.01.060>
78. Nasrollahzadeh M, Sajadi SM, Rostami-Vartooni A, Khalaj M (2014) Journey on greener pathways: use of *Euphorbia condylocarpa* M. bieb as reductant and stabilizer for green synthesis of Au/Pd bimetallic nanoparticles as reusable catalysts in the Suzuki and Heck coupling reactions in water. *RSC Adv* 4:43477–43484. <https://doi.org/10.1039/C4RA07173E>

79. Nasrollahzadeh M, Banaei A (2015) Hybrid Au/Pd nanoparticles as reusable catalysts for heck coupling reactions in water under aerobic conditions. *Tetrahedron Lett* 56:500–503. <https://doi.org/10.1016/j.tetlet.2014.12.041>
80. de Souza ROMA, Bittar MS, Mendes LVP, da Silva CMF, da Silva VT, Antunes OAC (2008) Copper-free Sonogashira reaction using gold nanoparticles supported on Ce₂O₃, Nb₂O₅ and SiO₂ under microwave irradiation. *Synlett* 2008:1777–1780. <https://doi.org/10.1055/s-2008-1078565>
81. Nafria R, Luo Z, Ibáñez M, Martí-Sánchez S, Yu X, de la Mata M, Llorca J, Arbiol J, Kovalenko MV, Grabulosa A et al (2018) Growth of Au–Pd₂Sn nanorods via galvanic replacement and their catalytic performance on hydrogenation and sonogashira coupling reactions. *Langmuir* 34:10634–10643. <https://doi.org/10.1021/acs.langmuir.8b02023>
82. Peshkov VA, Pereshivko OP, van der Eycken EV (2012) A walk around the A₃-coupling. *Chem Soc Rev* 41:3790–3807. <https://doi.org/10.1039/C2CS15356D>
83. Ermolat'ev DS, Bariwal JB, Steenackers HPL, de Keersmaecker SCJ, Van der Eycken EV (2010) Concise and diversity-oriented route toward polysubstituted 2-aminoimidazole alkaloids and their analogues. *Angew Chem Int Ed* 49:9465–9468. <https://doi.org/10.1002/anie.201004256>
84. Xu Q, Rozners E (2005) Asymmetric synthesis of trans-3,4-dialkyl-γ-butyrolactones via an Acyl-Claisen and Iodolactonization route. *Org Lett* 7:2821–2824. <https://doi.org/10.1021/ol050578j>
85. Kidwai M, Bansal V, Kumar A, Mozumdar S (2007) The first Au-nanoparticles catalyzed green synthesis of propargylamines via a three-component coupling reaction of aldehyde, alkyne and amine. *Green Chem* 9:742–745. <https://doi.org/10.1039/B702287E>
86. Huang J-L, Gray DG, Li C-J (2013) A₃-coupling catalyzed by robust Au nanoparticles covalently bonded to HS-functionalized cellulose nanocrystalline films. *Beilstein J Org Chem* 9:1388–1396. <https://doi.org/10.3762/bjoc.9.155>
87. Chen Y, Liu C, Abroshan H, Li Z, Wang J, Li G, Haruta M (2016) Phosphine/phenylacetylide-ligated Au clusters for multicomponent coupling reactions. *J Catal* 340:287–294. <https://doi.org/10.1016/j.jcat.2016.05.023>
88. Veisi H, Farokhi M, Hamelian M, Hemmati S (2018) Green synthesis of Au nanoparticles using an aqueous extract of stachys lavandulifolia and their catalytic performance for alkyne/ aldehyde/amine A₃ coupling reactions. *RSC Adv* 8:38186–38195. <https://doi.org/10.1039/C8RA06819D>
89. Carretin S, Blanco MC, Corma A, Hashmi ASK (2006) Heterogeneous gold-catalysed synthesis of phenols. *Adv Synth Catal* 348:1283–1288. <https://doi.org/10.1002/adsc.200606099>
90. Gupta AK, Rhim CY, Oh CH, Mane RS, Han S-H (2006) Gold nanoparticle-catalysed [3 + 2] dipolar cycloaddition of 1,6-allenynebenzaldehydes: construction of polycyclic ring systems. *Green Chem* 8:25–28. <https://doi.org/10.1039/B512034A>
91. Gryparis C, Efe C, Raptis C, Lykakis IN, Stratakis M (2012) Cyclization of 1,6-enynes catalyzed by gold nanoparticles supported on TiO₂: significant changes in selectivity and mechanism, as compared to homogeneous Au-catalysis. *Org Lett* 14:2956–2959. <https://doi.org/10.1021/ol301212j>
92. U. S. Department of Health and Human Services, Food and Drug Administration, Center for Drug Evaluation and Research (CDER), Center for Biologics Evaluation and Research (CBER) (2015) Q3D elemental impurities guidance for industry
93. Gniewek A, Trzeciak AM (2013) Rh(0) nanoparticles: synthesis, structure and catalytic application in Suzuki–Miyaura reaction and hydrogenation of benzene. *Top Catal* 56:1239–1245
94. Guha NR, Reddy CB, Aggarwal N, Sharma D, Shil AK, Bandna, Das P (2012) Solid-supported rhodium(0) nano-/microparticles: an efficient ligand-free heterogeneous catalyst for microwave-assisted Suzuki–Miyaura cross-coupling reaction. *Adv Synth Catal* 354:2911–2915

95. Kanuru VK, Humphrey SM, Kyffin JMW, Jefferson DA, Burton JW, Armbrüster M, Lambert RM (2009) Evidence for heterogeneous Sonogashira coupling of phenylacetylene and iodobenzene catalyzed by well defined rhodium nanoparticles. *Dalton Trans* 37:7602–7605
96. Karakulina A, Gopakumar A, Akçok I, Roulier BL, LaGrange T, Katsyuba SA, Das S, Dyson PJ (2016) A rhodium nanoparticle–Lewis acidic ionic liquid catalyst for the chemoselective reduction of heteroarenes. *Angew Chem Int Ed* 55:292–296
97. Yasukawa T, Miyamura H, Kobayashi S (2012) Polymer-incarcerated chiral Rh/Ag nanoparticles for asymmetric 1,4-addition reactions of arylboronic acids to enones: remarkable effects of bimetallic structure on activity and metal leaching. *J Am Chem Soc* 134:16963–16966
98. Yasukawa T, Suzuki A, Miyamura H, Nishino K, Kobayashi S (2015) Chiral metal nanoparticle systems as heterogeneous catalysts beyond homogeneous metal complex catalysts for asymmetric addition of arylboronic acids to α,β -unsaturated carbonyl compounds. *J Am Chem Soc* 137:6616–6623
99. Yasukawa T, Miyamura H, Kobayashi S (2014) Chiral metal nanoparticle-catalyzed asymmetric C–C bond formation reactions. *Chem Soc Rev* 43:1450–1461. <https://doi.org/10.1039/C3CS60298B>
100. Yasukawa T, Miyamura H, Kobayashi S (2016) Chiral ligand-modified metal nanoparticles as unique catalysts for asymmetric C–C bond-forming reactions: how are active species generated? *ACS Catal* 6:7979–7988. <https://doi.org/10.1021/acscatal.6b02446>
101. Yasukawa T, Kuremoto T, Miyamura H, Kobayashi S (2016) Asymmetric arylation of imines catalyzed by heterogeneous chiral rhodium nanoparticles. *Org Lett* 18:2716–2718
102. Miyamura H, Suzuki A, Yasukawa T, Kobayashi S (2018) Polysilane-immobilized Rh–Pt bimetallic nanoparticles as powerful arene hydrogenation catalysts: synthesis, reactions under batch and flow conditions and reaction mechanism. *J Am Chem Soc* 140:11325–11334. <https://doi.org/10.1021/jacs.8b06015>
103. Park JH, Kim E, Chung YK (2008) Heterobimetallic cobalt/rhodium nanoparticle-catalyzed carbonylative cycloaddition of 2-alkynylanilines to oxindoles. *Org Lett* 10:4719–4721
104. Park KH, Jung IG, Chung YK (2004) A Pauson–Khand-type reaction between alkynes and olefinic aldehydes catalyzed by rhodium/cobalt heterobimetallic nanoparticles: an olefinic aldehyde as an olefin and CO source. *Org Lett* 6:1183–1186
105. Park JH, Chung YK (2008) Cobalt–rhodium heterobimetallic nanoparticle-catalyzed reactions. *Dalton Trans*:2369–2378
106. Park JW, Chung YK (2015) Hydrogen-free cobalt–rhodium heterobimetallic nanoparticle-catalyzed reductive amination of aldehydes and ketones with amines and nitroarenes in the presence of carbon monoxide and water. *ACS Catal* 5:4846–4850
107. Choi I, Chun S, Chung YK (2017) Bimetallic cobalt–rhodium nanoparticle-catalyzed reductive amination of aldehydes with nitroarenes under atmospheric hydrogen. *J Org Chem* 82:12771–12777
108. Choi I, Chung H, Park JW, Chung YK (2016) Active and recyclable catalytic synthesis of indoles by reductive cyclization of 2-(2-nitroaryl)acetonitriles in the presence of Co–Rh Heterobimetallic nanoparticles with atmospheric hydrogen under mild conditions. *Org Lett* 18:5508–5511
109. Chandra D, Inoue Y, Sasase M, Kitano M, Bhaumik A, Kamata K, Hosono H, Hara M (2018) A high performance catalyst of shape-specific ruthenium nanoparticles for production of primary amines by reductive amination of carbonyl compounds. *Chem Sci* 9:5949–5956. <https://doi.org/10.1039/C8SC01197D>
110. Komanoya T, Kinemura T, Kita Y, Kamata K, Hara M (2017) Electronic effect of ruthenium nanoparticles on efficient reductive amination of carbonyl compounds. *J Am Chem Soc* 139:11493–11499. <https://doi.org/10.1021/jacs.7b04481>

111. Konnerth H, Prechtl MHG (2017) Selective hydrogenation of N-heterocyclic compounds using Ru nanocatalysts in ionic liquids. *Green Chem* 19:2762–2767. <https://doi.org/10.1039/C7GC00513J>
112. Chen F, Surkus A-E, He L, Pohl M-M, Radnik J, Topf C, Junge K, Beller M (2015) Selective catalytic hydrogenation of heteroarenes with N-graphene-modified cobalt nanoparticles (Co₃O₄-Co/NGr@ α -Al₂O₃). *J Am Chem Soc* 137:11718–11724. <https://doi.org/10.1021/jacs.5b06496>
113. Chen F, Kreyenschulte C, Radnik J, Lund H, Surkus A-E, Junge K, Beller M (2017) Selective semihydrogenation of alkynes with N-graphitic-modified cobalt nanoparticles supported on silica. *ACS Catal* 7:1526–1532. <https://doi.org/10.1021/acscatal.6b03140>
114. Qi X, Liu X, Qu L-B, Liu Q, Lan Y (2018) Mechanistic insight into cobalt-catalyzed stereodivergent semihydrogenation of alkynes: the story of selectivity control. *J Catal* 362:25–34. <https://doi.org/10.1016/j.jcat.2018.03.016>
115. Wu W, Jiang CZ, Roy VAL (2016) Designed synthesis and surface engineering strategies of magnetic iron oxide nanoparticles for biomedical applications. *Nanoscale* 8:19421–19474. <https://doi.org/10.1039/C6NR07542H>
116. Gieshoff TN, Welther A, Kessler MT, Prechtl MHG, von Wangelin AJ (2014) Stereoselective iron-catalyzed alkyne hydrogenation in ionic liquids. *Chem Commun* 50:2261–2264
117. Tejada-Serrano M, Cabrero-Antonino JR, Mainar-Ruiz V, López-Haro M, Hernández-Garrido JC, Calvino JJ, Leyva-Pérez A, Corma A (2017) Synthesis of supported planar iron oxide nanoparticles and their chemo- and stereoselectivity for hydrogenation of alkynes. *ACS Catal* 7:3721–3729. <https://doi.org/10.1021/acscatal.7b00037>
118. Rawat VS, Sreedhar B (2014) Iron-catalyzed borylation reactions of alkynes: an efficient synthesis of E-vinyl boronates. *Synlett* 25:1132–1136
119. Maleki A (2012) Fe₃O₄/SiO₂ nanoparticles: an efficient and magnetically recoverable nanocatalyst for the one-pot multicomponent synthesis of diazepines. *Tetrahedron* 68:7827–7833. <https://doi.org/10.1016/j.tet.2012.07.034>
120. Kumar A, Parella R, Babu SA (2014) Magnetic nano Fe₃O₄ catalyzed solvent-free stereo- and regioselective -aminolysis of epoxides by amines; a green method for the synthesis of β -amino alcohols. *Synlett* 25:835–842
121. Mak CA, Ranjbar S, Riente P, Rodríguez-Escrich C, Pericas MA (2014) Hybrid magnetic materials (Fe₃O₄/k-Carrageenan) as catalysts for the Michael addition of aldehydes to nitroalkenes. *Tetrahedron* 70:6169–6173
122. Firouzi-Haji R, Maleki A (2019) L-proline-functionalized Fe₃O₄ nanoparticles as an efficient nanomagnetic organocatalyst for highly stereoselective one-pot two-step tandem synthesis of substituted cyclopropanes. *ChemistrySelect* 4:853–857. <https://doi.org/10.1002/slct.201802608>
123. Basavegowda N, Magar KBS, Mishra K, Lee YR (2014) Green fabrication of ferromagnetic Fe₃O₄ nanoparticles and their novel catalytic applications for the synthesis of biologically interesting benzoxazinone and benzthioxazinone derivatives. *New J Chem* 38:5415–5420
124. Saif S, Tahir A, Chen Y (2016) Green synthesis of iron nanoparticles and their environmental applications and implications. *Nano* 6:209. <https://doi.org/10.3390/nano6110209>

Precise Synthesis of Nanoparticles and Their Catalytic Behavior



Makoto Tanabe and Kimihisa Yamamoto

Contents

1	Introduction	132
2	Poly(amidoamine) (PAMAM) Dendrimers	135
3	Poly(propyleneimine) (PPI) Dendrimers	143
4	Click (Triazolyl) Dendrimers	147
5	Polybenzyl Ethers (Fréchet-Type) Dendrimer	150
6	Dendritic Poly(phenylazomethine) (DPA)	151
7	Bimetallic and Multimetallic Catalysts Within Dendrimers	157
8	Conclusion	166
	References	166

Abstract This review provides a summary of the main concepts employed to prepare nanoparticles (NPs) and clusters encapsulated by dendrimers, their catalytic applications, and interesting research and trends in this field. Dendrimers not only serve as synthesis templates for the preparation of NPs but also stabilize the NPs against leaching and aggregation, which makes it possible to tune the functionality of the peripheral groups and bridge the gap between homogeneous and heterogeneous catalyses. In particular, π -conjugated dendrimers, referred to as dendritic poly(phenylazomethine)s (DPA), are regarded as reactors for synthesizing sub-nanoscale clusters with atomic-level precision, even using different elements. This new synthesis technology has significant potentials for enabling enhanced activity, selectivity, and stability of catalysts.

M. Tanabe and K. Yamamoto (✉)

Laboratory for Chemistry and Life Science (CLS), Institute of Innovative Research (IIR), Tokyo Institute of Technology, Yokohama, Japan

ERATO-JST Yamamoto Atom Hybrid Project, Tokyo Institute of Technology, Yokohama, Japan

e-mail: yamamoto@res.titech.ac.jp

Keywords Catalysts · Dendrimers · Nanoparticles · Oxidation · Supramolecular chemistry

Abbreviations

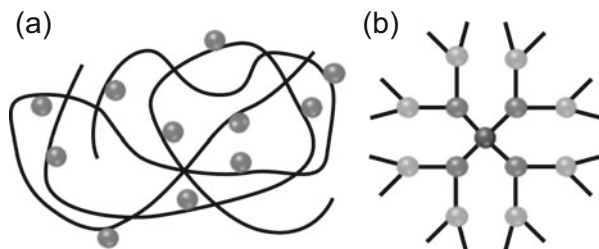
AAC	Alkyne-azide cycloaddition
CNT	Carbon nanotube
DEN	Dendrimer-encapsulated nanoparticles
DPA	Dendritic poly(phenylazomethine)
DSN	Dendrimer-stabilized nanoparticles
EDS	Energy-dispersive X-ray spectroscopy
EWG	Electron-withdrawing groups
GCE	Glassy carbon electrodes
GMC	Graphitized mesoporous carbon
NCD	Nanoparticle-cored dendrimers
NPs	Nanoparticles
ORR	Oxygen reduction reaction
PAMAM	Poly(amidoamine)
PPI	Poly(propyleneimine)
PyTPM	Pyridoxine(triphenylene)methane
STEM	Scanning transmission electron microscope
TEG	Triethylene glycol
TOF	Turnover frequency
TON	Turnover number
TPM	Tetraphenylmethane

1 Introduction

The advanced science and technology of catalysis is particularly important for overcoming the economic and environmental issues in our present society. Research in the 1990s, which revealed the surprising activity of Au nanoparticles (NPs), largely investigated novel catalytic materials on the nanoscale with properties different from their bulk counterparts [1]. Nanotechnology has since fascinated many researchers in fields of science such as catalysis, organic chemistry, surface science, molecular biology, semiconductor physics, etc. Interesting catalytic features of NPs have been revealed year by year, so that the number of publications on catalysis using NPs has exponentially increased.

The NPs used in catalysis have been synthesized with thermodynamic stability as a driving force, i.e., the particles are surrounded by organic ligands such as thiols, amines, carbonyls, or solvent molecules. These stabilized particles normally show low catalytic performance, because dissociation of the ligands takes place to generate the reactive surface sites. In contrast, metastable NPs and clusters composed of a

Fig. 1 (a) Macromolecular complex and (b) dendrimer complex



small number of metal atoms have been focused on as highly reactive catalysts in both homogeneous and heterogeneous systems. However, conventional synthesis of precisely size-controlled NPs is extremely difficult in solution.

The molecular complex composed of metal-organic hybrid components has widely been known as one of the conventional methods for the size-specified NPs (Fig. 1a). Synthetic macromolecules have a straight-chain structure, a distributed molecular weight, and a flexible backbone. Metal accumulation on the linear polymer exhibits a statistical distribution depending on the macromolecular structure. The synthesis of size-selected NPs or atom-specified clusters demands precise control of the higher-order structures of macromolecules as a synthesis template.

Dendrimers are nanosized, branched three-dimensional macromolecular frameworks, which are regularly repeated from the center, known as the core, with the number of branching repetitions referred to as the generation (Fig. 1b). In 1985, the first demonstration of the concept and synthesis of a dendrimer with a poly(amidoamine) (PAMAM) skeleton was published by Tomalia [2]. Starburst dendrimers were recognized as a new class polymer and expected to play a key role of a new emerging science of nanotechnology [3–6]. The following unique properties of dendrimers are suitable for a nanosized reactor.

1. Monodisperse nature: The number of coordination sites is determined by the size of the well-defined dendrimer structure.
2. Encapsulation effect: An inner nanospace within the dendrimer is produced by increasing the number of branching chains exponentially. The capsule-like nature is also referred to as “shell effect.”

The first synthesis of Cu NPs encapsulated by dendrimers within a cavity was reported independently by Crooks [7] and Tomalia [8] in 1998. Since these two pioneering papers were published, NPs stabilized by dendrimers have attracted attention in various research fields such as catalysis, magnetism, and chemical sensing. The synthesis procedure was thus demonstrated to be a large number of the preparation for NPs with well-defined sizes, compositions, and structures. Figure 2 shows a schematic of the general procedure. Lewis acidic metal ions (or halides) are added to a solution of the dendrimer. These metal species combine with the Lewis basic coordination sites, e.g., P, N, and S atoms, in the dendrimers to form metal-dendrimer complexes. The average number of metal ions in the dendrimer is determined by the molar ratio of metal ions to dendrimer. It should

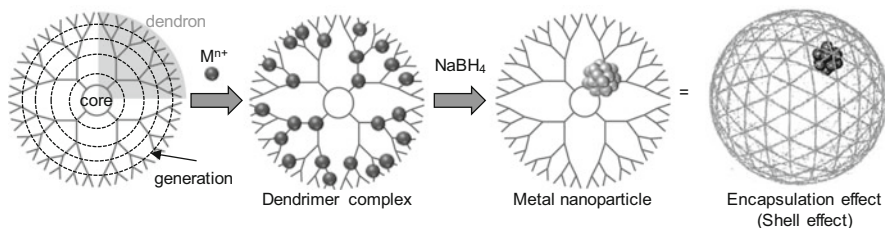


Fig. 2 Procedure for the synthesis of metal NPs encapsulated by a dendrimer

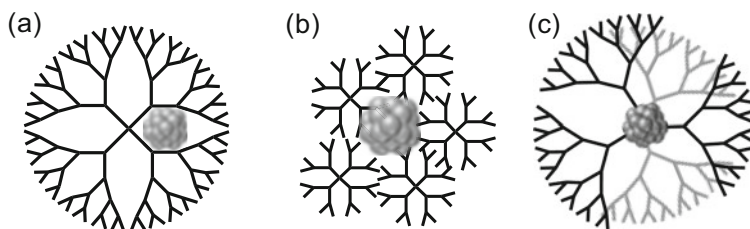


Fig. 3 Various metallodendritic structures of metal NPs for catalytic reactions with (a) interior, (b) exterior, and (c) core types

be noted that the average numbers represent a statistical distribution of the metal ions coordinated to the dendrimers. Chemical reduction of the metal ions to zero-valent metals by reducing agents (e.g., NaBH_4) provokes the agglomeration of metal atoms to form monodisperse NPs inside the dendrimer. Esumi reported a reagent-free photochemical reduction to form Au NPs in the same year [9], which had an advantage with the respect to the purification processes.

A great variety of dendritic nanocatalysts has been developed over the 20 years since the first discovery of metal NPs stabilized within dendrimers. The advantages of dendritic nanocatalysts include the following:

1. The most important role of the dendrimer is to act as a synthesis template for precisely controlled synthesis of NPs, whereby the number of atoms in the particles and the blending ratio of the different atoms are controlled. These factors significantly affect the catalytic activity and selectivity for catalysis.
2. The encapsulation effect provides catalytic stability to prevent the metastable NPs from aggregation, leaching, and passivation of metals during reactions. The dendrimer is functionalized as a size-selective molecular nanofilter of the reactants.
3. Dendrimer-encapsulated NPs can immobilize to organic polymer solids or inorganic solids on supports for heterogeneous applications. These heterogenized homogeneous catalysts are expected to surpass the catalytic performance of homogeneous catalysts and classical solid-state catalysts.

The catalytic properties of the dendritic NPs influent strongly on relationship between the particles and the dendrimers. Figure 3 summarizes the frequently

encountered locations (interior, exterior, or core) of NPs (or clusters) for catalysis in the dendrimer molecule.

- (a) Dendrimer-encapsulated NPs (DENs) – Encapsulation of NPs within a single dendrimer. DENs are the most popular location of NPs with an inner nanospace and are suitable for generation of the large dendrimers.
- (b) Dendrimer-stabilized NPs (DSNs) – Surrounding NPs with peripheral groups of several dendrimers. The formation of DSNs favors the generation of small dendrimers, followed by self-assembly of the dendrimer around the NP core. Therefore, the diameters of DSNs are slightly larger than those of DENs.
- (c) NP-cored dendrimers (NCDs) – NPs located in the core by the self-assembly of dendrons: The coordinating sites (e.g., P, N, and S atoms) at the focal point of the dendron are required as capping ligands for stabilization of the NPs. As the dendron size increases from G1 to G5, the number of dendritic units connected to the core decreases.

In this review, homogeneous and heterogeneous catalysis using NPs and clusters encapsulated by a series of dendrimers are presented. This review focuses on the unique catalytic activity, selectivity, and reusability of NPs, which are dependent on the size and location of the NPs in the dendrimer, as well as multimetallic NP materials, where the number of atoms and blend ratio of different elements has been precisely controlled.

2 Poly(amidoamine) (PAMAM) Dendrimers

The PAMAM dendrimers, prepared by Tomalia [10–12], are the most common dendrimers used to encapsulate NPs; they contain interior amido and amino groups and hydroxyl or amine groups at the peripheral position. The fourth-generation hydroxyl-terminated PAMAM dendrimer (G4-OH) are approximately 4.5 nm in diameter and contain 64 terminal OH groups and 62 tertiary amine groups (Fig. 4). The molecular weight becomes more than 14,000. The PAMAM dendrimer families with various generations are commercially available.

Crooks' group [13–16] pioneered catalysis using Pd DENs (1.3 ± 0.3 nm, Fig. 3a) within a hydroxyl-terminated PAMAM_{Gn}-OH dendrimer (where Gn represents the *n*th generation), which possessed high catalytic activity for hydrogenation of unbranched alkene (allyl alcohol) and branched alkene (*N*-isopropyl acrylamide) in water [17]. The size-selective catalytic activity during hydrogenation was dependent on dendrimer size and the reactants. The Pd₄₀ catalysts within dendrimers of lower generation (G4-OH), prepared from the ratio of Pd complex to dendrimer, exhibited the highest activities for the both reactants. Steric crowding on higher-generation dendrimers (G6-OH, G8-OH) hindered substrate penetration of the branched alkene, leading to only 10% and 5%, respectively. These results are possible to control reaction rates and do selective catalysis, which functioned as an adjustable-mesh “nanofilter” (Fig. 5) [18]. Incorporation of bulky groups

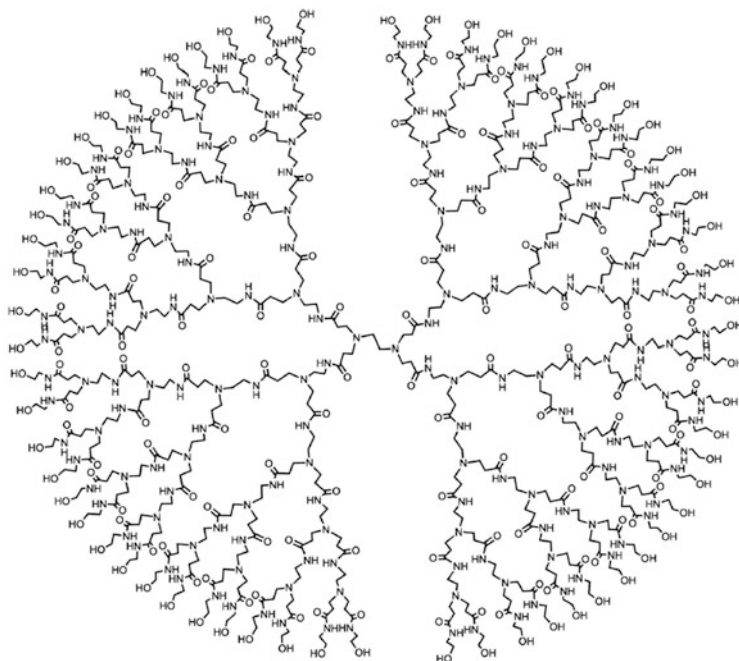


Fig. 4 Structure of a PAMAMG4-OH dendrimer

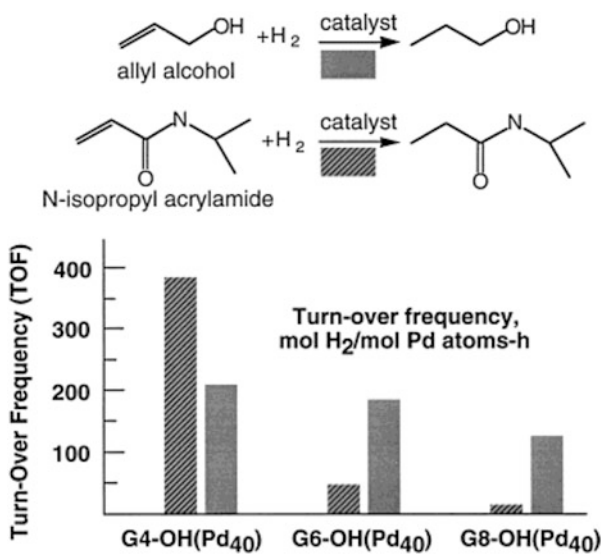


Fig. 5 Turnover frequencies for hydrogenation of alkenes obtained in water using Pd DENs. Adapted with permission from [13]. Copyright 2001 American Chemical Society

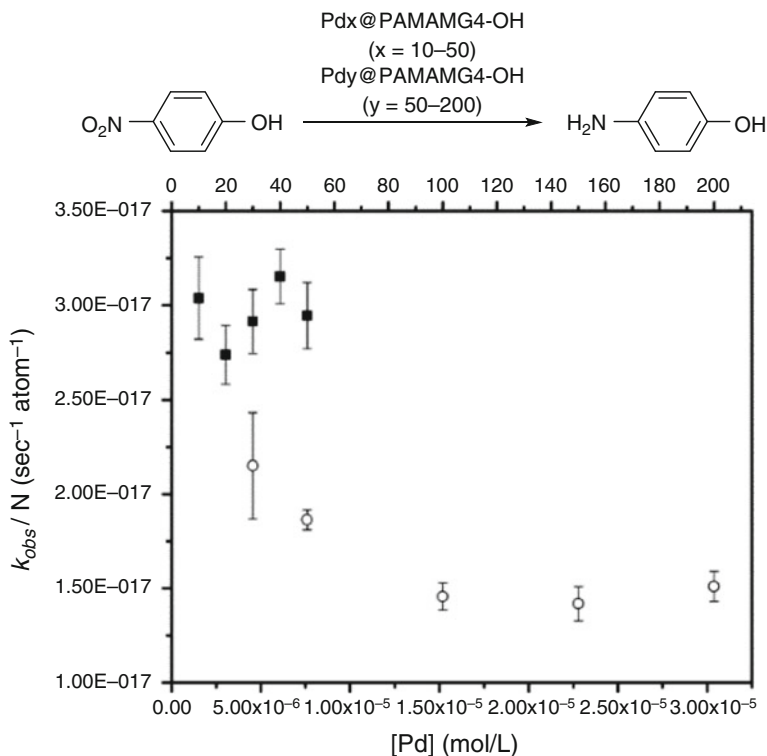
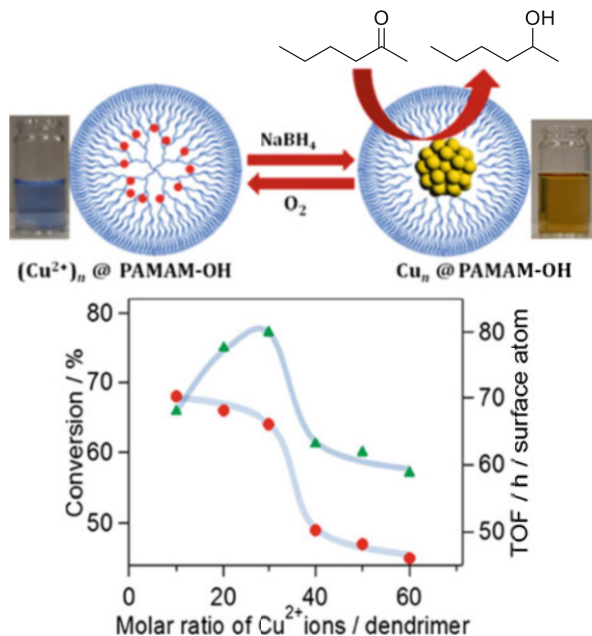


Fig. 6 Observed rate constants (k_{obs}) normalized by atoms of palladium in reaction of $\text{Pd}_x\text{@PAMAMG4-OH}$ (■: $x = 10-50$) and $\text{Pd}_y\text{@PAMAMG6-OH}$ (○: $y = 50-200$) for reduction of *p*-nitrophenol. Adapted with permission from [24]. Copyright 2013 American Chemical Society

functionalized various epoxide termini to the dendrimer end groups also influenced the catalytic activity of the Pd NPs [19]. These results suggest that more steric crowding on the dendrimer periphery resulted in lower activity for catalytic conversions. Amine-terminated PAMAM-NH₂ dendrimers are suitable to covalently link the dendrimer to the electrode surface because of the low reactivity of the peripheral hydroxyl groups [20]. Hydrogenation reactions catalyzed by a series of Pd NPs encapsulated by dendrimer derivatives are also available for organic [21], biphasic fluoruous/organic systems [22], and supercritical CO₂ solvents [23].

Stevenson et al. investigated the size dependence of the catalytic activity of Pd@PAMAMG_n-OH dendrimers for two different fourth and sixth generations (G4-OH, G6-OH) over a range of 10–200 atoms per nanoparticle using reduction of *p*-nitrophenol as a model reaction [24]. The rate constant normalized on a per-atom basis for NPs containing between 10 and 50 Pd atoms was relatively constant (Fig. 6), suggesting that all of the atoms in the particles were catalytically active and located on the surface of these small particles. However, for particles containing more than 50 Pd atoms, a decrease in rate of per-atom activity occurred

Fig. 7 Conversions (red) and TOF values (green) for hydrogenation of 2-hexanone as a function of the molar ratio of $[\text{Cu}^{2+}]/[\text{PAMAM-OH}(\text{G6})]$. Adapted with permission from [26]. Copyright 2013 American Chemical Society

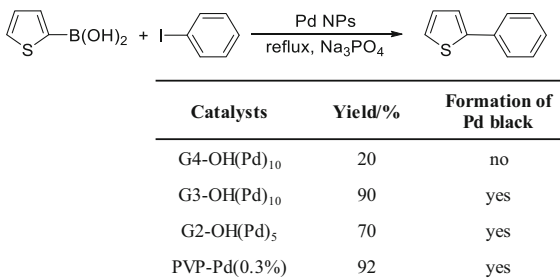


with increasing particle size, suggesting that some atoms were located in the catalytically inactive core. Similar size effect of Pd NPs on catalytic hydrogenation of allyl alcohol is sensitive to the electronic properties of the Pd NPs with a diameter < 1.5 nm, because the hydrogenation rates were not relative to any specific category of defect or face atom [25].

Tsukuda et al. provided size-specific Cu catalysts for hydrogenation of olefin and carbonyl groups in water which were performed by a series of Cu NPs within a sixth-generation PAMAM dendrimer, $\text{Cu}_n @ \text{PAMAMG6-OH}$ ($n = 10, 20, 30, 40, 50,$ and 60) [26]. As shown in Fig. 7, an estimated turnover frequency (TOF) of 2-hexanone per the molar ratio of Cu to the dendrimer is plotted, producing a volcano-shaped plot. Note that the Cu NPs were oxidized into Cu^{2+} ions under aerobic conditions but could be regenerated by reduction with NaBH_4 for catalytic application. The redox behavior of the Cu cluster could be repeated quantitatively. The coinage metal (Cu, Ag, Au) NPs [27] and Ru NPs [28] encapsulated by PAMAM dendrimers catalyzed the hydrogenation of 4-nitrophenol with NaBH_4 .

El-Sayed et al. investigated the stability of the Pd NPs within various generations of PAMAMGn-OH dendrimers ($n = 2, 3, 4$) and poly(*N*-vinyl-2-pyrrolidone) that performed as catalysts in the Suzuki-Miyaura reactions in an aqueous medium (Fig. 8) [29]. The Pd@PAMAMG4-OH (1.3 ± 0.1 nm) is found to be the best catalyst because the dendrimer stabilizes the Pd particles by preventing the formation of Pd black, but it does not fully passivate the metal surface. The mechanism for increasing the Pd particle in size involves the adsorption of phenylboronic acid to the NPs surface [30]. Christensen et al. examined Mizoroki-Heck [31] and Suzuki-

Fig. 8 Suzuki-Miyaura coupling reaction catalyzed by Pd@PAMAMGn-OH ($n = 2, 3, 4$) with different generation dendrimers and a PVP polymer



Miyaura [32] reactions in the presence of Pd catalysts encapsulated by PAMAMG4-OH dendrimers. The catalytic system is a very efficient catalyst giving good yields with 100–400 times less Pd than usual. Astruc et al. reported the Suzuki-Miyaura coupling reaction using Pd@PAMAMG4-NH₂ catalysts [33]. Crooks et al. report that Pd@PAMAM-OH dendrimers are catalytically active for Stille reactions. The reaction takes place under mild conditions (water, room temperature) and with good yields [34]. de Jesús suggested a possible mechanism for the Pd NPs within the nanospace of a PAMAM-OH dendrimer in the Stille reaction in water [35]. The plausible mechanism would involve small sizes of Pd species leached from the initial nanoparticle, which coordinated to the dendritic interior.

Esumi et al. reported that Au NPs within PAMAM dendrimer were prepared with different generations, resulting in the formation of the size-controlled particles of 3.0–4.1 nm [36]. The Au particles catalyzed the elimination of hydroxyl radicals in an H₂O₂/FeSO₄ system for biological applications, which exhibit 85 times greater catalytic activity than that of ascorbic acid. In contrast, Ag NPs assisted by photochemical reduction underwent aggregation of the particles with average size of about 7 nm in diameter [37].

Kaneda et al. reported preparation of Pd NCDs (Fig. 3c) by the self-assembly of PAMAM dendrons with different generations and alkyl chain lengths at the termini (Fig. 9). The largest third generation with longer alkyl chain (C12) became the smallest Pd NPs with a narrow size distribution (3.5 ± 1.3 nm), which provided highly selective performance for cyclic diene hydrogenations [38].

The development of methods for making heterogeneous catalysts is of interest because of the advantages of both homogeneous and heterogeneous catalysis. Although heterogeneous catalysts are often more easily recycled than their homogeneous counterparts, they are significantly less reactive and selective than homogeneous catalysts. Therefore, the immobilization of catalysts to organic polymer solids or inorganic materials has been widely studied. This strategy to incorporate dendritic structures into the “heterogenizing” homogeneous catalysts was expected to overcome these limitations. Conventional approach to supported dendritic catalysts was developed by Chandler’s group (Fig. 10) [39]. The PAMAM dendrimer-encapsulated Pt NPs were deposited onto the commercial silica support SBA-15. Gas-phase catalytic reactions using the encapsulated NPs usually proceeded slowly due to collapse of the flexible dendrimer without solvent. Calcination under O₂ and

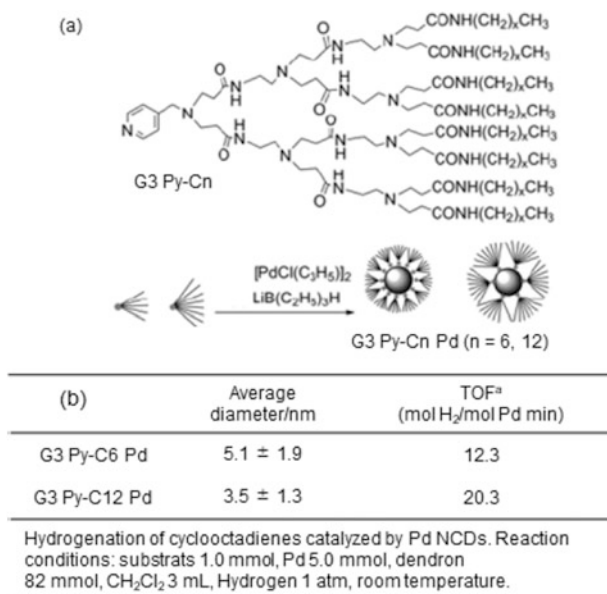


Fig. 9 (a) Formation of Pd NCDs stabilized by PAMAM dendrons. (b) Average diameters and TOFs for selective hydrogenation of cyclooctadiene to cyclooctene using the Pd NCD catalysts. Adapted with permission from [38]. Copyright 2008 The Royal Society of Chemistry

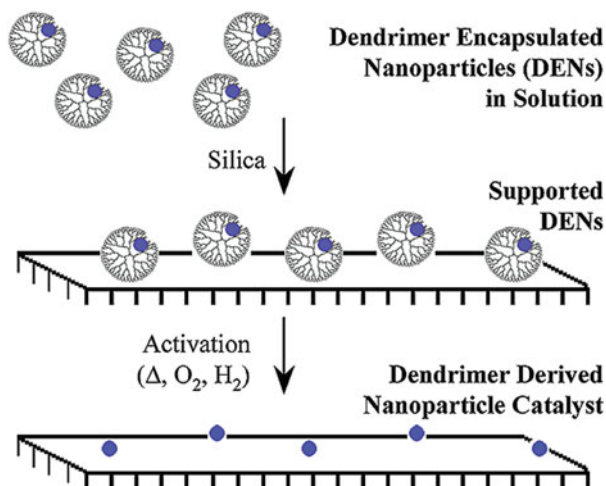


Fig. 10 Schematic route to dendrimer-derived supported NP catalysts. Adapted with permission from [39]. Copyright 2003 American Chemical Society

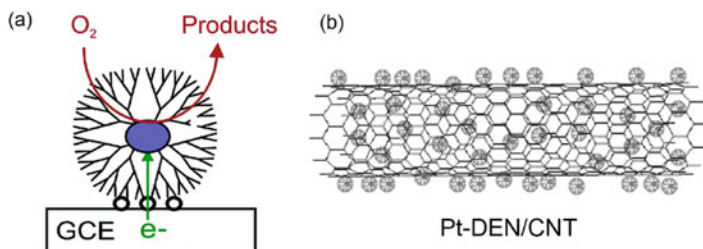


Fig. 11 Adsorption of Pt NPs (a) onto GCE and (b) onto CNT supports. Adapted with permission from [44, 46]. Copyright 2005 and 2007 American Chemical Society

H₂ flow at 300°C was used to remove the organic dendrimer without any significant aggregation. The Pt NP catalysts on the silica surface were more active for CO oxidation and toluene hydrogenation than a classic Pt/SiO₂ catalyst.

Amiridis et al. prepared Pt@PAMAM-OH dendrimer on porous silica support and removed the template for CO oxidation [40]. Later on, the Pt NPs provided the *trans-cis* conversion of 2-butene by Zaera group [41]. Size-controlled Ru NPs within PAMAM dendrimer were impregnated similarly on Al₂O₃ and maintained average particle size below 2.5 nm [42]. Li et al. reported preparation of hollow capsule-stabilized Au NPs through the encapsulation from the grafted dendrimers on the surface of the silica microspheres. The capsule-stabilized Au NPs catalyzed the reduction reaction of 4-nitrophenol to 4-aminophenol [43].

Platinum is considered the most effective catalyst for the oxygen reduction reaction (ORR), which is the cathode reaction in hydrogen-based fuel cells. However, Pt is not optimal in this application because of its scarcity and its high overpotential for the ORR. As the particle size is reduced, the efficiency of each atom in the particle is increased. However, it has been difficult to associate with synthesis and characterization of Pt particles in the <2 nm size range. The correlation between Pt particles and ORR kinetics is not well understood. The Pt NPs immobilized on glassy carbon electrodes (GCE, 1.4 ± 0.3 nm) [44, 45] and on N-doped carbon nanotubes (CNT, 2.2 ± 0.3 nm) [46] were electrochemically active in oxygen reduction reactions (Fig. 11). The Pt NPs were robust and retained their electrocatalytic activity within the dendrimers after consecutive scans. During electrochemical CO₂ reduction at -0.8 V in water, Au NPs stabilized with citrate of low-generation dendrimers (PAMAMG6-OH) rapidly grow up from the size of ~2 nm to 6–7 nm. The higher-generation G8-OH analogue stabilizes the Au NPs under the same condition. The initial size of 1.7 nm slightly increases to only 2.2 nm because of the encapsulation effect. The smaller, more stable Au NPs within G8-OH dendrimer exhibit higher activity and favor formation of H₂ over CO [47].

Somorjai et al. [48] have researched a series of heterogeneous metallic NPs (Au, Pd, Pt, Rh) supported on mesoporous silica (SBA-15), with sizes ranging from 1 to 2.7 nm, depending on the metal-to-dendrimer molar ratio. The “heterogenizing” homogeneous catalysts were prepared in three steps: complexation of the metallic

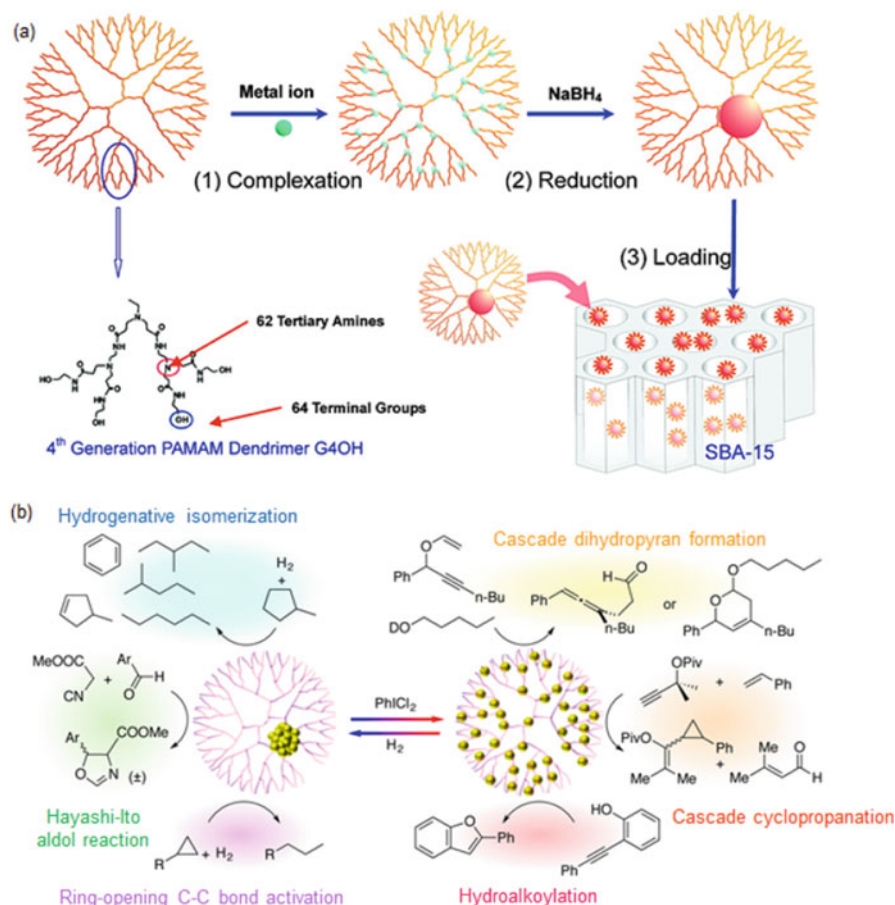


Fig. 12 (a) Preparation of PAMAM dendrimer-encapsulated NPs and subsequent immobilization on mesoporous support. (b) Catalytic reactions using "heterogenizing" homogeneous catalysts. Adapted with permission from [48, 49] Copyright 2008 and 2017 American Chemical Society, respectively

ions to a fourth-generation PAMAM dendrimer, chemical reduction of the metallic ions to the NPs (e.g., NaBH₄), and finally adsorption of the NPs onto the mesoporous SBA-15 support (Fig. 12). The reductive catalysts were efficient in promoting hydrogenation of ethylene and pyrrole (Rh, Pt) [49, 50], ring-opening C-C bond activation of strained three-membered rings (Rh) [51], reversible dehydrogenation/hydrogenation of *N*-heterocycles (Pd, Pt) [52], enhanced activity and selectivity in Hayashi-Ito aldol reaction of aldehydes and methyl isocyanacetate (Au) compared to the homogenous analogues [53], and ring-opening hydrogenative isomerization of methylcyclopentane (Rh, Pt) [54]. These metal NPs were oxidized by the hypervalent iodine species PhICl₂, and the electrophilic catalysts obtained,

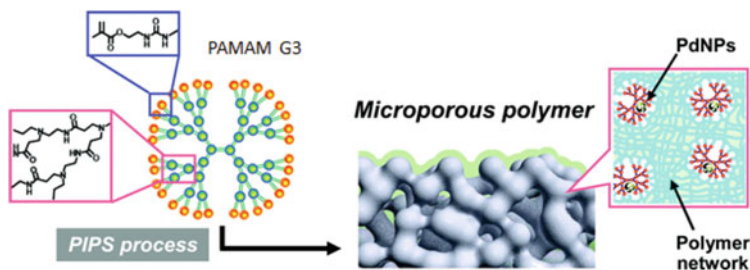


Fig. 13 Schematic outline of the preparation of microporous network polymers that contain Pd NPs. Adapted with permission from [60]. Copyright 2010 American Chemical Society

composed of Pt(II) and Pt(IV) chlorides and metallic Pt(0) as a mixture [55], were suitable for hydroalkoxylation via π -bond activation (Pt and Pd) [56, 57] and cascade cyclopropanation reactions and multistep formation of dihydropyrans (Au) [58, 59]. They also demonstrated advantages to use a flow reactor in the heterogeneous system to establish cascade reactions with the precise control of different temperatures and separation of the catalysts from reaction medium.

Kato et al. developed that Pd NPs in microporous network polymer, as shown in Fig. 13, exhibited great catalytic performance for a heterogeneous Suzuki-Miyaura reaction in water with a high turnover number ($\text{TON} = 8.5 \times 10^4$, 85%) [60]. Fabrication of the heterogeneous Pd catalysts was used by a traditional polymerization-induced phase separation (PIPS) techniques involving the Pd-PAMAM dendrimer complex. The resultant polymer has a mesoporous catalyst with a very high specific surface area and very small with a diameter of mainly around 2.0 nm.

Giacalone et al. reported the synthesis of single-walled carbon nanotubes and PAMAM dendrimers through straightforward convergent protocols [61]. The CNT-PAMAM dendrimers were used as a platform for the construction of Pd NPs with mean diameters of 1.6 ± 0.4 nm. The catalytic activity of the Pd NPs was best toward Suzuki-Miyaura and Mizoroki-Heck reactions. A low loading of the Pd catalyst (0.002 mol%) achieved a remarkable turnover frequency (TOF) of $546,000 \text{ h}^{-1}$, which is the highest reported for Pd NPs on nanocarbons. A “release and catch” mechanism of the Pd NPs was suggested during the catalytic cycle based on the experimental data. The single atoms or tiny clusters dissociated from the heterogeneous Pd particles would be highly active in heterogeneous cross-coupling reactions (Fig. 14).

3 Poly(propyleneimine) (PPI) Dendrimers

The first synthesis of poly(propyleneimine) (PPI) dendrimers was reported by Vögtle et al. in 1978 [62], which is one of common dendrimers used to encapsulate NPs (Fig. 15). PPI dendrimers do not contain internal amido groups and have been shown

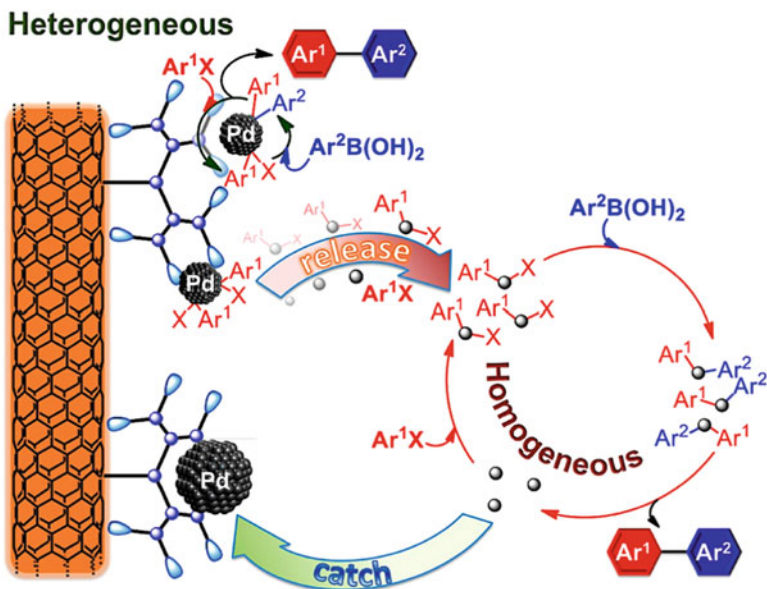


Figure 14 "Release and catch" mechanism of Pd NPs immobilized on CNT-PAMAM in Suzuki-Miyaura coupling reactions. Adapted with permission from [61]. Copyright 2016 American Chemical Society

to be stable at high temperature up to 470°C [63]. In contrast, thermal stability of PAMAM dendrimer is limited, because the retro-Michael reaction occurs at temperature beyond 100°C. As a result, PPI dendrimer allows the NPs to be used as high-temperature catalysts.

The first example of C-C coupling reactions using Pd NPs involved PPI dendrimers having perfluorinated polyether chains on their periphery to dissolve the dendrimers in a fluorocarbon/hydrocarbon solvent mixture [64]. The Pd NPs were effective for Mizorogi-Heck coupling in organic solvents. Although the Pd catalysts could be recovered fully after each reaction, catalytic activity decreased significantly with recovery/catalysis cycles. The PPI dendrimers functionalized by alkyl groups are soluble for organic solvents [65]. The Pd NPs within the PPI dendrimer are catalytically active for hydrogenation of 1-hexene, but they are less stable than those prepared by other routes.

Esumi et al. compared the catalytic activity of Au NPs within two different PAMAM and PPI dendrimers with surface amino groups in the reduction of 4-nitrophenol in an aqueous solution [66]. The diameters of Au NPs within two kinds of dendrimers, prepared using laser irradiation, are not different to each other to form the dendrimer-Au nanocomposites. A distinct difference in the catalytic activity was observed that the Au NPs within PPI dendrimers show higher activity for the chemical reduction of nitrophenol than those covered by PAMAM dendrimers (Fig. 16) [67]. This result was suggested that the rate constant is

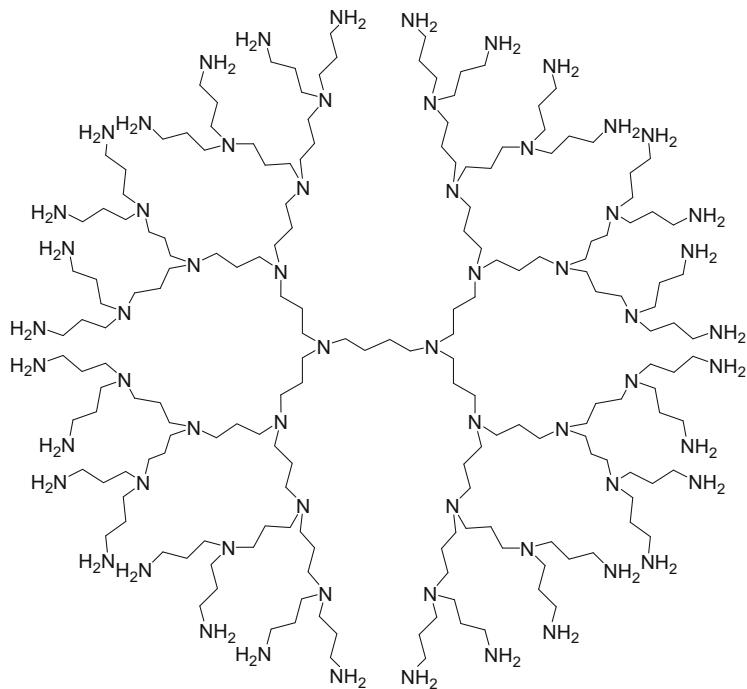


Fig. 15 Structure of a PPIG4 dendrimer

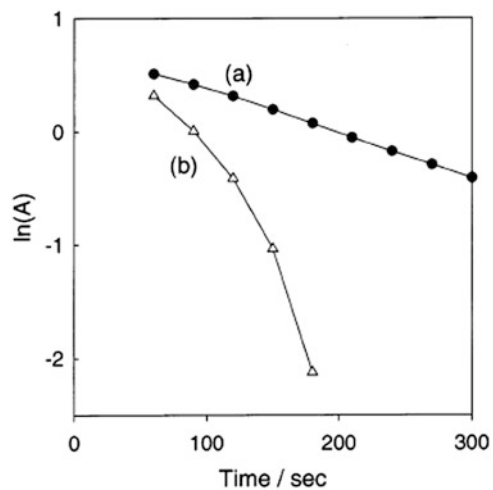


Fig. 16 Plots of $\ln A$ versus time for the reduction of 4-nitrophenol by Au NPs: (a) [PAMAM G3]/[Au³⁺] = 3 and (b) [PPI G3]/[Au³⁺] = 3. Adapted with permission from [67]. Copyright 2003 American Chemical Society

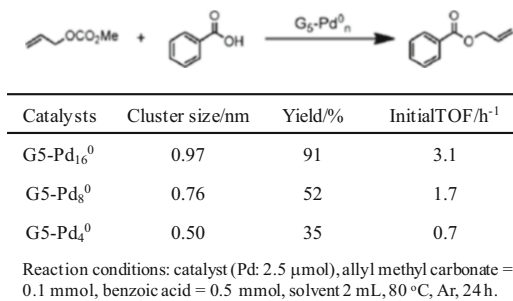


Fig. 17 Catalytic allylation in the presence of G5-Pd_n⁰ ($n = 4, 8, 16$). Adapted with permission from [72]. Copyright 2013 Royal Society Chemistry

attributed to the diffusion of 4-nitrophenol in the different sizes of two dendrimers. Three different metal NPs (Ag, Pt, and Pd) within PPI dendrimers were also conducted, resulting in the Pd-dendrimer nanocomposite which is the highest catalytic reduction [68].

Kaneda et al. investigated the catalytic properties of Pd NPs encapsulated within a fifth-generation PPI dendrimer functionalized with triethoxybenzamide on the termini. The dendrimer-encapsulated Pd NPs with a diameter of 2–3 nm are unique catalysts for substrate-specific hydrogenation of polar olefins, due to the strong interactions between the substrates and amino groups of the dendrimer [69]. The Pd_n NPs encapsulated within the PPI dendrimers (G5-Pd_n⁰) [70], prepared from the ratio of Pd complex to dendrimer, also exhibited catalytic activity for hydrogenation of hydrocarbons [71] and allylic substitution reactions [72]. The smallest Pd particle decreased the yield (35%) and initial turnover frequency (TOF = 0.7 h⁻¹) for allylation (Fig. 17).

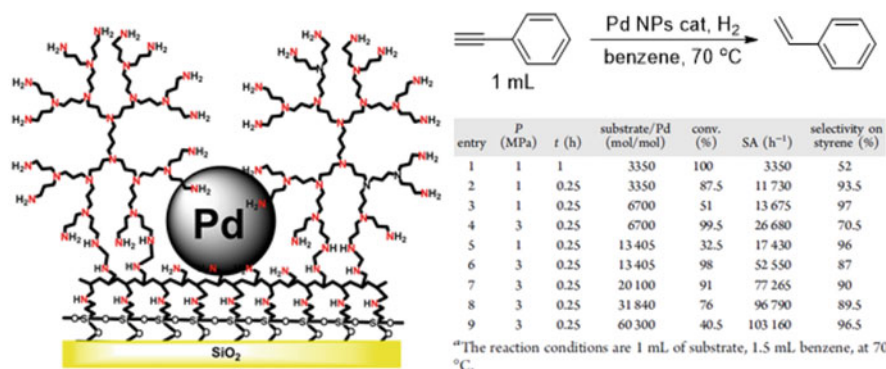


Fig. 18 Structure of Pd NPs encapsulated in a PPI dendrimer grafted to a silica surface modified with polyamine. Selective hydrogenation of phenylacetylene catalyzed by Pd NPs. Adapted with permission from [73]. Copyright 2014 American Chemical Society

New heterogeneous dendritic catalysts were tested using a combination of a silica polyamine composite with PPI dendrimers containing Pd NPs (1.95 ± 0.02 nm, Fig. 18) [73]. The Pd NPs were effective for catalytic hydrogenation of styrene, phenylacetylene, and dienes; their specific activities exceeded $100,000 \text{ h}^{-1}$ with the aid of nitrogen coordination of the PPI dendrimers. Optimal conditions for selective hydrogenation of phenylacetylene were at a substrate/Pd ratio equal to 20,100, which resulted in a conversion up to 91% and selectivity for styrene of 90% (Fig. 18, entry 7). The hybrid materials based on the Pd NPs effectively prevented metal leaching and could be used for several cycles. As a result, these catalyst systems possessed greater activity than Pd NPs combined with PPI dendrimers alone or Lindlar catalysts.

4 Click (Triazolyl) Dendrimers

Astruc et al. [74–81] prepared a series of “click” dendrimers composed of interior 1,2,3-triazolyl units and ferrocenyl, sulfonate or triethylene glycol (TEG) terminus, and so on. They investigated the encapsulation properties of the functionalized dendrimers containing hydrophobic and hydrophilic units. The functionalized click dendrimers are much interested in electrochemical, photochemical, and also catalytic performances.

Figure 19 shows two examples of “click” dendrimers, which contain tripodal branched with 9, 27, and 81 termini and 9, 36, and 117 triazole units, referred to as G0, G1, and G2, respectively. After reduction of Pd(II) complex in the dendrimer with ferrocenyl termini, dendrimers G1 and G2 gave small Pd DENs (G1,

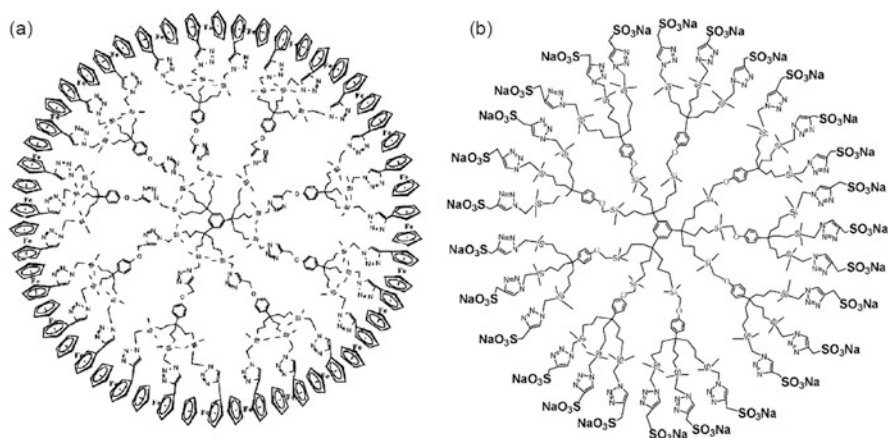


Fig. 19 Structures of “click” dendrimers with first generation (G1) with (a) hydrophobic ferrocenyl and (b) hydrophilic sulfonate terminus. Adapted with permission from [83, 86]. Copyright 2007 The Royal Society of Chemistry and 2008 Wiley-VCH Verlag GmbH & Co. KGaA, Weinheim

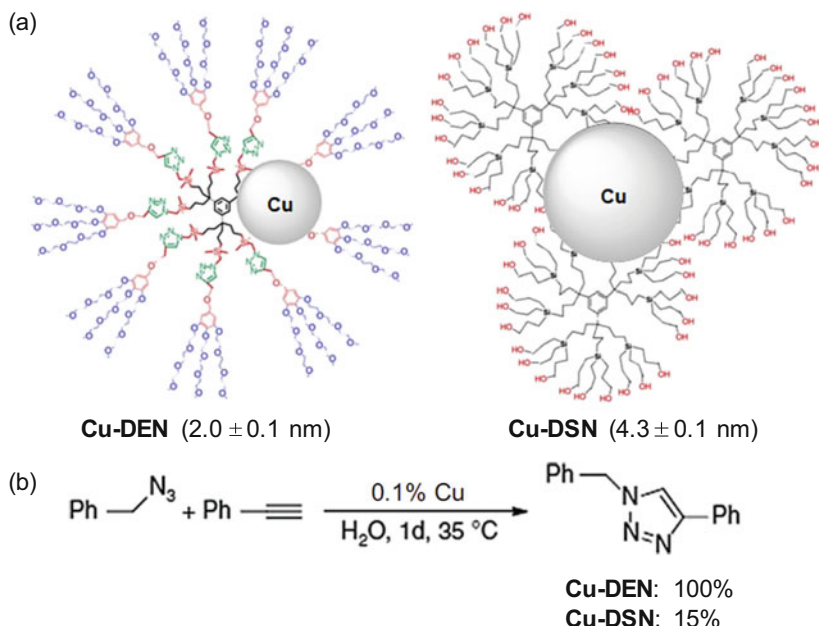


Fig. 20 (a) Proposed structures of Cu-DENs and Cu-DSNs. (b) Cu NPs-catalyzed AAC reaction. Adapted with permission from [92]. Copyright 2016 Macmillan Publishers Limited, part of Springer Nature

1.2 ± 0.2 nm; G2: 1.6 ± 0.3 nm). In contrast, the smallest dendrimer G0 formed a Pd DSN (1.2 ± 0.2 nm) due to its small size, with an open structure (Fig. 3b). The Pd NPs were stabilized by seven dendrimers [82, 83]. The interdendritic Pd DSNs were highly efficient, stable, and size-selective hydrogenation catalysts for various olefins in organic solvents [84] and Suzuki-Miyaura coupling reactions with 1 ppm of the Pd atom [85]. A water-soluble “click” dendrimer was achieved by incorporation of hydrophilic sulfonate. The Pd DSNs (2.3 ± 0.2 nm), formed by the smallest dendrimer (G0), were highly stable in air and were catalytically active for olefin hydrogenation and coupling reactions using a low amount of palladium (0.01 mol% Pd) [86].

Triethylene glycol (TEG) termini in the click dendrimer provide interdendritic assembly of DSNs, which protects the Pd NPs better than a single dendrimer [87–89]. The very small Pd NPs (1.4 ± 0.7 nm) were active in water/ethanol and catalyzed various cross-coupling reactions, such as Suzuki-Miyaura, Heck, and Sonogashira. The catalytic efficiency of Cu catalysts strongly depended on the location of the metal NPs inside or outside of the dendrimers (Fig. 20a) [90, 91]. In contrast, the inner Cu NPs (2.0 ± 0.1 nm), encapsulated by a dendrimer containing a triazole group (DEN), were protected from aerobic oxidation and catalyzed Huisgen-type alkyne-azide cycloaddition (AAC) quantitatively (Fig. 20b). The intradendritic Cu NPs (4.3 ± 0.1 nm) stabilized outside by a

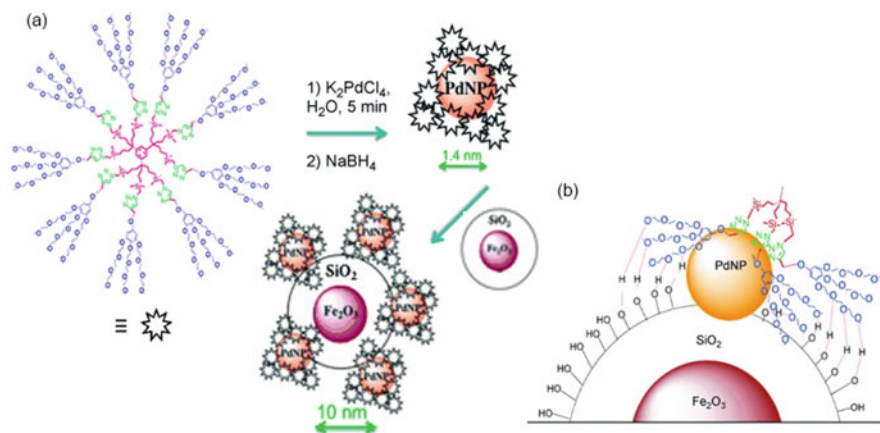


Fig. 21 (a) Impregnation of Pd NPs. (b) Fixation of the Pd NPs via hydrogen-bonding interactions of click dendrimers with the silica surface. Adapted with permission from [93]. Copyright 2015 Wiley-VCH Verlag GmbH & Co. KGaA, Weinheim

triazole-free dendrimer (DSN) were very rapidly oxidized at their surface, resulting in very poor catalytic conversion [92]. Therefore, the dendrimer ligands play a crucial role, which prevents aggregation of the NPs or air oxidation.

Magnetic dendritic catalysts have received attention because they can be recovered easily from reaction mixtures by exposure to an external magnetic field. Classical fixation of NPs on supports has been done mainly for the reduction of metal salts in the presence of the support. However, this process can cause aggregation of the NPs. Simple impregnation of SiO_2 -coated $\gamma-Fe_2O_3$ NPs with Pd NPs was succeeded by Astruc's group and produced stable, efficient, and recyclable heterogeneous catalysts for a variety of cross-coupling reactions at a low level of Pd loading (Fig. 21a) [93–95]. The very small Pd NPs (1.4 ± 0.7 nm) surrounded by triazolyl dendrimers with TEG termini immobilized onto the silica surface of $\gamma-Fe_2O_3$ NPs produced Pd NPs-located magnetic particles. The driving force for the strong Pd fixation onto the silica shell likely is provided by multiple supramolecular H-bonding interactions between the TEG termini and surface OH groups of the silica shell (Fig. 21b). In addition, the magnetic catalysts are so robust that the selective oxidation of benzylic alcohol by O_2 was quantitative in water, because the non-impregnated Pd NPs underwent immediate aggregation of Pd NPs in the presence of O_2 .

5 Polybenzyl Ethers (Fréchet-Type) Dendrimer

Fréchet-type dendrimer is based on polybenzyl ether hyperbranched skeleton based on 3,5-dihydroxybenzyl alcohol as the monomer unit (Fig. 22) [96]. The terminal groups act as good anchoring points for further functionalization. Fréchet-type dendrimers containing O atom have no coordination sites for metal ions. The dendron ligands with functionalized P or N atoms at the focal point form NP-cored dendrimers (NCDs), Fig. 3c which is easily prepared from the reduction of metal salts in the presence of the dendron ligands. The NCDs are effective catalysts in organic coupling reactions for readily approach of the reactants to the metal NPs.

Whitesell and Fox reported the first preparation of the Pd NCDs, surrounded by Fréchet-type polyaryl ether third-generation dendrons, had an average diameter of 2.0 nm composed of approximately 300 Pd atoms (Fig. 23) [97]. The Pd NPs surface was unpassivated and available for efficient phosphine-free Suzuki-Miyaura (TOF = 2,175) and Mizoroki-Heck (TOF = 1,738) reactions. Similar Pd NCDs stabilized by Fréchet-type phosphine dendrons of generations 1–3 were more active catalysts for Suzuki-Miyaura (TON = 65,000) and Stille coupling reaction, compared to the commonly used catalyst $[\text{Pd}(\text{PPh}_3)_4]$ [98, 99]. The Pt analogues (2.0–2.5 nm) with third generation are an active and reusable catalyst for the hydrogenation of nitrobenzenes [100].

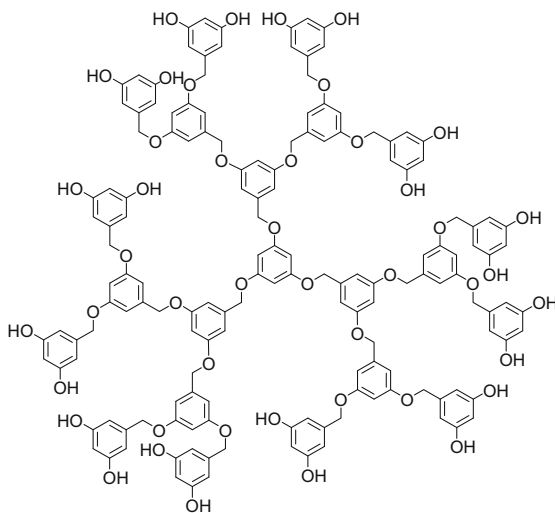


Fig. 22 Structures of Fréchet-type dendrimer

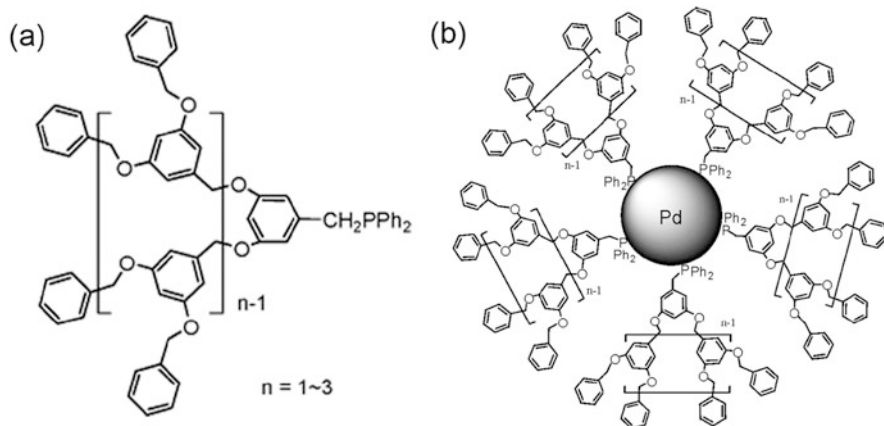


Fig. 23 (a) Structure of Fréchet-type polyaryl ether dendrons with a phosphine ligand. (b) Formation of Pd NCDs by self-assembly. Adapted with permission from [98]. Copyright 2006 American Chemical Society

6 Dendritic Poly(phenylazomethine) (DPA)

As described above, the dendrimers containing aliphatic chains possess the polydentate coordination sites with the same basicity. Precise accumulation of the metal halides is not possible even by specifying the loading ratio of the dendrimer and metal salts, resulting in statically distribution of the particle size. When accommodation of a metal ion to the N or P atoms of the common dendrimers was random, the number of metals accumulated in one dendrimer should be a Poisson distribution [101]. For example, in the case of random accumulation of the common monomer, the molar ratio of $[\text{metal ions}]/[\text{dendrimer}] = 5$ coexists not only with 5 but also with 3, 4, 6, and 7, resulting in a slightly broader distribution (Fig. 24). To obtain more narrow distribution of the accumulated numbers, the enthalpic driving force making the accumulation of metal ions should be used to reduce the distribution. Electronic gradient properties of the dendrimers can coordinate the metal ion to the suitable N sites in a regular order. In this case, the metal ion starts a stepwise assembly from the inner parts. The accumulated number of the metal leads to special numbers of 5, similar to the molar ratio at the calculated values ($25/5 = 5$).

To achieve an atomically monodispersed assembly of metals with a dendrimer, metal complexation to dendrimers should proceed in a stepwise, not random, fashion, which was developed by Yamamoto and co-workers [102–106]. Each imine nitrogen in the fourth-generation phenylazomethine dendrimer with *para*-phenylene unit (DPAG4-*p*Ph) formed a stepwise complex with SnCl_2 via a Lewis acid-base interaction (Fig. 25a) [107, 108]. Systematic analysis of this complexation revealed that SnCl_2 binds to imines of each generation of the dendrimer with different complexation constants. The fourth-generation dendrimer had four types of azomethines with slightly different basicity. This gradient enabled the stepwise

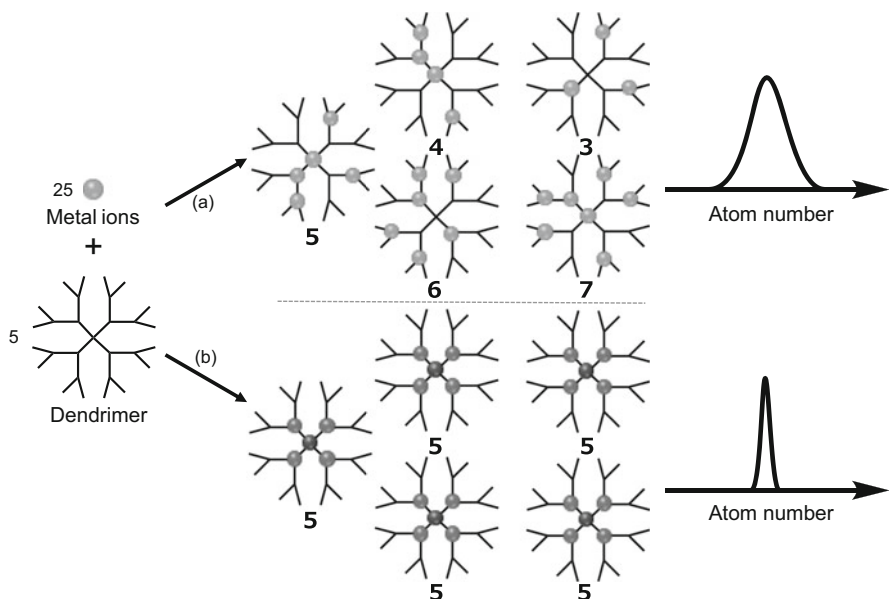


Fig. 24 Models to assemble the metal ion to dendrimers with (a) random accumulation and (b) precisely stepwise accumulation

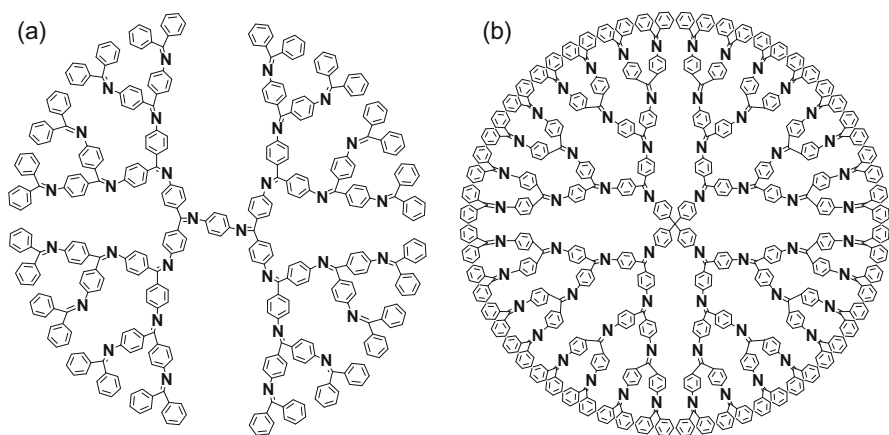


Fig. 25 Structures of dendritic poly(phenylazomethine) (DPA) with (a) a *p*-phenylene core (*p*Ph, two dendrons) and (b) a tetraphenylmethane core (TPM, four dendrons)

controlled assembly of multiple metals. Lewis acidic Sn halide starts a stepwise coordination to the imines with stronger basicity from the inner layer of the DPAG4-*p*Ph, to the adjacent outer layer. Fine-controlled metal assembly was established for various metal salts such as FeCl_3 and PtCl_4 , VCl_3 , $\text{TiCl}_3(\text{acac})$, and PtCl_4

[109]. After the accumulating metal salt, the following chemical reduction produced monodisperse metal clusters at the atomic level utilizing this principle [110]. A similar procedure of obtaining metal NPs was reported by using the PAMAM dendrimer containing amines and amides to undergo multidentate coordination or random accumulation of metal ions to the dendrimer. In contrast, the programmed clusters with the precise number of atoms can be established by stepwise accumulation of metal ions to the π -conjugated DPA dendrimers. This is only one example of the ability to control the precious number of atoms by changing the number of equivalents of dendrimer and metal salt. The DPAG4-*p*Ph with 2 dendrons consists of special magic numbers of 2, 6, 14, and 40 to assemble the metal ion with much narrow distribution. The DPAG4-TPM with 4 dendrons (Fig. 25b) involves similar magic numbers of 4, 12, 28, and 60, estimated as the sum of the number of N atom (Fig. 26).

A series of subnanosized Pt clusters with different atomicity values of 12, 28, and 60 using a DPAG4-TPM template and performed a fundamental electrochemical study dependent on the particle size of Pt for ORR [111]. When the particle size was decreased to the subnanometer scale, the resultant Pt clusters with ultrasmall sizes (<1 nm) exhibited molecule-like chemical properties derived from discrete electronic levels (Fig. 27). A comparison of the ORR activity of Pt₁₂, Pt₂₈, and Pt₆₀ showed greater activity for the smallest Pt₁₂ cluster than for Pt₂₈ and Pt₆₀, which exhibited 13 times higher catalytic activity than a conventional commercial carbon-supported Pt NPs (particle sizes 2–4 nm).

The Pt₁₂@DPAG4-TPM cluster also was a highly efficient catalyst for hydrogenation of low-reactive olefins that have an electron-withdrawing group [112] or steric hindrance and reductive amination of aldehydes with amines (Fig. 28) [113]. The catalytic performance of the Pt₁₂ cluster was attributed to the geometric and electronic properties of the atom-specific cluster, compared to commercially available Pt catalysts supported on activated carbon (2.2 ± 0.8 nm). Moreover, these subnanosized Pt_{*n*} clusters ($n = 12, 28, \text{ and } 60$) catalyzed aerobic oxidation of aromatic alcohols in the presence of organic peroxidant (*tert*-butyl hydroperoxide, TBHP) as room temperature (Fig. 29) [114].

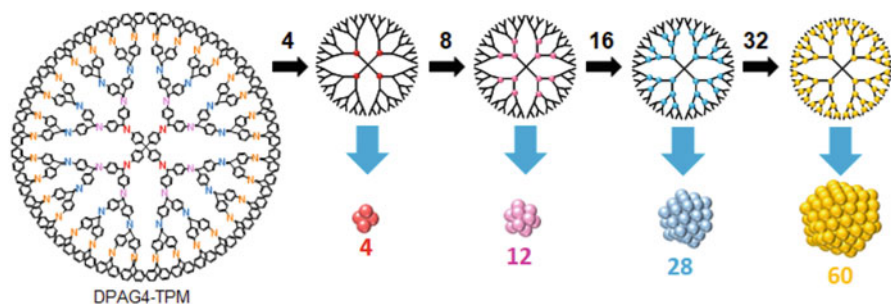


Fig. 26 Schematic representation of stepwise accumulation of metal ion in DPAG4-TPM

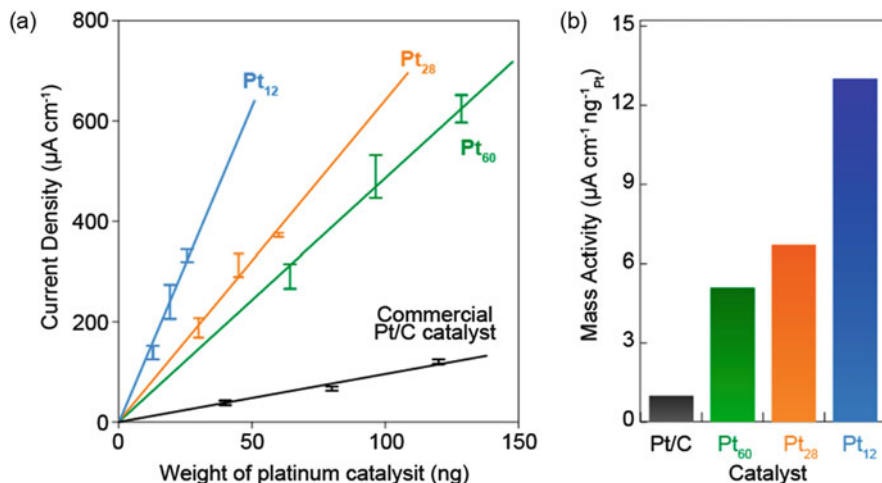


Fig. 27 (a) Dependence of kinetic current density on the weight of platinum modified on a glassy carbon electrode for Pt_n@DPAG4-TPM ($n = 12, 28, \text{ or } 60$) and for commercially available Pt catalyst. (b) Comparison of catalytic performances normalized by the weight of Pt_n clusters and the Pt/C catalysts. Adapted with permission from [111]. Copyright 2014 American Chemical Society

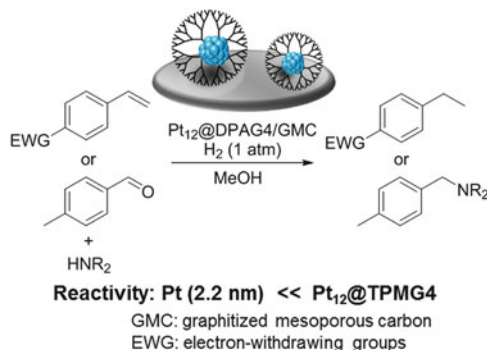


Fig. 28 Hydrogenation of low-reactive olefins and reductive amination of aldehydes catalyzed by Pt₁₂@DPAG4-TPM/GMC

Size-controlled tin oxide clusters, Sn_nO_x ($n = 12\text{--}60$), were prepared using accumulation of SnCl₂ to a DPA-TPM dendrimer, loaded into mesoporous silica, followed by chemical reduction and calcination under air to remove the dendritic template. The Sn_nO_x clusters are catalytically active for CO oxidation reactions (Fig. 30) [115–117]. The synthesized clusters contained not only stable Sn(IV) but also metastable divalent Sn(II) species, which act as an active site for CO adsorption. The increased ratio of Sn(II)/Sn(IV) that decreased the particle size enhanced CO oxidation reactivity.

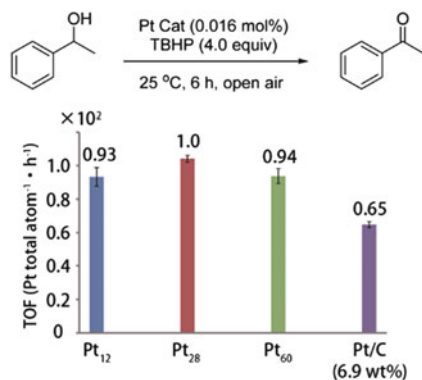


Fig. 29 Aerobic oxidation of aromatic alcohol as a function of the number of the Pt_{*n*} clusters (*n* = 12, 28, 60). Adapted with permission from [114]. Copyright 2015 The Royal Society of Chemistry

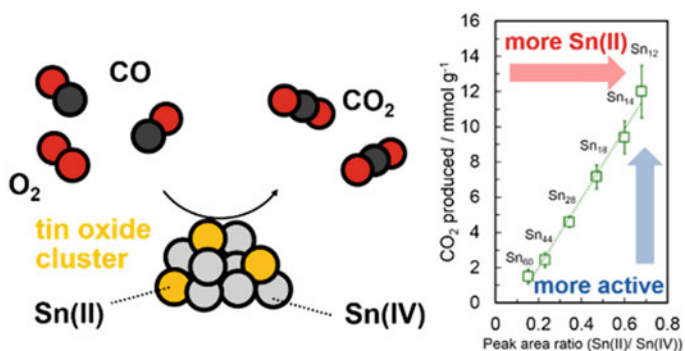


Fig. 30 CO oxidation reactivity relative to size-selected Sn_{*n*}O_{*x*} clusters. Adapted with permission from [115]. Copyright 2018 American Chemical Society

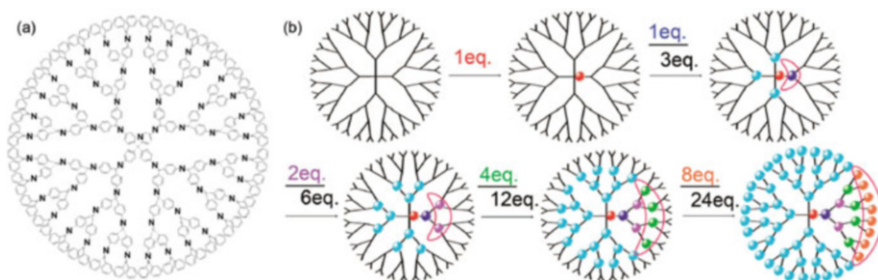


Fig. 31 (a) Structure of a DPAG4-PyTPM dendrimer and (b) unsymmetrical stepwise complexation of the metal ion to the dendrimer. Adapted with permission from [118]. Copyright 2012 The Chemical Society of Japan

In order to investigate the ORR catalytic performance dependent on the atomicity of the Pt_n ($n = 12-28$) cluster, a special dendrimer, DPAG4-PyTPM [118], was prepared by incorporation of a pyridoxine(triphenylene)methane core (Fig. 31). Unsymmetrical structure of the dendrimer increases the magic numbers of 1, 2, 5, 7, 13, 17, 29, 37, and 61 to coordinate the metal ion with narrow distribution. One incorporated pyridine changed the basicity of the imines on one dendron and increased coordinating sites having different basicities.

The Pt_{12} possessed significantly greater activity than that expected from the difference in the surface area. In contrast, the Pt_{13} cluster resulted in 2.5 times lower catalytic activity than Pt_{12} , which is no less than non-scalable physical properties which greatly differ depending on the atom number [119]. While the atomicity of Pt_{13} is the geometrically defined magic number, the shortage of one atom from the magic number of Pt_{13} was proposed to affect the exceptional activity of Pt_{12} through structural defects. Finally, experiments concluded that Pt_{19} cluster is the greatest oxygen reduction activity in the subnanometer region (Fig. 32) [120]. The ORR performance of the Pt NPs synthesized by PAMAM dendrimer did not reveal any difference on atomicity. In the case of DPA-PyTPM, however, a clear difference in ORR activity was observed for clusters with different numbers of Pt atoms. The atomicity dependence of catalytic activity revealed a big difference in scalability, which is attributed to “quantum effects” of the ultrasmall clusters. Thus, the accuracy of the cluster obtained by each dendrimer is different at the atomic level.

Selective oxidation of hydrocarbons is an important chemical reaction in both academic research and industry, because it can convert raw materials into value-added products in the fields of pharmaceuticals, polymers, and specialty chemicals. The $Pt_{19}@DPAG4-PyTPM$ with a narrow particle size distribution exhibits the highest catalytic performance with a turnover frequency of $3,238 \text{ atom}^{-1} \text{ h}^{-1}$, which is 1,700 times greater than that obtained by commercial Pt/C catalysts

Fig. 32 Catalytic activity for electrochemical oxygen reduction on platinum clusters with different atomicity. Clusters were synthesized using PAMAM or DPA-PyTPM dendrimers as the template. Adapted with permission from [120]. Copyright 2015 Wiley-VCH Verlag GmbH & Co. KGaA, Weinheim

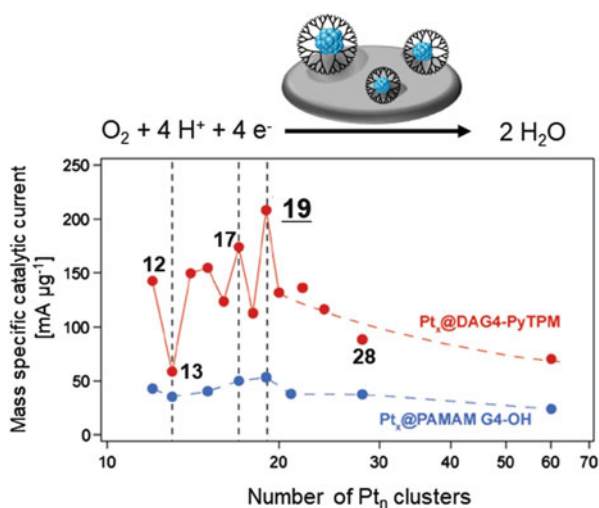
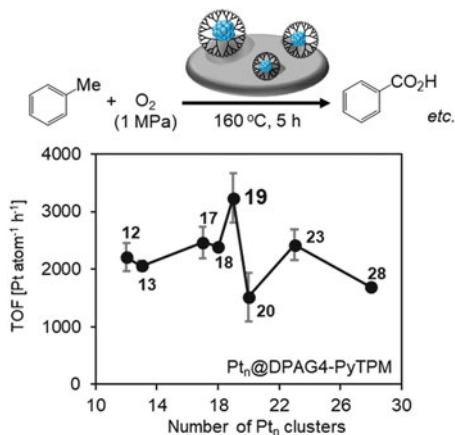


Fig. 33 Catalytic performance of subnanosized Pt_n particles ($n = 12, 28, \text{ and } 60$) in aerobic toluene oxidation. TOFs estimated from the sum of the TOFs for each product. Adapted with permission from [121]. Copyright 2019 Wiley-VCH Verlag GmbH & Co. KGaA, Weinheim



(Fig. 33) [121, 122]. A size-dependent oxygen activation pathway was proposed on the basis of the extended surface areas and irregular electron distributions, involving the formation of a hydroperoxide species on the surface. Similar characteristics were observed not only for oxygen reduction but also for aerobic oxidation of toluene, for which Pt_{19} was reported to be the best catalyst.

7 Bimetallic and Multimetallic Catalysts Within Dendrimers

Bimetallic NPs and clusters have attracted the interest of scientists because of the synergic effects that emerge from the compositional ratio between two distinct metals. These novel alloy materials provide catalytic selectivity, activity, and stability that are different from those for monometallic NPs. Three different approaches (co-complexation, sequential loading, and partial displacement methods) to prepare dendrimer-stabilized NPs are shown in Fig. 34. (1) The co-complexation method involves coordination of two metals in the dendrimer, followed by simultaneously chemical reduction to form alloy NPs. The composite ratios can be controlled by the amounts of the two metal ions added. This method is suitable for synthesizing multinuclear NPs composed of more than three metals. (2) The sequential loading method is effective for the preparation of core@shell NPs. Core@shell NPs are also interesting because their electronic and catalytic properties can be tuned by manipulating their structure. (3) The particle sizes in the partial displacement method are increased after the second reduction step. The partial displacement methods are dependent on the properties of transition metals. Cu NPs undergo galvanic exchange with less than a stoichiometric amount of Ag^+ , Au^{3+} , Pt^{2+} , and Pd^{2+} to give bimetallic NPs composed of Cu and these noble metals.

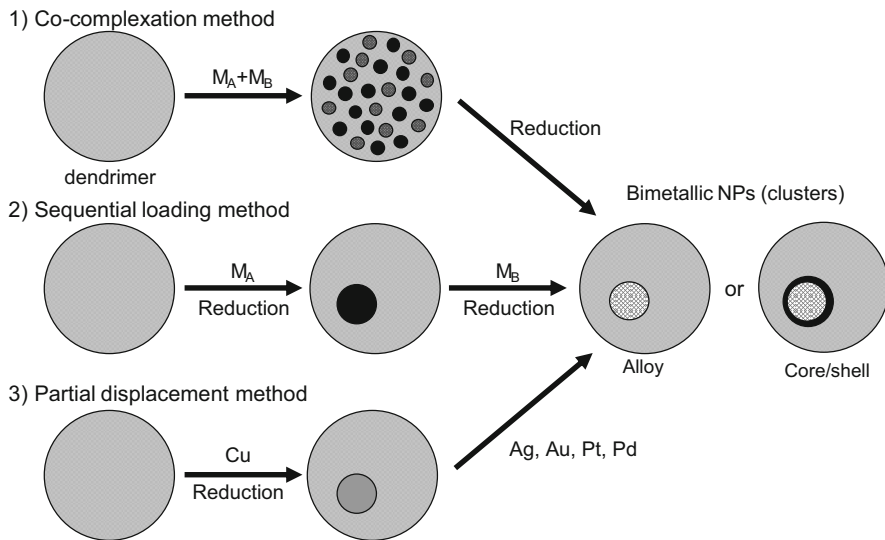


Fig. 34 Major synthesis schemes for bimetallic NPs (clusters) in a dendrimer

Crooks et al. reported the preparation of bimetallic PdPt alloys with sizes of <2 nm via a co-complexation method using K_2PdCl_4 and K_2PtCl_4 with the PAMAM-OH dendrimer as a synthesis template, and the product was characterized using energy-dispersive X-ray spectroscopy (EDS) [123]. The catalytic performance of these bimetallic alloys shows a synergistic effect in the hydrogenation of allyl alcohol, compared to physical mixtures containing Pd-only and Au-only catalysts. Both alloy and core/shell PdAu NPs of 1–3 nm in diameter were prepared by the co-complexation and sequential loading methods [124]. The hydrogenation rates with the PdAu alloys are enhanced compared to physical mixtures of the single-atom catalysts (Fig. 35). Rhee reported synergistic effects for the hydrogenation of cyclohexane over PdPt alloys [125] and the partial hydrogenation of 1,3-cyclooctadiene over PdRh alloys [126]. The highest activities for bimetallic PdPt and PdRh catalysts were achieved at ratios of 4:1 and 1:2, respectively.

Heterogeneous bimetallic systems have also been prepared by the immobilization of dendrimer-stabilized NPs on solid materials. Chandler et al. reported that dendrimer-stabilized PtAu NPs were adsorbed onto a high surface area SiO_2 support and thermally activated to remove the dendrimer ($300^\circ C$) under O_2 atmosphere and the following H_2 treatment (Fig. 36) [127]. The supported alloy NPs remained small at less than 3 nm, while monometallic Au particles readily form very large particles under such thermal conditions. The prepared $Pt_{16}Au_{16}$ NPs obtained from the intradendrimer exchange [128] of Cu with Pt and Au in a 1:1 stoichiometry enhanced the reaction rate for the catalysis of CO oxidation compared to that for single-metal Pt_{32} and Au_{32} particles and that for a physical mixture of $Pt_{32} + Au_{32}$. The same authors investigated the effects of the support for PtAu dendrimer-encapsulated NPs and found that a TiO_2 -supported catalyst showed resistance to

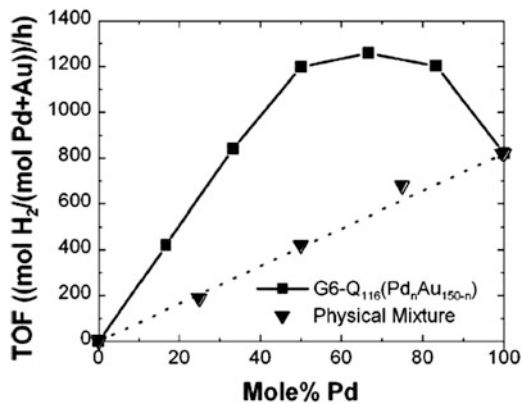


Fig. 35 Turnover frequencies (TOFs) for the hydrogenation of allyl alcohol as a function of the Pd mole percent in Pd-Au alloys and physical mixtures containing Pd-only and Au-only particles. The ■ symbols represent the bimetallic NPs, while the ▼ symbols represent data obtained from physical mixtures of Pd and Au. Adapted with permission from [124]. Copyright 2004 American Chemical Society

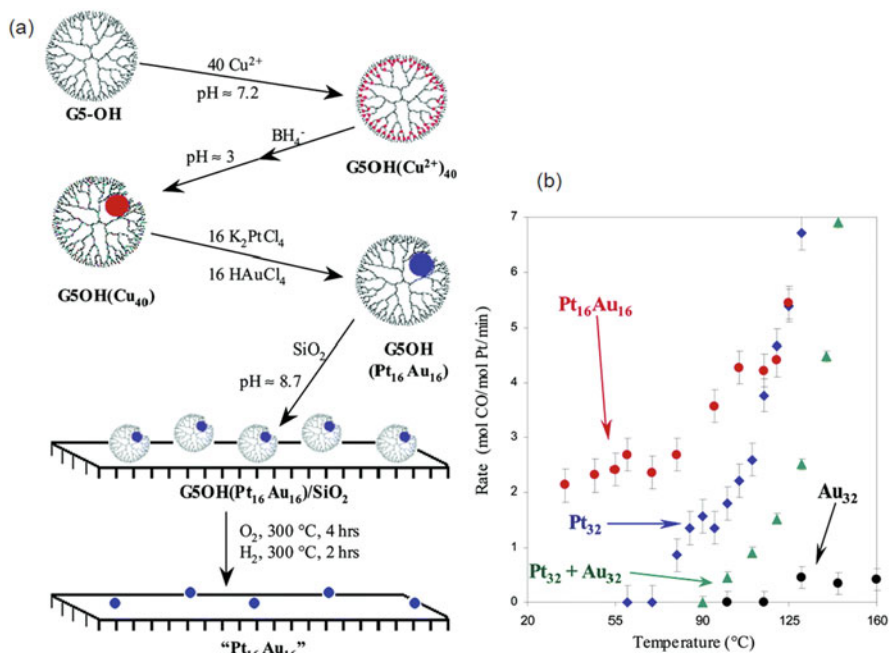


Fig. 36 (a) Schematic procedure for catalysis over a dendrimer-templated bimetallic Pt-Au alloy NPs on a support and (b) CO oxidation catalysis by silica-supported Pt₁₆Au₁₆, Pt₃₂, Au₃₂, and Pt₃₂ + Au₃₂. Adapted with permission from [127]. Copyright 2004 American Chemical Society

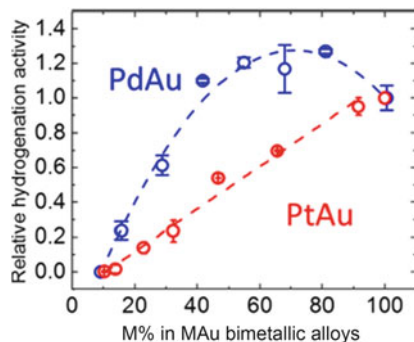


Fig. 37 TOF as a function of the ratio of M in MAu alloys. Adapted with permission from [131]. Copyright 2017 American Chemical Society

deactivation during an extended high-temperature oxidation treatment [129]. The TiO_2 -supported PdAu bimetallic catalyst also exhibited a synergetic catalytic effect toward CO oxidation compared to the supported Pd-only and Au-only catalysts [130].

PtAu and PdAu random alloy dendrimer-encapsulated NPs with an average size of about 1.6 nm exhibit different catalytic activity trends for alloy alcohol hydrogenation [131]. PtAu NPs exhibited a linear increase in activity with Pt content, whereas PdAu dendrimer-encapsulated NPs showed a maximum activity at a Pd content of about 60% (Fig. 37). Experimental and theoretical results suggested that this trend is caused by different positions of the H atoms on the PtAu and PdAu surfaces. H atoms are restricted to Pt-only surface sites on the PtAu NP surfaces, while H atoms interact with both Pd and Au atoms on the PdAu NP surfaces.

Qian et al. reported a novel AuPt bimetallic flower-shape nanostructure fabricated on a PAMAM dendrimer on an indium tin oxide support by electrochemical deposition [132]. Crooks investigated electrochemical reactions using bimetallic catalysts encapsulated by PAMAM dendrimers. Bimetallic PtPd NPs with 2:1 and 3:1 ratios and with an average of 180 atoms exhibited superior activity compared to monometallic Pt catalysts [133]. Au@Pt core/shell NPs were prepared via electrochemical underpotential deposition of Cu to an Au core on a glassy carbon electrode, followed by galvanic exchange of the Cu shell with Pt [134]. The electrocatalytic activity of $\text{Au}_{147}@\text{Pt}_n$ NPs ($n = 102$, full shell, and 54, part shell) was found to be similar [135], whereas the same bimetallic NPs showed efficient electrocatalytic oxidation of HCOOH [136]. This is due to deformation of the small particles, which resulted in the enhanced catalytic activity. The unique nanostructure contributed to the electrocatalytic activity toward the oxygen reduction reaction (ORR). In addition, trimetallic alloy-core-shaped AuPd@Pt NPs covered with an atomically thin Pt surface layer were stable [137]. Electrochemical measurements of the ORR activity of the AuPd@Pt NPs revealed a volcano-shaped trend with the peak top for a 28% Au/72% Pd alloy core, which is in a good agreement with the theoretical prediction (Fig. 38).

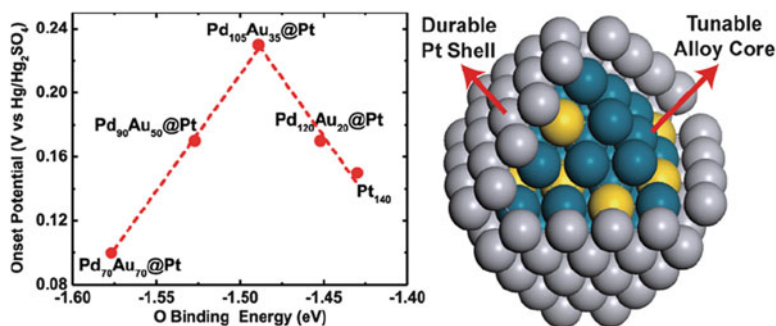


Fig. 38 Illustration of the trimetallic AuPd@Pt NP and the ORR catalytic activity. Adapted with permission from [137]. Copyright 2013 American Chemical Society

Bimetallic NPs composed of noble and base metal alloys are expected to exhibit interesting physical and chemical properties. Astruc et al. investigated the catalytic performance of AgCu and AuCu alloys that were prepared by the partial displacement method in G1 click dendrimer with a TEG termini [138]. Exposure of the AgCu alloy to air led only to Cu(0) oxidation to Cu(I), whereas Cu(0) was not oxidized in AuCu alloyed NPs. The AgCu catalyst underwent an almost quantitative reaction during the catalytic ACC reaction due to the efficient formation of Cu(I) species under air (Fig. 39). The PtCo nanoalloys in a 1:1 ratio stabilized by the same click dendrimer are much more efficient for hydrolysis of ammonia borane than either the dendrimer-stabilized Co or Pt analogue alone [139]. The synergy effect of the alloy is suggested to involve its intradendritic triazole ligands that activate the NP surface.

Incorporation of Cu into Pt NPs in the bimetallic NPs caused a CO adsorption peak that was red-shifted by 10–15 cm^{-1} from the original Pt₄₅-CO peak at 2075 cm^{-1} (Fig. 40) [140]. The peak shift is attributed to weak donation from Cu, which is more electropositive than Pt. The bimetallic CuPt catalysts enhanced the CO oxidation rate and decreased the activation energy due to the fluxional nature of the CO ligand. A possible explanation is that surface Cu atoms provide new sites that bind CO more weakly than monometallic Pt sites. In contrast, toluene hydrogenation was suppressed by Cu addition, and the catalysis was effectively shut off at a 2:1 Cu/Pt ratio. TiO₂-supported bimetallic AuNi NPs with sizes of approximately 2 nm, which were prepared using PAMAM dendrimer templates, enhanced oxygen activation for CO oxidation [141]. Incorporation of Ni into Au resulted in stronger adsorption of O and CO on the Au surfaces, as estimated by theoretical calculations. At the same time, the introduction of Ni reduced the relative number of catalytically active sites. Pt_n@Cu core@shell NPs (average *n* of 55, 147, and 255) encapsulated by PAMAMG6-OH were prepared via underpotential deposition of a Cu monolayer on a Pt core, which was immobilized on glassy carbon [142]. A small amount of Cu (only 2%) on Pt NPs accelerated the CO oxidation rate, compared to that for Cu-free Pt NPs. The isolated Cu atoms on Pt surface possess OH groups and act as binding

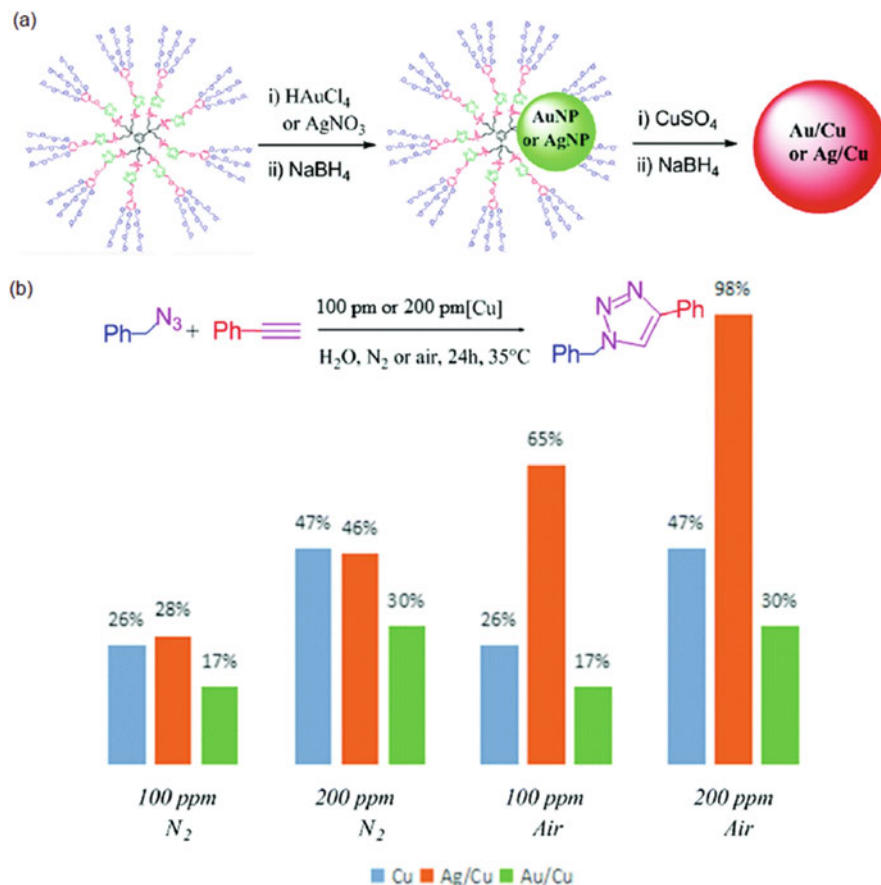


Fig. 39 (a) Procedure for the synthesis of the AuCu and AgCu alloys within a click dendrimer. (b) Catalytic activity of the alloys and Cu NPs in the catalytic AAC reaction. Adapted with permission from [140]. Copyright 2017 The Royal Society of Chemistry

sites for CO. This suggests that a trace amount of a cocatalytic metal leads to a significant improvement in catalytic performance [143].

Yamamoto et al. successfully prepared an atom-specified bimetallic Rh₃₂Fe₂₈ cluster using a fourth-generation phenylazomethine dendrimer derivative (DPAG4) [144]. The DPA enables the number and composition of different metals to be defined at the atomic level through layer-by-layer stepwise complexation of imine sites with metal ions (Fig. 41). The Rh₃₂Fe₂₈ cluster showed synergistic catalysis toward the hydrogenation of olefins and nitroarenes and demonstrated enhanced activity that surpassed that of a single Rh catalyst [145] and Wilkinson catalysts.

Multimetallic hybrid clusters with three elements were also prepared using a DPAG4-TPM template. Heterometal assemblies of AuCl₃, PtCl₄, and CuCl₂ in an

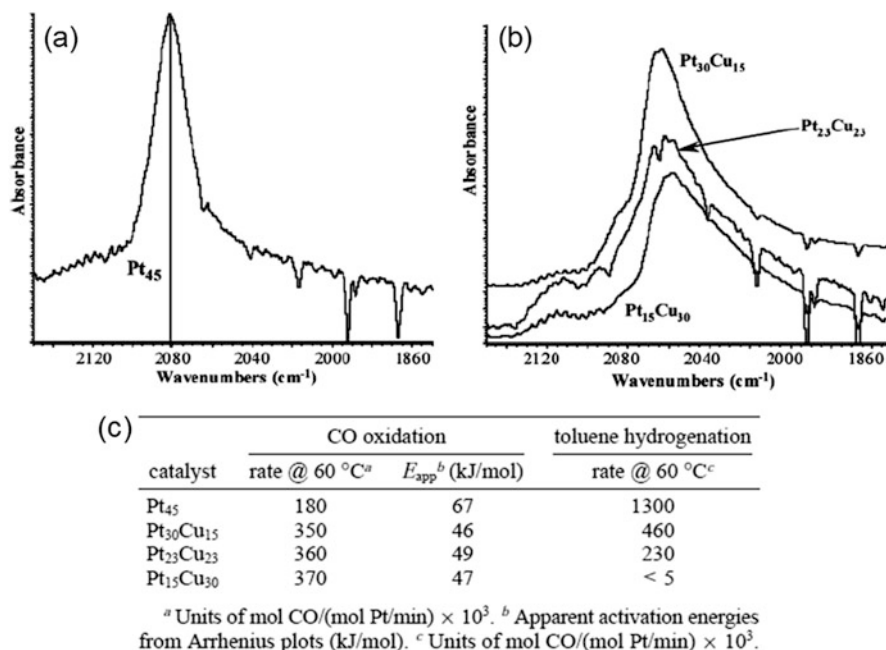


Fig. 40 (a) Infrared spectra of CO adsorbed on Pt₄₅ and on (b) Pt₃₀Cu₁₅, Pt₂₃Cu₂₃, and Pt₁₅Cu₃₀. (c) Summary of catalytic activity data. Adapted with permission from [140]. Copyright 2006 American Chemical Society

order were produced from the inner imines to the outer imines of the dendrimer, which was dominated by the Lewis acidity of the metal halide and the gradient Lewis basicity of the imine sites on each layer. The trimetallic CuPtAu cluster supported on carbon materials, obtained after chemical reduction, possessed greater catalytic activity than those of the single or bimetallic catalysts for the solvent-free aerobic oxidation of aromatic hydrocarbons [146]. Hybridization of copper atoms into the multimetallic clusters resulted in enhancement of the catalytic performance, which was 24 greater times than that for a commercially available Pt/C catalyst (Fig. 42).

Multimetallic sub-nanoclusters were successfully synthesized using a DPA-PyTPM template [147]. Precisely controlled multimetallic accumulation of five metal salts with different Lewis acidities: GaCl₃ > InBr₃ > AuCl₃ > BiCl₃ > SnBr₂, provided the location to coordinate five metal halides with a narrow distribution (Fig. 43). The multimetallic clusters, formed by chemical reduction of the complex, were confirmed using scanning transmission electron microscopy (STEM) and EDS, which revealed the spectral peaks of the five elements. This synthesis technique for multimetallic sub-nanoclusters could also be utilized for other metal species such as Fe, Pd, Rh, Sb, Cu, and Pt and is referred to as “atom hybridization.”

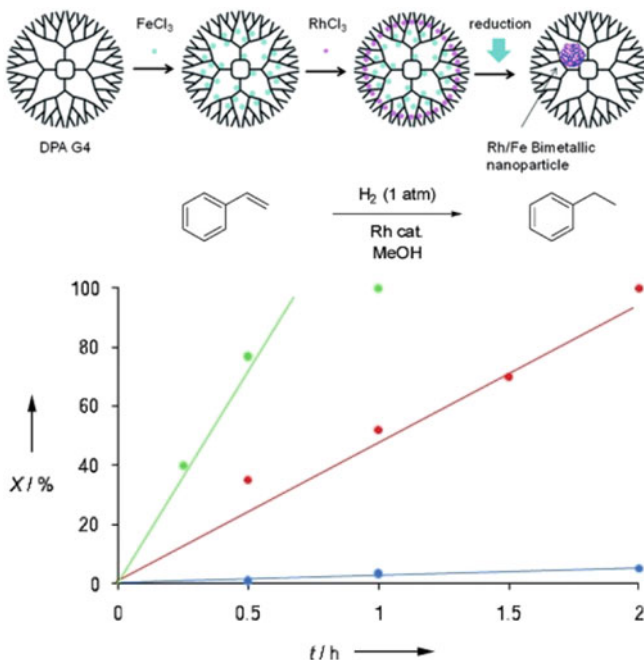


Fig. 41 Conversion (X) as a function of the reaction time (t) for the catalytic hydrogenation of styrene. Wilkinson catalyst (blue), Rh₆₀@DPAG4 (red), and Rh₃₂Fe₂₈@DPAG4 (green). Adapted with permission from [144]. Copyright 2011 Wiley-VCH Verlag GmbH & Co. KGaA, Weinheim

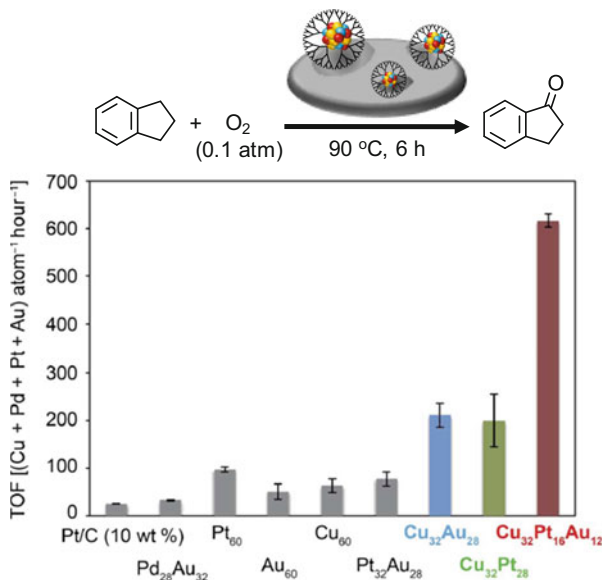


Fig. 42 Comparison of the catalytic activities of various catalysts based on TOF for the solvent-free aerobic oxidation of indane under an O₂ atmosphere. Adapted with permission from [146]. Copyright 2017 The American Association for the Advancement of Science (AAAS)

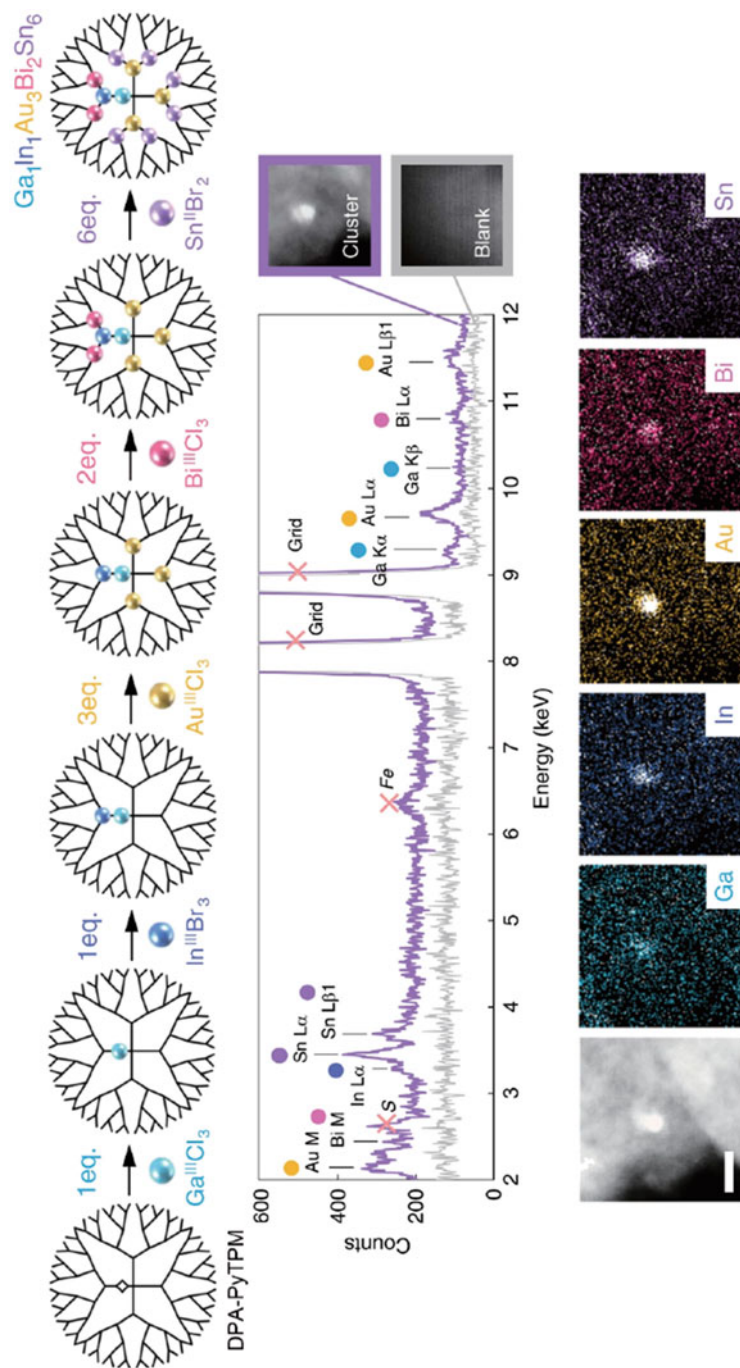


Fig. 43 Stepwise multimetallic accumulation of five metal salts on DPAG4-PyTPM and STEM/EDS analysis of five-element sub-nanocluster on carbon material. Adapted with permission from [147]. Copyright 2018 Macmillan Publishers Limited, part of Springer Nature

8 Conclusion

This article has provided an overview of the precisely controlled synthesis of NPs encapsulated by dendrimers and their catalytic applications. Since the first preparation of size-controlled NPs in the 1990s by Crooks, the use of dendritic nanocatalysts has increased rapidly and has provided a variety of catalytic reactions such as hydrogenation, C-C bond forming reactions, the oxidation of hydrocarbons and alcohols, and the ORR. Monometallic and bimetallic NPs stabilized by various dendrimers have been widely investigated with respect to catalytic application in both homogeneous and heterogeneous systems. Catalysis generally proceeds in the dendritic interior; therefore, the dendrimer plays a role as a nanoreactor to prevent aggregation of the NPs. Functionalized dendrimers containing triazolyl units, developed by Astruc, led to the achievement of sub-parts per million levels of metal loading catalysts and immobilization on magnetic NPs in pursuit of practical green chemistry. Precise control of the atom-specified clusters has been achieved with π -conjugated DPA derivatives. The sub-nanoclusters enhanced catalytic performance for electrochemical and organic reactions because of the reactive amorphous structure and irregular electronic distribution of the cluster surface [148]. Although recent enthusiasm with regard to multimetallic NPs leads to effective synergetic effects in catalysis, the synthesis technique for control of the size and components has been difficult at the sub-nanometer scale. The approach to synthesize heteroatom clusters using the DPA template is much expected to develop the uncultivated field for sophisticated catalysis [149, 150].

Acknowledgments This study was supported in part by JST ERATO Grant Number JPMJER1503, Japan (K. Y.), JSPS KAKENHI Grant No. JP 15H05757 (K. Y.). We would like to show our respect for the great efforts of all authors, whose names were listed in the references.

References

1. Okumura M, Fujitani T, Huang J, Ishida T (2015) *ACS Catal* 5:4699
2. Tomalia DA, Baker H, Dewald J, Hall M, Kallos G, Martin S, Roeck J, Ryder J, Smith P (1985) *Polym J* 17:117
3. Tomalia DA, Dvornic PR (1994) *Nature* 372:617
4. Tomalia DA, Naylor AM, Goddard WA (1990) *Angew Chem Int Ed Engl* 29:138
5. Tomalia DA (1996) *Macromol Symp* 101:243
6. Tomalia DA, Fréchet JMJ (2002) *J Polym Sci A Polym Chem* 40:2719
7. Zhao M, Sun L, Crooks RM (1998) *J Am Chem Soc* 120:4877
8. Balogh L, Tomalia DA (1998) *J Am Chem Soc* 120:7355
9. Esumi K, Suzuki A, Aihara N, Usui K, Torigoe K (1998) *Langmuir* 14:3157
10. Tomalia DA, Hall M, Hedstrand DM (1987) *J Am Chem Soc* 109:1601
11. Tomalia DA, Berry V, Hall M, Hedstrand DM (1987) *Macromolecules* 20:1164
12. Naylor AM, Goddard III WA, Kiefer GE, Tomalia DA (1989) *J Am Chem Soc* 111:2339
13. Crooks RM, Zhao M, Sun L, Chechik V, Yeung LK (2001) *Acc Chem Res* 34:181
14. Scott RWJ, Wilson OM, Crooks RM (2005) *J Phys Chem B* 109:692

15. Myers VS, Weir MG, Carino EV, Yancey DF, Pande S, Crooks RM (2011) *Chem Sci* 2:1632
16. Anderson RM, Yancey DF, Zhang L, Chill ST, Henkelman G, Crooks RM (2015) *Acc Chem Res* 48:1351
17. Zhao M, Crooks RM (1999) *Angew Chem Int Ed* 38:364
18. Niu Y, Yeung LK, Crooks RM (2001) *J Am Chem Soc* 123:6840
19. Oh S-K, Niu Y, Crooks RM (2005) *Langmuir* 21:10209
20. Ye H, Scott RWJ, Crooks RM (2004) *Langmuir* 20:2915
21. Chechik V, Zhao M, Crooks RM (1999) *J Am Chem Soc* 121:4910
22. Chechik V, Crooks RM (2000) *J Am Chem Soc* 122:1243
23. Yeung LK, Lee Jr CT, Johnston KP, Crooks RM (2001) *Chem Commun* 21:2290
24. Johnson JA, Makis JJ, Marvin KA, Rodenbusch SE, Stevenson KJ (2013) *J Phys Chem C* 117:22644
25. Wilson OM, Knecht MR, Garcia-Martinez JC, Crooks RM (2006) *J Am Chem Soc* 128:4510
26. Maity P, Yamazoe S, Tsukuda T (2013) *ACS Catal* 3:182
27. Nemanashi M, Meijboom R (2013) *J Colloid Interface Sci* 389:260
28. Antonels NC, Meijboom R (2013) *Langmuir* 29:13433
29. Li Y, El-Sayed MA (2001) *J Phys Chem B* 105:8938
30. Narayanan R, El-Sayed MA (2004) *J Phys Chem B* 108:8572
31. Rahim EH, Kamounah FS, Frederiksen J, Christensen JB (2001) *Nano Lett* 1:499
32. Pittelkow M, Moth Poulsen K, Boas U, Christensen JB (2003) *Langmuir* 19:7682
33. Lemo J, Heuzé K, Astruc D (2006) *Inorg Chim Acta* 359:4909
34. García-Martínez JC, Lezutekong R, Crooks RM (2005) *J Am Chem Soc* 127:5097
35. Bernechea M, de Jesus E, López-Mardomingo C, Terreros P (2009) *Inorg Chem* 48:4491
36. Esumi K, Houdatsu H, Yoshimura T (2004) *Langmuir* 20:2536
37. Kéki S, Török J, Deák G, Daróczy L, Zsuga M (2000) *J Colloid Interface Sci* 229:550
38. Mizugaki T, Murata M, Fukubayashi S, Mitsudome T, Jitsukawa K, Kaneda K (2008) *Chem Commun* 2:241
39. Lang H, May RA, Iversen BL, Chandler BD (2003) *J Am Chem Soc* 125:14832
40. Deutsch DS, Lafaye G, Liu D, Chandler B, Williams CT, Amiridis MD (2004) *Catal Lett* 97:139
41. Albiter MA, Morales R, Zaera F (2011) *Appl Catal A* 391:386
42. Lafaye G, Siani A, Marecot P, Amiridis MD, Williams CT (2006) *J Phys Chem B* 110:7725
43. Wu H, Liu Z, Wang X, Zhao B, Zhang J, Li C (2006) *J Colloid Interface Sci* 302:142
44. Ye H, Crooks RM (2005) *J Am Chem Soc* 127:4930
45. Ye H, Crooks JA, Crooks RM (2007) *Langmuir* 23:11901
46. Vijayaraghavan G, Stevenson KJ (2007) *Langmuir* 23:5279
47. Trindell JA, Clausmeyer J, Crooks RM (2017) *J Am Chem Soc* 139:16161
48. Ye R, Zhukhovitskly AV, Deraedt C, Toste FD, Somorjai GA (2017) *Acc Chem Res* 50:1894
49. Huang W, Kuhn JN, Tsung CK, Zhang Y, Habas SE, Yang P, Somorjai GA (2008) *Nano Lett* 8:2027
50. Kuhn JN, Huang W, Tsung C-K, Zhang Y, Somorjai GA (2008) *J Am Chem Soc* 130:14026
51. Ye R, Yuan B, Zhao J, Ralston WT, Wu C-Y, Barin EU, Toste DF, Somorjai GA (2016) *J Am Chem Soc* 138:8533
52. Deraedt C, Ye R, Ralston WT, Toste FD, Somorjai GA (2017) *J Am Chem Soc* 139:18084
53. Ye R, Zhao J, Yuan B, Liu W-C, De Araujo JR, Faucher FF, Chang M, Deraedt CV, Toste FD, Somorjai GA (2017) *Nano Lett* 17:584
54. Deraedt C, Melaet G, Ralston WT, Ye R, Somorjai GA (2017) *Nano Lett* 17:1853
55. Li Y, Liu JH-C, Witham CA, Huang W, Marcus MA, Fakra SC, Alayoglu P, Zhu Z, Thompson CM, Arjun A, Lee K, Gross E, Toste FD, Somorjai GA (2011) *J Am Chem Soc* 133:13527
56. Witham CA, Huang W, Tsung C-K, Kuhn JN, Somorjai GA, Toste DF (2010) *Nat Chem* 2:36
57. Huang W, Liu JH-C, Alayoglu P, Li Y, Witham CA, Tsung C-K, Toste FD, Somorjai GA (2010) *J Am Chem Soc* 132:16771

58. Gross E, Lui JH-C, Toste FD, Somorjai GA (2012) *Nat Chem* 4:947
59. Gross E, Shu X-Z, Alayoglu S, Bechtel HA, Martin MC, Toste FD, Somorjai GA (2014) *J Am Chem Soc* 136:3624
60. Ogasawara S, Kato S (2010) *J Am Chem Soc* 132:4608
61. Giacalone F, Campisciano V, Calabrese C, La Parola V, Syrgiannis Z, Maurizio P, Gruttadauria M (2016) *ACS Nano* 10:4627
62. Buhleier E, Whener W, Vögtle F (1978) *Synthesis* 2:155
63. de Brabander-van den Berg EMM, Nijenhuis A, Mure M, Keulen J, Reintjens R, Vandenbooren F, Bosnian B, de Raat R, Frijns T, van Den Wal S, Castelijns M, Put J, Meijer EW (1994) *Macromol Symp* 77:51
64. Yeung LK, Crooks RM (2001) *Nano Lett* 1:14
65. Niu Y, Crooks RM (2003) *Chem Mater* 15:3463
66. Esumi K, Miyamoto K, Yoshimura T (2002) *J Colloid Interface Sci* 254:402
67. Hayakawa K, Yoshimura T, Esumi K (2003) *Langmuir* 19:5517
68. Esumi K, Isono R, Yoshimura T (2004) *Langmuir* 20:237
69. Ooe M, Murata M, Mizugaki T, Ebitani K, Kaneda K (2002) *Nano Lett* 2:999
70. Mizugaki T, Kibata T, Ota K, Mitsudome T, Ebitani K, Jitsukawa K, Kaneda K (2009) *Chem Lett* 38:1118
71. Maeno Z, Kibata T, Mitsudome T, Mizugaki T, Jitsukawa K, Kaneda K (2011) *Chem Lett* 40:180
72. Kibata T, Mitsudome T, Mizugaki T, Jitsukawa K, Kaneda K (2013) *Chem Commun* 49:167
73. Karakhanov E, Maximov A, Kardasheva Y, Semernina V, Zolotukhina A, Ivanov A, Abbott G, Rosenberg E, Vinokurov V (2014) *ACS Appl Mater Interfaces* 6:8807
74. Astruc D, Lu F, Aranzaes JR (2005) *Angew Chem Int Ed* 44:7852
75. Astruc D, Ornelas C, Ruiz J (2008) *Acc Chem Res* 41:841
76. Astruc D, Boisselier E, Ornelas C (2010) *Chem Rev* 110:1857
77. Astruc D (2010) *Tetrahedron Asymmetry* 21:1041
78. Astruc D, Liang L, Rapakousiou A, Ruiz J (2012) *Acc Chem Res* 45:630
79. Zhao P, Li N, Astruc D (2013) *Coord Chem Rev* 257:638
80. Wang D, Astruc D (2013) *Coord Chem Rev* 257:2317
81. Wang D, Deraedt C, Ruiz J, Astruc D (2015) *Acc Chem Res* 48:1871
82. Ornelas C, Aranzaes JR, Cloutet E, Alves S, Astruc D (2007) *Angew Chem Int Ed* 46:872
83. Ornelas C, Salmon L, Aranzaes JR, Astruc D (2007) *Chem Commun* 43:4946
84. Ornelas C, Aranzaes JR, Salmon L, Astruc D (2008) *Chem Eur J* 14:50
85. Diallo AK, Ornelas C, Salmon L, Aranzaes JR, Astruc D (2007) *Angew Chem Int Ed* 46:8644
86. Ornelas C, Ruiz J, Salmon L, Astruc D (2008) *Adv Synth Catal* 350:837
87. Diallo AK, Boisselier E, Liang L, Ruiz J, Astruc D (2010) *Chem Eur J* 16:11832
88. Deraedt C, Salmon L, Etienne L, Ruiz J, Astruc D (2013) *Chem Commun* 49:8169
89. Deraedt C, Salmon L, Astruc D (2014) *Adv Synth Catal* 356:2525
90. Li N, Echeverría M, Moya S, Ruiz J, Astruc D (2014) *Inorg Chem* 53:6954
91. Deraedt C, Pinaud N, Astruc D (2014) *J Am Chem Soc* 136:12092
92. Liu X, Gregurec D, Irigoyen J, Martinez A, Moya S, Ciganda R, Hermange P, Ruiz J, Astruc D (2016) *Nat Commun* 7:60
93. Deraedt C, Wang D, Salmon L, Etienne L, Labrugère C, Ruiz J, Astruc D (2015) *ChemCatChem* 7:303
94. Wang D, Deraedt C, Salmon L, Labrugère C, Etienne L, Ruiz J, Astruc D (2015) *Chem Eur J* 21:1508
95. Wang Y, Latouche C, Rapakousiou A, Lopez C, Ledoux-Rax I, Ruiz J, Saillard J-Y, Astruc D (2014) *Chem Eur J* 20:8076
96. Hawker CJ, Fréchet JMJ (1990) *J Am Chem Soc* 112:7638
97. Gopidas KR, Whitesell JK, Fox MA (2003) *Nano Lett* 3:1757
98. Wu L, Li B-L, Huang Y-Y, Zhou H-F, He Y-M, Fan Q-H (2006) *Org Lett* 8:3605
99. Wu L, Li Z-W, Zhang F, He Y-M, Fan Q-H (2008) *Adv Synth Catal* 350:846

100. Yang P, Zhang W, Du Y, Wang X (2006) *J Mol Catal A* 260:4
101. Flory PJ (1940) *J Am Chem Soc* 62:1561
102. Higuchi M, Yamamoto K (2004) *Bull Chem Soc Jpn* 77:853
103. Yamamoto K, Imaoka T (2006) *Bull Chem Soc Jpn* 79:511
104. Yamamoto K, Imaoka T (2014) *Acc Chem Res* 47:1127
105. Imaoka T, Yamamoto K (2019) *Bull Chem Soc Jpn* 92:941
106. Yamamoto K, Imaoka T, Tanabe M, Kambe T (2020) *Chem Rev* 120:1397
107. Yamamoto K, Higuchi M, Shiki S, Tsuruta M, Chiba H (2002) *Nature* 415:509
108. Higuchi M, Tsuruta M, Chiba H, Shiki S, Yamamoto K (2003) *J Am Chem Soc* 125:9988
109. Takanashi K, Fujii A, Nakajima R, Chiba H, Higuchi M, Einaga Y, Yamamoto K (2007) *Bull Chem Soc Jpn* 80:1563
110. Enoki O, Imaoka T, Yamamoto K (2006) *Bull Chem Soc Jpn* 79:621
111. Yamamoto K, Imaoka T, Chun W-J, Enoki O, Katoh H, Takenaga M, Sono A (2009) *Nat Chem* 1:397
112. Takahashi M, Imaoka T, Hongo Y, Yamamoto K (2013) *Angew Chem Int Ed* 52:7419
113. Takahashi M, Imaoka T, Hongo Y, Yamamoto K (2013) *Dalton Trans* 42:15919
114. Takahashi M, Imaoka T, Yamamoto K (2015) *RSC Adv* 5:100693
115. Inomata Y, Albrecht K, Yamamoto K (2018) *ACS Catal* 8:451
116. Inomata Y, Albrecht K, Haruta N, Yamamoto K (2019) *Chem Mater* 31:8373
117. Kuzume A, Ozawa M, Tang Y, Yamada Y, Haruta N, Yamamoto K (2019) *Sci Adv* 5: eaax6455
118. Kitazawa H, Albrecht K, Yamamoto K (2012) *Chem Lett* 41:828
119. Imaoka T, Kitazawa H, Chun W-J, Omura S, Albrecht K, Yamamoto K (2013) *J Am Chem Soc* 135:13089
120. Imaoka T, Kitazawa H, Chun W-J, Yamamoto K (2015) *Angew Chem Int Ed* 54:9810
121. Huda M, Minamisawa K, Tsukamoto T, Tanabe M, Yamamoto K (2019) *Angew Chem Int Ed* 58:1002
122. Sonobe K, Tanabe M, Yamamoto K (2020) *ACS Nano* 14:1804
123. Scott RWJ, Datye AK, Crooks RM (2003) *J Am Chem Soc* 125:3708
124. Scott RWJ, Wilson OM, Oh S-K, Kenik EA, Crooks RM (2004) *J Am Chem Soc* 126:15583
125. Chung Y-M, Rhee H-K (2003) *Catal Lett* 85:159
126. Chung Y-M, Rhee H-K (2003) *J Mol Catal A* 206:291
127. Lang H, Maldonado S, Stevenson KJ, Chandler BD (2004) *J Am Chem Soc* 126:12949
128. Zhao M, Crooks RM (1999) *Chem Mater* 11:3379
129. Auten BJ, Lang H, Chandler BD (2008) *Appl Catal B* 81:225
130. Scott RWJ, Sivadinarayana C, Wilson OM, Yan Z, Goodman DW, Crooks RM (2005) *J Am Chem Soc* 127:1380
131. Luo L, Duan Z, Li H, Kim J, Henkelman G, Crooks RM (2017) *J Am Chem Soc* 139:5538
132. Qian L, Yang X (2006) *J Phys Chem B* 110:16672
133. Ye H, Crooks RM (2007) *J Am Chem Soc* 129:3627
134. Yancey DF, Carino EV, Crooks RM (2010) *J Am Chem Soc* 132:10998
135. Yancey DF, Zhang L, Crooks RM, Henkelman G (2012) *Chem Sci* 3:1033
136. Iyyamperumal R, Zhang L, Henkelman G, Crooks RM (2013) *J Am Chem Soc* 135:5521
137. Zhang L, Iyyamperumal R, Yancey DF, Crooks RM, Henkelman G (2013) *ACS Nano* 7:9168
138. Liu X, Ruiz J, Astruc D (2017) *Chem Commun* 53:11134
139. Wang Q, Fu F, Yang S, Moro MM, de los Angeles Ramirez M, Moya S, Salmon L, Ruiz J, Astruc D (2019) *ACS Catal* 9:1110
140. Hoover NN, Auten BJ, Chandler BD (2006) *J Phys Chem B* 110:8606
141. Chandler BD, Long CG, Gilbertson JD, Pursell CJ, Vijayaraghavan G, Stevenson KJ (2010) *J Phys Chem C* 114:11498
142. Carino EV, Crooks RM (2011) *Langmuir* 27:4427
143. Luo L, Zhang L, Duan Z, Lapp AS, Henkelman G, Crooks RM (2016) *ACS Nano* 10:8760

144. Nakamura I, Yamanoi Y, Imaoka T, Yamamoto K, Nishihara H (2011) *Angew Chem Int Ed* 50:5830
145. Nakamura I, Yamanoi Y, Imaoka T, Yamamoto K, Nishihara H (2008) *Chem Commun* 44:5716
146. Takahashi M, Koizumi H, Chun W-J, Kori M, Imaoka T, Yamamoto K (2017) *Sci Adv* 3: e1700101
147. Tsukamoto T, Kambe T, Nakao A, Imaoka T, Yamamoto K (2018) *Nat Commun* 9:3873
148. Liu L, Corma A (2018) *Chem Rev* 118:4981
149. Ding K, Cullen DA, Zhang L, Cao Z, Roy AD, Ivanov IN, Cao D (2018) *Science* 362:560
150. Chen P-C, Liu M, Du JS, Meckes B, Wang S, Lin H, Dravid VP, Wolverton C, Mirkin CA (2019) *Science* 363:959

Pd Nanoparticles in C–H Activation and Cross-coupling Catalysis



Ian James Stewart Fairlamb and Neil Walter James Scott

Contents

1	Introduction: Background to Cross-Coupling and C–H Bond Activation and Functionalisation Chemistry	172
2	Evidence for Catalytically Active Heterogeneous Species in <i>Classic</i> Cross-Coupling Processes	174
3	The Case for <i>Quasi</i> -Heterogeneous Catalysis in C–H Activation: Importance of Reaction Conditions in the Evolution of Heterogeneous Species from Homogeneous Sources	180
4	A Practical Guide for Confirming Heterogeneity in Cross-Coupling Reactions	184
5	Case Studies Involving Supported Nanoparticle-Catalysed C–H Bond Functionalising Reactions	186
5.1	Case Study I) Reusable, Site-Selective Direct C–H Arylation of Heteroarenes Enabled by CuO/Fe ₃ O ₄ Nanoparticles	186
5.2	Case Study II) Direct C–H Acetoxylation, Methoxylation, Halogenation and Arylation of Heterocycles Catalysed by Pd ^{II} /MWCNT Carbon Nanotubes . . .	189
5.3	Case Study III) Pd/C-Catalysed C–H Alkenylations in Continuous Flow, Using γ -Valerolactone as a Green Reaction Medium	191
5.4	Case Study IV) A Pd–Polypyrrole Nanocomposite-Catalyst for Direct C–H Activation of Heteroaromatics	192
5.5	Case Study V) 2-Arylpyridine Coupling with Alkylbenzene PdNPs on a γ -Al ₂ O ₃ Support	195
5.6	Case Study VI) Development and Optimisation of Conditions for Pd/C-Catalysed Site-Selective C–H Activation Reactions	197
6	Future Perspectives and Conclusions	199
	References	200

Abstract This chapter reviews the state of the art in the use of nanoparticles in cross-coupling catalysis, with a focus on C–H activation chemistry. Current understanding of the mechanistic role of heterogeneous catalyst sources as applied to classic cross-coupling process is discussed. Understanding of the factors that influence speciation of catalysts under conditions commonly employed in C–H activation/functionalisation chemistry is highlighted. An overview of the tests that an

I. J. S. Fairlamb (✉) and N. W. J. Scott
Department of Chemistry, University of York, York, UK
e-mail: ian.fairlamb@york.ac.uk; nwjs500@york.ac.uk

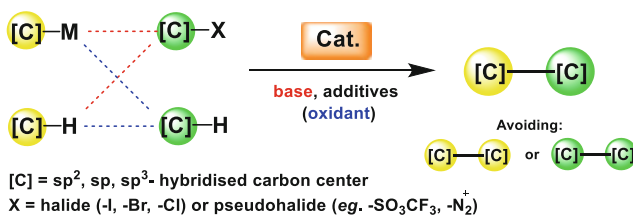
experimentalist can perform to gain insights on whether a reaction is heterogeneously or homogeneously catalysed is given, along with their respective caveats. Six detailed case studies are presented, aimed at introducing the reader to the breadth and variety of recent developments of both synthetic utility and mechanistic understanding of nanoparticles applied to the field of C–H activation/functionalisation chemistry.

Keywords C–H bond activation · Catalysis · Cross-coupling catalysis · Heterogeneous C–H functionalisation catalysis · Mechanism · Nanoparticles · Palladium · Pd nanoparticles · Pd speciation · Quasi-heterogeneous catalysis

1 Introduction: Background to Cross-Coupling and C–H Bond Activation and Functionalisation Chemistry

The activation of C–H bonds by transition metals has been of interest to organometallic chemists for many years [1]. Indeed, the intimate involvement of various transition metals with C–H bonds, with carbon centres of varying hybridisation, has been well studied over the past 30 years or so [2–3]. The advantage of this approach is that a functional group is not necessarily required for functionalisation through successive reaction(s). Indeed, over the last 10–15 years, the field of transition metal-catalysed C–H bond functionalisation has emerged with great vigour and application [4–7]. Researchers in catalysis and chemical synthesis have gone on to explore well beyond proof-of-concept transformations, seemingly making the impossible quite possible [8–10]. It is clear that a true paradigm shift in chemical synthesis, through explicit use of C–H bond functionalisation reactions, has been seen. A guiding example is in the field of catalytic cross-coupling chemistry (Scheme 1).

A typical (textbook) transformation involves reaction of an organometallic reagent “C–M” with an organohalide/pseudohalide “C–X” species, unifying two carbon-containing organic components (usually organic, but not limited to) to bring



Scheme 1 Showing a range of cross-coupling possibilities which can be used to forge C–C bonds

about the formation of a carbon–carbon bond. Such a transformation relies on the prefunctionalisation of the starting reagents, leading to the generation of waste (usually metal salt by-products). Such reactions need to avoid formation of homocoupled products, deriving from each starting reagent. It should be noted that coupling of two different organohalide partners has also been reported and has been practically examined by Lipshutz et al. [11–12]. During the mid-2000s [13–16], building on initial work reported in 1993 [17], more direct approaches were developed, as potential replacements for classical cross-coupling reactions. An example is the reaction of a suitable substrate containing a suitable C–H bond with an organohalide, generating a carbon–carbon bond, by the so-called *direct* approach. A variant of this process involves oxidative reaction of an organometallic reagent, again with a reagent possessing a suitable reactive C–H bond. Generally speaking, an oxidant is required for such a process. The “holy grail” in such chemistry is to bring together the oxidative cross-coupling reaction of two different C–H bonds, with metal salts such as AgX or CuX₂ being obvious oxidants, or more ideally oxygen (O₂). The disadvantage of using metal salts is the generation of stoichiometric by-products (e.g. either Ag metal or CuX) [18].

Site (regio)selectivity is of paramount importance in the context of C–H bond functionalisation reactions, which is often implicit, but usually guided by principles of underlying reactivity, be that of an intrinsic nature or through metal (catalyst) proximity (i.e. through a directed orientation of a metal centre to the C–H bond of interest, for functionalisation) [19–21]. While the obvious metal catalyst for such reactions processes is Pd-containing, many other metals can mediate formation of new carbon-carbon bonds [4], either by classical coupling, direct coupling or oxidative coupling strategies.

Many methodologies have been developed for C(sp)–H, C(sp²)–H and C(sp³)–H bond functionalisation reactions; indeed, the most promising examples have been discussed in recent comprehensive reviews, which are beyond the scope and focus of the current discussion described herein, but add great value in terms of an understanding and appreciation of the field as a whole. Without doubt the most challenging reactions are selective C(sp³)–H cross-coupling reactions, noting several remarkable methodologies that have been developed in recent years, for which further progress in terms of application, over the next 10 years or so, is likely.

By far and away the best studied catalysts for the functionalisation of C–H bonds are based on homogeneous systems, i.e. starting with a fully soluble metal catalyst system, either preformed or generated in situ. It is straightforward to come up with appropriate catalysts that fit the homogeneous regime; however the true nature of the active metal catalysts remains hotly debated [22–24]. In this context, quasi-homogeneous–heterogeneous catalyst systems are likely involved in many reactions, especially those involving Pd, but by no means limited to. When heterogeneous catalyst species are involved, inevitably there is the question can the catalyst be immobilised and recycled, minimising loss of catalytic activity and loss of metal (e.g. through leaching processes, leading also to non-desirable product contamination). With elemental sustainability in mind, and the pragmatic consideration that precious metals are likely to be used in chemical processes for at least the next 25 years, then it is incumbent on the scientific community to develop heterogeneous

catalyst systems for C–H bond functionalisation reactions. Gomez et al. wrote a critical review a few years ago [25], defining the new field of study as “molecular transformation of unactivated C–H bonds present in feedstock and readily available hydrocarbons into valuable chemicals by nanoparticle-leveraged C–H activation”.

2 Evidence for Catalytically Active Heterogeneous Species in *Classic* Cross-Coupling Processes

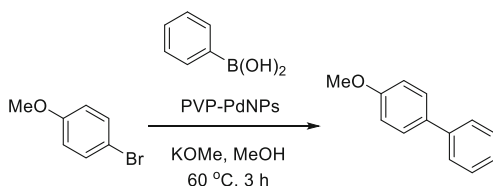
From a green and sustainable chemistry perspective, there is a clear benefit of direct C–H activation, over the classic C–X/C–M cross-coupling regime. This book chapter will focus on heterogeneous C–H cross-coupling processes. There is however still limited mechanistic understanding of how heterogeneous cross-coupling reactions occur, particularly regarding C–H bond activation and functionalisation processes. Understanding heterogeneous catalysis in classical cross-coupling systems is broader and may hence allow to inform an approach to mechanistic understanding in heterogeneous C–H bond activation systems. This section discusses literature evidence for a heterogeneous catalytic activity in *classic* cross-coupling reactions.

Direct Evidence for Surface-Catalysed Cross-Coupling

Fairlamb and Lee closely studied the competence of heterogeneous Pd nanoparticles stabilised by the polymer polyvinylpyrrolidone (PVP-PdNPs) as a catalyst in the Suzuki–Miyaura cross-coupling of 4-iodoanisole with phenylboronic acid (Scheme 2) [26–27].

Deploying a colloidal seeding synthetic method, PVP-supported PdNPs of four distinct sizes (average sized from 1.8 to 4 nm; truncated cuboctahedra, confirmed by TEM imaging) could be selectively prepared. The catalytic efficacy in the model reaction showed a decreasing activity based on turnover frequency (TOF) as particle size was increased. If, however, particle size was normalised to the total number of Pd atoms on *defect sites* of the truncated cuboctahedra nanoparticles, a linear correlation was observed between particle size and TOF (Fig. 1). Hence surface reactivity is governed by the number of low coordination number defect sites on the particle. This however does not answer the question of whether the reaction is occurring on the surface, as defect sites may simply be sites at which leached Pd atoms may be more soluble and therefore more prone to leaching, thereafter operating homogeneously. The authors thus employed in operando X-ray absorption

Scheme 2 Model reagents and conditions employed in the study of the PVP-PdNP-catalysed Suzuki–Miyaura cross-coupling



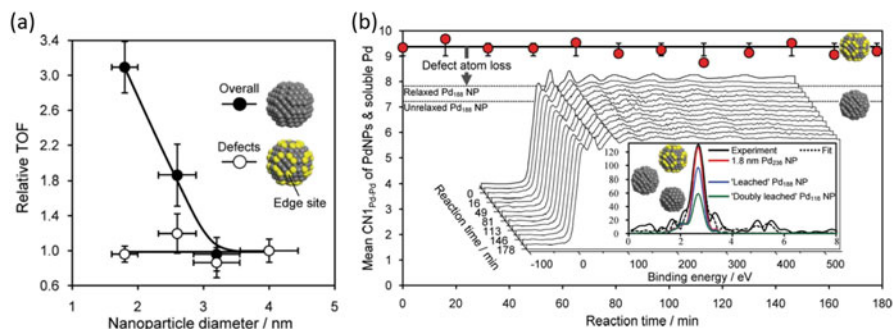


Fig. 1 (a) Showing the size dependence of TOF in a Suzuki–Miyaura cross-coupling, normalised to either total surface Pd atoms (•) or defect surface Pd atoms (○) (b) Figure showing that no significant change in surface Pd coordination number as the model Suzuki–Miyaura cross-coupling reaction proceeds. Reproduced with permission from *Angew. Chem., Int. Ed.*, 2010, 49, 1820. Copyright 2019 Wiley-VCH Verlag GmbH & Co

spectroscopy (XAS) method to monitor the coordination environment of the surface Pd (Fig. 1). These measurements showed that no significant change in coordination environment occurred on the surface Pd throughout the entire reaction process. These findings agree with XAFS, XPS and TEM measurements which, taken together, showed no evidence for leaching under the reaction conditions.

Kinetic analysis of the reaction showed no presence of an induction period, indicating that the PVP-PdNPs were not simply acting as a pre-catalyst or a reservoir for a true active species. Immediate, complete inhibition of catalyst activity was observed upon adding elemental mercury, further supporting a heterogeneous catalytic manifold in this reaction. This study provides significant evidence that cross-coupling can occur on the surface of a heterogeneous catalyst.

Xie et al. presented further compelling evidence for surface-mediated cross-coupling catalysis in Suzuki–Miyaura cross-coupling reactions [28]. Au-Pd core-satellite superstructures: structures featuring an inner core of AuNPs and an outer layer of PdNPs, separated by an ultrathin layer of silica (Fig. 2a, b) were fabricated. PdNP outer layer was decorated with 4-bromothiophenol which was chemisorbed to the Pd surface via disulfide linkages. The chemisorbed bromobenzene was found to be able to cross-couple with phenylboronic acid introduced via a K_2CO_3 aqueous solution (Fig. 2c). Surface-enhanced Raman spectroscopy (SERS) was used to track the depletion of reactants and concomitant formation of products, both of which remained anchored to the surface over time (Fig. 2d). Kinetic profiles of the reactions could be made, which indicated that independently synthesised smaller nanoparticles (5 nm) reacted faster than larger nanoparticles (15 nm), which was rationalised to be a result of increased exposure of surface Pd. Additionally, it was found that the reaction was faster when the C–Br bond of the aryl bromide was closer to the Pd surface. It was postulated that, in this case, the aryl halides can meet the catalyst by “swinging” or “rolling” around their sulphide anchor, and therefore the shorter the distance of the C–Br bond is to the surface, the more likely an interaction with the surface will occur.

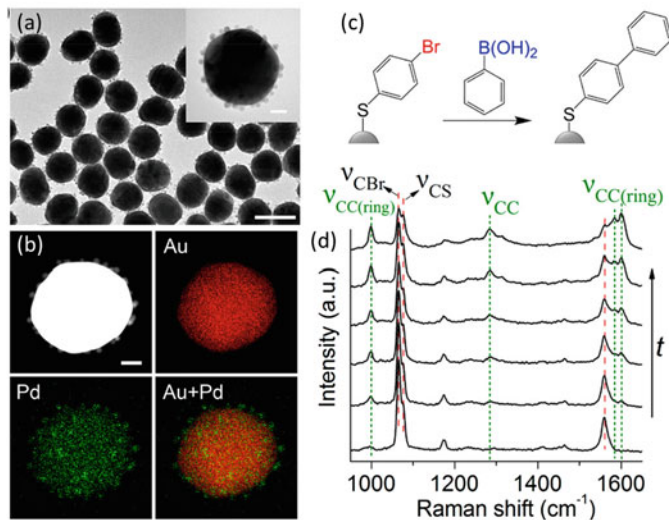


Fig. 2 Showing (a) A TEM image of Au–Pd core-satellite superstructures (b) High-angle annular dark-field scanning transmission electron microscopy (HAADF-STEM) image showing distribution of different elements on Au–Pd core-satellite superstructures (c) Reaction scheme for proposed surface-catalysed Suzuki–Miyaura cross-coupling, showing chemisorbed aryl bromide reacting with in the presence of aqueous phenylboronic acid in the presence of K_2CO_3 (d) Surface-enhanced Raman spectroscopy (SERS) showing conversion of chemisorbed aryl bromide to chemisorbed biaryl. *J. Phys. Chem. Lett.* 2019, 10, 1286–1291. Copyright [2019] American Chemical Society

The reaction was attempted exclusively employing Au in absence of Pd as the surface metal, with anchored 4-bromothiophenol starting material as the substrate in the presence of a solution known to contain Pd ($\sim 200 \mu\text{gL}^{-1}$ determined by ICP-AES) leached from a standard Au–Pd-catalysed post-reaction solution. As no conversion was observed under these control conditions, the authors ruled out the notion that leached Pd species were responsible for this cross-coupling. These results provide another strand of evidence to indicate that a Pd surface can activate an aryl halide to react heterogeneously with boronic acid to form the biaryl product.

Not only particle size, but the morphology of heterogeneous Pd can have an important influence on catalyst activity in Suzuki–Miyaura cross-coupling reactivity. McGlacken et al. compared the performance of Pd nanocubes (PdNCs), octahedra (PdOCTs) and cuboctahedra (PdCUOCs), which could be selectively synthesised (Fig. 3) [29]. In this study, the numbers of defect sites did not relate to the catalyst efficacy. Correlation between efficacy and the number of (100) facets present was however evident. Similar reaction profiles were observed with the different catalyst systems, where the Pd concentration controlled for the number of surface Pd atoms. It was thereby reasoned that the difference in reactivity observed was due to the number of (100) facets, which allowed Pd to be leached through oxidative etching by O_2 present under the reaction conditions (Fig. 3).

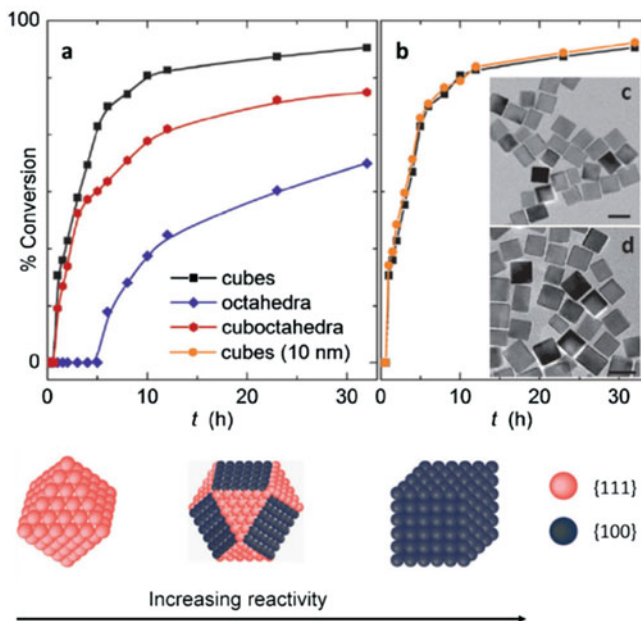


Fig. 3 Showing how morphology of PdNPs affect catalytic outcome. The number of 100 facets directly correlates with the catalytic activity of PdNPs copyright permission required [Angew. Chem. Int. Ed. 2014, 53, 4142–4145]

This work, taken with that reported by Fairlamb et al. (*vide supra*), shows that the specific system employed has significant bearing on whether or not a reaction is surface-catalysed. The change in morphology of heterogeneous catalyst resulted in an apparent switch from a fully heterogeneous to a quasi-heterogeneous catalytic manifold (i.e. a leached active species stemming from a heterogeneous source). This observation has ramifications for heterogeneous manifolds which stem from homogeneous sources, where particle morphology is not well controlled. Under these regimes there may be multiple sizes and morphologies of PdNP, each potentially having its own mode of activity: fully heterogeneous or quasi-heterogeneous. The picture (summarised in Fig. 4) is further complicated when there may additionally be competing homogeneous components to catalytic activity. Ananikov and Eremin have written a comprehensive review which discusses the complexity of such speciation dynamics in cross-coupling catalytic processes [23].

Qualitative Evidence for Surface-Catalysed Cross-Coupling

Several studies have pointed towards inverse correlations (negative-order dependence on loading) between catalyst concentration and efficacy. A study by DSM Pharma Chemicals found that the optimal loading of Pd(OAc)₂ for the Mizoroki–Heck cross-coupling of bromobenzene and *n*-butyl acrylate was 0.08 mol% (39 ppm) [31]. It was found that either increasing or decreasing the catalyst concentration resulted in reduced activity. Fairlamb et al. came across a similar finding in a Sonogashira cross-coupling of 4-bromoacetophenone and phenylacetylene using a variety of different succinimide-containing palladacycles as catalysts (Fig. 5).

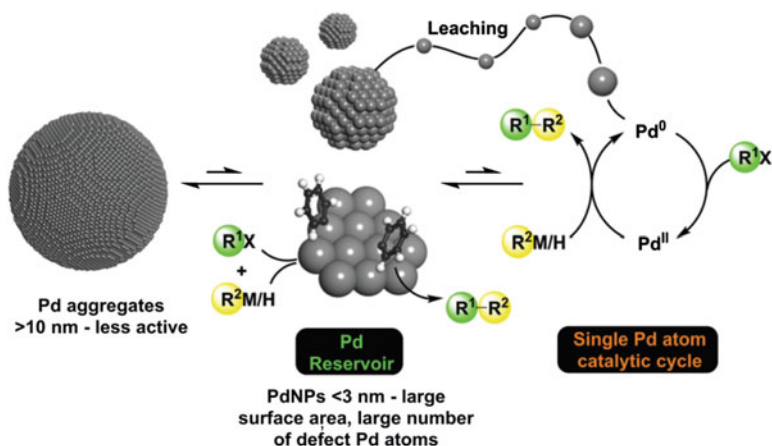
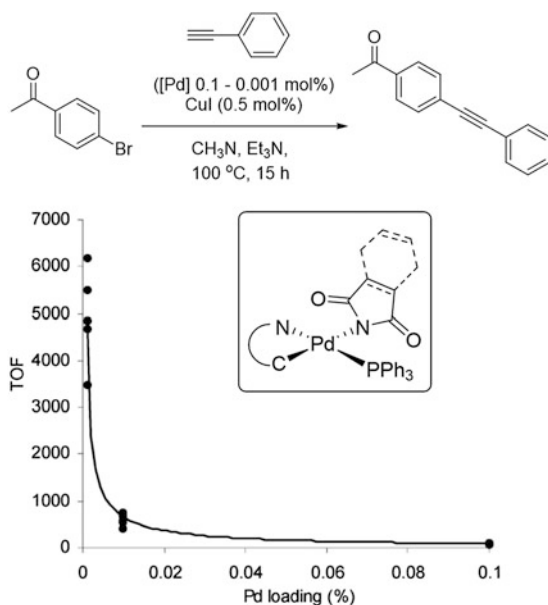


Fig. 4 Showing a range of known possibilities for active catalyst speciation during cross-coupling, with a potential role for homogeneous, heterogeneous, homogeneous leached from heterogeneous systems. Reproduced from Ref. [30] with permission from The Royal Society of Chemistry

Fig. 5 Summarising conditions used for the Sonogashira coupling of 4-bromoacetophenone and phenylacetylene, catalysed by a succinimide-containing palladacycle. An example of an inverse relationship between catalyst loading and turnover frequency TOF was recorded



Optimal catalyst performance was found at a loading of 0.01 mol% (92 ppm), and increasing the catalyst loading acted to reduce the activity. It is of significance that in both of these highly activated systems (featuring markedly different reactions and conditions), optimal Pd concentration is very low (< 100 ppm).

These results show that incredibly low concentrations of Pd can enable cross-coupling. Indeed, catalytically active concentrations of Pd metal, dubbed

“homeopathic”, have been shown to be able to catalyse cross-coupling processes, for example, employing activated aryl halide substrates under microwave conditions [32]. Moreover, it has been demonstrated that higher Pd concentrations can lead to catalytic deactivation, most likely due to aggregation to inactive Pd particles.

Evidence for Leaching of Metal from Heterogeneous Sources

When aggregated, Pd is not necessarily irreversibly bound to the aggregated material. Clear evidence of leaching of catalytically active material from heterogeneous sources into the solution phase has been documented. Common heterogeneous catalytic sources have been proven to operate via leached species (e.g. Pd/C, Pd/SiO₂ and Pd/SiO₂) [33–35]. In some cases, such as that reported by Arai et al., leaching can be followed by redeposition at the surface, upon completion of the reaction, allowing for efficient recycling of the heterogeneous catalyst [33]. Reactions that follow this regime can be said to operate via a leaching–redeposition catalytic mechanism (see Sect. 5.1, for an example in C–H functionalising chemistry).

Dupont et al. found that PdNPs, generated from a palladacyclic, homogeneous source could be stabilised and conveniently analysed in imidazolium ionic liquids [36]. These PdNPs, after successful mediation of a Mizoroki–Heck cross-coupling reaction, were shown to have released significant amount of Pd in the reaction solution, due to leaching brought about via oxidative addition on a particle surface.

Rothenberg et al. utilised UV/visible spectroscopic methods to track dynamics of reduction and concomitant aggregation of heterogeneous Pd from homogeneous sources [37]. The same group were able to demonstrate leaching of catalytically active material from relatively large nanoparticles (~ 15 nm) [38]. By design of a special reactor containing a porous membrane which would only allow passage of smaller particles, they proved that leached species can be active in cross-coupling processes. This does not however confirm that the leached species are operating as homogeneous catalysts, since nanoparticles of this size could theoretically contain several thousand Pd atoms, and thus, the reaction could still be occurring on a surface. Baiker et al. used X-ray absorption spectroscopic methods to track, in situ, the leaching of Pd from a heterogeneous source (Pd/Al₂O₃) under Mizoroki–Heck reaction conditions. In situ probing also revealed the presence of solution-suspended, colloidal, PdNPs as well as molecular species [PdBr₄]²⁻ and [Pd₂Br₆]²⁻, leached into the liquid phase. These results implied that Pd colloids are involved in catalysis and not merely a catalytic reservoir.

A key message which can be derived from these examples is the evidence that particulate metal can act as *reservoirs*, from which leaching of catalytically competent active species can arise.

Additionally, irreversible catalyst leaching can result in loss of expensive metal catalyst, to either waste streams or contamination of products. The problem of leaching is of further significance for the pharmaceutical sector, which sets stringent limits (<10 ppm for oral consumption) on the trace levels of Pd which can contaminate drug products. Thus, there is significant research drive to develop scavenger systems which can efficiently reclaim Pd lost to reaction solutions [39–40].

Obora et al. have synthesised and characterised highly catalytically active DMF-stabilised PdNPs and Cu/PdNPs; these catalysts can be prepared in a facile manner by simply refluxing PdCl₂ in DMF [41–43]. As palladophilic solvents such as DMF along with high-temperature conditions are commonly employed in C–H activation processes, a role for DMF-stabilised PdNPs (either as a catalyst reservoir) for catalytically active *leached* catalyst species or as a directly acting heterogeneous species should not be dismissed. Generally speaking, solvents do play an important role in cross-coupling chemistry – a recent review discusses these roles in detail [44].

Given the evidence that metal particles can mediate cross-coupling processes via surface catalysis, highly active Pd particles (*/*clusters) forming en route to the inactive Pd black are likely strong contenders for being the active catalytic species in these cases.

3 The Case for *Quasi*-Heterogeneous Catalysis in C–H Activation: Importance of Reaction Conditions in the Evolution of Heterogeneous Species from Homogeneous Sources

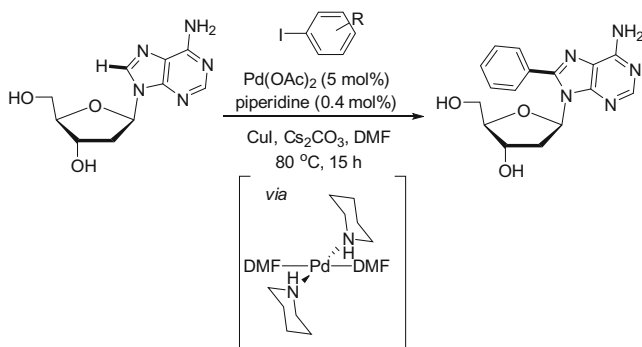
Common, soluble metal salts, e.g. Pd(OAc)₂ (which is most often derived from its trimer; Pd₃(OAc)₆) [45], have long been the “go-to” catalysts for homogeneous catalytic processes, including C–H activation, due to their relative cheapness and activity as simple Pd^{II} salts. It is important to note that soluble (homogeneous) species like Pd(OAc)₂ may be acting as a reservoir for the formation of higher-order species such as Pd⁰ clusters or nanoparticles (PdNPs), which may be the true active species in a given process.

The prevalence of such PdNPs (and whether they are indeed catalytically active) can vary as a function of the reaction conditions. For example, Fairlamb et al. investigated a site-selective Pd/Cu-mediated direct C–H arylation reaction of the nucleotide 2′-deoxyadenosine (Scheme 3) [46–48].

It was initially found that the trace impurity in DMF, dimethylamine, was critical for synthetically significant yields. Another secondary amine, piperidine, which was observed to bring about a similar activity, was investigated closely. Direct reaction of Pd₃(OAc)₆ with an excess of piperidine resulted in the formation of *trans*-Pd(OAc)₂(*N*-piperidyl)₂ which was found to degrade via a hypothesised DMF-ligated intermediate to well-defined DMF-stabilised PdNPs (around 1.7 nm, analysed by TEM) under the C–H arylation reaction conditions (80°C). Thus, the presence of amines was found to be able to promote the reduction of Pd^{II} to catalytically active Pd⁰NPs. Alami et al. showed that the heterogeneous source Pd(OH)₂/C could be employed in the C–H arylation of unprotected 8-adenenines using aryl halides in polar aprotic solvents DMF and NMP [49–50].

The Role of Polar Solvents in Pd Speciation and Propagation

Polar solvents such as DMF, DMAc, NMP (polar aprotic) and H₂O are commonly employed as solvents in catalytic C–H bond functionalising processes. There is



Scheme 3 Showing conditions employed for the direct C–H functionalisation of 2'-deoxyadenosine, which is suspected to occur via a DMF-stabilised Pd intermediate

significant evidence that such polar solvents can have influence on stabilisation and propagation of nanoparticles in cross-coupling processes. Obora et al. have synthesised and characterised highly catalytically active DMF-stabilised PdNPs and Cu/PdNPs; these catalysts can be produced in a facile manner by simply refluxing PdCl_2 in DMF [41]. Since palladophilic solvents, such as DMF, along with high-temperature conditions are commonly employed in C–H bond activation process, a role for DMF-stabilised PdNPs for catalytically active *leached* species or as directly acting heterogeneous surfaces should not be dismissed. PdNPs in DMF have additionally been observed in direct arylations of benzothiazole [51]. Choi et al. have developed a HPLC-MS-based method to analyse DMF-PdNPs, which may be too small (and thus perhaps highly active) to be visualised by TEM imaging [52]. Building on results from Dupont et al. (*vide supra*), highly polar ionic liquids have additionally been used to stabilise catalytically competent PdNPs of a narrow size-distribution (around 2 nm), generated from both $\text{Pd}_2(\text{dba})_3$ and $\text{Pd}(\text{OAc})_2$ [36, 53].

An important study by Hii et al. discovered a link between polar solvent and Pd^0 proliferation from $\text{Pd}(\text{OAc})_2$ under ligand-free Suzuki–Miyaura cross-coupling conditions [54]. It was found that a water-mediated dissociation of $\text{Pd}_3(\text{OAc})_6$ occurred prior to reduction to Pd^0 by arylboronic acid. Thus stoichiometry (relative to Pd) of water present has a direct bearing on the amount of catalytically available Pd^0 . The bulk solvent present additionally constitutes a factor, with the nuclearity of Pd(OAc)₂ being correlated to the dipole moment of the tested solvent. These results marry with structural studies subsequently carried out by Bedford et al. who found that alcohols and H₂O induce facile dissociation of the $\text{Pd}_3(\text{OAc})_6$ trimer [55]. A direct effect of trace levels of H₂O on *trans*- $\text{Pd}(\text{OAc})_2(\text{piperidyl})_2$ active catalyst speciation has also been so observed in Pd-catalysed arylcyanation reactions [56].

γ -Valerolactone (GVL), a lignocellulose-derived solvent, has been put forth as a green alternative to toxic and less environmentally friendly polar aprotic solvents such as DMF and NMP [57] (Fig. 6).

Computational analysis (DFT) has indicated that GVL had a similar co-ordination affinity to Pd as DMAc and thus is likely to behave similarly in activation and

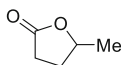
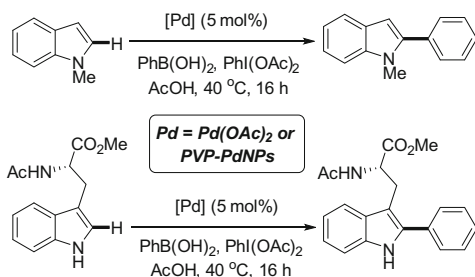


Fig. 6 The chemical structure of γ -valerolactone, a biomass-derived polar aprotic solvent

Scheme 4 Reaction conditions employed for the direct C–H arylation of *N*-methyl indole and a tryptophan derivative, catalysed by both PVP-PdNPs and Pd(OAc)₂



propagation of PdNPs (see Sect. 5.3 for an example of an application in heterogeneous C–H functionalisation chemistry). If appropriate to a process of interest, GVL should be considered as a green, non-toxic alternative to other polar aprotic solvents [58].

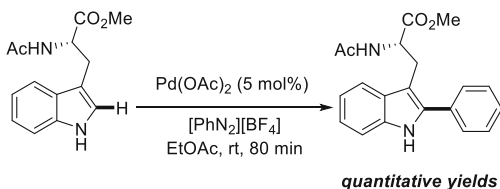
Given the importance of polar solvents (e.g. DMF, DMAc, NMP, H₂O, alcohols) in the proliferation and stabilisation of PdNPs, in reactions involving the degradation of metal catalyst precursors and concomitant growth of catalytically active Pd particles, interaction of polar solvents must be considered intrinsic to Pd speciation mechanisms in C–H bond functionalising reactions (Scheme 4).

Fairlamb et al. explored the site-selective direct C–H arylation of the C2-position of indole-containing compounds (*N*-methyl indole and tryptophan derivatives, using boronic acid as an arylating agent (Scheme 4) [59]. In all cases, employing a homogeneous Pd(OAc)₂ precursor, PdNPs were shown to form quickly upon reaction initiation. For these processes, both homogeneous Pd(OAc)₂ and heterogeneous PVP-PdNPs pre-catalyst sources demonstrated good catalyst activity.

An optimised C–H bond arylation of tryptophan derivatives, using aryldiazonium salt as the arylating coupling partner, was probed in detail (Scheme 5) [60]. A sigmoidal kinetic profile indicated an autocatalytic catalyst activation indicative of a quasi-heterogeneous mechanism. Again, small nanoparticles (~1 nm, analysed by TEM) formed under working conditions; however the mercury-poisoning test (Sect. 4) tentatively indicated that these were not participatory in the catalytic cycle.

It should be emphasised that the presence of heterogeneous species under the working reaction conditions does not necessarily mean the reaction is occurring on a

Scheme 5 Reaction conditions employed for the direct C–H arylation of *N*-methyl indole and a tryptophan derivative, catalysed by Pd(OAc)₂



surface. In some cases, although small nanoparticles form under reaction conditions, evidence points towards such species not being catalytically active. An example of which is the direct C–H bond activation of tryptophan derivatives with aryl boronic acids, in the presence of both Cu^{II} and Pd^0 [60]. The fact that both PVP-supported PdNPs and $\text{Pd}(\text{OAc})_2$ can catalyse these reactions is indicative of leached Pd catalysing the process from a higher-order catalyst reservoir, which does not directly participate as a catalyst species itself, i.e. by surface catalysis.

The examples above demonstrate that under working reaction conditions, employing $\text{Pd}(\text{OAc})_2$ can lead to the generation of catalytically viable PdNPs forming under the reaction conditions. The activity of such nanoparticles most likely varies according to the specific reaction conditions employed.

Kinetic analysis of catalyst performance can be valuable in comparison of catalysts, rather than simply assessing performance as a function of yield. Fairlamb et al. compared a variety of distinct heterogeneous: Pd/C, PVP-PdNPs and homogeneous $\text{Pd}(\text{OAc})_2$ and $\text{Pd}_2(\text{dba})_3 \cdot \text{CHCl}_3$ catalyst precursors in a direct C–H arylation at various heterocycles, including the site-selective C3 arylation of 2-butylthiophene [61] (Fig. 7; Scheme 6; Table 1).

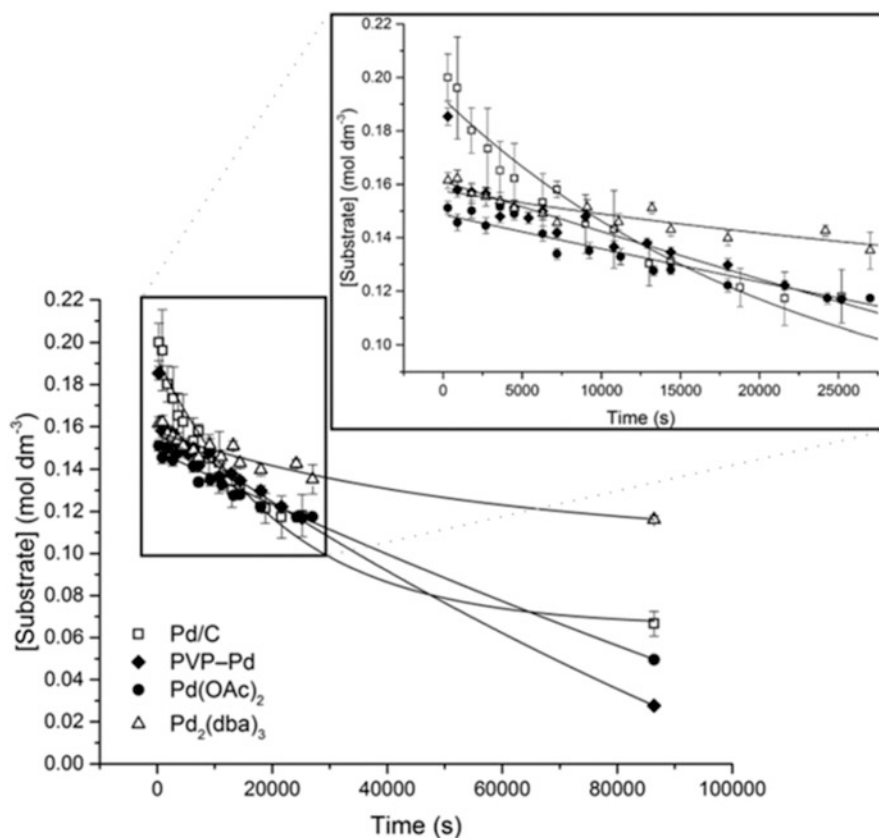
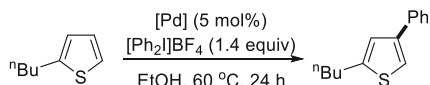


Fig. 7 Showing similarity of kinetic profiles stemming from distinct Pd catalytic sources observed in the direct arylation of 2-*n*-Bu-thiophene. © Georg Thieme Verlag



Scheme 6 Showing conditions employed for the direct C–H arylation of *n*-butyl thiophene

Table 1 Showing the observed rate constants (k_{obs}) determined from exponential fit of kinetic data for a range of different catalysts in a C–H bond functionalising reaction

Pd/C	PVP–Pd	Pd(OAc) ₂	Pd ₂ (dba) ₃
$(6.1 \pm 0.6) \times 10^{-6}$	$(1.6 \pm 0.2) \times 10^{-6}$	$(1.9 \pm 0.3) \times 10^{-6}$	$(2.6 \pm 0.3) \times 10^{-6}$

The remarkable similarity of the kinetic profiles and initial rates observed indicates a comparable active catalyst manifold, accessed from these quite different catalyst precursors. This could imply that a similar active species is settled upon, whether a homogeneous or heterogeneous precursor is used.

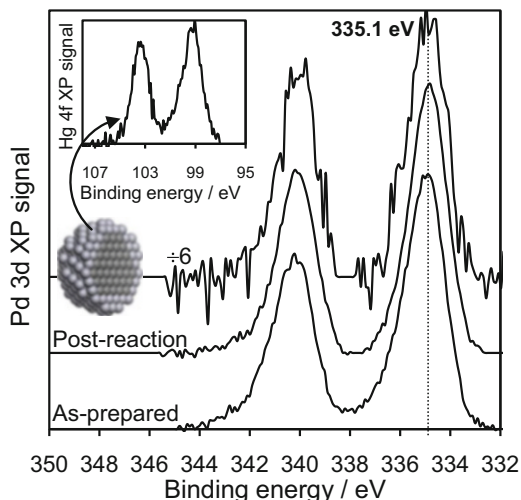
4 A Practical Guide for Confirming Heterogeneity in Cross-Coupling Reactions

In order to be able to fully optimise a given process, it is critical to know the fundamental nature of the catalytically active species. Several reviews have addressed the challenge of determining the extent of a heterogeneous component in a given reaction [62–63]. The picture is complicated because, in a *quasi*-heterogeneous process, a homogeneous pre-catalyst can aggregate to a heterogeneous active species. Conversely, a heterogeneous pre-catalyst may operate by leaching of the catalytically active species into the solution phase. There is no absolute empirical test for catalytic heterogeneity, and, generally, each test which can be employed carries caveats. An investigator must therefore carry out as many of the tests available for heterogeneity as possible, with appropriate controls, to gain the best possible assurance of catalytic homogeneity vs. heterogeneity.

Catalyst recyclability studies can be useful in determining whether leaching is occurring. If a catalyst's activity changes upon recycling, leaching may be indicated. Characterisation (e.g. by TEM, XPS, XRD) of prepared catalyst before and after use can show whether morphological changes occur during the catalytic process. If morphological changes do occur, this may be indicative of leaching of metal. Analysis of the metal content of the post-reaction mixture can additionally determine whether leaching has occurred. However further tests are needed to confirm whether it is the leached species which is responsible for observed activity.

A test that can shed light on the activity of leached Pd species is the hot-filtration test. This test involves filtering the entire reaction through a pre-heated Celite[®] (or other diatomaceous earth) pad during catalyst turnover. This removes (large) particulate metal from the reaction mixture while allowing homogeneous species to

Fig. 8 XPS characterisation of Pd/Hg heterometallic nanoparticles formed upon performing a Hg-poisoning test
 Reproduced from Ref. [27] with permission from The Royal Society of Chemistry



pass through. The filtrate is swiftly reintroduced to the reaction conditions (reaction temperature, reaction recharged with other insoluble components, e.g. bases or oxidants), and analysis of the filtrate will indicate whether the reaction has continued post-filtration. If turnover is inhibited by the filtration, it can be said that the particulates have a direct role in catalysis.

The Hg-poisoning test (aka Hg-drop test) involves spiking a reaction mixture of interest with elemental Hg at initiation, or more often during catalytic turnover. Elemental Hg has been shown to be able to bind selectively to heterogeneous metal surfaces to produce an inactive amalgam [64]. Thus if turnover is inhibited by Hg addition, then heterogeneous catalysis is indicated [65]. The inactive heterometallic particulate product of the reaction between PdNPs and elemental Hg was characterised using X-ray photoelectron spectroscopy (XPS) by Fairlamb et al. (Fig. 8) [27].

Recently, some work has pointed towards certain homogeneous species (palladacycles) being able to react directly with elemental Hg [66–67]. As a consequence, extreme caution and appropriate controls are advised when interpreting the result of the Hg-poisoning test. The impact of this finding against typical Pd^{II} oxidative addition/transmetallation intermediates from a classical cross-coupling has not yet been confirmed (at the time of writing in 2019).

The three-phase test makes use of a solid-supported substrate, the majority of which would only be accessible to a homogeneous species, not a heterogeneous species. The solid support could be an inert polymer, e.g. Wang resin. Thus, if analysis of the solid support and the reaction solution indicates product formation, then a homogeneous active species is indicated. It is possible that the active catalyst could have formed via leaching of a metal catalysis species from a heterogeneous source. An appropriate control involves the analysis of the solution for metal leaching (e.g. using ICP-MS). The support's permeability is a factor in the three-

phase test validity and does not determine whether the active species is mononuclear species or small metal nanoparticles (i.e. has the ability to penetrate the resin). For example, Fagnou et al. showed that the pore size of a Wang resin is sufficient to allow seeding and propagation of small nanoparticles [68].

5 Case Studies Involving Supported Nanoparticle-Catalysed C–H Bond Functionalising Reactions

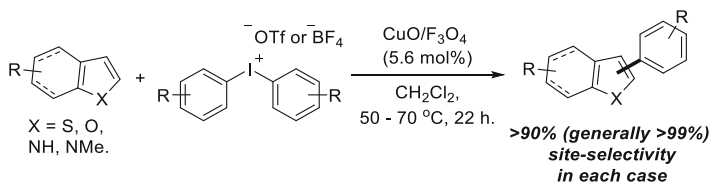
C–H bond functionalisation by heterogeneous catalysis is a currently burgeoning field, and there is a wealth of diversity in reactivity being uncovered. With a view to facilitate the reader to gain a strong foothold on the field, six *case studies* of published examples of representative, cutting-edge heterogeneously catalysed C–H bond functionalisation reactions have been specially selected and will be discussed in detail herein. In each case study, emphasis will be placed on (1) exhibiting the variety of reactivity of such systems and thus the broadness of their synthetic utility; (2) detailing what is known about the mechanism of reactivity, with emphasis on what is known about active catalyst speciation in order to prime the reader for reactivity trends, where possible the reader's attention will be drawn to the variety of techniques that can be employed to characterise the catalyst and probe its mode of activity; and (3) detailing and critiquing the overall greenness of each process (e.g. catalyst recyclability, solvents and reagents, overall efficiency, etc.). With each case study taken together, we aim to illustrate the power and diversity of heterogeneous C–H functionalisation chemistry.

We have found that most examples of supported heterogeneous catalysts for use in C–H functionalisation fall under four broad categories:

1. Metal–metal frameworks
2. Metal–organic frameworks
3. Silica and alumina-based frameworks
4. Carbon-based frameworks (including Pd/C)

5.1 Case Study I) Reusable, Site-Selective Direct C–H Arylation of Heteroarenes Enabled by CuO/Fe₃O₄ Nanoparticles

In an example of a metal–metal framework, Glorius et al. employed CuO nanoparticles supported on Fe₃O₄ (magnetite) as a catalyst in direct arylations of a variety of heterocycles [69]. A fascinating and rigorous mechanistic study was carried out, which, taken together, pointed towards a soluble (homogeneous)



Scheme 7 Showing generalised conditions used for the CuO/Fe₃O₄-catalysed C–H functionalisation of heteroaromatics

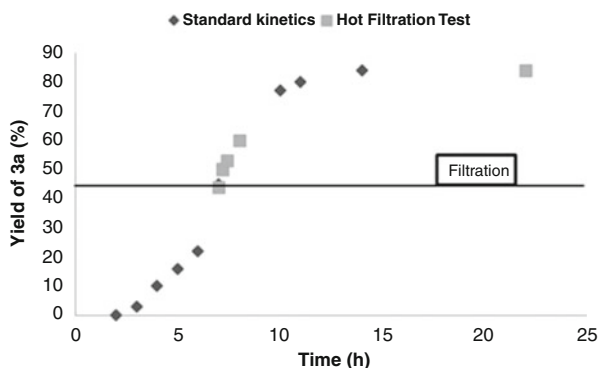


Fig. 9 Kinetic profile of a reaction under standard conditions (3a = product), showing a ~2 h induction period and sigmoidal reaction profile. The figure also shows the results of a positive “hot-filtration” test. Vásquez-Céspedes, S.; Chepiga, K. M.; Möller, N.; Schäfer, A. H.; Glorius, ACS Catalysis 2016, 6, 5954–5961. Copyright [2019] American Chemical Society

species, generated from a heterogeneous source, being the catalytically active species. Employing the conditions detailed in Scheme 7, a variety of electron-rich heterocycles could be arylated, using diaryliodonium salts as an arylating source, to bring about highly site-selective, direct arylation of some common heterocycles.

The aromatic heterocycles reported were electron-rich thiophenes, furans and benzofurans, as well as indoles (both Me-protected and unprotected). Both electron-withdrawing and electron-donating *para*- and *meta*-substituted diaryliodonium salts were well tolerated; however yields were higher with electron-poor aryl groups.

The CuO/Fe₃O₄, composed of earth-abundant materials, could be easily prepared by heating CuCl₂ with Fe₃O₄ under basic conditions, albeit in a low 17% yield. The superparamagnetic nature of the Fe₃O₄ support allowed for the use of a magnet to remove the spent catalyst from the post-reaction mixture.

A kinetic analysis of some standard reaction conditions showed the reaction to follow a sigmoidal reaction profile featuring an induction period of 2 h (Fig. 9). The hot-filtration test was administered and did not significantly alter the kinetic profile. This indicated that, under the reaction conditions, the heterogeneous catalyst forms a soluble active catalyst.

Additionally, it was observed that the later the hot-filtration test was employed in the reaction process, the higher the conversion subsequent to filtration. Kinetic

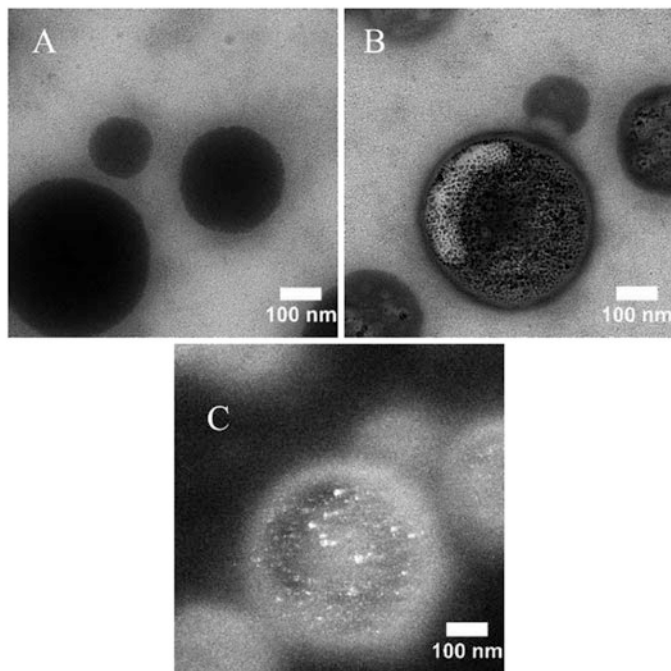


Fig. 10 TEM images of a sample of reaction mixture showing (a) aggregates before and (b) bright-field and (c) dark-field images after visualisation by EFTEM; showing the electron beam to have destroyed the amorphous material in the outer layer, revealing small CuO nanoparticles beneath. Vásquez-Céspedes, S.; Chepiga, K. M.; Möller, N.; Schäfer, A. H.; Glorius, ACS Catalysis 2016, 6, 5954–5961. Copyright [2019] American Chemical Society [69]

tracking of the reaction post-filtration showed the absence of an induction period, confirming that the active catalyst had already formed prior to the filtration.

TEM and XFTEM images taken from samples of the reaction mixture at 40% conversion showed that aggregates of CuO nanoparticles ($\sim < 5$ nm) were present in the reaction mixture (Fig. 10); this was further confirmed by X-ray diffraction.

These mechanistic results, taken together, indicate that small CuO nanoparticles, leached from the original heterogeneous source, are the active species in this process. This constitutes somewhat rare strong evidence of a *release–catch catalytic manifold*, where the active catalyst is leached from the heterogeneous source before returning to the heterogeneous source by the end of the process. This hypothesis was corroborated by measurement of the metal concentration in solution (using TXRF) which was seen to increase during the reaction and decrease towards the end of the reaction. A “release–catch” mechanism was further supported by the fact that, post reaction, the heterogeneous catalyst could be recycled and reused effectively five times before loss of activity. Intriguingly, experiments indicated that reaction between CuO and diaryliodonium cation may be responsible for the leaching of negatively charged CuONPs from the heterogeneous source during the reaction process.

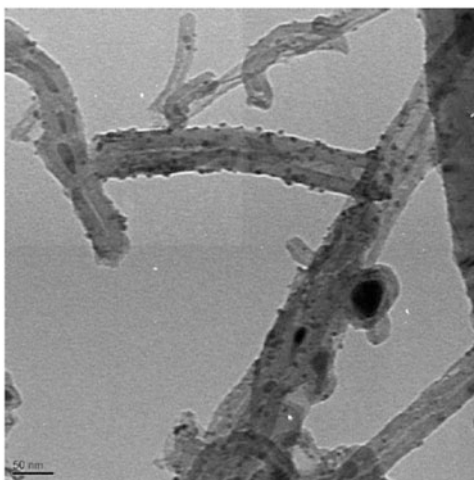
This study shows that a highly recyclable catalyst, composed of earth-abundant materials, can be employed in a relatively mild, operationally straightforward C–H bond arylation reaction involving industrially relevant aromatic heterocycles. This work includes somewhat rare evidence of a release–capture catalytic manifold.

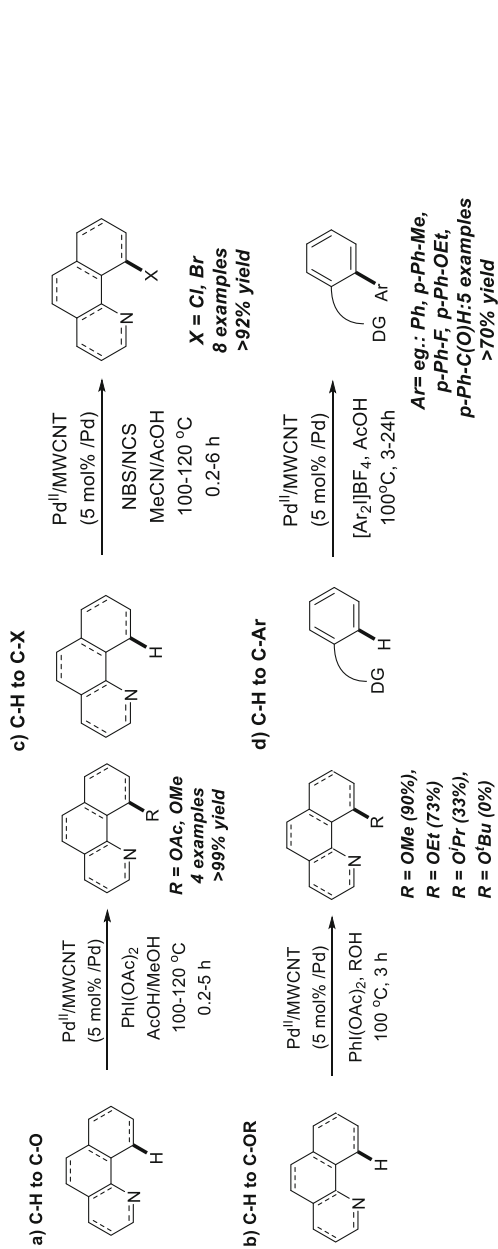
5.2 Case Study II) Direct C–H Acetoxylation, Methoxylation, Halogenation and Arylations of Heterocycles Catalysed by Pd^{II}/MWCNT Carbon Nanotubes

Ellis et al. have worked extensively on Pd^{II} nanoparticles supported on a multiwalled carbon nanotube system (Pd^{II}/MWCNT) (Fig. 11) for application in various directed C(sp²)–H bond functionalisation reactions. Acetoxylation, etherifications (e.g. methoxylation, ethoxylation) halogenations [70] and arylations [71], directed by *ortho*-substituted *N*-containing arene substrates (e.g. phenylpyridines and benzo [*h*]quinolines), were successfully carried out using the Pd^{II}/MWCNT catalyst (Scheme 8). Such transformations have been proposed to occur via a Pd^{II}/Pd^{IV} catalytic cycle [72]. Fine control of synthesis of Pd/MWCNT by a ball mill-mediated process allowed for selective embedding of Pd^{II} (over Pd⁰) onto a multiwalled carbon nanotube structure, thus allowing for a supported heterogeneous catalytic system that could carry out these transformations [73].

Some differing reactivity from the Pd^{II}/MWCNT catalyst preparation was observed when compared to Pd(OAc)₂ deployed under the same conditions. Increased yields but lower substrate tolerance was observed in some acetoxylation reactions. Reduced rates were observed in some alkoxylation reactions. However,

Fig. 11 TEM image showing Pd^{II}NPs embedded in a multiwalled carbon nanotube (MWCNT) structure, a supported heterogeneous catalyst which can be employed in a range of synthetically useful functionalisation reactions. Reproduced from Ref. [73] with permission from The Royal Society of Chemistry





Scheme 8 Showing the range of conditions and substrates used in the N-directed C-H functionalisation of heterocycles by a multiwalled carbon nanotube-supported Pd^{II} nanoparticles

employing Pd^{II}/MWCNT, markedly increased yields were observed in halogenations employing *N*-bromo- and *N*-chlorosuccinimide as the X⁺ source.

For arylations of a range of *N*-directing substrates, the Pd^{II}/MWCNT catalyst performed to an equivalent level or was poorer than Pd(OAc)₂. On a model substrate, 2-phenyl-3-methylpyridine and *para*-substituted electron-withdrawing and donating as well as neutral aromatic substituents were well tolerated, with good yields (aryl group being transferred from the diaryliodonium salt derivative).

Catalyst recycling studies in a specific reaction, methoxylation of 8-methylquinoline showed a minimal loss of activity, with a remarkable drop of only 8% conversion after 16 recycles. ICP-MS showed extremely low levels of leached Pd (<250 ppb) into the reaction solution post-reaction. No further conversion was observed after hot-filtration tests were administered. Taken together, these experiments constitute some evidence of a heterogeneous catalytic manifold being responsible for this transformation.

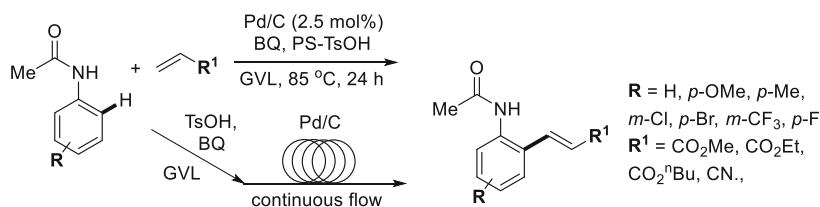
Recycling studies were additionally carried out with a model arylation reaction where reactivity was conserved for the first three cycles but found to drop significantly after the third. ICP-MS analysis of the reaction mixture showed 38.4 ppm of leached Pd, significantly higher than that with the model methoxylation reaction. It is worthy to note that the catalytic recyclability and the amount of leaching of catalytic metal vary significantly depending on the type of reaction carried out, thus underlining that the supported catalysts can behave differently, depending on the reaction conditions deployed.

This work constitutes a supported heterogeneous analogue of synthetically useful C–H functionalisation reactions, previously carried out with Pd(OAc)₂. While generally not performing better than the homogeneous catalyst precursor per reaction, this system does exhibit the benefit of being able to be recycled and reused multiple times.

5.3 Case Study III) Pd/C-Catalysed C–H Alkenylations in Continuous Flow, Using γ -Valerolactone as a Green Reaction Medium

Vaccaro and Ackermann et al. have focused on boosting the sustainability of a direct C–H alkenylation process, namely, in the Fujiwara–Moritani reaction [74]. The simple, widely available heterogeneous supported catalyst Pd/C was deployed. Acetanilides were functionalised in a site-selective manner at the *ortho*-C–H position, with activated alkenes in the presence of an acid and oxidant additives. In optimised reaction conditions, substrates were deployed alongside a polymer-supported tosic acid, which allowed for more efficient recycling. γ -Valerolactone (GVL), a biomass-derived reaction medium, was used as the solvent (Scheme 9).

All reactions reported showed good to excellent yields. *Meta*- and *para*-substituted acetanilides were well tolerated in addition to a variety of different electron-withdrawing substituents on the alkene coupling partner.



Scheme 9 Showing reaction conditions, including scope of substrates tested in a Pd/C-catalysed Fujiwara–Moritani C–H activation reaction. The process was compatible in both batch and flow

Table 2 Showing modest improvements in yield when the Pd/C-catalysed Fujiwara–Moritani alkenylation reactions were carried out under continuous-flow conditions

Substrates used	Yield/% (batch)	Yield/% (continuous flow)
R = H, R ¹ = CO ₂ nBu	95	97
R = H, R ¹ = CO ₂ Et	97	99
R = <i>m</i> -Cl, R ¹ = CO ₂ ⁿ Bu	80	89
R = <i>p</i> -F, R ¹ = CO ₂ ⁿ Bu	82	87

The process showed good recyclability of both the Pd/C catalyst and the polymer-supported tosic acid additive, both of which could be reused with the same activity four times, with some loss of activity on a fifth run. The quantity of Pd released into the reaction medium was assessed to be low: ~4 ppm (using ICP-OES). Hot-filtration and the Hg-poisoning tests both pointed towards a heterogeneous mechanism in this case.

The efficiency of the process led was improved when placed under *continuous-flow* conditions which gave a production rate of 4 gh⁻¹ with a 97% overall yield (Table 2). ICP-AES analysis of the GVL reaction solution, as with the batch process, indicated minimal leaching (~4 ppm), the level of which remained remarkably constant throughout the process. Under flow conditions, the GVL solvent proved to be less prone to the leaching of Pd than more toxic less safe and environmentally friendly solvents tested: DMF and NMP (GVL/DMF/NMP = 4/80/31 ppm).

Several aspects of this process, such as the use of the plant-derived GVL, exhibit strong green credentials. Additionally, Pd/C which is relatively cheap and widely commercially available employed with a polymer-supported acid, both of which could be recycled, contributes towards a highly sustainable process. Furthermore, the efficiency and yields were improved through use of continuous-flow conditions, with low levels of leaching of contaminant metal to the reaction solution observed.

5.4 Case Study IV) A Pd–Polypyrrole Nanocomposite-Catalyst for Direct C–H Activation of Heteroaromatics

Hierso et al. developed and honed an organic polymer-supported heterogeneous catalytic system: a Pd–polypyrrole (Pd@PPy) enabling arylation at a variety of

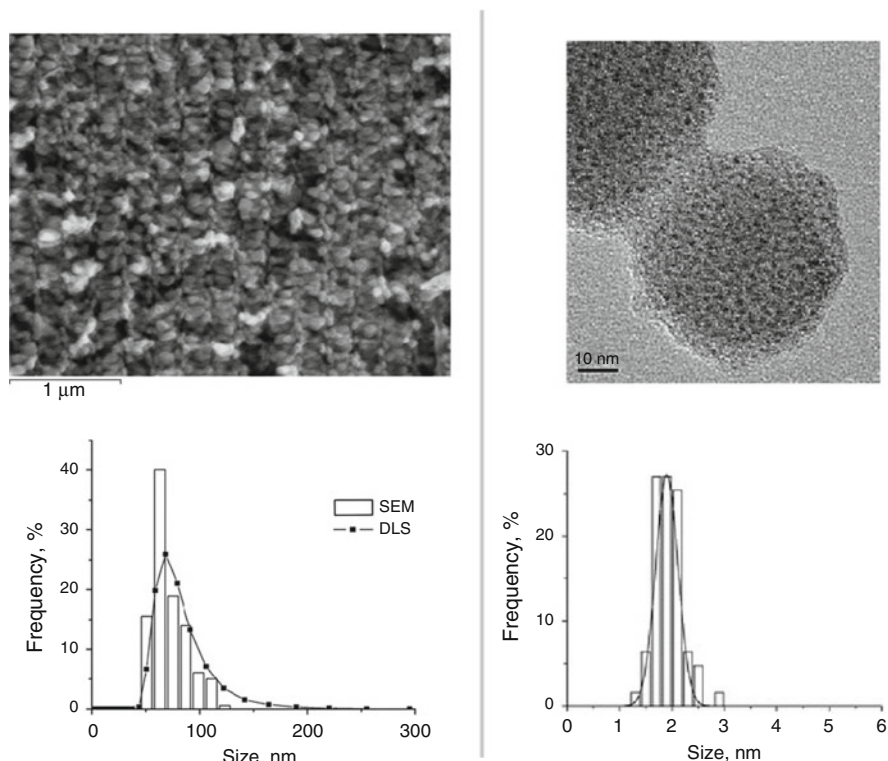
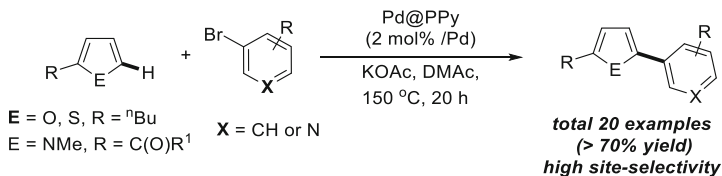


Fig. 12 [Left] Showing (above) SEM image of PPy spherical support; (below) showing concordant DLS/SEM results in determination of PPy-support particle size. [Right] Showing (top) TEM image of PdNPs embedded on spherical pPy support (bottom) showing size distribution of PdNPs < permission not obtained here (very expensive)

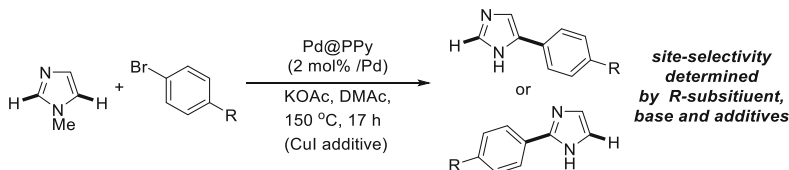
5-membered heteroarenes [75–77]. The catalyst was easily prepared in water by reduction of $\text{Pd}^{\text{II}}(\text{NH}_3)_4\text{Cl}_2$ in the presence of excess pyrrole (a reductant), with sonication. This procedure affords a highly nanoparticulate, high Pd loading material (35 wt%, determined by ICP-AES), with PdNPs (1.8–2.2 nm, determined by TEM) embedded on and within polypyrrole spheres (50–90 nm, determined by SEM) with a high ratio of surface to bulk Pd (measured using XPS analysis). DLS (dynamic light scattering) was additionally used to characterise the spherical polypyrrole support; these results were in good agreement with that gained by SEM (Fig. 12).

The nanocomposite was applied to the C–H arylation of furans and thiophenes using a fairly wide range of bromoarene as the aryl-donating coupling partner, albeit under relatively harsh conditions (Scheme 10). Notably, heterocyclic bromopyridines could couple efficiently in good yields, without significant catalyst poisoning.

In a subsequent development, 2-carboxy-aldehyde and ketone-substituted *N*-Methylpyrroles could be directly arylated in good to excellent yields and site-selectively for



Scheme 10 showing conditions used C–H arylation of oxazoles, thiophenes and pyrroles, enabled by a Pd@PPy nanocomposite

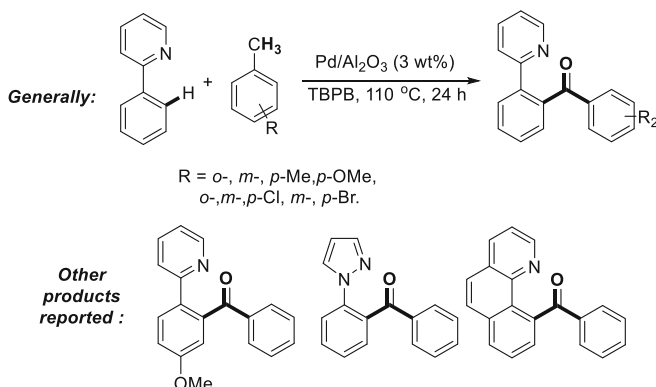


Scheme 11 Showing generalised conditions used for controlling the site-selectivity in direct C–H arylation of N-Me-imidazole by Pd@PPy nanocomposite

the 5-position [77]. *N*-Me-imidazoles could additionally be coupled with both electron-rich and electron-poor bromoarenes (Scheme 11). Site-selectivity (C2 vs. C4 position) was found to be governed by the *para*-substituent on bromoarene substrate, type of base and additive. However, a narrower scope of bromoarenes was tested in this case, and thus no significant structure–activity correlations could be fully made.

The performances of C–H arylations at *N*-Me-pyrroles and imidazoles enabled by Pd@PPy nanocomposites were compared with and observed to be equal if not more effective than that catalysed by either the homogeneous catalyst precursor Pd(OAc)₂ and the ubiquitous heterogeneous catalyst Pd/C.

Catalyst recycling experiments in this case yielded inconsistent results, which were found to vary depending on the specific substrates used. For example, the coupling of 2-*n*-butylfuran and 4-bromobenzonitrile could be repeated after recycling of the catalyst, with no loss of activity; however the analogous process failed when deploying 4-bromoacetophenone as the bromoarene and a similarly recycled catalyst. This observation underlines the fact that recycling studies should not be limited to a model reaction, as different substrates can have vastly different effects on potential for catalyst recyclability. It was observed that growth of PdNPs (measured by TEM) from 4 to 7 nm occurred during the course of a reaction, without any change in morphology of the polypyrrole support (measured by SEM). This was taken to indicate that catalytically relevant PdNPs are not merely superficial to the polypyrrole support and the reaction solution likely penetrates into the depths of the support to access buried catalytically active PdNPs, resulting in concomitant Ostwald ripening of PdNPs. ICP-AES analysis of a filtrate post-reaction 260 ppm (2.7%/Pd) indicated that a not insignificant amount of Pd is leached into the reaction mixture during the reaction. No hot-filtration experiment was reported in this case; thus it is unclear whether the leached Pd is catalytically competent.



Scheme 12 Reaction conditions and reagents used for the direct cross-dehydrogenative coupling (CDC) of 2-arylpyridines with alkylbenzenes, catalysed by γ - Al_2O_3

This study demonstrates the catalyst efficacy of PdNPs on a well-characterised organic framework which could effectively catalyse direct C–H arylations in a range of pharmaceutically relevant substrates.

5.5 Case Study V) 2-Arylpyridine Coupling with Alkylbenzene PdNPs on a γ - Al_2O_3 Support

Bao and Zhaorigetu et al. found that PdNPs supported on γ - Al_2O_3 (γ -alumina) were able to mediate C–H/C–H cross-dehydrogenative coupling (CDC) of 2-arylpyridines with alkylbenzenes [78]. This report builds on reactivity uncovered by Patel et al. [79].

Three different types of *ortho*-directing arylpyridine moiety were found to be able to be coupled with alkylbenzenes to afford aromatic ketones (Scheme 12).

A *tert*-butyl-peroxybenzoate oxidant was required, and the reactions were performed neatly, with a high excess of the alkylbenzene substrate as the reaction solvent. It was found that either increasing or decreasing the catalyst loading resulted in a reduction of catalyst activity.¹ Employing different supports (Sm_2O_3 and CeO_2) resulted in reduced activity; this was rationalised to be a result of the superior porosity and increased surface of the γ - Al_2O_3 compared to the alternative oxide superstructures tested.

¹See Sect. 2 for a discussion of the inverse relationships between catalyst loading and performance in heterogeneous cross-coupling reactions.

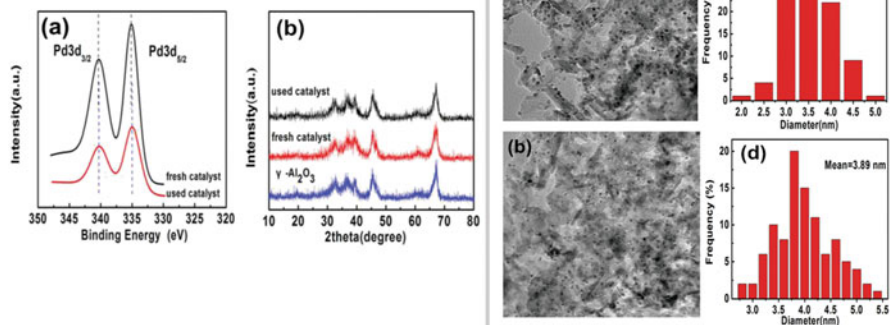
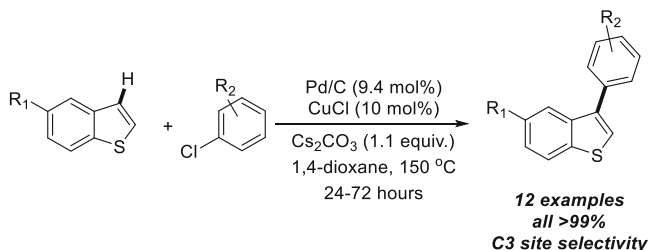


Fig. 13 Characterisation evidence for γ -Al₂O₃-supported PdNPs; [Left] (a) XPS spectrum (b) XRD spectrum. Right (a) and (b) TEM images of supported PdNPs before and after one use (respectively). (c) and (d) Size distribution of supported PdNPs before and after one use (respectively), (determined by TEM). Reproduced from Ref. [78] with permission from the Royal Society of Chemistry

The catalyst system was prepared by NaBH₄ reduction of PdCl₂ in the presence γ -Al₂O₃ powder (from an “impregnation–reduction” method). XPS (X-ray photoelectron spectroscopy) indicated that Pd⁰ was the dominant oxidation state, with the signal significantly reduced after one catalytic use (left (a) Fig. 13). XRD (X-ray diffraction) showed no distinct signal from the Pd, which implied that the nanoparticles were small and well-dispersed (left (b) Fig. 13). TEM analysis confirmed a mean Pd particle diameter of 3.21 and 3.89 nm for fresh and used catalyst, respectively (right (a) and (b) Fig. 13). The recyclability of the catalyst was assessed in a model reaction between 2-phenylpyridine and toluene. The catalyst could be reused three times without loss of activity, with a drop of a mere 13% on the fifth use. The radical inhibitor TEMPO attenuated the model reaction, giving indication that the oxidant may have a dual radical initiator/oxidiser role. A Pd⁰/Pd^{II}/Pd^{IV} catalytic cycle was proposed.

In summary, this report constitutes a good example of the use of a well characterised, easily prepared and recyclable supported heterogeneous catalyst for application in C–H/C–H bond functionalisation, introducing significant molecular complexity from simple starting materials, in good yields. A similar approach to reaction screening and catalyst characterisation was employed when the same group investigated the Pd/ γ -Al₂O₃-catalysed amidation of esters and another C–H bond functionalising process [80].



Scheme 13 Showing the conditions employed for the C3 site-selective direct C–H arylation of benzo[b]thiophenes

5.6 Case Study VI) Development and Optimisation of Conditions for Pd/C-Catalysed Site-Selective C–H Activation Reactions

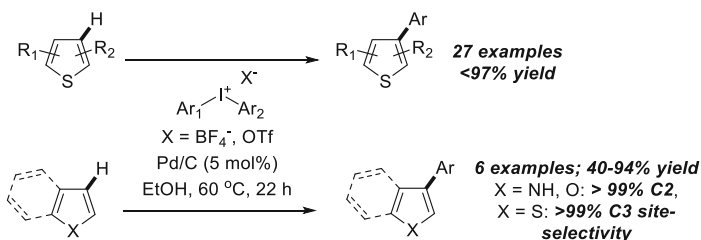
It is well-established that Pd/C can be used as a heterogeneous hydrogenation catalyst, but only relatively recently has Pd/C seen application in cross-couplings involving C–H bond functionalisation. To this end, Glorius et al. have recently led the way. Methodologies for direct C–H arylation at benzothiophenes were discovered and later developed and optimised, expanding the scope to a wider variety of heterocyclic coupling partners. These conditions were later adapted for the C–H arylation of polyaromatic hydrocarbon compounds.

In the first example, aryl chlorides could be used as an arylating coupling partner, and a dual catalytic system of Pd/C and CuCl (a proposed Lewis acidic co-catalyst) was employed, with Cs₂CO₃ as a base (Scheme 13) [81]. Most intriguingly, C3 site-selectivity was achieved in each case, in stark contrast to the nominal homogeneous catalysts [e.g. Pd(PPh₃)₄ and PdCl₂(PPh₃)₂], which afford the C2 product. This constitutes an unprecedented example of homogeneous to heterogeneous switch in site-selectivity.

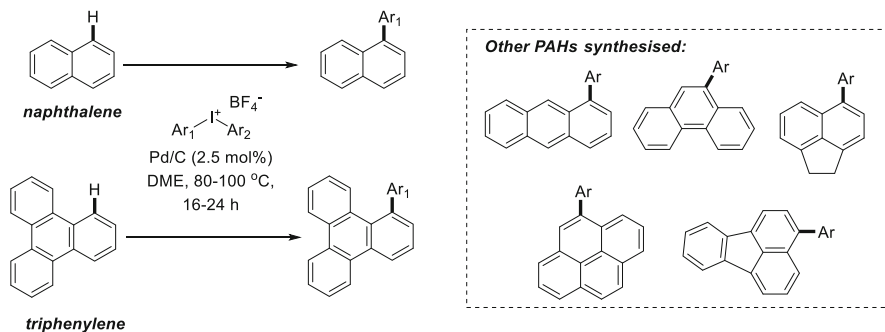
Broader employment of this methodology required higher temperatures and long reaction times for synthetically useful substrate conversions. In spite of these harsher conditions, which could be expected to give rise to a leached active species, both the hot-filtration test and the three-phase test pointed towards a heterogeneous catalytic manifold. Additionally, leaching was determined to be minimal, using TXRF (total reflection X-ray fluorescence) spectroscopy.

Changing the coupling partner to a diaryliodonium salt allowed for the reactions to proceed under significantly milder conditions, in alcoholic solvent (Scheme 14) [82]. This change of substrate allowed the reaction to work in absence of additive CuCl and base. Using this methodology, efficient C3 site-selective arylation of thiophenes and benzothiophenes was possible.

Site-selective coupling using wider scope of aromatic heterocyclic substrate was also possible under these reaction conditions, with furans, benzofurans and unprotected indoles additionally being able to undergo arylation at the C2 position. In spite



Scheme 14 Showing the conditions employed for the highly site-selective direct C–H arylation of varying heterocyclic aromatic compounds



Scheme 15 Showing the conditions employed for the C–H arylation of a variety polyaromatic hydrocarbon compounds

of the highly oxidising reaction conditions employed (which may be expected to result in oxidative leaching of metal), standard heterogeneity tests (Hg-poisoning test, the three-phase test and the hot-filtration test) all point towards a heterogeneous active catalyst. After each catalyst use, yields dropped by 41%, indicating a severe change in catalyst morphology after a single cycle.

This method was subsequently modified for the efficient direct arylation of naphthalene triphenylene and related polyaromatic hydrocarbons (PAHs) (Scheme 15) [83]. In these examples, arylation was seen to proceed with good site-selectivity at the most sterically hindered position (albeit the more acidic position). A range of electron-deficient and electron-donating substituents on the aromatic coupling partner were well tolerated under reaction conditions. However, tuning of the substituent electronics on the model PAH (naphthalene) resulted in significantly reduced reaction efficiency. In all cases polyarylated aromatics arose as undesired by-products under the reaction conditions. $\text{Pd/Al}_2\text{O}_3$ additionally was shown to be an active catalyst in this process, but not as active as Pd/C .

The reaction was determined to be first order in Pd, with an induction period that decreases in length as a function of higher catalyst loading. This finding indicates that the active catalyst is formed over time from an inactive pre-catalyst. Critically, employing standard tests (e.g. Hg-poisoning test, three-phase test and hot-filtration), a heterogeneous catalytic manifold was indicated. Also, reactivity was attenuated by

addition of radical inhibitors; TEMPO, BHT and BQ indicating a radical aryl species are involved in the catalytic cycle. With these mechanistic studies in mind, the authors concluded that a heterogeneous species is formed either by leaching and re-aggregation or by breaking off from the heterogeneous source.

An important observation to note is that the Pd/C source (i.e. the manufacturer) had a significant bearing on reactivity, indicating variability in activity of the catalyst samples. This case study demonstrates how a set of reaction conditions can be tuned and adapted and then applied to a variety of different aromatic substituents. It also gives indication of the ability for the widely accessible catalyst, Pd/C, to be employed in an operationally simple manner to carry out cross-coupling reactions for the synthesis of valuable chemicals, thus bypassing the need to prepare complex Pd catalyst scaffolds.

6 Future Perspectives and Conclusions

In this review we have highlighted the importance of heterogeneous/quasi-heterogeneous–homogeneous metal-catalysed cross-coupling reactions, with many important breakthroughs being made in synthetic chemistry. Considerably more mechanistic work has been completed on classical cross-coupling reactions, such as Suzuki–Miyaura cross-coupling and Heck alkenylation reactions. We decided to set out this groundwork for classical cross-coupling reactions to assist researchers in building and assessing more fully the potential of metal surfaces and aggregated metal species in functionalising C–H bonds, in suitable substrates. Numerous promising synthetic methodologies have been reported over the last few years, and some preliminary mechanistic work are completed. However, for the field to move to the next step, it is necessary to conduct more detailed and comprehensive studies using techniques such as XAS (XANES/EXAFS) on reactions conducted in operando, particularly if higher oxidation state Pd^{IV} species are proposed. Such studies arguably require access to synchrotron facilities and specific expertise, which is difficult for most research groups working in this field to conduct. In this context collaboration with surface scientists can be highly beneficial.

From our point view we have benefited as a synthetic organic and organometallic chemistry group by collaborating with physical chemists working in surface catalysis. This has helped gained valuable mechanistic insight in cross-coupling catalysis, which can also inform future directions in terms of catalyst design. Critically, it is necessary for the catalysis community at large to seriously consider the role of aggregated metal catalyst species in frontier-leading C–H bond functionalisation reactions. Typically, many groups will assess this with a few tests, but the closer one looks, evidence will usually emerge showing that aggregated metal species form from homogeneous metal catalyst species. Whether such aggregated species are active in their own right, a reservoir of catalytically active species or a moribund form needs to be assessed fully. The increasing evidence showing a role for metal catalyst surfaces and aggregated species (i.e. nanoparticles) in catalytic cross-

coupling reactions, of a myriad of substrates containing C–H bonds, highlights that the field ought to be fully examining homogeneous, heterogeneous and quasi-heterogeneous–homogeneous behaviour. Having more developed and definite tests will aid the catalysis and synthetic chemistry community at large in this respect.

At the time of writing, it is clear that the future is a very bright one for catalytic cross-coupling chemistry, and there are many benefits and opportunities for the employment of heterogeneous catalyst-type species. It remains to be seen whether such catalysts will be more broadly applied in target-orientated synthesis, such as in complex natural product synthesis. Hydrogenation on Pd/C is a mainstream reaction in chemical synthesis, and it is the opinion of the authors that a step-change would be seen in the broader adoption of similar catalysts in tricky synthetic transformations (i.e. substrates containing a plethora of functionality and stereochemical information). Of particular note is that Pd/C is a preferred catalyst used in process chemistry. The pioneering work by Glorius et al. has highlighted that conditions can be tuned to grant Pd/C the ability to mediate complex C–H bond functionalisations. Thus, there are many opportunities for this fascinating field going forwards, which can additionally be exploited in the synthesis of agrochemicals, pharmaceuticals and advanced materials.

References

1. Adrio LA, Nguyen BN, Guilera G, Livingston AG, Hii KK (2012) Speciation of Pd(OAc)₂ in ligandless Suzuki–Miyaura reactions. *Cat Sci Technol* 2:316–323
2. Bao Y-S, Zhang D, Jia M, Zhaorigetu B (2016) Replacing Pd(OAc)₂ with supported palladium nanoparticles in ortho-directed CDC reactions of alkylbenzenes. *Green Chem* 18:2072–2077
3. Bao Y-S, Wang L, Jia M, Xu A, Agula B, Baiyin M, Zhaorigetu B (2016) Heterogeneous recyclable nano-palladium catalyzed amidation of esters using formamides as amine sources. *Green Chem* 18:3808–3814
4. Bedford RB, Bowen JG, Davidson RB, Haddow MF, Seymour-Julen AE, Sparkes HA, Webster RL (2015) Facile hydrolysis and alcoholysis of palladium acetate. *Angew Chem Int Ed* 54:6591–6594
5. Bizouard P, Testa C, Zinovyeva VA, Roger J, Hierso J-C (2016) Palladium–Polypyrrole nanocomposites Pd@PPy for direct C–H functionalization of pyrroles and imidazoles with bromoarenes. *Synlett* 27:1227–1231
6. Bray JTW, Ford MJ, Karadakov PB, Whitwood AC, Fairlamb IJS (2019) The critical role played by water in controlling Pd catalyst speciation in arylocyanation reactions. *React Chem Eng* 4:122–130
7. Brazier JB, Nguyen BN, Adrio LA, Barreiro EM, Leong WP, Newton MA, Figueroa SJA, Hellgardt K, Hii KKM (2014) Catalysis in flow: operando study of Pd catalyst speciation and leaching. *Catal Today* 229:95–103
8. Campeau L-C, Rousseaux S, Fagnou K (2005) A solution to the 2-Pyridyl organometallic cross-coupling problem: regioselective catalytic direct arylation of pyridine N-oxides. *J Am Chem Soc* 127:18020–18021
9. Carole WA, Colacot TJ (2016) Understanding palladium acetate from a user perspective. *Chem Rev* 22:7686–7695
10. Cassol CC, Umpierre AP, Machado G, Wolke SI, Dupont J (2005) The role of Pd nanoparticles in ionic liquid in the Heck reaction. *J Am Chem Soc* 127:3298–3299

11. Chernyshev VM, Astakhov AV, Chikunov IE, Tyurin RV, Eremin DB, Ranny GS, Khrustalev VN, Ananikov VP (2019) Pd and Pt catalyst poisoning in the study of reaction mechanisms: what does the mercury test mean for catalysis? *ACS Catal* 9:2984–2995
12. Chiba M, Thanh MN, Hasegawa Y, Obora Y, Kawasaki H, Yonezawa T (2015) Synthesis of binary solid solution Cu–Pd nanoparticles by DMF reduction for enhanced photoluminescence properties. *J Mater Chem C* 3:514–520
13. Clark JR, Feng K, Sookezian A, White MC (2018) Manganese-catalysed benzylic C(sp³)–H amination for late-stage functionalization. *Nat Chem* 10:583–591
14. Collins G, Schmidt M, O’Dwyer C, Holmes JD, McGlacken GP (2014) The origin of shape sensitivity in palladium-catalyzed Suzuki–Miyaura cross coupling reactions. *Angew Chem Int Ed* 53:4142–4145
15. Collins KD, Honeker R, Vásquez-Céspedes S, Tang D-TD, Glorius F (2015) C–H arylation of triphenylene, naphthalene and related arenes using Pd/C. *Chem Sci* 6:1816–1824
16. Crabtree RH (2012) Resolving heterogeneity problems and impurity artifacts in operationally homogeneous transition metal catalysts. *Chem Rev* 112:1536–1554
17. Crabtree RH, Lei A (2017) Introduction: CH activation. *Chem Rev* 117:8481–8482
18. Crabtree RH, Mingos DM (2007) *Comprehensive organometallic chemistry III: from fundamentals to applications*, vol 5. Elsevier Science, Amsterdam
19. De Ornellas S, Williams TJ, Baumann CG, Fairlamb IJS (2013) Chapter 12. Catalytic C–H/C–X bond functionalisation of nucleosides, nucleotides, nucleic acids, amino acids, peptides and proteins. In: C–H and C–X bond functionalization: transition metal mediation. RSC Publishing, Cambridge, pp 409–447
20. de Vries AHM, Mulders JMCA, Mommers JHM, Henderickx HJW, de Vries JG (2003) Homeopathic ligand-free palladium as a catalyst in the heck reaction. A comparison with a palladacycle. *Org Lett* 5:3285–3288
21. Deraedt C, Astruc D (2014) “Homeopathic” palladium nanoparticle catalysis of cross Carbon–Carbon coupling reactions. *Acc Chem Res* 47:494–503
22. Dey A, Sinha SK, Achar TK, Maiti D (2018) Game of directors: accessing remote meta- and Para-C–H bonds with covalently attached directing groups. *Angew Chem Int Ed* 58(32):10820–10843
23. Eisenstein O, Milani J, Perutz RN (2017) Selectivity of C–H activation and competition between C–H and C–F bond activation at fluorocarbons. *Chem Rev* 117:8710–8753
24. Ellis PJ, Fairlamb IJS, Hackett SFJ, Wilson K, Lee AF (2010) Evidence for the surface-catalyzed Suzuki–Miyaura reaction over palladium nanoparticles: an operando XAS study. *Angew Chem Int Ed* 49:1820–1824
25. Eremin DB, Ananikov VP (2017) Understanding active species in catalytic transformations: from molecular catalysis to nanoparticles, leaching, “cocktails” of catalysts and dynamic systems. *Coord Chem Rev* 346:2–19
26. Fairlamb IJS (2005) Palladium catalysis in synthesis: where next? *Tetrahedron* 61:9661–9662
27. Fairlamb IJS (2016) Chapter 11. Pd-catalysed cross-couplings for the pharmaceutical sector and a move to cutting-edge C–H bond functionalization: is palladium simply too precious? In: *Green and sustainable medicinal chemistry*. Royal Society of Chemistry (RSC) Publishing, Cambridge, pp 129–139
28. Fairlamb IJS, Lee AF (2013) Chapter 3. Fundamental Pd⁰/Pd^{II} redox steps in cross-coupling reactions: homogeneous, hybrid homogeneous–heterogeneous to heterogeneous mechanistic pathways for C–C couplings. In: Ribas X (ed) *C–H and C–X bond functionalization: transition metal mediation*. RSC, Cambridge, pp 72–107
29. Ferlin F, Santoro S, Ackermann L, Vaccaro L (2017) Heterogeneous C–H alkenylations in continuous-flow: oxidative palladium-catalysis in a biomass-derived reaction medium. *Green Chem* 19:2510–2514
30. Gaikwad AV, Rothenberg G (2006) In-situ UV-visible study of Pd nanocluster formation in solution. *Phys Chem Chem Phys* 8:3669–3675

31. Gandeepan P, Müller T, Zell D, Cera G, Warratz S, Ackermann L (2019) 3d transition metals for C–H activation. *Chem Rev* 119:2192–2452
32. Gensch T, Hopkinson MN, Glorius F, Wencel-Delord J (2016) Mild metal-catalyzed C–H activation: examples and concepts. *Chem Soc Rev* 45:2900–2936
33. Gorunova ON, Novitskiy IM, Grishin YK, Gloriovov IP, Roznyatovsky VA, Khrustalev VN, Kochetkov KA, Dunina VV (2018) When applying the mercury poisoning test to Palladacycle-catalyzed reactions, one should not consider the common misconception of mercury(0) selectivity. *Organometallics* 37:2842–2858
34. Guin S, Rout SK, Banerjee A, Nandi S, Patel BK (2012) Four tandem C–H activations: a sequential C–C and C–O bond making via a Pd-catalyzed cross dehydrogenative coupling (CDC) approach. *Org Lett* 14:5294–5297
35. Hartwig JF (2010) *Organotransition metal chemistry: from bonding to catalysis*. University Science Books, Sausalito
36. Hartwig JF, Larsen MA (2016) Undirected, homogeneous C–H bond functionalization: challenges and opportunities. *ACS Central Sci* 2:281–292
37. Huang L, Ang TP, Wang Z, Tan J, Chen J, Wong PK (2011) On the roles of solid-bound ligand scavengers in the removal of palladium residues and in the distinction between homogeneous and heterogeneous catalysis. *Inorg Chem* 50:2094–2111
38. Hyotanishi M, Isomura Y, Yamamoto H, Kawasaki H, Obora Y (2011) Surfactant-free synthesis of palladium nanoclusters for their use in catalytic cross-coupling reactions. *Chem Commun* 47:5750–5752
39. Kapdi AR (2014) Organometallic aspects of transition-metal catalysed regioselective C–H bond functionalisation of arenes and heteroarenes. *Dalton Trans* 43:3021–3034
40. Korwar S, Brinkley K, Siamaki AR, Gupton BF, Ellis KC (2015) Selective N-chelation-directed C–H activation reactions catalyzed by Pd(II) nanoparticles supported on multiwalled carbon nanotubes. *Org Lett* 17:1782–1785
41. Korwar S, Burkholder M, Gilliland SE, Brinkley K, Gupton BF, Ellis KC (2017) Chelation-directed C–H activation/C–C bond forming reactions catalyzed by Pd(ii) nanoparticles supported on multiwalled carbon nanotubes. *Chem Commun* 53:7022–7025
42. Krasovskaya V, Krasovskiy A, Bhattacharjya A, Lipshutz BH (2011) “On water” sp³–sp² cross-couplings between benzylic and alkenyl halides. *Chem Commun* 47:5717–5719
43. Krasovskiy A, Thomé I, Graff J, Krasovskaya V, Konopelski P, Duplais C, Lipshutz BH (2011) Cross-couplings of alkyl halides with heteroaromatic halides, in water at room temperature. *Tetrahedron Lett* 52:2203–2205
44. Lafrance M, Fagnou K (2006) Palladium-catalyzed benzene arylation: incorporation of catalytic pivalic acid as a proton shuttle and a key element in catalyst design. *J Am Chem Soc* 128:16496–16497
45. Lafrance M, Rowley CN, Woo TK, Fagnou K (2006) Catalytic intermolecular direct arylation of perfluorobenzenes. *J Am Chem Soc* 128:8754–8756
46. Leadbeater NE, Marco M (2002) Ligand-free palladium catalysis of the Suzuki reaction in water using microwave heating. *Org Lett* 4:2973–2976
47. Lee AF, Ellis PJ, Fairlamb IJS, Wilson K (2010) Surface catalysed Suzuki–Miyaura cross-coupling by Pd nanoparticles: an operando XAS study. *Dalton Trans* 39:10473–10482
48. Liu W, Ali SZ, Ammann SE, White MC (2018) Asymmetric Allylic C–H alkylation via palladium(II)/cis-ArSOX catalysis. *J Am Chem Soc* 140:10658–10662
49. Liu W, Huang X, Placzek MS, Kraska SW, McQuade P, Hooker JM, Groves JT (2018) Site-selective 18F fluorination of unactivated C–H bonds mediated by a manganese porphyrin. *Chem Sci* 9:1168–1172
50. Lyons TW, Sanford MS (2010) Palladium-catalyzed ligand-directed C–H functionalization reactions. *Chem Rev* 110:1147–1169
51. Martínez AV, Leal-Duaso A, García JI, Mayoral JA (2015) An extremely highly recoverable clay-supported Pd nanoparticle catalyst for solvent-free Heck–Mizoroki reactions. *RSC Adv* 5:59983–59990

52. Murai S, Kakiuchi F, Sekine S, Tanaka Y, Kamatani A, Sonoda M, Chatani N (1993) Efficient catalytic addition of aromatic carbon-hydrogen bonds to olefins. *Nature* 366:529–531
53. Parisien M, Valette D, Fagnou K (2005) Direct arylation reactions catalyzed by Pd(OH)₂/C: evidence for a soluble palladium catalyst. *J Org Chem* 70:7578–7584
54. Pla D, Gómez M (2016) Metal and metal oxide nanoparticles: a lever for C–H functionalization. *ACS Catal* 6:3537–3552
55. Raluy E, Favier I, López-Vinasco AM, Pradel C, Martin E, Madec D, Teuma E, Gómez M (2011) A smart palladium catalyst in ionic liquid for tandem processes. *Phys Chem Chem Phys* 13:13579–13584
56. Reay AJ, Fairlamb IJS (2015) Catalytic C–H bond functionalisation chemistry: the case for quasi-heterogeneous catalysis. *Chem Commun* 51:16289–16307
57. Reay AJ, Neumann LK, Fairlamb IJS (2016) Catalyst efficacy of homogeneous and heterogeneous palladium catalysts in the direct Arylation of common heterocycles. *Synlett* 27:1211–1216
58. Reay AJ, Hammarback LA, Bray JTW, Sheridan T, Turnbull D, Whitwood AC, Fairlamb IJS (2017) Mild and regioselective Pd(OAc)₂-catalyzed C–H Arylation of Tryptophans by [ArN₂] X, promoted by Tonic acid. *ACS Catal* 7:5174–5179
59. Saha D, Adak L, Ranu BC (2010) Palladium(0) nanoparticles-catalyzed ligand-free direct arylation of benzothiazole via C–H bond functionalization. *Tetrahedron Lett* 51:5624–5627
60. Sahnoun S, Messaoudi S, Peyrat J-F, Brion J-D, Alami M (2008) Microwave-assisted Pd(OH)₂-catalyzed direct C–H arylation of free-(NH₂) adenines with aryl halides. *Tetrahedron Lett* 49:7279–7283
61. Sahnoun S, Messaoudi S, Brion J-D, Alami M (2009) A site selective C–H arylation of free-(NH₂) adenines with aryl chlorides: application to the synthesis of 6,8-disubstituted adenines. *Org Biomol Chem* 7:4271–4278
62. Santoro S, Kozhushkov SI, Ackermann L, Vaccaro L (2016) Heterogeneous catalytic approaches in C–H activation reactions. *Green Chem* 18:3471–3493
63. Santoro S, Ferlin F, Luciani L, Ackermann L, Vaccaro L (2017) Biomass-derived solvents as effective media for cross-coupling reactions and C–H functionalization processes. *Green Chem* 19:1601–1612
64. Sherwood J, Clark JH, Fairlamb IJS, Slattery JM (2019) Solvent effects in palladium catalysed cross-coupling reactions. *Green Chem* 21(9):2164–2213
65. Siamaki AR, Lin Y, Woodberry K, Connell JW, Gupton BF (2013) Palladium nanoparticles supported on carbon nanotubes from solventless preparations: versatile catalysts for ligand-free Suzuki cross coupling reactions. *J Mater Chem A* 1:12909–12918
66. Slavík P, Kurka DW, Smith DK (2018) Palladium-scavenging self-assembled hybrid hydrogels – reusable highly-active green catalysts for Suzuki–Miyaura cross-coupling reactions. *Chem Sci* 9:8673–8681
67. Storr TE, Firth AG, Wilson K, Darley K, Baumann CG, Fairlamb IJS (2008) Site-selective direct arylation of unprotected adenine nucleosides mediated by palladium and copper: insights into the reaction mechanism. *Tetrahedron* 64:6125–6137
68. Storr TE, Baumann CG, Thatcher RJ, De Ornellas S, Whitwood AC, Fairlamb IJS (2009) Pd(0)/Cu(I)-mediated direct arylation of 2'-deoxyadenosines: mechanistic role of Cu(I) and reactivity comparisons with related purine nucleosides. *J Org Chem* 74:5810–5821
69. Tabasso S, Calcio Gaudino E, Rinaldi L, Ledoux A, Larini P, Cravotto G (2017) Microwave-assisted, ligand-free, direct C–H arylation of thiophenes in biomass-derived γ -valerolactone. *New J Chem* 41:9210–9215
70. Tang D-TD, Collins KD, Glorius F (2013) Completely regioselective direct C–H functionalization of Benzo[b]thiophenes using a simple heterogeneous catalyst. *J Am Chem Soc* 135:7450–7453
71. Tang D-T, Collins KD, Ernst JB, Glorius F (2014) Pd/C as a catalyst for completely regioselective C–H functionalization of thiophenes under mild conditions. *Angew Chem Int Ed Engl* 53:1809–1813

72. Thathagar MB, ten Elshof JE, Rothenberg G (2006) Pd Nanoclusters in C-C coupling reactions: proof of leaching. *Angew Chem Int Ed* 45:2886–2890
73. Vásquez-Céspedes S, Chepiga KM, Möller N, Schäfer AH, Glorius F (2016) Direct C–H Arylation of Heteroarenes with copper impregnated on magnetite as a reusable catalyst: evidence for CuO nanoparticle catalysis in solution. *ACS Catal* 6:5954–5961
74. Whitesides GM, Hackett M, Brainard RL, Lavalleye JPPM, Sowinski AF, Izumi AN, Moore SS, Brown DW, Staudt EM (1985) Suppression of unwanted heterogeneous platinum(0)-catalyzed reactions by poisoning with mercury(0) in systems involving competing homogeneous reactions of soluble organoplatinum compounds: thermal decomposition of bis(triethylphosphine)-3,3,4,4-tetramethylplatinacyclopentane. *Organometallics* 4:1819–1830
75. Widegren JA, Finke RG (2003) A review of the problem of distinguishing true homogeneous catalysis from soluble or other metal-particle heterogeneous catalysis under reducing conditions. *J Mol Catal A Chem* 198:317–341
76. Zinovyeva VA, Vorotyntsev MA, Bezverkhyy I, Chaumont D, Hierso J-C (2011) Highly dispersed palladium–polypyrrole nanocomposites: in-water synthesis and application for catalytic arylation of heteroarenes by direct C–H bond activation. *Adv Funct Mater* 21:1064–1075
77. Widegren JA, Bennett MA, Finke RG (2003) Is it homogeneous or heterogeneous catalysis? Identification of bulk ruthenium metal as the true catalyst in benzene hydrogenations starting with the monometallic precursor, Ru(II)(η^6 -C₆Me₆)(OAc)₂, plus kinetic characterization of the heterogeneous nucleation, then autocatalytic surface-growth mechanism of metal film formation. *J Am Chem Soc* 125:10301–10310
78. Williams TJ, Reay AJ, Whitwood AC, Fairlamb IJS (2014) A mild and selective Pd-mediated methodology for the synthesis of highly fluorescent 2-arylated tryptophans and tryptophan-containing peptides: a catalytic role for Pd⁰ nanoparticles? *Chem Commun* 50:3052–3054
79. Yano H, Nakajima Y, Obora Y (2013) *N,N*-Dimethylformamide-stabilized palladium nanoclusters as catalyst for Migita–Kosugi–Stille cross-coupling reactions. *J Organomet Chem* 745:258–261
80. Zhang M, Zhang Y, Jie X, Zhao H, Li G, Su W (2014) Recent advances in directed C–H functionalizations using monodentate nitrogen-based directing groups. *Org Chem Front* 1:843–895
81. Zhang L, Li Z, Zhang Y, Chin Paa M, Hu Q, Gong X, Shuang S, Dong C, Peng X, Choi MMF (2015) High-performance liquid chromatography coupled with mass spectrometry for analysis of ultrasmall palladium nanoparticles. *Talanta* 131:632–639
82. Zhao F, Bhanage BM, Shirai M, Arai M (2000) Heck reactions of Iodobenzene and methyl acrylate with conventional supported palladium catalysts in the presence of organic and/or inorganic bases without ligands. *Chem Eur J* 6:843–848
83. Zhao Y, Du L, Li H, Xie W, Chen J (2019) Is the Suzuki–Miyaura cross-coupling reaction in the presence of Pd nanoparticles heterogeneously or homogeneously catalyzed? An interfacial surface-enhanced Raman spectroscopy study. *J Phys Chem Lett* 10:1286–1291

Further Reading²

Eremin DB, Ananikov VP (2017) *Coord Chem Rev* 346:2–19. A discussion of possibilities of the nature of the catalyst species in cross-coupling reactions

²The following references are recommended further reading in the form of book chapters and reviews.

- Fairlamb IJS, Lee AF (2013) Chapter 3. Fundamental Pd0/PdII redox steps in cross-coupling reactions: homogeneous, hybrid homogeneous–heterogeneous to heterogeneous mechanistic pathways for C–C couplings. In: C–H and C–X bond functionalization. RSC, Cambridge, pp 72–107. Discusses homogeneous and potential heterogeneous and components to catalytic reactivity, focusing on classical cross-coupling processes
- Pla D, Gomez M (2016) Metal and metal oxide nanoparticles: a lever for C–H functionalization. ACS Catal 6:3537–3552. Heterogeneous C–H-bond activation and functionalisation catalysis, including Pd, Ru and CuNPs, focussing on ‘unactivated’ C–(sp³)H (a few examples) and C–(sp²)H bonds
- Reay A, Fairlamb IJS (2015) Catalytic C–H bond functionalisation chemistry: the case for quasi-heterogeneous catalysis. Chem Commun 51:16289–16307. A discussion of heterogeneous includes a wealth of practical examples of heterogeneous catalytic C–H bond functionalisation chemistry
- Santoro S, Ferlin F, Luciani L, Ackerman L, Vaccaro L (2017) Biomass-derived solvents as effective media for cross-coupling reactions and C–H functionalization processes. Green Chem 19:1601–1612. A review on use of green biomass-derived solvents or cross-coupling, includes some heterogeneous catalytic examples
- Santoro S, Kozhushkov SI, Ackermann L, Vaccaro L (2016) Heterogeneous catalytic approaches in C–H activation reactions. Green Chem 18:3471

Nanoparticle Catalysts in Flow Systems



Hiroyuki Miyamura and Shū Kobayashi

Contents

1	Introduction: Nanoparticles as Heterogeneous Catalysts in Flow “Fine” Synthesis	208
2	Metal Nanoparticle Catalysts Immobilized in Microchannels and Microreactors	211
2.1	Polymer-Incarcerated Palladium Nanoparticles Immobilized in Microchannels for Hydrogenation	211
2.2	Polysilane-Supported Palladium Nanoparticles Immobilized in Microchannels for Hydrogenation	212
2.3	Gold Nanoparticles Immobilized in a Capillary for Aerobic Oxidation	214
2.4	Polymeric Palladium Nanoparticle Membrane-Installed Microflow Devices for Hydrodehalogenation	215
3	Continuous-Flow Reactions Using Metal Nanoparticles Packed in Columns (Fixed-Bed Reactors)	218
3.1	Continuous-Flow Hydrogenation Using Polysilane-Supported Palladium Catalysts	219
3.2	Poly(dimethyl)silane-Supported Palladium Nanoparticles for Continuous-Flow Hydrogenation	221
3.3	Reductive Amination Through Hydrogenation Using Metal Nanoparticle Catalysts Under Continuous-Flow Conditions	225
3.4	Hydrogenation of Arenes and Heteroarenes Using Metal Nanoparticle Catalysts Under Continuous-Flow Conditions	228
3.5	Aerobic Oxidation of Alcohols Under Continuous-Flow Conditions Using Metal Nanoparticle Catalysts	233
3.6	Control of Selectivity in Heterogeneous Gold Catalysis Under Flow Conditions . .	237
4	Summary	240
	References	241

Abstract By taking advantage of the high catalytic activity and high turnover frequency (TOF) of heterogeneous metal nanoparticle catalysts, continuous-flow systems, in which introduced reactants are converted into the desired product in high yield, can be realized. These continuous-flow reactors possess high compatibility with sequential continuous-flow systems, which enable multistep flow

H. Miyamura and S. Kobayashi (✉)

Department of Chemistry, Graduate School of Science, The University of Tokyo, Tokyo, Japan
e-mail: shu_kobayashi@chem.s.u-tokyo.ac.jp

synthesis of biologically active compounds such as active pharmaceutical ingredients (APIs) and natural products.

Keywords Continuous-flow reaction · Heterogeneous catalyst · Packed-bed reactor

1 Introduction: Nanoparticles as Heterogeneous Catalysts in Flow “Fine” Synthesis

Modern organic synthesis, the so-called fine organic synthesis, is used for the synthesis of a wide range of useful compounds, and many synthetic reactions can be used to achieve high yields and selectivities. These chemical syntheses are mainly carried out using either a batch or a flow method. Batch methods, in which all starting components, substrates, catalysts, additives, solvents, etc. are charged into a flask before starting the reaction (Fig. 1a), are currently the most commonly used approach in most laboratories of organic chemistry and synthetic organic chemistry; the production of fine chemicals such as active pharmaceutical ingredients (APIs), agrochemicals, electronic chemicals, fragrances, etc. is generally performed by repeating batch methods. In contrast, in flow methods, materials are simultaneously charged and discharged. Starting materials are continuously introduced at one end of a column or a hollow loop, and the product is continuously eluted from the other end of the column or loop (Fig. 1b). Flow methods have been used in the large-scale synthesis of basic chemicals by reactions of gas molecules; the synthesis of ammonia through the Haber–Bosch process is a typical example. However, it has been considered that flow methods are difficult to apply to the synthesis of complex molecules such as APIs. Nevertheless, since Kobayashi proposed the concept of

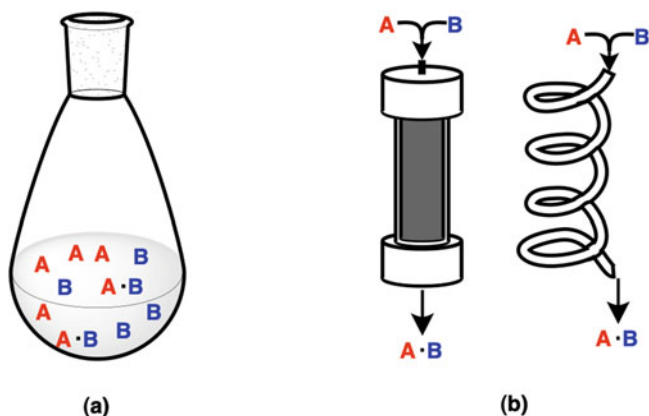


Fig. 1 Batch reaction (a) and continuous-flow reaction (b)

flow “fine” synthesis in 2016 [1], increasing numbers of syntheses and reactions that attain high yields and high selectivities for complex molecules using flow methods have been reported. Flow “fine” synthesis can be defined as “reaction and synthesis that attain high yields and high selectivities by a flow method.” Furthermore, because a characteristic of the flow method is that it is continuous, flow “fine” synthesis should construct multistep flow systems by combining individual flow reactions to synthesize structurally complex molecules. Flow “fine” synthesis has several advantages over conventional organic synthesis. (1) High-energy productivity and energy saving compared with batch methods can be realized. (2) The compact nature of a reactor means that space saving can be realized in addition to energy saving. (3) The low-volume reaction space means that the risk of out-of-control reactions can be minimized by rapid heat exchange and it is possible to suppress damage caused in the event of leakage even when high-risk substances are used; therefore, flow “fine” synthesis ensures high safety. (4) It is possible to adjust the quantity of production by controlling the rate of introduction of starting materials; such “just-in-time” production can reduce the amount of waste generated, which can lead to reduced costs. (5) Automation is easier, and it is possible to minimize the exposure of operators to hazardous chemicals. (6) Using columns packed with a suitable catalyst (fixed-bed reactor), the separation of catalyst from the product is not required.

Kobayashi divided reactions of flow “fine” synthesis into types I–IV (Fig. 2).

Type I: Substrates (A and B) are passed through a column or hollow loop, etc. during which reactions occur. Although the product is obtained continuously, unreacted A and B, as well as by-products, are also eluted as contaminants.

Type II: One of the substrates (B) is supported in a column. If an excess amount of B is used, the second substrate (A) is consumed. Although contamination of the

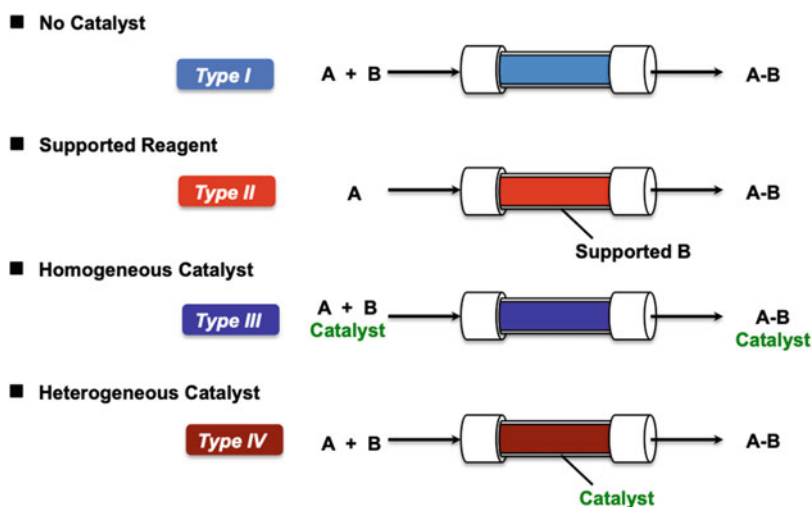


Fig. 2 Four types of continuous-flow systems

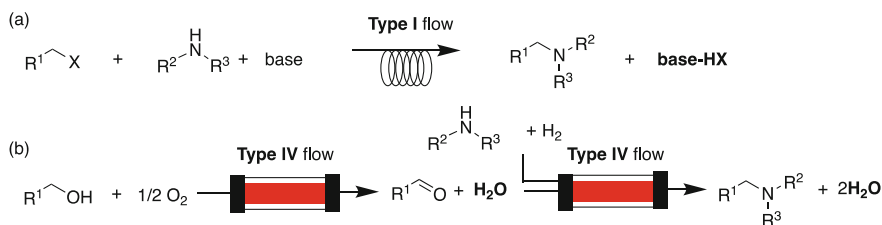
product by unreacted A or B may be avoided, overreactions may occur. In addition, once supported B is consumed, the column must be changed.

Type III: Substrate A reacts with B in the presence of a homogeneous catalyst. Although catalysis proceeds smoothly, the catalyst cannot be easily separated, and it elutes as a contaminant in the product.

Type IV: Substrate A reacts with B in the presence of a heterogeneous catalyst. If catalysis proceeds smoothly, no separation of the catalyst from the product is required.

Considering the recent guidelines on green sustainable chemistry, synthesis with catalysts is preferred to synthesis without catalysts because the former can lead to energy saving and waste reduction. From this viewpoint, flow systems of types II and IV are recommended. Furthermore, whereas the products are contaminated by homogeneous catalysts in type III flow systems, no contamination of catalysts is expected under ideal conditions of type IV systems. If multistep continuous-flow systems are designed for the synthesis of complex molecules, the generation of by-products and contamination of catalysts may be problematic for downstream flow reactions. Therefore, type IV flow systems may have some advantages over other types of flow reactions, and type IV flow systems that produce no by-products or only by-products that can be easily removed by phase separation, such as gas or water, are ideal. For example, Scheme 1 shows two different methods (a and b) to obtain the same secondary amine from starting materials at the same oxidation levels. The reaction shown in Scheme 1a is a one-step process that uses type I flow, which generates salt as a by-product. On the other hand, the sequential reaction shown in Scheme 1b is a two-step process combining type IV flow systems of aerobic oxidation and hydrogenation, and only water is generated as a by-product. From the viewpoint of flow “fine” synthesis, (b) is preferred over (a) because water can be easily removed by phase separation and it can be potentially connected to other downstream flow systems without any concerns.

Heterogeneous catalysts used in type IV flow are required to be robust over long periods of reaction time, to exhibit high tolerance against various functional groups, and to have appropriate physical properties for the construction of flow reactors. In this chapter, heterogeneous metal nanoparticle catalysts that can be used in type IV flow systems for flow “fine” synthesis are introduced and discussed.



Scheme 1 Two methods to obtain secondary amine under continuous-flow conditions

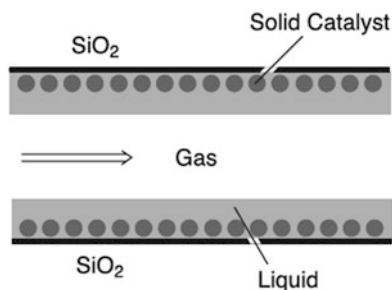
2 Metal Nanoparticle Catalysts Immobilized in Microchannels and Microreactors

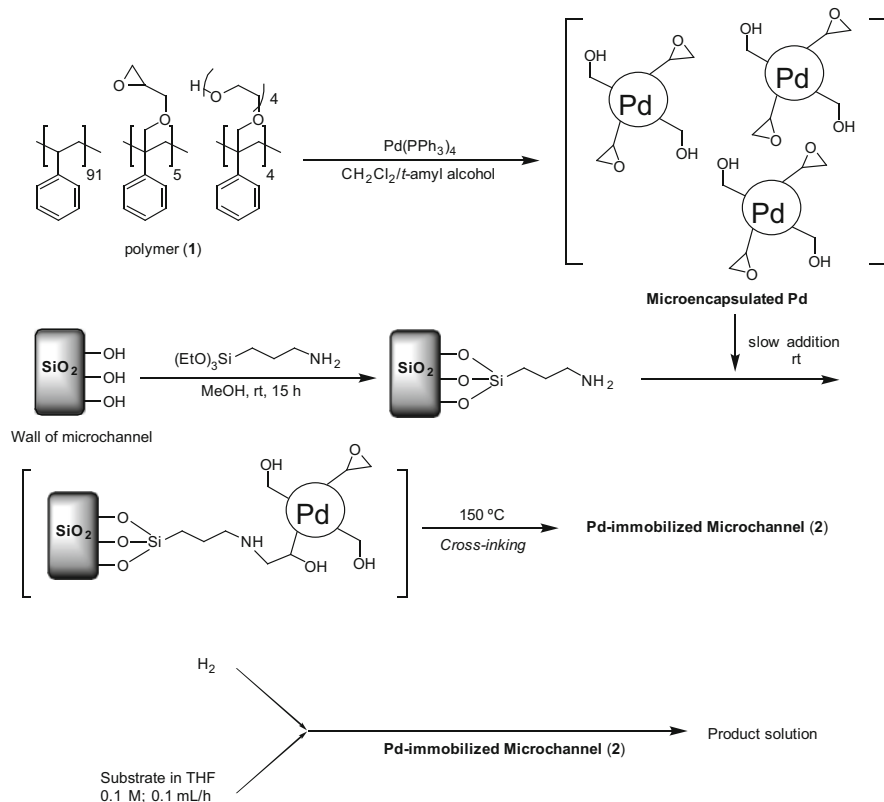
Redox reactions are key for flow “fine” synthesis. Especially, type IV flow reactors for aerobic oxidation and hydrogenation are useful and ideal to flow “fine” synthesis as discussed above. However, multi-interfacial reaction environments involving gas–liquid–solid multiphase reaction conditions are needed for continuous-flow systems. Microchannels and microreactors are ideal devices for such purpose because they can maximize the specific surface area. Therefore, methods that can be applied to immobilize heterogeneous metal nanoparticle catalysts in such microfluidic devices are crucial for success.

2.1 Polymer-Incarcerated Palladium Nanoparticles Immobilized in Microchannels for Hydrogenation

In 2004, Kobayashi and co-workers designed a microchannel reactor that has a very large specific interfacial area per unit of volume (10,000–50,000 m²/m³), in which Pd nanoparticles stabilized by cross-linking polymer (1), the so-called polymer-incarcerated catalysts [2], were immobilized on the wall of the surface-modified microchannel (2) through covalent bonds (Fig. 3, Scheme 2) [3]. A hydrogenation reaction was conducted under continuous-flow conditions at ambient temperature by introducing a tetrahydrofuran solution of a benzalacetone (0.1 M) through one inlet and introducing H₂ through the other inlet via a mass-flow controller (Scheme 2). When the flow rate of H₂ was relatively slow, alternate slugs of the liquid and gas were observed, and the yield was insufficient [63% yield with a flow rate of the liquid substrate of 0.8 mL/h and a flow rate of H₂ of 0.15 mL/min]. On the other hand, with increased flow rate of H₂ (1.0 mL/min) and a decreased flow rate of substrate (0.1 mL/h), as the desired flow conditions, the liquid flowed close to the channel surface where the catalyst was immobilized, and the gas flowed through the center (Fig. 4).

Fig. 3 Polymer-incarcerated catalysts immobilized on the wall of the surface-modified microchannel





Scheme 2 Preparation of Pd-immobilized microchannel for continuous-flow hydrogenation

2.2 Polysilane-Supported Palladium Nanoparticles Immobilized in Microchannels for Hydrogenation

In 2006, Kobayashi and co-workers developed a poly(methylphenylsilane)-encapsulated Pd nanoparticle catalyst for hydrogenation reactions as well as cross-coupling reactions [4]. Polysilane is a polymer with particular electronic properties that derive from the σ -conjugated electrons of the silicon backbone. σ -Conjugated electrons show reduction ability to generate metal nanoparticles from metal salts and stabilize metal nanoparticles by multiple, weak interactions as well as those of aromatic π -electrons. Polysilane is also commercially available and inexpensive. In addition, polysilane is a highly stable and safe material that does not swell with organic solvents. Polysilane operated not only as a backbone for the immobilized catalysts but also as a connecting material between the surface of the glass wall and catalyst via silicon–oxygen networks. To improve the activity and stability, a range of metal oxides were used as a second support to construct polysilane–metal oxide

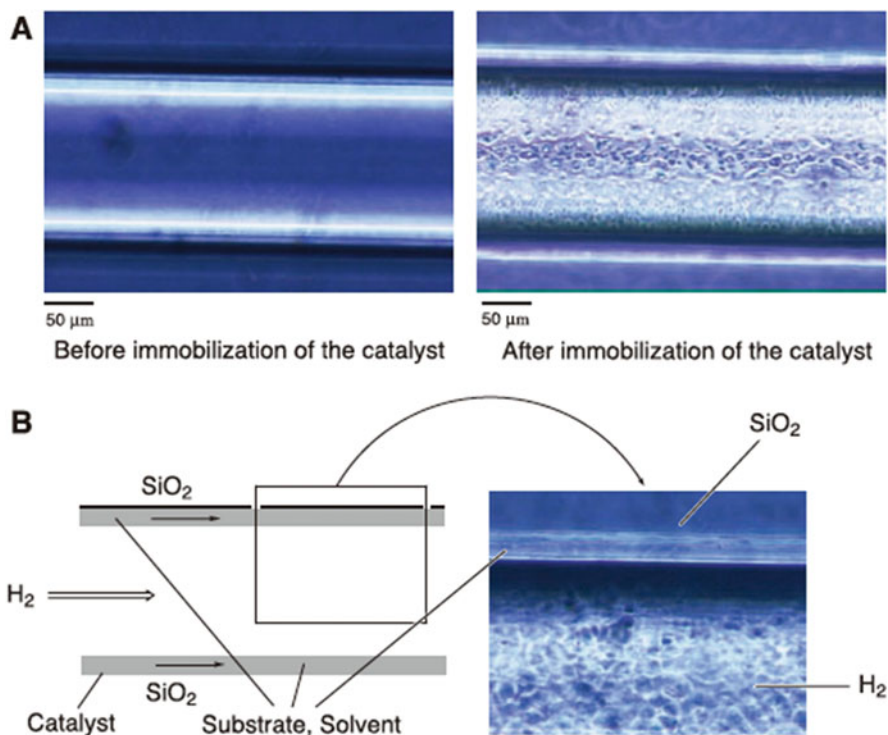
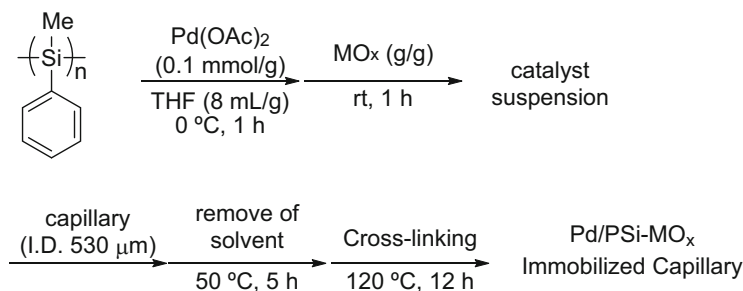
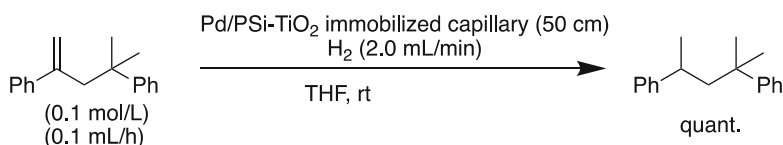


Fig. 4 Photographic image of the Pd-immobilized microchannel reactor under pipe-flow conditions

composite materials. In 2008, Kobayashi and co-workers developed Pd nanoparticle-immobilized capillary reactors based on polysilane encapsulation techniques [5]. Palladium(II) acetate was added to a THF solution of polysilane followed by the addition of metal oxide, and the mixture was stirred for 1 h. Capillaries (530 μm i.d.) were filled with the catalyst solution, and the solvent was removed in a dry over (50°C, 5 h). After cross-linking (120°C, 12 h), Pd/PSi-MO_x immobilized capillary was obtained (Scheme 3). Substrate solution and hydrogen gas were directly passed through the capillary to conduct hydrogenation. When TiO₂ was employed as a second support, 2,4-diphenyl-4-methyl-1-pentanone was hydrogenated quantitatively; 11 substrates were also hydrogenated in good to excellent yields. The Pd/PSi-MO_x immobilized capillary was reused 12 times without loss of activity after simple treatment (Scheme 4).



Scheme 3 Preparation of capillary-immobilized Pd nanoparticle catalyst



Scheme 4 Hydrogenation reaction using capillary-immobilized Pd nanoparticle catalyst

2.3 Gold Nanoparticles Immobilized in a Capillary for Aerobic Oxidation

In 2007, Kobayashi and co-workers developed Au nanoparticle catalysts immobilized on polystyrene-based copolymer with a cross-linking moiety (**4**) (Fig. 5), the so-called polymer-incarcerated Au nanoparticle catalyst (PI-Au) [6]. In 2009, the same group developed Au nanoparticle-immobilized capillary reactors for aerobic oxidation of alcohols to the corresponding carbonyl compounds [7]. In general, aerobic oxidation of alcohols using heterogeneous catalysts is slower than hydrogenation of olefins, and a reaction environment with a large gas–liquid–solid interfacial surface area is required to complete the reaction within the limited length of the reaction channel under continuous-flow conditions. Commercially available polysiloxane-coated capillary (**3**) (50 cm length, 250 μm i.d.) that contained 50% phenyl and 50% *n*-cyanopropyl functionalities on silicon atoms with a film thickness of 0.25 μm on the walls was employed as the base of the reactors (Fig. 6). The cyanopropyl group was reduced to the corresponding primary amine group using lithium aluminum hydride (Scheme 5a). Microencapsulated gold nanoparticles (MC-Au), which were prepared by reduction of chlorotriphenylphosphine gold using sodium borohydride in the presence of copolymer with alcohol and epoxide moieties as a stabilizer (**4**), were used for the immobilization (Scheme 5b). The colloidal solution of the MC-Au was slowly pumped into the modified capillary, and the capillary was heated at 170 $^\circ\text{C}$ for 5 h. Cross-linking and covalent bond formation between the copolymer and the capillary surface occurred to afford the Au nanoparticle-immobilized capillary (Scheme 5c). The prepared Au nanoparticle-immobilized capillary was attached to a T-shaped

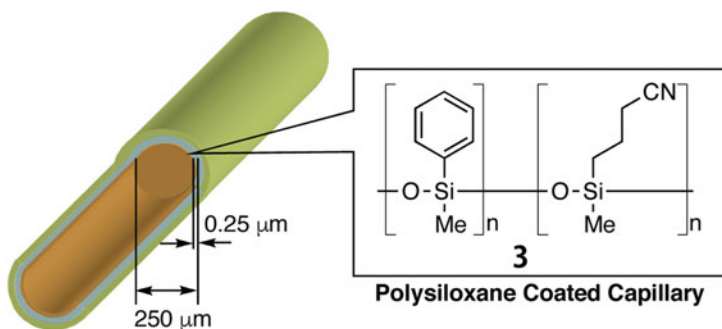


Fig. 5 Surface-modified capillary

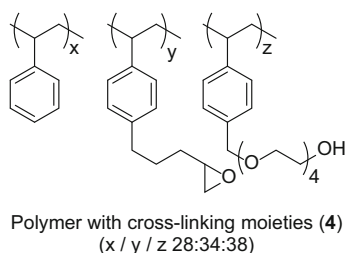
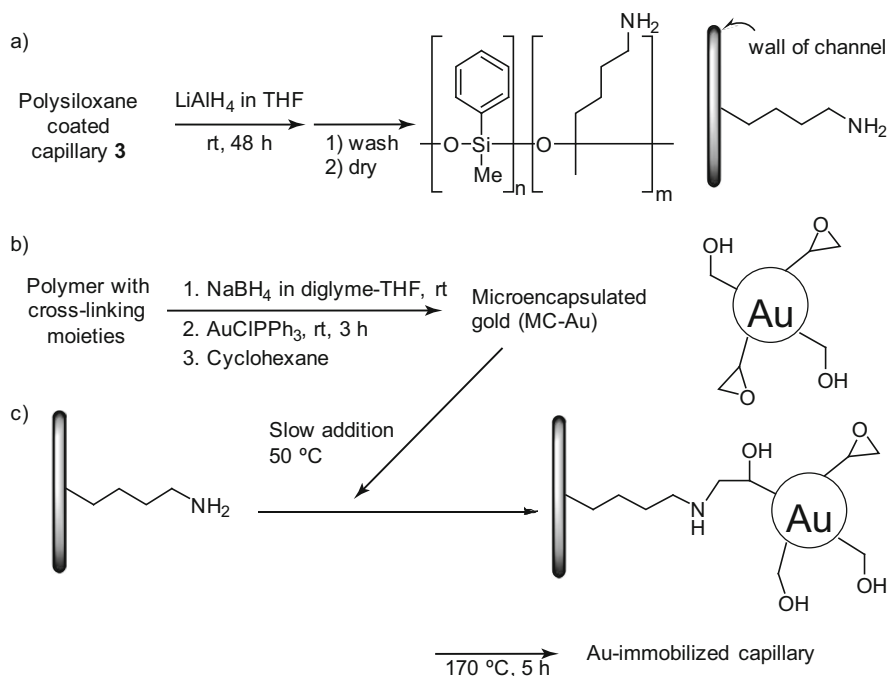


Fig. 6 Styrene-based polymer with cross-linking moieties

connector, which was connected to another T-shaped connector by a Teflon tube. Solutions of substrates in 1,2-dichloroethane and an aqueous solution of potassium carbonate were introduced at a flow rate of 0.1 mL/h and 0.03 mL/h, respectively (Fig. 7). Oxygen gas was introduced through a mass-flow controller at a flow rate of 1.5 mL/min. When 1-phenylethanol was used as the substrate, quantitative conversion to acetophenone was maintained over 4 days. Nine other substrates were successfully oxidized in good to excellent yields using the same capillary reactors.

2.4 Polymeric Palladium Nanoparticle Membrane-Installed Microflow Devices for Hydrodehalogenation

In 1999, Whitesides and co-workers found that polymer deposition resulted from the acid–base reaction at the laminar interface of two flows: polymeric sulfonate salt and a polymeric ammonium salt [8]. In 2006, Uozumi and co-workers developed a microchannel reactor with a catalytic membrane containing a Pd complex based on the strategy of polymeric deposition at a laminar interface [9]. A polymer membrane of a Pd complex was formed inside a microchannel reactor through



Scheme 5 Immobilization of Au nanoparticles on surface-modified capillary

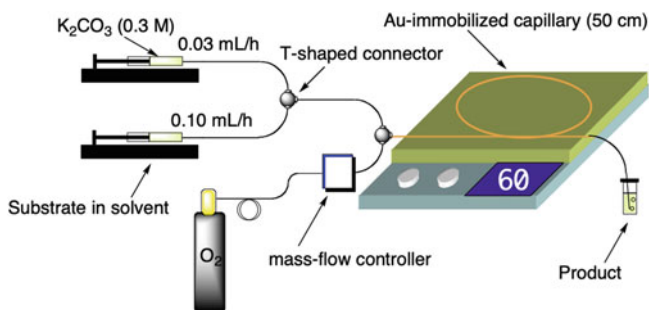


Fig. 7 Continuous oxidation using capillary-immobilized Au nanoparticle catalyst

self-assembling complexation of a polymeric phosphine ligand and a Pd species at the interface of two parallel laminar layers flowing through the microchannel. The developed microchannel with a polymeric membrane containing an immobilized Pd complex could be successfully used to perform a Suzuki–Miyaura coupling reaction. In 2012, the same group found that a Pd complex immobilized on a polymeric membrane in a microchannel could be reduced to form Pd nanoparticles

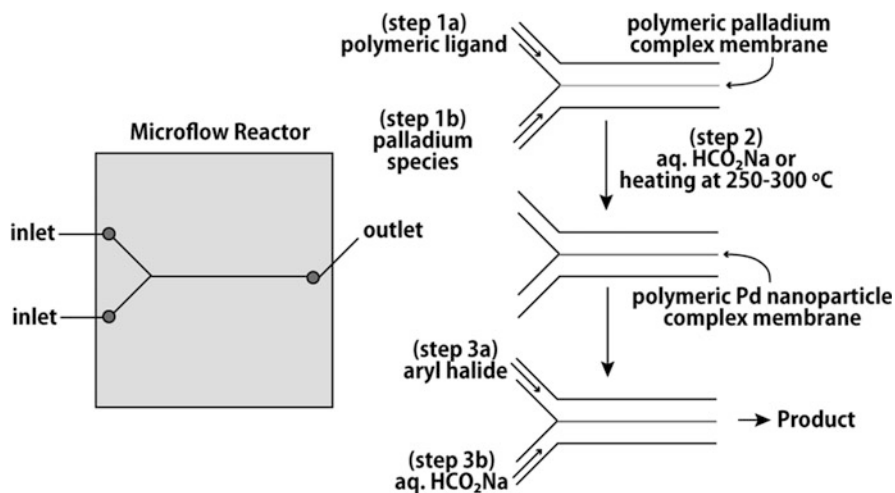


Fig. 8 Preparation of polymeric Pd nanoparticle membrane in microflow reactors

[10]. Polymeric laminar membranes of composites 5a–5c in the microchannel were prepared by complexation of PdCl_2 salts with poly(4-vinylpyridine), poly[(*N*-isopropylacrylamide)₅-co-(4-diphenylstyrylphosphine)], and pyridinium polymer, respectively (Fig. 8). A saturated aqueous solution of HCO_2Na was streamed into these microchannels at $50\text{ }^\circ\text{C}$ for 30 min at a flow rate of $0.5\ \mu\text{L}/\text{min}$. Black-colored polymeric palladium nanoparticle membrane-installed microchannel devices were prepared from composites 5a and 5c with average Pd nanoparticle sizes of 6 and 12 nm, respectively (Fig. 9). On the other hand, neither color change nor formation of Pd nanoparticles was observed from composite 5b. Thermal decomposition of composites 5a–5c in microchannel devices at $250\text{--}300\text{ }^\circ\text{C}$ led to the formation of Pd nanoparticles in all cases (Fig. 10). The thickness of the membrane in the microchannel device under dry and wet (iPrOH/ H_2O) conditions was 14.3 and $17.1\ \mu\text{m}$, respectively. These microchannel devices containing Pd nanoparticle membranes were subjected to hydrodehalogenation of aryl halides. A solution of 1-chloro-3,5-dimethoxybenzene in iPrOH and an aqueous solution of HCO_2Na were streamed into the microchannel devices 6a–6f at $50\text{ }^\circ\text{C}$ from two separate inlets, with both flow rates of $0.5\ \mu\text{L}/\text{min}$ and a residence time of 8 s (Scheme 6). Microchannel devices prepared from composite membrane 5a through either HCO_2Na reduction or thermal decomposition gave quantitative conversions. Although devices derived from composite 5c gave moderate conversions, devices derived from 5b gave poor conversions. Not only aryl chloride but also bromide, iodide, and triflate were successfully dehalogenated using the microchannel device derived from composite 5a.

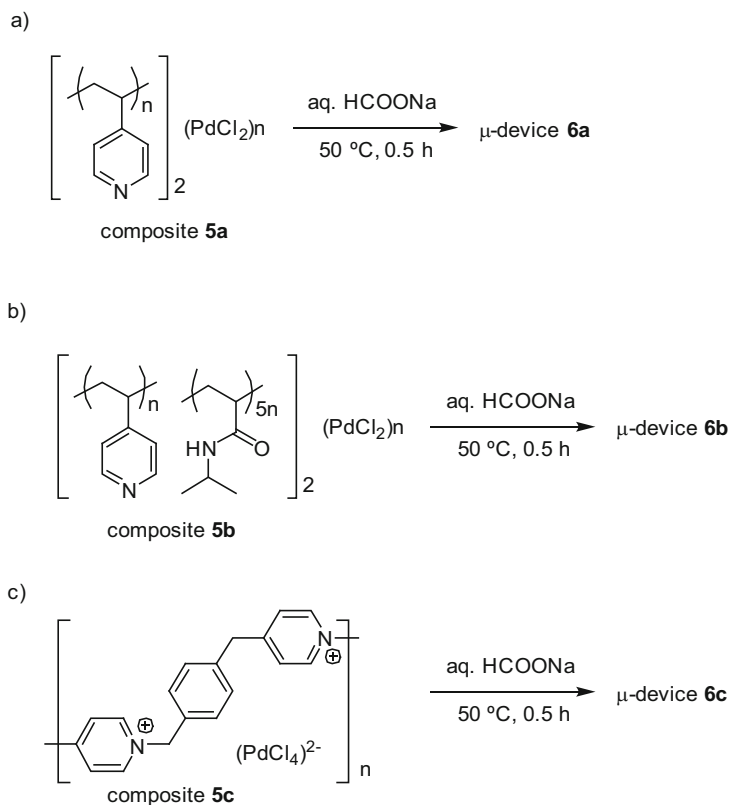


Fig. 9 Preparation of Pd nanoparticle membrane in a microflow reactor

3 Continuous-Flow Reactions Using Metal Nanoparticles Packed in Columns (Fixed-Bed Reactors)

Microreactors have advantages of high interfacial specific surface area for multiphase reactions; however, the productivity of a single microreactor is low. Although increasing the number of single microreactors increases the productivity, this approach is expensive. The most straightforward and cost-efficient method for continuous-flow reactors using a heterogeneous catalyst on a lab to industrial scale is using a column packed with appropriate heterogeneous catalyst as the reactor. When finely powdered heterogeneous catalysts are packed into a column and both gas and liquid are streamed, the heterogeneous catalyst itself can work as a “mixer” of the two phases, and efficient mixing and large interfacial surface area can be expected. The speed of each stream, the physical properties of the solid catalyst, and the design of the inlet of the column can be very important to achieve both efficient mixing and smooth streams of both phases.

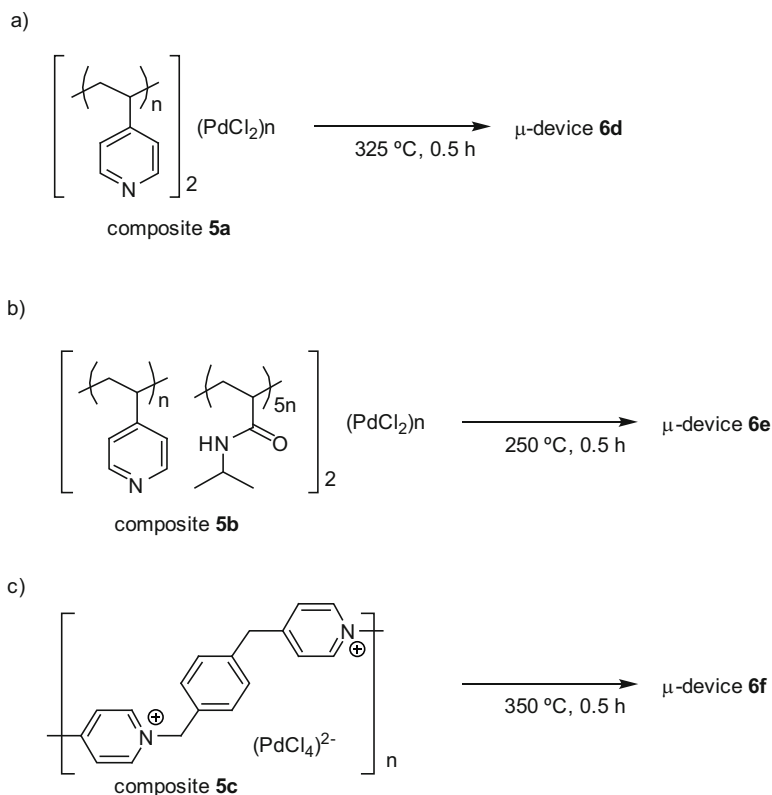
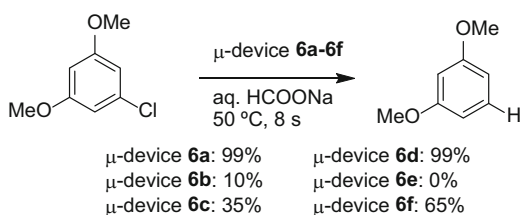


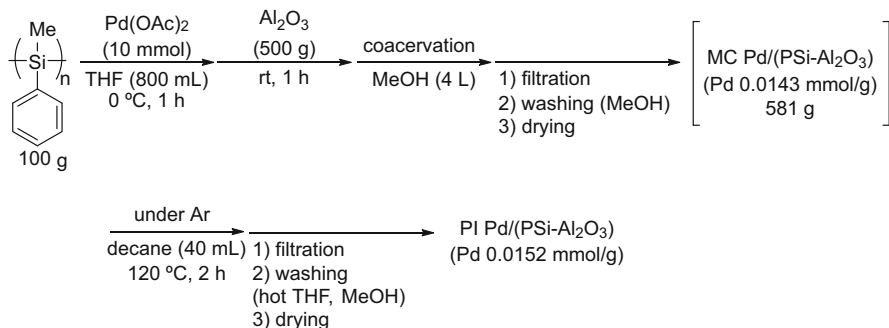
Fig. 10 Preparation of Pd nanoparticle membrane in a microflow reactor

Scheme 6 Pd-catalyzed reaction using Pd nanoparticle membranes in microflow reactors



3.1 Continuous-Flow Hydrogenation Using Polysilane-Supported Palladium Catalysts

In 2008, Kobayashi and co-workers developed poly(methylphenylsilane)-supported palladium nanoparticles on metal oxide hybrid catalysts (Pd/(PSi-MO_x)), and they worked as hydrogenation catalysts without leaching of palladium (Scheme 7) [11]. The hybrid catalysts were insoluble, did not swell in any solvent, and were predicted to be applicable to continuous-flow reactors. In 2011, Kobayashi and



Scheme 7 Preparation of polysilane-immobilized Pd nanoparticle catalyst

co-workers designed a continuous-flow reactor for hydrogenation reaction using heterogeneous polysilane-supported palladium/alumina hybrid catalysts [12]. The efficient mixing of gas and liquid before the catalyst region might be important for efficient reaction. A high-performance liquid chromatography (HPLC) pump was used to feed the substrate into the central hole in the top of the column, which was filled with the Pd/(PSi-Al₂O₃) catalyst (Fig. 11). Hydrogen gas was introduced into the six holes surrounding the central hole using a mass-flow controller. The column was heated in a water bath as required. The substrate reacted with H₂ gas inside the column, and the product was collected downstream of the column. Hydrogenation reaction of ethyl cinnamate was performed with this continuous-flow reactor under neat conditions, and the hydrogenated product was collected for 8 h without contamination of the starting material. The catalyst retained high activity for at least 8 h, and the turnover number (TON) reached 8,700 (Scheme 8). Seven other liquid substrates were hydrogenated quantitatively under neat conditions with this continuous-flow reactor, and solid substrates were also applicable after dissolving in an appropriate solvent.

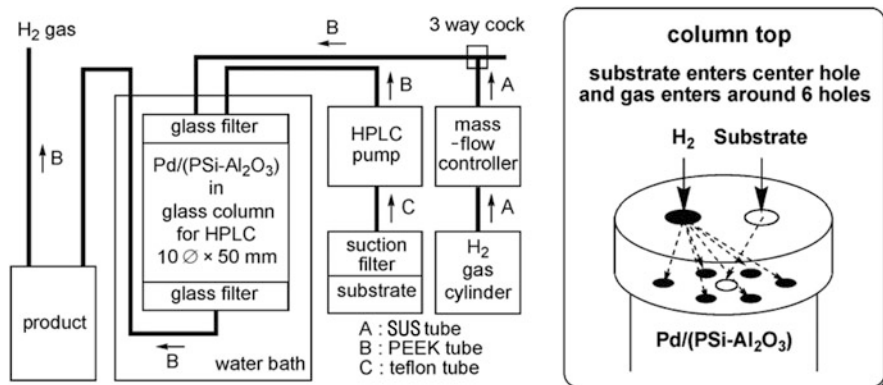
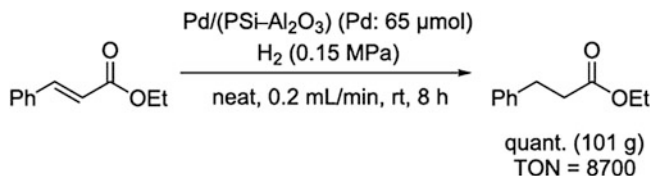


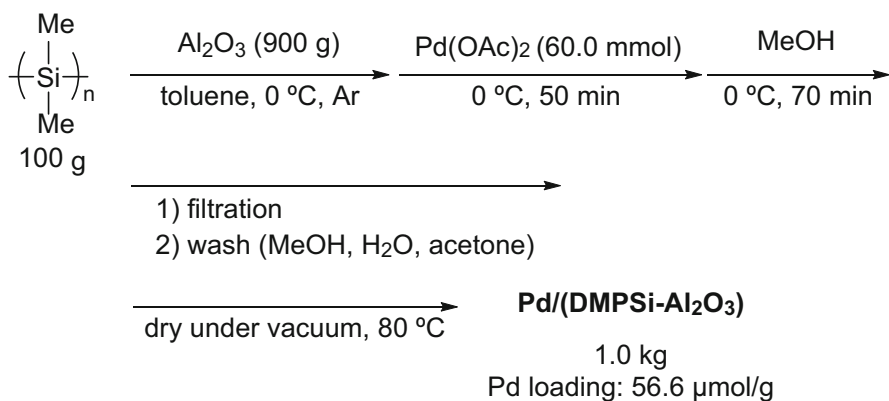
Fig. 11 Continuous-flow hydrogenation using polysilane-immobilized Pd nanoparticle catalyst in column



Scheme 8 Reactivity of continuous-flow hydrogenation

3.2 Poly(dimethyl)silane-Supported Palladium Nanoparticles for Continuous-Flow Hydrogenation

In 2015, Kobayashi and co-workers developed a poly(dimethyl)silane-supported palladium/alumina hybrid catalyst [Pd/(DMPSi- Al_2O_3)] [13]. Poly(dimethyl)silane is readily available and inexpensive, although poly(methylphenyl)silane is relatively limited and expensive. The catalysts were prepared from poly(methylphenyl)silane and palladium acetate without the use of external reductant (Scheme 9). Pd nanoparticles with an average size of (6.4 ± 3.4) nm were found using scanning transmission electron microscopy (STEM) and energy-dispersive X-ray spectroscopy (EDS) to exist on silicon-rich areas rather than on aluminum- or oxygen-rich areas. This observation suggested that these nanoparticles were formed through reduction by the polysilane support and were simultaneously immobilized on the polymer through electronic interactions. Approximately 900 mg of the catalyst was packed in a SUS column (5 mm diameter, 50 mm length), which was then placed in an aluminum heating block to control the reaction temperature (Fig. 12). The substrate, either neat or in solution, was introduced into the SUS column packed with the catalyst using a peristaltic pump, and, simultaneously, H_2 gas was introduced at atmospheric pressure into the catalyst column through a mass-flow



Scheme 9 Preparation of Pd nanoparticles immobilized on a composite support of poly(dimethyl)silane and alumina

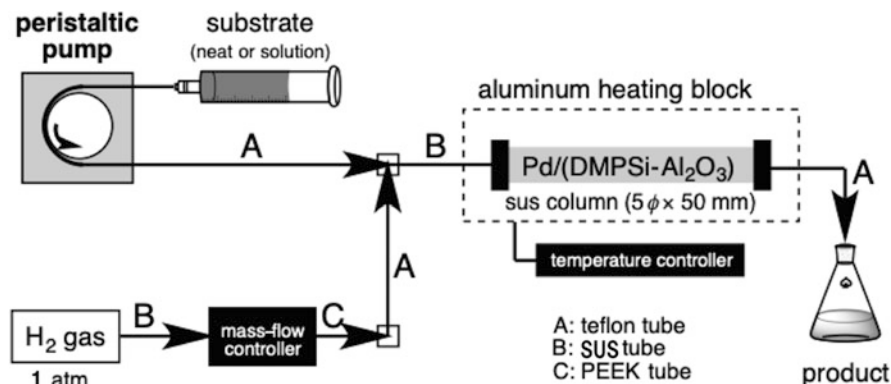








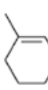




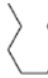
Fig. 12 Continuous-flow hydrogenation using Pd nanoparticles immobilized on a composite support of poly(dimethyl)silane and alumina

controller. H_2 gas and substrate solution were mixed in a SUS mesh filter placed at the inlet of the column. The product was collected downstream of the column. Various substrates were hydrogenated quantitatively, and 5–100 g scale production was achieved for a 5 h reaction period. The catalytic turnover frequency (TOF) exceeded $3,000 \text{ h}^{-1}$, and TON reached more than 16,000 (Table 1, entries 1 and 2). Furthermore, a selection of vegetable oils (olive oil, macadamia nut oil, castor oil, and jojoba oil) was successfully hydrogenated to afford the desired saturated oils, which are commercial products, with high efficiency, using a SUS column (10 mm diameter, 150 mm length). One of the advantages of continuous-flow systems with a catalyst-packed column is the ease with which the systems can be scaled up. The production of castor oil could be increased to 1.5 kg/h using a large SUS column (100 mm diameter, 1,000 mm length), and the system was found to be stable for more than 1 month.

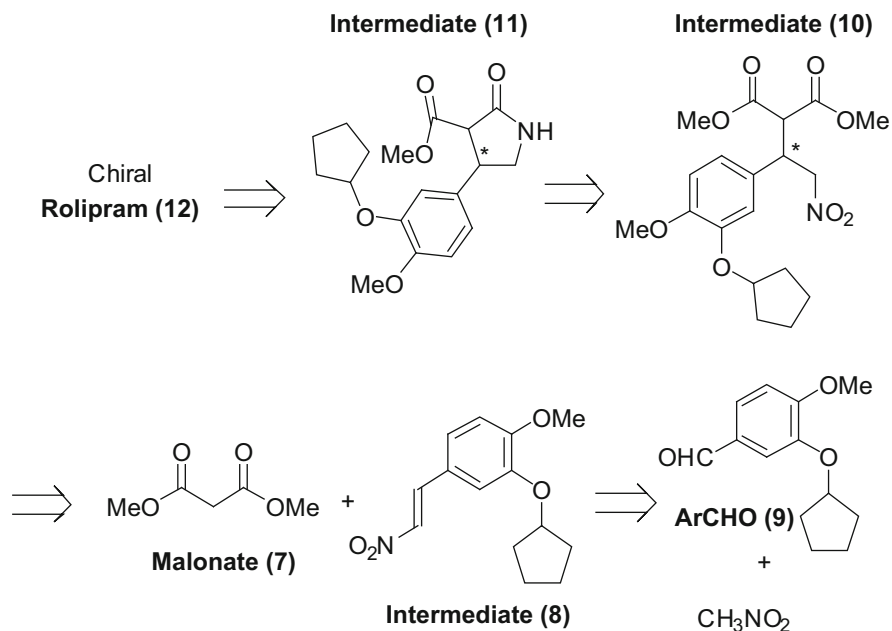
In addition, the same group developed other poly(dimethyl)silane-supported palladium hybrid catalysts [Pd/(DMPSi-bone charcoal-Celite) and Pd/(DMPSi-SiO₂)] that were successfully used for hydrogenation of nitro compounds [14, 15] and nitriles [16], respectively, under continuous-flow conditions.

In 2015, Kobayashi and co-workers achieved the synthesis of (*S*)-Rolipram (**12**) using a multistep continuous-flow system including an eight-step sequence of chemical transformations (Scheme 10) [17]. Commercially available starting materials were successively passed through the columns containing achiral and chiral catalysts to produce the drug directly with high enantioselectivity. All four columns packed with heterogeneous catalysts were type IV flow systems (Fig. 13). The flow synthesis of intermediate **8** from **9** and nitromethane was conducted with a SUS column I (10 mm i.d., 300 mm length) packed with a silica-supported amine (Chromatorex DM1020; Fuji Silysia; 4.5 g, 0.73 mmol/g) and finely crushed anhydrous calcium chloride (13.5 g). A toluene solution of **9** and nitromethane was introduced from the bottom of the column, and the desired product **8** was obtained in >90% yield over at least 1 week. The next flow synthesis of intermediate **10** was

Table 1 Substrate scope of continuous-flow hydrogenation

Entry	Substrate	Substrate flow [$\mu\text{L min}^{-1}$]	H_2 [equiv.]	T [$^{\circ}\text{C}$]	Product	Yield ^d [%]	TON/TOF [h^{-1}]
1		300	1.5	30		91.8 ^b	16,475/3,295
2		300	1.5	30		86.5 ^b	16,839/3,368
3		100	1.5	30		26.5 ^b	6,016/1,203
4		50	2.0	70		12.7 ^b	2,516/498
5 ^c		40	15.0	120		6.5 ^b	304/101
6		100	3.0	30		23.2 ^b	3,951/790

^aYield of isolated product^bQuant^cReaction time: 3 h



Scheme 10 Retrosynthetic scheme to access chiral Rolipram

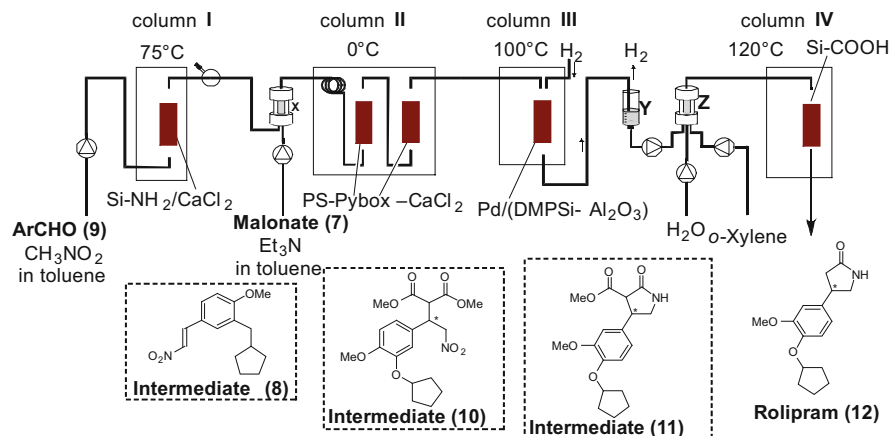


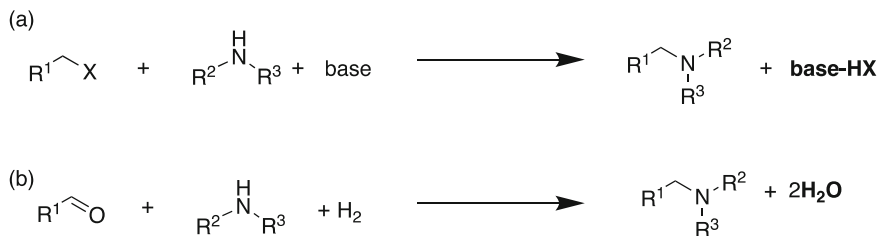
Fig. 13 Sequential continuous-flow synthesis of chiral Rolipram

conducted with a sequence of three columns; column X was filled with MS4A, and columns II-1 and II-2 were filled with polymer-supported chiral calcium catalyst (PS-(*S*)-pybox-calcium chloride, where pybox is pyridinebisoxazoline). The reaction was conducted at 0°C, introducing a solution of nitroalkene **8** synthesized in

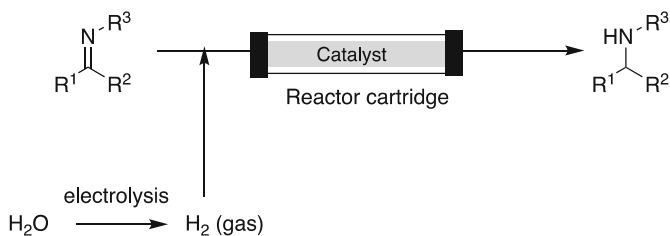
column I, a toluene solution of malonate **7**, and triethylamine into a sequence of column X and column II. The desired γ -nitro ester **10** was obtained in 84% yield with 94% enantiomeric excess at this step after workup. The crude solution of **10** eluted from column II and atmospheric pressure H₂ was passed through column III, which was packed with poly(dimethyl)silane-supported palladium/carbon, to afford γ -lactam **11** in 74% yield with 94% enantiomeric excess. The final stage in the synthesis of Rolipram involved the hydrolysis and decarboxylation of the ester part of **11**. This flow synthesis was conducted with column IV, which was packed with silica-supported carboxylic acid (Chromatorex ACD, Fuji Silysia), passing through the mixture of crude solution of **11** after separation of H₂ gas, water, and *o*-xylene, from the top down at 120°C. Finally, (*S*)-Rolipram (**12**) was obtained in 50% yield from **9** (997.8 mg/h, 96% enantiomeric excess). In this sequential continuous-flow system, the hydrogenation step using a palladium nanoparticle catalyst was placed at a later stage of the sequential transformation. This means that the crude mixture that was introduced to the heterogeneous catalyst was potentially a mixture of various compounds including remaining starting materials and small amounts of side-products. Therefore, robust catalysts that were not poisoned by other compounds were required for this purpose. During the screening of the hydrogenation catalyst, neither several commercially available Ni and Pd catalysts nor poly(methylphenylsilane)-supported palladium/alumina catalyst worked at all.

3.3 *Reductive Amination Through Hydrogenation Using Metal Nanoparticle Catalysts Under Continuous-Flow Conditions*

C–N bond-formation reactions are among the most important transformations for the synthesis of APIs and other biologically important compounds. Substitution reactions with alkyl halides are a common approach for this purpose; however, in addition to overreaction issues, this reaction is not suitable from a green organic synthesis point of view because of the massive amount of inorganic salts that are generated as waste (Scheme 11a). On the other hand, reductive amination of carbonyl compounds using H₂ is a promising approach because only water is generated (Scheme 11b). This approach is not only recommended from a green organic synthesis point of view but also offers the potential of application to sequential continuous-flow systems because water is readily removed by phase separation during flow. However, problems often arise due to reversibility, compound/functional group incompatibility, and overreduction. In particular, the reduction of aryl imines often gives secondary amines that are contaminated with the corresponding primary amine, derived from overreduction and debenzylation of the desired product. In 2005, Ley and co-workers realized continuous-flow hydrogenation of imines to the corresponding amines using a commercially available H-Cube[®] flow hydrogenator (Scheme 12) [18]. H-Cube[®] mixes hydrogen gas with a flowing



Scheme 11 Two synthetic schemes to access tertiary amine



Scheme 12 Continuous-flow reductive amination

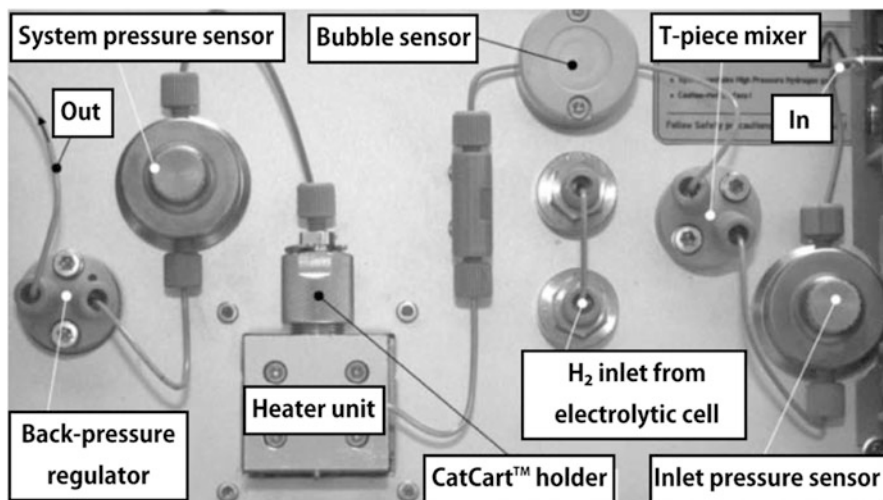
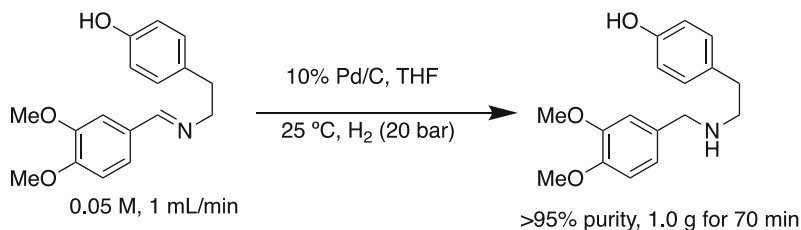


Fig. 14 Photographic image of H-Cube[®]

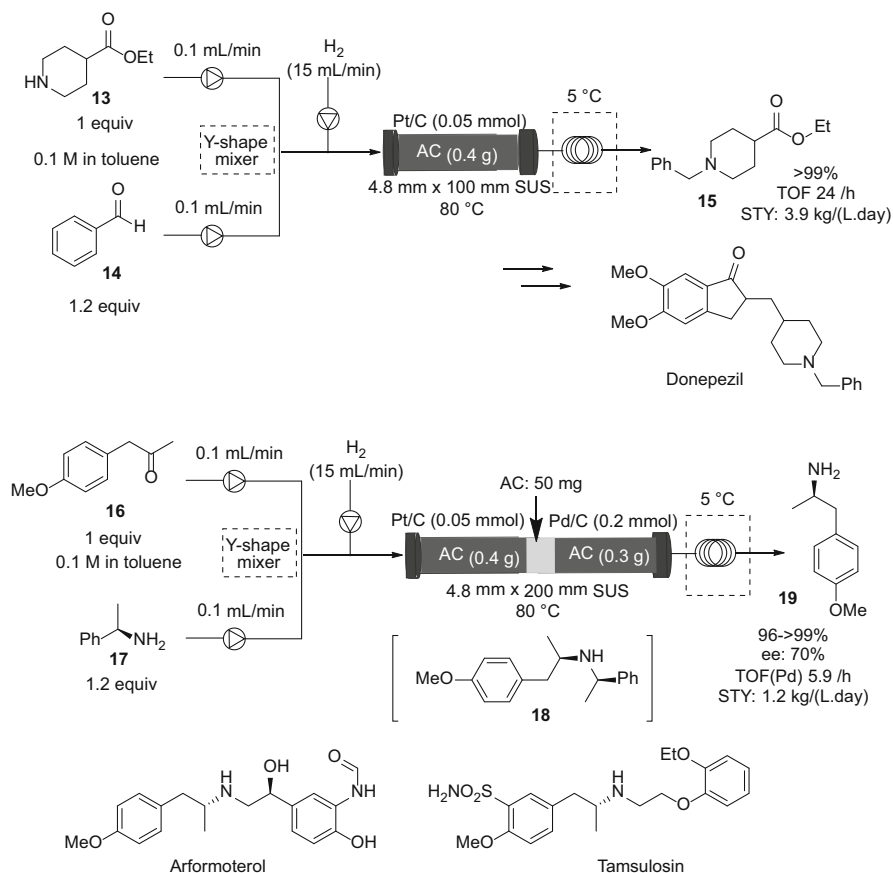
substrate stream in a T-piece mixer that contains a titanium frit to ensure efficient gas dispersion (Fig. 14). The hydrogen is generated internally on demand by the electrolysis of water and the gas–liquid mixture is pumped through a suitable catalyst contained in an interchangeable metal cartridge. An integral Peltier heater



Scheme 13 Continuous-flow reductive amination using H-Cube[®]

enables the cartridge to be heated to 100°C, and a responsive back-pressure regulator allows flow hydrogenation to be performed up to 100 bar. Reductive amination reaction was systematically optimized using varying solvents, concentration, flow rate, pressure, and temperature. As a result of optimization, the authors found that 1.0 g of analytically pure secondary amine could be obtained under the conditions 10% Pd/C packed in 30 mm × 4 mm cartridge, 0.05 M THF solution, 25°C, 20 bar H₂, and 10 mL/min flow rate for 70 min (Scheme 13).

For the synthesis of secondary amines through reductive amination, isolated imines can be available. However, isolation of some aliphatic imines and iminium intermediates for the preparation of tertiary amines is sometimes difficult. Direct reductive amination, in which imine or iminium intermediates generated in situ from carbonyl compounds and amines, is more efficient and ideal, although problems of side-reactions, such as reduction of carbonyl compounds, are expected. In 2018, Kobayashi and co-workers found that platinum nanoparticles on carbon (Pt/C) had high activity, selectivity, and durability for direct reductive amination under continuous-flow conditions [19]. Secondary amine **13** and benzaldehyde **14** in toluene solution (0.1 M) were pumped at the same flow rate and mixed using a Y-shaped mixer. A stream of 15 mL/min of hydrogen regulated by a mass-flow controller was connected to the system through a T-shaped mixer fixed at an inlet of a flow reactor (SUS column, 4.8 mm diameter × 100 mm length) (Scheme 14). The bed reactor was packed with 0.05 mmol of a catalyst premixed with 0.4 g of activated carbon as a diluting agent and heated at 80°C with an aluminum heating block. Benzylated amine **15**, which is an intermediate of donepezil, could be synthesized continuously in quantitative yield over 20 h, and the Pt/C catalyst exhibited a TOF of 24 h⁻¹, and the system had a high space-time yield of 3.9 kg/L/day. In addition, the stereoselective direct reductive amination of a carbonyl compound with hydrogen gas, which had been reported only in a batch method, was achieved under continuous-flow conditions. Flowing the chiral amine **17** with a ketone **16** at 60°C promoted a quantitative yield of the corresponding chiral amine **18** in an 85% diastereomeric ratio in favor of the anti-conformation. Telescoping this transformation with a stereoretentive chiral auxiliary removal catalyzed by Pd/C in the same column reactor afforded chiral amine **19**, which is the direct precursor of two commercialized drugs: arformoterol and tamsulosin (Scheme 14).

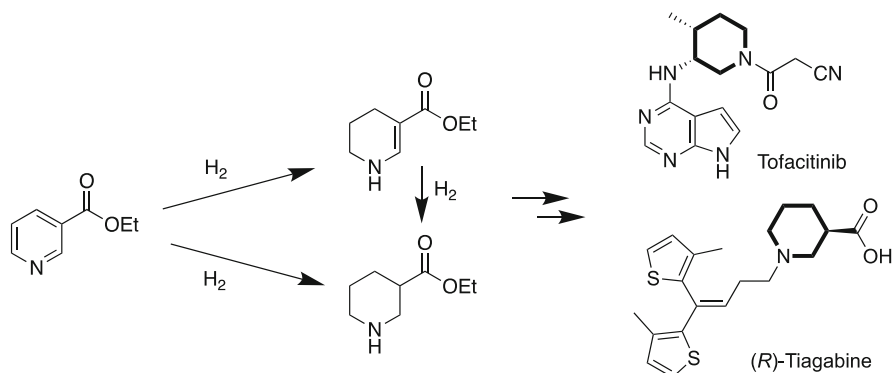


Scheme 14 Continuous-flow reductive amination for the synthesis of APIs

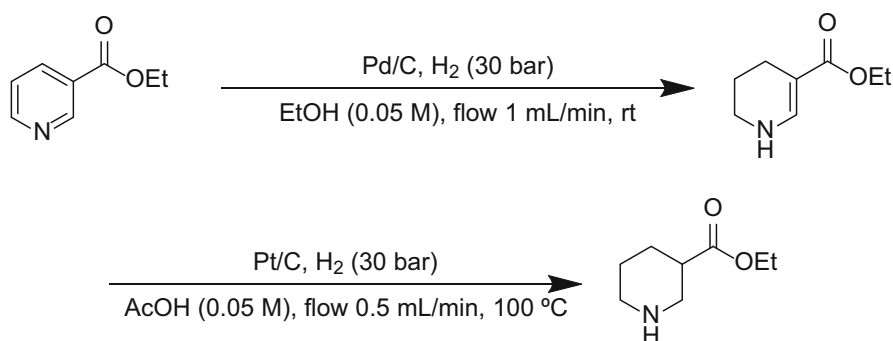
3.4 Hydrogenation of Arenes and Heteroarenes Using Metal Nanoparticle Catalysts Under Continuous-Flow Conditions

Hydrogenation of arenes and heteroarenes is an important reaction in a variety of fields of organic synthesis, including drug and natural product synthesis, and petroleum chemistry, as well as for the transition to a hydrogen-based society. In addition, selective hydrogenation of arene and heteroarene moieties in more complex compounds bearing various functionalities is a challenge that must be overcome for the synthesis of biologically active compounds such as APIs.

The selective and efficient partial and full hydrogenation of pyridine derivatives to provide valuable intermediates of APIs is particularly interesting (Scheme 15). Hydrogenation of 3-nicotinate is one of the most challenging tasks. The partial



Scheme 15 Hydrogenation of 3-nicotinate for API synthesis



Scheme 16 Continuous-flow hydrogenation of 3-nicotinate

hydrogenation product of 3-nicotinate is the vinylogous carbamate, which is stabilized by conjugation of the lone pair of electrons on the nitrogen atom with the C=C bond and carbonyl group. This conjugation allows the hydrogenation to be stopped at this stage. In 2009, Kappe and co-workers developed continuous-flow hydrogenation of 3-nicotinate using the commercially available H-Cube[®] Flow Hydrogenator [20]. Using ethanol as the solvent and a Pd/C catalyst, the partially hydrogenated product was selectively formed at room temperature with 30 bar of H₂ (Scheme 16). To achieve full hydrogenation of partially hydrogenated vinylogous carbamate, harsh conditions using Pt/C instead of Pd/C were required: acetic acid as solvent, 100 bar of H₂, 100 °C (Scheme 16).

In 2014, Ley and co-workers improved the productivity of this process using the commercially available HEL FlowCAT reactor [21]. This reactor is a compact, benchtop unit that is run under fixed-bed, trickle-flow conditions. This reactor is more suitable for scale-up and process intensification studies than the H-Cube reactor because the capacity of the trickle bed reactor is larger: reactor column

1 (RC1), 6 mm i.d., 3 mL internal volume, charge of 4 g of catalyst; reactor column 2 (RC2), 12 mL internal volume, charge of 13 g of catalyst (Fig. 15). The hydrogenation of 3-ethylnicotinate was conducted using a HEL FlowCAT reactor with 13 g of Pd/Al₂O₃ packed in RC2 under the reaction conditions: 1.0 M EtOAc, 7 mL/min flow rate of substrate solution at 160°C, 0.6 L/min of 100 bar H₂. Analytically pure fully hydrogenated product was obtained with a throughput of 1,524 g/day for 3.75 h (Scheme 17). When Rh/Al₂O₃ was used instead of Pd/Al₂O₃, a throughput of 1959 g/day was realized with less catalyst; 4 g of Rh/Al₂O₃ in RC1 (Scheme 18).

In 2018, Kobayashi and co-workers developed a poly(dimethyl)silane-supported Rh–Pt/alumina bimetallic nanoparticle catalyst [Rh–Pt/(DMPSi–Al₂O₃)] for arene hydrogenation reaction [22]. The catalyst could be used in both batch and continuous-flow systems with high performance under mild conditions, 50–70°C, neat, and atmospheric (1 atm) H₂, and showed wide substrate generality to demonstrate its high tolerance for various functionalities. In addition, the high durability of

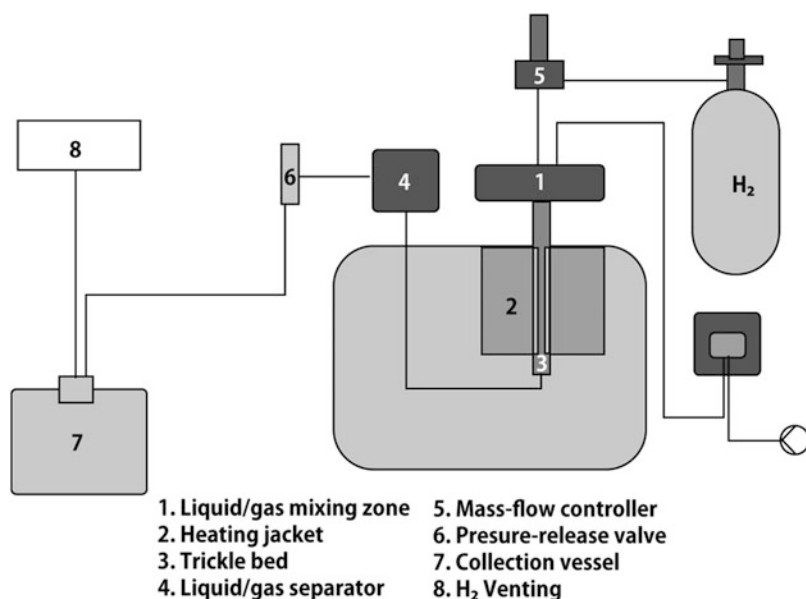
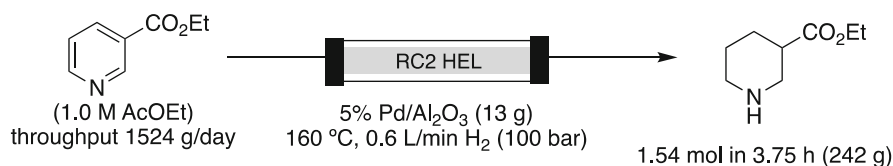
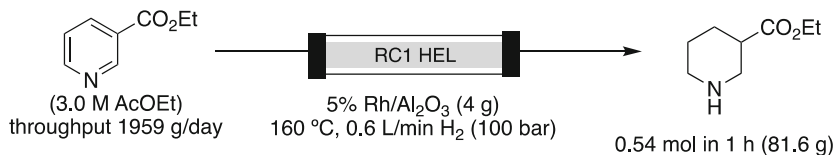


Fig. 15 HEL FlowCAT reactor



Scheme 17 Continuous-flow hydrogenation of 3-nicotinate using the RC2 column



Scheme 18 Continuous-flow hydrogenation of 3-nicotinate using the RC1 column

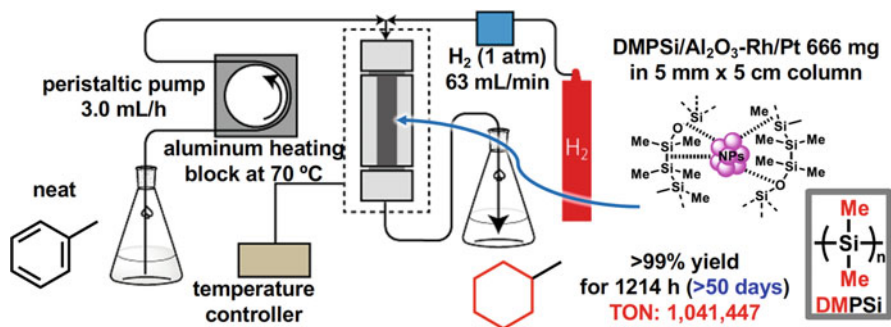
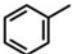

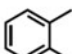



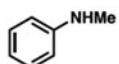
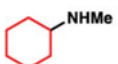


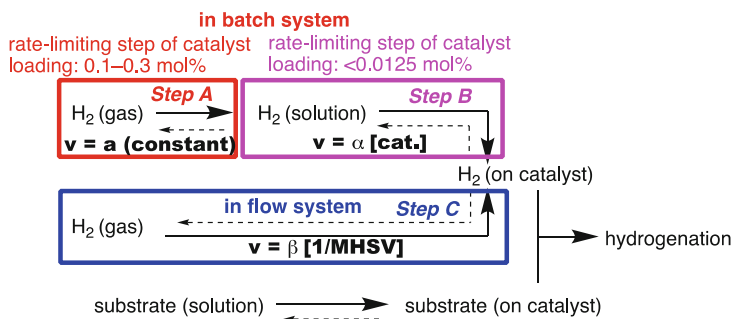
Fig. 16 Continuous-flow hydrogenation of arene using Rh–Pt bimetallic nanoparticle immobilized on a composite support of poly(dimethyl)silane and alumina

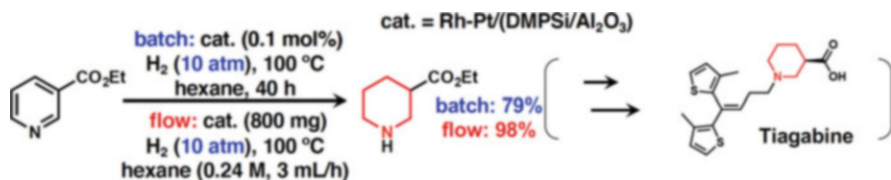
the catalyst under continuous-flow conditions over 50 days was demonstrated (Fig. 16). Substrate and hydrogen, as liquid and gas substrates, respectively, were simultaneously passed through a column containing Rh–Pt/(DMPSi–Al₂O₃) without a back-pressure controller at the outlet. The inlet of the column was constructed as a double-layered structure with a metallic mesh through which both the liquid and gas components pass and intermix well before entering the catalyst-packed region. When the liquid substrate was delivered with a flow rate of 0.05 mL/min together with 63 mL/min hydrogen (corresponding to 1.86 equiv. of the amount theoretically required for quantitative conversion) through Rh–Pt/(DMPSi–Al₂O₃) (666 mg), packed in a stainless steel column maintained at 70 °C, using an aluminum heating block, the substrate, toluene, was fully converted, and analytically pure methylcyclohexane was obtained quantitatively. The conversion ratio of the flow reaction, which was analyzed at regular intervals, was maintained quantitatively throughout a run of >50 days; a total TON of 347,149 (9,981,553 reacted H₂/active site) was achieved (Fig. 16). Kinetic studies both in batch and flow systems revealed that the reaction followed zero-order kinetics with respect to the substrate. Catalytic TOFs for four types of substrates were compared in batch systems and continuous-flow systems (Table 2). TOFs of flow systems were much greater than those of batch systems for all substrates, and a limited amount of hydrogen was used in the flow system. For *N*-methylaniline and pyrrole, TOFs were 27 times greater in flow than in batch systems. Enhanced catalytic activity in flow systems can be explained by the difference in the pathway of hydrogen access to the surface of the nanoparticles from

Table 2 Rate acceleration of arene hydrogenation under continuous-flow conditions compared with a batch system

Conditions (for both batch and flow): 50 °C, neat, H ₂ (1 atm)				
Substrate	Product	TOF (Batch)	TOF (Flow)	TOF (Flow)/TOF (Batch)
		604 h ⁻¹	3390 h ⁻¹	5.6
		90 h ⁻¹	681 h ⁻¹	7.6
		41 h ⁻¹	1118 h ⁻¹	27
		43 h ⁻¹	1507 h ⁻¹	25

the gas phase (steps A and B vs C in Fig. 17). In the batch system, a catalyst exists with a liquid substrate, and only dissolved hydrogen in the solution has access to the surface of the nanoparticles (steps A and B). On the other hand, in the flow system, hydrogen gas and liquid substrate are directly introduced to the column packed with solid catalyst, and hydrogen can access the surface of the nanoparticles from the gas-phase hydrogen directly (step C). In the cases of *N*-methylaniline and pyrrole, stronger adsorption of substrates and products to the surface of the catalyst is expected than with the case of toluene because of the influence of the heteroatom. The efficiency of hydrogen adsorption that is competing with substrate/product adsorption has a greater impact on the reaction rate, and a much higher catalytic enhancement in the flow system is observed. The catalyst worked for the full

**Fig. 17** Mechanism of reaction acceleration under continuous-flow conditions



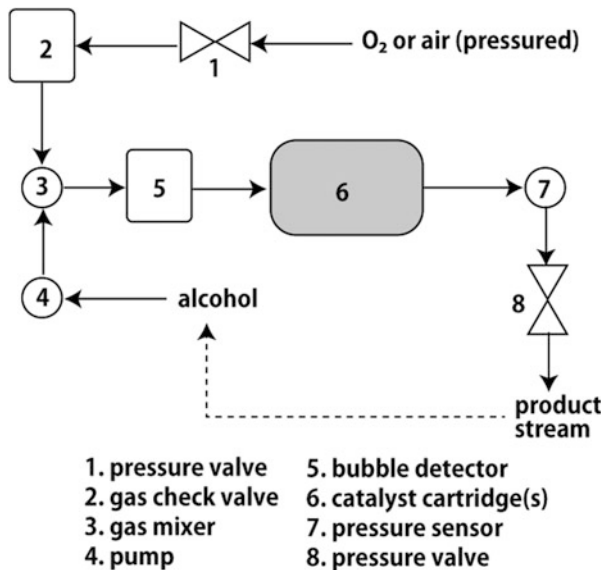
Scheme 19 Hydrogenation of 3-nicotinate using Rh–Pt bimetallic nanoparticle immobilized on a composite support of poly(dimethyl)silane and alumina

hydrogenation of 3-ethyl nicotinate at 100 °C with 10 atm H_2 under both batch systems and flow systems. In this case, continuous-flow conditions showed superior performance (almost quantitative conversion) to the batch system (79% conversion) (Scheme 19).

3.5 Aerobic Oxidation of Alcohols Under Continuous-Flow Conditions Using Metal Nanoparticle Catalysts

Selective oxidation of alcohols is one of the most important transformations in organic synthesis. This is because the resulting carbonyl compounds possess higher energy and reactivity, allowing many types of carbon–carbon and other bond-forming reactions. Aerobic oxidation of alcohol using heterogeneous catalysts is one of the most ideal processes. However, because aerobic oxidation of alcohols catalyzed by metal nanoparticle catalysts under mild conditions is a slower process than hydrogenation reactions, it is challenging to complete oxidation reactions within the limited space of a column packed with the catalyst under continuous-flow conditions. In 2010, Hii and co-workers developed aerobic oxidation of alcohols to aldehydes or ketones using a commercially available X-Cube flow reactor with a catalyst cartridge packed with Ru/Al₂O₃ catalyst [23]. Reactions were conducted in continuous recirculating mode rather than continuous-flow conditions because the single-pass reactions are not enough to complete the oxidation in most cases (Fig. 18). In 2010, Kobayashi and co-workers developed Au–Pt and Au–Pd bimetallic nanoparticle catalysts stabilized by the composite support of cross-linking polymer and spherical carbon black (PI-CB/Au–Pt and PI-CB/Au–Pd) for aerobic oxidation of alcohols to aldehydes/ketones and methyl esters, respectively, based on the polymer incarceration technique [24]. In 2012, the same group applied these catalysts to continuous-flow systems [25]. In these reactions, both organic phase (substrate in organic solvents) and aqueous phase (water or aqueous base solution) are used for high catalytic turnover, and gas–liquid–solid multiphase reaction conditions are required for the continuous-flow reactors. The catalysts were packed with a certain amount of Celite in the glass column to prevent obstruction of the column by swelling of the catalysts (Fig. 19). The reaction temperature was controlled with an aluminum heating block, molecular oxygen

Fig. 18 Continuous-flow aerobic oxidation system



(1 atm) was regulated with a mass-flow controller, and the organic and aqueous phases were regulated using conventional HPLC pumps and introduced simultaneously. The column had a head with three inlets. All the components were passed through the downflow column only once. Under trifluorotoluene/water biphasic conditions using PI-CB/Au-Pt as catalyst, 3-phenyl-1-propanol was selectively oxidized to the corresponding aldehyde constantly over a long period (81% yield for 4 days) (Fig. 19). On the other hand, under methanol/aqueous potassium carbonate solvent conditions, direct methyl ester formation proceeded using

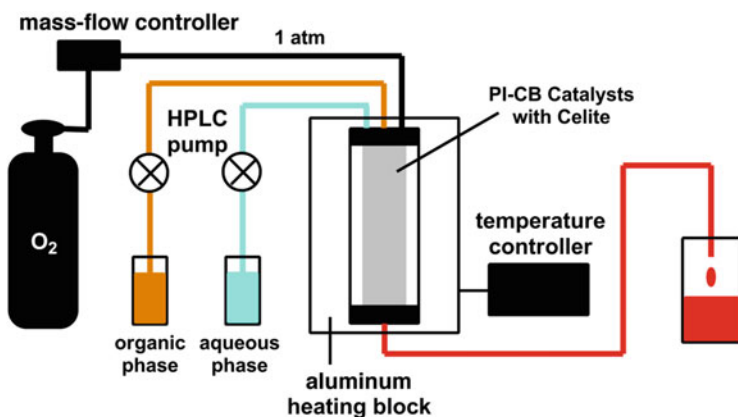
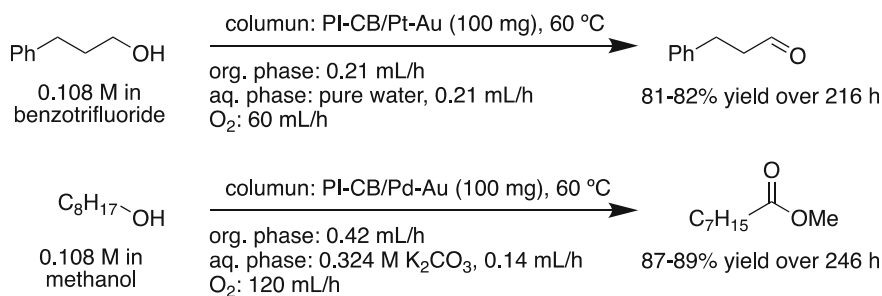


Fig. 19 Continuous-flow aerobic oxidation system using polymer-incarcerated metal nanoparticle catalysts

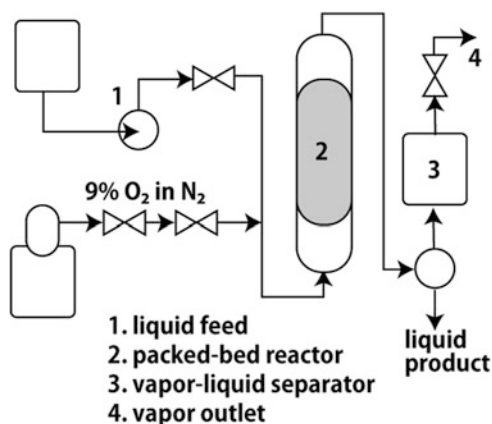


Scheme 20 Aerobic oxidation of alcohols under continuous-flow conditions

1-octanol as the substrate to afford the corresponding ester constantly for a long period (89% for 11 days) (Scheme 20).

In 2017, Root, Stahl, and co-workers found that $\text{PdBi}_x\text{Te}_y/\text{C}$ multicomponent heterogeneous catalysts showed high activity and selectivity for direct aerobic oxidative methyl esterification with alcohols [26]. The identification of possible catalysts for oxidative methyl ester formation from alcohols was initiated by the screening of simple binary and ternary admixtures of Pd/C in combination with one or two metal and/or metalloid components as catalysts. The authors established the optimized catalyst components by examining over 400 admixture combinations rapidly using this method. Two very effective catalysts, $\text{PdBi}_{0.47}\text{Te}_{0.09}/\text{C}$ (PBT-1) and $\text{PdBi}_{0.35}\text{Te}_{0.23}/\text{C}$ (PBT-2), were found, and they were applied to the continuous-flow process by incorporating the catalyst into a packed-bed reactor (Fig. 20). A solution of the primary alcohol was mixed with a diluted O_2/N_2 gas stream at a T-junction, and the gas-liquid mixture was fed into a packed-bed reactor. The catalytic activities were evaluated by weight hourly space velocity (WHSV) for the long-term assessment of oxidation of benzyl alcohol to the corresponding methyl ester (Fig. 21). The activity of PBT-1 steadily decreased over 33 h under continuous-

Fig. 20 Reactor for continuous-flow aerobic oxidation



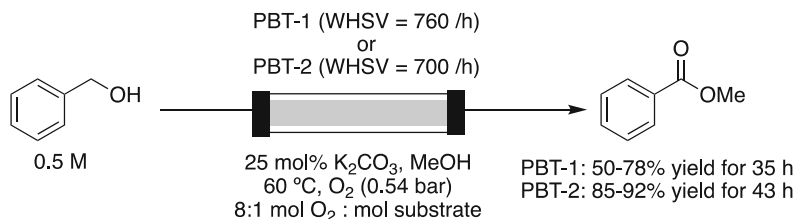


Fig. 21 Comparison of PBT-1 and PBT-2 under continuous-flow aerobic oxidation system

flow conditions. In contrast, the PBT-2 catalyst showed excellent long-term stability over 43 h at a WHSV of 700 h^{-1} . Analysis of the reaction rate at different temperatures ($50\text{--}80^\circ\text{C}$) under continuous-flow conditions provided the basis for Arrhenius analysis of PBT-2-catalyzed oxidation of benzyl alcohol, which revealed that the reaction exhibits an activation energy of 79 kJ/mol and pre-exponential factor of $1.1 \times 10^{12} \text{ s}^{-1}$ (Fig. 22). These values correspond to a TOF of $1,600 \text{ h}^{-1}$ at a reaction temperature of 60°C .

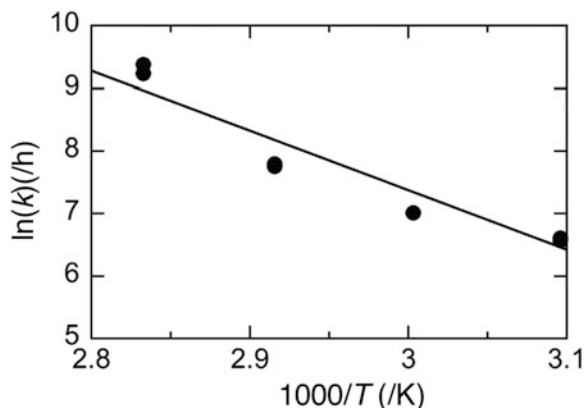
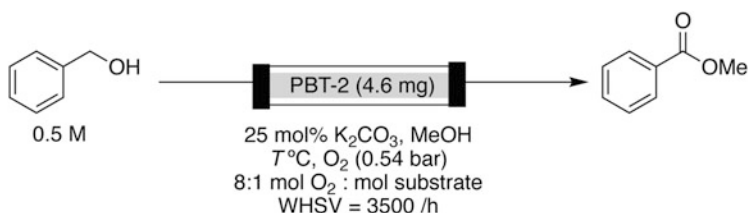


Fig. 22 Arrhenius analysis of continuous-flow aerobic oxidation

3.6 Control of Selectivity in Heterogeneous Gold Catalysis Under Flow Conditions

In 2012, Toste, Somorjai, and co-workers developed heterogeneous Au nanoparticle catalysts in which highly active species were generated by the reversible oxidation of metal nanoparticles to ions, which were stabilized by both the encapsulating dendrimer and the mesoporous silica support [27]. Au nanoparticles (2.0 ± 0.3 nm) were encapsulated in a fourth-generation (G4) polyamidoamine (PAMAM) dendrimer and loaded on SBA-15 (Au-G4OH/SBA-15), a mesoporous SiO_2 support with a surface area of $790 \text{ m}^2/\text{g}$ (Fig. 23). The catalytic activity of Au-G4OH/SBA-15 was tested for cyclopropanation reactions using propargyl pivalate **20** and styrene as reactants for the formation of *cis*- and *trans*-diastereomers of cyclopropane **21**. After the addition of PhICl_2 to the reaction mixture, which generates catalytically active species via oxidation, high catalytic reactivity of the catalyst was achieved with more than 99% conversion in toluene within 12 h at room temperature. The formation of undesired 3-methyl-2-butenal was minimized, and

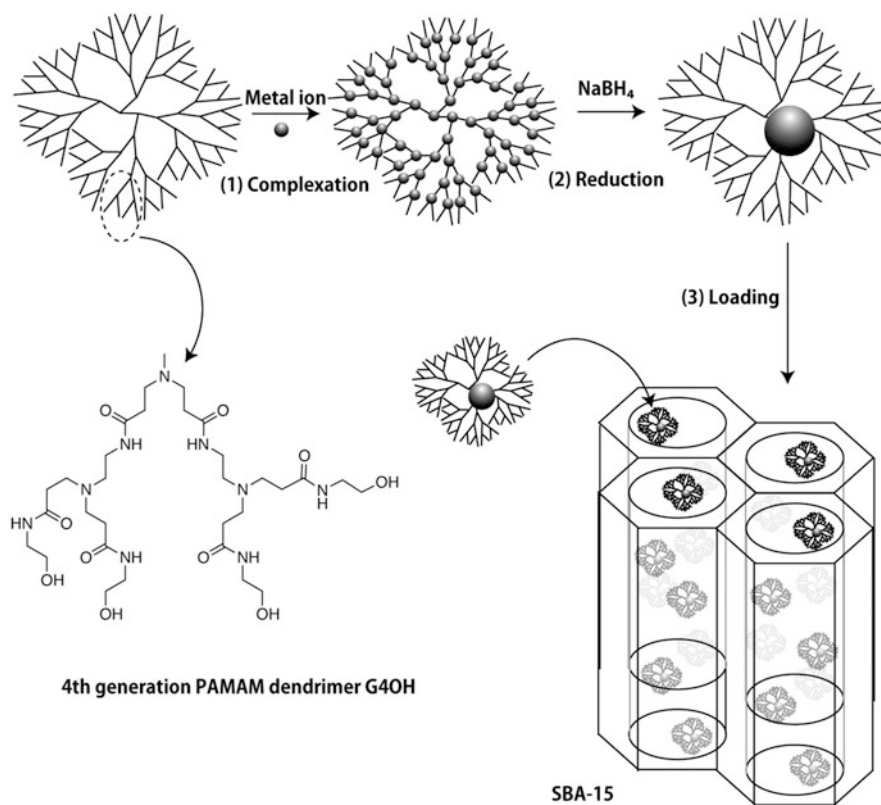
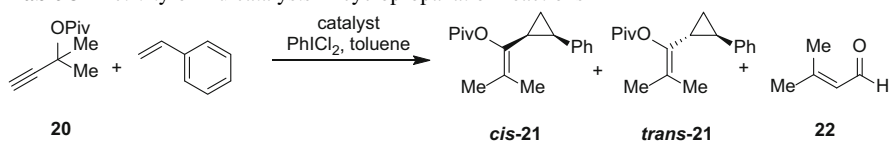


Fig. 23 Au nanoparticles immobilized on SBA-15 with dendrimer as a stabilizer

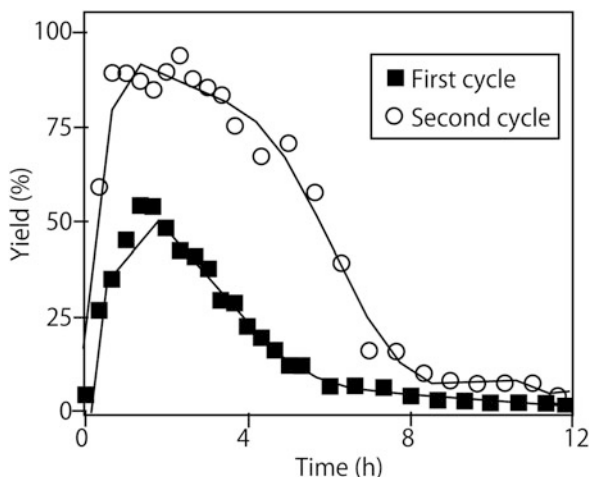
Table 3 Activity of Au catalysts in cyclopropanation reactions

Entry	Catalyst	Conversion (%)	Selectivity (<i>cis/trans</i> - 21 :aldehyde (22)) (%/%)	Diastereoselectivity (<i>cis</i> - 21 : <i>trans</i> - 21)	Au in solution (ppm)
1	2.0 ± 0.3 nm Au-G4OH/SBA-15	>99	95:5	17:1	0.1
2	AuCl ₃	>99	95:5	3.5:1	80
3	2.2 ± 0.4 nm Au-PAG4/SBA-15	>99	93:7	6:1	0.1
4	2.1 ± 0.3 nm Au@OA/SBA-15	>99	80:20	4:1	15
5	AuCl ₃ @G4/SBA-15	5	93:7	17:1	0.8
6	2.0 ± 0.3 nm Au-G4OH/SBA-15 (flow)	58	100:0	18:1	NA
7	2.1 ± 0.3 nm Au@OA/SBA-15 (flow)	>99	87:13	3.5:1	NA

high *cis*-diastereoselectivity was observed under the conditions (Table 3, entry 1). XPS measurements indicated that, with the addition of PhICl₂, Au nanoparticles were oxidized to Au(III) species that interacted with chloride ions. No leaching of Au ions to the solution phase was detected by inductively coupled plasma-mass spectrometry measurements (<0.1 ppm). In a comparison between homogeneous and heterogeneous systems, the diastereomeric *cis/trans* ratio of the heterogeneous system (Au-G4OH/SBA-15) was increased by fivefold from that of the homogeneous system (AuCl₃) (entries 1 vs 3). In the heterogeneous system, the support would produce enhanced steric effects around the Au centers, which results in the observed improvement in diastereoselectivity.

To take full advantage of the heterogeneous nature and high catalytic activity and selectivity of the dendrimer-encapsulated Au nanoparticles, the catalyst was tested in a flow reactor. The high yield and diastereoselectivity of the Au-G4OH/SBA-15 catalyst were maintained when the catalytic reaction was transferred from the batch to the flow mode. Using Au-G4OH/SBA-15 as the catalyst in a fixed-bed plug-flow reactor, in a given injection the maximum yield of cyclopropane **21** was 58% with a *cis/trans* ratio of 18:1 (entry 6). The catalyst was deactivated after 6 h through the reduction of the oxidized Au nanoparticles back to their metallic state; however, the active catalyst could be regenerated by a flow of PhICl₂ (Fig. 24). Using the regenerated catalyst, the conversion was increased to 90%, and the catalyst stayed active for 9 h. The percentage of highly oxidized metal ions increased considerably with reoxidation of the dendrimer-encapsulated metal nanoparticles, which

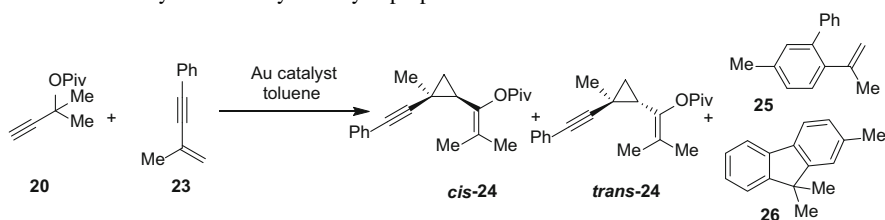
Fig. 24 Catalytic activity of Au-G4OH/SBA-15 during recovery and reuse



produced the observed increase in reactivity. The enhancement in the catalytic yield and activity after reoxidation of the catalyst proves the reversibility of the active oxidation state of the metal without any leaching of Au ions to the solution phase. In addition, the high diastereoselectivity in the batch mode can be maintained in the flow system, which further highlights the truly heterogeneous nature of the dendrimer-encapsulated Au nanoparticles.

The highly stereoselective Au-G4OH/SBA-15 catalyst was employed for the sequential cyclopropanation rearrangement of propargyl pivalate **21** and enyne **23** (Table 4). In this reaction, the primary product, *cis*-cyclopropane **24**, is reported

Table 4 Activity of Au catalysts in cyclopropanation reactions under continuous-flow conditions



Entry	Catalyst	Total conversion (%)	Cyclopropane 24 (%) (<i>cis</i> - 24 : <i>trans</i> - 24)	Secondary products (%) (25 : 26)
1	AuCl ₃	50	40 (3:1)	10 (3:2)
2	2.0 ± 0.3 nm Au-G4OH (batch)	40	38 (12:1)	2 (1:1)
3	2.0 ± 0.3 nm Au-G4OH (flow) (5 mL/h)	20	18 (100:0)	2 (100:0)
4	2.0 ± 0.3 nm Au-G4OH (flow) (0.1 mL/h)	72	0	72 (100:0)

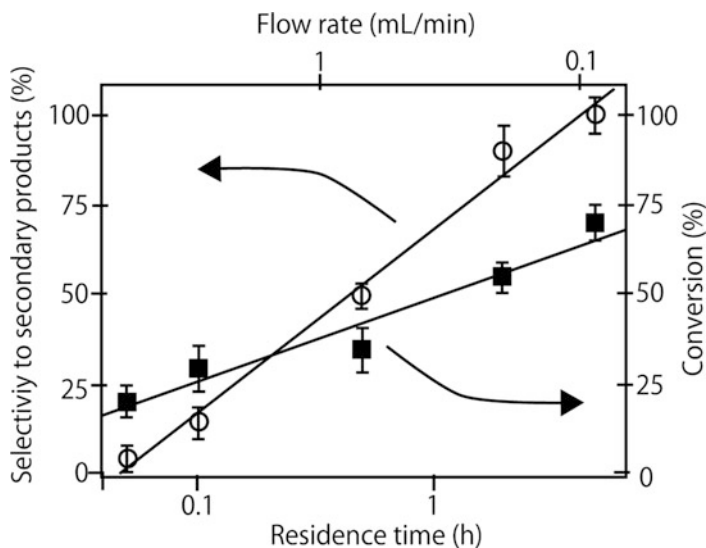


Fig. 25 Effect of residence time on selectivity and conversion

to rearrange catalytically into two secondary products, styrene **25** and fluorene **26**. When using a homogeneous AuCl_3 catalyst at room temperature, a 40% yield of cyclopropane **24** was obtained, with a *cis/trans* ratio of 3:1, accompanied by a 10% yield of products **25** and **26** (in a 3:2 ratio) formed by the rearrangement of the product *cis*-**24**. Switching to the heterogeneous Au-G4OH/SBA-15 catalyst in the batch mode led to a better selectivity, with a *cis/trans* ratio of 12:1 for **24** and only a small amount of the rearrangement products **25** and **26** (1% each). The same catalyst was employed in the flow system. An interesting correlation of product distribution with the reactant's residence time was observed. With a flow rate of 5 mL/h, 18% yield of *cis*-cyclopropane **24** was measured (*cis/trans* ratio of 100:0), along with 2% of secondary products. By reducing the flow rate to 0.1 mL/h and thereby increasing the residence time, the conversion was increased by more than threefold to 72%, and an exclusive selectivity for the rearrangement product **25** was obtained. By systematically changing the residence time of the reactants, a linear increase in the reactivity coupled with a linear enhancement in the selectivity toward the rearrangement product **25** was observed (Fig. 25). In this reaction, the reaction residence time thus played an important role in achieving better selectivity and reactivity with the heterogeneous catalyst.

4 Summary

By taking advantage of the high catalytic activity and high TOF of heterogeneous metal nanoparticle catalysts, continuous-flow systems, in which the introduced reactants are converted into the desired product in high yield, can be realized. For

example, in gas–liquid–solid multiphase reactions, continuous-flow systems employing microchannel and fixed-bed reactors provide high specific interfacial surface area to afford efficient reaction environments. These continuous-flow reactors possess high compatibility with sequential continuous-flow systems, which enables multistep flow synthesis of biologically active compounds such as APIs and natural products. In addition, these continuous-flow systems are easily scaled up by increasing either the size of the column or the number of reactors. Moreover, continuous-flow systems can be used to realize unique chemoselectivities that cannot be achieved in batch reactors, by controlling the residence time of reactants in the catalyst column.

References

1. Kobayashi S (2016) *Chem Asian J* 11:425–436
2. Kobayashi S, Miyamura H (2013) *Aldrichimica Acta* 46:3–19
3. Kobayashi J, Mori Y, Okamoto K, Akiyama R, Ueno M, Kitamori T, Kobayashi S (2004) *Science* 304:1305–1308
4. Oyamada H, Akiyama R, Hagio H, Naito T, Kobayashi S (2006) *Chem Commun*:4297–4299
5. Ueno M, Suzuki T, Naito T, Oyamada H, Kobayashi S (2008) *Chem Commun*:1647–1649
6. Miyamura H, Matsubara R, Miyazaki Y, Kobayashi S (2007) *Angew Chem Int Ed* 46:4151–4154
7. Wang N, Matsumoto T, Ueno M, Miyamura H, Kobayashi S (2009) *Angew Chem Int Ed* 48:4744–4746
8. Kenis PJA, Ismagilov RF, Whitesides GM (1999) *Science* 285:83
9. Uozumi Y, Yamada YMA, Beppu T, Fukuyama N, Ueno M, Kitamori T (2006) *J Am Chem Soc* 128:15994–15995
10. Yamada YM, Watanabe T, Ohno A, Uozumi Y (2012) *ChemSusChem* 5:293–299
11. Oyamada H, Naito T, Miyamoto S, Akiyama R, Hagio H, Kobayashi S (2008) *Org Biomol Chem* 6:61–65
12. Oyamada H, Naito T, Kobayashi S (2011) *Beilstein J Org Chem* 7:735–739
13. Kobayashi S, Okumura M, Akatsuka Y, Miyamura H, Ueno M, Oyamada H (2015) *ChemCatChem* 7:4025–4029
14. Saito Y, Ishitani H, Kobayashi S (2016) *Asian J Org Chem* 5:1124–1127
15. Ishitani H, Saito Y, Tsubogo T, Kobayashi S (2016) *Org Lett* 18:1346–1349
16. Saito Y, Ishitani H, Ueno M, Kobayashi S (2017) *ChemistryOpen* 6:211–215
17. Tsubogo T, Oyamada H, Kobayashi S (2015) *Nature* 520:329–332
18. Saaby S, Knudsen KR, Ladlow M, Ley SV (2005) *Chem Commun*:2909–2911
19. Laroche B, Ishitani H, Kobayashi S (2018) *Adv Synth Catal* 360:4699–4704
20. Irfan M, Petricci E, Glasnov TN, Taddei M, Kappe CO (2009) *Eur J Org Chem* 2009:1327–1334
21. Ouchi T, Battilocchio C, Hawkins JM, Ley SV (2014) *Org Process Res Dev* 18:1560–1566
22. Miyamura H, Suzuki A, Yasukawa T, Kobayashi S (2018) *J Am Chem Soc* 140:11325–11334
23. Zotova N, Hellgardt K, Kelsall GH, Jessiman AS, Hii KK (2010) *Green Chem* 12:2157
24. Kaizuka K, Miyamura H, Kobayashi S (2010) *J Am Chem Soc* 132:15096–15098
25. Kaizuka K, Lee K-Y, Miyamura H, Kobayashi S (2012) *J Flow Chem* 2:1
26. Mannel DS, Ahmed MS, Root TW, Stahl SS (2017) *J Am Chem Soc* 139:1690–1698
27. Gross E, Liu Jack H-C, Toste FD, Somorjai GA (2012) *Nat Chem* 4:947–952

Nanocatalysis Meets Biology



Oscar Verho and Jan-E. Bäckvall

Contents

1	Introduction	244
2	Nano Meets Bio in Organic Synthesis	245
2.1	Dynamic Kinetic Resolution: A Major Driver for the Development of Nanometal-Enzyme Hybrids	246
2.2	The Application of Nanometal-Enzyme Hybrids for Other Organic Transformations ...	250
2.3	Future Outlook on the Applications of Nanometal-Enzyme Hybrids in Organic Synthesis	253
3	Bioelectrocatalysis: An Exciting Arena for Nanometal-Enzyme Hybrids	254
3.1	Biofuel Cells Based on the Interfacing of Metal Nanoparticles and Enzymes	255
3.2	Outlook on the Future Applications of Enzymatic Biofuel Cells	260
4	Harnessing Microbes for Nanoparticle Synthesis	262
4.1	Biosynthesized Transition Metal Nanoparticles and Biometallic Whole Cell Systems in Catalysis	262
4.2	Future Outlook on Biometallic Whole Cell Catalysts	268
5	General Conclusions	269
	References	270

Abstract This chapter will review the currently available strategies for interfacing transition metal nanoparticles with enzymes and other more complex biological systems, as well as the applications of such biometal hybrids in the areas of catalysis, energy production, environmental remediation, and medicine. In the first part of this chapter, the focus will be on the many nanometal-enzyme hybrids that have been developed for applications in organic synthesis. Within the field of organic chemistry, nanometal-enzyme hybrids are often used as bifunctional catalysts to mediate

O. Verho (✉)

Department of Organic Chemistry, Stockholm University, Stockholm, Sweden

Department of Medicinal Chemistry, Uppsala Biomedical Centre, Uppsala University, Uppsala, Sweden

e-mail: oscar.verho@su.se

J.-E. Bäckvall (✉)

Department of Organic Chemistry, Stockholm University, Stockholm, Sweden

e-mail: jeb@organ.su.se

different multistep transformations, as for example the dynamic kinetic resolution of alcohols and amines. The second part of this chapter will offer an overview of nanometal-enzyme hybrids that are used as bioelectrodes in biofuel cells. This area of research has grown significantly during the past decades, much because of the many potential future applications of such devices for medical purposes. Here, nanometal-enzyme hybrid based biofuel cells hold particular promise for biosensing applications, as well as for replacing battery-based solutions in actuator devices such as mechanical valves and pacemakers. In the final part of this chapter, the different strategies to use bacteria to synthesize metal nanoparticles will be reviewed. As will be shown by the many examples in this part, biologically synthesized and supported transition metal nanoparticles constitute interesting catalytic systems that could for example be used for energy production, pollutant degradation, and small molecule synthesis.

Keywords catalysis · nanoparticles · nanometal-enzyme hybrids · biofuel cells · biosynthesis

1 Introduction

With the rapid progress of the nanotechnology field in the past decades, there has been an explosion in the number of available methods for interfacing nanomaterials with biocatalysts or other more complex biological systems. When it comes to the interfacing of nanocatalysts with enzymes, it has been shown to be a very powerful strategy for creating efficient hybrid catalytic systems, which display functions that are more than the sum of their parts [1–3]. Nanoparticles (NPs) or other nanometal species have, for example, been used to modify the functions of enzymes or stabilize their structures, which have opened the door to new and more efficient biocatalytic processes. Conversely, enzymes can be utilized to tailor the structure and catalytic properties of nanometal species. For instance, enzymes can provide a coordinative environment that stabilizes nanocatalysts, preventing them from agglomerating. Because of this intriguing synergy between nanometal species and enzymes, such hybrid systems have found a wide range of applications related to biosensing, catalysis, energy production, environmental monitoring, and medicine [2]. However, researchers in these fields have continued to push the boundaries for the creation of advanced hybrid systems, and today there also exists a number of examples where nanomaterials have even been interfaced with complex biological systems such as living bacteria [4].

The aim of this chapter is to review some selected research topics at the intersection of nanotechnology and biology. The first part of this chapter will give an overview of those nanometal-enzyme hybrids that have been used as catalysts for different organic transformations, and here our intention is to showcase the current state of the art of the field and outline future research directions. The second

part of this chapter will be devoted to bioelectrodes based on the combination of nanometal species and enzymes, which are devices that are expected to have many future applications within the field of medicine. These bioelectrodes could, for example, be integrated into biofuel cells that are supposed to power different medical implants or biosensors [5, 6]. The final part of this chapter will be dedicated to bacteria that are able to reduce metal salts into metal NPs, and here we will give examples on how these bacteria can be exploited for the design of biometallic whole cell systems. The research in such “living bioinorganic hybrids” constitutes a very exciting frontier in catalysis, and as we will show in this part, they could very well be harnessed for applications in the fields of organic synthesis, environmental remediation, and energy research [7].

2 Nano Meets Bio in Organic Synthesis

Nature has always been a major source of inspiration and fascination to chemists. Despite the impressive progress that has been made within the field of organic chemistry during the past century, we are still in many regards far behind Nature. For example, when it comes to the practice of executing synthetic sequences, we still have a lot to learn from the natural systems. In contrast to our synthetic sequences that are often done in a stepwise fashion, and which require isolation and purification of each chemical intermediate, Nature makes use of well-organized multienzymatic systems in which each chemical step is coupled to the next, to enable more efficient and selective cascade processes [8]. Furthermore, many of the enzymes involved in these intricate cascades are equipped with metal-containing cofactors that help them to carry out chemical transformations that are not possible to achieve with the chemistry of the amino acids. Thus, these so-called metalloenzymes are often used by biological systems in highly challenging chemical processes, such as photosynthesis, respiration, and nitrogen fixation [9–11].

With the ambition to construct reaction sequences that are as well-orchestrated as those seen in Nature, chemists have explored many different strategies for combining different kinds of catalytic processes, in order to create more efficient cascade reactions. One approach that has proven to be particularly fruitful has been the combination of transition metal catalysis and enzyme catalysis [12]. Here, the rapidly developing nanotechnology field has been one of the most important driving forces, as it has continuously provided chemists with new and intriguing ways of bringing metal nanocatalysts and enzymes together. Especially interesting are those approaches that allow for the conservation of the catalytic functions of both entities. This is in many cases not possible to achieve with the conventional “artificial metalloenzyme” design approach [3, 13], where insertion of a catalytically active metal center into the active site of the enzyme often abolishes the native catalytic function of the latter.

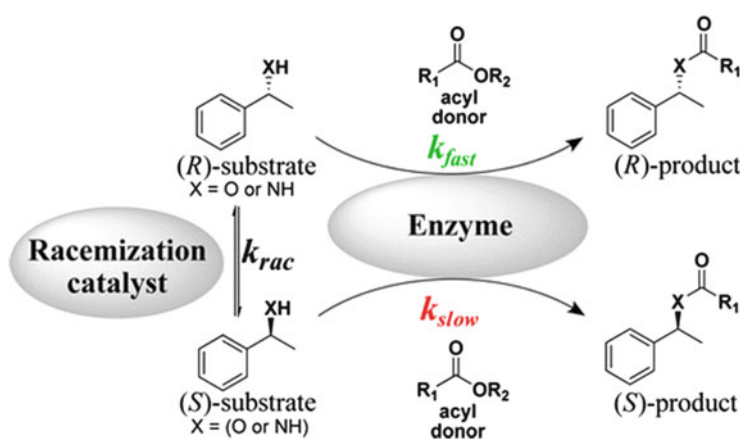
In this part, different strategies for bringing metal NPs and enzymes together for applications in organic synthesis will be highlighted. These examples generally

fall within two main categories, which is either the so-called co-immobilization approach where the nanocatalyst and the enzyme are attached next to one another on a support material or the more challenging bioconjugation approach where the two catalytic species are directly merged together. The overall goal of this part is not only to review the applications of such hybrid systems but also to shine light on their respective advantages and shortcomings. By doing so, we aim to outline future research directions that would be helpful for the development of even more efficient and intricate coupled catalytic systems for organic chemistry applications.

2.1 *Dynamic Kinetic Resolution: A Major Driver for the Development of Nanometal-Enzyme Hybrids*

In organic synthesis, the transformation that has perhaps benefitted the most from coupled catalytic systems involving both transition metals and enzymes is the dynamic kinetic resolution (DKR) of alcohols and amines [14, 15]. In these so-called chemoenzymatic DKR processes, enzymatic resolution that occurs via a transacylation reaction is coupled to transition metal-catalyzed racemization, to allow for complete conversion of a racemic starting material into an enantiomerically pure product (Scheme 1). With this approach, one elegantly overcomes the major limitation of a classical kinetic resolution (KR), where the maximum yield of the enantiomerically pure product never can exceed 50%, as one of the substrate enantiomers will ideally remain unreacted.

The first efficient procedure for DKR of alcohols involved the use of a heterogeneously immobilized lipase together with a homogeneous ruthenium



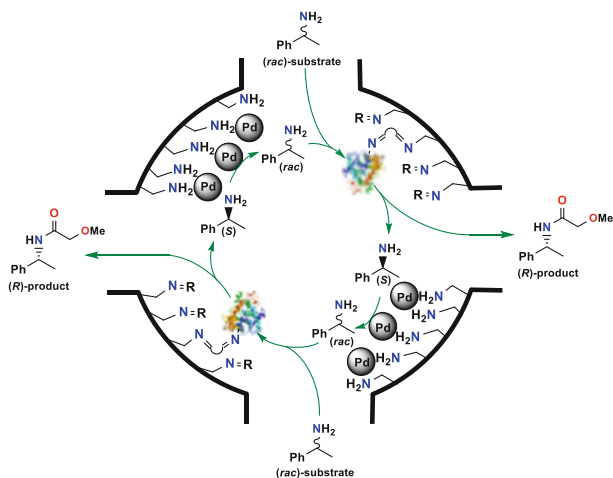
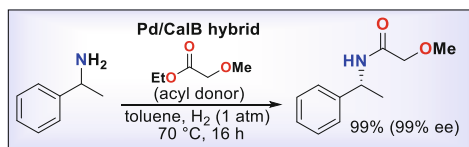
Scheme 1 General depiction of a (R)-selective chemoenzymatic DKR of secondary alcohols and primary amines (Verho et al. [14]. Reprinted with permission of American Chemical Society)

cyclopentadienyl complex [16]. In a related study about the same time, $\text{Rh}_2(\text{OAc})_4$ had been used as racemization catalyst leading to a less efficient DKR [17] [For a DKR of allylic acetates using a lipase and $\text{PdCl}_2(\text{MeCN})_2$, see 18]. Following these early studies, a great portion of the recent research in alcohol and amine DKR has focused on catalytic systems that combine heterogeneously immobilized hydrolases with homogeneous Ru cyclopentadienyl complexes, because of their high efficiency and broad substrate scope [14, 19–22]. However, with the recent increasing interest in more green and efficient catalytic processes, there has been a push to develop fully heterogeneous DKR systems that are easier to separate and recycle. Thus, significant efforts have lately been dedicated toward the development of more efficient heterogeneous racemization catalysts [14, 23].

Of the heterogeneous racemization catalysts developed so far, those based on Pd NPs that operate through a transfer hydrogenation mechanism have been the most successful, both in terms of efficiency and substrate scope. Following the seminal discovery by the Reetz group already in 1996 [24], that commercial Pd/C could be used as a racemization catalyst in a DKR, a number of research groups started to evaluate and develop different kinds of nanopalladium-based racemization catalysts. This work has yielded a wide range of Pd-based racemization catalysts for amine DKR, in which the Pd NPs have been immobilized on different support materials, such as alkaline earth salts [25, 26], aluminum oxyhydroxide [27–29], sulfate-anion modified layered double hydroxide [30], and mesoporous silicas [31–34].

Following the success of these fully heterogeneous DKR systems with separately immobilized Pd NPs and enzymes, researchers soon became interested in studying if it was possible to further improve the performance of such DKR systems by bringing the two catalytic components closer together into so-called nanometal-enzyme hybrids. The groups of Filice and Palomo were the first to create such a nanometal-enzyme hybrid for DKR purposes, and they did so by simply mixing *Candida antarctica* lipase B (CalB) with $\text{Pd}(\text{OAc})_2$ in an aqueous media [35]. Here, the enzyme worked as the reducing agent for the Pd(II) ions, which mainly produced small Pd NPs with an average diameter of 1.3 nm. Once formed, these Pd NPs got entrapped within the enzyme structure, generating a heterogeneous nanometal-enzyme hybrid composite that could be separated by centrifugation. This Pd/CalB hybrid allowed for a quite effective DKR of 1-phenylethylamine with 6 equiv. ethyl acetate as the acyl donor, resulting in 98% yield and >99% ee of the corresponding (*R*)-amide within 4 h. Although this DKR was carried out at a very small scale and under dilute conditions, it constituted the first proof of concept that a single bifunctional hybrid catalyst could be used to mediate both reactions of a DKR. Apart from showing the DKR application of this Pd/CalB hybrid, the authors also demonstrated that it could be used as a catalyst for cross-coupling reactions and an ester hydrolysis/nitro reduction cascade of 4-nitrophenyl butyrate as well.

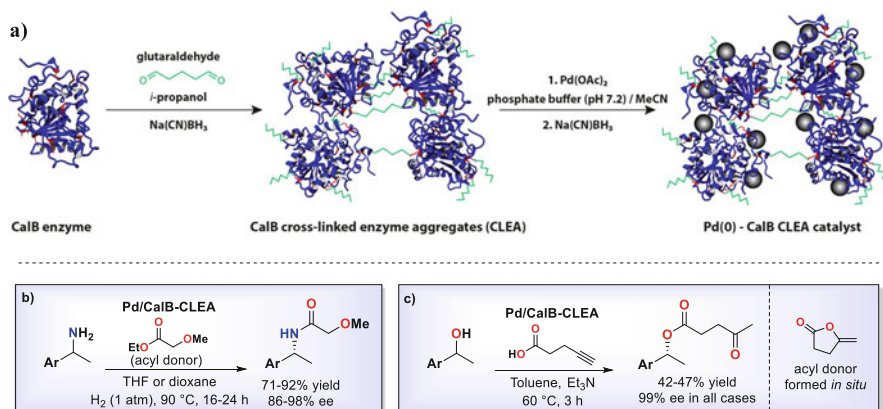
A more practical Pd/CalB hybrid was subsequently reported by the group of Bäckvall, where the Pd NPs and the enzyme were co-immobilized on the same support material [36]. The Bäckvall group had previously developed a heterogeneous catalyst based on Pd NPs immobilized on aminopropyl-



Scheme 2 DKR of 1-phenylethylamine by a bifunctional Pd/CalB hybrid catalyst developed by the Bäckvall group

functionalized siliceous mesocellular foam (Pd(0)-AmP-MCF) and shown that it could be used to efficiently racemize amines under a H_2 atmosphere [34]. Apart from being able to racemize amines, this versatile Pd(0) nanocatalyst has also been used for a number of other transformations, as, for example, oxidations [37, 38], reductions [39–41], oxidative cyclizations [42, 43], and cross-couplings [41, 44]. The authors had noted that not all of the aminopropyl groups on the support surface of this Pd(0)-AmP-MCF nanocatalyst was involved in the coordination of the Pd NPs, and thus they hypothesized that these free aminopropyl groups could be exploited for co-immobilization of CalB. The anchoring of the enzyme to the Pd(0)-AmP-MCF nanocatalyst was achieved by first reacting the free aminopropyl groups with a dialdehyde linker (glutaraldehyde) and then covalently attaching the enzyme to the free aldehyde group of the linker via a Schiff-base forming reaction.

This Pd/CalB hybrid allowed for an efficient DKR of 1-phenylethylamine with 2 equiv. ethyl methoxy acetate as the acyl donor at 70°C under 1 atm H_2 , giving the corresponding (*R*)-amide product in 99% yield and 99% ee after 20 h (Scheme 2). Interestingly, when compared to the corresponding separate components systems, i.e., Pd NPs and CalB, separately immobilized on the MCF to give Pd-AmP-MCF and CALB-AmP-MCF (which was mixed), the Pd-CALB hybrid catalyst displayed superior efficiency for this DKR reaction. The hybrid catalyst could be recycled; however, already at the third recycling, the enzyme component was found to be deactivated, which led to a much slower reaction.



Scheme 3 Synthesis of a Pd/CalB-CLEA biohybrid (**a**) and its application for the DKR of amines (**b**) and for the synthesis of chiral 1-phenylethyl 4-oxopentaoate derivatives via a cycloisomerization/KR cascade (**c**). Modified graphic from Görbe et al. with permission from American Chemical Society [46]

To develop a hybrid catalyst with improved recyclability, the Bäckvall group later explored an alternative way of interfacing CalB with Pd NPs, which omitted the need of a support material [45, 46]. In this synthetic approach, CalB was first converted into a cross-linked enzyme aggregate (CLEA) [For a review of cross-linked enzyme aggregates, please see 47] by the use of glutaraldehyde and Na(CN)BH_3 . Then, the formed CLEA was treated with Pd(OAc)_2 followed by Na(CN)BH_3 to allow for the generation of Pd NPs within the enzyme matrix (Scheme 3a). Characterization by transmission electron microscopy (TEM) revealed that Pd NPs in the size range 2–4 nm were well-dispersed within the heterogeneous enzyme composite, and from elemental analysis, the authors could show that the Pd loading was quite high (4.7 wt%).

This Pd/CalB-CLEA hybrid was successfully used for the DKR of seven different benzylic amines, where it produced the corresponding (*R*)-amides in 71–92% yield and 86–98% *ee* (Scheme 3b) [45]. These DKR reactions were performed at 90°C for 16–24 h under a H_2 atmosphere, with 2 equiv. ethyl methoxy acetate as the acyl donor. Gratifyingly, this support-less Pd/CalB-CLEA displayed considerably better reusability than their previous hybrid [36], as shown by a recycling study in which it could be reused five times for the DKR of 1-phenylethylamine with only a minor decrease in performance over each cycle.

Apart from the DKR of amines, this bifunctional Pd/CalB-CLEA hybrid has also been used to synthesize (*R*)-1-phenylethyl 4-oxopentaoate derivatives via one-pot cascades (Scheme 3c) [46]. In these cascades, the Pd NPs first catalyzed the cycloisomerization of 4-pentynoic acid into a lactone, which served as an *in situ* generated acyl donor for the CalB-catalyzed KR of the secondary alcohol.

Later, Zhang et al. reported on the development of another Pd/CalB hybrid for the DKR of 1-phenylethylamine, which involved a hierarchical yolk-shell/shell nanoreactor assembly in which the two catalytic species were spatially positioned in separate domains [48]. Similar to the preparation method used by the group of

Bäckvall for their first hybrid catalyst, the authors started from a pre-synthesized Pd nanocatalyst to which the enzyme was incorporated in the final step of the synthetic sequence. However, in this system the CalB was not covalently attached, but directly absorbed on the outer surface of the support particles. In DKR experiments with 2 equiv. ethyl methoxy acetate as the acyl donor, this catalyst showed good activity and enantioselectivity, although the chemoselectivity toward the desired product was modest (98% conv, 63% yield, >99% ee after 8 h at 70°C under 1 atm H₂). Also, the recyclability of this hybrid was found to be limited, which was most likely due to the non-covalent enzyme immobilization method used.

A series of Pd/CalB-CLEA hybrids with a remarkably high activity in the DKR of amines was also very recently described by Li et al. [49]. These hybrids were prepared in analogous manner to the Pd/CalB-CLEA developed by the group of Bäckvall, but instead of glutaraldehyde as the cross-linking agent, the authors of this study used the aldehyde-functionalized triblock polymer of propylene oxide to covalently link CalB together. The protein-polymer conjugate that formed was then treated with different amounts of Pd(OAc)₂ and reduced, to give Pd/CalB hybrids of varying Pd loadings and NP sizes. These hybrids allowed for a highly efficient DKR of three benzylic amines at 55–65°C with 3 equiv. ethyl acetate as the acyl donor, furnishing the corresponding (*R*)-amides in 60–99% yield and in perfect ee. A noteworthy feature of this Pd/CalB hybrid catalyst was that it enabled the racemization of amines in the absence of a H₂ atmosphere. Furthermore, it exhibited a remarkable recyclability and allowed for the DKR of 1-phenylethylamine to be carried out ten times, giving >80% yield and 99% ee in each cycle.

A conceptually different bifunctional hybrid catalyst for the DKR of amines and alcohols was also recently described by the group of Chen [50]. This hybrid catalyst was obtained by co-encapsulating Shvo's dimeric Ru complex and CalB into a soft nanocomposite consisting of 2-methylimidazole, Co ions, and the biosurfactant sodium deoxycholate. Shvo's dimeric Ru complex is a commonly employed transfer hydrogen catalyst that has been used for a wide range of oxidation and reduction reactions in organic synthesis [51], and in this hybrid this complex was responsible for racemizing the alcohol and amine substrates. Although this hybrid catalyst showed modest performance in the DKR of 1-phenylethylamine, the DKR of 1-phenylethanol worked fairly well and gave the corresponding (*R*)-acetate product in 98% yield and 99% ee after 4 h at 70°C. However, the recyclability of this Ru/CalB DKR hybrid catalyst was modest, and over five cycles it was found to continuously lose activity.

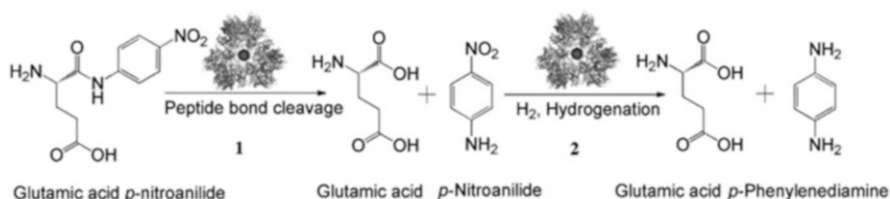
2.2 *The Application of Nanometal-Enzyme Hybrids for Other Organic Transformations*

Nanometal-enzyme hybrids have not only been applied for DKR reactions, but they have also been used as catalysts for other organic transformations as

well. For example, one of the earlier examples was developed for the use in Suzuki-Miyaura reactions by the group of Cacchi [52]. This hybrid, which had been constructed via the conjugation approach, consisted of Pd NPs that had been immobilized in the protein Dps, isolated from the thermophilic bacterium *Thermosynechococcus elongatus*. Although this hybrid catalyst did not make use of any catalytic activity from the protein component, it was still important for controlling the size of the NPs and enabling the cross-coupling reaction to be performed in water. Furthermore, because of the possibility to run the Suzuki reactions in water, the authors were also able to design chemoenzymatic one-pot cascades for the synthesis of chiral biraryl alcohols, by pairing this hybrid with an alcohol dehydrogenase from *Lactobacillus brevis*.

Another elegant example of a nanometal-enzyme assembly prepared via the conjugation approach was the Pt/aminopeptidase hybrid reported by Kim et al. [53]. Unlike the hybrid previously developed by the group of Cacchi, this Pt/aminopeptidase hybrid made use of both the nanometal and the enzyme components for coupled tandem catalysis. For the synthesis of their hybrid, the authors deliberately chose an aminopeptidase from *Streptococcus pneumoniae* that is known to self-assemble into well-defined tetrahedral dodecameric superstructures. On the inside of these aminopeptidase superstructures, there is a cavity with a diameter of ca 6 nm that can be exploited for the entrapping of metal NPs. To incorporate the Pt NPs into the interior of these aminopeptidase superstructures, the authors simply exposed them to an aqueous solution of K_2PtCl_4 and then slowly reduced the Pt(II) with $NaBH_4$. The Pt NPs that formed on the inside of aminopeptidase superstructures were found to be crystalline and have an average diameter of ca 2 nm, as determined by TEM analysis. To demonstrate the dual functions of their hybrid, the authors chose a cascade reaction involving the substrate glutamic acid *p*-nitroanilide. In this two-step reaction, the aminopeptidase catalyzed the hydrolysis of the amide bond, and the Pt NPs catalyzed the hydrogenation of the nitro group in the liberated *p*-nitroanilide leaving group (Scheme 4).

Ganai et al. subsequently reported on another interesting approach for interfacing enzymes with metals, in which Au NPs with a mesoporous coating of SiO_2 were employed as the support for a glucosidase [54]. The anchoring of the glucosidase to the surface of these Au/ SiO_2 support particles was done covalently, using a grafted epoxide linker that reacted with the exposed lysine residues of the enzyme. Although the Au NPs are buried in the core of the support particle, the mesoporous

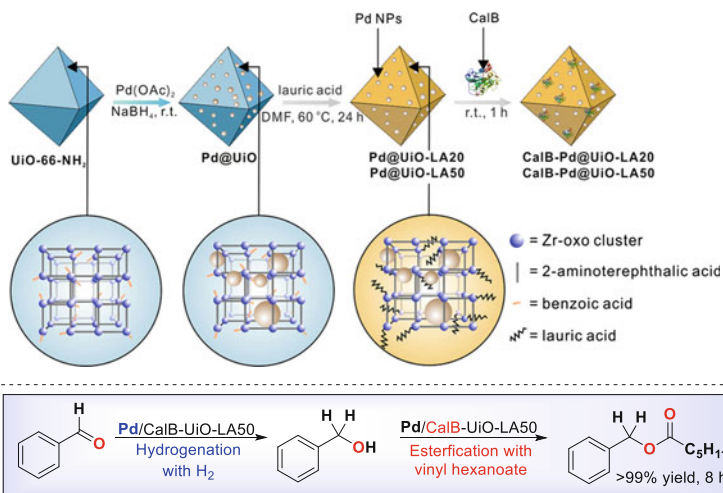


Scheme 4 Cascade reaction catalyzed by a Pt/aminopeptidase hybrid (San et al. [53]. Reprinted with permission of John Wiley and Sons)

nature of the SiO₂ shell made it possible for the reactants to reach the nanoparticles, which enabled this hybrid catalyst to be used in a relay sequence where its dual modes of reactivity could be showcased. For their demonstration, the authors used 4-nitrophenyl- β -glucopyranoside as the substrate, which was first hydrolyzed by the glucosidase into glucose and 4-nitrophenol. Once the hydrolysis reaction was complete, NaBH₄ was added to the reaction mixture, and then the Au NPs catalyzed the reduction of the 4-nitrophenol into 4-hydroxyaniline.

The interfacing of Cu NPs and CalB for tandem catalysis purposes has also been recently described by Ge and coworkers [55]. In their study, the authors demonstrated that the addition of copper sulfate to a phosphate buffer saline (PBS) solution containing CalB led to the self-assembly of a three-dimensional copper phosphate-enzyme composite. The driving force for this assembly process was the Cu(II) ions that created a well-ordered enzyme-metal ion network. Interestingly, the authors found that it was possible to re-assemble this copper phosphate-enzyme composite into well-defined Cu/CalB NPs, by reducing the Cu(II) with NaBH₄. Furthermore, they showed that polyvinyl pyrrolidone (PVP) could be used as an additive in this re-assembly process to control the degree of aggregation, which allowed them to prepare smaller and more active Cu/CalB NPs. The dual catalytic function of this Cu/CalB hybrid was demonstrated in a two-step chemoenzymatic cascade, involving CalB-catalyzed hydrolysis of *p*-nitrophenyl butyrate and Cu-catalyzed nitro-group reduction of the liberated 4-nitrophenol.

Very recently, Wang et al. reported on the design of another Pd/CalB hybrid [56], which was obtained by co-immobilizing the two catalytic species within separate compartments of the metal-organic framework (MOF) UiO-66-NH₂. This particular MOF can be conveniently synthesized by mixing ZrCl₄, 2-aminoterephthalic acid, and benzoic acid in DMF, and allowing the reaction mixture to incubate for 24 h at 120°C. A useful feature of this MOF is that the benzoic acid ligands are exchangeable, which makes it a flexible platform for interfacing different catalysts since its structure and chemical properties can be sequentially tuned to fit each catalytic species that is being immobilized. In their synthesis of this Pd/CalB hybrid, the authors started from the unmodified MOF UiO-66-NH₂ and generated Pd NPs within its inner pores. Next, the authors performed a ligand exchange of the benzoic acid for lauric acid, which dramatically changed the polarity of the MOF and made it significantly more hydrophobic. The increase in the hydrophobic nature of the MOF was not only of benefit for its catalytic applications in organic solvents, but it also allowed for more efficient immobilization of the CalB. The authors carried out this enzyme immobilization by simply stirring the Pd@UiO with CalB at room temperature for 1 h. The CalB enzyme was too large to enter the pores of the MOF, and instead it deposited on the outer surface of the support particles, well-separated from the Pd NPs. The authors prepared two different Pd/CalB hybrids that differed in the amount of lauric acid, and the most efficient one named CalB-Pd@-UiO-LA50 exhibited good activity in a one-pot hydrogenation/esterification cascade (Scheme 5). In this cascade, benzaldehyde could be efficiently converted into benzyl hexanoate in >99% yield within 8 h at room temperature. The recyclability of this hybrid also proved to be good, and it could be reused three times with only a minor loss in activity of the CalB component.



Scheme 5 Synthesis and application of a MOF-based Pd/CalB hybrid. Modified graphic from Wang et al. [56], with permission from John Wiley and Sons)

2.3 Future Outlook on the Applications of Nanometal-Enzyme Hybrids in Organic Synthesis

During the past decade, there has been an emerging interest in the organic chemistry community of novel nanometal-enzyme hybrids because of their potential as multifunctional catalysts in complex cascade sequences. Although some very impressive contributions have already been made in this area, as, for example, the many bifunctional Pd/CalB hybrids developed for the DKR of amines [36, 45, 48, 49], there is still significant room for further developments in terms of both hybrid design and the cascades they are used in. So far, only very few enzymes have been used to construct nanometal-enzyme hybrids, and simply expanding the portfolio of enzymes used would open up new opportunities to broaden the potential catalytic applications of these hybrids. Some enzymes that would be exciting to study in interfaces with different transition metal NPs would, for example, be different aldolases, decarboxylases, dehydrogenases, oxidases, proteases, pyrophosphatases, and transferases. In terms of the transition metals to be integrated into future hybrids, it would be interesting to study the performance of NPs based on the first row transition metals Fe, Mn, Co, and Ni, as they are attractive from both an economical and environmental point of view. Moreover, it would be exciting to see how far this hybrid catalyst concept could be pushed in terms of the maximum number of catalytic species that could be co-immobilized on the same support. So far, most examples have involved the pairing of only one nanometal species and one enzyme, but in principle there is nothing that prevents three or more different catalytic species to be co-immobilized

in one hybrid catalyst. However, this will most likely require the development of more elaborate synthetic methods and novel support materials.

By having access to large libraries of hybrids with wide variation of the enzyme and metal NP components, it will be much easier to design new cascades that have the potential to deliver elaborate products that are synthetically useful. Unfortunately, many of the cascade reactions involving nanometal-enzyme hybrid catalyst that has been reported so far have primarily been designed to just showcase their dual catalytic functions. As a result, the products formed from such cascades have often been quite simple and not really valuable from a synthetic point of view. Moving forward, it would be exciting to see hybrid catalysts being applied in more intricate cascades, which can enable access to more elaborate and synthetically useful target molecules in a fashion that is reminiscent of how complex natural products are sequentially assembled in Nature. Here, it is important to point out that we chemists have the possibility to go beyond Nature in the future, as we are privileged to have the vast chemistry of all the transition metals at our full disposal. As have already been demonstrated with the hybrids developed for DKR of amines, it is possible to create artificial metalloenzymes that display overall catalytic functions that have no precedence in Nature [36]. From this perspective, it will be highly interesting to follow the continued research in this area over the coming decades and to see what complex organic compounds that could soon be synthesized, thanks to novel nanometal-enzyme hybrids.

3 Bioelectrocatalysis: An Exciting Arena for Nanometal-Enzyme Hybrids

Within the field of electrocatalysis, there has been a recent increase in the interest for nanometal-enzyme hybrids that can be used as electrodes in enzymatic biofuel cells (EBCs). In the medicinal sciences, there is a considerable interest for EBCs since they constitute promising power sources for microelectronic systems such as actuators and sensors [57]. The electricity needed to power such devices would be produced by the EBC through electrochemical reactions that makes use of endogenous substrates within the users' bodies as the fuels. Here, the oxidation of different saccharides at the anode coupled to the reduction of oxygen at the cathode has been explored as the main way to generate electricity *in vivo*. Of the endogenous saccharides, glucose has become by far the one most vividly studied since it is abundant in relatively high concentrations in several different body fluids [6, 57]. In addition to glucose, bioanodes have also been developed for other substrates, such as cholesterol [58], creatinine [59], ethanol [60–62], fructose [63, 64], lactate [65, 66], pyruvate [65, 67], urea [68, 69], and vitamin C [70].

However, it should be emphasized that the research in EBCs still have a long way to go before these devices can be considered as a realistic substitute for batteries

in medical implants intended for long-term use. Besides challenges associated with biocompatibility and sterilization, the full potential of EBCs is primarily held back by their unsatisfactory operational stabilities, which typically ranges from a few hours to months (this can be compared to sealed batteries with lifetimes of about 5–8 years) [57]. On the other hand, if EBCs would be made more durable than batteries, they would certainly constitute a much more attractive alternative to batteries since they are easier to miniaturize and they would theoretically never run out of their source of energy. Despite the limitations and challenges associated with the use of EBCs for medicinal applications, the field of bioelectrocatalysis still represents an interesting research area to review in this chapter, since it has contributed significantly to the design of new nanometal-enzyme hybrids.

3.1 Biofuel Cells Based on the Interfacing of Metal Nanoparticles and Enzymes

In contrast to conventional fuel cells that make use of different metal catalysts for the conversion of chemical energy into electricity, EBCs instead rely on redox-active enzymes as the key catalytic components. This latter approach is preferable for use in implantable devices since enzyme catalysts operate efficiently in physiological conditions (i.e., low temperatures and at near-neutral pH) [71]. Moreover, enzymes are highly selective for organic substrates present in living organisms. For these reasons, EBCs are especially suited for incorporation into implantable or microscale biomedical devices. However, the major challenge for constructing efficient EBCs is to ensure for an efficient electron transfer between the enzymes and the electrode surface. It is known that electron transfer rate decreases rapidly as the distance between the enzymes' active sites and the electrode surface increases. Given the facts that enzymes are large molecules with catalytically active sites often confined in a small pocket, EBC design is challenging from both a chemistry and engineering point of view. As a result, EBCs generally exhibit power outputs ($10\ \mu\text{W}$ – $1\ \text{mW cm}^{-2}$) that are much lower than those of conventional fuel cells [57]. However, it should be emphasized that such low power outputs could still be sufficient to power many different sorts of microscale devices, and thus EBCs should be evaluated based on their long-term stability rather than on how high power densities they can reach.

As shown in Fig. 1, EBCs can be divided into two main groups depending on how the electrons are being shuttled between the enzyme and the electrode: (1) mediated electron transfer (MET) devices where different electron transfer mediators are used as relays in the electron transfer (this includes inorganic complexes of Fe [72, 73], Os [74, 75], and Ru [76, 77]; organic compounds such as quinones [78, 79], phenothiazines [80, 81], and viologens [82, 83]; or more recently also polyoxometalate nanoclusters [84]) and (2) direct electron transfer (DET) devices where the electrons are being directly transported between the enzyme components and the electrodes. Although MET generally exhibits higher power densities

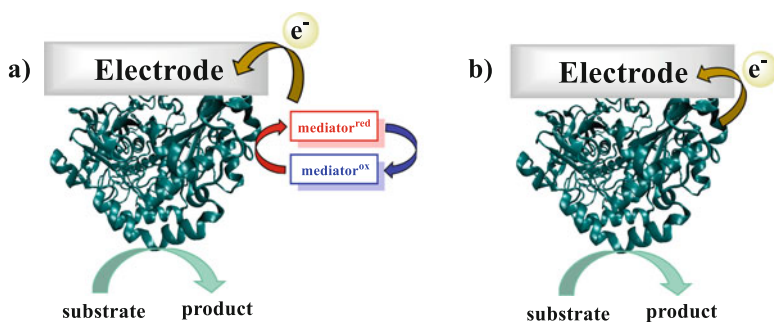


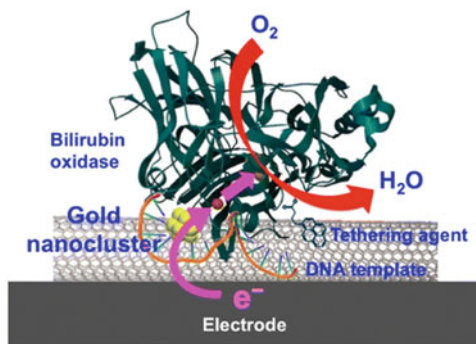
Fig. 1 Illustration of mediated electron transfer (a) and direct electron transfer (b)

than DET devices, they are less attractive for biomedical applications since they always come with the risk of the electrolyte solution leaking out, which is associated with severe health risks [85]. Hence, the research that has been aimed at developing energy solutions for smaller microscale devices has in recent years focused on DET devices. Approaches to improve the performances of DET-based EBCs have, for example, included the development of different immobilization methods that not only enable high loadings of enzymes onto the electrode surfaces but which also allow for control of the orientation of the enzymes, which translate into enhanced electron transfer processes. This research area has benefited tremendously from the fast-growing nanotechnology field, which has provided many new conductive nanomaterials used for coating electrodes.

An important milestone in the development of DET devices was the discovery that the interfacing of enzyme-based electrodes with Au NPs could greatly enhance the electron transfer process. In 2011, the groups of Atanassov and Banta rationally designed a hybrid glucose oxidase (GOx) from *Aspergillus niger* with a site-specific modification (H447C), which allowed it to efficiently coordinate to an Au NP [86]. Immobilization of this GOx:Au NP hybrid onto an electrode surface resulted in a DET bioanode with significantly improved oxygen reduction kinetics. Although the electrochemical output of this particular electrode was poor, it provided an important proof of concept that showed that the integration of transition metal NPs with enzyme-based electrodes could be a promising strategy for designing more efficient EBCs.

The full potential of this strategy was later demonstrated by the groups of Atanassov and Martinez in 2015, with the design of a bioelectrode composed of bilirubin oxidase (BOx) and DNA-templated Au nanoclusters (Fig. 2) [87]. The used DNA ligand was found to be very effective in controlling the growth of the Au particles, as characterization experiments by TEM revealed that the Au nanoclusters were only ~ 0.9 nm in size on average. Furthermore, the X-ray photoelectron spectroscopy (XPS) analysis indicated that the Au formed mixed-valence clusters of Au(0) and Au(I) in a ratio 1:3.7. Interestingly, the interfacing of the electrode surface with these Au nanoclusters led to dramatically reduced overpotentials for the BOx-catalyzed O_2 reduction (by ~ 15 mV). Additionally, the

Fig. 2 A bioelectrode composed of hybrid DNA-templated Au nanoclusters and bilirubin oxidase (BOD) for improved enzymatic reduction of O_2 (Charkraborty et al. [91]. Reprinted with permission of American Chemical Society)



Au nanoclusters enhanced the electronic communication between the electrode and the enzyme. The measured $E_{\text{onset}} = 0.525$ V and $E_{1/2} = 0.430$ V vs Ag/AgCl, values were considerably higher than those of earlier reported BOx-based electrodes [88–90]. Also, the presence of the Au NPs was found to significantly improve the current density by $\sim 50\%$ (cf. $735 \mu\text{A cm}^{-2}$ vs $493 \mu\text{A cm}^{-2}$ for the corresponding gold-free electrode).

Inspired by the seminal studies by Atanassov and coworkers on Au NP-doped bioanodes, several other groups quickly followed by constructing complete EBCs based on this nanometal-enzyme hybrid concept. For example, the group of Kokoh reported on a series of EBCs with different Au NP/BOx-bioanodes paired with a GOx biocathode [91]. The best performing glucose/ O_2 EBC presented in this study was interfaced with trimetallic $\text{Au}_{60}\text{Pt}_{20}\text{Pd}_{20}$ NPs immobilized on electrospun Vulcan XC72R carbon nanofibers. This device displayed a power density of $91 \mu\text{W cm}^{-2}$ and a current density of $249 \mu\text{W cm}^{-2}$, respectively, when operated at pH 7.4 with 10 mM glucose at 37°C . However, a major drawback of this device was that only the bioanode operated through DET, while the biocathode required 2,2'-azino-bis(3-ethylbenzothiazoline-6-sulfonate) diammonium salt (ABTS) as a mediator for efficient electron transfer. This mediator-dependent cathode proved to be a critical limitation of this EBC assembly in terms of long-time performance, since the ABTS was found to leach substantially over time, which caused the device to lose 85% of its activity over the first 7 days of operation. Following the work of Kokoh et al., the group of Zhu developed a structural similar EBC with more durable performance, which was composed of a mediator-less bioanode based on GOx/Au NP@graphene and a ABTS/laccase/Au NP@graphene biocathode [92]. This EBC displayed an impressive maximum power density of 2 mW cm^{-2} , and in a longevity experiment where it was used to power LED diodes, it was found to retain 66% of its power output after 70 days.

The group of Zhu subsequently reported on a completely mediator- and membrane-less EBC with good long-time stability, in which both electrode surfaces were made from a conductive ternary hybrid material of carbon nanotubes, carbon nitride nanosheets, and Au NPs [93]. This EBC, which featured a pyrroloquinoline quinone-dependent glucose dehydrogenase for glucose oxidation and a BOx for O_2

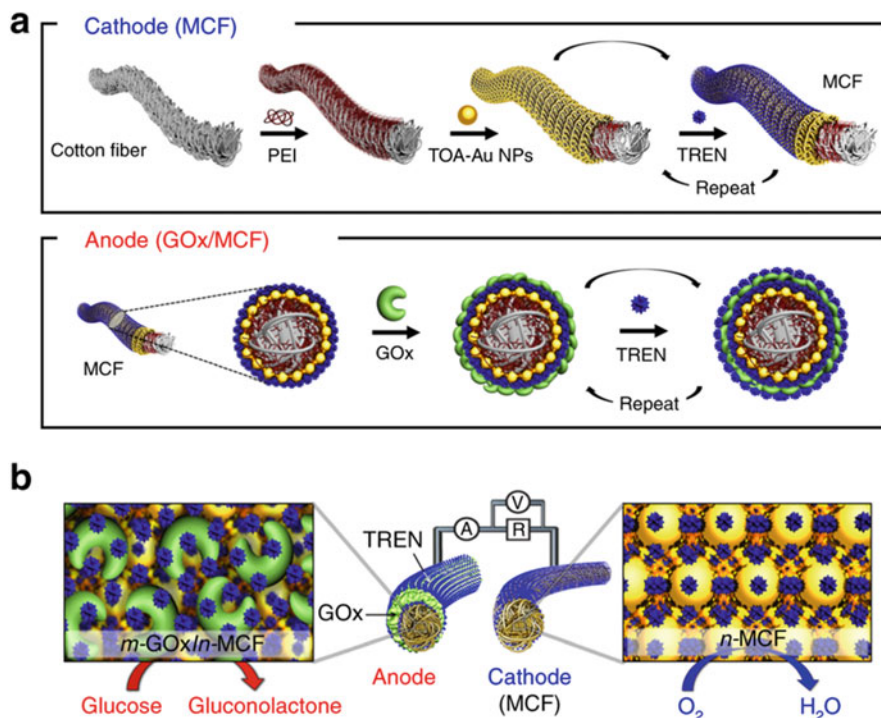


Fig. 3 General outline of the synthesis of the metallic cotton fiber bioelectrodes (a) and an illustration of the complete EBC assembly (b) (Kwon et al. [95]. Image reprinted from an open-access article available from Nat. Commun, Springer Nature)

reduction, was capable of reaching an open current voltage of 0.55 V and a high maximum power density of $249 \mu\text{W cm}^{-2}$, when subjected to an O₂-saturated PBS solution containing 5 mM glucose at pH 7.4. This work by the group of Zhu was not only an important contribution because it presented a DET device that rivaled the performance of EBCs relying on electron transfer mediators, i.e., MET devices. Their work was also important because it demonstrated how new nanomaterials can enable the development of new and highly efficient EBCs. Shortly after this study, the group of Zhou reported on the development of another mediator-less glucose/O₂ EBC in which the electrodes had been fabricated from a carbon nanofiber/Fe₃O₄/Au NP hybrid material [94]. Also this DET device exhibited a respectable performance and a good long-time durability.

However, when it comes to the highest power outputs of DET devices, the groups of Lee and Cho have certainly pushed the boundaries of what is possible with their EBC. In 2018, they reported on a mediator- and membrane-less glucose/O₂ EBC that exhibited an astonishing maximum power density of 3.7 mW cm^{-2} , when subjected to a PBS solution containing 300 mM glucose (Fig. 3) [95]. It should be noted, however, that this glucose concentration is significantly higher than those typically employed when testing EBCs, but interestingly this device was also found to

reach a very high power density when operated under more biologically relevant conditions ($\sim 0.9 \text{ mW cm}^{-2}$ at 10 mM glucose). The high performance of this EBC was enabled by an elaborate manufacturing method in which 8 nm-sized Au NPs were layer-by-layer (LBL) assembled with small organic linkers onto cotton fibers to produce a highly porous metallic cotton fiber electrode material with extremely high conductivity ($> 2.1 \times 10^4 \text{ S cm}^{-1}$).

Interestingly, this engineered metallic cotton fiber material was found to be a highly efficient oxygen reduction catalyst by itself, which enabled the final EBC assembly to have an “enzyme-free” cathode. On the anode side, these metallic cotton fibers were used as a support material to which a GOx enzyme was immobilized. To improve the electrical communication between the enzyme and the Au NPs at the anode, the authors employed tris-(2-aminoethyl)amide (TREN) as a small molecule adhesive. By both binding covalently to the Au NPs and interacting electrostatically with the enzyme, TREN was able to bring both of the components into a very close proximity, which greatly improved the DET rate. Additionally, TREN was also found to have a beneficial effect on the overall operational stability of the electrode, and the entire device was found to maintain more than half of its initial power density over 35 days. This study by the groups of Lee and Cho provided another excellent example of how the design of new nanomaterials with high internal surface areas and good superconducting properties can drive EBC development forward. The same authors subsequently used this LBL assembly technique to prepare a related EBC based on a carbon fiber electrode material [96]. Although this device also showed a relatively high performance, it still proved to be less efficient than the EBC described in their first study.

As can be seen from the examples presented so far, Au is evidently the main transition metal of choice when it comes to the doping of electrode materials with different metal NPs. As indicated by the great body of work in this field, Au NPs appear to be superior to other metal NPs concerning the ability to promote electron transfer processes. However, it should be noted that also some other transition metal NPs have been studied for this purpose. Platinum, a transition metal mainly employed in non-enzymatic fuel cells [97–99], has also been used to generate nanostructured materials for bioelectrode applications [100–102]. For example, Tel-Vared and coworkers very recently reported on a complete EBC setup, which featured a mesoporous carbon-based hybrid anode with Pt nanoclusters and GOx NPs, paired with a BOx-based cathode [103]. Although the described DET device reached a modest maximal power output and current density ($45 \mu\text{W cm}^{-2}$ and $105 \mu\text{A cm}^{-2}$ when operated at glucose concentrations of 60 mM), this study is interesting from a synthetic perspective since it outlined a new paradigm for assembling bioelectronic elements, which could also be interesting to apply to Au-based systems. Here, the reduction of the metal precursor PtCl_5^- was carried out by the immobilized GOx which had already been confined into the mesopores of the carbonaceous matrix on beforehand. With this synthetic approach, the authors managed to form the Pt nanoclusters in a very close proximity to the FAD redox active center of the GOx, which allowed for a good contact surface between the two catalytic components. This close wiring of the GOx and

the Pt NPs was found to be highly beneficial for the electron transfer, as indicated by the unusually high turnover rate of electrons of $2,580 \text{ e}^- \text{ s}^{-1}$ that was measured.

In addition to Pt, several other metals have been studied as modifiers for bioelectrodes, as, for example, Ag [104], Co [105], and Pd [106], but perhaps one of the most interesting metals to study further is Fe, given its low toxicity, low cost, and high availability. The group of Poo-arporn recently described a glucose/ O_2 EBC that was manufactured from a reduced graphene oxide electrode material, which was only doped with superparamagnetic Fe_3O_4 NPs [107]. Although the measured maximum power density was modest ($73.7 \mu\text{W cm}^{-2}$ at 5 mM glucose), the open circuit voltage of +0.63 V was more impressive and demonstrates that Fe-based electrode materials could be used in the future to fabricate EBCs that are viable for real-life applications.

3.2 Outlook on the Future Applications of Enzymatic Biofuel Cells

Future applications of bioelectrodes and complete EBC assemblies in the medicinal field are predicted to increase. However, in order for these devices to become widely applied, their long-term performance need to be further improved if they are to compete with state-of-the-art batteries. Encouragingly, this research field has progressed at an impressive pace during the past decade, much thanks to innovations related to the engineering of new nanomaterials and clever solutions for interfacing enzymes with nanometallic species. Thus, it will most likely not take long until we can see the first examples of implantable medical devices that are powered by EBCs. Such devices could, for example, be self-powered biosensors that over a period of days detect certain analytes in the patient's blood and where the measured analyte at the same time acts as a fuel for the EBC. As has been showcased herein, biosensors have already been developed for a wide range of analytes such as cholesterol, glucose, lactate, urea, and vitamin C, and all of these are relevant to a variety of medical conditions and diseases. However, in recent years several ingenious bioanalytical devices have been reported in which hybrid glucose/ O_2 EBCs have been connected to more elaborate sensing platforms to enable the detection of a much wider range of species.

For example, the group of Li has reported on a self-powered and ultrasensitive aptasensing platform for detection of antibiotic residues in the nM range (Fig. 4) [108]. In this system, the bioanode of the EBC is coated with $\text{SiO}_2@ \text{Au}$ NP-DNA conjugates that interact with the electrode surface via complementary and pre-attached aptamers. The function of these DNA conjugates is to block the access of glucose to the bioanode surface in the absence of the analyte and thus restrict the power output of the EBC. However, once the analyte is present in the surrounding solution, the analyte will interact with the aptamers and trigger the release of the DNA conjugates, which will expose the electrode surface to the glucose, and as a result, the power output of the EBC will increase. The authors showcased the practical applicability of this aptasensing

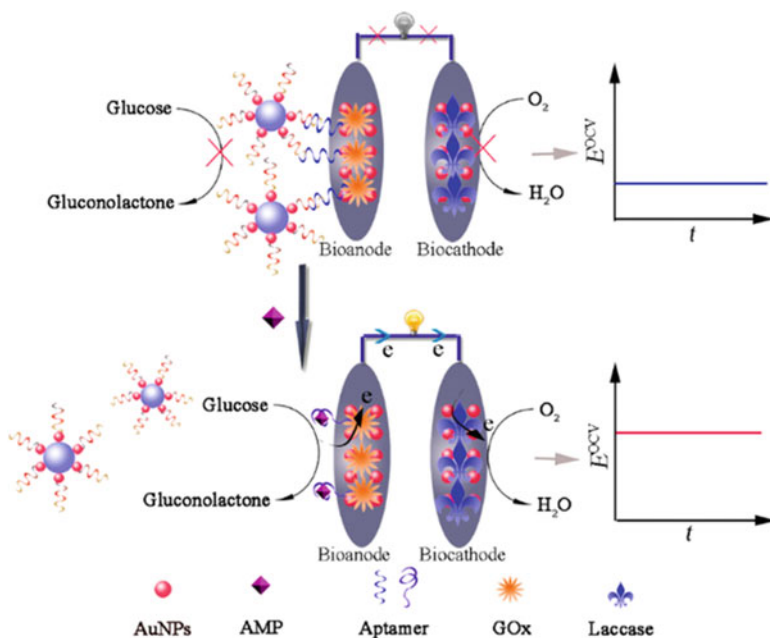


Fig. 4 Illustration of the EBC-powered aptasensing platform of ampicillin (Gai et al. [108]. Reprinted with permission of American Chemical Society)

platform by demonstrating that it could be used for measuring ampicillin in milk samples.

This aptasensing platform also exhibited an impressive selectivity, thanks to the high binding specificity of the aptamer component, which enabled discrimination of ampicillin from six other antibiotics. Seen overall, this study by the group of Li constitutes an excellent example of how glucose/ O_2 EBCs could be integrated into more advanced sensing platforms, which by careful choice of the analyte-recognition element could be used to detect essentially any analyte in a biological sample. Examples of such analytes could be anything from other small molecules such as melamine, which has been quantified by an immunosensing platform developed by the group of Li [109], all the way up to larger biomolecules such as microRNA, which has been measured in high sensitivity with a colorimetric sensing platform designed by the groups of Cui and Zhao [110].

Apart from expanding the repertoire of analytes that can be measured, a considerable amount of research has also been dedicated to miniaturizing these devices and reducing the need for surgical procedures, as a means to improve the user-friendliness and broaden the range of applications. Here, non-invasive, EBC-powered devices that do not need to be implanted and which make use of fuels in, for example, saliva [111, 112], sweat [113, 114], and tears [115, 116] could open up for new applications related to general health monitoring or sports.

Apart from being used to power various biosensors, EBCs have also for a long time been put forward as potential power sources for actuator systems such

as pacemakers or mechanical valves. However, in order for such applications to be realized, EBCs have to be greatly improved in terms of both power output and long-term performance. Therefore, it will most likely take additional decades of research before EBCs are able to compete with battery-based solutions for these kinds of applications. Despite currently lagging behind in this area, the future of EBCs still looks very bright, and it is likely that these devices will revolutionize the health care in the near future and become a daily part of our lives.

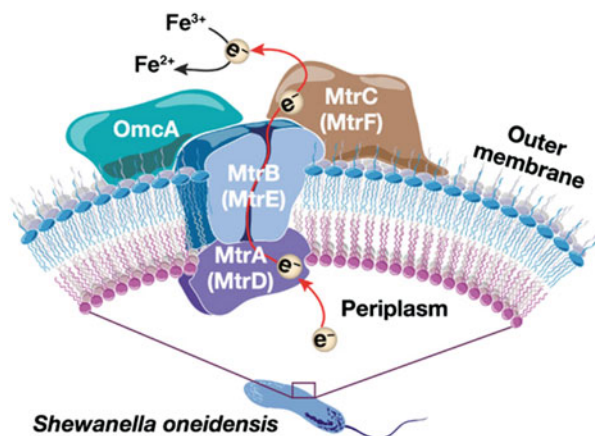
4 Harnessing Microbes for Nanoparticle Synthesis

As is evident from the many examples presented in this chapter so far, a wide range of synthetic protocols for preparing nanostructured catalysts with tailored properties are available. Most often, these protocols rely on the work by chemists, who use specific combinations of chemical reagents and different synthetic techniques for the rational design of nanomaterials. However, lately it has been found that bacteria can aid the production of nanometal species [4, 7]. Apart from offering a green alternative for generating metal NPs that is free of toxic chemical reagents, this approach also provides direct access to biometallic whole cell systems (BWCSs) in which the bacteria also act as supports for the formed metal NPs. As will be shown in this part, such BWCSs are far from being merely academic curiosities. In fact, such “living” catalytic systems are very interesting for a number of applications related to, for example, environmental remediation, energy research, and organic chemistry [4, 7].

4.1 *Biosynthesized Transition Metal Nanoparticles and Biometallic Whole Cell Systems in Catalysis*

The interest for biosynthesized transition metal NPs within the chemistry community was sparked in 1998, when the group of Macaskie demonstrated that the sulfate-reducing bacterium *Desulfovibrio desulfuricans* could be used for the preparation of Pd NPs. This bacterium was found to produce Pd NPs in sizes of approximately 50 nm, when it was subjected to an aqueous solution containing $\text{Pd}(\text{NH}_3)_4\text{Cl}_2$ and different electron donors (H_2 , formate, and pyruvate) [117]. After this seminal study, many researchers became interested in searching for other microorganisms that could be harnessed for the biosynthesis of metal NPs that are commonly used as catalysts in organic transformations. Soon, it was found that several other bacteria were also capable of mediating the bioreduction of metal salts, as, for example, *Aeromonas hydrophila* [118, 119], *Cupriavidus necator* [120], *Geobacter sulfurreducens* [121, 122], *Pseudomonas putida* [120], *Pseudomonas stutzeri* [123], and *Shewanella oneidensis* [124, 125]. Of these,

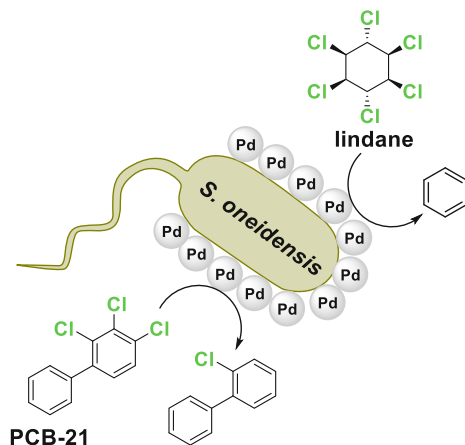
Fig. 5 Schematic overview of the electron transport chain in *Shewanella oneidensis* that is responsible for metal reduction (Wang et al. [126]. Image adapted from an open-access article available from Sci Adv, Springer Nature, American Association for the Advancement of Science)



S. oneidensis has received particular attention over the years since it has proved to be very efficient in reducing many different catalytically relevant transition metals, and moreover the electron transfer pathway responsible for its extraordinary electrochemical activity is well-characterized [126–128]. To achieve the metal reduction, *S. oneidensis* makes use of an extracellular electron transfer pathway that involves the so-called MtrCAB conduit. This is a collection of electron transfer proteins that are responsible for shuttling some of the metabolically generated electrons from the cytoplasm all the way to the extracellular space (Fig. 5). Here, the outer membrane *c*-type cytochromes, MtrC and OmcA, are the primary mediators of the electron transfer to the metal substrate. The fact that the metal reduction occurs at the outer membrane of *S. oneidensis* is highly convenient, since it allows for the metal NPs to deposit on the exterior surface of the bacteria as they form, which leads to the concomitant creation of a BWCS.

BWCSs derived from *S. oneidensis* have been shown to hold potential as catalysts for different organic transformations. For example, the group of Verstraete has in a series of publications studied *S. oneidensis*-supported Pd nanocatalysts for the degradation of various pollutants for environmental remediation purposes (Fig. 6). In their first study in 2005, they reported on the use of a BWCS based on Pd NPs and *S. oneidensis* for the dechlorination of polychlorinated biphenyls (PCBs) [129]. In this work, the authors studied in great detail the Pd(II) biosorption and bioreduction capability of *S. oneidensis*, and they could demonstrate that it was possible to obtain recoveries of Pd exceeding 90% with several different electron donors (H_2 , EtOH, lactate, and pyruvate). Furthermore, the authors were able to show that this Pd/*S. oneidensis* BWCS was capable of reductively dehalogenate several lightly and highly chlorinated PCB congeners in water and sediment samples with good efficiency. Here, the authors could, for example, demonstrate that it is possible to reduce the PCB content of a soil suspension sample by 73% within 48 h at 28°C, by using a bioPd-loading of 50 mg/L and H_2 as the hydrogen donor. Interestingly, when the authors attempted to perform the same experiment with

Fig. 6 Degradation of chlorinated pollutants by a biometallic whole cell catalyst based on Pd NPs and *S. oneidensis*



commercial Pd(0) powder, it was found that Pd loadings of 500 mg/L were required to give similar results as those of the *S. oneidensis*-generated bioPd. From this comparison study, it was evident that the *S. oneidensis*-based bioreduction approach allowed for the generation of remarkably efficient Pd nanocatalysts. In a follow-up study, Verstraete and coworkers showed that this Pd/*S. oneidensis* BWCS could also be applied for the efficient degradation of the pesticide lindane. By using a fed-batch process configuration with formate as the hydrogen donor, 98% of the lindane could be removed from a lindane-saturated water solution (10 mg/L) within 24 h [130].

In 2011, the joint efforts of the Verstraete and Boon groups made further progress in this area by demonstrating for the first time that *S. oneidensis* can be used to create bimetallic BWCSs and that this represents a promising approach for extending scope of chlorinated pollutants that can be dehalogenated [131]. In this study, the authors showed that a Pd/Au-*S. oneidensis* system allowed for efficient removal of the drug diclofenac (78%) and the solvent trichloroethylene (83%) from aqueous solutions within 24 h, when using H₂ as hydrogen donor. These results were in sharp contrast to those of the monometallic BWCSs, which showed very low clearance rates of these two chlorinated compounds. Although the authors concluded that an even more efficient BWCS could possibly be designed by further optimization of the Au/Pd ratio, the disclosed Pd/Au-*S. oneidensis* system still constituted a very nice example on how the degradation of recalcitrant pollutants can be achieved through the combination of different transition metals in BWCSs.

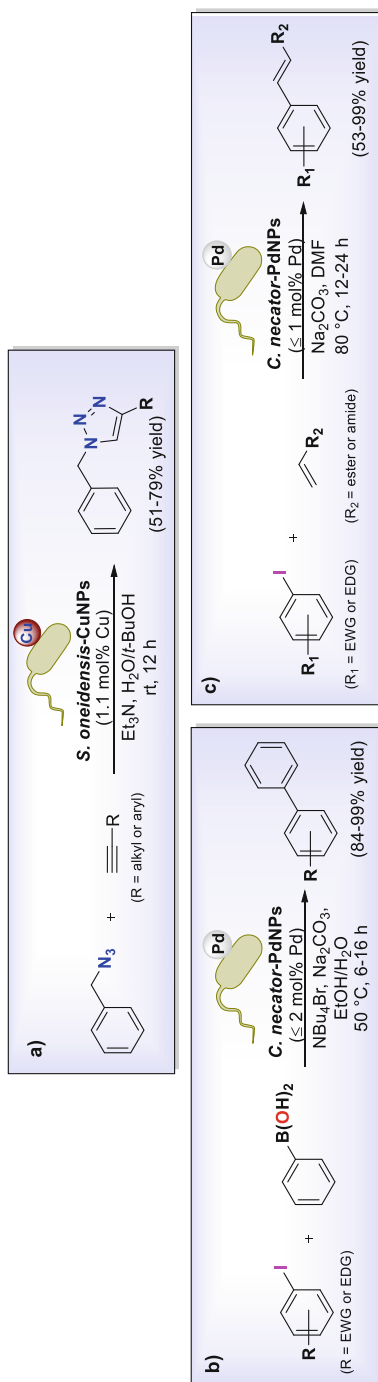
More recently, the group of Zhang demonstrated the potential of Pd/*S. oneidensis* BWCSs to be used as electrocatalysts for the oxidation of biofuels [132]. In their study, the authors showed that *S. oneidensis* coated with ~6 nm-sized Pd NPs could allow for efficient electrocatalytic oxidation of formate, when deposited onto a glassy carbon electrode. Remarkably, this BWCS displayed a high catalytic activity that was found to be superior to that of conventionally electrodeposited Pd, as indicated by the anodic formate oxidation peak which was 220 mV more negative for the *S. oneidensis*-generated Pd NPs. Unfortunately, the authors were not able to

elucidate the origin of this high catalytic activity experimentally, but they speculated that the Pd NPs could benefit from being near the bacteria's membrane proteins with their multiple electronic centers and electron transfer systems. Apart from the high catalytic activity, this BWCS also exhibited an excellent substrate selectivity for formate, and no electrocatalysis could be observed in the presence of other related compounds such as MeOH, EtOH, or acetate. In contrast, current responses were observed in the presence of all of these compounds when electrodeposited Pd was used as the catalyst.

Kimber et al. also showed that it is possible to prepare Cu-based BWCSs through the use of *S. oneidensis*, and additionally, they demonstrated that this BWCS could be used as a catalyst for "Click reactions" [133]. The biosynthesis of the Cu NPs was achieved by supplying the bacteria with a solution containing 50×10^{-6} M CuSO₄ and 30×10^{-3} M lactate, from which they were capable of extracting and reducing all Cu(II) within 96 h. Analysis by TEM revealed that the majority of the Cu NPs were in the size range of 20–50 nm, and furthermore it was found that they were primarily located intracellularly. From X-ray absorption near edge structure (XANES) spectroscopy, the authors were able to determine that the Cu NPs were mainly composed of Cu(0), although they were covered with a surface layer of Cu₂O. In the catalytic evaluations of this Cu-based BWCS, it was tested as a catalyst for the cycloaddition of benzyl azide with various alkynes. By using BWCS quantities that corresponded to a Cu loading of 1.1 mol%, the authors were able to prepare a number of triazoles in good to high yields (51–79%) within 12 h at room temperature (Scheme 6a).

Although much of the focus of this part of the chapter has so far been dedicated to *S. oneidensis* and its rather remarkable ability to reduce different transition metal ions, it is important to point out that other microorganisms have also been employed for the preparation of BWCS-based catalysts. For example, in 2009, the group of Skrydstrup reported on the design of two different Pd-based BWCSs involving the Gram-negative bacteria *Cupriavidus necator* and *Pseudomonas putida* [134]. By TEM characterization of these BWCSs, the authors could establish that the morphology of the biosorbed Pd differed significantly between the two bacteria species. *Cupriavidus necator* was found to give rise to very small and well-dispersed Pd NPs, while the Pd formed large aggregates on the cell surface of *Pseudomonas putida*. Because of the more desirable Pd morphology generated by the *Cupriavidus necator*, the authors chose to focus most of their catalytic study on this BWCS, and here they could show that it was a highly competent catalyst for both Suzuki-Miyaura and Mizoroki-Heck reactions (Scheme 6b,c). For the Suzuki-Miyaura reaction between *p*-iodotoluene and phenylboronic acid, they were also able to demonstrate the recyclability of this BWCS catalyst by showing that it could be reused four times without any signs of activity loss. The Pd(0)-*Pseudomonas putida* BWCS was also briefly tested in their study, and despite its non-ideal Pd morphology, it still showed good catalytic activity for both transformations.

The group of Macaskie has also reported on the preparation of Pd NP-based BWCSs involving a variety of Gram-negative and Gram-positive



Scheme 6 Catalytic applications of different BWCSs. A Cu/*S. oneidensis*-based BWCS as a catalyst for “Click reactions” (a) and a Pd/*C. necator*-based BWCS as a catalyst for Suzuki-Miyaura cross-couplings (b) and Mizoroki-Heck reactions (c)

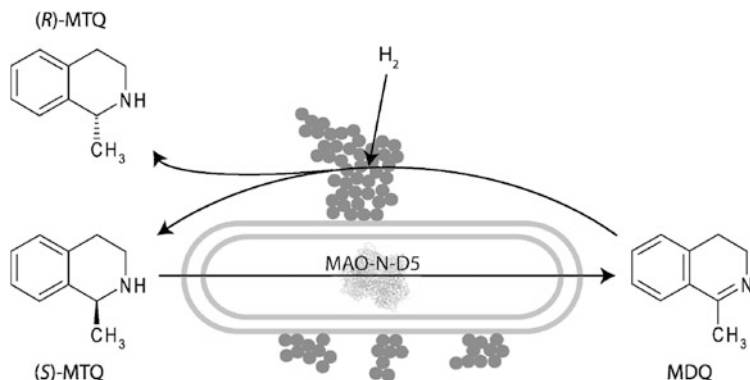
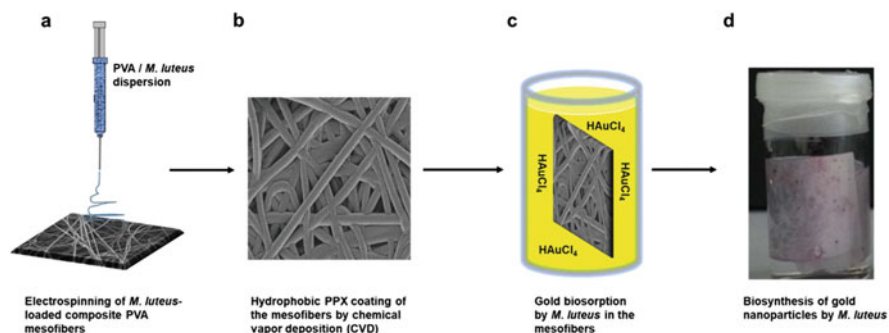


Fig. 7 Deracemization of a cyclic amine by a bifunctional biometallic whole cell catalyst. (Foulkes et al. [139] Reprinted with permission of American Chemical Society)

bacteria, and these have, for example, been studied as catalysts for the hydrogenation of alkenes [135], reduction of chromium species [136, 137], as well as H_2 generation from hypophosphite [138]. Another very impressive example of an elaborately designed BWCS with dual catalytic functions was described by the group of Lloyd in 2011 (Fig. 7) [139]. In this work, the authors first genetically engineered *E. coli* to overproduce a monoamine oxidase (MAO) that exhibited high enantioselectivity in the oxidation of chiral amines. These bacteria were subsequently coated with nanoscale Pd(0) by taking advantage of their ability to catalyze the reduction of Pd(II) when exposed to H_2 . The bifunctional BWCS obtained, proved to be a highly efficient catalyst for the deracemization of the cyclic amine, 1-methyltetrahydroisoquinoline (MTQ), which over multiple cycles of oxidations and reductions gave enantio-enriched product. Here, the intracellular MAO is responsible for the highly enantioselective oxidation of (S)-MTQ to the prochiral imine, while the Pd NPs catalyze the reduction of this imine back to *rac*-MTQ. When these cycles of oxidation and reduction are allowed to occur repeatedly, the desired product (R)-MTQ is gradually enriched in a cyclic deracemization process. The authors also compared the performance of this BWCS with a separate component system involving Pd-free cells and a commercial Pd/C catalyst, by allowing both catalytic systems to take part in five cycles of oxidation and reduction each. Interestingly, the BWCS catalyst was found to offer several advantages over the separate component system, as, for example, higher product recovery and lower Pd leaching.

Another interesting strategy for interfacing Au NPs with bacteria was very recently described by the group of Greiner [140]. In their study, they manufactured a *Micrococcus luteus*/Au NP/polymer nonwoven-type composite via a stepwise protocol that is depicted in Scheme 7. In the first step, *M. luteus* was charged onto poly(vinylalcohol) (PVA) microfibers using electrospinning. Next, the bacteria-loaded PVA was coated with hydrophobic poly(*p*-xylylene)



Scheme 7 Biosynthesis of Au NPs in a *M. luteus*/PVA composite nonwoven material. (a) Electrospinning of *M. luteus*-loaded composite PVA mesofibers, (b) hydrophobic PPX coating of the mesofibers by chemical vapor deposition, (c) Au biosorption by *M. luteus* in the mesofibers, and (d) Au NP biosynthesis by *M. luteus*. (Reichs et al. [140] Reprinted with permission of John Wiley and Sons)

(PPX) by chemical vapor deposition. Finally, this composite material was put in a HAuCl_4 -solution, and the entrapped *Micrococcus luteus* biosorbed the Au(III) salt and reduced it to Au NPs. Interestingly, this bioinorganic hybrid material proved to be a competent catalyst for the hydrolysis of dimethylphenylsilane. Although the reaction required a long reaction time of 350 h to reach completion, the Au loading used was extremely low (0.001 mol%). Therefore, if one takes this small Au loading into account, this catalyst was actually quite efficient. Moreover, another peculiar and highly interesting observation made by the authors was that the well-being of the *M. luteus* seemed important for the observed catalytic activity. Remarkably, when control experiments were performed with this hybrid material containing dead *M. luteus*, no catalytic activity was observed from the Au NPs.

Although the usefulness of this hybrid material for catalytic applications can be debated, this study still constitutes an intriguing way for synthesizing interfaced systems between bacteria and metal NPs. Such systems could become very interesting for further catalytic studies, if the metal loading could be increased further.

4.2 Future Outlook on Biometallic Whole Cell Catalysts

The main conclusion that can be drawn from this overview of BWCSs is that their preparation is certainly justified and further research on their use is motivated. Although it might at first glance appear unnecessary and overly complicated to immobilize metal nanocatalysts on living organisms instead of on conventional support material, some of the studies highlighted herein show intriguing indications that this BWCS approach might confer a number of advantages. In many of

the studies highlighted above, various bacteria are capable of reducing different catalytically important transition metal ions and biosorbing the formed metal NPs with high efficiency. Moreover, the formed NPs are often very small and tightly bound to the microorganism's membrane, which is highly advantageous from a catalysis perspective. Also, it seems to be possible to recycle BWCSs efficiently, as, for example, demonstrated by the study of the Skrydstrup group where their BWCS could be separated by centrifugation as any other conventional heterogeneous catalyst [134].

Another finding that is especially intriguing and that has been found to be true for most of the studied BWCSs so far is that the interaction between the metal NPs and the bacterial membrane proteins enable improved catalytic activity compared to conventional heterogeneous metal catalysts in many cases. It will be very exciting to follow the future developments in this area. Here, it would be particularly interesting to see more demonstrations of new BWCSs as catalysts for different organic transformations. There is certainly a huge potential for more elaborate BWCS designs similar to the one reported by Foulkes et al. [139], where biosorbed Pd NPs and an intracellularly expressed enzyme are used to achieve an overall deracemization of an amine. By following this approach, it should be possible to design more intricate cascade processes, which in turn could open up for the synthesis of even more complex molecules. This synthetic approach would certainly have the potential to bring organic chemists closer to the dream of being able to design efficient cascade processes that can compete with the efficiency and selectivity of Nature's highly spectacular coupled enzymatic pathways.

5 General Conclusions

Many different strategies for interfacing nanometal species with biological systems have been presented in this chapter. As has been demonstrated herein, bioinorganic hybrid systems have found a wide range of applications in several different research disciplines. In organic synthesis, metal NPs interfaced with either enzymes or bacteria have been extensively studied as catalysts for different transformations. Here, a particular focus has been dedicated to bioinorganic hybrids that display multiple catalytic functions, as they have the potential to be applied in intricate cascades that can be used to access highly complex organic compounds of value for the fine chemical and pharmaceutical industry. In the field of bioelectrocatalysis, the design of nanometal-enzyme hybrids is currently a major research frontier, which is already yielding a variety of new efficient and robust EBCs that are being evaluated as power sources for biosensors and actuators. This research is expected to have a transformative impact on the field of medicine in a near future, by enabling for the development of new implantable and wearable biomedical devices that will be of useful for the treatment and monitoring of different diseases. However, it is perhaps also safe to say that bioinorganic hybrid systems will most likely see many more applications than those outlined in this chapter. As the fields of nanotechnology and biology continue to move forward, new research

frontiers will certainly emerge, which are not apparent for us now with our current knowledge. Regardless, it will be very exciting to follow this research at the intersection of nanotechnology and biology and to see where it takes us in the upcoming decades.

References

1. San BH, Gusthart J, Lee SS, Kim KK (2018) Metal–enzyme hybrid catalysts in cascade and multicomponent processes. In: Montserrat D, Bäckvall JE, Pàmies O (eds) *Artificial metalloenzymes and metalloDNAzymes in catalysis: from design to applications*. Wiley-VCH, Weinheim, pp 321–351. <https://doi.org/10.1002/9783527804085.ch11>
2. Chen M, Zeng G, Xu P, Lai C, Tang L (2017) How do enzymes ‘meet’ nanoparticles and nanomaterials? *Trends Biochem Sci* 42:914–930. <https://doi.org/10.1016/j.tibs.2017.08.008>
3. Pàmies O, Diéguez M, Bäckvall JE (2015) Artificial metalloenzymes in asymmetric catalysis: key developments and future directions. *Adv Synth Catal* 357:1567–1586. <https://doi.org/10.1002/adsc.201500290>
4. Macaskie LE, Mkiheenko IP, Omajai JB, Stephen AJ, Wood J (2017) Metallic bionanocatalysts: potential applications as green catalysts and energy materials. *Microb Biotechnol* 10:1171–1180
5. Pinyou P, Blay V, Muresan LM, Nogue T (2019) Enzyme-modified electrodes for biosensors and biofuel cells. *Mater Horiz* 6:1336–1358. <https://doi.org/10.1039/c9mh00013e>
6. Kärkäs MD, Verho O, Åkermark B (2018) Metalloenzyme-inspired systems for alternative energy harvest. In: Montserrat D, Bäckvall JE, Pàmies O (eds) *Artificial metalloenzymes and metalloDNAzymes in catalysis: from design to applications*. Wiley-VCH, Weinheim, pp 353–381. <https://doi.org/10.1002/9783527804085.ch12>
7. Lloyd JR, Byrne JM, Coker VS (2011) Biotechnological synthesis of functional nanomaterials. *Curr Opin Biotechnol* 22:509–515. <https://doi.org/10.1016/j.copbio.2011.06.008>
8. Bruggink A, Schoevaart R, Kieboom T (2003) Concepts of nature in organic synthesis: cascade catalysis and multistep conversions in concert. *Org Process Res Dev* 7:622–640. <https://doi.org/10.1021/op0340311>
9. Liu J, Chakraborty S, Hosseinzadeh P, Yu Y, Tian S, Petrik I, Bhagi A, Lu Y (2014) Metalloproteins containing cytochrome, iron-sulfur, or copper redox centers. *Chem Rev* 114:4366–4469. <https://doi.org/10.1021/cr400479b>
10. Hoffman BM, Lukoyanov D, Dean DR, Seefeldt LC (2013) Nitrogenase: a draft mechanism. *Acc Chem Res* 46:587–595. <https://doi.org/10.1021/ar300267m>
11. Barber J (2006) Photosystem II: an enzyme of global significance. *Biochem Soc Trans* 34:619–631. <https://doi.org/10.1042/BST0340619>
12. Köhler V, Turner NJ (2015) Artificial concurrent catalytic processes involving enzymes. *Chem Commun* 51:450–464. <https://doi.org/10.1039/C4CC07277D>
13. Schwizer F, Okamoto Y, Heinisch T, Gu Y, Pellizzoni MM, Lebrun V, Reuter R, Köhler V, Lewis JC, Ward TR (2018) Artificial metalloenzymes: reaction scope and optimization strategies. *Chem Rev* 118:142–231. <https://doi.org/10.1021/acs.chemrev.7b00014>
14. Verho O, Bäckvall JE (2015) Chemoenzymatic dynamic kinetic resolution: a powerful tool for the preparation for the preparation of enantiomerically pure alcohols and amines. *J Am Chem Soc* 137:3996–4009. <https://doi.org/10.1021/jacs.5b01031>
15. Marcos R, Martín-Matute B (2012) Combined enzyme and transition-metal catalysis for dynamic kinetic resolution. *Isr J Chem* 52:639–652. <https://doi.org/10.1002/ijch.201200012>

16. Larsson ALE, Persson BA, Bäckvall JE (1997) Enzymatic resolution of alcohols coupled with ruthenium-catalyzed racemization of the substrate alcohol. *Angew Chem Int Ed* 36:211–1212
17. Dinh PM, Howarth JA, Hudnott AR, Williams MJ, Harris W (1996) Catalytic racemization of alcohols: applications to enzymatic resolution reactions. *Tetrahedron Lett* 37:7623–7626. [https://doi.org/10.1016/0040-4039\(96\)01677-2](https://doi.org/10.1016/0040-4039(96)01677-2)
18. Allen JV, Williams MJ (1996) Dynamic kinetic resolution with enzyme and palladium combinations. *Tetrahedron Lett* 37:1859–1862. [https://doi.org/10.1016/0040-4039\(96\)00136-0](https://doi.org/10.1016/0040-4039(96)00136-0)
19. Martín-Matute B, Edin M, Bogár K, Bäckvall JE (2004) Highly compatible metal and enzyme catalysts for efficient dynamic kinetic resolution of alcohols at ambient temperature. *Angew Chem Int Ed* 43:6535–6539. <https://doi.org/10.1002/anie.200461416>
20. Fernández-Salas JA, Manzini S, Nolan SP (2014) A cationic ruthenium complex for the dynamic kinetic resolution of secondary alcohols. *Chem Eur J* 20:13132–13135. <https://doi.org/10.1002/chem.201404096>
21. Mavrynsky D, Päiviö M, Lundell K, Sillanpää R, Kanerva LT, Leino R (2009) Dicarboxylchloro(pentabenzylcyclopentadienyl)ruthenium as racemization catalyst in the dynamic kinetic resolution of secondary alcohols. *Eur J Org Chem* 2009:1317–1320. <https://doi.org/10.1002/ejoc.200801248>
22. Kim MJ, Chung YI, Choi YK, Lee HK, Kim D, Park J (2003) (S)-selective dynamic kinetic resolution of secondary alcohols by the combination of subtilisin and an aminocyclopentadienylruthenium complex as the catalysts. *J Am Chem Soc* 125:11494–11495. <https://doi.org/10.1021/ja036766r>
23. Parvulescu A, Janssens J, Vanderleyden J, De Vos D (2010) Heterogeneous catalysts for racemization and dynamic kinetic resolution of amines and secondary alcohols. *Top Catal* 53:931–941. <https://doi.org/10.1007/s11244-010-9512-x>
24. Reetz MT, Schimossek K (1996) Lipase-catalyzed dynamic kinetic resolution of chiral amines. Use of palladium as the racemization catalyst. *Chimia* 50:668–669
25. Parvulescu AN, Jacobs PA, De Vos DE (2007) Palladium catalysts on alkaline-earth supports for racemization and dynamic kinetic resolution of benzylic amines. *Chem Eur J* 13:2034–2043. <https://doi.org/10.1002/chem.200600899>
26. Parvulescu A, De Vos D, Jacobs P (2005) Efficient dynamic kinetic resolution of secondary amines with Pd on alkaline earth salts and a lipase. *Chem Commun* (42):5307–5309. <https://doi.org/10.1039/B509747A>
27. Engström K, Shakeri M, Bäckvall JE (2011) Dynamic kinetic resolution of β -amino esters by a heterogeneous system of a palladium nanocatalyst and *Candida antarctica* lipase A. *Eur J Org Chem* 2011:1827–1830. <https://doi.org/10.1002/ejoc.201001714>
28. Choi YK, Kim Y, Han K, Park J, Kim MJ (2009) Synthesis of optically active amino acid derivatives via dynamic kinetic resolution. *J Org Chem* 74:9543–9545. <https://doi.org/10.1021/jo902034x>
29. Kim MJ, Kim WH, Han K, Choi YK, Park J (2007) Dynamic kinetic resolution of primary amines with a recyclable Pd nanocatalyst for racemization. *Org Lett* 9:1157–1159. <https://doi.org/10.1021/ol070130d>
30. Xu G, Dai X, Fu S, Wu J, Yang L (2014) Efficient dynamic kinetic resolution of arylamines with Pd/layered double-hydroxide-dodecyl sulfate anion for racemization. *Tetrahedron Lett* 55:397–402. <https://doi.org/10.1016/j.tetlet.2013.11.041>
31. Xu Y, Wang M, Feng B, Li Z, Li Y, Li H, Li H (2017) Dynamic kinetic resolution of aromatic sec-alcohols by using a heterogeneous palladium racemization catalyst and lipase. *Cat Sci Technol* 7:5838–5842. <https://doi.org/10.1039/C7CY01954H>
32. Jin Q, Jia G, Zhang Y, Li C (2014) Modification of supported Pd catalysts by alkalic salts in the selective racemization and dynamic kinetic resolution of primary amines. *Cat Sci Technol* 4:464–471. <https://doi.org/10.1039/C3CY00535F>
33. Gustafson KPJ, Lihammar R, Verho O, Engström K, Bäckvall JE (2014) Chemoenzymatic dynamic kinetic resolution of primary amines using a recyclable palladium nanoparticle catalyst together with lipases. *J Org Chem* 79:3747–3751. <https://doi.org/10.1021/jo500508p>

34. Shakeri M, Tai CW, Göthelid E, Oscarsson S, Bäckvall JE (2011) Small Pd nanoparticles supported in large pores of mesocellular foam: an excellent catalyst for racemization of amines. *Chemistry–A Eur J* 17(47):13269–13273. <https://doi.org/10.1002/chem.20110126>
35. Filice M, Marciello M, del Puerto Morales M, Palomo JM (2013) Synthesis of heterogeneous enzyme–metal nanoparticle biohybrids in aqueous media and their applications in C–C bond formation and tandem catalysis. *Chem Commun* 49:6876–6878. <https://doi.org/10.1039/C3CC42475H>
36. Engström K, Johnston EV, Verho O, Gustafson KPJ, Shakeri M, Tai CW, Bäckvall JE (2013) Co-immobilization of an enzyme and a metal into the compartments of mesoporous silica for cooperative tandem catalysis: an artificial metalloenzyme. *Angew Chem Int Ed* 52:14006–14010. <https://doi.org/10.1002/anie.201306487>
37. Verho O, Åkermark T, Johnston EV, Gustafson KPJ, Tai CW, Svengren H, Kärkäs MD, Bäckvall JE, Åkermark B (2015) Well-defined palladium nanoparticles supported on siliceous mesocellular foam as heterogeneous catalysts for the oxidation of water. *Chem Eur J* 21:5909–5915
38. Johnston EV, Verho O, Kärkäs MD, Shakeri M, Tai CW, Palmgren P, Eriksson K, Oscarsson S, Bäckvall JE (2012) Highly dispersed palladium nanoparticles on mesocellular foam: an efficient and recyclable heterogeneous catalyst for alcohol oxidation. *Chem Eur J* 18:12202–12206. <https://doi.org/10.1002/chem.201202157>
39. Nagendiran A, Pascanu V, Bermejo Gómez A, González Miera G, Tai CW, Verho O, Martín-Matute B, Bäckvall JE (2016) Mild and selective catalytic hydrogenation of the C=C Bond in α,β -unsaturated carbonyl compounds using supported palladium nanoparticles. *Chem Eur J* 22:7184–7189. <https://doi.org/10.1002/chem.201600878>
40. Verho O, Gustafson KPJ, Nagendiran A, Tai CW, Bäckvall JE (2014) Mild and selective hydrogenation of nitro compounds using palladium nanoparticles supported on amino-functionalized mesocellular foam. *ChemCatChem* 6:3153–3159. <https://doi.org/10.1002/cctc.201402488>
41. Verho O, Nagendiran A, Johnston EV, Tai CW, Bäckvall JE (2012) Nanopalladium on amino-functionalized mesocellular foam: an efficient catalyst for Suzuki reactions and transfer hydrogenations. *ChemCatChem* 5:612–618. <https://doi.org/10.1002/cctc.201200247>
42. Li MB, Posevins D, Gustafson KPJ, Tai CW, Shchukarev A, Qiu Y, Bäckvall JE (2019) Diastereoselective cyclobutenol synthesis: a heterogeneous palladium-catalyzed oxidative carbocyclization-borylation of enallenols. *Chem Eur J* 25:210–215. <https://doi.org/10.1002/chem.201805118>
43. Deiana L, Jiang Y, Palo-Nieto C, Afewerki S, Incerti-Pradillos CA, Verho O, Tai CW, Johnston EV, Córdova A (2014) Combined heterogeneous metal/chiral amine: multiple relay catalysis for versatile eco-friendly synthesis. *Angew Chem Int Ed* 53:3447–3451. <https://doi.org/10.1002/anie.201310216>
44. Bratt E, Verho O, Johansson MJ, Bäckvall JE (2014) A general Suzuki cross-coupling reaction of heteroaromatics catalyzed by nanopalladium on amino-functionalized siliceous mesocellular foam. *J Org Chem* 79:3946–3954. <https://doi.org/10.1021/jo500409r>
45. Gustafson KPJ, Görbe T, de Gonzalo-Calvo G, Yuan N, Schreiber CL, Shchukarev A, Tai CW, Persson I, Zou X, Bäckvall JE (2019) Chemoenzymatic dynamic kinetic resolution of primary benzylic amines using Pd⁰-CalB CLEA as a biohybrid catalyst. *Chem Eur J* 25:9174–9179. <https://doi.org/10.1002/chem.201901418>
46. Görbe T, Gustafson KPJ, Verho O, Kervefors G, Zheng H, Zou X, Johnston EV, Bäckvall JE (2017) Design of a Pd(0)-CalB CLEA biohybrid catalyst and its application in a one-pot cascade reaction. *ACS Catalysis* 7(3):1601–1605. <https://doi.org/10.1021/acscatal.6b03481>
47. Sheldon RA (2011) Cross-linked enzyme aggregates as industrial biocatalysts. *Org Process Res Dev* 15:213–223. <https://doi.org/10.1021/op100289f>
48. Zhang X, Jing L, Chang F, Chen S, Yang H, Yang Q (2017) Positional immobilization of Pd nanoparticles and enzymes in hierarchical yolk-shell@shell nanoreactors for tandem catalysis. *Chem Commun* 53:7780–7783. <https://doi.org/10.1039/C7CC03177G>

49. Li X, Cao Y, Luo K, Sun Y, Xiong J, Wang L, Liu Z, Li J, Ma J, Ge J, Xiao H, Zare RN (2019) Highly active enzyme-metal nanohybrids synthesized in protein-polymer conjugates. *Nat Catal* 2:718–725. <https://doi.org/10.1038/s41929-019-0305-8>
50. Li H, Qiu C, Cao X, Lu Y, Li G, He X, Lu Q, Chen K, Ouyang P, Tan W (2019) Artificial nanometalloenzymes for cooperative tandem catalysis. *ACS Appl Mater Interfaces* 11:15718–15726. <https://doi.org/10.1021/acsami.9b03616>
51. Conley BL, Pennington-Boggio MK, Boz E, Williams TJ (2010) Discovery, applications, and catalytic mechanisms of Shvo's catalyst. *Chem Rev* 110:2294–2312. <https://doi.org/10.1021/cr9003133>
52. Prastaro A, Ceci P, Chiancone E, Cirilli R, Colone M, Fabrizi G, Stringaro A, Cacchi S (2009) Suzuki-Miyaura cross-coupling catalyzed by protein-stabilized palladium nanoparticles under aerobic conditions in water: application to a one-pot chemoenzymatic enantioselective synthesis of chiral biaryl alcohols. *Green Chem* 11:1929–1932
53. San BH, Kim S, Moh SH, Lee H, Jung DY, Kim KK (2011) Platinum nanoparticles encapsulated by aminopeptidase: a multifunctional bioinorganic nanohybrid catalyst. *Angew Chem Int Ed* 50:11924–11929. <https://doi.org/10.1002/anie.201101833>
54. Ganai AK, Shinde P, Dhar BB, Sen Gupta S, Prasad BLV (2013) Development of a multifunctional catalyst for a “relay” reaction. *RSC Adv* 3:2186–2191. <https://doi.org/10.1039/C2RA22829G>
55. Li Z, Ding Y, Wu X, Ge J, Ouyang P, Liu Z (2016) An enzyme-copper nanoparticle hybrid catalyst prepared from disassembly of an enzyme-inorganic nanocrystal three-dimensional nanostructure. *RSC Adv* 6:20772–20776. <https://doi.org/10.1039/C5RA27904F>
56. Wang Y, Zhang N, Zhang E, Han Y, Qi Z, Ansorge-Schumacher M, Ge Y, Wu C (2019) Heterogeneous metal-organic frameworks-based biohybrid catalysts for cascade reaction in organic solvent. *Chem Eur J* 25:1716–1721. <https://doi.org/10.1002/chem.201805680>
57. Cosnier S, Gross AJ, Giroud F, Holzinger M (2018) Beyond the hype surrounding biofuel cells: What's the future of enzymatic fuel cells? *Curr Opin Electrochem* 12:148–155. <https://doi.org/10.1016/j.coelec.2018.06.006>
58. Sekretaryova AN, Beni V, Eriksson M, Karyakin AA, Turner APF, Vagin MY (2014) Cholesterol self-powered biosensor. *Anal Chem* 86:9540–9547. <https://doi.org/10.1021/ac501699p>
59. Lad U, Khokhar S, Kale GM (2008) Electrochemical creatinine biosensors. *Anal Chem* 80:7910–7917. <https://doi.org/10.1021/ac801500t>
60. Aquino Neto S, Milton RD, Hickey DP, De Andrade AR, Minteer SD (2016) Membraneless enzymatic ethanol/O₂ fuel cell: transitioning from an air-breathing Pt-based cathode to a bilirubin oxidase-based biocathode. *J Power Sources* 324:208–214. <https://doi.org/10.1016/j.jpowsour.2016.05.073>
61. Gouranlou F, Ghourchian H, Kheirmand M, Salimi A (2017) Effect of support on power output of ethanol/O₂ biofuel cell. *Nanochem Res* 2:214–222. <https://doi.org/10.22036/ncr.2017.02.008>
62. Aquino Neto S, Almeida TS, Palma LM, Minteer SD, de Andrade AR (2014) Hybrid nanocatalysts containing enzymes and metallic nanoparticles for ethanol/O₂ biofuel cell. *J Power Sources* 259:25–32. <https://doi.org/10.1016/j.jpowsour.2014.02.069>
63. Bollella P, Hibino Y, Kano K, Gorton L, Antiochia R (2018) Highly sensitive membraneless fructose biosensor based on fructose dehydrogenase immobilized onto aryl thiol modified highly porous gold electrode: characterization and application in food samples. *Anal Chem* 90:12131–12136. <https://doi.org/10.1021/acs.analchem.8b03093>
64. Trivedi UB, Lakshminarayana D, Kothari IL, Patel PB, Panchal CJ (2009) Amperometric fructose biosensor based on fructose dehydrogenase enzyme. *Sensors Actuators B Chem* 136:45–51. <https://doi.org/10.1016/j.snb.2008.10.020>
65. Kucherenko IS, Topolnikova SOO (2019) Advances in the biosensors for lactate and pyruvate detection for medical applications: a review. *Trends Anal Chem* 110:160–172. <https://doi.org/10.1016/j.trac.2018.11.004>

66. Rassaei L, Olthuis W, Tsujimura S, Sudhölter EJR, van der Berg A (2014) Lactate biosensors: current status and outlook. *Anal Bioanal Chem* 406:123–137. <https://doi.org/10.1007/s00216-013-7307-1>
67. Malik AM, Chaudhary R, Pundir CS (2019) An improved enzyme nanoparticles based amperometric pyruvate biosensor for detection of pyruvate in serum. *Enzyme Microb Technol* 123:30–38. <https://doi.org/10.1016/j.enzmictec.2019.01.006>
68. Chaudhary R, Joshi A, Srivastava R (2017) pH and urea estimation in urine samples using single fluorophore and ratiometric fluorescent biosensors. *Sci Rep* 7:5840. <https://doi.org/10.1038/s41598-017-06060-y>
69. Singh M, Verma N, Garg AK, Redhu N (2008) Urea biosensors. *Sensors Actuators B Chem* 134:345–351. <https://doi.org/10.1016/j.snb.2008.04.025>
70. Wen Y, Xu J, Liu M, Li D, He H (2012) Amperometric vitamin C biosensor based on the immobilization of ascorbate oxidase into the biocompatible sandwich-type composite films. *Appl Biochem Biotechnol* 167:2023–2038. <https://doi.org/10.1007/s12010-012-9711-y>
71. Xu Q, Zhang F, Xu L, Leung P, Yang C, Li H (2017) The applications and prospect of fuel cells in medical field: a review. *Renew Sust Energy Rev* 67:574–580. <https://doi.org/10.1016/j.rser.2016.09.042>
72. Arslan F, Beskan U (2014) An amperometric biosensor for glucose detection from glucose oxidase immobilized in polyaniline-polyvinylsulfonate-potassium ferricyanide film. *Artif Cells Nanomed Biotechnol* 42:284–288. <https://doi.org/10.3109/21691401.2013.812650>
73. Meredith MT, Kao DY, Hickey D, Schmidtke DW, Glatzhofer DT (2011) High current density ferrocene modified linear poly(ethylenimine) bioanodes and their use in biofuel cells. *J Electrochem Soc* 158:B166–B174. <https://doi.org/10.1149/1.3505950>
74. Nakabayashi Y, Omayu A, Morii S, Yagi S (2000) Evaluation of osmium(II) complexes as mediators accessible for biosensors. *Sensors Actuators B Chem* 66:128–130. [https://doi.org/10.1016/S0925-4005\(00\)00324-5](https://doi.org/10.1016/S0925-4005(00)00324-5)
75. Ohara TJ (1995) Osmium bipyridyl redox polymers used in enzyme electrodes. *Platin Met Rev* 39(2):54–62.
76. Raymundo-Pereira PA, Mascarenhas ACV, Teixeira MFS (2016) Evaluation of the oxo-bridged dinuclear ruthenium ammine complex as redox mediator in an electrochemical biosensor. *Electroanalysis* 28:562–569. <https://doi.org/10.1002/elan.201500479>
77. Kosela E, Elzanowska H, Włodzimierz K (2002) Charge mediation by ruthenium poly(pyridine) complexes in ‘second-generation’ glucose biosensors based on carboxymethylated β -cyclodextrin polymer membranes. *Bioanal Chem* 373:724–734. <https://doi.org/10.1007/s00216-002-1308-9>
78. Milton RD, Hickey DP, Abdellaoui S, Lim K, Wu F, Tan B, Minter SD (2015) Rational design of quinones for high power density biofuel cells. *Chem Sci* 6:4867–4875. <https://doi.org/10.1039/C5SC01538C>
79. Reuillard B, Le Goff A, Agnes C, Holzinger M, Zebda A, Gondran C, Elouarzaki K, Cosnier S (2013) High power enzymatic biofuel cell based on naphthoquinone-mediated oxidation of glucose by glucose oxidase in a carbon nanotube 3D matrix. *Phys Chem Chem Phys* 15:4892–4896. <https://doi.org/10.1039/C3CP50767J>
80. Sekretaryova AN, Vagin MY, Beni V, Turner AP, Karyakin AA (2014) Unsubstituted phenothiazine as a superior water-insoluble mediator for oxidases. *Biosens Bioelectron* 53:275–282. <https://doi.org/10.1016/j.bios.2013.09.071>
81. Pöller S, Shao M, Sygmund C, Ludwig R, Schuhmann W (2013) Low potential biofuel cell anodes based on redox polymers with covalently bound phenothiazine derivatives for wiring flavin adenine dinucleotide-dependent enzymes. *Electrochim Acta* 110:152–158. <https://doi.org/10.1016/j.electacta.2013.02.083>
82. Lee D, Kim YH, Park S (2016) Enzyme electrode platform using methyl viologen electrochemically immobilized on carbon materials. *J Electrochem Soc* 163:G93–G98. <https://doi.org/10.1149/2.0521608jes>

83. Liu X, Hao M, Feng M, Zhang L, Zhao Y, Du X, Wang G (2013) A one-compartment direct glucose alkaline fuel cell with methyl viologen as electron mediator. *Appl Energy* 106:176–183. <https://doi.org/10.1016/j.apenergy.2013.01.073>
84. Boussema F, Gross AJ, Hmida F, Ayed B, Majdoub H, Cosnier S, Maaref A, Holzinger M (2018) Dawson-type polyoxometalate nanoclusters confined in a carbon nanotube matrix as efficient redox mediators for enzymatic glucose biofuel cell anodes and glucose biosensors. *Biosens Bioelectron* 109:20–26. <https://doi.org/10.1016/j.bios.2018.02.060>
85. Falk M, Blum Z, Shleev S (2012) Direct electron transfer based enzymatic fuel cells. *Electrochim Acta* 82:191–202. <https://doi.org/10.1016/j.electacta.2011.12.133>
86. Holland JT, Lau C, Brozik S, Atanassov P, Banta S (2011) Engineering of glucose oxidase for direct Electron transfer via site-specific gold nanoparticle conjugation. *J Am Chem Soc* 133:19262–19265. <https://doi.org/10.1021/ja2071237>
87. Charkraborty S, Babanova S, Rocha RC, Desireddy A, Artyushkova K, Boncella AE, Atanassov P, Martinez JS (2015) A hybrid DNA-templated gold nanocluster for enhanced enzymatic reduction of oxygen. *J Am Chem Soc* 137:11678–11687. <https://doi.org/10.1021/jacs.5b05338>
88. Ramasamy RP, Luckarift HR, Ivnitiski DM, Atanassov PB, Johnson GR (2010) High electrocatalytic activity of tethered multicopper oxidase-carbon nanotube conjugates. *Chem Commun* 46:6045–6047. <https://doi.org/10.1039/C0CC00911C>
89. Weigel MC, Tritscher E, Lisdat F (2007) Direct electrochemical conversion of bilirubin oxidase at carbon nanotube-modified glassy carbon electrodes. *Electrochem Commun* 9:689–693. <https://doi.org/10.1016/j.elecom.2006.10.052>
90. Shleev S, El Kasmi A, Ruzgas T, Gorton L (2004) Direct heterogeneous electron transfer reactions of bilirubin oxidase at a spectrographic graphite electrode. *Electrochem Commun* 6:934–939. <https://doi.org/10.1016/j.elecom.2004.07.008>
91. Holade Y, Both Engel A, Tingry S, Cherifi A, Cornu D, Servat K, Napporn TW, Kokoh KB (2014) Insights on hybrid glucose biofuel cells based on bilirubin oxidase cathode and gold-based anode nanomaterials. *ChemElectroChem* 1:1976–1987. <https://doi.org/10.1002/celec.201402142>
92. Chen Y, Gai P, Zhang J, Zhu JJ (2015) Design of an enzymatic biofuel cell with large power output. *J Mater Chem A* 3:11511–11516. <https://doi.org/10.1039/C5TA01432H>
93. Gai P, Song R, Zhu C, Ji Y, Chen Y, Zhang JR, Zhu JJ (2015) A ternary hybrid of carbon nanotubes/graphitic carbon nitride nanosheets/gold nanoparticles used as robust substrate electrodes in enzyme biofuel cells. *Chem Commun* 51:14735–14738. <https://doi.org/10.1039/C5CC06062A>
94. Ji Y, Gai P, Feng J, Wang L, Zhang J, Zhu JJ (2017) A Fe₃O₄-carbon nanofiber/gold nanoparticle hybrid for enzymatic biofuel cells with larger power output. *J Mater Chem A* 5:11026–11031. <https://doi.org/10.1039/C7TA01931A>
95. Kwon CH, Ko Y, Shin D, Kwon M, Park J, Bae WK, Lee SW, Cho J (2018) High-power hybrid biofuel cells using layer-by-layer assembled glucose oxidase-coated metallic cotton fibers. *Nat Commun* 9:4479. <https://doi.org/10.1038/s41467-018-06994-5>
96. Kwon CH, Ko Y, Shin D, Lee SW, Cho J (2019) Highly conductive electrocatalytic gold nanoparticle-assembled carbon fiber electrode for high-performance glucose-based biofuel cells. *J Mater Chem A* 7:13495–13505. <https://doi.org/10.1039/C8TA12342J>
97. Navae A, Narimani M, Korani A, Ahmadi R, Salimi A, Soltanian S (2016) Bimetallic Fe₁₅Pt₈₅ nanoparticles as an effective anodic electrocatalyst for non-enzymatic glucose/oxygen biofuel cell. *Electrochim Acta* 208:325–333. <https://doi.org/10.1016/j.electacta.2016.05.033>
98. Zhao Y, Fan L, Gao D, Ren J, Hong B (2014) High-power non-enzymatic glucose biofuel cells based on three-dimensional platinum nanoclusters immobilized on multiwalled carbon nanotubes. *Electrochim Acta* 145:159–169. <https://doi.org/10.1016/j.electacta.2014.09.006>
99. Wang Y, Chen J, Zhou C, Zhou L, Kong Y, Long H, Zhong S (2014) A novel self-cleaning, non-enzymatic glucose sensor working under a very low applied potential based on a Pt nanoparticle-decorated TiO₂ nanotube array electrode. *Electrochim Acta* 115:269–276. <https://doi.org/10.1016/j.electacta.2013.09.173>

100. Maity D, Rajendra Kumar RT (2019) Highly sensitive amperometric detection of glutamate by glutamic oxidase immobilized Pt nanoparticle decorated multiwalled carbon nanotubes (MWCNTs)/polypyrrole composite. *Biosens Bioelectron* 130:307–314. <https://doi.org/10.1016/j.bios.2019.02.001>
101. Sardesai NP, Karimi A, Andreescu S (2014) Engineered Pt-doped Nanoceria for oxidase-based bioelectrodes operating in oxygen-deficient environments. *ChemElectroChem* 1:2082–2088. <https://doi.org/10.1002/celec.201402250>
102. Li Y, Chen SM, Chen WC, Li YS, Ajmal Ali M, AlHemaid FMA (2011) Platinum nanoparticles (PtNPs) – laccase assisted biocathode reduction of oxygen for biofuel cells. *Int J Electrochem Sci* 6:6398–6409
103. Trifonov A, Stemmer A, Tel-Vered R (2019) Enzymatic self-wiring in nanopores and its applications in direct electron transfer biofuel cells. *Nanoscale Adv* 1:347–356. <https://doi.org/10.1039/C8NA00177D>
104. Bollella P, Mazzei F, Favero G, Fusco G, Ludwig R, Gorton L, Antiochia R (2017) Improved DET communication between cellobiose dehydrogenase and a gold electrode modified with a rigid self-assembled monolayer and green metal nanoparticles: the role of an ordered nanostructuration. *Biosens Bioelectron* 88:196–203. <https://doi.org/10.1016/j.bios.2016.08.027>
105. Liu L, Ci S, Bi L, Jia J, Wen Z (2017) Three-dimensional nanoarchitectures of co nanoparticles inlaid on N-doped macroporous carbon as bifunctional electrocatalysts for glucose fuel cells. *J Mater Chem A* 5:14763–14774. <https://doi.org/10.1039/C7TA04114D>
106. Sun L, Ma Y, Zhang P, Chao L, Huang T, Xie Q, Chen C, Yao S (2015) An amperometric enzyme electrode and its biofuel cell based on a glucose oxidase-poly (3-anilineboronic acid)-Pd nanoparticles bionanocomposite for glucose biosensing. *Talanta* 138:100–107. <https://doi.org/10.1016/j.talanta.2015.02.011>
107. Pakongpan S, Tuantranont A, Poo-arporn RP (2017) Magnetic nanoparticle-reduced graphene oxide nanocomposite as a novel bioelectrode for mediatorless-membraneless glucose enzymatic biofuels cells. *Sci Rep* 7:12882. <https://doi.org/10.1038/s41598-017-12417-0>
108. Gai P, Gu C, Hou T, Li F (2017) Ultrasensitive self-powered aptasensor based on enzyme biofuel cell and DNA bioconjugate: a facile and powerful tool for antibiotic residue detection. *Anal Chem* 89:2163–2169. <https://doi.org/10.1021/acs.analchem.6b05109>
109. Gu C, Gai P, Hou T, Li H, Xue C, Li F (2017) Enzymatic fuel cell-based self-powered homogeneous immunosensing platform via target-induced glucose release: an appealing alternative strategy for turn-on melamine assay. *ACS Appl Mater Interfaces* 9:35721–35728. <https://doi.org/10.1021/acsami.7b07104>
110. Wang Y, Zhang L, Cui K, Ge S, Zhao P, Yu J (2019) Paper-supported self-powered system based on a glucose/O₂ biofuel cell for visual microRNA-21 sensing. *ACS Appl Mater Interfaces* 11:5114–5122. <https://doi.org/10.1021/acsami.8b20034>
111. Bollella P, Fusco G, Stevar D, Gorton L, Ludwig R, Ma S, Boer H, Koivula A, Tortolini C, Favero G, Antiochia R, Mazzei F (2018) A glucose/oxygen enzymatic fuel cell based on gold nanoparticles modified graphene screen-printed electrode. Proof-of-concept in human saliva. *Sensors Actuators B Chem* 256:921–930. <https://doi.org/10.1016/j.snb.2017.10.025>
112. Göbel G, Beltran ML, Mudhenk J, Heinlein T, Schneider J, Lisdat F (2016) Operation of a carbon nanotube-based glucose/oxygen biofuel cell in human body liquids-performance factors and characteristics. *Electrochim Acta* 218:278–284. <https://doi.org/10.1016/j.electacta.2016.09.128>
113. Anastasova S, Crewther B, Bemnowicz P, Curto V, Ip HMD, Rosa B, Yang GZ (2017) A wearable multisensing patch for continuous sweat monitoring. *Biosens Bioelectron* 93:139–145. <https://doi.org/10.1016/j.bios.2016.09.038>
114. Jia W, Valdés-Ramírez G, Bandokar AJ, Windmiller JR, Wang J (2013) Epidermal biofuel cells: energy harvesting from human perspiration. *Angew Chem Int Ed* 52:7233–7236. <https://doi.org/10.1002/anie.201302922>

115. Xiao X, Siepenkotter T, Ó Conghaile P, Leech D, Magner E (2018) Nanoporous gold-based biofuel cells on contact lenses. *ACS Appl Mater Interfaces* 10:7107–7116. <https://doi.org/10.1021/acsami.7b18708>
116. Falk M, Andoralov V, Silow M, Toscano MD, Shleev S (2013) Miniature biofuel cell as a potential power source for glucose-sensing contact lenses. *Anal Chem* 85:6342–6348. <https://doi.org/10.1021/ac4006793>
117. Lloyd JR, Yong P, Macaskie LE (1998) Enzymatic recovery of elemental palladium by using sulfate-reducing bacteria. *Appl Environ Microbiol* 66:543–548
118. Jayaseelan C, Rahuman AA, Mohana Roopan S, Vishnu Kirthi A, Venkatesan J, Kim SK, Iyappan M, Siva C (2013) Biological approach to synthesize TiO₂ nanoparticles using *Aeromonas hydrophila* and its antibacterial activity. *Spectrochim Acta A* 107:82–89. <https://doi.org/10.1016/j.saa.2012.12.083>
119. Jayaseelan C, Rahuman AA, Vishnu Kirthi A, Marimuthu S, Santhoshkumar T, Bagavan A, Gaurav K, Karthik L, Bhaskara Rao KV (2012) Novel microbial route to synthesize ZnO nanoparticles using *Aeromonas hydrophila* and their activity against pathogenic bacteria and fungi. *Spectrochim Acta A* 90:78–84. <https://doi.org/10.1016/j.saa.2012.01.006>
120. Bunge M, Søbjerger LS, Rotaru AE, Gauthier D, Lindhardt AT, Hause G, Finster K, Kingshott P, Skrydstrup T, Meyer RL (2010) Formation of palladium(0) nanoparticles at microbial surfaces. *Biotechnol Bioeng* 107:206–215. <https://doi.org/10.1002/bit.22801>
121. Levar CE, Hoffman CL, Dunshee AJ, Toner BM, Bond DR (2017) Redox potential as a master variable controlling pathways of metal reduction by *Geobacter sulfurreducens*. *ISME J* 11:741–752. <https://doi.org/10.1038/ismej.2016.146>
122. Law N, Ansari S, Livens FR, Renshaw JC, Lloyd JR (2008) Formation of nanoscale elemental silver particles via enzymatic reduction by *Geobacter sulfurreducens*. *Appl Environ Microbiol* 74:7090–7093. <https://doi.org/10.1128/aem.01069-08>
123. Klaus T, Joerger R, Olsson E, Granqvist CG (1999) Silver-based crystalline nanoparticles, microbially fabricated. *Proc Natl Acad Sci U S A* 96:13611–13614. <https://doi.org/10.1073/pnas.96.24.13611>
124. De Corte S, Hennebel T, De Gussem B, Verstraete W, Boon N (2012) Bio-palladium: from metal recovery to catalytic applications. *Microb Biotechnol* 5:5–17. <https://doi.org/10.1111/j.1751-7915.2011.00265.x>
125. Shi L, Rosso KM, Clarke TA, Richardson DJ, Zachara JM, Fredrickson JK (2012) Molecular underpinnings of Fe(III) oxide reduction by *Shewanella oneidensis* MR-1. *Front Microbiol* 3:50. <https://doi.org/10.3389/fmicb.2012.00050>
126. Wang Q, Jones III AAD, Gralnick JA, Lin L, Buie CR (2019) Microfluidic dielectrophoresis illuminates the relationship between microbial cell envelope polarizability and electrochemical activity. *Sci Adv* 5:eaat5664. <https://doi.org/10.1126/sciadv.aat5664>
127. Dundas CM, Graham AJ, Romanovicz K, Keitz BK (2018) Extracellular electron transfer by *Shewanella oneidensis* controls palladium nanoparticle phenotype. *ACS Synth Biol* 7:2726–2736. <https://doi.org/10.1021/acssynbio.8b00218>
128. Fredrickson JK, Romine MF, Beliaev AS, Auchtung JM, Driscoll ME, Gardner TS, Nealon KH, Osterman AL, Pinchuk G, Reed JL, Rodionov DA, Rodrigues JLM, Saffarini DA, Serres MH, Spormann AM, Zhulin IB, Tiedje JM (2008) Towards environmental systems biology of *Shewanella*. *Nat Rev Microbiol* 6:592–603. <https://doi.org/10.1038/nrmicro1947>
129. De Windt W, Aelterman P, Verstraete W (2005) Bioreductive deposition of palladium (0) nanoparticles on *Shewanella oneidensis* with catalytic activity towards reductive dechlorination of polychlorinated biphenyls. *Environ Microbiol* 7:314–325. <https://doi.org/10.1111/j.1462-2920.2005.00696.x>
130. Mertens B, Blothe C, Windey K, De Windt W, Verstraete W (2007) Biocatalytic dechlorination of lindane by nano-scale particles of Pd(0) deposited on *Shewanella oneidensis*. *Chemosphere* 66:99–105. <https://doi.org/10.1016/j.chemosphere.2006.05.018>

131. De Corte S, Hennebel T, Fitts JP, Sabbe T, Bliznuk V, Verschuere S, van der Lelie, Verstraete W, Boon N (2011) Biosupported bimetallic Pd-Au nanocatalysts for dechlorination of environmental contaminants. *Environ Sci Technol* 45:8506–8513. <https://doi.org/10.1021/es2019324>
132. Wu R, Tian X, Xiao Y, Ulstrup J, Mølager Christensen HE, Zhao F, Zhang J (2018) Selective electrocatalysis of biofuel molecular oxidation using palladium nanoparticles generated on *Shewanella oneidensis* MR-1. *J Mater Chem A* 6:10655–10662. <https://doi.org/10.1073/10.1039/C8TA01318G>
133. Kimber RL, Lewis EA, Parmeggiani F, Smith K, Bagshaw H, Starborg T, Joshi N, Figueroa AI, van der Laan G, Cibirin G, Gianolio D, Haigh SJ, Patrick RAD, Turner NJ, Lloyd JR (2018) Biosynthesis and characterization of copper nanoparticles using *Shewanella oneidensis*: applications for click chemistry. *Small* 14:1703145. <https://doi.org/10.1002/smll.201703145>
134. Sveidal Søbberg L, Gauthier D, Thyboe Lindhardt A, Bunge M, Finster K, Meyer RL, Skrydstrup T (2009) Bio-supported palladium nanoparticles as a catalyst for Suzuki-Miyaura and Mizoroki-heck reactions. *Green Chem* 11:2041–2046. <https://doi.org/10.1039/B918351P>
135. Creamer NJ, Mikheenko IP, Yong P, Deplanche K, Sanyahumbi D, Wood J, Pollmann K, Merroun M, Selenska-Pobell S, Macaskie LE (2007) Novel supported Pd hydrogenation bionanocatalyst for hybrid homogeneous/heterogeneous catalysis. *Catal Today* 128:80–87. <https://doi.org/10.1016/j.cattod.2007.04.014>
136. Mabbett AN, Sanyahumbi D, Yong P, Macaskie LE (2006) Biorecovered precious metals from industrial wastes: single-step conversion of a mixed metal liquid waste to a bioinorganic catalyst with environmental application. *Environ Sci Technol* 40:1015–1021. <https://doi.org/10.1021/es0509836>
137. Mabbett AN, Macaskie LE (2002) A new bioinorganic process for the remediation of Cr(VI). *J Chem Technol Biotechnol* 77:1169–1175. <https://doi.org/10.1002/jctb.693>
138. Yong P, Rowson NA, Farr JPG, Harris IR, Macaskie LE (2002) Bioreduction and biocrystallization of palladium by *Desulfovibrio desulfuricans* NCIMB 8307. *Biotechnol Bioeng* 80:369–379. <https://doi.org/10.1002/bit.10369>
139. Foulkes JM, Malone KJ, Coker VS, Turner NJ, Lloyd JR (2011) Engineering a biometallic whole cell catalyst for enantioselective deracemization reactions. *ACS Catal* 1:1589–1594. <https://doi.org/10.1021/cs200400t>
140. Reich S, Agarwal S, Greiner A (2019) Electrospun bacteria-gold nanoparticle/polymer composite mesofiber nonwovens for catalytic applications. *Macromol Chem Phys* 220:1900007. <https://doi.org/10.1002/macp.201900007>

Chiral Metal Nanoparticles for Asymmetric Catalysis



Tomohiro Yasukawa and Shū Kobayashi

Contents

1	Introduction	280
2	Chiral Amine-Modified Nanoparticle Catalysts	281
2.1	Cinchona Alkaloids and Their Derivatives Modified Nanoparticle Catalysts	282
2.2	Chiral Diamine-Modified Nanoparticle Catalysts	284
2.3	Amino Acid-Modified Nanoparticle Catalysts	286
3	Chiral Phosphine-Modified Nanoparticle Catalysts	289
3.1	Asymmetric Hydrogenation	289
3.2	Asymmetric Hydrosilylation	292
3.3	Asymmetric C–C Bond-Forming Reaction	294
3.4	Miscellaneous	298
4	Chiral N-Heterocyclic Carbene-Modified Nanoparticle Catalysts	299
5	Chiral Diene-Modified Nanoparticle Catalysts	302
6	Other Chiral Molecules as Modifiers	306
7	Chiral Polymer-Stabilized Nanoparticle Catalysts	307
8	Conclusion	310
	References	311

Abstract Metal nanoparticles modified by chiral ligands or chiral polymers, called as “chiral metal nanoparticles,” are promising catalysts for asymmetric organic transformations. In this chapter, the class of chiral modifiers is focused to overview advance in the field of metal nanoparticle-catalyzed asymmetric reactions.

T. Yasukawa

Green and Sustainable Chemistry Social Cooperation Laboratory, Graduate School of Science,
The University of Tokyo, Bunkyo-ku, Tokyo, Japan

S. Kobayashi (✉)

Green and Sustainable Chemistry Social Cooperation Laboratory, Graduate School of Science,
The University of Tokyo, Bunkyo-ku, Tokyo, Japan

Department of Chemistry, School of Science, The University of Tokyo, Bunkyo-ku, Tokyo,
Japan

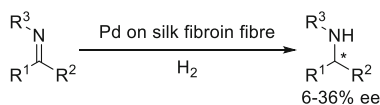
e-mail: shu_kobayashi@chem.s.u-tokyo.ac.jp

Keywords Asymmetric catalysis · Chiral metal nanoparticles · Chiral modifier · Heterogeneous catalysts

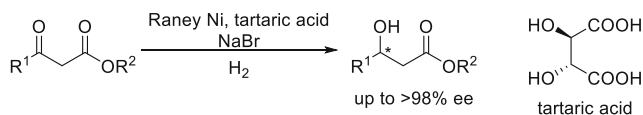
1 Introduction

Development of enantioselective catalysis is an important subject as it is an effective process to synthesize target chiral molecules that are further led to useful compounds such as medicines and pesticides [1, 2]. Research using small chiral molecules including metal complexes and organocatalysts as catalysts is a current mainstream in the field of asymmetric catalysis. Numerous homogeneous small molecule catalysts were developed to date, and various transformations were achieved with excellent enantioselectivity. On the other hand, use of chiral molecule-modified surface of metal nanoparticles or supported metal species for asymmetric catalysis was overwhelmingly less developed, though this strategy is attractive because supported metal species are easily separated from a reaction mixture and reused. Indeed, this concept was realized in the early stage of investigations for asymmetric catalysis. In 1956, Akabori et al. reported a Pd catalyst immobilized on silk fibroin fiber for asymmetric hydrogenation of imines as a first example of surface asymmetric catalysis (Scheme 1) [3]. In this reaction, enantioselectivity was still low, and the structure of a chiral modifier was not well-defined. Several years later, the same group reported small chiral molecules such as amino acid- or tartaric acid-modified Raney Ni-catalyzed asymmetric hydrogenations of carbonyl compounds achieving high enantioselectivity (Scheme 1) [4–6]. These studies proved that highly enantioselective catalysis by a chiral ligand-modified metal surface was possible. In 1979, Orito et al. reported asymmetric hydrogenation of methyl pyruvate or

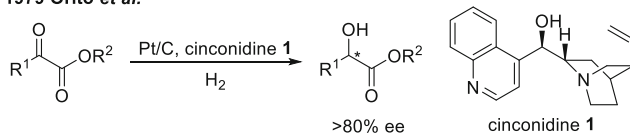
1956 Akabori *et al.*



1963 Akabori *et al.*

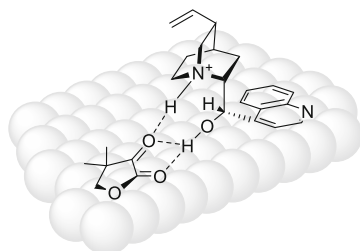


1979 Orito *et al.*



Scheme 1 Early examples of asymmetric catalysis using supported metals and chiral modifiers

Scheme 2 Proposed reaction mechanism of Orito reaction

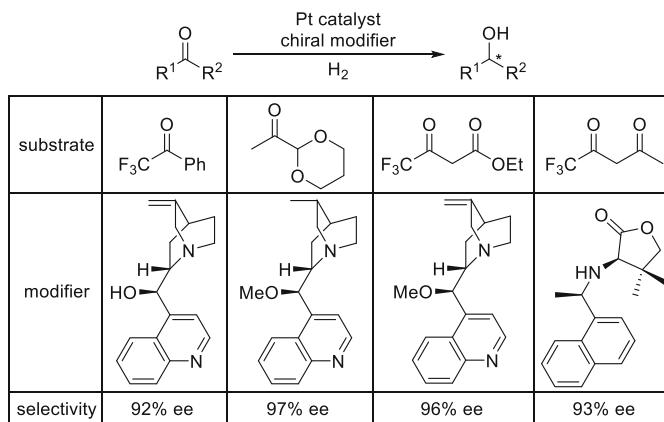


methyl benzoylformate catalyzed by cinchonidine **1**-modified Pt on carbon (Scheme 1) [7, 8]. This reaction has attracted interests of many researchers in surface chemistry as well as organic chemistry and catalytic chemistry and was extensively studied even almost 40 years after the discovery to improve the catalyst system and to clarify the reaction mechanism [9–15]. Since there are several excellent review papers that summarize studies of Orito-type reactions and related reactions [16–20], this chapter just briefly introduces it and does not explain more details.

Thanks to these pioneering studies, chiral ligand-modified nanoparticle catalysts, called as chiral nanoparticles in this chapter, were gradually studied, and several reactions including more challenging asymmetric C–C bond-forming reactions could be achieved in high enantioselectivity. Undoubtedly, structures of chiral modifiers are the most important factor, and their role is sometimes not just creation of chiral environments. For example, it was suggested that a cinchonidine modifier in Orito reaction chemisorbed on the metal surface through the interaction of an aromatic moiety and interacted with a substrate on the metal surface to form the individual 1:1 diastereomeric complex through hydrogen bonds (Scheme 2) [21–23]. Therefore, in this chapter, we categorized a class of chiral modifier by structure and overviewed advance of chiral nanoparticle catalysis. Several examples prove a great potential of chiral metal nanoparticles as heterogeneous asymmetric catalyst systems because of their robustness, activity, and unique selectivity. It should be noted that although the true active species was difficult to identify in most cases, several examples described the characteristic nature of chiral nanoparticle catalysts, which show different behavior from the corresponding homogeneous metal complex catalysts. On the other hand, catalytically active species should be carefully discussed since it is possible that a leached homogeneous metal complex is an actual active species. To examine it, several control experiments to evaluate heterogeneity of each catalysis were suggested [24], and we also cover such discussions.

2 Chiral Amine-Modified Nanoparticle Catalysts

Inspired by Orito's asymmetric hydrogenation reaction, cinchona alkaloids derivatives or simpler amines such as 1-(1-naphthyl)ethylamine [25–28] were examined for asymmetric hydrogenation of α -ketoesters [19]. By changing modifier structures,

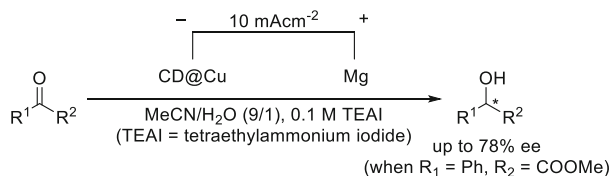


Scheme 3 Representative examples of suitable chiral modifier for Pt-catalyzed asymmetric hydrogenation of various activated ketones

applicable activated ketones were also broadened to a wide variety of activated ketones [29] including α -keto acetals [30], β -ketoesters [31], and trifluoromethyl-substituted ketones [32] (Scheme 3). However, substrate generality in each catalyst system was usually narrow. To expand the scope or develop new reactions, other types of chiral amine modifiers such as chiral diamine and amino acid derivatives were studied for chiral nanoparticle catalyst systems.

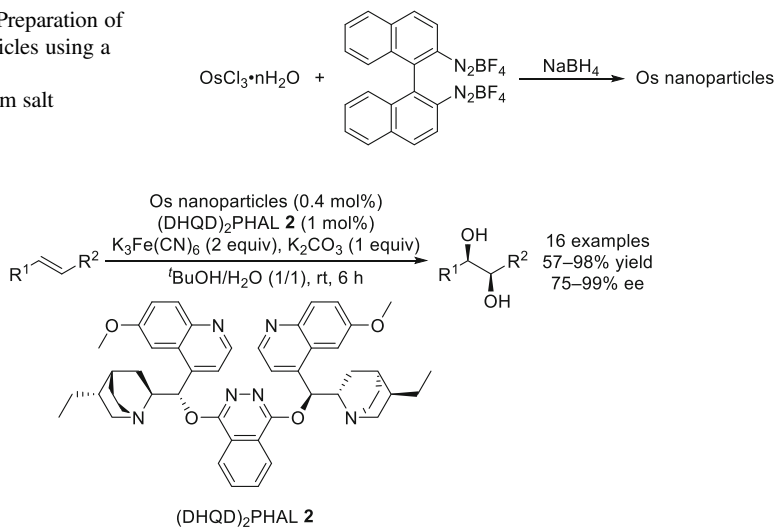
2.1 Cinchona Alkaloids and Their Derivatives Modified Nanoparticle Catalysts

In 2015, Wang and Lu et al. reported an alkaloid adsorbed on Cu nanoparticles for electrochemical asymmetric hydrogenation [33]. Cu nanoparticles were prepared by chemical reduction of Cu salts and pressed into a coin to use it as a cathode. In the presence of an alkaloid, cinchonidine **1** or cinchonine, asymmetric reduction of α -ketoesters proceeded in high yields and moderate enantioselectivities (up to 63% ee) under electrochemical conditions. Water was employed as a hydrogen source, and the reaction could be performed under mild conditions. In 2016, the same group improved the system to achieve the same reaction in good enantioselectivities (Scheme 4) [34]. The entrapment of alkaloids within Cu nanoparticles was attempted by the preparation of Cu nanoparticles in an aqueous solution of cinchonidine **1**. The average size of nanoparticles was 100 nm, and they were aggregated into a macroporous solid. EDX spectra and powder XRD pattern indicated cinchonidine **1** was immobilized within small cages of aggregated nanocrystals. Cinchonidine **1** was not washed out in an MeCN/H₂O co-solvent system, and the alkaloid/Cu composite (CD@Cu) could be reused for ten times without loss of activity and selectivity. In 2017, the same group developed bimetallic Pr@Cu nanoparticle



Scheme 4 Alkaloid@Cu nanoparticle composites for electrochemical asymmetric hydrogenation of ketones

Scheme 5 Preparation of Os nanoparticles using a binaphthyl bis-diazonium salt



Scheme 6 Bis-cinchona alkaloid-modified Os nanoparticles catalyzed asymmetric dihydroxylation of olefins

cathodes prepared by chemical reduction of Pt salts on Cu nanoparticles for electrochemical asymmetric hydrogenation [35]. The reactions with unactivated ketones were also performed in the presence of cinchonidine **1**; however, poor yields and moderate enantioselectivities were observed.

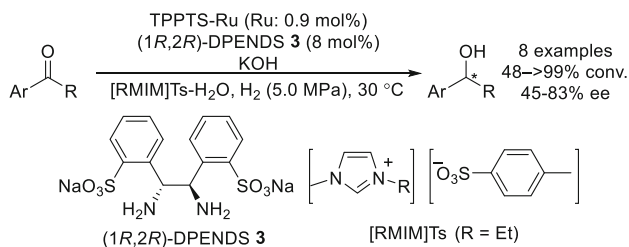
In 2018, Wu reported bis-cinchona alkaloid-modified Os nanoparticles catalyzed asymmetric dihydroxylation of olefins [36]. Os nanoparticle catalysts were prepared from a binaphthyl bis-diazonium salt as a precursor of stabilizer (Scheme 5). The absence of the diazonium group in the prepared Os nanoparticles was confirmed by FTIR analysis, and the formation of small nanoparticles (1.5–2.0 nm) was confirmed by TEM analysis. Bis-cinchona alkaloid (DHQD)₂PHAL **2** was found to be the best chiral modifier for asymmetric dihydroxylation. The ratio of Os loading and the amount of binaphthyl-based stabilizer were critical for both catalytic activity and enantioselectivity. Many substrates including styrene derivatives and unsaturated carbonyl compounds could be converted to the corresponding diols in high to excellent enantioselectivities (Scheme 6), while nitroolefin and unsaturated nitrile

could not react. The heterogeneous nature of the catalysis was verified by a Hg-poisoning experiment and a hot filtration experiment. And the catalyst could be reused for five cycles without significant loss of activity and aggregation of nanoparticles.

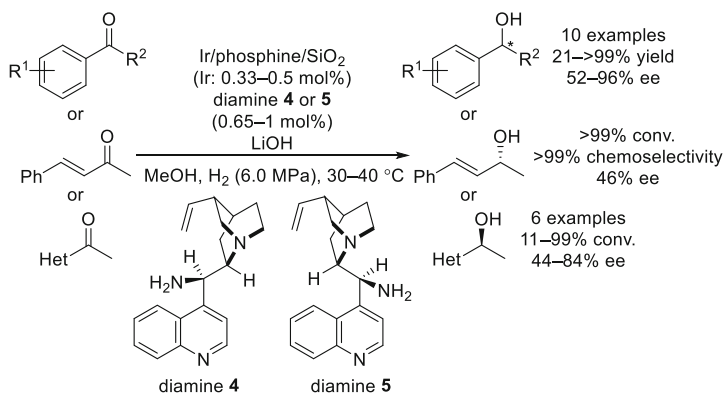
2.2 Chiral Diamine-Modified Nanoparticle Catalysts

Asymmetric hydrogenation of nonactivated aromatic ketones is an atom economical process to prepare chiral alcohols. However, early attempts using chiral ligand-modified heterogeneous catalysts, such as proline-modified Pd/C, cinchona-modified Pt/C, and chiral organotin-modified Pt or Rh, could not achieve high enantioselectivity ($\sim 20\%$ ee) [37–40].

In 2007, Zhao et al. reported *R,R*-1,2-diphenylethylene diamine ((*R,R*)-DPEN)-modified Ru on γ -Al₂O₃-catalyzed asymmetric hydrogenation of acetophenone [41]. A phosphine ligand was additionally employed to effect on the conversion and enantioselectivity, and a relatively high ee (60.5%) was obtained. In the same year, Chen et al. reported asymmetric hydrogenation of aromatic ketones in an ionic liquid using a monophosphine TPPTS [P(*m*-C₆H₄SO₃Na)]-stabilized Ru catalyst and chiral diamine **3** as a modifier [42]. RuCl₃·3H₂O was reduced by H₂ in the presence of TPPTS as a stabilizer to generate Ru nanoparticles whose size was about 5 nm. The reactions were performed in a co-solvent system with ionic liquid [RMIM]Ts (1-alkyl-3-methylimidazolium *p*-methylphenylsulfonates, R = ethyl, butyl, octyl, dodecyl, hexadecyl), and various aromatic ketones were hydrogenated with high conversions and moderate to high enantioselectivities (Scheme 7). The ionic liquid substituted with the longer alkyl chain decreased enantioselectivity because the Ru catalyst modified with hydrophilic chiral diamine **3** was reduced due to its high solubility in water. This Ru nanoparticle catalyst system was more active than the corresponding metal complex (RuCl₂(TPPTS)₂) under the same conditions, although similar high enantioselectivities were obtained by the metal complex. The chiral alcohol products could be separated by extraction with



Scheme 7 TPPTS-stabilized Ru in ionic liquids catalyzed asymmetric hydrogenation of aromatic ketones

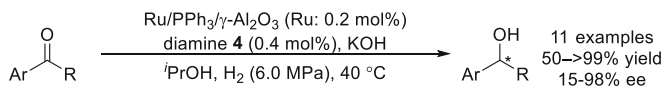


Scheme 8 Chiral diamine-modified Ir/phosphine/SiO₂ catalyzed asymmetric hydrogenation of various ketones

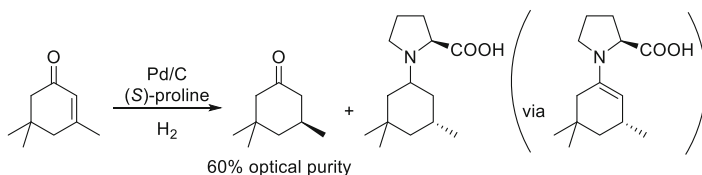
n-hexane, while the catalyst and diamine **4** remained in ionic liquid and water, and they were reused several times.

In 2008, Chen et al. reported a SiO₂-supported Ir catalyst for asymmetric hydrogenation of aromatic ketones [43]. The catalyst was stabilized by an additional phosphine and modified by cinchona alkaloid-derived chiral diamine **4** or **5** to facilitate the reaction with good to excellent enantioselectivities (Scheme 8). Addition of the phosphine is essential for both conversion and enantioselectivity. The corresponding homogeneous Ir/phosphine/diamine catalyst gave low enantioselectivity. The filtering test and mercury-poisoning test also supported the heterogeneous nature of this catalyst system. This catalyst system was applicable for asymmetric hydrogenation of an unsaturated ketone [44] and heteroaromatic methyl ketones (Scheme 8) [45]. In the former reaction, the corresponding allylic alcohol was obtained selectively with moderate enantioselectivity. In the latter reactions, the desired chiral alcohols were obtained with moderate to high enantioselectivities. The same group further investigated asymmetric hydrogenation of acetophenone using the cinchonidine **1**-stabilized Ir particles on SiO₂ with (1*S*,2*S*)-diphenylethylenediamine (DPEN) as a modifier [46]. The synergy between cinchonidine **1** and DPEN improved the reaction rate and enantioselectivity (up to 79.8% ee), while poor results were obtained in the absence of one of them. In 2014, they improved the Ir/PPh₃/SiO₂ system by using monodispersed and silanol-rich silica and 9-amino-(9-deoxy)epicinchonine as a chiral modifier [47]. They demonstrated that silanols enhanced the activity and enantioselectivity via hydrogen bonding between substrates and silanols in the heterogeneous asymmetric hydrogenation of aromatic ketones to achieve excellent enantioselectivities (up to 99.9% ee).

In 2010, Chen et al. reported phosphine-stabilized Ru on γ -Al₂O₃ for asymmetric hydrogenation of aromatic ketones in the presence of chiral diamine **4** as a modifier (Scheme 9) [48]. Under the optimized conditions, various acetophenone and propiophenone derivatives were reduced to the corresponding chiral alcohols with high to excellent enantioselectivities, while low enantioselectivity was observed in



Scheme 9 Chiral diamine-modified Ru/phosphine/ Al_2O_3 catalyzed asymmetric hydrogenation of aromatic ketones



Scheme 10 Pd on carbon with proline catalyzed asymmetric hydrogenation of isophorone

the case that R group was butyl. Control experiments using other modifiers such as cinchonine, cinchonidine **1**, and quinine indicated that the amine group in the 9-position of the modifier was essential.

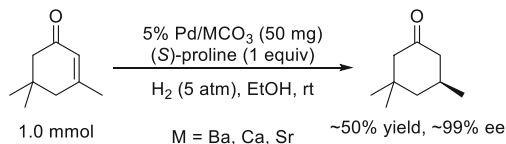
2.3 Amino Acid-Modified Nanoparticle Catalysts

Direct use of amino acids for chiral induction is attractive because amino acids are readily available chiral sources.

In 1989, Tungler et al. examined asymmetric hydrogenation of unsaturated ketones in the presence of Pd on carbon (Pd/C) with a stoichiometric amount of proline (Scheme 10) [49]. They found that dihydroisophorone can be obtained from isophorone in good enantioselectivity (60% optical purity). Initially, they proposed that enantioselectivity arise from the formation of a proline-/substrate-condensed product that adsorbed on the Pd surface [49, 50]. However, in 2006, Lambert et al. pointed out that this mechanism was not appropriate and the enantioselectivity was resulted from kinetic resolution [51, 52]. In this revised mechanism, initially hydrogenation on a heterogeneous catalyst affords a racemic product, and proline reacts preferentially with one enantiomer to form an enamine, which is further reduced to produce an amine, while an excess of the other enantiomer remains unreacted. Thus, the heterogeneous process is not an enantioselection step in this reaction system. In 2009, Lambert et al. attempted to design surface-tethered chiral modifiers to achieve a truly heterogeneous enantioselective process for the same reaction [53]. Pyrrolidine-contained chiral sulfide ligands that can robustly anchor to Pd nanoparticles were investigated, and the desired products were obtained in good yields and low enantioselectivities (up to 15% ee) in the presence of a catalytic amount of modifier.

In 2006, Török et al. examined proline-modified base-supported Pd catalysts for asymmetric hydrogenation of isophorone [54]. They found that the activity of

Scheme 11 Proline-modified, base-supported Pd catalyzed asymmetric hydrogenation of isophorone



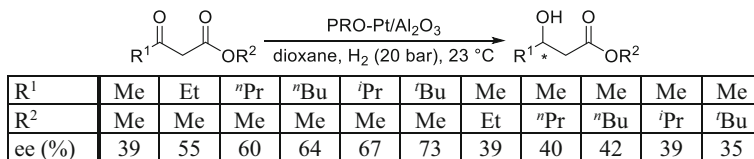
alkaline earth metal carbonate-supported catalysts produced significant secondary kinetic resolution with excellent enantioselectivity (Scheme 11). The use of basic supports enhanced proline adsorption on the Pd catalyst through an ionic interaction, and a modifier adsorption was a crucial factor in asymmetric hydrogenation. In 2015, the same group investigated aminomethylated polystyrene-supported Pd catalysts for asymmetric hydrogenation of isophorone [55]. In these catalyst systems, a direct enantioselective proline-modified hydrogenation of isophorone occurred without the contribution of a secondary kinetic resolution; however, enantioselectivity was moderate (up to 51% ee).

In 2015, Meemken et al. studied the surface processes occurring at the methanol-Pd catalyst interface using attenuated total reflection infrared spectroscopy to clarify the role of the heterogeneous catalyst in asymmetric hydrogenation of isophorone [56]. They revealed the existence of two competing reaction pathways that were kinetic resolution and Pd-catalyzed stereoselective hydrogenation. The reaction was controlled by these pathways depending on surface coverage of the Pd catalyst.

Use of catalytic amounts of amino acids as chiral modifiers for asymmetric catalysis is also possible.

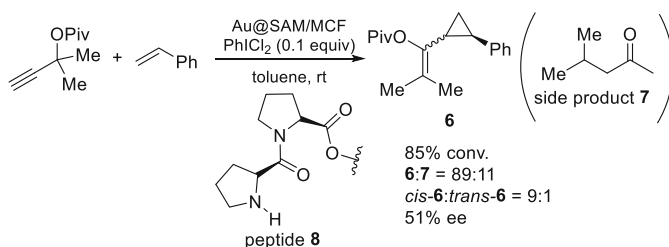
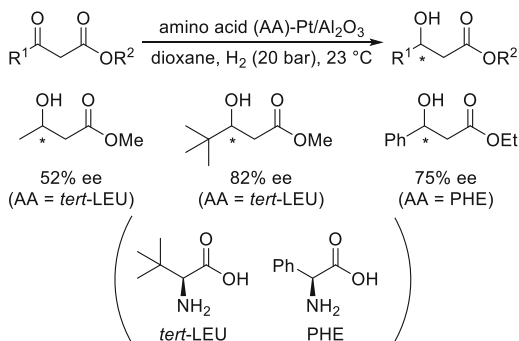
In 2013, Kunz et al. examined cysteine and its derivatives to functionalize Pt nanoparticles, and asymmetric hydrogenation of 2-butanone was demonstrated [57]. Chiral induction occurred in this system although enantioselectivity was very low (up to 9% ee). In 2015, the same group studied proline-functionalized Pt nanoparticles supported on alumina (PRO-Pt/Al₂O₃) for asymmetric hydrogenation of acetophenone [58]. Phenyl-1-ethanol was selectively obtained with low enantioselectivity (14% ee), while unprotected Pt nanoparticles gave a mixture of phenyl-1-ethanol and cyclohexyl-1-ethanol. An enhanced rate toward phenyl-1-ethanol was found for proline-functionalized Pt nanoparticles in comparison with unprotected ones. They also investigated the effect of particle size on the asymmetric catalytic properties of supported proline-functionalized Pt nanoparticles [59]. An asymmetric hydrogenation of ethylacetoacetate was chosen as a model, and moderate enantioselectivity (up to 34% ee) was obtained. The enantioselectivity was not altered by the particle size, suggesting that the selectivity was primarily determined by the ligand-reactant interaction that worked between the carbonyl group of the substrate and the N-H group of proline. On the other hand, the activity was determined by the particle size.

In 2017, Kunz et al. applied PRO-Pt/Al₂O₃ for asymmetric hydrogenation of β -ketoesters [60]. The effect of R¹ substituents was studied, and good enantioselectivity (73% ee) was obtained when R¹ group was bulky *tert*-butyl group (Scheme 12). In 2018, the same group reported further examination of the effects of amino acids for the same reaction system [61]. Various combinations of substrates and amino acids



Scheme 12 PRO-Pt nanoparticles catalyzed asymmetric hydrogenation of β -ketoesters

Scheme 13 Amino acid-functionalized Pt nanoparticles catalyzed asymmetric hydrogenation of β -ketoesters

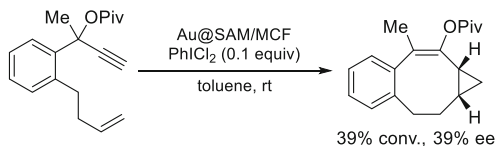


Scheme 14 Au@SAM/MCF-17 catalyzed asymmetric intermolecular cyclopropanation

as chiral ligands for nanoparticles were screened to enhance enantioselectivity. High enantioselectivity (up to 82% ee) was observed when bulky substituents were introduced to both substrate and chiral ligand (Scheme 13). Experimental results and simulations suggested that the NH group and the COOH group of the ligand might interact with two carbonyl groups of the reactant.

In 2013, Toste and Somorjai et al. developed Au nanoparticle catalysts immobilized on a chiral self-assembled monolayer (SAM) on the surface of a mesoporous silica support for asymmetric cyclopropanation reactions [62]. Amino acids were attached to the surface of the mesoporous silica (MCF-17) through the OH functionalities to create a chiral SAM. Au ions were introduced to the support, and the encapsulated Au ions were reduced to nanoparticles by exposure to H₂ atmosphere. The obtained Au nanoparticles catalyst (Au@SAM/MCF) was employed in the intermolecular cyclopropanation reaction of styrene with propargyl pivalate (Scheme 14). In order to generate real active Au catalysts within the

Scheme 15 Au@SAM/MCF-17 catalyzed asymmetric intramolecular cyclopropanation



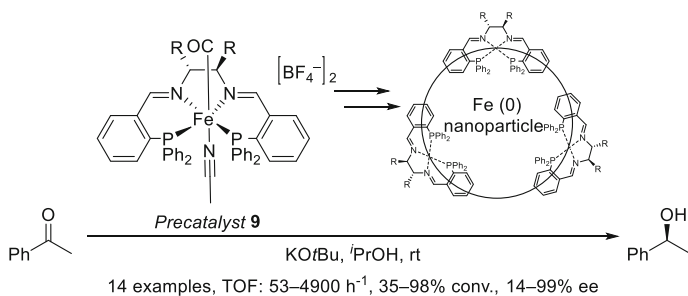
heterogeneous support, 0.1 equiv. of an oxidizer was used for the reaction. The desired product **6** was obtained in good diastereoselectivity and moderate enantioselectivity, when peptide **8** was immobilized on the surface of the mesoporous silica. The corresponding homogeneous system using AuCl₃ and unsupported diproline in the intermolecular reaction showed low yield and no enantioselection. While no leaching of Au complexes to a solution phase was confirmed by ICP analysis, in situ near-edge X-ray adsorption fine structure (NEXAFS) measurements under the reaction conditions proved the formation of Au(III) ions as active species, which were generated from Au(0) nanoparticles by oxidation with an externally added oxidant, PhICl₂. The same catalyst could be also used for the asymmetric intramolecular cyclopropanation reactions, although moderate conversion and enantioselectivity were observed (Scheme 15). Although the enantioselectivity was not enough high, the advantages of the surrounding chiral SAM for the formation of a mesoscale enantioselective catalyst were noted.

3 Chiral Phosphine-Modified Nanoparticle Catalysts

Chiral phosphorus ligands have played an important role in the development of asymmetric catalysis. Since early investigations of asymmetric hydrogenation in the period of 1970–1980, thousands of efficient chiral phosphine ligands with diverse structures have been developed [63–65]. They have been extensively utilized in both academic research and industry for not only asymmetric hydrogenation but also asymmetric C–C bond-forming reactions. Inevitably, chiral phosphines were examined as a modifier for metal nanoparticles, and various asymmetric catalysis including asymmetric C–C bond-forming reactions were developed. This section also covered phosphine modifiers that contain amine or hydroxy group as a coordination site. Since there are many types of chiral phosphine modifiers, subsections were categorized by type of reactions.

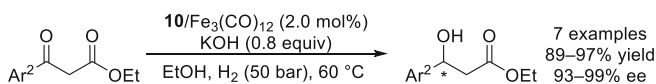
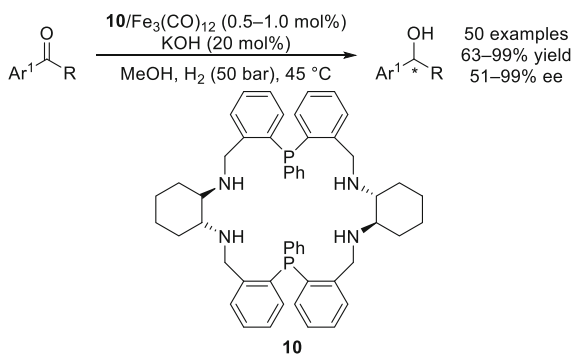
3.1 Asymmetric Hydrogenation

In 2009, Morris et al. developed chiral Fe complex **9** with a PNNP-type tetradentate ligand-catalyzed asymmetric transfer hydrogenation of ketones (Scheme 16) [66]. They found that these Fe pre-catalysts showed an induction period during catalysis [67], and in 2012, their further mechanistic investigations strongly



Scheme 16 Chiral Fe nanoparticles as proposed active species catalyzed asymmetric transfer hydrogenation of ketones

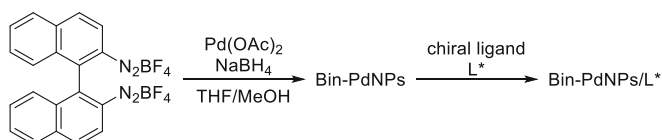
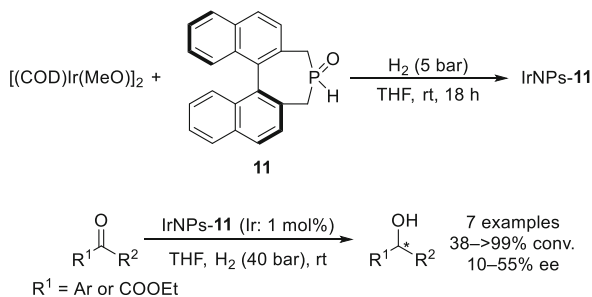
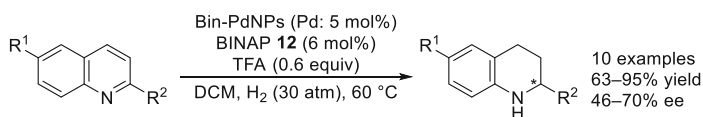
Scheme 17 Chiral Fe species catalyzed asymmetric hydrogenation of aromatic ketones



Scheme 18 Chiral Fe species catalyzed asymmetric hydrogenation of β -ketoesters

suggested PNNP ligand-modified Fe(0) nanoparticles as the active species in the reaction system [68, 69]. STEM analysis showed that Fe nanoparticles were approximately 4.5 nm in diameter, SQUID analysis revealed that the catalytic mixture contained a superparamagnetic species, and XPS analysis confirmed the formation of Fe(0) species. Poisoning test using PMe_3 completely inhibited the reaction, and the result of the reaction with a polymer-immobilized substrate also supported that Fe nanoparticles were active species. This is a rare example of highly active chiral zerovalent nanoparticles not based on precious metals. According to DFT studies, the process, in which the pre-catalyst **9** loses its acetonitrile ligand and is reduced to an Fe(0) species, is energetically favorable [70].

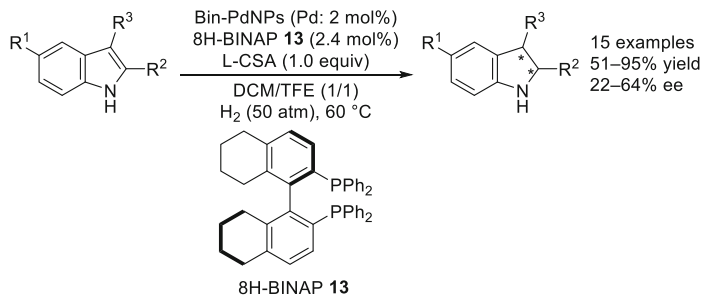
In 2014, Gao et al. reported asymmetric hydrogenation reactions catalyzed by chiral Fe catalysts [71]. An iron carbonyl complex with chiral 22-membered macrocyclic ligand **10** was found to be effective for asymmetric hydrogenation of aryl ketones including heteroaromatics (Scheme 17) and β -ketoesters (Scheme 18) under

Scheme 19 Chiral iridium nanoparticles catalyzed asymmetric hydrogenation of ketones**Scheme 20** Preparation of Pd nanoparticles using a binaphthyl bis-diazonium salt**Scheme 21** Bin-PdNPs catalyzed asymmetric hydrogenation of quinolines

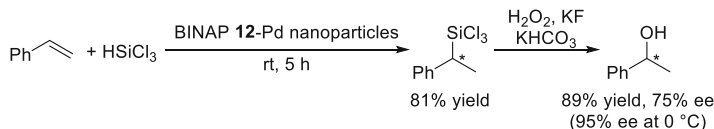
basic conditions. Broad substrate generality was achieved with good to excellent enantioselectivities. Several mechanistic observations indicated that active species in the Fe catalyst system might be heterogeneous with **10**-modified Fe particles. For examples, dynamic light scattering confirmed the existence of Fe particles, and a significant poisoning effect was observed.

In 2016, Leeuwen et al. reported a chiral secondary phosphine oxide-modified Ir nanoparticle catalyst for asymmetric hydrogenation of ketones [72]. Ir nanoparticles (IrNPs-**11**) were prepared by H_2 reduction of an Ir salt in the presence of 0.5 eq. (based on Ir) of enantiopure phosphine oxide **11** (Scheme 19). The non-supported IrNPs-**11** could catalyze asymmetric hydrogenation of aromatic ketones and ethyl pyruvate to afford the corresponding alcohols in low to moderate enantioselectivities (Scheme 19). A mercury-poisoning experiment led to the complete inhibition of the reaction, indicating that the nanoparticles were responsible for the catalysis.

In 2017, Wu et al. reported chiral diphosphine-modified Pd nanoparticle catalysts for asymmetric hydrogenation of N-heteroaromatics [73]. Pd nanoparticle catalysts were prepared from a binaphthyl bis-diazonium salt as a precursor of a stabilizer and were modified by chiral ligands (Scheme 20). Chiral Pd nanoparticles modified by 2,2'-bis(diphenylphosphino)-1,1'-binaphthyl (BINAP) **12** were effective for asymmetric hydrogenation of quinolines in the presence of an acid, and the corresponding tetrahydroquinolines were obtained in moderate to good enantioselectivities (Scheme 21). When the chiral ligand was changed to 8H-BINAP **13**, the catalyst



Scheme 22 Bin-PdNPs catalyzed asymmetric hydrogenation of indoles



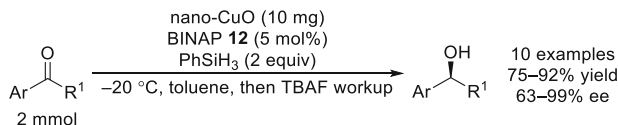
Scheme 23 BINAP 12-Pd nanoparticles catalyzed asymmetric hydrosilylation of styrene

system could be applied to asymmetric hydrogenation of indoles with moderate enantioselectivities (Scheme 22).

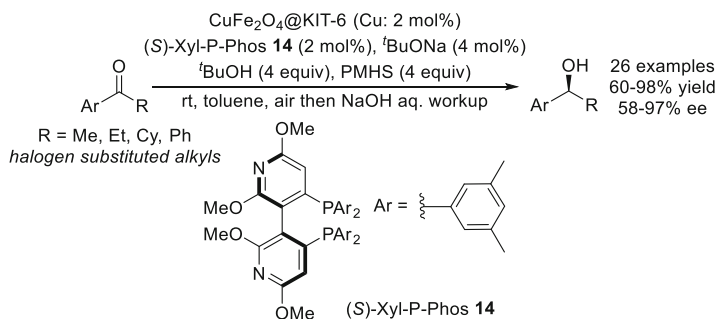
3.2 Asymmetric Hydrosilylation

Asymmetric hydrosilylation is a powerful method to synthesize chiral alcohols from prochiral compounds such as ketones and olefins, because the C–Si bonds can be easily oxidized and O–Si bonds can be easily hydrolyzed to afford the corresponding alcohols [74]. In 2003, Fujihara et al. reported BINAP 12-modified Pd nanoparticles catalyzed asymmetric hydrosilylation of styrene (Scheme 23) [75]. Chiral Pd nanoparticles were prepared from K_2PdCl_4 by the reduction with $NaBH_4$ in the presence of BINAP 12, and a small size of nanoparticles with narrow dispersity (2.0 ± 0.5 nm) was confirmed by TEM analysis. The BINAP 12-stabilized Pd nanoparticles could catalyze asymmetric hydrosilylation of styrene, and an excellent enantioselectivity was observed, while the corresponding BINAP 12-Pd complex could not catalyze this reaction under the same reaction conditions.

In 2007, Kantam et al. reported nanocrystalline copper oxide (nano-CuO), which possessed high surface area ($136 \text{ m}^2/\text{g}$) and a small particle size (7–9 nm), catalyzed asymmetric hydrosilylation of aromatic ketones [76]. In the presence of BINAP 12 as a chiral modifier, the reactions with phenylsilane proceeded well for various aromatic ketones to afford the corresponding chiral alcohols in good to excellent enantioselectivities after workup with TBAF (Scheme 24). The catalyst could be reused for four times without significant loss of activity and selectivity. No reaction occurred in the filtrate obtained after removal of the solid catalyst indicating that the



Scheme 24 Nano-CuO with BINAP **12** catalyzed asymmetric hydrosilylation of aromatic ketones



Scheme 25 CuFe_2O_4 @KIT-6 with Xyl-P-Phos **14** catalyzed asymmetric hydrosilylation of aromatic ketones

active species were not leached out. XPS analysis revealed that both +2 and +1 oxidation states of Cu were observed after treatment with BINAP **12** and silane, while the fresh catalyst and the used catalyst showed the peak corresponding to +2 oxidation state. In 2009, the same group reported copper ferrite nanoparticles (CuFe_2O_4) for asymmetric hydrosilylation of aromatic ketones with polymethylhydrosiloxane (PMHS) as an inexpensive, nontoxic, and air-stable hydride source [77]. In the presence of the nanoparticles and BINAP **12**, various aromatic ketones and ketoesters were converted to the corresponding alcohols in moderate to excellent enantioselectivities at room temperature. The Cu catalyst could be magnetically separable and could be reused for three times without significant loss of activity and selectivity.

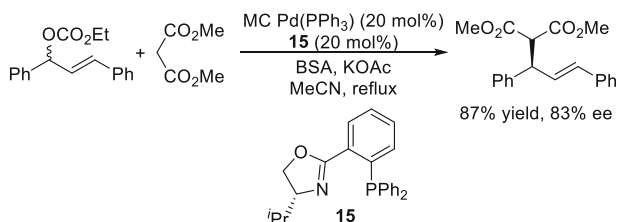
In 2014, Wu and Shi et al. developed CuFe_2O_4 nanoparticles supported on mesoporous silica (KIT-6) matrix for asymmetric hydrosilylation of aromatic ketones [78]. The reaction with PMHS proceeded in the presence of Xyl-P-Phos **14** as a chiral modifier at room temperature under air, and wide substrate generality including halo-substituted alkyl aryl ketones was demonstrated with good to excellent enantioselectivities (Scheme 25). The magnetically separated catalyst could be reused for four cycles; however, the enantioselectivity decreased slightly. Nitrogen sorption analysis indicated that the specific surface and the pore volume area decreased after the catalytic reaction. TGA analysis showed that more than 8 wt% organic species were recorded for the reused catalyst. These results indicated that the chiral ligands were strongly bound to the nanoparticles, and they were difficult to wash out.

3.3 Asymmetric C–C Bond-Forming Reaction

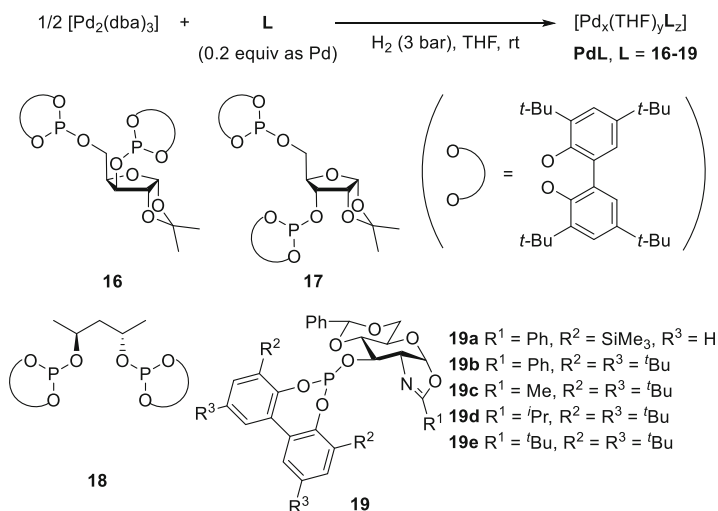
3.3.1 Palladium Nanoparticle Catalysis

In 2001, Kobayashi et al. developed a Pd(0) catalyst encapsulated by polystyrene (MC Pd(PPh₃)), which was successfully used for a catalytic asymmetric allylation reaction (Scheme 26) [79]. In the presence of chiral phosphine-oxazoline **15**, the allylated adduct was obtained in high yield with high enantioselectivity.

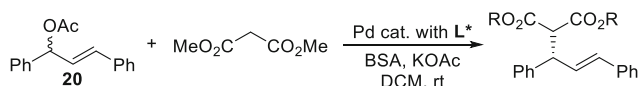
In 2004, Gómez, Philippot, and Chaudret et al. reported asymmetric allylic alkylation reactions catalyzed by colloidal Pd nanoparticles stabilized with chiral diphosphite **16** derived from a xylose backbone (Scheme 27) [80]. The catalytic performance of a molecular Pd complex prepared in situ from [Pd(C₃H₅)Cl]₂ with **16** was compared with that of nanoparticles (Scheme 28). In the case of a nanoparticle catalyst system, the reaction mainly proceeded with only one of the enantiomers of substrate **20**, and a very efficient kinetic resolution was demonstrated. On the other hand, no kinetic resolution was observed in the presence of the molecular complex.



Scheme 26 Microencapsulated (MC) Pd-catalyzed asymmetric allylation

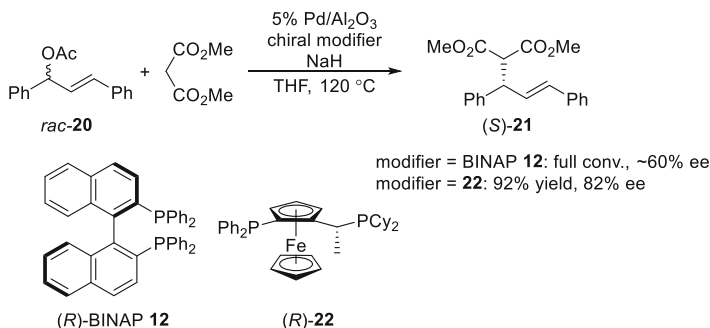


Scheme 27 Preparation of chiral diphosphite ligands stabilized Pd nanoparticles



Pd nanoparticle **16**: ~60% conv., 97% ee (recovered **20**: 89% ee)
 molecular complex: ([Pd(C₃H₅)Cl]₂ + **16**): 95% conv., 90% ee

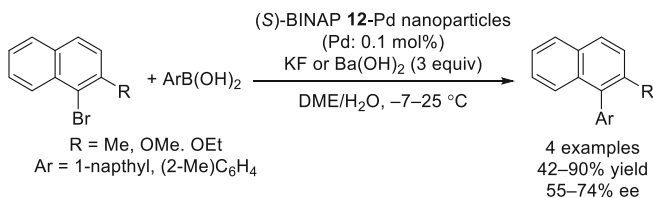
Scheme 28 Chiral diphosphite ligand **16**-based Pd catalysts for asymmetric allylic alkylation



Scheme 29 Chiral phosphine-modified Pd/Al₂O₃ catalyzed asymmetric allylic alkylation

In 2007, the same group reported detailed studies of this reaction with different chiral modifiers and substrates [81]. Three types of ligands **16–18** were examined, and Pd-**16** and Pd-**18** could give the product in excellent enantioselectivities. On the other hand, Pd-**17** easily decomposed into metal complex species and could not induce high enantioselectivity, while Pd-**16** and Pd-**18** did not decompose. Alkyl-substituted allyl acetates were not alkylated by using Pd-**16** or Pd-**18**, while the corresponding metal complex catalyst systems gave high conversions. In 2008, Diéguez, Gómez, and Leeuwen et al. reported chiral oxazolinyl-phosphite ligands **19a–19e**- modified Pd nanoparticle systems for the same reaction [82]. The nature of active species was studied using continuous-flow membrane reactor (CFMR), transmission electron microscope (TEM) observations, classical poisoning experiments, and kinetic measurements. Those studies proved the molecular nature of the truly active species that was leached out from the catalyst.

Heterogeneous Pd nanoparticle catalysts with chiral modifiers were also examined for asymmetric allylic alkylation. In 2005, Felpin and Landais reported the combination of Pd/C and (*R*)-BINAP **12** for the reaction of racemic **20** with diethylmalonate in water, and high enantioselectivity (80% ee) was achieved, while the yield was low (21%) [83]. In 2007, Baiker et al. reported BINAP **12**-modified Pd/Al₂O₃ catalyst systems for the reaction of racemic **20** with the sodium salt of dimethylmalonate (Scheme 29) [84]. Pd/Al₂O₃ treated under hydrogen gas showed good chemoselectivity (94%) and moderate enantioselectivity (~60% ee) in the presence of BINAP **12**. The enantioselectivity of this system was independent on reaction temperatures (60 and 120 °C), while the corresponding homogeneous complex catalyst showed poor enantioselectivity to give the opposite enantiomer of the

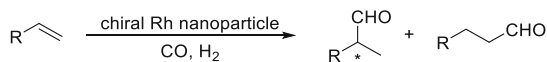


Scheme 30 BINAP **12**-modified Pd nanoparticles catalyzed asymmetric Suzuki-Miyaura coupling

product (*R*-**21**) at 60°C or above. In 2008, the same group improved the enantioselectivity of this reaction to 82% ee by changing the chiral modifier to ferrocenyl phosphine ligand **22** (Scheme 29) [85]. No temperature dependence on the enantioselectivity was observed again (at 60 and 120°C). In the corresponding homogeneous metal complex system, the same enantiomer of the product (*S*-**21**) was produced; however, the enantioselectivity was decreased by increasing the reaction temperature from 85% ee at 60°C to 55% ee at 120°C. In 2010, the same group reported detailed studies of the nature of the active species in Pd/Al₂O₃-BINAP **12** system and emphasized heterogeneity [86]. The oxidation state of Pd was elucidated by in situ X-ray absorption near-edge structure (XANES) analysis in a reaction mixture. Partially oxidized surface of Pd nanoparticles could be reduced by the reaction components, such as the solvent and sodium dimethyl malonate to maintain their reduced state during the reaction without Pd leaching. In contrast, the addition of a chlorinated solvent, such as chloroform, favored dissolution of metallic Pd to form homogeneous catalyst species.

In 2008, Fujihara et al. reported chiral bisphosphine-modified chiral Pd nanoparticles and their application to asymmetric Suzuki-Miyaura coupling reactions (Scheme 30) [87]. Pd nanoparticles were prepared by reduction of K₂PdCl₄ with NaBH₄ in the presence of a chiral phosphine. Several bisphosphine ligands were tested for the coupling reactions, and (*S*)-BINAP **12** was found to be the best chiral modifier in terms of activity, enantioselectivity, and stability of chiral Pd nanoparticles to afford axially chiral biaryl compounds in good enantioselectivities at low temperature (−7 to 25°C).

In 2009, Yamashita et al. reported that BINAP **12**-modified bimetallic Fe/Pd nanoparticles with core-shell structure catalyzed asymmetric Suzuki-Miyaura coupling reaction [88]. The catalyst worked for the coupling reaction between 1-bromo-2-methoxynaphthalene and 2-naphthyl boronic acid with moderate enantioselectivity (up to 48% ee). The nanoparticles were easily recovered by magnet and could be reused with keeping identical enantioselectivity without an external addition of a chiral modifier. The hot leaching test was conducted, and the reaction hardly occurred in the filtrate after removal of the catalyst.



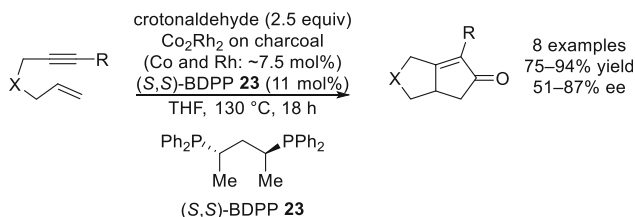
Scheme 31 Chiral Rh nanoparticles catalyzed asymmetric hydroformylation

3.3.2 Rh Nanoparticle Catalysis

Asymmetric hydroformylation of olefins using inexpensive syngas is a useful method to synthesize optical active aldehydes. While a chiral Rh complex was often used for this reaction [89] and Rh nanoparticles were also studied for non-asymmetric hydroformylation [90], development of chiral Rh nanoparticle systems for asymmetric hydroformylation is still a challenging topic (Scheme 31).

In 2000, Anderson et al. reported chiral diphosphine ligand-modified Rh/SiO₂·Al₂O₃ catalyzed asymmetric hydroformylation of styrene although enantioselectivity was low (up to 9% ee) [91]. In 2006, Li et al. reported asymmetric hydroformylation of styrene or vinyl acetate catalyzed by BINAP **12**-modified Rh/SiO₂ [92]. A good enantioselectivity (up to 72% ee) and 100% selectivity of a branched aldehyde for the hydroformylation was obtained; however, the conversion was poor (<10%). In 2008, the same group reported a different method to prepare modified Rh nanoparticles by one-pot chemical reduction of aqueous rhodium chloride dispersed in toluene in the presence of amphiphilic tetraoctylammonium bromide (TOAB) and (*R*)-BINAP **12** [93]. These BINAP **12**-modified Rh nanoparticles could be also immobilized on SiO₂ in vacuum by adsorption; however, no significant improvement of catalytic performance was observed. In 2008, Axet, Claver, and Philippot reported asymmetric hydroformylation of styrene using colloidal Rh nanoparticles modified with carbohydrate-derived diphosphite ligands [94]. With the addition of an excess amount of the ligand, high conversion, high regioselectivity, and moderate enantioselectivity (31% ee) were observed. In situ high-pressure (HP) NMR spectroscopic studies under catalytic conditions in the presence of chiral Rh nanoparticles led to detection of the hydridorhodium diphosphite complex [RhH(CO)₂(L)]. These results indicated that metal complex species generated from nanoparticles also worked as active species. Given that the difference of enantioselectivity between the molecular complex system and the nanoparticle system, a possibility that some activity comes from nanoparticles cannot be excluded. In 2018, Trzeciak et al. reported DNA-stabilized Rh nanoparticle catalysts for asymmetric hydroformylation [95]. In the presence of BINAP **12**, asymmetric hydroformylation of vinyl acetate proceeded to afford the corresponding branched product in moderate yield (~30%) and moderate enantioselectivity (49% ee). The analyses of the organic phase of the post-reaction mixtures by ³¹P NMR and IR indicated that a hydridorhodium complex, HRh(CO)₂(BINAP **12**), formed when Rh nanoparticles were dissolved under hydroformylation conditions.

Another way to utilize carbon monoxide for organic synthesis is Pauson-Khand reaction that is a [2 + 2 + 1] cycloaddition among an alkyne, an alkene, and carbon monoxide to construct cyclopentenone skeleton. In 2005, Chung et al. reported charcoal-immobilized Co/Rh heterobimetallic nanoparticles catalyzed asymmetric

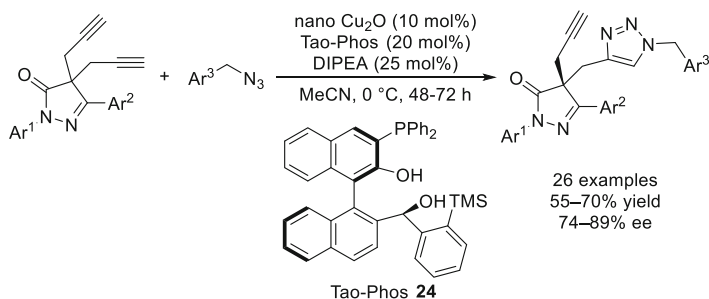


Scheme 32 Chiral diphosphine **23**-modified Co/Rh on charcoal catalyzed asymmetric Pauson-Khand reactions

Pauson-Khand-type reactions with a chiral diphosphine modifier [96]. Chiral diphosphine **23**-modified Co/Rh catalysts worked well for the reactions of several enynes with crotonaldehyde as a source of carbon monoxide proceeded, and the corresponding bicyclic cyclopentenones were obtained in high yields with moderate to good enantioselectivities (Scheme 32). The catalyst could be reused with the addition of a new chiral modifier in each run for five times without significant loss of yield and enantioselectivity. ICP-AES analysis of the reaction mixture obtained after three cycles detected 3.9 ppm of Co and 0.3 ppm of Rh species; however, the results of mercury-poisoning test supported heterogeneous nature of active species as Hg(0) completely eliminated further catalysis after the addition of Hg(0) to the reaction mixture.

3.4 Miscellaneous

In 2018, Xu et al. reported chiral Cu nanoparticles catalyzed desymmetrization of pyrazolone-derived bisalkynes through catalytic asymmetric Huisgen [3 + 2] cycloaddition [97]. CuF₂ was initially used for the screening of chiral ligands, and Tao-Phos **24** was found to be the best ligand. Several Cu salts were then examined, and Cu₂O whose particle size was ~20 nm gave also similar good performance with that of CuF₂. A Tao-Phos **24**-Cu nanoparticle system worked for several aromatic substrates with good to high enantioselectivities (Scheme 33). The nonlinear relationship between enantiopurity of the ligand and the product was observed. In contrast to a CuF₂ system, ESI-MS analysis in the Cu₂O system could not detect the corresponding Cu complex-derived peak indirectly suggesting that the formation and absorption of Cu/Tao-Phos **24** complex on the surface of nano Cu₂O could be recognized. A hot filtration test also supported the stable adsorption of Tao-Phos **24** on nano Cu₂O.



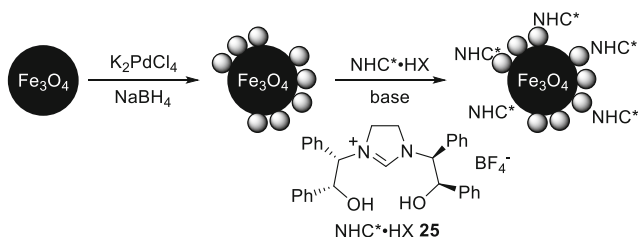
Scheme 33 Tao-Phos **24**-Cu nanoparticles catalyzed asymmetric Huisgen alkyne-azide cycloaddition of bisalkynes

4 Chiral N-Heterocyclic Carbene-Modified Nanoparticle Catalysts

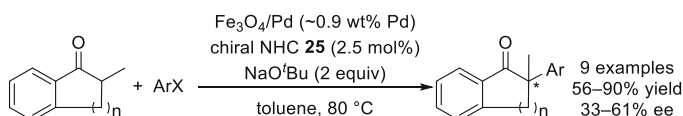
N-Heterocyclic carbenes (NHCs) have been widely studied not only as ligands for metal complexes and organocatalysts but also as stabilizers for metal nanoparticles because of their strong surface binding [98, 99].

In 2010, Glorius et al. reported the first successful application of chiral NHC for metal nanoparticle-catalyzed asymmetric reactions [100]. Chiral NHC **25** bearing hydroxy groups was utilized to modify Pd nanoparticles supported on magnetite ($\text{Fe}_3\text{O}_4/\text{Pd}$) (Scheme 34), and this system showed good catalytic performance for asymmetric α -arylation of ketones with aryl halides (Scheme 35). Various types of cyclic ketones and aryl halides could be employed to afford the corresponding α -arylated ketones in moderate enantioselectivities. Intramolecular α -arylation reactions of amide substrates could also proceed smoothly, and relatively high enantioselectivities were observed (Scheme 36). In the latter reaction (when $\text{X} = \text{Cl}$, $\text{R}^1 = \text{Bn}$, $\text{R}^2 = \text{Et}$, $\text{Ar} = \text{Ph}$), the corresponding homogeneous Pd complex catalyst system ($\text{Pd}(\text{allyl})\text{Cl}$)₂ and chiral NHC **25** gave a poor result (32% yield, 23% ee), indicating that an activity principle of the chiral nanoparticle system is different from that of a homogeneous complex system. The heterogeneous nature of the active species was further confirmed by a hot filtration test, a mercury-poisoning test, and trace-metal analysis by ICP-OES. The paramagnetic catalyst could be recovered using a magnet and reused for five cycles without significant loss of activity and selectivity.

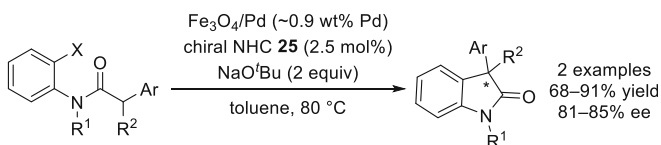
Several characterization of the obtained NHC-modified Pd catalyst ($\text{Fe}_3\text{O}_4/\text{Pd}/\mathbf{25}$) was conducted. XPS analysis confirmed that zero valency of Pd was maintained even after the surface modification. Attenuated total reflection infrared spectroscopy (ATR-IR) analysis could detect the NHC-modified surface by comparison of the spectra obtained from the free salt **25** and that of $\text{Fe}_3\text{O}_4/\text{Pd}/\mathbf{25}$, and marked differences were observed. Different BET surfaces were obtained for Fe_3O_4 , $\text{Fe}_3\text{O}_4/\text{Pd}$, and $\text{Fe}_3\text{O}_4/\text{Pd}/\mathbf{25}$.



Scheme 34 Preparation of chiral NHC **25** modified Fe₃O₄/Pd nanoparticles



Scheme 35 Chiral NHC **25**-Pd nanoparticle catalyzed asymmetric α -arylation of ketones with aryl halides

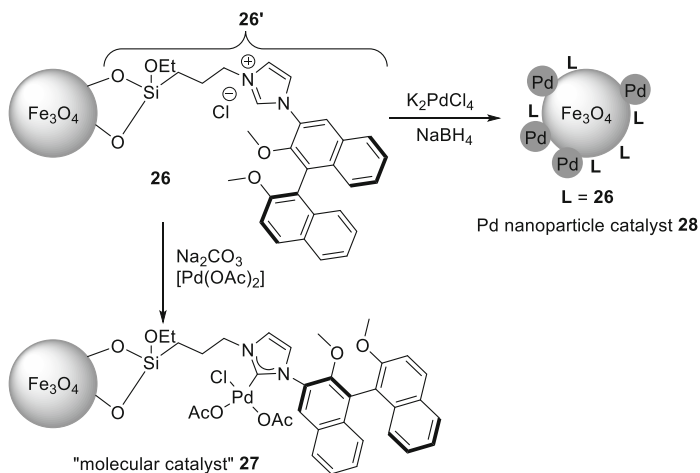


Scheme 36 Chiral NHC **25**-Pd nanoparticle catalyzed intramolecular asymmetric α -arylation of amides with aryl halides

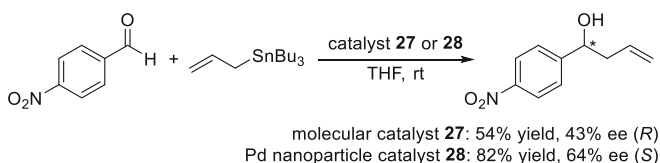
The same group examined a combination of Fe₃O₄/Pd and quinine as a chiral modifier for the asymmetric α -arylation reaction [101]. Good yields and enantioselectivities were obtained; however, a mercury-poisoning test and a filtration test indicated that the nature of the active species was not heterogeneous. These results emphasized the important role of NHC as a modifier for both stability and activity of the Pd nanoparticle catalysts.

In 2011, Glorius et al. developed Fe₃O₄-supported chiral NHC-based catalysts [102]. Molecular catalyst **27** was prepared by complexation of supported chiral NHC **26** with Pd(OAc)₂, while Pd nanoparticle catalyst **28** was prepared by the reduction of K₂PdCl₄ in the presence of the same supported NHC **26** (Scheme 37). The oxidation states of Pd in these catalysts were determined by XPS analysis to confirm the formation of a Pd complex or Pd(0) nanoparticles. These two heterogeneous Pd catalysts were applied to the asymmetric allylation of 4-nitrobenzaldehyde with allyltributyltin, and the results were compared (Scheme 38). The nanoparticle catalyst **28** gave better results for both yield and enantioselectivity, and surprisingly, the product was obtained with the opposite absolute configuration to that obtained with the molecular catalyst **27**.

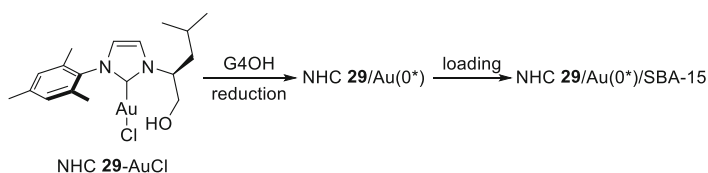
In 2018, Toste and Somorjai et al. reported heterogeneous Au nanoparticle catalysts with NHC ligands prepared by a strategy of supported dendrimer-



Scheme 37 Preparation of a molecular catalyst and a Pd nanoparticle catalyst from Fe_3O_4 -supported chiral NHC **26**



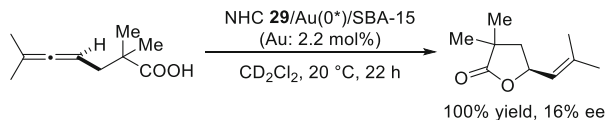
Scheme 38 Chiral NHC-Pd nanoparticle catalyzed asymmetric allylation of 4-nitrobenzaldehyde with allyltributyltin



Scheme 39 Preparation of supported Au nanoparticles with NHC ligand **29**

encapsulated metal clusters (DEMCs) [103]. *L*-Amino acid-derived chiral NHCs with a hydroxyl group were chosen as a modifier. The hydroxy group was expected to strengthen interactions of the NHC-ligated Au nanoparticle with SBA-15 and to facilitate proto-deauration that had been postulated to be turnover-limiting step [104]. Au nanoparticles were prepared from a chiral NHC-Au complex in the presence of a dendrimer (G4OH) that enhances the stability of the nanoparticles to aggregation, and they were further loaded on SBA-15 (Scheme 39). XPS, XANES, and time-of-flight secondary ion mass spectrometry (ToF-SIMS) analysis revealed that the Au nanoparticles prepared from the NHC complex were coated with monolayers of Au(I) species, presumably NHC-Au(I) complexes.

Scheme 40 Chiral NHC
29-Au nanoparticle
 catalyzed asymmetric
 lactonization



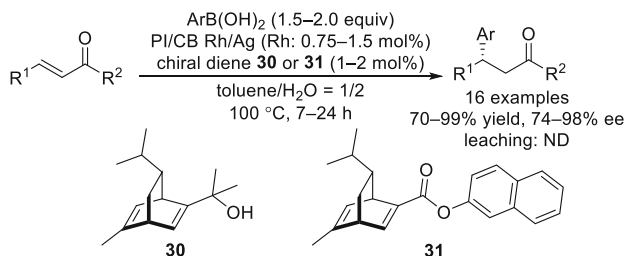
These chiral Au nanoparticle catalysts were applied to asymmetric lactonization of allene-carboxylic acids (Scheme 40). Eleven types of chiral NHCs were screened, and the desired products were obtained in quantitative yields and maximally 16% ee. Although the enantioselectivity was low, the metal complex NHC **29**-AuCl itself could not catalyze the reaction, and the reaction using NHC **29**-AuCl with AgBF₄ afforded the product in only 2% ee, indicating that NHC anchoring at the nanoparticle surface is crucial for enantioselectivity.

5 Chiral Diene-Modified Nanoparticle Catalysts

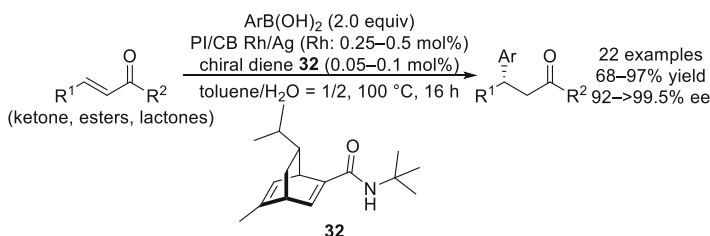
Chiral diene ligands were developed by Hayashi et al. for the first time and were applied for Rh-catalyzed asymmetric reactions [105]. While they initially utilized a bicyclo[2,2,1]heptadiene framework, Carreira et al. concurrently reported other chiral diene ligands with a bicyclo[2,2,2]octadiene framework for Ir-catalyzed asymmetric reactions [106]. Since higher activity of chiral diene-Rh complexes for asymmetric arylation reactions than chiral phosphine Rh complexes was realized, intensive researches of chiral dienes were promoted to develop new structures of chiral dienes and new ligands with hybrid structures including olefins [107–109].

One of the representative applications of chiral diene ligands is asymmetric 1,4-addition of arylboronic acids to unsaturated carbonyl compounds [110, 111]. Thanks to highly active chiral diene Rh complex catalysts, this type of reaction was widely studied to achieve various substrates including not only α - β -unsaturated carbonyl compounds but also aldehydes, imines, strained alkenes, and alkenyl arenes with excellent enantioselectivities [112]. Not only academic research but also a large-scale (>20 kg) process was demonstrated [113, 114]. However, active, reusable, and robust heterogeneous Rh catalysts for these reactions without metal leaching are demanded because of the high cost of Rh.

In 2012, Kobayashi et al. reported Rh nanoparticle catalysts immobilized on a composite of polystyrene-based copolymer with a cross-linking moiety and carbon black (PI/CB Rh) for asymmetric 1,4-addition of boronic acids to α , β -unsaturated ketones in the presence of a chiral modifier (Scheme 41) [115]. They initially examined chiral phosphine, (*S*)-BINAP **12**, as a chiral modifier for PI/CB Rh; however, a significant amount of Rh leaching was observed during the reaction. On the other hand, the use of a chiral diene as a modifier not only improved catalytic activity and enantioselectivity but also suppress a metal leaching to the detection limit of ICP-AES. Secondly, they examined bimetallic structures to achieve reactions with less reactive acyclic substrates. A bimetallic catalyst consisting of Rh and Ag (PI/CB Rh/Ag) was found to be the most active catalyst, and various enones were



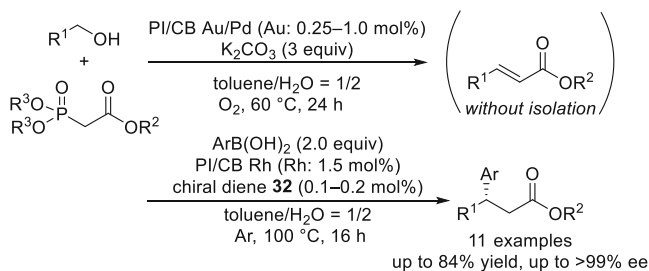
Scheme 41 Chiral diene-modified Rh nanoparticle catalysts for asymmetric 1,4-addition of arylboronic acids to enones



Scheme 42 Secondary amide-substituted chiral diene **32** modified Rh nanoparticle catalysts for asymmetric 1,4-addition of arylboronic acids to unsaturated esters

coupled to the desired α -arylated ketones in high yields with high enantioselectivities in the presence of a chiral modifier **30** or **31** without leaching of the metals. STEM analysis and EDS mapping revealed that alloy nanoparticles formed, and aggregation of Rh nanoparticles was not observed in PI/CB Rh/Ag. PI/CB Rh/Ag could be reused while keeping high yields and high enantioselectivities for 14 times.

In 2015, Kobayashi et al. improved their chiral Rh nanoparticle systems by employing a bifunctional chiral diene bearing a secondary amide moiety (Scheme 42) [116]. The new modifier **32** was supposed to possess a diene part for coordination to metal and a secondary amide group to interact with carbonyl substrates through hydrogen bonding. While the previous chiral diene **30** gave a low enantioselectivity (33% ee) for an asymmetric 1,4-addition to an α,β -unsaturated ester, chiral diene **32**-modified Rh nanoparticle systems dramatically improve the yield and enantioselectivity. Control studies using a tertiary amide-substituted chiral diene that gave a lower enantioselectivity (66% ee) suggested that the secondary amide moiety in diene **32** played an important role in achieving the excellent yield and enantioselectivity. Moreover, the amount of a diene loading could be reduced to 0.05–0.1 mol%, and broad substrate scope including formal synthesis of biologically important compounds was achieved with outstanding enantioselectivities. The Rh catalyst could be reused with the addition of a new portion of the chiral ligand, and no significant loss of the catalytic activity and enantioselectivity was observed over six runs. No metal leaching was confirmed by ICP-AES analysis of the crude



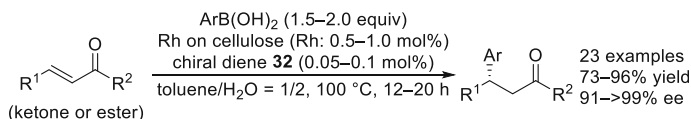
Scheme 43 One-pot oxidation/HWE reaction/asymmetric 1,4-addition reactions catalyzed by Au/Pd nanoparticle and chiral Rh nanoparticle

mixture, and a hot-filtration test confirmed that no reaction proceeded in the filtrate that was obtained in the middle of the reaction.

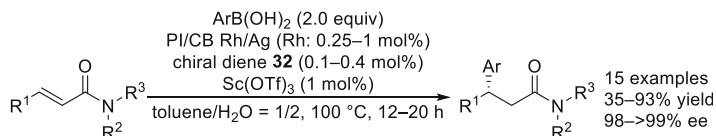
In this work, several unique natures of Rh nanoparticle systems that were different from the nature of the corresponding homogeneous Rh(I)-diene **32** complex were found. The comparison of the catalytic activity in a homogeneous Rh(I) complex system and the chiral Rh nanoparticle system showed that superior performance of the nanoparticle system in terms of activity and/or enantioselectivity was observed for several substrates. Nonlinear effect analysis [117], which is a plot of enantiopurity of a product against enantiopurity of a chiral ligand, was also conducted in both systems. A positive nonlinear effect was observed in the heterogeneous nanoparticle system, whereas a linear relationship between enantiomeric excess of a ligand and that of a product was observed in the homogeneous metal complex system.

In 2015, Kobayashi et al. applied chiral diene **32**-modified Rh nanoparticle catalysts to an integrated process of oxidation-olefination-asymmetric 1,4-addition reactions (Scheme 43) [118]. Polymer-incarcerated Au/Pd bimetallic catalyst (PI/CB Au/Pd), developed by the authors [119], was used for a tandem process of aerobic oxidation and Horner-Wadsworth-Emmons (HWE) olefination to convert primary alcohols to the corresponding unsaturated esters. After the two-step reaction, PI/CB Rh, arylboronic acid, and chiral diene **32** were added to perform the asymmetric 1,4-addition in the same pot. These three-step, one-pot sequential reactions catalyzed by two different heterogeneous nanoparticle catalysts can produce β -arylated esters in high yields with excellent enantioselectivities from readily available alcohols. Such an integration of reactions has great advantages that can reduce the number of purification steps, and unstable intermediates can be treated in situ.

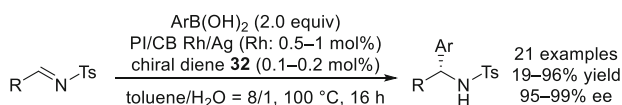
In the same year, Kobayashi et al. also developed cellulose-supported Rh nanoparticle catalysts for asymmetric 1,4-addition reactions (Scheme 44) [120]. Unlike PI/CB catalysts, Rh nanoparticles were well dispersed over the support without Ag, and this monometallic catalyst showed high catalytic activity in the presence of chiral diene **32** for the reaction with α,β -unsaturated ketones and esters. They analyzed the catalyst with chiral diene **32** by solid-state NMR with the addition of a solvent to swell the sample, so-called swollen-resin magic-angle spinning (SR-MAS) NMR [121]. The pulse sequence consisting of a diffusion filter and isotropic



Scheme 44 Cellulose-supported Rh nanoparticle catalysts for asymmetric 1,4-addition reactions



Scheme 45 Cooperative catalyst system using chiral Rh nanoparticle and Lewis acid catalysts for asymmetric 1,4-addition to unsaturated amides

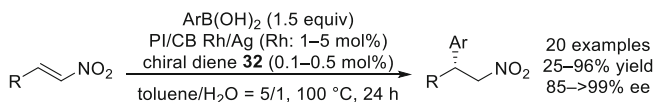


Scheme 46 Chiral Rh nanoparticle catalyzed asymmetric arylation of imines

mixing was used to suppress signals from chiral diene **32** in the solution phase and to exchange the remaining magnetization of cellulose with nearby molecules that would be anchored in the catalyst. The result suggested that the chiral diene **32** adsorbed on the Rh nanoparticles was observed selectively using this method. Similar to the PI/CB Rh/Ag system, a positive nonlinear effect was observed in this cellulose-supported Rh nanoparticle system.

In 2016, Kobayashi et al. reported a cooperative catalyst system using a chiral Rh nanoparticle catalyst and a metal Lewis acid catalyst for asymmetric 1,4-additions to α,β -unsaturated amides (Scheme 45) [122]. α,β -Unsaturated amides are significantly less reactive substrates than α,β -unsaturated ketones and esters because of their high LUMO energy. They employed Sc(OTf)₃ as a water-compatible Lewis acidic co-catalyst to activate amide substrates for chiral Rh nanoparticle systems. The reactions proceeded to afford the corresponding β -chiral amides with excellent enantioselectivity without leaching of Rh. The role of Sc(OTf)₃ was assumed to lower the LUMO level of the amide substrate to accelerate a C–C bond-forming step and/or accelerate a protonation (product release and catalyst regeneration) step by inner-sphere water ligands of the water-compatible Lewis acid. In the presence of Sc(OTf)₃, a higher yield in the heterogeneous nanoparticle catalyst system than that in the corresponding homogeneous Rh-diene **32** complex system was observed, indicating that the heterogeneous nanoparticle catalyst system enhanced the efficiency of the cooperative catalysis.

In 2016, Kobayashi et al. expanded the applicability of chiral Rh nanoparticle systems to asymmetric arylation of aldimines (Scheme 46) [123]. The ratio of



Scheme 47 Chiral Rh nanoparticle catalyzed asymmetric arylation of nitroolefins

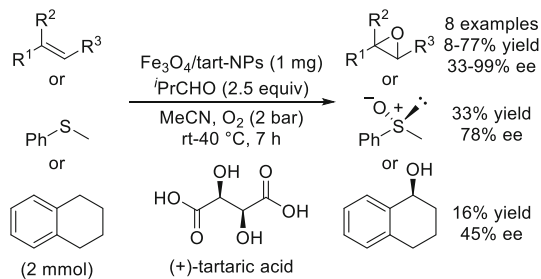
toluene and water was optimized to 8:1 to prevent hydrolysis of imines. Asymmetric arylation of aromatic tosylamines proceeded smoothly to afford the corresponding chiral (diarylmethyl)amines in high yields with excellent enantioselectivities in the presence of PI/CB Rh/Ag and chiral diene **32**. On the other hand, as aliphatic imines are more sensitive to water than aromatic imines, the desired products of aliphatic imines were obtained in moderate yields, while enantioselectivities were excellent.

In 2017, Kobayashi et al. further applied chiral Rh nanoparticle systems to asymmetric arylation of nitroolefins (Scheme 47) [124]. The ratio of toluene and water was crucial not only to achieve high yields and enantioselectivities but also to prevent metal leaching. The system worked well even for heteroarene-substituted nitroolefins and aliphatic olefins in excellent enantioselectivity. The nature of active species was discussed in details. First of all, they denied the possibility of the leached homogeneous species as an active species by hot filtration tests. The kinetic behavior of the catalysts recovered at several timings was examined, and their XPS analysis was conducted. These studies suggested a generation of an active species through a redox process between phenyl boronic acid and metal nanoparticles. Considering the similarity of the outcomes of enantioselectivities in homogeneous and heterogeneous systems, they concluded the scenario, in which the reaction proceeded on metal complexes or on very small nanoclusters within the polymer phase, was more likely than the scenario in which the reaction proceeded on the surface of the metal nanoparticles.

6 Other Chiral Molecules as Modifiers

In 2016, Hosseini-Monfared developed magnetite nanoparticles stabilized by L-(+)-tartaric acid ($\text{Fe}_3\text{O}_4/\text{tart-NPs}$) for asymmetric oxidation of olefins, thioanisole, and tetralin (Scheme 48) [125]. The catalyst was prepared by heating a diethylene glycol solution of $\text{FeCl}_3 \cdot 6\text{H}_2\text{O}$, tartaric acid, and urea at 200°C . Asymmetric oxidation of olefins was performed under oxygen atmosphere in the presence of the catalyst and isobutyl aldehyde as a reductant for the reduction of dioxygen at the beginning of the reaction. Aliphatic substrates gave the corresponding chiral epoxides in moderate to good yields with good to excellent enantioselectivities, while styrene derivatives afforded the products in poor yields and low to moderate enantioselectivities. In the latter case, aldehyde or ketone by-products were observed. The reactions of thioanisole to give the sulfoxide and of tetralin to afford the alcohol also proceeded under the same conditions. The catalysts could be collected by magnetic decantation

Scheme 48 Asymmetric oxidation of olefins, thioanisole, and tetralin by $\text{Fe}_3\text{O}_4/\text{tart}$ -NPs



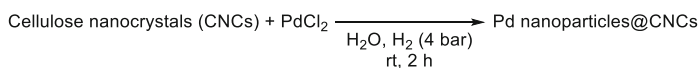
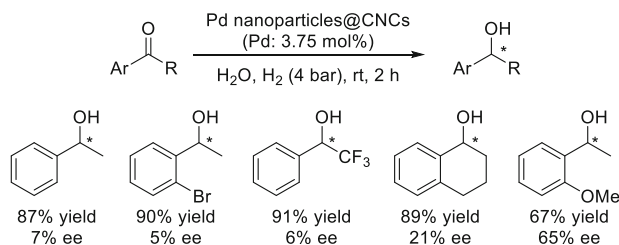
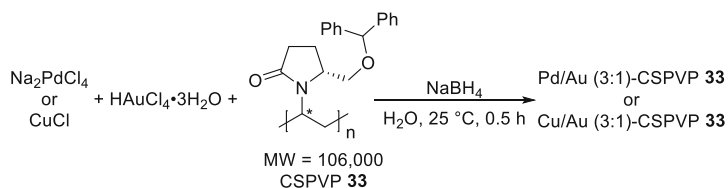
and reused five times with increasing catalytic activity after each use in the aerobic oxidation of tetralin.

7 Chiral Polymer-Stabilized Nanoparticle Catalysts

Use of polymer with chiral functionality as a chiral modifier is an attractive subject, as a chiral modifier is expected to be easily recovered. Although silk, as a chiral polymer, supported Pd catalyst was found to be active in asymmetric hydrogenation of benzylidene oxazolidone in the 1950s [3], no successful example of chiral polymer-supported nanoparticle catalysts for asymmetric catalysis was reported until recent studies.

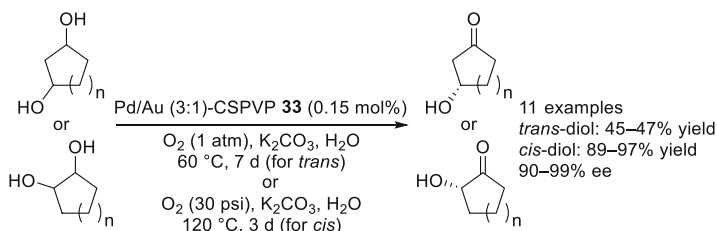
In 2015, Moores et al. utilized cellulose nanocrystals (CNCs) as chiral inducers [126]. Pd nanoparticles were deposited on highly crystalline and well-defined CNCs via treatment of an aqueous mixture of a CNC suspension and a PdCl_2 solution under mild H_2 pressure (Scheme 49). Several aromatic ketones were tested as substrates in asymmetric hydrogenation by the Pd nanoparticles on CNCs, and maximally a 65% ee could be obtained from the reaction with *ortho*-methoxy acetophenone (Scheme 50). The aqueous suspension could be recovered by simple phase separation and reused up to three times with no loss of activity and enantioselectivity. The fourth and fifth cycles did lead to a drop in activity, but the enantioselectivity was preserved. Heterogeneity of the catalyst system was also confirmed by a poisoning experiment with CS_2 . The 3D structure of the catalyst was studied by cryo-electron microscopy, high-resolution transmission electron microscopy, and tomography. It revealed that sub-nanometer-thick Pd patches are located at the surface of CNCs.

In 2016, Hua et al. reported chiral-substituted poly-*N*-vinylpyrrolidinones (CSPVP **33**) supported bimetallic Pd/Au and Cu/Au nanoparticle catalysts for various asymmetric oxidation reactions [127]. Chiral pyrrolidinone monomers were prepared from *N*-Boc *L*-(*S*)-amino acids, and the corresponding polymers were used for deposition of bimetallic nanoparticles (Scheme 51). Various structures of monomers were examined in asymmetric oxidation of 1,3-diol, and CSPVP **33** was found to be the best chiral inducer. Pd/Au bimetallic nanoparticle catalysts on CSPVP **33** were applied to kinetic resolution of *trans*-1,2 and 1,3-diols and asymmetric mono oxidation of *cis*-1,2 and 1,3-diols to produce the corresponding

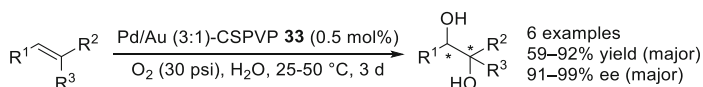
**Scheme 49** Preparation of cellulose nanocrystals supported Pd nanoparticles**Scheme 50** Pd nanoparticles on CNCs catalyzed asymmetric hydrogenation of ketones**Scheme 51** Preparation of chiral-substituted poly-*N*-vinylpyrrolidinones **33** supported bimetallic catalysts

hydroxy ketones in excellent enantioselectivity (Scheme 52). The same catalyst was also utilized for asymmetric oxidation of alkenes to afford diols with excellent enantioselectivities (Scheme 53). Interestingly, resulting diols did not undergo further oxidation even though benzylic alcohols were easily oxidized by Au nanoparticle catalysts [128]. Furthermore, Cu/Au bimetallic nanoparticle catalysts on CSPVP **33** were applied to asymmetric C–H oxidation of cycloalkanes to produce ketones with excellent enantioselectivities (Scheme 54).

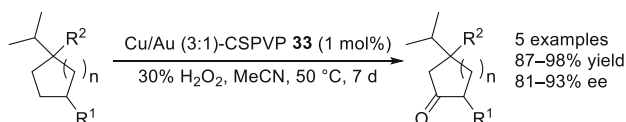
In 2017, Chen and Dong et al. reported Pd nanoparticles loaded on a homochiral covalent organic framework (COF) for asymmetric catalysis [129]. The chiral COF support (CCOF-MPC) was synthesized from cyanuric chloride and *S*-(+)-2-methylpiperazine at 90°C, and the Pd nanoparticles were loaded on CCOF-MPC via sequential solution impregnation and reduction of a Pd salt by NaBH₄ to afford the catalyst (Pd@CCOF-MPC) (Scheme 55). High-resolution transmission electron microscopy (HRTEM) analysis of the catalyst showed highly dispersed Pd nanoparticles with a particle size of 2–5 nm. The size of the Pd nanoparticles was larger than that of the pore size (1.5 nm) in Pd@CCOF-MPC indicating that Pd nanoparticles might be located between the 2D COF layers. An increase in the interlayer spacing of COF was also demonstrated by the PXRD pattern of the catalyst.



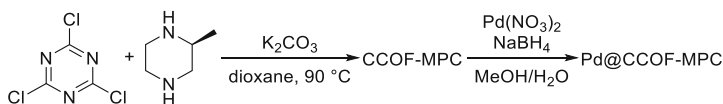
Scheme 52 Pd/Au-CSPVP **33** catalyzed asymmetric oxidation of 1,3-diols and 1,2-diols



Scheme 53 Pd/Au-CSPVP **33** catalyzed asymmetric oxidation of alkenes



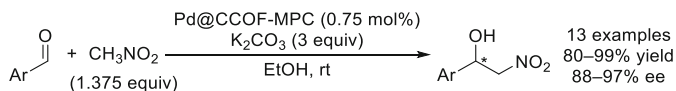
Scheme 54 Cu/Au-CSPVP **33** catalyzed asymmetric oxidation of cycloalkanes



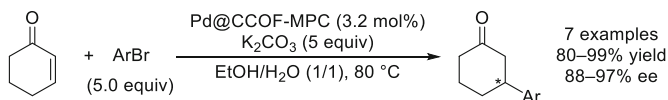
Scheme 55 Preparation of Pd@CCOF-MPC

Pd@CCOF-MPC was applied to asymmetric Henry reactions, and various aromatic aldehydes were converted to the corresponding β -nitro alcohols in high enantioselectivity (Scheme 56). CCOF-MPC itself hardly catalyzed the reaction indicating that Pd nanoparticles in the CCOF-MPC matrix are responsible for the catalytic activity. The catalyst was also applied to asymmetric reductive Heck reactions of 2-cyclohexen-1-one with aryl halides (Scheme 57). Although Pd nanoparticles were aggregated and leached out after five runs in both reactions, relatively high levels of yield and enantioselectivity were maintained.

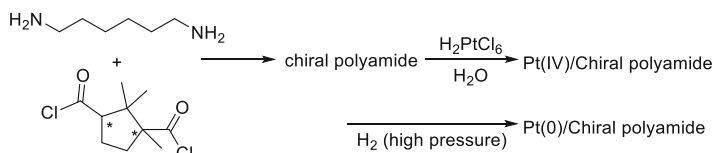
In 2017, Sharma et al. reported Pt nanoparticles incorporated chiral polyamide for asymmetric hydrogenation of an α -ketoester [130]. Chiral polyamides were synthesized from camphoric dichloride and diamine monomers by interfacial condensation reactions. A Pt(IV) salt was loaded on the polymer followed by reduction under high-pressure hydrogen to afford the catalyst, Pt(0)/chiral polyamide (Scheme 58). Several diamine linkers were examined, and the catalyst prepared from hexamethylenediamine showed the best performance in asymmetric hydrogenation



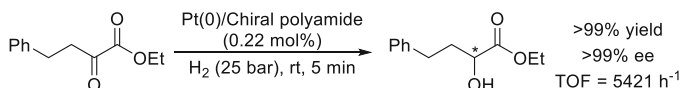
Scheme 56 Pd@CCOF-MPC catalyzed asymmetric Henry reaction



Scheme 57 Pd@CCOF-MPC catalyzed asymmetric reductive Heck reaction



Scheme 58 Preparation of chiral polyamide supported Pt nanoparticle catalysts



Scheme 59 Pt(0)/chiral polyamide catalyzed asymmetric hydrogenation of ethyl 2-oxo-4-phenylbutanoate

of ethyl 2-oxo-4-phenylbutanoate with excellent enantioselectivity (Scheme 59). The catalyst could be reused for ten cycles with slight loss of enantioselectivity. This chiral polyamide supports have helical structure with molecular chirality examined by the CD and UV-vis spectroscopies.

8 Conclusion

As introduced in this chapter, chiral nanoparticle catalytic systems have a potential to construct robust asymmetric catalysts. Thanks to diverse choice of chiral modifiers, which were originally used for homogeneous metal complex catalysis, applicable reactions catalyzed by chiral metal nanoparticles were dramatically expanded especially since 2000. Several reports proved that not only small molecules but also chiral polymers would be good candidates of chiral modifiers for nanoparticles. Some examples demonstrated excellent enantioselectivities with broad substrate generality and reusability, and they must be useful heterogeneous catalysts. Moreover, chiral metal nanoparticles showed unique catalytic behaviors that are different from the corresponding homogeneous metal complex systems. It indicates that the

active species in nanoparticle catalysis are not leached molecular complexes although true active species are unclear in most cases. This is an emerging area of research, and we expect that further studies lead to achievement of more efficient and unique chiral nanoparticle catalysis.

References

1. Ojima I (2010) *Catalytic asymmetric synthesis*. Wiley, Hoboken
2. Christmann M, Bräse S (2012) *Asymmetric synthesis II: more methods and applications*. Wiley, Hoboken
3. Akabori S, Sakurai S, Izumi Y, Fujii Y (1956) *Nature* 178:323
4. Izumi Y, Imaida M, Fukawa H, Akabori S (1963) *Bull Chem Soc Jpn* 36:21
5. Izumi Y, Imaida M, Fukawa H, Akabori S (1963) *Bull Chem Soc Jpn* 36:155
6. Tatsumi S, Imaida M, Fukuda Y, Izumi Y, Akabori S (1964) *Bull Chem Soc Jpn* 37:846
7. Orito Y, Imai S, Niwa S (1979) *Nippon Kagaku Kaishi*:1118
8. Orito Y, Imai S, Niwa S, Nguyen GH (1979) *J Synth Org Chem Jpn* 37:173
9. Rodríguez-García L, Hungerbühler K, Baiker A, Meemken F (2017) *ACS Catal* 7:3799
10. Xue XR, Wang YH, Han FS (2017) *Chem Commun* 53:3346
11. Yang T, Lou LL, Yu WJ, Feng YJ, Li H, Yu K, Liu SX (2017) *ChemCatChem* 9:458
12. Mao C, Zhang J, Xiao MT, Liu YJ, Zhang XQ (2018) *Curr Appl Phys* 18:1480
13. Meemken F, Rodríguez-García L (2018) *J Phys Chem Lett* 9:996
14. Xue XR, Chen P, Xu P, Wang YH (2018) *Catal Commun* 110:55
15. Xue XR, Zhao ZH, Wang YH (2018) *Org Chem Front* 5:3585
16. Blaser H-U, Studer M (2007) *Acc Chem Res* 40:1348
17. Zhan E, Chen C, Li Y, Shen W (2015) *Cat Sci Technol* 5:650
18. Baiker A (2015) *Chem Soc Rev* 44:7449
19. Meemken F, Baiker A (2017) *Chem Rev* 117:11522
20. Tang Z (2018) *Chiral nanomaterials: preparation, properties and applications*. Wiley, Hoboken
21. Maeda N, Hungerbühler K, Baiker A (2011) *J Am Chem Soc* 133:19567
22. Meemken F, Maeda N, Hungerbuehler K, Baiker A (2012) *Angew Chem Int Ed* 51:8212
23. Goubert G, McBreen PH (2013) *ChemCatChem* 5:683
24. Crabtree RH (2012) *Chem Rev* 112:1536
25. Demers-Carpentier V, Goubert G, Masini F, Lafleur-Lambert R, Dong Y, Lavoie S, Mahieu G, Boukouvalas J, Gao H, Rasmussen AMH, Ferrighi L, Pan Y, Hammer B, McBreen PH (2011) *Science* 334:6057
26. Orglmeister E, Mallat T, Baiker A (2005) *Adv Synth Catal* 347:78
27. Dong Y, Svane K, Lemay JC, Groves MN, McBreen PH (2017) *ACS Catal* 7:1757
28. Goubert G, Dong Y, Groves MN, Lemay JC, Hammer B, McBreen PH (2017) *Nat Chem* 9:531
29. Lavoie S, Laliberté M-A, Temprano I, McBreen PH (2006) *J Am Chem Soc* 128:7588
30. Studer M, Burkhardt S, Blaser H-U (1999) *Chem Commun*:1727
31. von Arx M, Mallat T, Baiker A (2002) *Catal Lett* 78:267
32. Diezi S, Hess M, Orglmeister E, Mallat T, Baiker A (2005) *Catal Lett* 102:121
33. Yang HP, Wang H, Lu JX (2015) *Electrochem Commun* 55:18
34. Yang HP, Fen Q, Wang H, Lu JX (2016) *Electrochem Commun* 71:38
35. Yue YN, Wu D, Zeng S, Yang MP, Wang H, Lu JX (2017) *New J Chem* 41:7853
36. Zhu J, Sun X-T, Wang X-D, Wu L (2018) *ChemCatChem* 10:1788
37. Tungler A, Tarnai T, Máthé T, Petró J (1991) *J Mol Catal* 67:277
38. Perosa A, Tundo P, Selva M (2002) *J Mol Catal A Chem* 180:169
39. Vetere V, Faraoni MB, Santori GF, Podestá J, Casella ML, Ferretti OA (2004) *J Catal* 226:457

40. Vetere V, Faraoni MB, Santori GF, Podestá JC, Casella ML, Ferretti OA (2005) *Catal Today* 107–108:266
41. Cheng H, Hao J, Wang H, Xi C, Meng X, Cai S, Zhao F (2007) *J Mol Catal A Chem* 278:6
42. Wang J, Feng H, Qin R, Fu H, Yuan M, Chen H, Li X (2007) *Tetrahedron Asymmetry* 18:1643
43. Jiang HY, Yang CF, Li C, Fu HY, Chen H, Li RX, Li XJ (2008) *Angew Chem Int Ed* 47:9240
44. Jiang H-Y, Sun B, Zheng X-X, Chen H (2012) *Appl Catal A* 421:86
45. Li C, Zhang L, Zheng C, Zheng X, Fu H, Chen H, Li R (2014) *Tetrahedron Asymmetry* 25:821
46. Yang CF, Jiang HY, Feng J, Fu HY, Li RX, Chen H, Li XJ (2009) *J Mol Catal A Chem* 300:98
47. Li C, Zhang L, Liu H, Zheng X, Fu H, Chen H, Li R (2014) *Catal Commun* 54:27
48. Jiang H-Y, Chen H, Li R-X (2010) *Catal Commun* 11:584
49. Tungler A, Kajtar M, Mathe T, Toth G, Fogassy E, Petro J (1989) *Catal Today* 5:159
50. Tungler A, Máthé T, Petró J, Tarnai T (1990) *J Mol Catal* 61:259
51. McIntosh AI, Watson DJ, Burton JW, Lambert RM (2006) *J Am Chem Soc* 128:7329
52. Mhadgut SC, Török M, Dasgupta S, Török B (2008) *Catal Lett* 123:156
53. Watson DJ, Jesudason RJBRJ, Beaumont SK, Kyriakou G, Burton JW, Lambert RM (2009) *J Am Chem Soc* 131:14584
54. Mhadgut SC, Török M, Esquibel J, Török B (2006) *J Catal* 238:441
55. Schafer C, Mhadgut SC, Kugyela N, Torok M, Torok B (2015) *Cat Sci Technol* 5:716
56. Rodríguez-García L, Hungerbühler K, Baiker A, Meemken F (2015) *J Am Chem Soc* 137:12121
57. Kunz S, Schreiber P, Ludwig M, Maturi MM, Ackermann O, Tschurl M, Heiz U (2013) *Phys Chem Chem Phys* 15:19253
58. Schrader I, Warneke J, Backenköhler J, Kunz S (2015) *J Am Chem Soc* 137:905
59. Schrader I, Neumann S, Himstedt R, Zana A, Warneke J, Kunz S (2015) *Chem Commun* 51:16221
60. Schrader I, Neumann S, Sulce A, Schmidt F, Azov V, Kunz S (2017) *ACS Catal* 7:3979
61. Šulce A, Backenköhler J, Schrader I, Piane MD, Müller C, Wark A, Ciacchi LC, Azov V, Kunz S (2018) *Cat Sci Technol* 8:6062
62. Gross E, Liu JH, Alayoglu S, Marcus MA, Fakra SC, Toste FD, Somorjai GA (2013) *J Am Chem Soc* 135:3881
63. Tang W, Zhang X (2003) *Chem Rev* 103:3029
64. Li YM, Kwong FY, Yu WY, Chan ASC (2007) *Coord Chem Rev* 251:2119
65. Pereira MM, Calvete MJF, Carrilho RMB, Abreu AR (2013) *Chem Soc Rev* 42:6990
66. Mikhailine A, Lough AJ, Morris RH (2009) *J Am Chem Soc* 131:1394
67. Meyer N, Lough AJ, Morris RH (2009) *Chem Eur J* 15:5605
68. Sonnenberg JF, Morris RH (2014) *Cat Sci Technol* 4:3426
69. Sonnenberg JF, Coombs N, Dube PA, Morris RH (2012) *J Am Chem Soc* 134:5893
70. Prokopchuk DE, Sonnenberg JF, Meyer N, Zimmer-De Iuliis M, Lough AJ, Morris RH (2012) *Organometallics* 31:3056
71. Li Y, Yu S, Wu X, Xiao J, Shen W, Dong Z, Gao J (2014) *J Am Chem Soc* 136:4031
72. Cano I, Tschan MJL, Martinez-Prieto LM, Philippot K, Chaudret B, van Leeuwen P (2016) *Cat Sci Technol* 6:3758
73. Xia YT, Ma J, Wang XD, Yang L, Wu L (2017) *Cat Sci Technol* 7:5515
74. Riant O, Mostefai N, Courmarcel J (2004) *Synthesis*:2943
75. Tamura M, Fujihara H (2003) *J Am Chem Soc* 125:15742
76. Kantam ML, Laha S, Yadav J, Likhari PR, Sreedhar B, Choudary BM (2007) *Adv Synth Catal* 349:1797
77. Kantam ML, Yadav J, Laha S, Srinivas P, Sreedhar B, Figueras F (2009) *J Org Chem* 74:4608
78. Li M, Li B, Xia H-F, Ye D, Wu J, Shi Y (2014) *Green Chem* 16:2680
79. Akiyama R, Kobayashi S (2001) *Angew Chem Int Ed* 40:3469
80. Jansat S, Gómez M, Philippot K, Muller G, Guiu E, Claver C, Castillon S, Chaudret B (2004) *J Am Chem Soc* 126:1592

81. Favier I, Gómez M, Muller G, Axet MR, Castillon S, Claver C, Jansat S, Chaudret B, Philippot K (2007) *Adv Synth Catal* 349:2459
82. Dieguez M, Pamies O, Mata Y, Teuma E, Gomez M, Ribaudó F, van Leeuwen PWNM (2008) *Adv Synth Catal* 350:2583
83. Felpin FX, Landais Y (2005) *J Org Chem* 70:6441
84. Reimann S, Mallat T, Baiker A (2007) *J Catal* 252:30
85. Reimann S, Mallat T, Baiker A (2008) *J Catal* 254:79
86. Reimann S, Grunwaldt J-D, Mallat T, Baiker A (2010) *Chem Eur J* 16:9658
87. Sawai K, Tatum R, Nakahodo T, Fujihara H (2008) *Angew Chem Int Ed* 47:6917
88. Mori K, Kondo Y, Yamashita H (2009) *Phys Chem Chem Phys* 11:8949
89. Klosin J, Landis CR (2007) *Acc Chem Res* 40:1251
90. Neves ACB, Calvete MJF, Melo T, Pereira MM (2012) *Eur J Org Chem*:6309
91. Coronado JM, Coloma F, Anderson JA (2000) *J Mol Catal A Chem* 154:143
92. Han D, Li X, Zhang H, Liu Z, Li J, Li C (2006) *J Catal* 243:318
93. Han D, Li X, Zhang H, Liu Z, Hu G, Li C (2008) *J Mol Catal A Chem* 283:15
94. Axet MR, Castillon S, Claver C, Philippot K, Lecante P, Chaudret B (2008) *Eur J Inorg Chem* 2008:3460
95. Alsalahi W, Trzeciak AM (2018) *ChemistrySelect* 3:1727
96. Park KH, Chung YK (2005) *Adv Synth Catal* 347:854
97. Chen MY, Xu Z, Chen L, Song T, Zheng ZJ, Cao J, Cui YM, Xu LW (2018) *ChemCatChem* 10:280
98. Hopkinson MN, Richter C, Schedler M, Glorius F (2014) *Nature* 510:485
99. Zhukhovitskiy AV, MacLeod MJ, Johnson JA (2015) *Chem Rev* 115:11503
100. Ranganath KVS, Kloesges J, Schäfer AH, Glorius F (2010) *Angew Chem Int Ed* 49:7786
101. Richter C, Ranganath KVS, Glorius F (2012) *Adv Synth Catal* 354:377
102. Ranganath KVS, Schaefer AH, Glorius F (2011) *ChemCatChem* 3:1889
103. Ye R, Zhukhovitskiy AV, Kazantsev RV, Fakra SC, Wickemeyer BB, Toste FD, Somorjai GA (2018) *J Am Chem Soc* 140:4144
104. Shu X-Z, Nguyen SC, He Y, Oba F, Zhang Q, Canlas C, Somorjai GA, Alivisatos AP, Toste FD (2015) *J Am Chem Soc* 137:7083
105. Hayashi T, Ueyama K, Tokunaga N, Yoshida K (2003) *J Am Chem Soc* 125:11508
106. Fischer C, Defieber C, Suzuki T, Carreira EM (2004) *J Am Chem Soc* 126:1628
107. Defieber C, Gruetzmacher H, Carreira EM (2008) *Angew Chem Int Ed* 47:4482
108. Dong HQ, Xu MH, Feng CG, Sun XW, Lin GQ (2015) *Org Chem Front* 2:73
109. Nagamoto M, Nishimura T (2017) *ACS Catal* 7:833
110. Hayashi T, Yamasaki K (2003) *Chem Rev* 103:2829
111. Takaya Y, Ogasawara M, Hayashi T, Sakai M, Miyaura N (1998) *J Am Chem Soc* 120:5579
112. Tian P, Dong H-Q, Lin G-Q (2012) *ACS Catal* 2:95
113. Howell GP (2012) *Org Process Res Dev* 16:1258
114. Brock S, Hose D, Moseley J, Parker A, Patel I, Williams A (2008) *Org Process Res Dev* 12:496
115. Yasukawa T, Miyamura H, Kobayashi S (2012) *J Am Chem Soc* 134:16963
116. Yasukawa T, Suzuki A, Miyamura H, Nishino K, Kobayashi S (2015) *J Am Chem Soc* 137:6616
117. Satyanarayana T, Abraham S, Kagan HB (2009) *Angew Chem Int Ed* 48:456
118. Miyamura H, Suzuki A, Yasukawa T, Kobayashi S (2015) *Adv Synth Catal* 357:3815
119. Kobayashi S, Miyamura H (2013) *Aldrichimica Acta* 46:3
120. Yasukawa T, Miyamura H, Kobayashi S (2015) *Chem Sci* 6:6224
121. Kobayashi S, Akiyama R, Furuya T, Moriwaki M (1998) *Molecules* 2:35
122. Yasukawa T, Saito Y, Miyamura H, Kobayashi S (2016) *Angew Chem Int Ed* 55:8058
123. Yasukawa T, Kuremoto T, Miyamura H, Kobayashi S (2016) *Org Lett* 18:2716
124. Miyamura H, Nishino K, Yasukawa T, Kobayashi S (2017) *Chem Sci* 8:8362
125. Hadian-Dehkordi L, Hosseini-Monfared H (2016) *Green Chem* 18:497

126. Kaushik M, Basu K, Benoit C, Cirtiu CM, Vali H, Moores A (2015) *J Am Chem Soc* 137:6124
127. Hao B, Gunaratna MJ, Zhang M, Weerasekara S, Seiwald SN, Nguyen VT, Meier A, Hua DH (2016) *J Am Chem Soc* 138:16839
128. Takale BS, Bao M, Yamamoto Y (2014) *Org Biomol Chem* 12:2005
129. Ma HC, Kan JL, Chen GJ, Chen CX, Dong YB (2017) *Chem Mater* 29:6518
130. Sharma P, Sharma RK (2017) *ChemistrySelect* 2:513